

**Design, synthesis and evaluation of novel and
clinically used anti-cancer agents targeted
intracellularly**

Omar Mohammed

**Thesis submitted in partial fulfilment of the requirements of
Edinburgh Napier University for the degree of Doctor of Philosophy**

Abstract of Thesis

The development of drug resistance, notably multidrug resistance (MDR) and adverse side effects due to treatment with current anticancer drugs are considerable obstacles in cancer therapy and together with dose-limiting toxicity lead to therapeutic failure in the cancer clinic. The aim of this study is to design and deliver new anticancer agents selectively to the tumour site to increase efficacy and reduce toxic side effects to normal cells, thereby increasing the therapeutic index; this would afford significant improvement for patients. The P-glycoprotein (P-gp; p-170) efflux pump is the most notable factor contributing to MDR. In one approach, a series of novel ester-linked aminoanthraquinone-triphenylphosphonium (AQ-TPP) conjugates, structurally related to the DNA-binding, Pgp- substrate anticancer drug mitoxantrone, was synthesised and characterized by mass spectrometry, ^1H and ^{13}C NMR spectroscopy. AQ-conjugates of the lipophilic cation TPP^+ were designed and shown to utilize the large mitochondrial membrane potential ($\Delta\Psi\text{m}$) in cancer cells to drive drug accumulation inside the mitochondria and concomitantly circumvent Pgp-mediated resistance. Correspondingly, enhanced DNA-binding affinity and cytotoxicity were achieved for the AQ-TPP conjugate series compared with unconjugated precursors, exemplified by conversion of the non-DNA binding, non-cytotoxic hydroxyalkylanthraquinone NU:UB 238 to its TPP conjugate SH1; that bound strongly to DNA ($K_{\text{app}} 0.1 \times 10^7 \text{M}^{-1}$) and was equitoxic in the highly resistant Pgp-expressing HCT 15 colon carcinoma and sensitive MCF7 breast carcinoma cell lines. [IC_{50} (μM) 9.48 ± 0.32 and 9.69 ± 3.35 , respectively, by MTT assay]. Confocal microscopy live cell imaging in HCT116 colon cells, using MitoTrackerFM tracer dye showed significant colocalisation of cationic and lipophilic SH1 ($\text{Log D: } 2.68 \pm 0.04$) to mitochondria and not to lysosomes, whereas precursor NU:UB 238 ($\text{Log D: } 1.97 \pm 0.12$) was not taken up by cells, establishing proof of principle.

In another approach to achieve selective targeting of anthraquinone-based cytotoxics to cancer cells, a novel theranostic (therapeutic and diagnostic) anticancer prodrug Rho-Pro-Ala-Asn-Gly-APA-AQ(4,8-di-OH) (OM50) and FRET substrate of the endoprotease legumain, highly overexpressed in cancer, was designed and synthesized, using solution

phase and solid phase peptide synthesis, to incorporate experimental anticancer drug NU:UB 51, a cytotoxic bis-hydroxylated, propyl-spaced, aminoanthraquinone glycine conjugate with in vivo activity to confer cancer cell selectivity by legumain-mediated prodrug OM50 activation in the tumour microenvironment. The active drug was attached to the C-terminal asparagine (Asn) residue of the peptide substrate to exploit the unique proteolytic cleavage specificity of the enzyme for the acid terminus of Asn. Incubation of OM50 (10 μ M) with rh-legumain (0.40 ng/ μ L) at 37 °C for 2 h in MES assay buffer (pH 5.0) afforded a time-dependent increase in relative fluorescence intensity, monitored at the emission wavelength (λ_{em} 583 nm) of rhodamine-labelled peptide, confirming proof of principle for activation of the prodrug and direct release of the active anthraquinone NU:UB 51.

The above approaches offer the prospect of improved methods for selectively targeting the anthraquinone class of cytotoxics to cancer cells with therapeutic potential.

Declaration

It is hereby declare that this thesis and the research work upon which it is based were conducted by the author, Omar Mohammed.

Omar Mohammed

Acknowledgements

Foremost, I would like to express the deepest appreciation and my sincere gratitude to my supervisors, Dr David Mincher, Dr Agnes Turnbull and Dr Janis MacCallum, who have supported me throughout my PhD study and research project with their motivation, patience, enthusiasm and enormous knowledge. I could not have imagined having a better advisor for my PhD study and not have been possible to write this doctoral thesis without their help, support and patience.

I would like to thank the ESPRC National Mass Spectrometry Facility, University of Swansea. Thanks are also due to the NMR-facility at Heriot-Watt University.

Thanks are also due to past and present lab mates and members of the molecular drug design group, in particular Dr Yao Ding, Dr Sunil Mathur, Maria Gauci, Aiman Rehan and Olga Biskou for their assistance and friendship during my study and my time in the lab.

I would like to thank the research technician team and postgraduate research society members for their support and help during my time at Edinburgh Napier University.

Last but not the least, a special thanks to my family for their great support encouragements throughout my study. Special thanks to my father and mother who gave me the support during my study and I am grateful for them for all of the sacrifices they had made. At the end, I would like to express appreciation to my wife who is always trying to cheer me up and support me throughout all my studies.

Contents

Abstract of Thesis.....	i
Declaration	iii
Acknowledgements	iv
List of tables	xxii
Abbreviations	xxiii
Preface.....	xxvii
Nomenclature.....	xxvii
1 Chapter 1	2
1.1 Aim and Hypothesis	2
1.2 Introduction	3
1.2.1 Mitochondrial structure and function.....	3
1.2.2 Mitochondrial membrane potential ($\Delta\Psi_m$).....	5
1.2.3 Mitochondrial DNA and topoisomerases.....	6
1.2.4 Mitochondria and cancer	10
1.2.5 Mitochondrial targeting for cancer therapy.....	11
1.2.5.1 Examples of drugs targeted to mitochondria	12
1.2.5.2 Triphenylphosphonium bromide (TPP) vector targeted to mitochondria.....	14
1.2.5.3 Examples of TPP conjugates targeted to Mitochondria.....	16
1.2.5.4 Examples of other vectors targeted to mitochondria	22
1.2.6 Drug resistance	25
1.2.7 Anthraquinones and anthracyclines.....	30
1.2.8 Lysosomal sequestration	34
1.3 Results and discussion	39
1.3.1 Rational design.....	39
1.3.2 Synthetic strategy	44
1.3.3 Synthesis of the mitoxantrone derivatives-TPP conjugates.....	47
1.3.3.1 Synthesis of HO-EAE-AQ(4-OH) (OM1)	47

1.3.3.2	Synthesis of HO-EAE-Boc-AQ (4-OH) (OM2)	49
1.3.3.3	Synthesis of TPP-EAE-Boc-AQ-(4-OH) (OM22-Boc)	51
1.3.3.4	Synthesis of TPP-EAE-AQ(4-OH) (OM22 TFA)	52
1.3.3.5	Synthesis of OH-Butyl-AQ (4-OH) (NU:UB 252)	59
1.3.3.6	Synthesis of TPP-Butyl-AQ(4-OH) (OM30)	65
1.3.3.7	Synthesis of HO-pentyl-AQ(4-OH) (OM28)	72
1.3.3.8	Synthesis of TPP-Pentyl-AQ(4-OH) (OM31)	73
1.3.3.9	Synthesis of HO-EOE-AQ(4-OH) (OM29)	80
1.3.3.10	Synthesis of TPP-EOE-AQ(4-OH) (OM32)	81
1.3.3.11	Synthesis of OH-butyl-AQ (NU:UB 238)	88
1.3.3.12	Synthesis of (TPP-Butyl-AQ) (SH1)	89
1.3.3.13	Synthesis of mono-TPP-NU:UB 65 (OM25)	96
1.3.3.14	Synthesis of bis-TPP-NU:UB 65 (OM26)	97
1.3.4	Synthesis of mitoxantrone derivatives rhodamine B conjugates	100
1.3.4.1	Synthesis of Rho- β -ala-O ^t Bu (OM6) and Rho- β -ala-OH (OM7)	101
1.3.4.2	Synthesis of Rho- β -ala-EAE-Boc-AQ (4-OH) (OM17) and Rho- β -ala-EAE-AQ (4-OH) (OM18)	102
1.3.4.3	Synthesis of Rho-pip-Boc (OM4) and Rho-piperazine TFA (OM4 TFA)	105
1.3.4.4	Synthesis of Rho-pip-succinate (OM5)	106
1.3.4.5	Synthesis of Rho-pip-succ-EAE-Boc-AQ(4-OH) (OM15) and Rho-pip-succ-EAE-AQ(4-OH) (OM16)	106
1.3.5	Synthesis of mitoxantrone and ametantrone-linked conjugate	109
1.3.5.1	Synthesis of Mitoxantrone-Boc (OM19)	110
1.3.5.2	Attempted synthesis of Rho-pip-succ-mitoxantrone-Boc (OM20) and Rho-pip-succ-mitoxantrone (OM21)	111
1.3.5.3	Attempted synthesis of TPP-mitoxantrone-Boc (OM23) and bis-TPP-mitoxantrone-Boc (OM24)	115
1.3.5.4	Synthesis of ametantrone (NK1)	117
1.3.5.5	Synthesis of Ametantrone-Boc (NK4)	118
1.3.5.6	Synthesis of TPP-ametantrone-Boc (NK6) and TPP-ametantrone-TFA (NK8)	119
1.3.6	DNA binding assay	123
1.3.6.1	Mitoxantrone 2HCl DNA binding	126
1.3.6.2	OM2 [AQ-EAE-OH (4-OH)] TFA DNA binding	127

1.3.6.3	OM22 [AQ-EAE-TPP(4-OH)] TFA DNA binding	128
1.3.6.4	OM30 [AQ-Butyl-TPP(4-OH)] DNA binding	129
1.3.6.5	OM31 [AQ-Pentyl-TPP(4-OH)] DNA binding	130
1.3.6.6	OM32 [AQ-EOE-TPP(4-OH)] DNA binding	131
1.3.6.7	SH1 (AQ-Butyl-TPP) DNA binding	132
1.3.6.8	OM26 (bis-TPP-NU:UB 65) DNA binding	133
1.3.6.9	Ametantrone DNA binding.....	134
1.3.7	Distribution Coefficient.....	139
1.3.8	MTT Assay	145
1.3.9	Cellular uptake and localization	151
1.3.10	Morphological evaluation	160
1.3.11	Conclusion.....	168
1.4	Experimental	171
1.4.1	Analytical methods	171
1.4.1.1	Instruments.....	171
1.4.1.2	Thin layer chromatography (TLC).....	171
1.4.1.3	Column chromatography	171
1.4.1.4	Mass spectrometry	171
1.4.1.5	High performance liquid chromatography (HPLC).....	171
1.4.1.6	Proton and carbon nuclear magnetic resonance (¹ H and ¹³ C NMR)	172
1.4.2	General method A: For dichloromethane or chloroform / water solvent extraction	172
1.4.3	Synthesis of the mitoxantrone derivative-TPP conjugates.....	172
1.4.3.1	Synthesis of 1-hydroxy-4-((2-((2-hydroxyethyl)amino)ethyl)amino)anthracene-9,10-dione (HO-EAE-AQ(4-OH) (OM1).....	172
1.4.3.2	Synthesis of tert-butyl (2-((4-hydroxy-9,10-dioxo-9,10-dihydroanthracen-1-yl)amino)ethyl)(2-hydroxyethyl)carbamate (HO-EAE-Boc-AQ (4-OH) (OM2).173	
1.4.3.3	Synthesis of (5-(2-((tert-butoxycarbonyl)(2-((4-hydroxy-9,10-dioxo-9,10-dihydroanthracen-1-yl)amino)ethyl)amino)ethoxy)-5-oxopentyl)triphenylphosphonium (TPP-EAE-Boc-AQ-(4-OH)) (OM22-Boc)	173
1.4.3.4	Synthesis of (5-(2-((2-((4-hydroxy-9,10-dioxo-9,10-dihydroanthracen-1-yl)amino)ethyl)ammonio)ethoxy)-5-oxopentyl)triphenylphosphonium TPP-EAE-AQ(4-OH) (OM22)	174

1.4.3.5 Synthesis of 1-hydroxy-4-((4-hydroxybutyl)amino)anthracene-9,10-dione (OH-Butyl-AQ (4-OH) (NU:UB 252).....	175
1.4.3.6 Synthesis of (5-(4-((4-hydroxy-9,10-dioxo-9,10-dihydroanthracen-1-yl)amino)butoxy)-5-oxopentyl)triphenylphosphonium (TPP-Butyl-AQ(4-OH) (OM30).....	175
1.4.3.7 Synthesis of 1-hydroxy-4-((5-hydroxypentyl)amino)anthracene-9,10-dione (HO-pentyl-AQ(4-OH) (OM28).....	176
1.4.3.8 Synthesis (5-((5-((4-hydroxy-9,10-dioxo-9,10-dihydroanthracen-1-yl)amino)pentyl)oxy)-5-oxopentyl)triphenylphosphonium (TPP-Pentyl-AQ(4-OH) (OM31).....	177
1.4.3.9 Synthesis of 1-hydroxy-4-((2-(2-hydroxyethoxy)ethyl)amino)anthracene-9,10-dione (HO-EOE-AQ(4-OH) (OM29).....	178
1.4.3.10 Synthesis of (5-(2-(2-((4-hydroxy-9,10-dioxo-9,10-dihydroanthracen-1-yl)amino)ethoxy)ethoxy)-5-oxopentyl)triphenylphosphonium (TPP-EOE-AQ(4-OH) (OM32).....	179
1.4.3.11 Synthesis of 1-((4-hydroxybutyl)amino)anthracene-9,10-dione (OH-butyl-AQ) (NU:UB 238).....	180
1.4.3.12 Synthesis of (5-(4-((9,10-dioxo-9,10-dihydroanthracen-1-yl)amino)butoxy)-5-oxopentyl)triphenylphosphonium (TPP-Butyl-AQ) (SH1)	180
1.4.3.13 Synthesis of (5-((5-((4-((5-hydroxypentyl)amino)-9,10-dioxo-9,10-dihydroanthracen-1-yl)amino)pentyl)oxy)-5-oxopentyl)triphenylphosphonium TPP-NU:UB 65 (OM25)	182
1.4.3.14 Synthesis of (((((9,10-dioxo-9,10-dihydroanthracene-1,4-diyl)bis(azanediyl))bis(pentane-5,1-diyl))bis(oxy))bis(5-oxopentane-5,1-diyl))bis(triphenylphosphonium) bis-TPP-NU:UB 65 (OM26).....	182
1.4.4 Synthesis of mitoxantrone derivatives rhodamine B conjugates.....	183
1.4.4.1 Synthesis of tert-butyl 3-(3',6'-bis(diethylamino)-3-oxospiro[isindoline-1,9'-xanthen]-2-yl)propanoate (Rho-β-ala-O ^t Bu) (OM6)	183
1.4.4.2 Synthesis of N-(9-(2-((2-carboxyethyl)carbamoyl)phenyl)-6-(diethylamino)-3H-xanthen-3-ylidene)-N-ethylethanaminium (Rho-β-ala-OH) (OM7).....	183
1.4.4.3 Synthesis of N-(9-(2-((3-(2-((tert-butoxycarbonyl)(2-((4-hydroxy-9,10-dioxo-9,10-dihydroanthracen-1-yl)amino)ethyl)amino)ethoxy)-3-oxopropyl)carbamoyl)phenyl)-6-(diethylamino)-3H-xanthen-3-ylidene)-N-ethylethanaminium Rho-β-ala-EAE-Boc-AQ(4-OH) (OM17).....	184
1.4.4.4 Synthesis of 2-((3-(2-(6-(diethylamino)-3-(diethyliminio)-3H-xanthen-9-yl)benzamido)propanoyl)oxy)-N-(2-((4-hydroxy-9,10-dioxo-9,10-dihydroanthracen-1-yl)amino)ethyl)ethan-1-aminium (Rho-β-ala-EAE-AQ(4-OH) (OM18)	185

1.4.4.5	Synthesis of N-(9-(3-(4-(tert-butoxycarbonyl)piperazine-1-carbonyl)phenyl)-6-(diethylamino)-3H-xanthen-3-ylidene)-N-ethylethanaminium (Rho-pip-Boc) (OM4)	185
1.4.4.6	Synthesis of N-(6-(diethylamino)-9-(3-(piperazine-1-carbonyl)phenyl)-3H-xanthen-3-ylidene)-N-ethylethanaminium (Rho-piperazine TFA) (OM4 TFA)....	186
1.4.4.7	Synthesis of 4-(4-(3-(6-(diethylamino)-3-(diethyliminio)-3H-xanthen-9-yl)benzoyl)piperazin-1-yl)-4-oxobutanoate (Rho-pip-succinate) (OM5)	186
1.4.4.8	Synthesis of N-(9-(3-(4-(4-(2-((tert-butoxycarbonyl)(2-((4-hydroxy-9,10-dioxo-9,10-dihydroanthracen-1-yl)amino)ethyl)amino)ethoxy)-4-oxobutanoyl)piperazine-1-carbonyl)phenyl)-6-(diethylamino)-3H-xanthen-3-ylidene)-N-ethylethanaminium (Rho-pip-succ-EAE-Boc-AQ(4-OH) (OM15).....	186
1.4.4.9	Synthesis of 2-((4-(4-(3-(6-(diethylamino)-3-(diethyliminio)-3H-xanthen-9-yl)benzoyl)piperazin-1-yl)-4-oxobutanoyl)oxy)-N-(2-((4-hydroxy-9,10-dioxo-9,10-dihydroanthracen-1-yl)amino)ethyl)ethan-1-aminium (Rho-pip-succ-EAE-AQ(4-OH) (OM16).....	187
1.4.5	Synthesis of mitoxantrone and ametantrone-linked prodrugs.....	188
1.4.5.1	Synthesis of di-tert-butyl (((5,8-dihydroxy-9,10-dioxo-9,10-dihydroanthracene-1,4-diyl)bis(azanediyl))bis(ethane-2,1-diyl))bis((2-hydroxyethyl)carbamate) (Mitoxantrone-Boc) (OM19)	188
1.4.5.2	Attempted synthesis of Rho-pip-succ-mitoxantrone-Boc (OM20).....	188
1.4.5.3	Attempted synthesis of 2,2'-((5,8-dihydroxy-9,10-dioxo-9,10-dihydroanthracene-1,4-diyl)bis(azanediyl))bis(N-(2-((4-(4-(3-(6-(diethylamino)-3-(diethyliminio)-3H-xanthen-9-yl)benzoyl)piperazin-1-yl)-4-oxobutanoyl)oxy)ethyl)ethan-1-aminium) (Rho-pip-succ-mitoxantrone) (OM21)	189
1.4.5.4	Attempted synthesis of TPP-mitoxantrone-Boc (one arm) (OM23) and TPP-mitoxantrone (two arm) (OM24)	189
1.4.5.5	Synthesis of ametantrone (NK1)	190
1.4.5.6	Synthesis of di-tert-butyl (((9,10-dioxo-9,10-dihydroanthracene-1,4-diyl)bis(azanediyl))bis(ethane-2,1-diyl))bis((2-hydroxyethyl)carbamate) (ametantrone-Boc) (NK4)	190
1.4.5.7	Synthesis of ((((((9,10-dioxo-9,10-dihydroanthracene-1,4-diyl)bis(azanediyl))bis(ethane-2,1-diyl))bis((tert-butoxycarbonyl)azanediyl))bis(ethane-2,1-diyl))bis(oxy))bis(5-oxopentane-5,1-diyl))bis(triphenylphosphonium) (TPP-ametantrone-Boc) (NK6)	191
1.4.5.8	Synthesis of ((((((9,10-dioxo-9,10-dihydroanthracene-1,4-diyl)bis(azanediyl))bis(ethane-2,1-diyl))bis(ammoniumdiyl))bis(ethane-2,1-diyl))bis(oxy))bis(5-oxopentane-5,1-diyl))bis(triphenylphosphonium) (TPP-ametantrone tfa) (NK8).....	192

1.4.6	DNA binding assay	192
1.4.6.1	Materials.....	192
1.4.6.2	DNA quantification.....	193
1.4.6.3	Method	193
1.4.7	Distribution Coefficient Assay	194
1.4.7.1	Materials.....	194
1.4.7.2	Calibration curve methods.....	194
1.4.7.3	Distribution coefficient	194
1.4.8	MTT assay.....	195
1.4.8.1	Materials.....	195
1.4.8.2	Cell culture method	195
1.4.8.3	MTT assay method.....	196
1.4.9	Confocal microscopy	197
1.4.9.1	Materials.....	197
1.4.9.2	Method	197
1.4.10	Morphology studies	198
1.4.10.1	Materials	198
1.4.10.2	Method.....	198
1.5	Structure library.....	200
1.6	References.....	213
2	Chapter 2.....	239
2.1	Aim.....	239
2.2	Introduction	240
2.2.1	Tumour Microenvironment.....	240
2.2.2	Proteases	240
2.2.3	Legumain.....	241
2.2.4	Protease activated probes.....	242
2.2.5	Fluorescence resonance energy transfer (FRET).....	243
2.2.6	Rhodamine B.....	244
2.2.7	Protease activated prodrugs.....	248
2.2.8	NU:UB 51 (Gly-APA-AQ).....	252
2.3	Results and discussion	255

2.3.1	Rational design.....	255
2.3.2	Synthetic strategy	257
2.3.2.1	NU:UB 51 quencher	257
2.3.3	Peptide coupling.....	258
2.3.3.1	Fluorophore coupling.....	261
2.3.4	Synthesis of legumain targeted theranostic prodrug Rho-Pro-Ala-Asn-Gly-APA-AQ(4,8-di-OH) (OM50)	261
2.3.4.1	Synthesis of anthraquinone spacer compound APA- AQ(4,8-di-OH) (NU:UB 59).....	262
2.3.4.2	Synthesis of Boc-Gly-APA-AQ(4,8-di-OH) (NU:UB 51-Boc).....	263
2.3.4.3	Synthesis of Gly-APA-AQ(4,8-di-OH) (NU:UB 51)	264
2.3.5	Synthesis of prodrug OM50, Rho-Pro-Ala-Asn-Gly- APA-AQ(4,8-di-OH), by solution phase peptide synthesis	265
2.3.5.1	Synthesis of Fmoc-Asn(Trt)-Gly-APA-AQ(4,8-di-OH) (OM43)	265
2.3.5.2	Synthesis of H-Asn(Trt)-Gly-APA-AQ(4,8-di-OH) (OM44).....	269
2.3.5.3	Synthesis of Fmoc-Ala-Asn(Trt)-Gly-APA-AQ(4,8-di-OH) (OM45)....	270
2.3.5.4	Synthesis of H-Ala-Asn(Trt)-Gly-APA-AQ(4,8-di-OH) (OM46)	271
2.3.5.5	Synthesis of Fmoc-Pro-Ala-Asn(Trt)-Gly-APA-AQ(4,8-di-OH) (OM47).....	273
2.3.5.6	Synthesis of H-Pro-Ala-Asn(Trt)-Gly-APA-AQ(4,8-di-OH) (OM48) ...	274
2.3.5.7	Synthesis of Rho-Pro-Ala-Asn(Trt)-Gly-APA-AQ(4,8-di-OH) (OM49)	275
2.3.5.8	Removal of the trityl (Trt) group	277
2.3.6	Synthesis of the target compound Rho-Pro-Ala-Asn-Gly-APA-AQ(4,8-di-OH) (OM50) by solid phase peptide synthesis.....	279
2.3.6.1	Resin swelling	280
2.3.6.2	Deprotection of amino acid	280
2.3.6.3	Colour test.....	280
2.3.6.4	Peptide coupling	281
2.3.6.5	Rho-Pro-Ala-Asn(TRT)-resin cleavage	283
2.3.6.6	Reaction of Rho-Pro-Ala-Asn(Trt)-OH with Gly-APA-AQ(4,8-di-OH) [NU:UB 51] to give OM49.....	285
2.3.7	FRET and legumain studies	287
2.3.7.1	UV-Visible absorption assays.....	287
2.3.7.2	Rhodamine B-Pro-Ala-Asn-OH and NU:UB 51	287

2.3.7.3	Fluorescence spectroscopy assays.....	288
2.3.7.4	Incubation of OM50 with legumain	290
2.3.8	Cellular uptake and localization	292
2.3.9	Conclusion.....	295
2.4	Experimental	298
2.4.1	Synthesis of legumain targeted theranostic prodrug Rho-Pro-Ala-Asn-Gly-APA-AQ(4,8-di-OH) (OM50)	298
2.4.1.1	Synthesis of anthraquinone spacer compound APA-AQ(4,8-di-OH) (NU:UB 59).....	298
2.4.1.2	Synthesis of Boc-Gly-APA-AQ(4,8-di-OH) (NU:UB 51-Boc).....	298
2.4.1.3	Synthesis of Gly-APA-AQ(4,8-di-OH) [(NU:UB 51)	299
2.4.2	Synthesis of Synthesis of prodrug OM50, Rho-Pro-Ala-Asn-Gly-APA-AQ(4,8-di-OH), by solution phase peptide synthesis	299
2.4.2.1	Synthesis of Fmoc-Asn(Trt)-Gly-APA-AQ(4,8-di-OH) (OM43)	299
2.4.2.2	Synthesis of Asn(Trt)-Gly-APA-AQ(4,8-di-OH) (OM44)	300
2.4.2.3	Synthesis of Fmoc-Ala-Asn(Trt)-Gly-APA-AQ(4,8-di-OH) (OM45)....	300
2.4.2.4	Synthesis of Ala-Asn(Trt)-Gly-APA-AQ(4,8-di-OH) (OM46)	300
2.4.2.5	Synthesis of Fmoc-Pro-Ala-Asn(Trt)-Gly-APA-AQ(4,8-di-OH) (OM47).....	301
2.4.2.6	Synthesis of Pro-Ala-Asn(Trt)-Gly-APA-AQ(4,8-di-OH) (OM48)	301
2.4.2.7	Synthesis of Rho-Pro-Ala-Asn(Trt)-Gly-APA-AQ(4,8-di-OH) (OM49)	301
2.4.2.8	Synthesis of Rho-Pro-Ala-Asn-Gly-APA-AQ(4,8-di-OH) (OM50)	302
2.4.3	Synthesis of the target compound Rho-Pro-Ala-Asn-Gly-APA-AQ(4,8-di-OH) (OM50) by solid phase peptide synthesis.....	302
2.4.3.1	Resin swelling	302
2.4.3.2	Fmoc deprotection	303
2.4.3.3	Colour test.....	303
2.4.3.4	Peptide coupling and Fmoc deprotection addition of alanine residue	303
2.4.3.5	Peptide coupling and Fmoc deprotection: addition of proline residue	303
2.4.3.6	Synthesis of Rho-Pro-Ala-Asn(Trt)-resin.....	304
2.4.3.7	Rho-Pro-Ala-Asn(Trt)-resin cleavage	304
2.4.3.8	Synthesis of Rho-Pro-Ala-Asn(Trt)-Gly-APA-AQ(4,8-di-OH) (OM49)...	304
2.4.3.9	Synthesis of Rho-Pro-Ala-Asn-Gly-APA-AQ(4,8-di-OH) (OM50).....	305
2.4.4	UV-visible absorption assay	305

2.4.4.1	Materials.....	305
2.4.4.2	Method	306
2.4.5	Fluorescence spectroscopy assay.....	306
2.4.5.1	Materials.....	306
2.4.5.2	Methods	306
2.4.6	Fluorescence spectroscopy assay of OM50 with recombinant human legumain	307
2.4.6.1	Materials.....	307
2.4.6.2	Method	307
2.4.7	Confocal microscopy	308
2.4.7.1	Materials.....	308
2.4.7.2	Method	308
2.5	Structure library.....	311
2.6	References.....	315
3	Chapter 3: Summary Discussion of Research Results	341
3.1	Overview	341
3.2	Proof of Concepts	341
3.2.1	Proof of Concept 1: selectivity for cancer cell mitochondria.....	341
3.2.2	Biological significance of mitochondrial targeting and mechanistic considerations.....	342
3.2.3	Proof of Concept 2: selective prodrug activation at the cancer cell surface.....	346
3.2.4	Biological significance.....	347
3.3	Multiple uses of rhodamine B in this research.....	349
3.4	Structure-activity relationships	350
3.5	References.....	354
3.6	Appendix	360

List of figures

Figure 1.1: mitochondria structure.....	4
Figure 1.2: Mitochondrial membrane potential ($\Delta\Psi_m$) and accumulation of lipophilic cationic-conjugates inside the mitochondrial matrix of a cancer cell.	6
Figure 1.3: Topoisomerase types.....	8
Figure 1.4: Topoisomerase inhibitor.....	9
Figure 1.5: General concept for TPP Carrier-Drug Targeting of mitochondria	12
Figure 1.6: Gamitrinib-TPP structure.....	13
Figure 1.7: Nitrooxy-doxorubicin structure.....	14
Figure 1.8: Rhodamine 123 structure (a mitochondrial vector).....	15
Figure 1.9: Triphenylphosphonium (TPP) structure (a mitochondrial vector)	16
Figure 1.10: Doxorubicin-triphenylphosphonium (DOX-TPP) structure	17
Figure 1.11: Structures of the (hexachloro-fluorescein)-TPP and TPP modified conjugates: (hexachloro-fluorescein)-triphenylethylphosphonium (1a), (hexachloro-fluorescein)-tri-p-tolyylethylphosphonium (2a), and (hexachloro-fluorescein)-tris(3,5-xylyl)ethylphosphonium (3a).....	18
Figure 1.12: TPP conjugate with G4NH ₂ PAMAM Dendrimer.....	20
Figure 1.13: Chemical structure of mitoquinone (MitoQ ₁₀)	21
Figure 1.14: Chemical structure of a CTPP-PE conjugate	21
Figure 1.15: Chemical structure of TPP-MH-PLL-NPs	22
Figure 1.16: Chemical structure of 4FDT-RhB	24
Figure 1.17: Role of P-gp transporters in the development of the MDR phenotype in cancer cells	27
Figure 1.18: The mechanism of P-gp inhibitor XR9576 inhibiting the activity of ATPase which is required to open P-gp, therefore decrease efflux and increase accumulation of anticancer drugs.....	29
Figure 1.19: Mitoxantrone structure	32
Figure 1.20: Structure of 9b and 9c compounds	34
Figure 1.21: Structure of pixantrone	34
Figure 1.22: Structure of sunitinib	36
Figure 1.23: Chemical structure of mefloquine.....	37
Figure 1.24: The general design of a mitochondrial targeting prodrug system.....	40
Figure 1.25: Structure of the NU:UB series of anthraquinone-amino acid conjugates ..	41
Figure 1.26: Chemical structure of NU:UB 73, 76 and SH1. Red is butyl spacer.	42
Figure 1.27: <i>In Vivo</i> Chemosensitivity against MAC15A colon adenocarcinoma: Comparison of NU:UB 73 (194), NU:UB 76 (196) and Mitoxantrone (7)	43
Figure 1.28: synthesis of rhodamine B tertiary amide by reacting rhodamine B with piperazine.....	46
Figure 1.29: Structures of model compounds and the attachment showing the site of the subsequent Boc-protection and site(s) for attachment of carriers upon esterification. Where R ₁ = OH or H and R ₂ = NH or O or CH ₂	46
Figure 1.30: Reaction scheme showing the amination of leucoquinizarin	48

Figure 1.31: Reaction of leucoquinizarin (1) with N-(2-hydroxyethyl)ethylenediamine (2). (a) N-(2-hydroxyethyl)ethylenediamine, dichloromethane, 50°C 1 h. (b) triethylamine, O ₂ , 4 h	49
Figure 1.32: Reaction of OM1 with Boc ₂ O. (a) Boc ₂ O, methanol, 1 h	50
Figure 1.33: Reaction of OM2 with TPP. (a) TPP, DCC, DMAP, dichloromethane, 1 h	52
Figure 1.34: Reaction of OM22 Boc with (TFA). (a) TFA, room temperature, 30 min ...	52
Figure 1.35: The ESI (+) mass spectrum of OM22 TFA	53
Figure 1.36: ¹ H NMR signals (ppm) for OM22 TFA	54
Figure 1.37: ¹ H NMR spectrum (DMSO, 300 MHz) of OM22 TFA.....	55
Figure 1.38: ¹³ C NMR signals (ppm) for OM22 TFA.....	56
Figure 1.39: ¹³ C NMR spectrum (DMSO, 75.5 MHz) of OM22 TFA	57
Figure 1.40: ¹³ C NMR DEPT90 spectrum (DMSO, 75.5 MHz) of OM22 TFA.....	58
Figure 1.41: Synthesis of NU:UB 252 by reaction of Leucoquinizarin (1) with 4-amino-1-butanol. (a) 4-amino-1-butanol, dichloromethane, 50°C, 1 h, triethylamine, O ₂ , overnight.	59
Figure 1.42: ¹ H NMR signals (ppm) of NU:UB 252.....	60
Figure 1.43: ¹ H NMR spectrum (DMSO, 300 MHz) of NU:UB 252	61
Figure 1.44: ¹³ C NMR signals (ppm) of NU:UB 252	62
Figure 1.45: ¹³ C NMR spectrum (DMSO, 75.5 MHz) of NU:UB 252.....	63
Figure 1.46: ¹³ C NMR DEPT90 spectrum (DMSO, 75.5 MHz) of NU:UB 252	64
Figure 1.47: Synthesis of OM30 by of reaction of NU:UB 252 with TPP. (a) TPP, DCC, DMAP, dichloromethane, 1 h.	65
Figure 1.48: The ESI (+) mass spectrum of OM30.....	66
Figure 1.49: ¹ H NMR signals (ppm) of OM30.....	67
Figure 1.50: ¹ H NMR spectrum (DMSO, 300 MHz) of OM30	68
Figure 1.51: ¹³ C NMR signals (ppm) of OM30.....	69
Figure 1.52: ¹³ C NMR spectrum (DMSO, 75.5 MHz) of OM30.....	70
Figure 1.53: ¹³ C NMR DEPT90 spectrum (DMSO, 75.5 MHz) of OM30	71
Figure 1.54: Synthesis of OM28 by reaction of Leucoquinizarin (1) with 5-amino-1-pentanol. (a) 5-amino-1-pentanol, dichloromethane, 50°C, 1 h, triethylamine, O ₂ , 4 h..	72
Figure 1.55: Synthesis of OM31 by reaction of OM28 with TPP. (a) TPP, DCC, DMAP, dichloromethane, 1 h.....	73
Figure 1.56: The ESI (+) mass spectrum of OM31	74
Figure 1.57: ¹ H NMR signals (ppm) of OM31	75
Figure 1.58: ¹ H NMR spectrum (DMSO, 300 MHz) of OM31	76
Figure 1.59: ¹³ C NMR signals (ppm) of OM31.....	77
Figure 1.60: ¹³ C NMR spectrum (DMSO, 75.5 MHz) of OM31	78
Figure 1.61: ¹³ C NMR DEPT90 spectrum (DMSO, 75.5 MHz) of OM31	79
Figure 1.62: Synthesis of OM29 by reaction of Leucoquinizarin (1) with 2-(2-aminoethoxy)ethanol. (a) 2-(2-aminoethoxy)ethanol, dichloromethane, 50°C, 1 h, triethylamine, O ₂ , overnight.	80
Figure 1.63: Synthesis of OM31 reaction of OM29 with TPP. (a) TPP, DCC, DMAP, dichloromethane, 1 h.....	81

Figure 1.64: The ESI (+) mass spectrum of OM32.....	82
Figure 1.65: ¹ H NMR signals (ppm) of OM32.....	83
Figure 1.66: ¹ H NMR spectrum (DMSO, 300 MHz) of OM32	84
Figure 1.67: ¹³ C NMR signals (ppm) of OM32.....	85
Figure 1.68: ¹³ C NMR spectrum (DMSO, 75.5 MHz) of OM32.....	86
Figure 1.69: ¹³ C NMR DEPT90 spectrum (DMSO, 75.5 MHz) of OM32	87
Figure 1.70: Synthesis of NU:UB 238 by reaction of 1-chloroanthraquinone (1) with 4-amino-1-butanol. (a) 4-amino-1-butanol, DMSO, 95°C, 30 min, water	88
Figure 1.71: Synthesis of SH1 by reaction of NU:UB 238 with TPP. (a) TPP, DCC, DMAP, dichloromethane, 1 h.	90
Figure 1.72: The ESI (+) mass spectrum of SH1.....	90
Figure 1.73: ¹ H NMR signals (ppm) of SH1.....	91
Figure 1.74: ¹ H NMR spectrum (DMSO, 300 MHz) of SH1	92
Figure 1.75: ¹³ C NMR signals (ppm) of SH1	93
Figure 1.76: ¹³ C NMR spectrum (DMSO, 75.5 MHz) of SH1.....	94
Figure 1.77: ¹³ C NMR DEPT90 spectrum (DMSO, 75.5 MHz) of SH1	95
Figure 1.78: Reaction of NU:UB 65 with TPP. (a) TPP, DCC (2 x 0.5 eq) and DMAP in dilute solution of dichloromethane, 1 h.	97
Figure 1.79: Reaction of NU:UB 65 with TPP. (a) high equivalent (6 eq) of TPP, DCC and DMAP in concentrated solution of dichloromethane, 1 h.	98
Figure 1.80: The ESI (+) mass spectrum of NU:UB 65	99
Figure 1.81: synthesis of OM6 and OM7. (a) HN-β-ala-O ^t Bu, PyBop, DIPEA, DMF, 2 h. (b) TFA, overnight.	102
Figure 1.82: Reaction of OM2 with OM7 followed by reaction of OM17 with TFA. (a) OM2, DCC, DMAP, dichloromethane, overnight. (b) TFA, 30 min.	104
Figure 1.83: Reaction of Rho B with Boc-piperazine (a) Boc-piperazine, HATU, DIPEA, DMF/dichloromethane, overnight. (b) TFA, overnight.	105
Figure 1.84: Reaction of OM4 with succinic anhydride to give OM5, (a) succinic anhydride, DIPEA, DMF, 1 h.	106
Figure 1.85: Reaction of OM2 with OM5 to give OM15 followed by deprotection of OM15 to give OM16. (a) OM2, DCC, DMAP, dichloromethane, 12 h. (b) TFA, 30 min.	108
Figure 1.86: Reaction of mitoxantrone with Boc ₂ O. (a) Boc ₂ O, DIPEA, methanol, 1 h.	111
Figure 1.87: Reaction of OM19 with Rho-pip-succinate. (a) Rho-pip-succinate, DCC, DMAP, dichloromethane, 1 h.	113
Figure 1.88: Reaction of OM20 with TFA. (a) TFA, 30 min	114
Figure 1.89: Reaction of OM19 with TPP. (a) high equivalent of TPP, DCC and DMAP. dichloromethane, 1 h.	116
Figure 1.90: Reaction of leucoquinizarin with N-(2-hydroxyethyl)ethylenediamine. (a) N-(2-hydroxyethyl)ethylenediamine, dichloromethane, 50°C, condensation, 1 h. (b) triethylamine, O ₂ , 4.5 h.	117
Figure 1.91: Reaction of ametantrone (NK1) with Boc ₂ O. (a) Boc ₂ O, methanol, 1 h.	118

Figure 1.92: Reaction of TPP with NK4. (a) TPP, HATU, 4-methylmorpholine, DMF, room temperature for 1 h, 40°C for 1.5 h, room temperature for 18 h.	120
Figure 1.93: Reaction of NK6 with TFA. (a) TFA, 30 min	121
Figure 1.94: The ESI (+) mass spectrum of NK8.....	122
Figure 1.95: Chemical structure of ethidium bromide (EtdBr).....	125
Figure 1.96: Variation of relative fluorescence intensity of CT-DNA (60 μ M) with pre-bound EtdBr (30 μ M) when treated with different concentrations of mitoxantrone in PBS buffer. λ_{ex} 480 nm; λ_{em} 610 nm (n = 3).	126
Figure 1.97: : Variation of relative fluorescence intensity of CT-DNA (60 μ M) with pre-bound EtdBr (30 μ M) when treated with different concentrations of OM2 TFA in PBS buffer. (n = 3). λ_{ex} 480 nm; λ_{em} 610 nm.	127
Figure 1.98: Variation of relative fluorescence intensity of CT-DNA (60 μ M) with pre-bound EtdBr (30 μ M) when treated with different concentrations of OM22 TFA in PBS buffer. (n = 3) λ_{ex} 480 nm; λ_{em} 610 nm.	128
Figure 1.99: Variation of relative fluorescence intensity of CT-DNA (60 μ M) with pre-bound EtdBr (30 μ M) when treated with different concentrations of OM30 in PBS buffer. (n = 3). λ_{ex} 480 nm; λ_{em} 610 nm.	129
Figure 1.100: Variation of relative fluorescence intensity of CT-DNA (60 μ M) with pre-bound EtdBr (30 μ M) when treated with different concentrations of OM31 in PBS buffer. (n = 3). λ_{ex} 480 nm; λ_{em} 610 nm.	130
Figure 1.101: Variation of relative fluorescence intensity of CT-DNA (60 μ M) with pre-bound EtdBr (30 μ M) when treated with different concentrations of OM32 in PBS buffer. (n=3). λ_{ex} 480 nm; λ_{em} 610 nm.	131
Figure 1.102: Variation of relative fluorescence intensity of CT-DNA (60 μ M) with pre-bound EtdBr (30 μ M) when treated with different concentrations of SH1 in PBS buffer. (n = 3). to λ_{ex} 480 nm; λ_{em} 610 nm.	132
Figure 1.103: Variation of relative fluorescence intensity of CT-DNA (60 μ M) with pre-bound EtdBr (30 μ M) when treated with different concentrations of OM26 in PBS buffer. (n = 3). λ_{ex} 480 nm; λ_{em} 610 nm.	133
Figure 1.104: Variation of relative fluorescence intensity of CT-DNA (60 μ M) with pre-bound EtdBr (30 μ M) when treated with different concentrations of ametantrone in PBS buffer. (n = 3). λ_{ex} 480 nm; λ_{em} 610 nm.	134
Figure 1.105: Relative lipophilicity/ hydrophobicity of OM2, OM22, NU:UB 252, OM30, SH1, NU:UB 238, OM16 and mitoxantrone.....	144
Figure 1.106: Conversion of MTT to formazan (the basis of the colourimetric method)	146
Figure 1.107: Survival rate of MCF-7 breast cancer cells treated with OM2, OM22, NU:UB 65 and OM26 for 48 h (n = 8) in comparison with untreated cells.	147
Figure 1.108: Survival rate of HCT-15 colon carcinoma cell lines treated with OM2, OM22, NU:UB 65 and OM26 for 48 h (n = 8) in comparison with untreated cells.	147
Figure 1.109: Survival rate of HCT-15 colon carcinoma cell lines treated with Mitoxantrone, OM30, OM31 and OM32 for 96 h (n = 8) in comparison with untreated cells.	148

Figure 1.110: Localisation of SH1 in HCT-116 cells. SH1 (2 μ M) localised to the mitochondria within 90 min as measured by live cell imaging. (i) SH1 stained with LysoTracker Green DND26, (A) SH1, (B) LysoTracker and (C) merged image. (ii) SH1 stained with MitoTracker Green FM, (A) SH1, (B) MitoTracker and (C) merged image. Images were captured as 63 x magnification. 154

Figure 1.111: Localisation of OM22 in the HCT-116 cells. OM22 (2 μ M) localised to the lysosome within 90 min as measured by live cell imaging. (i) OM22 stained with LysoTracker Green DND26, (A) OM22, (B) LysoTracker and (C) merged image. (ii) OM22 stained with MitoTracker Green FM, (A) OM22, (B) MitoTracker and (C) merged image. Images were captured as 63 x magnification..... 156

Figure 1.112: Localization of OM30 (2 μ M), OM31 (2 μ M) and OM32 (2 μ M) with mitochondria in HCT-116 cells within 90 min as measured by live cell imaging. (A) OM30, OM31 and OM32, (B) MitoTracker and (C) merged images. Images were captured as 63 x magnification..... 158

Figure 1.113: Structure and localization of mitoxantrone (1 μ M) with lysosome in HCT-116 cells within 90 min of live cell imaging. (A) mitoxantrone, (B) LysoTracker and (C) merged images. Images were captured as 63 x magnification..... 159

Figure 1.114: Structure and localization of ametantrone with nucleus in stained HCT-116 cell line with MitoTracker Green FM within 90 min of live cell imaging. (A) ametantrone, (B) MitoTracker and (C) merged images. Images were captured as 63 x magnification. 159

Figure 1.115: Schematic representation of the morphological changes during apoptosis 161

Figure 1.116: Cytotoxic effects of SH1 on HCT-116 cells. Bright field microscopy changes in cell morphology after 2 h post-treatment with SH1 at 10 μ M with no changes at other concentrations and control cells. 163

Figure 1.117: Cytotoxic effects of SH1 on HCT-116 cells. Bright field microscopy changes in cell morphology after 4 h post-treatment with SH1 at 5 μ M and 10 μ M with no changes at other concentration and control cells. 163

Figure 1.118: Cytotoxic effects of SH1 on HCT-116 cells. Bright field microscopy changes in cell morphology after 6 h post-treatment with SH1 at 1 μ M, 5 μ M and 10 μ M with no changes in control cells..... 164

Figure 1.119: Cytotoxic effects of SH1 on HCT-116 cells. Bright field microscopy changes in cell morphology after 24 h post-treatment with SH1 at 1 μ M, 5 μ M and 10 μ M with no changes in control cells..... 164

Figure 1.120: Cytotoxic effects of SH1 on HCT-116 cells. Bright field microscopy changes in cell morphology after 2 h post-treatment with OM22 at 10 μ M with no changes at other concentrations and control cells. 165

Figure 1.121: Cytotoxic effects of SH1 on HCT-116 cells. Bright field microscopy changes in cell morphology after 4 h post-treatment with OM22 at 5 μ M and 10 μ M with no changes at other concentrations and control cells..... 166

Figure 1.122: Cytotoxic effects of SH1 on HCT-116 cells. Bright field microscopy changes in cell morphology after 6 h post-treatment with OM22 at 1 μ M, 5 μ M and 10 μ M with no changes in control cells.....	166
Figure 1.123: Cytotoxic effects of SH1 on HCT-116 cells. Bright field microscopy changes in cell morphology after 24 h post-treatment with OM22 at 1 μ M, 5 μ M and 10 μ M with no changes in control cells.....	167
Figure 2.1: Representation of the FRET concept.	244
Figure 2.2:Chemical structures of three forms of rhodamine B. cationic and zwitterionic forms are fluorescent whereas the lactone form is nonfluorescent.	245
Figure 2.3: Fluorescence emission of (a) Rho-Pro-OH (10 μ M) and (b) FAM-Pro-OH in phosphate-citrate buffer, pH 3-8.....	246
Figure 2.4: The structures of the four rhodamine core fluorophores	248
Figure 2.5: Structure of Suc-Ala-Ala-Asn-Val-colchicine	250
Figure 2.6: Structure of CBZ-AAN-Dox	250
Figure 2.7: Structure of ALS5.....	251
Figure 2.8: Chemical structure of NU:UB 51	252
Figure 2.9: Comparison of NU:UB 51, doxorubicin and mitoxantrone <i>in vivo</i> chemosensitivity against MAC15A adenocarcinoma of the colon.	253
Figure 2.10: General structure of Rhodamine labeled prodrug OM50 (a theranostic).	256
Figure 2.11: Schematic presentation of NU:UB 51 synthesis.....	258
Figure 2.12: Solution phase peptide synthesis schematic representation	259
Figure 2.13: Solid phase peptide synthesis schematic representation	260
Figure 2.14: Chemical structure of the target compound Rho-Pro-Ala-Asn-Gly-APA-AQ(4,8-di-OH) (OM50)	262
Figure 2.15: Reaction of leuco-5-hydroxyquinizarin (1) with 1,3-diaminopropane. (a) 1,3-diaminopropane, dichloromethane, 40°C, triethylamine, O ₂ , 1.5 h.....	263
Figure 2.16: Reaction of NU:UB 59 with Boc-Gly-OH. (a) Boc-Gly-OH, PyBOP, DIPEA, DMF, 1.5 h.	264
Figure 2.17: Reaction of NU:UB 51-Boc with TFA. (a) TFA, 30 min, room temperature	265
Figure 2.18: Reaction of NU:UB 51 with Fmoc-Asn(Trt)-OH. (a) Fmoc-Asn(Trt)-OH, PyBOP, HOBt, DIPEA, DMF, 1.5 h.	267
Figure 2.19: The mass spectrum of the OM43	268
Figure 2.20: Reaction of OM43 with piperidine (20% in DMF). (a) piperidine (20% in DMF), 15 min, room temperature.	269
Figure 2.21: Reaction of OM44 with Fmoc-Ala-OH. (a) Fmoc-Ala-OH, PyBOP, HOBt, DIPEA, DMF, 1.5 h.....	271
Figure 2.22: Reaction of OM45 with piperidine (20% in DMF). (a) piperidine (20% in DMF), 15 min, room temperature.	273
Figure 2.23: Reaction of OM46 with Fmoc-Pro-OH. (a) Fmoc-Pro-OH, PyClock, DIPEA, DMF, 1.5 h.	274
Figure 2.24: Reaction of OM47 with piperidine (20% in DMF). (a) piperidine (20% in DMF), 15 min, room temperature.	275

Figure 2.25: Reaction of OM48 with rhodamine B. (a) rhodamine B, PyClock, DIPEA, DMF, 1.5 h.	277
Figure 2.26: Reaction of OM49 with TFA. (a) TFA, ~ 3 h, room temperature.....	278
Figure 2.27: The mass spectrum for OM50.....	279
Figure 2.28: The mechanism of colour test.....	281
Figure 2.29: The five steps of the solid phase peptide synthesis.	283
Figure 2.30: The chemical structure of the Rho-Pro-Ala-Asn(TRT)-OH.....	284
Figure 2.31: Mass spectrum for Rho-Pro-Ala-Asn(Trt)-OH.....	285
Figure 2.32: The mass spectrum for OM50 from solid phase peptide synthesis.....	286
Figure 2.33: UV-Vis absorption assay of Rho B-Pro-Ala-Asn-OH and NU:UB 51. Concentration: 20 μ M of NU:UB 51 and 5 μ M of rho B-Pro-Ala-Asn- in legumain assay buffer (50 mM MES hydrate, 250 mM NaCl, pH 5.0) , Red arrow indicates the maximum absorbance.....	287
Figure 2.34: Fluorescence intensity spectrum of Rho-Pro-Ala-Asn-OH. Concentration: 0.5 μ M in legumain assay buffer (50 mM MES hydrate, 250 mM NaCl, pH 5.0). Excitation wavelength: 562 nm. Red arrow: maximum fluorescence intensity at 583 nm.	289
Figure 2.35: Fluorescence emission spectrum of OM50 (red line) compared with Rho-Pro-Ala-Asn-OH (blue line). Concentration 0.5 μ M each in legumain assay buffer. Excitation wavelength: 562 nm.....	290
Figure 2.36: The cleavage site of legumain at the C-terminal of asparagine.....	291
Figure 2.37: Cleavage of Prodrug OM50 by recombinant human legumain. Variation in RFI (Relative Fluorescence Intensity) with time for OM50 [Rho-Pro-Ala-Asn-Gly-APA-AQ(4,8-di-OH)] upon incubation with legumain (40 ng) in legumain assay buffer (50 mM MES hydrate, 250 mM NaCl, pH 5.0), 2 h.....	292
Figure 2.38: Localization of NU:UB 51 in HCT-116 cell. NU:UB 51(5 μ M) localized to the mitochondria and lysosome within 90 min as measured by live cell imaging. The localisation of NU:UB 51 in mitochondria shown in (i) (A) NU:UB 51 stained with(B) MitoTracker Green FM and (c) merged image. The localisation of NU:UB 51 in lysosomes shown in (ii) (A) NU:UB 51 stained with (B) LysoTracker Green DND26 and (c) merged image. Images were captured at 63 x magnification.	293
Figure 2.39: live cell imaging of OM50 in HCT-116 cell lines stained with LysoTracker Green DND26. The colocalization of OM50 with LysoTracker Green shows the localization of OM50 (1 μ M) outside the cell with no localization in the mitochondria and lysosome within 90 min as measured by live cell imaging. (A) OM50, (B) LysoTracker Green DND26 and (C) merged image. Images were captured at 63 x magnification..	294
Figure 3.1: Illustration of Proof of Concept for mitochondrial targeted drugs. A. Chemical synthesis of mitochondrial targeted drug; B. mitochondrial targeted drug and C. confocal image which shows the localization of a TPP conjugate drug in mitochondria.....	342
Figure 3.2: Illustration of Proof of Concept for the theranostic prodrug Rho-Pro-Ala-Asn-Gly-APA-AQ(4,8-di-OH) (OM50) and showing legumain-mediated activation of the prodrug and simultaneous release of a rhodamine B-labelled peptide (fluorescent reporter of prodrug activation) and cytotoxic agent NU:UB 51 at the tumour cell.	347

Figure 3.3: Different uses of rhodamine B in this research.....	350
Figure 3.4: Selective delivery of novel anticancer drugs that have been synthesised in this research.....	351

List of tables

Table 1.1: Summary of QE_{50} and K_{app} values for tested compounds. #ND (not determined)	137
Table 1.2: LOG D values for tested compound in PBS buffer 7.4 and saturated octanol	144
Table 1.3: The mean IC_{50} values for different compounds (μM) in MCF-7 and HCT-16 cell lines, after 48 h and 96 h incubation. #ND (not determined)	149
Table 2.1: Arrangement on black 96-well plate for Fluorimetric Assay.....	307

Abbreviations

4FDT	Fluorinated docetaxel
ABC	ATP-binding cassette
ADP	Adenosine diphosphate
AEP	Asparaginyl endopeptidase
Ala	Alanine
AMC	Aminomethylcoumarin
AQ	Anthraquinone
ASM	Acid sphingomyelinase
Asn	Asparagine
ATP	Adenosine triphosphate
Boc ₂ O	tert-Butyloxycarbonyl
CaRG	Carboxyrhodamine 6G
CHF	Congestive heart failure
CsA	Cyclosporine A
CT DNA	Calf thymus DNA
DCC	1,3-Dicyclohexylcarbodiimide
DCU	<i>N,N'</i> -dicyclohexylurea
DIPEA	<i>N,N'</i> -diisopropylethylamine
DMAP	<i>N,N'</i> -Dimethylpyridine-4-amine
DMF	<i>N,N'</i> -Dimethylformamide
DMSO	Dimethyl sulfoxide
DOX	Doxorubicin
DTX	Docetaxel
ECM	Extracellular matrix
Eq	Molar equivalent(s)
ESI(+) or (-)	Electrospray ionisation/positive or negative mode

EtdBr	Ethidium bromide
FDT	Fluorinated docetaxel derivative
Fmoc	Fluorenylmethoxycarbonyl
FRET	Fluorescence resonance energy transfer
g	Gram(s)
Gly	Glycine
GmSA	Galactosamine serum albumin
GTP	Guanosine triphosphate
h	Hour(s)
HOBt	Hydroxybenzotriazole
HPLC	High performance liquid chromatography
IMM	Inner mitochondrial membrane
IMS	Intermembrane space
K_{app}	DNA binding constant
M	Molar
MDR	Multidrug resistance
Min	Minutes
MitoQ ₁₀	Mitoquinone Q ₁₀
mmol	Millimole(s)
MOMP	Mitochondrial outer membrane permeabilization
MPPs	Mitochondria-penetrating peptides
MS	Mass spectrum
MSD	Membrane-spanning domains
mtDNA	Mitochondrial DNA
MTT	3-(4,5-dimethylthiazol-2-yl)-2,5 diphenyl tetrazolium bromide
NADH	Nicotinamide adenine dinucleotide
NBDs	Nucleotide-binding domains
NCI	National Cancer Institute

nDNA	Nuclear DNA
NHS	N-hydroxysuccinimide
NMR	Nuclear magnetic resonance
NP	Nanoparticle
NR	Nonradiative
OMM	Outer mitochondrial membrane
PAMAM	Poly(amidoamine)
PDT	Photodynamic therapy
PE	Phosphatidylethanolamine
PEG	polyethylene glycol
PEG-PE	Polyethylene glycol-phosphatidylethanolamine
PET	Photoinduced electron transfer
P-gp	P-glycoprotein
PLL	Poly-L-lysine
Pro	Proline
PyBOP	Benzotriazol-1-yl-oxytripyrrolidinophosphonium hexafluorophosphate
PyClock	6-Chloro-benzotriazole-1-yl-oxy-tris-pyrrolidinophosphonium hexafluorophosphate
QD	Quantum dots
R _f	Retention factor
Rho B	Rhodamine B
ROS	Reactive oxygen species
rRNA	Ribosomal RNA
SPPS	Solid phase peptide synthesis
TAMRA	Carboxytetramethylrhodamine
TCA	Tricarboxylic acid cycle
TFA	Trifluoroacetic acid
TLC	Thin-layer chromatography

Top	Topoisomerase
Top2cc	Top2 cleavage complexes
TPMP	Triphenylmethylphosphonium
TPP	Triphenylphosphonium
tRNA	Transfer ribonucleic acid
Trt	Triphenylmethyl (trityl)
UV	Ultraviolet
VDAC	Voltage dependent anion channel
ZnPc	Zinc phthalocyanine
$\Delta\Psi_m$	Mitochondrial membrane potential

Preface

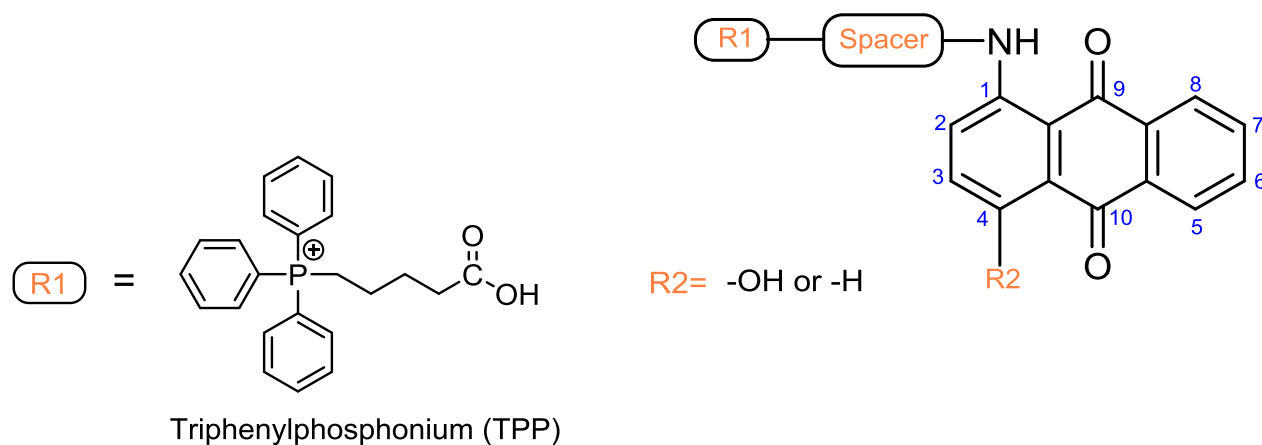
Results from this research programme have been reported in part in the following publication:

Mohammed, O., Turnbull, A., MacCallum, J. and Mincher, J. D. (2016) Design, synthesis and evaluation of novel and clinically used anti-cancer agents targeted to mitochondria. Proceedings of the EACR24, European J Cancer. **61**, p. S126. doi: 10.1016/S0959-8049(16)61446-6.

Nomenclature

During this research, different series of novel compounds have been synthesised to specifically target anticancer drugs inside the cancer cells. The structures below show examples of the compounds designed and synthesised in this study in their simplest format.

TPP-anthraquinone conjugate compounds



The numbering system (blue colour) was used in this research for the anthraquinone chromophore, to support the NMR characterization (i.e. the compounds were considered to be 1-amino-4-hydroxyanthraquinones).

Example

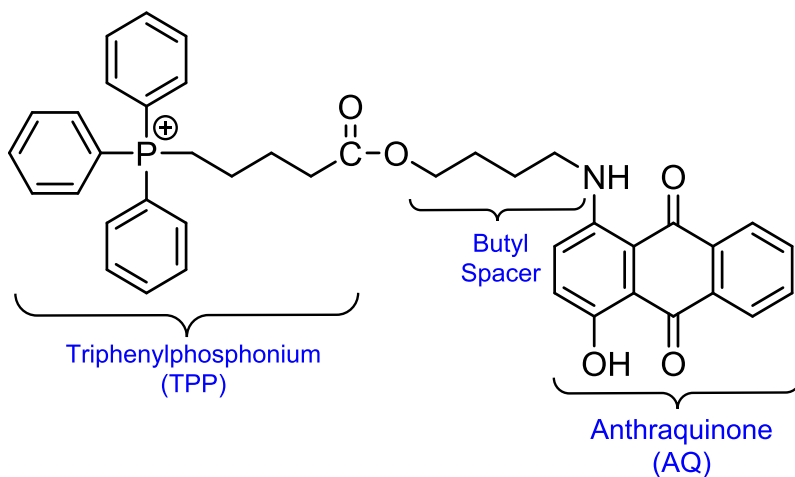
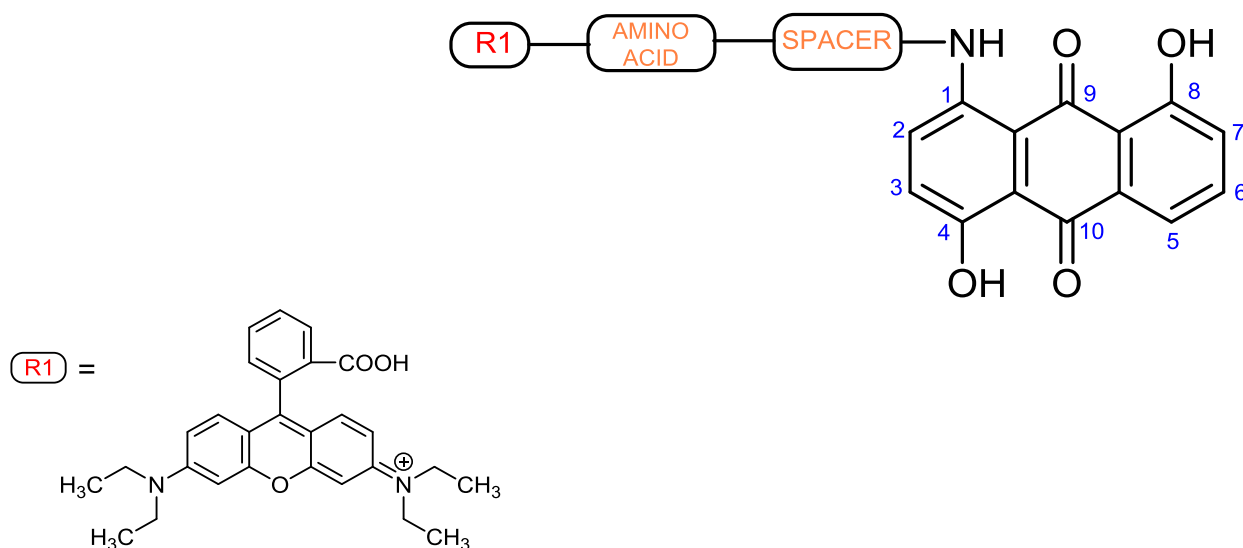


Figure A1: Structural representation of TPP-aminoanthraquinone [TPP-butyl-AQ(4-OH)]

The abbreviation AQ was used for the anthraquinones. The vector triphenylphosphonium has been represented by the standard abbreviation TPP. The spacer in the TPP-conjugate compounds has been further abbreviated for convenience; for example, the spacer $\text{-HO-(CH}_2\text{)}_4\text{-NH-}$ (hydroxybutylamino) is presented as Butyl in **Figure A1**. In other instances, for example, the spacer $\text{-OH-(CH}_2\text{)}_2\text{-O-(CH}_2\text{)}_2\text{-NH-}$ (hydroxyethoxyethylamino) is represented as EOE.

Rhodamine-conjugate prodrug



Example

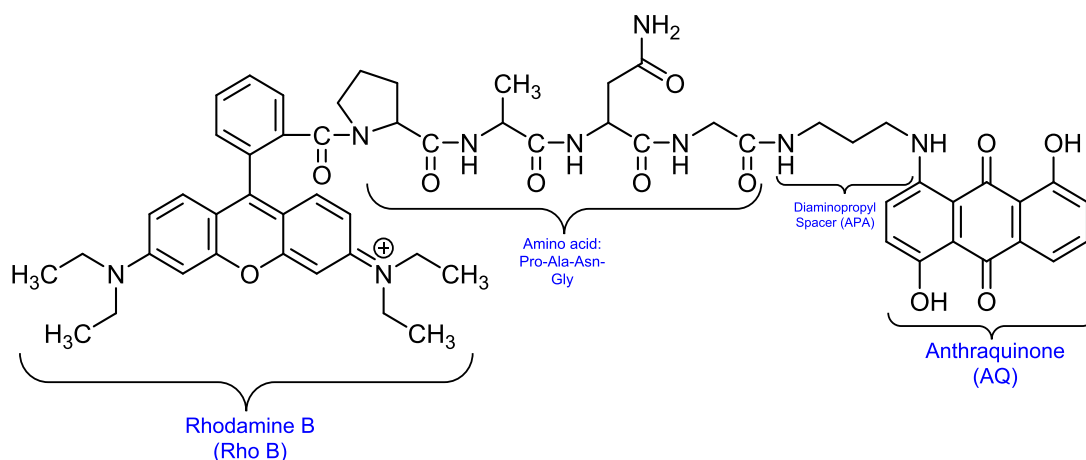


Figure A2: Structural representation of rhodamine B prodrug [Rho-Pro-Ala-Asn-Gly-APA-AQ(4,8-di-OH)]

In addition, in the rhodamine B prodrug, the spacer group [-HN-(CH₂)₃-NH-] (aminopropylamino) has been further abbreviated to APA. Gly-APA-AQ(4,8-di-OH) has been further abbreviated to NU:UB 51 (active agent component of the prodrug). The peptide is described using standard 3-letter codes Pro-Ala-Asn **Figure A2**. The fluorophore rhodamine B has been further abbreviated to Rho for convenience

Chapter 1

1 Chapter 1

1.1 Aim and Hypothesis

Aim

The principal aims of this project are the synthesis and characterization of a series of novel anti-cancer drugs targeted selectively to mitochondria. Specifically, to develop novel compounds containing the mitochondrial carriers triphenylphosphonium (TPP) and rhodamine, ester-linked with anthraquinone derivatives structurally related to the topoisomerase inhibitor mitoxantrone. Furthermore, to evaluate the DNA-binding, cytotoxicity, lipophilicity, cellular uptake and subcellular localization of members of the series.

Hypothesis

The higher membrane potential ($\Delta\Psi_m$) of cancer cells compared with healthy cells can be exploited to achieve selective delivery of anticancer drugs to mitochondria using specific lipophilic cations, with the potential to avoid drug resistance, reduce side effects and increase the therapeutic index.

1.2 Introduction

1.2.1 Mitochondrial structure and function

The observation that mitochondria are vital organelles in eukaryotic cells has been highlighted more than one Century ago. They were originally described as “bioplasts”, then were soon renamed due to their threadlike appearance during spermatogenesis (mitos = thread, chondros = granule). Mitochondria are known as a powerhouse by playing a central role in energy generating processes [adenosine triphosphate (ATP)] via oxidative phosphorylation and produce more than 90% of intracellular ATP in healthy eukaryotic cells (Galluzzi *et al.*, 2010). However, mitochondria are also involved in secondary cellular functions such as the production of nicotinamide adenine dinucleotide (NADH) and guanosine triphosphate (GTP) in the citric acid cycle, synthesis of phospholipids for membrane biogenesis (Kühlbrandt, 2015) , fatty acid oxidation, amino acid metabolism and tricarboxylic acid and urea cycle (Duchen, 2004; Smith *et al.*, 2012; Smith *et al.*, 2011). All these functions make mitochondria an organelle to target in cancer therapy.

Mitochondria consist of an outer mitochondrial membrane (OMM) and an inner mitochondrial membrane (IMM) with folded cristae that separate two aqueous compartments; the intermembrane space (IMS), which is the space between OMM and IMM, and the inner mitochondrial matrix, which is surrounded by the inner mitochondrial membrane (Endo and Yamano, 2010) **Figure 1.1**. The OMM is porous and freely passed by small, uncharged molecules and ions through pore-forming membrane proteins (porins), such as the voltage dependent anion channel VDAC, which regulates the entry of different cellular components into the mitochondria. Any larger molecules, such as proteins, have to be transferred by special translocases. Because of its porosity, there is no membrane potential across the outer membrane (Kühlbrandt, 2015). The outer membrane also plays an important role in cell apoptosis by process called mitochondrial outer membrane permeabilization (MOMP), resulting in pore formation leading to the

release of proteins normally found in the space between the inner and outer mitochondrial membranes such as cytochrome C (Green and Kroemer, 2004).

However, the inner mitochondrial membrane (IMM) is highly folded into cristae and it is the most important part of mitochondria because it involves in the formation of ATP under. The IMM contains the components of the electron transport chain in which the oxidation/reduction reaction generates a proton that is used by ATP synthase to phosphorylate adenosine diphosphate (ADP) to ATP. Mitochondrial cristae folds allow a greater amount of enzymes and ATP synthase included in electron transport chain to be packed into the mitochondrion (Paumard, 2002).

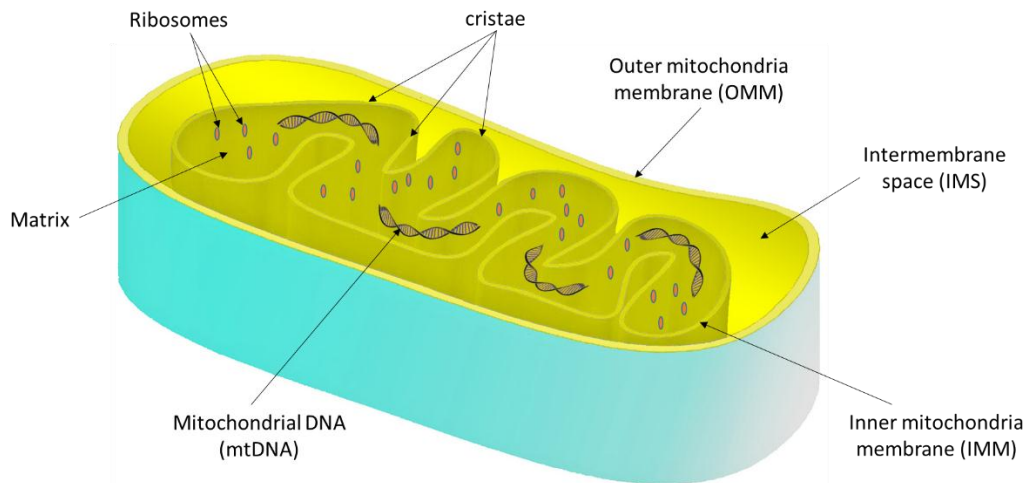


Figure 1.1: mitochondria structure

However, mitochondria are known to be dynamic organelles in which the shape and size of mitochondria are highly variable and are controlled by fusion and fission. Also, the internal structure (inner membrane) of mitochondria can change in response to their physiological state (Detmer and Chan, 2007). Many cristae are found in mitochondria from tissues where energy demand is high, whereas tissues with low energy have insignificant cristae (Higgs and Peterson, 2005). In addition, the mitochondrial inner membrane is not only morphologically different but also seems to have different functional demands. For example, proteins that are involved in the translocation of other proteins

through the inner membrane, are enriched in the inner boundary membrane close to the outer membrane, whereas proteins that are involved in oxidative phosphorylation are enriched in the cristae membranes. Also, the mitochondrial membrane structure is linked to the metabolic state of mitochondria. Mitochondria, which have limited respiration and are characterized by narrow cristae and few cristae junctions per cristae compartment have low ADP. Whereas, the mitochondria that have high respiratory activity and are characterized by larger cristae and several cristae junctions per cristae compartment have high ADP (Detmer and Chan, 2007). Therefore, these changes in mitochondrial structure and function make mitochondria dynamic organelles.

1.2.2 **Mitochondrial membrane potential ($\Delta\Psi_m$)**

Mitochondrial membrane potential ($\Delta\Psi_m$) is an electrochemical gradient that is generated across the inner mitochondrial membrane (IMM). The origin of this gradient is a consequence of the transfer of electrons through mitochondrial enzyme complexes I, III, and IV, coupled to the pumping of protons from the mitochondrial matrix into the intermembrane space. The $\Delta\Psi_m$ has a critical role in apoptosis, production of reactive oxygen species, energy translation, stability of mitochondrial encoded, protein synthesis and activation and translation of nuclear encoded proteins across mitochondrial membranes. However, $\Delta\Psi_m$ is dynamic and changes in response to apoptotic signals, changes in the microenvironment, location of an individual cell during growth and localization of particular mitochondria within a cell (Heerdt *et al.*, 2005).

Furthermore, mitochondria can create a transmembrane electric potential of approximately -180 mV in comparison with the plasma membrane which can produce approximately -60 mV (Rin Jean *et al.*, 2014). However, the most notable difference between healthy cells and cancer cells is that mitochondrial membrane potential ($\Delta\Psi_m$) is higher in cancer cells than healthy cells (Constance and Lim, 2012). Therefore, as the ($\Delta\Psi_m$) increases, more intracellular cationic species will penetrate the mitochondria membrane in comparison with mitochondria in healthy cells, consequently increasing the

accumulation of cationic drugs inside mitochondria and leading to cellular death **Figure 1.2.**

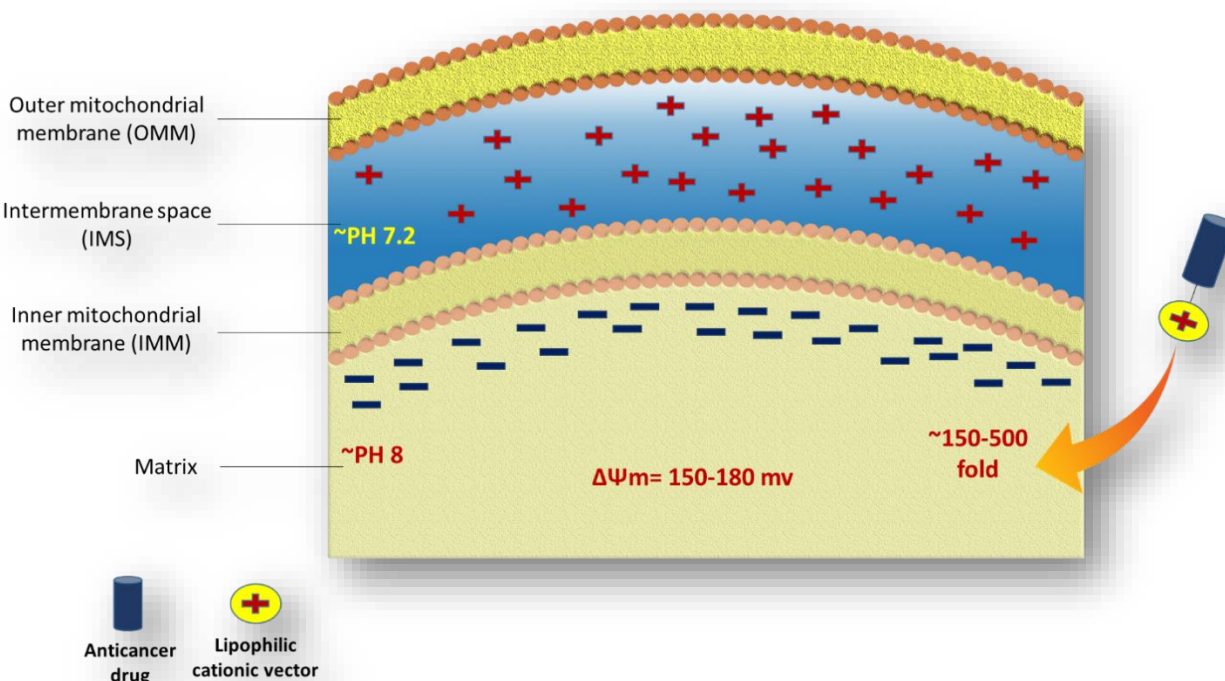


Figure 1.2: Mitochondrial membrane potential ($\Delta\Psi_m$) and accumulation of lipophilic cationic-conjugates inside the mitochondrial matrix of a cancer cell.

1.2.3 Mitochondrial DNA and topoisomerases

Each human cell contains nuclear DNA (nDNA) and a mitochondrial genome DNA (mtDNA). Mitochondria are the only cellular organelles containing DNA outside the nucleus (Khiati *et al.*, 2014). mtDNA was first discovered in 1963 by (Nass and Nass, 1963), they showed conclusively that chick embryo mitochondria contained DNA using electron microscopy. The mtDNA sequence was first published in 1981 as being 16,569 base pairs long (Anderson *et al.*, 1981). mtDNA is a circular double-stranded DNA molecule, capable of transcription, translation and protein assembly which are present at a high copy number per cell, and the number varies with the cell type. Human mtDNA encodes 13 polypeptides involved in respiration and oxidative phosphorylation, as well as 2 rRNAs and a set of 22 tRNAs that are essential for mitochondrial protein synthesis

(Chatterjee *et al.*, 2006). mtDNA has special features including high copy number, matrilineal inheritance, a higher evolutionary turnover rate when compared with nDNA and lack of recombination (Van Oven and Kayser, 2009). In addition, compared with nDNA, mtDNA is more susceptible to damage due to insufficient DNA repair capacity, the lack of protective histones, and a high rate of reactive oxygen species (ROS) generation in mitochondria. Because all of the genes in mtDNA are important for the bioenergetic and biogenesis function of mitochondria, any mtDNA change may result in impairment of oxidative phosphorylation and enhanced ROS production, therefore may accelerate the rate of mtDNA mutations, this has been linked to the early stages of carcinogenesis (Yu *et al.*, 2007).

On the other hand, mtDNA, like nuclear DNA, require DNA topoisomerases for transcription and replication (Wang *et al.*, 2002). DNA topoisomerases are ubiquitous enzymes that modify DNA topology by breaking the DNA phosphodiester backbone and resealing it, allowing DNA double helices or stands to pass through or rotate around each other. Hence, DNA topoisomerases play an essential role in modifying, maintaining and monitoring the topology of DNA transcription, replication, recombination, and repair of DNA (Zhang *et al.*, 2007).

DNA topoisomerases have been divided into two main types, type I and type II topoisomerases. Type I topoisomerases, which break one DNA strand at a time have been divided into two main groups: type IA and type IB. Type IA topoisomerases subdivided into (Top3 α and Top3 β) and Type IB subdivided into (Top1 and Top1mt). whereas, type II topoisomerases, which cut both strands of the DNA double helix (IIA) subdivided into (Top2 α and Top2 β) **Figure 1.3** (Zhang *et al.*, 2001). Mitochondria have type I topoisomerase (top I mt), which is similar to nuclear top I, composed of four domains: An N-terminal localization domain, a linker domain, a core domain, and a C-terminal domain containing the catalytic tyrosine. Type I topoisomerases have been classified type IA and IB according to the polarity of the cleavage reaction and the relaxation mechanism. Type IA enzymes have an opposite polarity that bind to the 5' end of the cleaved DNA by covalent linkage and then relaxation of DNA by strand passage like topoisomerase II. In contrast, Type IB enzymes split the DNA by transesterification

and forming a tyrosyl-DNA covalent catalytic intermediate at 3' end of the DNA breaks (Zhang *et al.*, 2007). Furthermore, nuclear top 2 is known to translocate from the nucleus to mitochondria and therefore can present another drug target in addition to mt-Top1. Mitochondrial DNA and topoisomerases have been the subject of a very recent review (Goffart *et al.*, 2019).

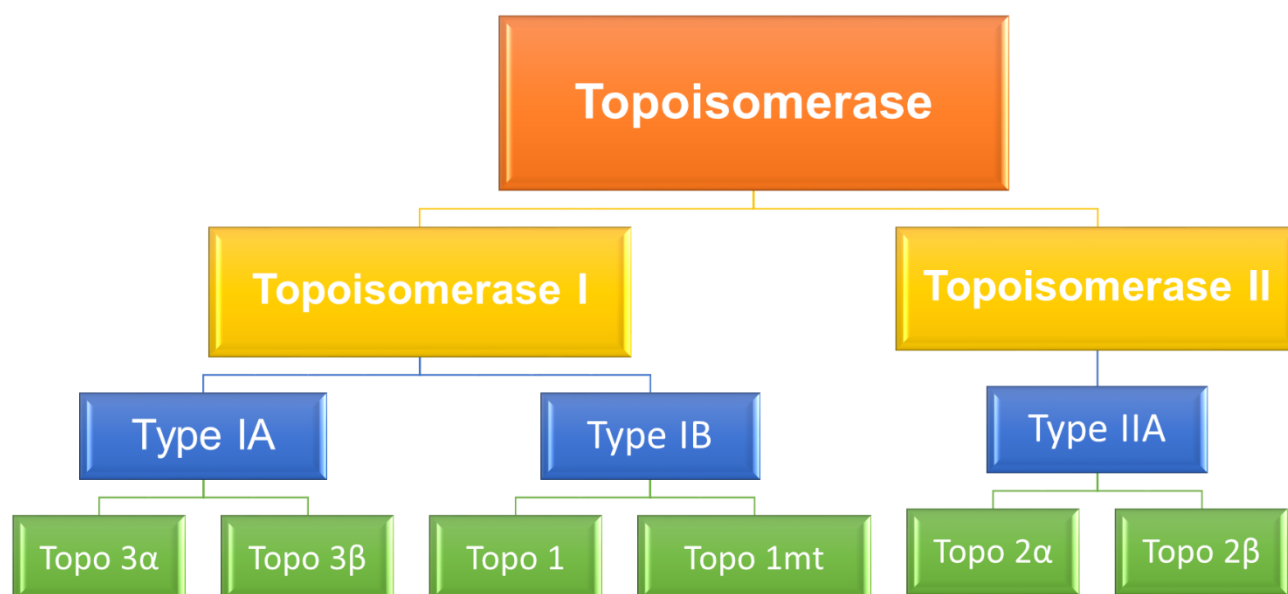


Figure 1.3: Topoisomerase types

Therefore, targeting drugs to mitochondrial DNA by inhibiting the activity of topoisomerases is a promising therapy to kill cancer cells. Many topoisomerase inhibitors, known as poisons, work by binding at the enzyme-DNA interface therefore trapping topoisomerase cleavage complexes which in turn, if not repaired, lead to cell death (Khiati *et al.*, 2014). These inhibitors poison Top2 cleavage complexes (Top2cc) by two mechanisms; by inhibiting DNA relegation, in a similar manner as etoposide, teniposide, the DNA intercalators doxorubicin, daunorubicin and amsacrine and by enhance the formation of Top2cc such as quinolones, ellipticines, azatoxins and the natural flavonoid genistein. These drugs not only poison Top2-mediated DNA double-strand breaks but

also single-strand breaks. Furthermore, doxorubicin poisons Top2cc at low drug concentrations due to its ability to inhibit Top2 catalytic activity without trapping cleavage complexes at drug concentrations that alter DNA structure, thereby preventing Top2 from binding to DNA or from forming Top2cc (Pommier *et al.*, 2010) **Figure 1.4.**

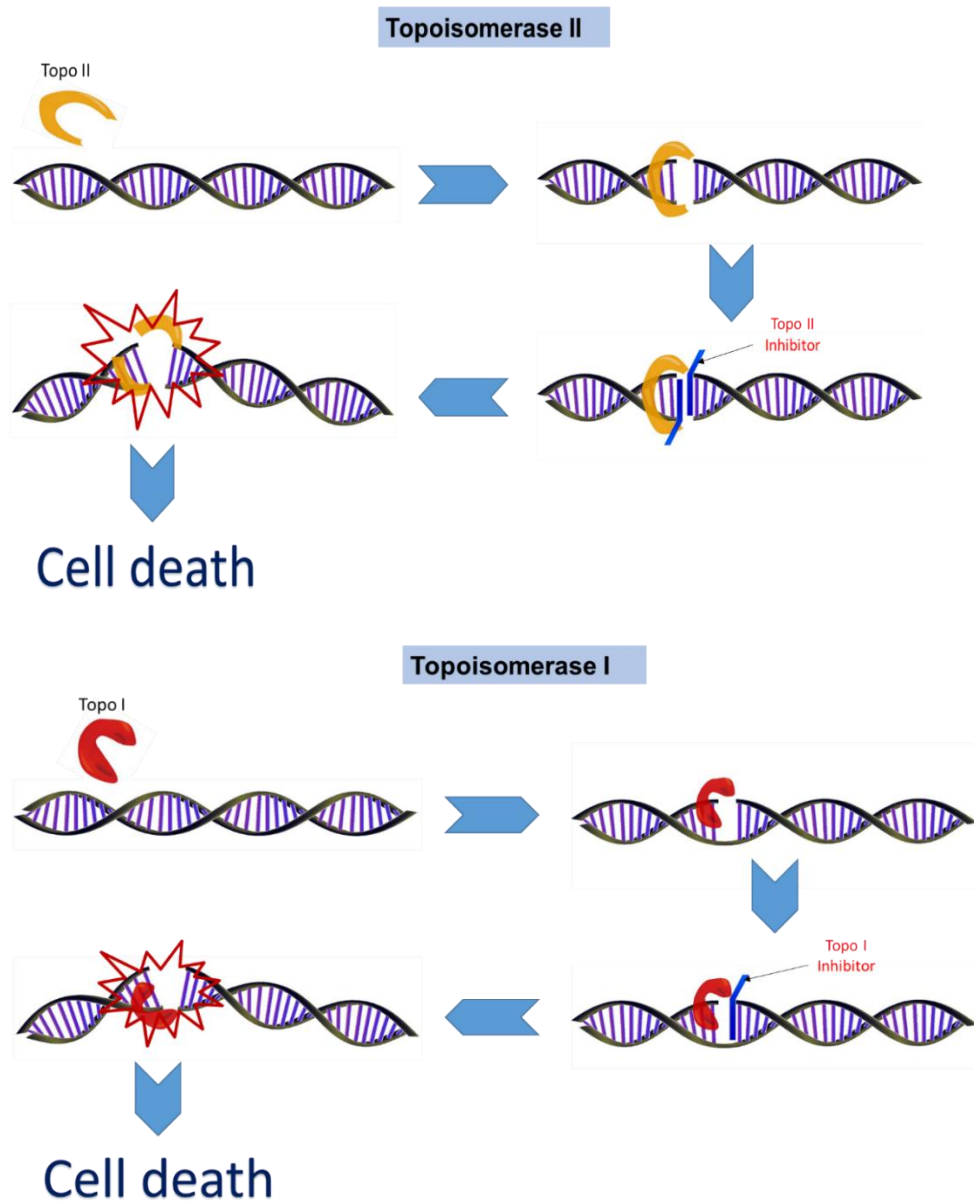


Figure 1.4: Topoisomerase inhibitor

1.2.4 **Mitochondria and cancer**

Mitochondria play a crucial role in the regulation of cellular function, metabolism, and cell death in cancer cells. Several functional changes to cancer cell mitochondria are involved in tumour formation including decreased oxidative phosphorylation, increased production of reactive oxygen species (ROS) and increase in glycolysis. However, in cancer cells, mutations in mitochondrial genomes can change the biochemical behaviour of mitochondrial and nuclear protein complexes which in turn increase reactive oxygen species (ROS), thereby enabling tumour growth. In healthy cells, the glycolysis process in which ATP is generated is mainly by oxidative breakdown of pyruvate following non-oxidative breakdown of glucose (Verschoor *et al.*, 2013). In contrast, cancer cells constitutively upregulate glucose metabolism, even in the presence of high oxygen, thus cancer cells synthesize ATP through 'aerobic glycolysis', which is a metabolic process in which glucose breaks down in the absence of oxygen to produce lactic acid and increase the acidity of cancer cells which may facilitate tumour invasion. On the other hand, increased glucose breakdown provides building blocks for the synthesis of nucleotides and amino and fatty acids (Kroemer, 2006). The differences in the ratio of glycolysis and respiration in healthy and cancer cells is known as the Warburg effect (Warburg, 1956).

Furthermore, it was discovered that the mitochondria of cancer cells are often resistant against the induction of mitochondrial outer membrane permeabilization (MOMP), which is a crucial process during apoptosis due to the release of proapoptotic factors such as cytochrome *c* from the mitochondrial intermembrane space to the cytosol, which in turn mediate the pathway of apoptosis. The inhibition of MOMP resulting in disabled apoptosis which is important for the development of solid tumours (Kroemer, 2006).

However, several growth advantages of cancer cells provided by aerobic glycolysis include growth of cells in unfavourable microenvironments, affording precursors for biosynthetic reactions and generation of substrates for glycosylation reactions. The metabolism of glycolytic enzymes has independent functions which in turn provide additional function to cancer cells such as resistance to apoptosis, transcriptional and malignancy regulation and invasiveness. Besides aerobic glycolysis, the malignant phenotype is distinguished by additional metabolic changes, new lipid and nucleotide

biosynthesis, and glutamine-dependent anaplerosis [renewal of tricarboxylic acid cycle (TCA cycle) intermediates]. These changes in metabolism are important in rapid cell proliferation. Furthermore, many forms of cancer reveal mitochondrial DNA (mtDNA) mutations that include, mutations deletions, duplications, copy number changes and insertions, which can cause inhibition of oxidative phosphorylation, an increase reactive oxygen species generation, and can lead in tumour adaptation under adverse conditions. Alterations in cancer mtDNA include, increase invasive metastatic potential, drug resistance and poorer prognosis of cancer cells have been observed and related with the type and range of mtDNA mutations (Pathania *et al.*, 2009).

1.2.5 **Mitochondrial targeting for cancer therapy**

Targeting compounds to mitochondria represents a promising approach in cancer chemotherapy due to its vital functions in survival of eukaryotic cells through energy production (ATP) via oxidative phosphorylation and its crucial role in regulation of apoptosis (Galluzzi and Kroemer, 2008). However, (Diehn *et al.*, 2009) demonstrated that modifications in the levels of reactive oxygen species (ROS) have been linked to the intrinsic chemotherapy resistance of cancer stem cells. These changes and functions make these organelles attractive drugs targets for cancer therapy.

The mitochondria of tumour cells are structurally and functionally different from those of normal cells. Tumour cells have extensive metabolic reprogramming that make cancer cells more liable to mitochondrial disorder than healthy cells. In addition, mitochondrial adaptations that take place in cancer range from simple to intense dysfunction, therefore any difference between healthy and tumour cells is an opportunity to be therapeutically targeted (Constance and Lim, 2012). On the other hand, to deliver active drugs to mitochondria, it is important first to understand the chemical properties of molecules that selectively localize inside mitochondria. Two generalized requirements for mitochondrial localization are: delocalized positive charge and lipophilicity **Figure 1.5** (Horobin *et al.*, 2007). Delocalized positive charge is important to control the uptake of delivery vectors

through mitochondrial membrane and cellular membrane, which have a negative membrane potential.

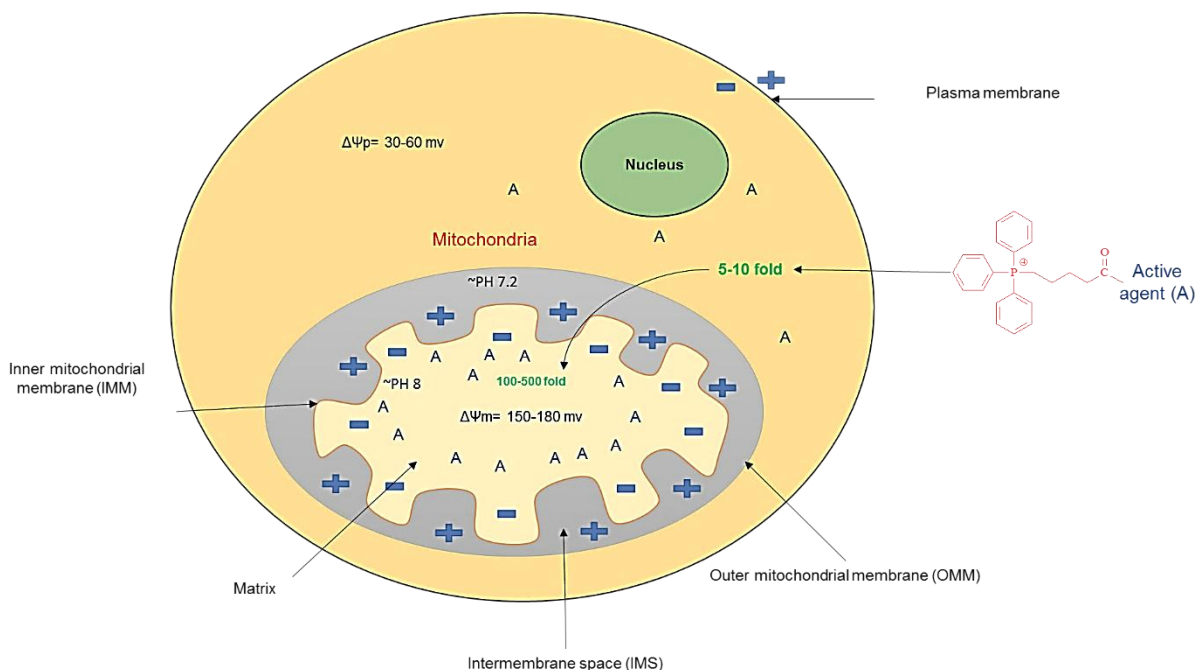


Figure 1.5: General concept for TPP Carrier-Drug Targeting of mitochondria

1.2.5.1 Examples of drugs targeted to mitochondria

Impermeability of mitochondria against a wide range of molecules, makes the design of an efficient mitochondria-targeting cell permeable compound a difficult challenge. Delocalized positive charge is important to control the uptake of delivery vectors through mitochondrial membrane and cellular membrane, which have a negative membrane potential. An example of a vector containing drug with a positive charge to increase its uptake by mitochondria is gamitrinib (a mitochondrial matrix inhibitor) **Figure 1.6**. Geldanamycin, which is the therapeutically active portion of gamitrinib, was conjugated with triphenylphosphonium (TPP) to increase the uptake by mitochondria. Two main advantages of delocalized positive charge of this molecule that allow it to across the large

negative potential of inner mitochondrial membrane (IMM) are: the positive charge reduces the activation energy related with de-solvating the ion that should occur to advance its uptake through the hydrophobic inner mitochondrial membrane (IMM) and reduction of the interaction of this molecule with surrounding water molecules due to the spreading of positive charge over a large surface area, increasing its ionic radius (Kang *et al.*, 2009; Kelley *et al.*, 2011).

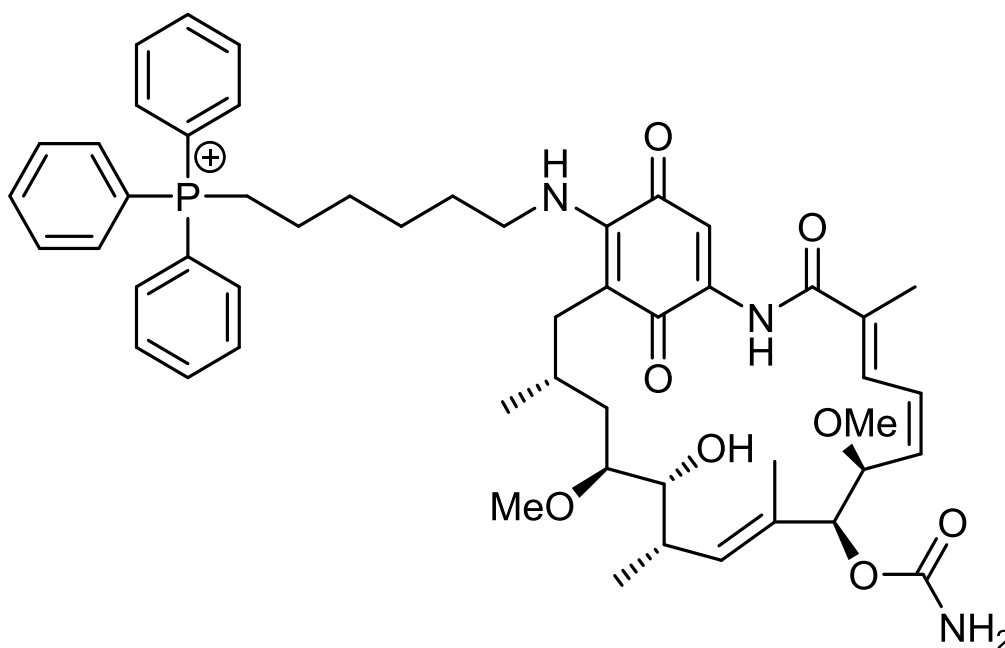


Figure 1.6: Gamitrinib-TPP structure

Furthermore, delocalized positive charge is not enough to make it cross the hydrophobic IMM, therefore introducing lipophilicity to the molecule will drive it to pass the hydrophobic IMM of mitochondria and accumulate. A hydrophobic nitrooxy-doxorubicin was designed to include a nitric oxide-releasing phenyl group that sufficiently increased its hydrophobicity compared with doxorubicin alone **Figure 1.7**. This structure modification drives the molecule to be localized in membrane-rich organelles such as mitochondria instead of localized in the nucleus (Riganti *et al.*, 2013). Moreover, mitochondria-targeted small molecules that are not conjugated with targeting vectors tend to accumulate within

metabolically active cells such as heart and brain (Rin Jean *et al.*, 2014). For this reason, by attaching mitochondrial targeting vectors, the anticancer active drugs will accumulate inside the mitochondria, which in turn reduces the side effects on normal cells.

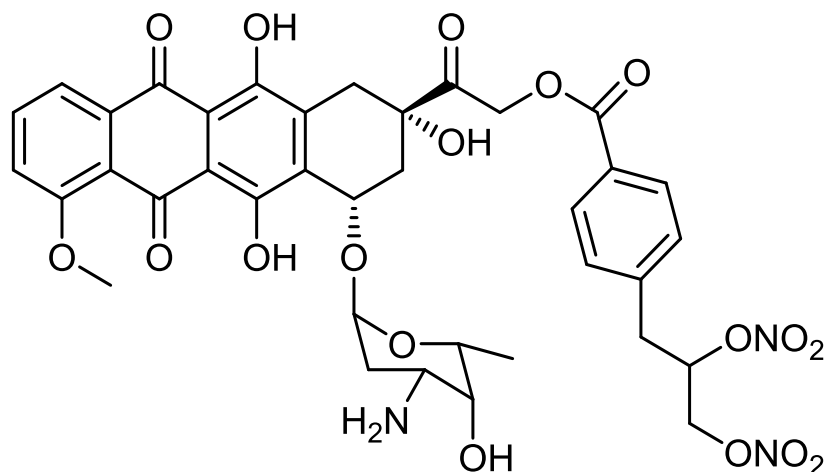


Figure 1.7: Nitrooxy-doxorubicin structure

1.2.5.2 Triphenylphosphonium bromide (TPP) vector targeted to mitochondria

The delivery of drugs to mitochondria is a promising avenue for therapeutics in many human diseases but specifically in cancer treatment. It improves the therapeutic efficacy of anticancer drugs through accumulation of the drug inside the mitochondria and reduction of the undesirable effects of its off-target subcellular localization. By designing specific targeted delivery systems to mitochondria certain characteristics of the drugs may be improved, such as decreasing drug resistance, increasing bioavailability, and poor solubility. However, as the mitochondria have crucial implications in human pathophysiology, design and construction of carrier vectors for efficient selective drug delivery inside the mitochondria by crossing several membranes to reach its final destination inside the mitochondrion is the main and current focus of molecular pharmacological research. In addition, passive targeting to mitochondria is difficult due to its morphology properties therefore, targeting strategies are being developed in addition

to conjugation to lipophilic cations, including encapsulation in liposomes and incorporation into mitochondria-targeted peptides (Apostolova and Victor, 2015).

The large membrane potential of mitochondria (-150 to -180 mV) provides a sufficient force for the selective targeting of lipophilic cations and accumulation inside the mitochondria. The distinct negative membrane potential present in mitochondria is not found in any other subcellular compartment and offers a unique molecular delivery opportunity for selectively targeting the mitochondrion (Hoye *et al.*, 2008). The delivery of lipophilic cations inside the cell was first shown with the lipophilic cation rhodamine 123 in combination with the anticancer drug cisplatin (Teicher *et al.*, 1987) **Figure 1.8**. On the other hand, the most notable and widely employed lipophilic cation for mitochondrial targeting is (4-carboxybutyl)triphenylphosphonium bromide (TPP) **Figure 1.9**. The lipophilic nature and delocalized positive charge of TPP, allows TPP to permeate lipid bilayers easily and accumulate within mitochondria with 100-500 fold difference in the accumulation of TPP in the cytoplasm (Bielski *et al.*, 2015). The selective uptake of TPP by mitochondria should greatly increase the specificity and efficacy of targeting molecules to mitochondria and moreover decreasing unwanted side effects (Smith *et al.*, 2003).

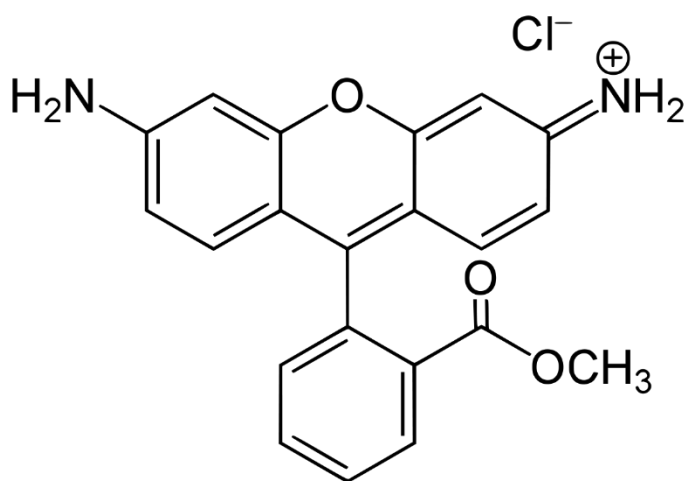


Figure 1.8: Rhodamine 123 structure (a mitochondrial vector)

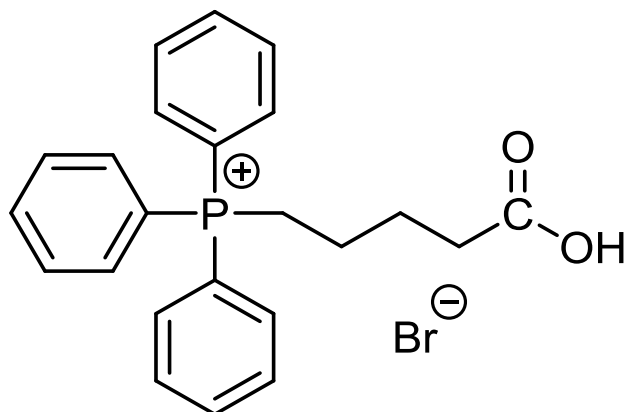


Figure 1.9: Triphenylphosphonium (TPP) structure (a mitochondrial vector)

1.2.5.3 Examples of TPP conjugates targeted to Mitochondria

Consequently, a number of TPP conjugates compounds have been designed to target the mitochondria for improve therapeutic index and reduce side effects. To improve this view, Chakraborty and Jana, (2015) synthesised quantum dots (QD) and iron oxide-based nanoprobe and they conjugated these compounds with TPP. They found that QDs distributed all over the cells, but QDs with TPP were found to be localized inside cells. Moreover, they reported that co-localization study for QD with or without TPP using mitotracker and lysotracker probes showed that the nanoprobe clearly co-localized inside the mitochondria but did not co-localize in lysosomes, thus QD-TPP produces high toxicity in comparison with QD due to their excessive binding with mitochondria and thus disturbing their function (Chakraborty and Jana, 2015).

In addition, Han *et al.*, (2014) synthesised doxorubicin (DOX) derivatives; doxorubicin has a similar mechanism of action to mitoxantrone (the model compound in this research) as both are DNA binding topoisomerase II inhibitors. They conjugated TPP directly to DOX by an amide bond to investigate mitochondrial targeting of DOX **Figure 1.10**. Han *et al.*, (2014) studied mitochondrial targeting, intracellular accumulation, cytotoxicity and resistance to DOX-TPP in human cancer cells and compared these with free DOX. They reported that cellular uptake of free DOX was lower than that of DOX-TPP in MDA-MB-435/DOX breast cancer cell line, due to the possibility of bypass of Pgp and other overexpressed efflux pumps in resistant cell lines by DOX-TPP. The subcellular

localization of free DOX when compared with DOX-TPP in MDA-MB-435/WT and MDA-MB-435/DOX cell lines showed the localization of free DOX in the nucleus of MDA-MB-435/WT cells without any observed presence in mitochondria or cytoplasm and in MDA-MB-435/DOX cells, free DOX was excluded from the nucleus. DOX-TPP showed similar distribution in both cell lines and colocalized with Mitotracker in mitochondria and no notable distribution in cytoplasm or nucleus in both cell lines, determining that TPP makes DOX more targeted to mitochondria, thus increases the preferential accumulation of DOX inside the mitochondria and not in the nucleus or cytoplasm leading to cellular death (Han *et al.*, 2014).

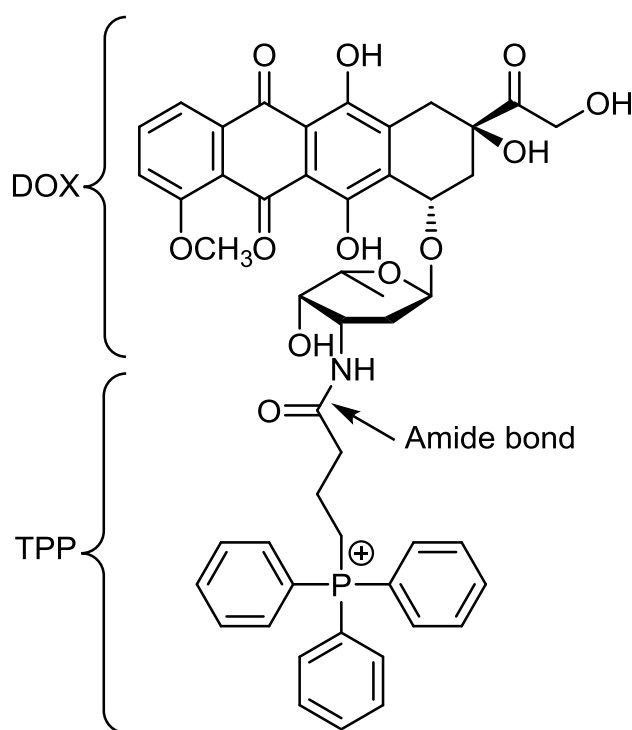


Figure 1.10: Doxorubicin-triphenylphosphonium (DOX-TPP) structure

However, to improve the activity and targeting efficiency of TPP, several modifications of the hydrophobicity of the TPP–drug conjugate system have been studied and investigated. Hu *et al.*, (2017) studied the effect of TPP phenyl substitution on the mitochondrial uptake properties of TPP. They indicated that increasing both the hydrophobicity of the cation and solvent accessible surface area by methyl substitution at

different positions of the TPP phenyl rings remarkably enhanced the partitioning of the modified TPP cation in a hydrophobic environment and improved the accumulation of conjugated cargo within the mitochondria. Hu *et al.*, (2017) conjugated TPP with hexachloro-fluorescein **Figure 1.11** for photodynamic therapy (PDT), which is the light irradiation of photosensitizer-stained cancer cells in the presence of molecular oxygen to produce reactive oxygen species that are capable of damaging and killing cells (Agostinis *et al.*, 2011). Hu *et al.*, (2017) prepared three hexachloro-fluorescein TPP-conjugates. First conjugate has no methyl substitution on phenyl rings of TPP, the second conjugate has one methyl substitution and the third conjugate has two methyl substitutions. They demonstrated that the accumulation level of the modified TPP species in the mitochondria of HeLa cells and FU97 gastric cancer cells increased significantly upon substitution of the phenyl rings. However, unconjugated fluorescein does not accumulate notably in the mitochondria and therefore does not display any PDT effect, while TPP-conjugates permeate both plasma and mitochondrial membranes and accumulate in the mitochondria. The more hydrophobic TPP cationic carrier with two methyl substituents on phenyl groups facilitates a better mitochondrial uptake of conjugated hexachloro-fluorescein which leads to a 2 fold improvement in PDT efficacy upon light irradiation (Hu *et al.*, 2017).

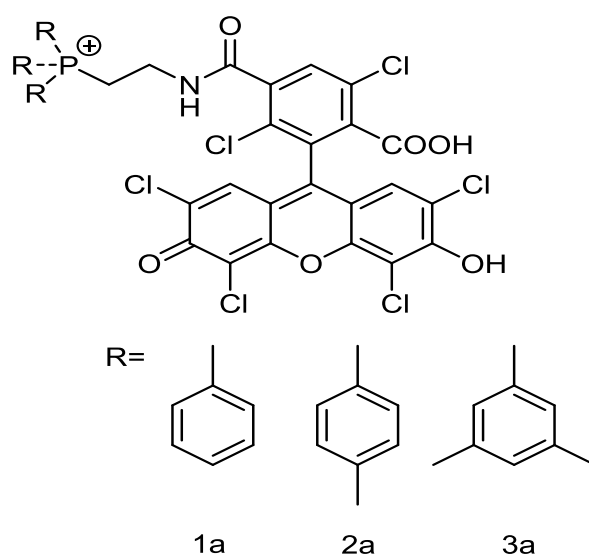
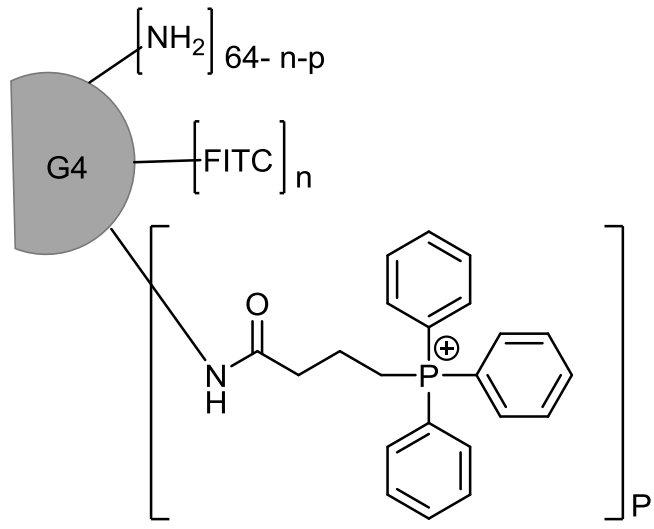


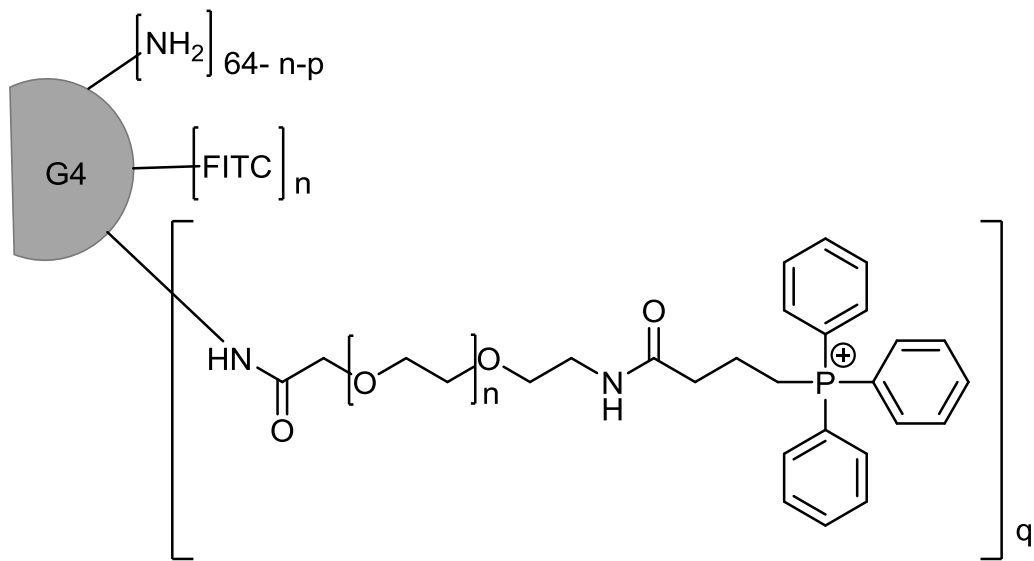
Figure 1.11: Structures of the (hexachloro-fluorescein)-TPP and TPP modified conjugates: (hexachloro-fluorescein)-triphenylethylphosphonium (1a), (hexachloro-fluorescein)-tri-p-tolyethylphosphonium (2a), and (hexachloro-fluorescein)-tris(3,5-xyllyl)ethylphosphonium (3a)

In addition, TPP density plays a significant role in the mitochondrial targeting when the number of TPP conjugates increases, which has been improved by (Bielski *et al.*, 2015). Bielski *et al.*, (2015) conjugated TPP with poly(amidoamine) (PAMAM) dendrimers. Dendrimers have highly reproducible pharmacokinetic profiles because of their structure and they are relevant strategies to deliver a combination therapy (Li *et al.*, 2013). Bielski *et al.*, (2015) designed two main TPP conjugates, they linked TPP directly to 4 PAMAM G4NH₂ dendrimer (G4NH₂-TPP) **Figure 1.12 (A)** and they used a polyethylene glycol PEG linker (G4NH₂-PEGTPP) **Figure 1.12 (B)**. Three TPP loadings were used; no (0 TPP), low (5 TPP) and medium (10 TPP) for G4NH₂-TPP and same density for G4NH₂-PEGTPP. They reported that both strategies make a significant enhancement in mitochondrial targeting compared with unconjugated compound. Direct TPP conjugation exhibited a direct correlation between targeting and TPP number density (G4NH₂-10TPP is higher than that of G4NH₂-5TPP which were both higher than G4NH₂-0TPP, while indirect conjugation resulted in high targeting for all TPP densities with no effect on targeting by the degree of PEGylation. Furthermore, the density of TPP showed a direct correlation with the toxicity. Bielski *et al.*, (2015) measured the IC₅₀ for three densities which showed that G4NH₂-10TPP has an IC₅₀ of 2.95 μM, while G4NH₂-0TPP's IC₅₀ was found at significantly higher concentrations (more than 20 μM) and the IC₅₀ for G4NH₂-5TPP does not affect the toxicity profile of the conjugate. Therefore, the maximum density of TPP is limited by its toxicity effect, which seems that the conjugate with 5 TPP represents the ideal number of TPP residues with significant improvement in targeting while the toxicity of the conjugate is not changed (Bielski *et al.*, 2015).

The alkyl chain between the TPP and its conjugate also have a significant effect in accumulation of the TPP-conjugates inside the mitochondria. Mitoquinone (MitoQ₁₀) **Figure 1.13**, is a TPP bound version of ubiquinone Q₁₀. The cellular uptake of MitoQ is more rapid than that of methylTPP, because the hydrophobicity of MitoQ is higher than that of methylTPP, which in turn reduces the activation energy available for passage across the plasma membrane. MitoQ₁₀, has a 10-carbon atom-alkyl chain, which shows optimum activity and accumulation in the mitochondria (Apostolova and Victor, 2015). This indicates the role of an alkyl chain in the colocalization of MitoQ₁₀ conjugate compound in the mitochondria.



A



B

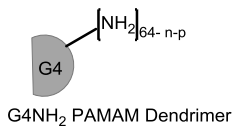


Figure 1.12: TPP conjugate with G4NH₂ PAMAM Dendrimer

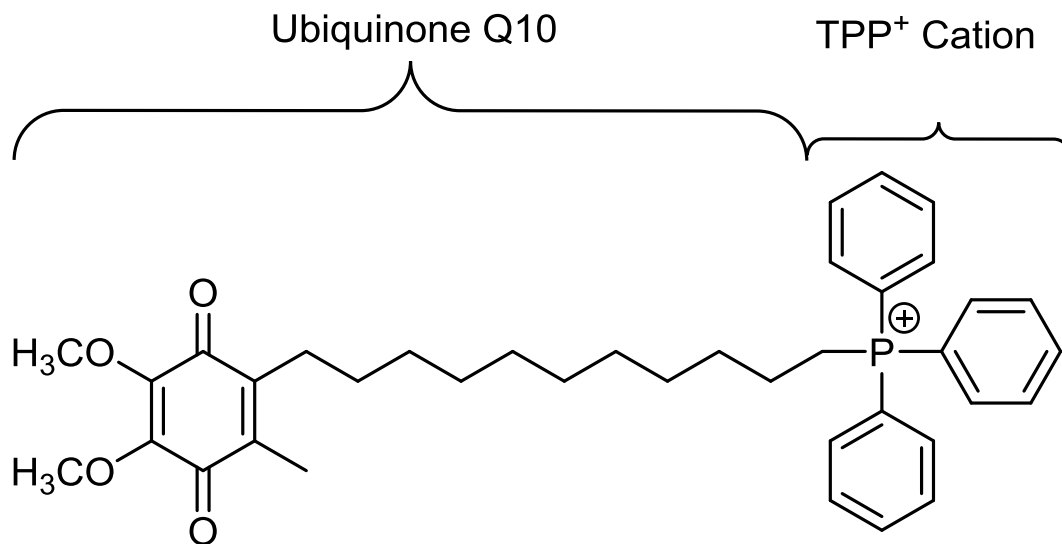


Figure 1.13: Chemical structure of mitoquinone (MitoQ₁₀)

In addition, Rin Jean *et al.*, (2014) reported that TPP conjugates in general have low toxicity and high level of uptake in vivo. However, (Guzman-villanueva *et al.*, 2015) reported that TPP has high cellular toxicity levels, which have limited its therapeutic use due to an excessive accumulation of TPP cation within mitochondria. However, to reduce the cytotoxicity of TPP, (Guzman-villanueva *et al.*, 2015) synthesised CTPP-PE by hydrophobization with two-tail phospholipid phosphatidylethanolamine (PE) via a carboxyl-to-amine conjugation reaction to reduce the cytotoxic effect of TPP **Figure 1.14**. They reported that CTPP-PE liposomes were less toxic than TPP and its derivatives at high concentration, and that the accumulation of TPP within the mitochondria was high, therefore the functionality of TPP cations was not altered by the hydrophobization reaction. This may be a benefit when using TPP to target cancer cells as the accumulation of TPP inside the cancer cells may cause cytotoxicity.

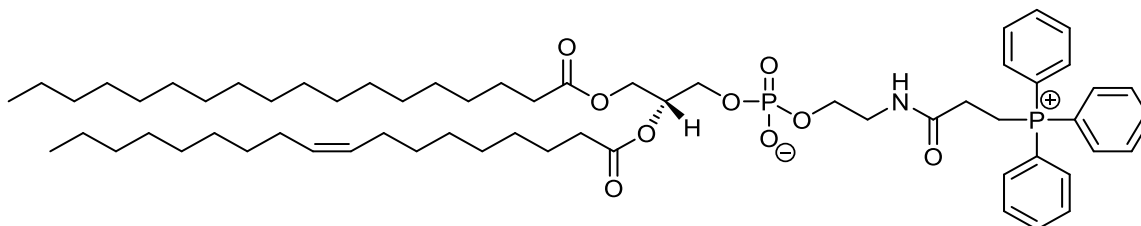


Figure 1.14: Chemical structure of a CTPP-PE conjugate

1.2.5.4 Examples of other vectors targeted to mitochondria

However, there are other vectors that can deliver anticancer drugs to mitochondria such as, nanoparticle, liposomes, cationic peptide and rhodamine B. Nanoparticle (NP) can be modified for mitochondrial targeting by attaching positively charged TPP carrier on the outer surface or within its structure (Weissig *et al.*, 2006). For example, Wang *et al.*, (2013) synthesised a novel nanoparticle system and conjugated it with TPP to enhance its activity. They used poly-L-lysine (PLL), which is a cationic nanocarrier that promotes cellular incorporation through adsorptive endocytosis via non-specific electrostatic association with an anionic membrane and helped their escape from endolysosomal compartments by the osmotic effect. The medium-sized PLL (MH-PLL) is considered to be the optimum one. TPP was conjugated to MH-PLL-NPs (TPP-MH-PLL-NPs) through a carbodiimide reaction process for selective mitochondrial targeting **Figure 1.15**. TPP-conjugates were found to be effectively taken up by cells and selectively accumulated in the mitochondria (Wang *et al.*, 2013). This indicated that the combination between two vectors can improve the activity and selectivity of targeting anticancer drugs.

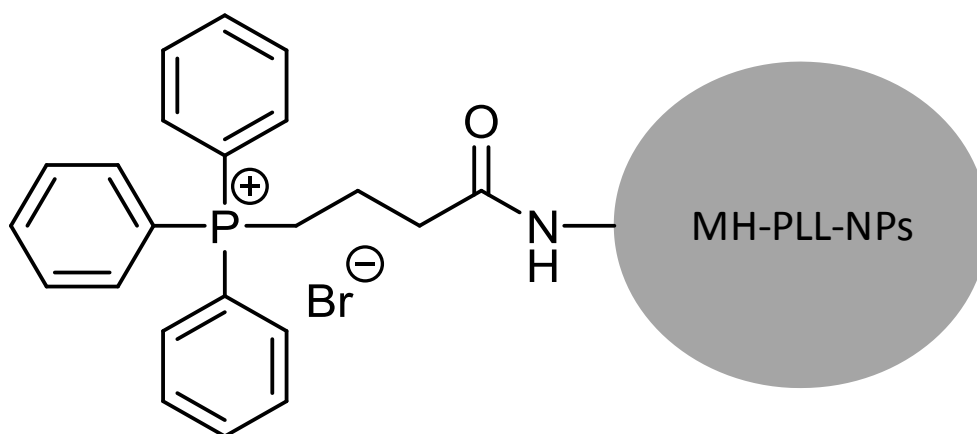


Figure 1.15: Chemical structure of TPP-MH-PLL-NPs

On the other hand, liposomes are another nanoparticle system that are used to deliver active drugs to mitochondria (Weissig *et al.*, 2006). Special advantages for using

liposomes are their biocompatibility and biodegradability, varied range of compositions and ability to carry and protect wide range of biomolecule (Torchilin, 2009). However, there are some limitations for using this carrier including complex synthesis, their toxicity in vivo and possible immune response (Filion and Phillips, 1998). To improve this, Biswas *et al.*, (2012) synthesised a novel polyethylene glycol-phosphatidylethanolamine (PEG-PE) attached with a TPP group (TPP-PEG-PE) and this conjugate was incorporated into the liposomal lipid bilayer. Liposome-TPP-conjugates were studied for the mitochondrial targeting, toxicity and potency delivering paclitaxel (PTX) to cancer cells in vitro and in vivo. They demonstrated that modified liposomes with novel polymer TPP-PEG-PE are non-toxic and effectively target mitochondria in cancer cells (Biswas *et al.*, 2012).

Peptide vectors have also been shown to provide efficient carriers for mitochondrial cargo delivery. The advantages of this vector include low toxicity, high specificity and an increase in the variety of interactions such as protein–lipid, protein–DNA and protein–protein, that are difficult to target with small molecules. However, peptide vectors can face some difficulties in delivery, such as rapid clearance, degradation by proteases (Constance and Lim, 2012) and cannot deliver cargo with high molecular weight (Rin Jean *et al.*, 2014). Horton *et al.*, (2008) engineered a type of cell-permeable peptide that expeditiously enters human cells and has specific mitochondrial localization. They indicated that these mitochondria-penetrating peptides (MPPs) have a characteristic favourable to use as a delivery vector because of straightforward synthesis and biocompatibility. Therefore, the MPPs may represent a class of transporters that effectively deliver cargo to mitochondria which are very suitable to cross an organelle membrane that is difficult to penetrate (Horton *et al.*, 2008).

Additionally, rhodamine B was also used as a carrier and fluorophore targeting to mitochondria. Rhodamine B is a member of delocalized lipophilic cations and it has been used as a carrier for molecules targeting to mitochondria because of preferential accumulation in this organelle (Muli *et al.*, 2014). Ngen *et al.*, (2009) reported that accumulation of conjugate dyes is higher than the unconjugated one due to the delocalized positive charge of rhodamine B. Also, they reported that the molecule conjugated with TPP (TPP-Rh) has greater intracellular accumulation in compared with

unconjugated TPP-OH or rhodamine B. Moreover, Xie *et al.*, (2013) synthesis and developed a fluorinated docetaxel derivative (4FDT) from docetaxel (DTX). Xie *et al.*, (2013) developed a novel anticancer prodrug targeted to mitochondria in which a fluorinated docetaxel derivative (4FDT) and rhodamine B were conjugated via a biodegradable ester bond **Figure 1.16**. They reported that the cytotoxicity of 4FDT-RhB is much lower than DTX and 4FDT and that the toxicity of the prodrug increased with time and IC₅₀ at 72 hours was 10 times more toxic of that at 48 hours in HepG2 cells, meaning that the prodrug needed time to release active drug. Also, the prodrug was specifically delivered to mitochondria and was stable in plasma or whole blood. It can be concluded that rhodamine B can also be used as a vector for molecules targeted to mitochondria (Xie *et al.*, 2013).

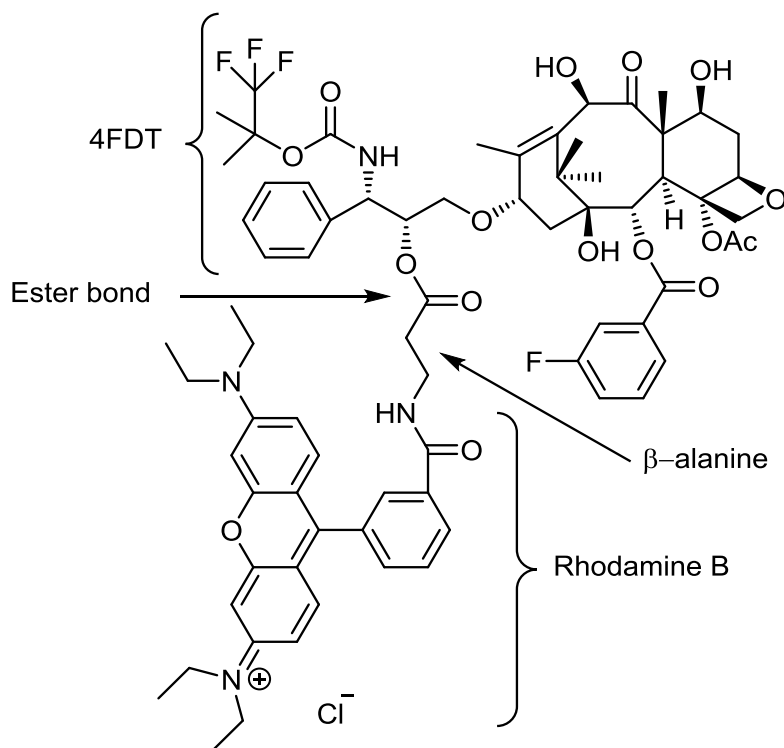


Figure 1.16: Chemical structure of 4FDT-RhB

1.2.6 Drug resistance

The failure of cancer patients to respond to specific therapeutic treatment can happen because of the host factor which is the general and most common factor leading to failure in cancer therapy. Host factors include rapid metabolism or poor absorption or excretion of a drug, resulting in low serum levels (Pluen *et al.*, 2001). However, each cancer cell responds to cytotoxic agents in their own way because each cancer cell has a different genetic make-up depending on the tissue of origin, the pattern of activation of oncogenes, variations in gene expression and inactivation of tumour suppressors, in turn resulting in a different array of drug-resistance gene expression by every cancer cell therefore leading to overgrowth of drug-resistant variants by many cancers (Gottesman, 2002). However, cancer cells can become resistant to anticancer agents by one of these mechanisms: specific metabolism of a drug, loss of a cell surface receptor or transporter for a drug and modification by mutation of the specific target of a drug, these mechanisms result in resistance to a single class of drugs (Longo-Sorbello and Bertino, 2001). However, cells express mechanisms of resistance that give simultaneous resistance to different classes of drugs that have unrelated structure and function. This phenomenon is known as multidrug resistance (MDR) (Sauna *et al.*, 2001).

There are five families of efflux-pump proteins that are correlated with MDR but the most notable and popular efflux-pump is the ATP-binding cassette (ABC) superfamily. MDR efflux pumps are classified based on the energy source that the pump uses, the number of components that the pump has (single or multiple), the types of substrate that the pump exports and the number of transmembrane-spanning regions of transporter protein (Piddock, 2006). Additionally, cellular multidrug resistance usually happens due to the resistance of cells to many substances, often hydrophobic drugs, which is known as classical multidrug resistance. This type of resistance results from expression of ATP-dependent efflux pumps with wide drug specificity. These pumps belong to the ATP-binding cassette (ABC) transporter family and have similar sequences and structure (Dean, Hamon and Chimini, 2001). Human ABC transporters consist of 48 family members, with well-studied members: P-glycoprotein (ABCB1), breast cancer resistance protein (BCRP/MXR/ ABC-P/ABCG2) and multidrug resistance-associated proteins

(MRP1/ABCC1 and MRP2/ABCC2) (Katayama *et al.*, 2014). The resistance of this family to a wide range of drug occurs because of their ability to increase drug efflux and decrease drug influx resulting in reduced intracellular drug concentrations. Many structurally unrelated drugs are affected by this family of ABC transporters, such as, vinca alkaloids (vinblastine and vincristine), anthracyclines (doxorubicin and daunorubicin), the microtubule-stabilizing drug paclitaxel and RNA transcription inhibitor actinomycin-D (Ambudkar *et al.*, 1999).

Furthermore, MDR also can be mediated by decreased drug uptake. Water soluble drugs might fail to accumulate inside the cells even without increased efflux. Example of these drugs include, antifolate methotrexate, cisplatin and nucleotide analogues (Shen *et al.*, 2000). MDR can also result from the activation of regulated detoxifying systems, such as DNA repair and the cytochrome P450, which in turn induces the P-glycoprotein (P-gp) transporter. Additionally, MDR can result from blocked apoptosis pathways, this might happen due to a malignant transformation, leading to decreased ceramide levels (Gottesman, 2002).

However, the majority of MDR is caused by the over expression of an energy dependent drug efflux pump, known as P-glycoprotein (P-gp). P-gp was the first ATP-dependent system discovered that was involved in MDR (Sauna *et al.*, 2001). P-gp is encoded by the multidrug resistance 1 (MDR1) gene, which is located on chromosome 7q21 and it is vastly over-expressed in many human cancers, including cancers of the gastrointestinal tract (small and large intestine, pancreatic cancer and liver cancer), cancers of the genitourinary system (kidney, ovary, testicle), cancers of the hematopoietic system (myeloma, lymphoma, leukemia), and childhood cancers (neuroblastoma, fibrosarcoma) (Goldstein *et al.*, 1989; Katayama *et al.*, 2014). P-gp has a molecular weight of 170 kDa and it contains two nucleotide-binding domains (NBDs) and three membrane-spanning domains (MSDs). The two NBDs are recognized by the presence of ATP-binding cassettes that are responsible for hydrolysis of ATP required to transport the solute outside the cells. Each MSDs contains 5-6 transmembrane segments which form the pore in the plasma membrane, in which the solutes are ejected from the cell (Cole, 2014).

P-gp can detect and bind a large number of hydrophobic natural product drugs when they cross and enter plasma membranes. These drugs include the commonly used natural anticancer drugs such as doxorubicin and daunorubicin, taxol, vinblastine and vincristine (Bogman *et al.*, 2001). When these drugs bind to P-gp, this results in activation of one of the ATP-binding domains and hydrolysis of ATP resulting in a large change in P-gp conformation, which in turn releases the drug into the extracellular space. Hydrolysis of a second ATP is required to restore P-gp to its original state (Gottesman, 2002) **Figure 1.17**. On the other hand, tumours that are derived from tissues that normally express P-gp usually express the highest level of P-gp resulting in high resistance to some cytotoxic agents. In contrast, the expression of P-gp may be low at the time of diagnosis in some tumours, but after chemotherapy, P-gp is induced resulting in the development of MDR (Thomas and Coley, 2003).

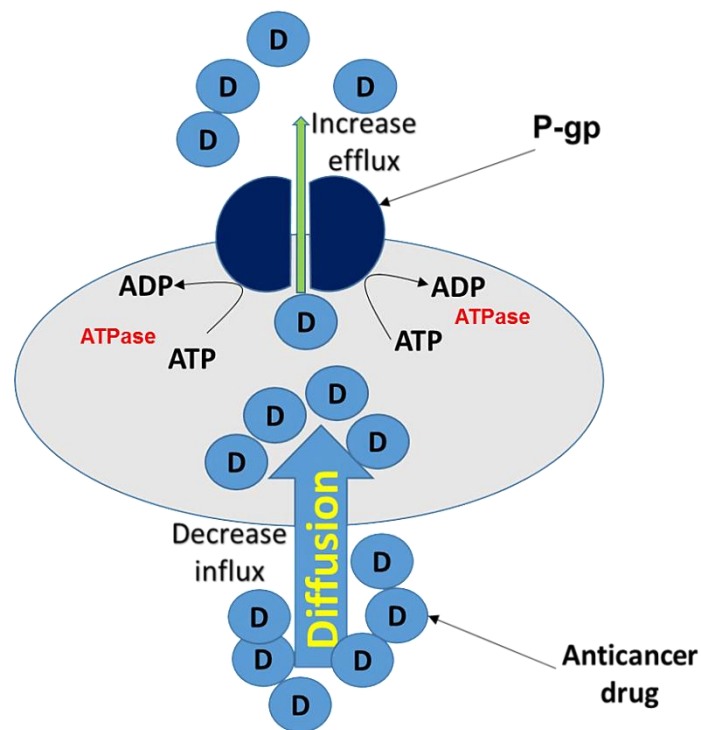


Figure 1.17: Role of P-gp transporters in the development of the MDR phenotype in cancer cells

Furthermore, it was reported that P-gp is not present in mitochondria. Paterson and Gottesman, (2007) presented data to show that P-gp is not localized to mitochondria. They used KB-V1 cells selected for resistance to vinblastine and MCF-7 cells selected for resistance to adriamycin that both express high levels of P-gp. They demonstrated that although P-gp is present in the crude mitochondrial fraction, further purification found that P-gp is not present in mitochondrial membranes, and its presence in the crude mitochondrial fraction was due to plasma membrane contamination (Paterson and Gottesman, 2007). However, Shen *et al.*, (2012) investigated the presence or absence of P-gp in mitochondria using Rhodamine123 as a mitochondria marker and cyclosporine A (CsA) as a mitochondria tracker and Pgp inhibitor in mitochondria isolated from MCF-7 and doxorubicin-resistant MCF-7 (MCF-7/ADM) cells. They indicated that the accumulation of Rho123 in MCF-7/ADM without the addition of CsA is dramatically lower than that of MCF-7 because of the localization of P-gp at the membrane of mitochondria in MCF-7/ADM. However, after pre-incubation of the mitochondria with CsA, they found a marked increase in the accumulation of Rho123 in mitochondria because P-gp was inhibited by CsA and there was no significant change in MCF-7 mitochondria following the addition of CsA. Shen *et al.*, (2012) suggested that Rho123 was pumped out of the mitochondria by an active transport process due to differences in concentration. To confirm this, they tested Rho123 in MCF-7/ADM mitochondria with lower accumulation and they placed it in solution without Rho123. They found that the remaining Rho123 in MCF-7/ADM was significantly lower than that in MCF-7 mitochondria before incubation with CsA and after incubation with CsA, Rho123 export was inhibited in MCF-7/ADM and no significant changes were found in MCF-7. However, this is the only study that shows the expression of P-gp at the mitochondrial membrane.

On the other hand, using drugs that can escape from ABC transporters and are not substrates of ABC transporters such as, alkylating drugs (cyclophosphamide), anthracycline modified drugs (anamycin and doxorubicin-peptide) and antimetabolites (5-fluorouracil) could circumvent drug resistance and allow the anticancer drug to accumulate inside the targeting cell (Choi, 2005). Another method to circumvent resistance to anticancer drugs is to administer nontoxic drugs that have the ability to inhibit ABC transporters **Figure 1.18**. The compounds that reverse resistance against

anticancer drugs are called MDR modulators, MDR inhibitors and MDR reversal agents or chemosensitizers (Liscovitch and Lavie, 2002). Hence, the combination of anticancer drugs together with an MDR inhibitor can be used to circumvent MDR. Two factors that should be determined in order to use this combination include, first, to identify the ABC transporter protein involved in drug resistance and to employ an MDR inhibitor and anticancer drug that should match the transporter protein to be inhibited. The second factor is to detect the plasma concentrations and *in vivo* activity of MDR inhibitor in order to determine the effective inhibitory concentration is attained *in vivo* (Ozben, 2006).

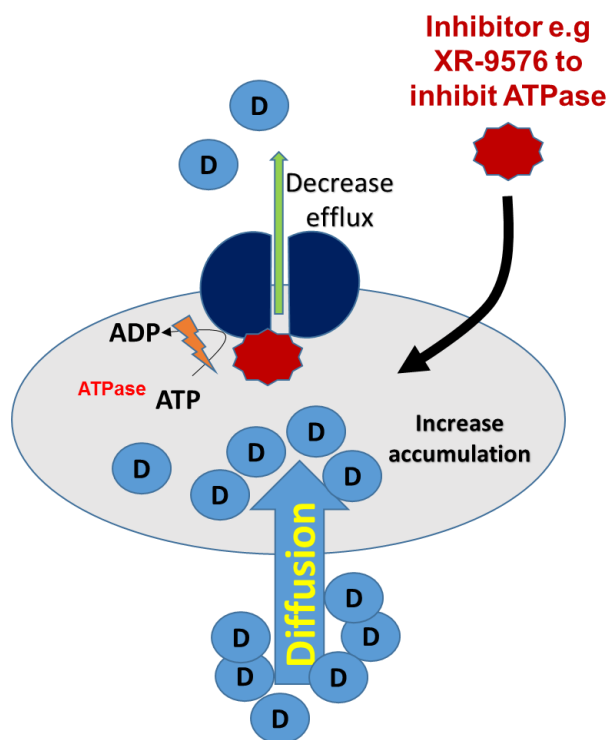


Figure 1.18: The mechanism of P-gp inhibitor XR9576 inhibiting the activity of ATPase which is required to open P-gp, therefore decrease efflux and increase accumulation of anticancer drugs.

In another approach, Settanni *et al.*, (2012) designed and synthesised a mitochondria-targeting carrier QCy7HA and conjugated it with doxorubicin (DOX). The conjugate has the ability to limit the effects of (P-gp) efflux pumps of MDR cells on DOX, indicating that targeting drug to mitochondria is a potential promising method for treatment of drug-

resistant cancers. They designed a fluorogenic probe AcQCy7 for specific mitochondria labelling. They attached the hexanoic acid linker to the phenolic oxygen of the Cy7-like moiety of AcQCy7 through an ether bond to give QCy7HA. Both QCy7HA and AcQCy7 are hydrophobic and have cationic properties (two positive charges on each molecule), which make it a potential mitochondria-targeting conjugate. Settanni *et al.*, (2012) conjugated DOX with QCy7HA because DOX has two practical advantages: first, it has a free –NH₂ functional group that can easily react with the activated carboxylic acid group on the carrier QCy7HA to form the DOX- QCy7HA conjugate. Second, DOX is fluorescent thus allowing for visualizing its intracellular localization by fluorescence microscopy. They studied the co-localization of QCy7HA-DOX conjugate. They indicated that QCy7HA-DOX conjugate was completely co-localized in mitochondria, whereas DOX (without carrier) was kept in cell nucleus over mitochondria or other subcellular, demonstrating that QCy7HA is able to deliver the conjugated DOX to mitochondria effectively (Settanni *et al.*, 2012).

Furthermore, two cell lines were chosen by (Settanni *et al.*, 2012) to determine the effects of the P-gp efflux pumps on the cytotoxicity of QCy7HA-DOX and free DOX, which is drug-sensitive human uterine sarcoma MES-SA cells and its multidrug-resistant subline MES-SA/Dx5. They indicated that the free DOX exhibited toxicity against MES-SA lines with 21-fold greater potency than MES-SA/Dx5 lines, whereas only a 6-fold difference was observed for mitochondria- targeting QCy7HA-DOX. Those results demonstrated that the toxicity of free DOX was reduced by P-gp efflux pumps when compared with mitochondria-targeting QCy7HA-DOX which was much less effected by P-gp efflux pumps (Settanni *et al.*, 2012). Therefore, specific targeting of anticancer drugs to mitochondria by using specific carriers could limit the power of P-gp efflux pumps, thus increasing the accumulation of anticancer drugs inside the mitochondria.

1.2.7 **Anthraquinones and anthracyclines**

Mitoxantrone (1,4-dihydroxy-5,8-bis{[2-[(2-hydroxyethyl)amino]-ethyl]amino]-9,10-anthracenedione) is a synthetic anticancer anthracycline analogue and it is classified as

antitumour antibiotic with significant efficiency in the treatment of different human cancers and multiple sclerosis (Enache *et al.*, 2015). In general, anthracyclines include some of the most potent anticancer drugs ever developed and they play an essential role in the treatment of a wide variety of solid tumours and haematological malignancies, alone or in combination with other cancer drugs (Mordente *et al.*, 2012). Anthracyclines have diverse cytotoxicity mechanisms against cancer cells including: inhibition of macromolecular biosynthesis by the inhibition of DNA replication and RNA transcription, generation of reactive oxygen species (ROS), resulting in DNA damage and/or lipid peroxidation, inhibition of topoisomerase II, direct membrane damages, DNA adduct formation, interference with DNA strand separation or DNA unwinding (Gewirtz, 1999). However, the exact mechanism of how anthracyclines kill tumour cells is still poorly understood, but the evidence of nuclear localization and high DNA affinity of anthracyclines suggest that their anticancer activity is linked to their ability to intercalate between nuclear DNA base pairs thus poisoning topoisomerase activity, leading to the death of dividing cancer cells (Swift *et al.*, 2006; Nitiss, 2009; Pommier *et al.*, 2010). On the other hand, the therapeutic activity of anthracyclines is limited by their toxicity for myocardial tissue, resulting in a progressive cardiomyopathy which can develop into congestive heart failure (CHF) (Mordente *et al.*, 2012).

In order to minimize the side effects relating with the naturally occurring anthracyclines doxorubicin and daunorubicin, mitoxantrone - a member of the anthracenedione class was designed as a simplified analogue of the anthracyclines (Feofanov *et al.*, 1997) to reduce cardiotoxicity associated with the anthracycline antibiotics (Parker *et al.*, 2004). Structurally, mitoxantrone is symmetrical and consists of a tricyclic planar chromophore and two basic side chains containing nitrogen that are positively charged at physiological pH 7.4 **Figure 1.19**. The two side chains of mitoxantrone are critical for intercalation into DNA and the role of the positively charged N-containing side chains is to stabilize the insertion of the ring between base pairs by forming electrostatic interactions with the negatively charged phosphate backbone of DNA (Varadwaj *et al.*, 2010). Several studies on the mechanism of mitoxantrone action have shown that nuclear DNA is the main target for the mitoxantrone where its function is as a potent topoisomerase II inhibitor (Cornbleet *et al.*, 1984). Mitoxantrone accumulates in cells and concentrates in the nucleus and

inhibits DNA replication and RNA transcription by binding with DNA and causes DNA condensation, cross-linking and strand breakage (Panousis and Phillips, 1994). Mitoxantrone shows activity against solid tumours, lung cancer, melanoma, advanced breast cancer, acute non-lymphocytic leukemia, non-Hodgkins lymphoma. In addition, mitoxantrone has similar activity with less toxicity in comparison with other active available agents used in treatment of advanced breast cancer (Cornbleet *et al.*, 1984; Feofanov *et al.*, 1997).

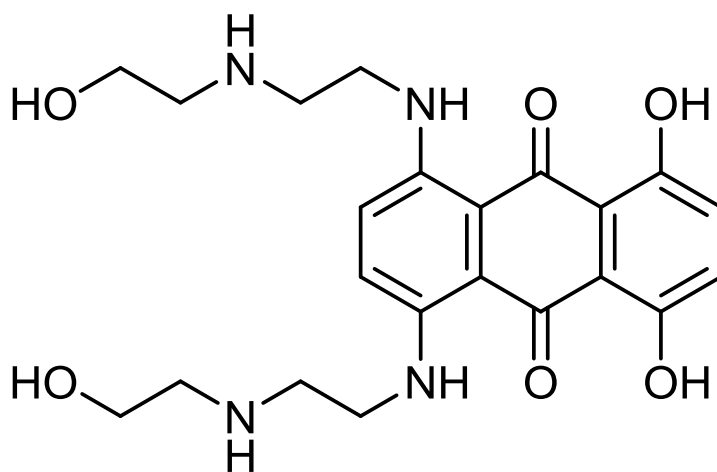


Figure 1.19: Mitoxantrone structure

Mitoxantrone became a widespread drug due to its lower risks of cardiotoxic effects compared with doxorubicin and daunorubicin (Kapuscinski *et al.*, 1981). However, it is now known that mitoxantrone can also induce cardiotoxicity which is dose-dependent, irreversible and it may occur after a long period of treatment (Ehninger *et al.*, 1990; Seiter, 2005). Furthermore, Rossato *et al.*, (2014) studied the effect of mitoxantrone on the cardiac mitochondria and they indicated that therapeutic concentrations of mitoxantrone (100 nM and 1 μ M) caused an energetic variation by hyperpolarization of the membrane potential of mitochondria, and a decrease in ATP levels and increase in the intracellular calcium levels after 24, 48, and 96 hours of mitoxantrone incubation in a H9c2 cells (cardiomyoblast cell model). Mitoxantrone also caused inhibition of ATP-synthase expression and activity with associated increase in the reactive species generation after

96 hours incubation at the same concentrations (100 nM and 1 μ M). Therefore, they revealed that mitoxantrone overlapped with mitochondrial functionality, resulting in an imbalance in the mitochondrial function and therefore late ATP depletion which in turn leads to heart dysfunction and impaired cardiac performance (Rossato *et al.*, 2014).

However, due to the severe side effects such as cardiotoxicity, myelosuppression and extravasation of mitoxantrone specially and anthracyclines in general, considerable efforts have been employed to enhance their curative effect and reduce the side effects. These enhancements include modification of the original anthraquinone backbones and variations in side chains which result in biological improvements (Mansour *et al.*, 2010). To improve this concept, Wang *et al.*, (2012) synthesised anthraquinone–polyamine conjugates to order to increase the cytotoxicity and reduce side effects of anthraquinones like mitoxantrone. Several compounds have been synthesised but the most notable compounds were **9b** and **9c**. Compound **9b** contained a terminal aminobutyl scaffold in the side chain, whereas **9c** contained a terminal aminopropyl scaffold **Figure 1.20**. Wang *et al.*, (2012) indicated that both compounds have high cytotoxicity on solid human cancer HepG2 and were less toxic on normal hepatic QSG7701 cells in an in vivo study, confirming that the presence of a polyamine motif will increase the tumour specific capability of the polyamine-conjugate drugs (Wang *et al.*, 2012). Furthermore, Mansour *et al.*, (2010) studied the effect of side chain length and the presence of primary and secondary amine in the side chain on the formation of DNA adducts and anticancer efficacy produced by these drugs. They demonstrated that pixantrone, which is a novel 2-aza-anthracenedione having a primary amino group in its side chain, has significant anticancer efficacy but fails to induce any detectable cardiotoxicity in comparison with mitoxantrone **Figure 1.21**. Pixantrone is similar to mitoxantrone in that it can be activated by formaldehyde to give formaldehyde-mediated adducts with DNA, due to its primary amino groups in the side chain, however these DNA adducts are formed much more effectively than mitoxantrone. They found also that the side chain length is not a major factor in adduct formation but the presence of a primary amino group is the most important factor because a primary amine is more reactive than secondary amine to form greater concentrations of reactive drug-Schiff base precursors. This complex is more stable than with a secondary amino group, hence the reaction with DNA will be more potent. On the

other hand, the pyridine ring present in the backbone of pixantrone makes it less effective than the corresponding mitoxantrone compound (Mansour *et al.*, 2010).

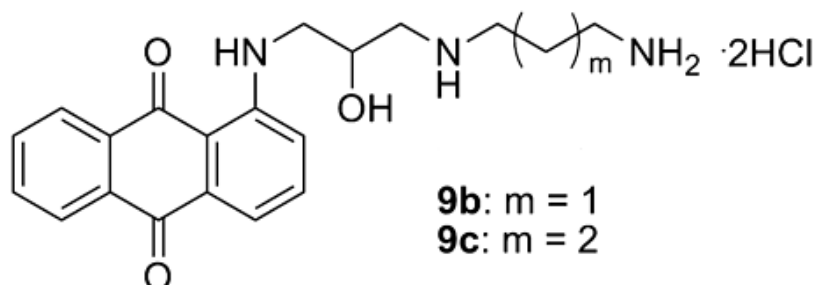


Figure 1.20: Structure of 9b and 9c compounds

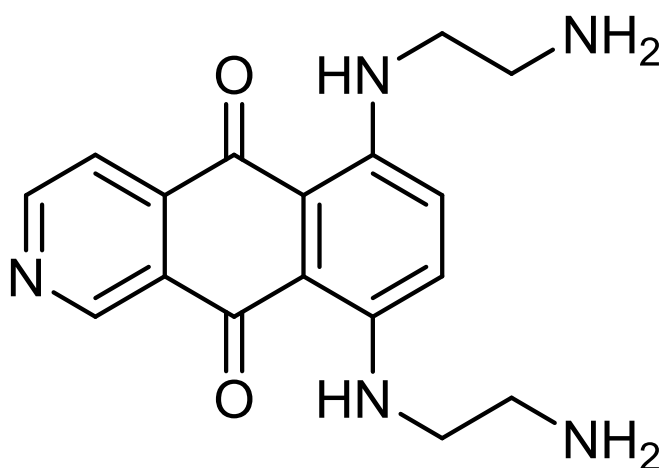


Figure 1.21: Structure of pixantrone

1.2.8 Lysosomal sequestration

Lysosomes are single membrane organelles that are found in all eukaryotic cells and were first described by Christian de Duve about 60 years ago. Lysosomes are the major digestive organelles in cells which degrade intracellular components and extracellular materials taken up by the cell including other organelles, proteins and lipids. These materials enter the lysosomes via endocytosis from outside the cell or via autophagy from inside the cell. The products generated by lysosome degradation either diffuse out of the

lysosome or are transported by lysosomal proteins to the cytosol for reuse by the cell (Mrschtik and Ryan, 2015). Lysosomes have more than 50 hydrolase enzymes, including glycosidases, proteases, nucleases, lipases, phospholipases, phosphatases, and sulfatases. Lysosomes are characterized by low acidic pH 4.5-5 which is maintained by vacuolar H⁺-ATPase. The acidic pH of lysosomes is essential for the maximum activity of hydrolase enzyme (Boya, 2012). In addition, lysosomes are involved in exocytosis, endocytosis, cholesterol homeostasis, macroautophagy, chaperone-mediated autophagy, promote tumourigenesis and trigger apoptosis and cell death. Furthermore, the lysosomes in cancer cells are relatively large and more fragile in comparison with normal lysosomes. Also, cancer cells are more vulnerable to lysosomal mediated cell death than normal cells which can be exploited in the design of new effective anticancer drugs that enhance lysosomal cell death by inhibition of caspase dependent cell death (Halaby, 2015).

Despite their important role in the cell, lysosomes can alter the accumulation of lipophilic amine drugs from their target site by sequestering or trapping them inside the acidic lysosomes by a process known as lysosomal sequestration or lysosomal trapping. One of the most important physiological parameters that predicted the degree of lysosomal accumulation is the pH of lysosomes relative to the pH of the cytosol. Because the larger the lysosome-to-cytosol pH gradient, the larger the extent of lysosomal sequestration is, therefore the considerable trapping of weak bases in lysosomes can greatly reduce drug target interaction which can in turn reduce drug activity (Ndolo *et al.*, 2012). However, because the lipophilic weak amine base drugs diffuse through cell membranes at physiological pH via passive diffusion, once they are inside the lysosomes, they become protonated and accumulate in lysosomes in their cationic state. Certain hydrophobic weak base chemotherapeutics found to be highly accumulated in lysosomes include the doxorubicin, mitoxantrone, daunorubicin, imidazoacridinones and sunitinib **Figure 1.22**. On the other hand, treating the cell with lysosome alkalinizing agents such as bafilomycin A1 and vesicular H⁺-ATPase inhibitor, could eradicate lysosomal drug sequestration and decrease the accumulation of drug in lysosomes, therefore increase cytotoxic drug efficacy (Zhitomirsky and Assaraf, 2015).

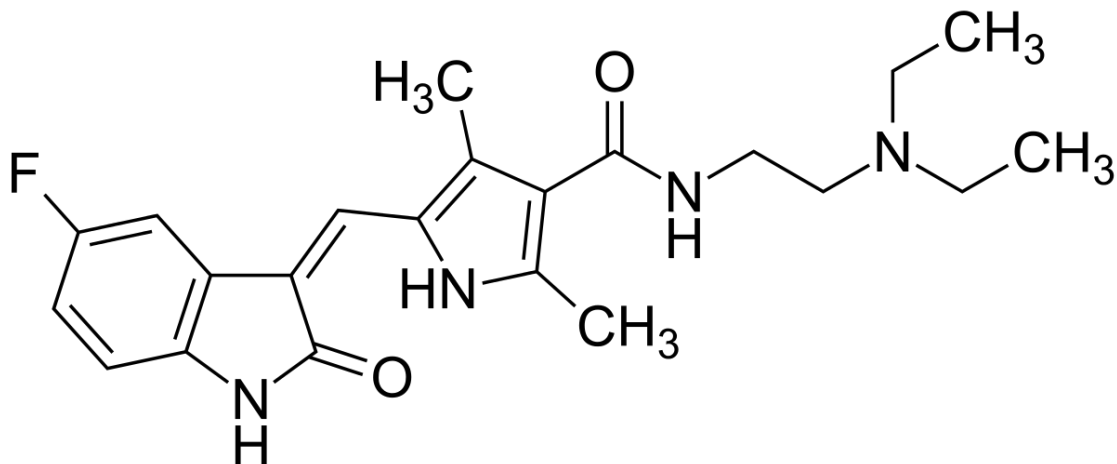


Figure 1.22: Structure of sunitinib

With regard to this, Gotink *et al.*, (2011) investigated resistance mechanisms for sunitinib, which is an antiangiogenic tyrosine kinase inhibitor. They found that resistance to sunitinib is mediated by lysosomal sequestration. They hypothesized that sunitinib might preferentially accumulate in acidic lysosomes because it is hydrophobic ($\log P = 5.2$) can easily cross plasma membranes and other intracellular membranes. Also, sunitinib is a weak base with $pK_a = 8.95$, therefore decreasing the pH below 9, it will be protonated and thereby losing its ability to cross membranes. At pH 5 or below such as in lysosomes, all sunitinib will be protonated and would not be able to cross the membranes, therefore will be trapped in lysosomes. To improve this, Gotink *et al.*, (2011) studied the co-localization of sunitinib in acidic lysosomes. They found clear co-localization of sunitinib in acidic lysosomes and there was no co-localization with other intracellular organs, indicating that resistant cells are able to sequester sunitinib from their cytoplasmic compartment into acidic lysosomes and provide a novel mechanism of resistance (Gotink *et al.*, 2011). In contrast, lysosomes can employ as a novel emerging target for anticancer treatment through different processes of lysosomal disruption by lysosomotropic agents such as mefloquine **Figure 1.23** (Sukhai *et al.*, 2013). Zhitomirsky and Assaraf, (2015), suggested that tumour cells that are rich in lysosomes and are resistant to many hydrophobic weak base drugs such as mitoxantrone, doxorubicin and sunitinib, may exhibit a favourable

response to treatment by targeting lysosomes in malignant cells by induction of lysosome-mediated apoptosis, disruption of lysosomes by lysosomotropic agents such as mefloquine and lysosomal photodestruction by lysosome accumulating photosensitizers such as imidazoacridinones (Zhitomirsky and Assaraf, 2015). This view was proved by (Petersen *et al.*, 2013), which they targeted lysosomes in cancer cells both in vitro and in vivo. They showed that lysosomes in cancer cells can be selectively targeted by targeting lysosomal membrane permeabilization and subsequent cell death, which may prove to be a valuable method in cancer treatment. They targeted acid sphingomyelinase (ASM) inhibition to destabilize lysosomes in cancer cells using lysosome-destabilizing experimental anticancer agent siramesine. Siramesine interferes with the binding of ASM to its essential lysosomal cofactor, bis(monoacylglycero)phosphate, leading to reduced tumour growth in vivo, reversion of multidrug resistance MDR, and cancer-specific lysosomal cell death (Petersen *et al.*, 2013).

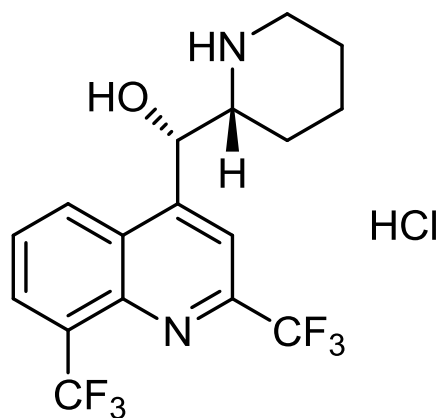


Figure 1.23: Chemical structure of mefloquine

Chapter 1

Results and discussion

1.3 Results and discussion

This chapter describes the design, synthesis and evaluation of novel anticancer drugs targeted intracellularly, specifically targeted to mitochondria. The mitochondrial targeted drugs were specifically designed to accumulate inside the mitochondria by targeting the high membrane potential ($\Delta\Psi_m$) of mitochondria in cancer cells. The following sections in this chapter explain the rational design and synthetic strategy of novel compounds. The synthesis, purification and characterization are also explained in detail followed by biological evaluation in *vitro* assays for the mitochondrial compounds. These assays include: DNA binding assays, distribution coefficient assays, cell viability (MTT) assays, cellular uptake and localization and morphology studies of the targeted compounds.

1.3.1 Rational design

In the last years, there was an improvement in the cancer diagnosis and treatments due to a better understanding of tumour biology (Pelicano *et al.*, 2006). These treatments include chemotherapy, radiation therapy and surgical intervention or a combination of these treatments (Aftab *et al.*, 2018). Most of the traditional chemotherapy works by interfering with DNA synthesis and mitosis leading to the death of cancer cells (Hosoya and Miyagawa, 2014). However, these anticancer drugs are nonselective and can also damage healthy normal tissue and have poor delivery to cancer cells which leads to undesirable side effects such as vomiting, nausea and becoming immunocompromised (Nurgali *et al.*, 2018). Also, the failure of the remedial treatment of cancer patients usually occurs by drug resistance of the tumour to chemotherapeutic agents (multidrug resistance) due to the drug being effluxed by the P-glycoprotein (P-gp) trans-membrane pumps that are overexpressed in cancer (Tanabe *et al.*, 2001; Callaghan *et al.*, 2014). Therefore, the therapeutic effect of anticancer drugs can be maximized, whilst also making the drug more selective resulting in more precise delivery of the drug to the tumour cells and potentially overcoming multidrug resistance by attaching cytotoxic drugs to a targeting vector.

In this programme of research, a prodrug system has been designed and developed to deliver novel experimental anticancer agents to the specific targeting site (mitochondria). Mitochondria are sometimes known as a power house and also have intrinsic mitochondrial DNA (mtDNA) and lack P-gp (Chatterjee *et al.*, 2006; Paterson and Gottesman, 2007; Fulda *et al.*, 2010). Therefore, specific delivery of an anticancer drug to mitochondria could avoid drug resistance and by interfering with mtDNA synthesis, lead to cell death and give the drug more selectivity. This prodrug system contains an active drug that is toxic and connected via a biodegradable linker to a targeting vector (either triphenylphosphonium TPP or rhodamine B) that takes the prodrug to the targeting site (mitochondria). The biodegradable vector will be cleaved by normal metabolic processes such as, specific enzyme-mediated hydrolytic cleavage or under specific conditions such as pH **Figure 1.24**.

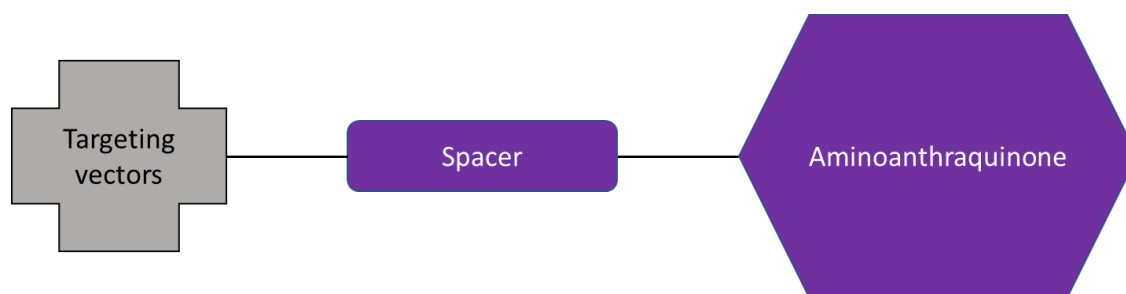


Figure 1.24: The general design of a mitochondrial targeting prodrug system

In this study, aminoanthraquinone derivatives, which are structurally related to clinically used mitoxantrone (topoisomerase II poison), were chosen as the potential active drugs for targeted delivery to mitochondria. For many years now, there has been a particular interest in our laboratory in aminoanthraquinones, both as topoisomerase inhibitors and DNA binding agents.

In the earliest studies, a series of anthraquinone-amino acid conjugates were synthesised in which the amino acid was linked via the *N*-terminus to the anthraquinone nucleus at the C-1 position to afford compounds with anti-topoisomerase activity (Meikle *et al.*, 1995; Mincher, 1999).

One compound (designated CAM 1 or, later, NU:ICRF 505), was shown to act as a clean topoisomerase I poison (although less potent than camptothecin) without affecting the catalytic activity of either DNA topo I or II and had promising *in vivo* activity against human lung and colon cancer xenograft models (Cummings *et al.*, 1996). NU:ICRF 505 was, however, and in common with the majority of compounds in the series, poorly soluble in aqueous media and poor bioavailability precluded its further development.

In order to overcome problems observed with the conjugates of this type, another series of **spacer-linked** anthraquinone-amino acid conjugates [designated NU:UB, **Figure 1.25**] was developed (Mincher, 1999; Turnbull, 2003) that possessed the following structural alterations:

- 1) The amino acid motif was reversed resulting in improved water solubility from possible amine salt formation.
- 2) A **spacer** group was inserted between the anthraquinone skeleton and the acid terminus of the amino acid (or peptide) via an amide or ester bond.

**STRUCTURAL TEMPLATE OF
THE EARLY NU:UB SERIES**

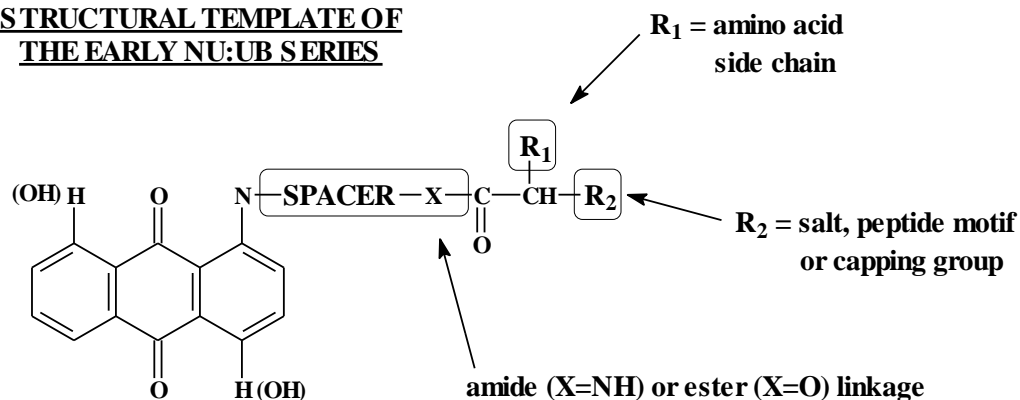


Figure 1.25: Structure of the NU:UB series of anthraquinone-amino acid conjugates

In contrast to the anthracenediones mitoxantrone and ametantrone, the vast majority of the NU:UB library was restricted to anthraquinones that are substituted by a single side-arm substituent, 'the spacer'. Importantly, it was observed that the nature of the spacer group itself was an important determinant of topoisomerase inhibitory properties; conformationally flexible spacers have a large degree of rotational freedom and are able

to adopt many conformations, facilitating their ability to bind to DNA and interact with topoisomerases. Leading members from the NU:UB series were found to inhibit DNA topoisomerases, have shown broad-spectrum activity *in vitro* at low micromolar concentrations in panels of human and animal tumour cell lines, including those of the NCI 60 cell line anticancer drug screen, and are active *in vivo* in experimental colon cancer (Mincher *et al.*, 1999).

Turnbull, (2003) designed and synthesized novel DNA topoisomerase inhibitors NU:UB 73 and NU:UB 76, which are both structurally related to AQ-Butyl-TPP (SH1) synthesized in this research project. Both NU:UB 73 and 76 contain the same aminobutanol spacer as in SH1 **Figure 1.26**. Additionally, the studies showed that the AQ-aminobutanol is inactive and once it was attached with L-alanine (NU:UB 73) and D-alanine (NU:UB 76) it became active *in vivo*. *In vivo* Chemosensitivity against MAC15A colon adenocarcinoma of NU:UB 73 and 76 produced the greatest reduction of tumour volume of any of the conjugates tested at toxic doses and a greater growth delay compared with mitoxantrone which produces growth delay but does not shrink tumours **Figure 1.27** (Turnbull, 2003; Mincher, 1999). Therefore, Taking the advantage of this study AQ-aminobutanol (NU:UB 238) which is inactive was conjugated with triphenylphosphonium bromide (TPP), which in turn make the compound active *in vitro*.

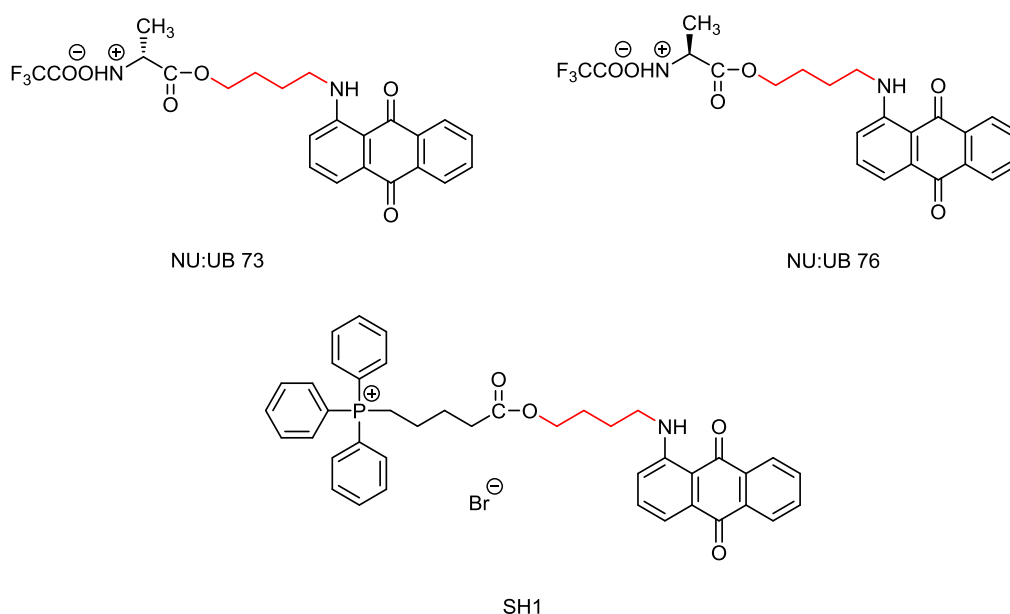


Figure 1.26: Chemical structure of NU:UB 73, 76 and SH1. Red is butyl spacer.

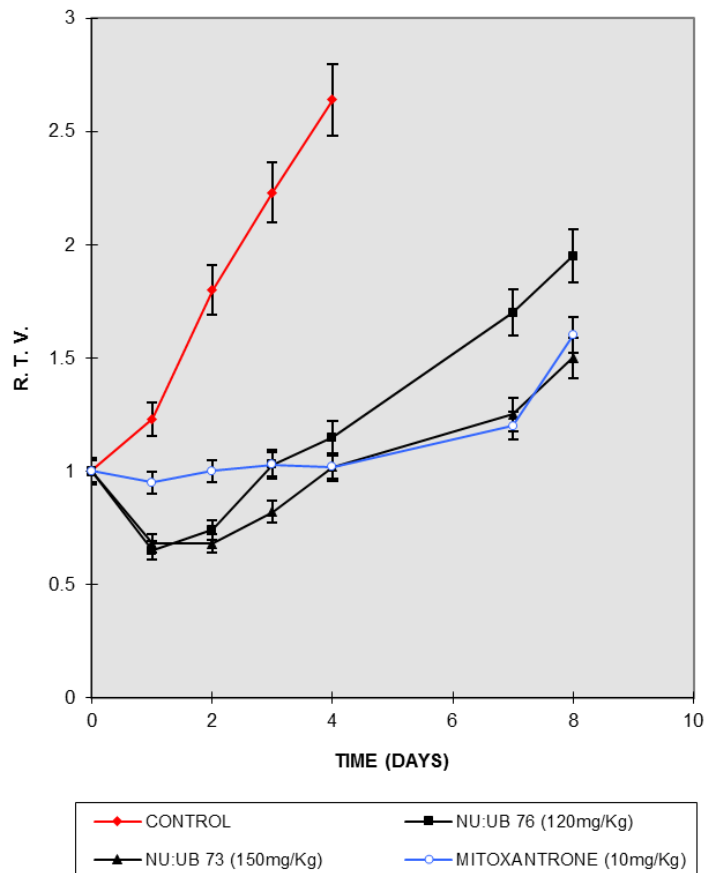


Figure 1.27: *In Vivo* Chemosensitivity against MAC15A colon adenocarcinoma: Comparison of NU:UB 73 (194), NU:UB 76 (196) and Mitoxantrone (7)

Furthermore, confocal microscopy studies on the subcellular localisation of selected lipophilic spacer-linked anthraquinone conjugates from the NU:UB series showed that they were rapidly taken up into cells (Pettersson, 2004). It was also suggested that a positive charge along with a degree of lipophilicity influenced whether or not the anthraquinones were recognised by P-gp and were able to overcome MDR, in line with observations by Lampidis *et al.*, (1997), that, with decreased affinity for binding DNA, related lipophilic anthracyclines shift in their primary localisation from nuclear to mitochondrial. Thus, as lipophilicity increased and nuclear DNA binding properties of the NU:UB compounds decreased, the analogues seemed to distribute in mitochondria (Pettersson, 2004), suggesting that mitochondria may pose an anthracycline target for the NU:UB compounds, notably, this was not the case for doxorubicin which showed no mitochondrial localisation.

Based on these findings, in this programme of research, both aminoanthraquinone derivatives from the NU:UB series and novel aminoanthraquinones were used as a point of attachment for mitochondrial targeting vectors.

Additionally, the ability of the chosen vector, TPP to enter mitochondrial membranes depends on hydrophobicity or lipophilicity properties, the functional group of TPP and linker unit (alkyl chain) length (Ross *et al.*, 2008; Reily *et al.*, 2013). However, the hydrophobicity properties play an important role for TPP to enter mitochondria and in the accumulation of charged TPP inside the mitochondria, which is related to the octanol/water partition coefficient of a given compound.

1.3.2 **Synthetic strategy**

In this research programme, several different model TPP conjugates have been synthesised containing different side-arms including the same side arm as in mitoxantrone **Figure 1.29**. These molecules have been synthesized by linking the aminoanthraquinone with a spacer. Molecules have a different spacer with different length in order to study the effect of these spacers on the cytotoxicity, DNA binding and localization of novel compounds in mitochondria. It has been reported that the presence of amino groups in the spacer of mitoxantrone and the presence of hydroxyl group in the anthraquinone chromophore have a crucial role in binding with DNA and also their role in stability of drug-DNA complexes (Bailly *et al.*, 1996). Therefore, different series of novel compounds were designed and synthesized in order to investigate the role of structural changes on the toxicity, DNA binding and localization of the compounds inside the mitochondria or inside the lysosomes.

The aminoanthraquinone-spacers were further ester linked with the mitochondria carriers using 1,3-dicyclohexylcarbodiimide (DCC) as the coupling (dehydrating agent) and 4-dimethylaminopyridine (DMAP) as acylation catalyst. The choice of these coupling agents were based on previous studies that demonstrates their role in the formation of ester bonds and the high percentage yield results from using it. Zhu *et al.*, (2008) studied the

effect of using DCC on the formation of ester bonds. They found that in the presence of DCC and with carboxylic acids as acylation agents, the esterification reaction after 10 hours proceeded smoothly with high to excellent yield. However, they demonstrated that without DMAP the esterification did not occur even after long period of time (Zhu *et al.*, 2008). Neises and Steglich, (1978), illustrated that the using of 3-10 mol% of DMAP with DCC would accelerate the esterification of carboxylic acid with alcohol giving a good yield at room temperature (Neises and Steglich, 1978). Furthermore, Han *et al.*, (2014), used DCC and N-hydroxysuccinimide (NHS) to successfully conjugate TPP with doxorubicin, where the amide bond was formed between the TPP and doxorubicin. Therefore, herein, DCC and DMAP were used to form the ester bond between the hydroxyl group of the spacer and the carboxylic acid group of the TPP.

In addition, rhodamine B was used as a mitochondrial targeting vector due to the presence of cationic charge and the lipophilic properties of rhodamine B which make it a selective vector to accumulate inside the mitochondria (Muli *et al.*, 2014). However, the locked form (nonfluorescent) and unlocked form (fluorescent) of rhodamine was the main consideration to choose a linker that can keep the Rhodamine in the open ring form and avoid cyclization. Therefore, it was important to prepare and link a photolabile groups (cage compounds) that can keep the rhodamine in its open-ring form to keep its fluorescence for further studies (Lavis and Raines, 2008). It has been reported that the formation of a tertiary amide with Rhodamine and/or functionalized rhodamine B with piperazine could inhibit the spirolactam formation of Rhodamines (Nguyen and Francis, 2003). Nguyen and Francis, (2003), reacted the lactone form of rhodamine B with piperazine which resulted in the formation of tertiary amide and kept the Rhodamine in its unlocked form (fluorescent) (Nguyen and Francis, 2003) **Figure 1.28**. Xie *et al.*, (2013) synthesized a Rhodamine mitochondrial targeting prodrug in which the rhodamine B and 4FDT (anti-hepatoma drug) were linked via a biodegradable linker through a β -alanine in which the rhodamine B and β -alanine were linked with a biodegradable amide bond to keep the open-ring form of rhodamine and a β -alanine was linked with 4FDT via biodegradable ester bond. They found that the prodrug was active and completely localized in the mitochondria (Xie *et al.*, 2013). Therefore, throughout this project,

piperazine was used to inhibit the spirolactam of the rhodamine B and keep its fluorescence.

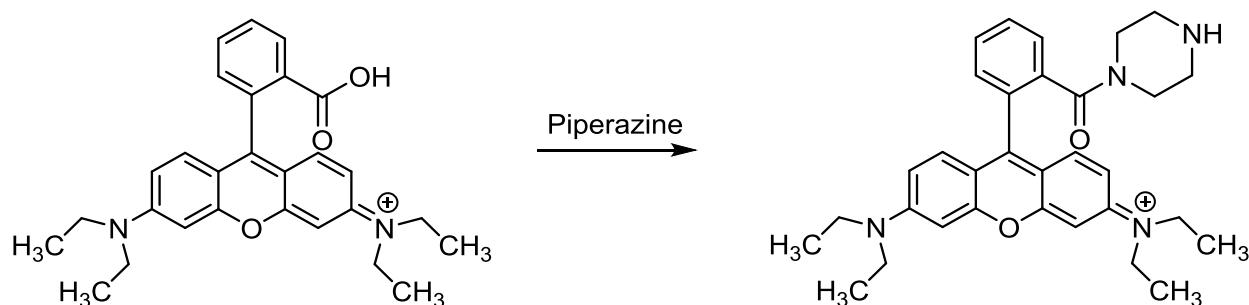


Figure 1.28: synthesis of rhodamine B tertiary amide by reacting rhodamine B with piperazine

Therefore, the aminoanthraquinone-spacers (structurally related to mitoxantrone) were synthesized and firstly were ester linked with the carriers Rho- β -ala-OH, Rho-piperazine-succinate and (4-carboxybutyl) triphenylphosphonium bromide (TPP). Second, NU:UB 65, a 2 armed mitoxantrone derivative was attached with TPP. Third, attempts were made to ester link mitoxantrone with TPP and Rho-piperazine-succinate vectors. Finally, ametantrone was synthesised and ester-linked with TPP **Figure 1.29**.

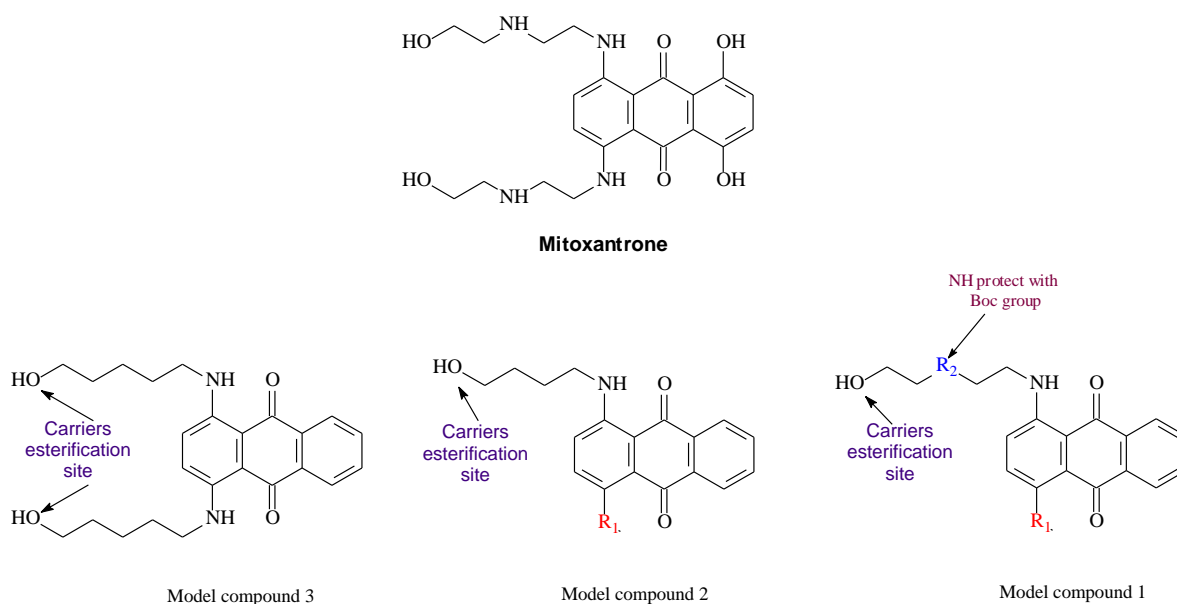


Figure 1.29: Structures of model compounds and the attachment showing the site of the subsequent Boc-protection and site(s) for attachment of carriers upon esterification. Where **R1= OH or H** and **R2= NH or O or CH₂**.

Due to the increased negative membrane potential of mitochondria in cancer cells (Constance and Lim, 2012), it was hypothesized that the attachment of the TPP group to mitoxantrone derivatives would increase the lipophilic properties of these compounds in order to improve the ability to pass through cell membranes. Also, it is hypothesized that the cationic, lipophilic TPP and rhodamine B carriers will allow the active molecule to accumulate in the mitochondria. Cleavage of the biodegradable ester link by esterases should release the cytotoxic drug which could potentially bind to DNA and subsequently inhibit the intrinsic DNA-topoisomerase or bind to mtDNA of mitochondria.

1.3.3 Synthesis of the mitoxantrone derivatives-TPP conjugates

1.3.3.1 Synthesis of HO-EAE-AQ(4-OH) (OM1)

The synthesis of the library of aminoanthraquinones, which were intended for use as active drugs targeted to mitochondria, was started by the amination of leucoquinizarin with *N*-(2-hydroxyethyl)ethylenediamine in dichloromethane (DCM), to afford anthraquinone-spacer compounds which were further ester-linked with mitochondrial vectors.

According to Kikuchi *et al.*, (1982), leucoquinizarin reacts with primary amines to give mono-amino and diaminoanthraquinone derivatives for which the percentage yields are condition dependent. The amination of leucoquinizarin is believed to proceed by an addition-elimination mechanism **Figure 1.30**, which is the addition of amine to a carbonyl group of a keto tautomer (a) leading to ionic intermediate (b) which is further transformed, after dehydration to (c) (Kikuchi *et al.*, 1982). However, in another study, Morris *et al.*, (1986) synthesized 5-hydroxyquinizarin and aminoanthraquinones from leuco-5-hydroxyquinizarin. They found that if the leuco-intermediates were stirred with trimethylamine in dichloromethane and aerial oxidation, the aminoanthraquinones were formed. However, if the intermediates were oxidized and then hydrolyzed using HCl or NaOH, they each gave 5-hydroxyquinizarin (Morris *et al.*, 1986).

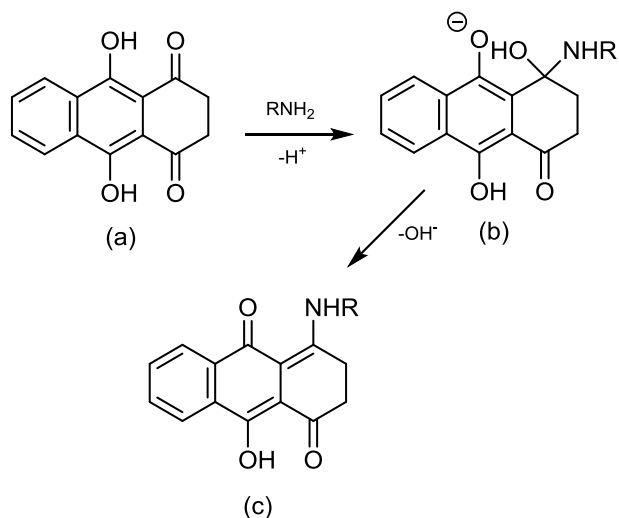


Figure 1.30: Reaction scheme showing the amination of leucoquinizarin

It is reasonable to assume that upon formation (C) would tautomerize to the 1-alkylamino- α -hydroxy tautomer preventing a bis-amination. By applying these methodologies in this project, HO-EAE-AQ(4-OH) (OM1) was synthesized by reaction of leucoquinizarin with N-(2-hydroxyethyl)ethylenediamine, for 1 hour at 50°C, to produce an intermediate (greenish-brown colour), which on oxidation (aeration) and addition of triethylamine produced (OM1) (purple colour) **Figure 1.31**. The change of colour from greenish-brown to purple demonstrated evidence of the oxidation of the intermediate leuco-form of the product to the target aminohydroxyanthraquinone ring system. The progress of the reaction was monitored by thin-layer chromatography on silica plates (TLC test) (4:1 chloroform: methanol) which showed a purple spot of presumed anthraquinone-spacer (OM1). The monoamination of leucoquinizarin with spacer was performed under specific conditions (1 hour at 50°C) to produce 4-hydroxylated aminoanthraquinone (purple compound) and to avoid formation of a diaminoanthraquinone (the 1,4- diaminated blue compound). Solvent extraction and evaporation afforded crude OM1. The introduction of a hydroxyl group into the anthracenedione ring generally improves cytotoxic potency, as in the case of mitoxantrone, due to stronger binding to DNA and slower dissociation kinetics therefore, an increase in the cytotoxicity due to the presence of the hydroxy groups (Smith *et al.*, 1990). It was decided that the secondary amino group in the side

chain of OM1 should be protected to avoid any side reaction of the secondary amine in further reactions (because of the reactive lone electron pair of the amine) which would compete with the free hydroxyl group intended for the site of attachment of the TPP carrier.

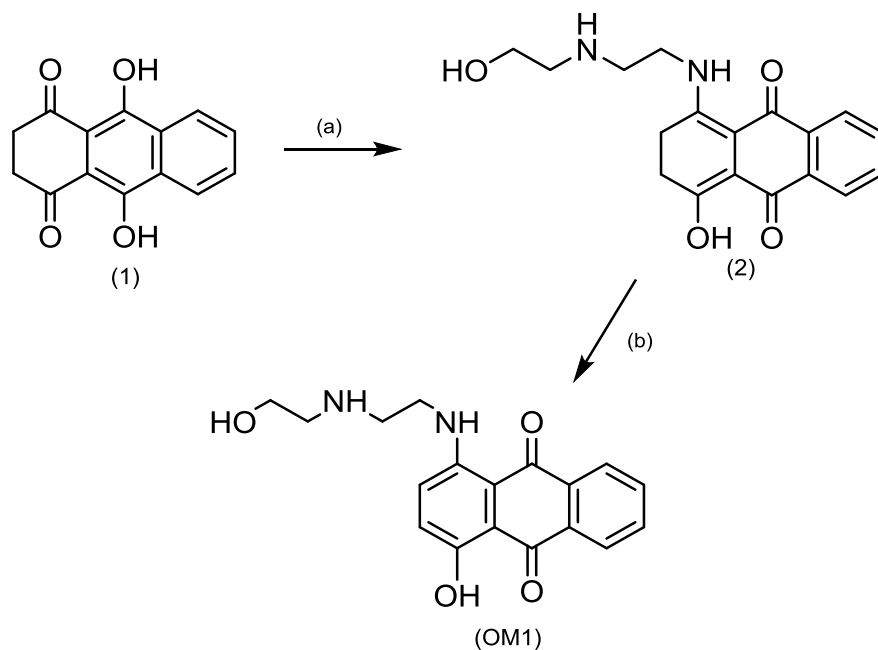


Figure 1.31: Reaction of leucoquinizarin (1) with N-(2-hydroxyethyl)ethylenediamine (2). (a) N-(2-hydroxyethyl)ethylenediamine, dichloromethane, 50°C 1 h. (b) triethylamine, O₂, 4 h

1.3.3.2 Synthesis of HO-EAE-Boc-AQ (4-OH) (OM2)

Introducing a protecting group to the secondary amino group in the side chain is a challenge because the protection group should be:

- I. Easy to introduce
- II. Stable to a wide range of reaction conditions
- III. Safely removed at the end of reaction process or when required
- IV. The removal should be fast and free of side reactions

By considering all these characteristics, it was decided the tert-butyloxycarbonyl (Boc₂O) group was the best protecting group to protect the amino group due to being easy to react

(Boc₂O) with a secondary amine in the side chain and safe to remove by adding trifluoroacetic acid (TFA) to the protected compound (typically for 30 minutes at room temperature (Isidro-Liobet *et al.*, 2009).

HO-EAE-Boc-AQ (4-OH) (OM2) was prepared by the reaction of OM1 with Boc₂O in cold methanol **Figure 1.32**. The mixture was kept over ice and the reaction continued for an hour. Purification of the crude product, firstly by solvent extraction using chloroform/water (to destroy the unreacted Boc₂O with water), then column chromatography, using chloroform at the beginning to get rid of all unreacted leucoquinizarin (orange). The polarity of the solvent was increased using 4:1 chloroform: ethyl acetate + 2-5% methanol to give an analytically pure sample of the title compound (OM2) **Figure 1.32**. The structure of OM2 was confirmed by its high resolution electrospray (+) mass spectrum which showed a clear signal at m/z 427.1864 [M + H]⁺ which corresponded to the expected molecular mass of the 426.1791. Furthermore, there was a good correlation between the observed data and the theoretical isotope model for C₂₃H₂₆N₂O₆. This showed that the Boc₂O protecting group was successfully attached in OM2.

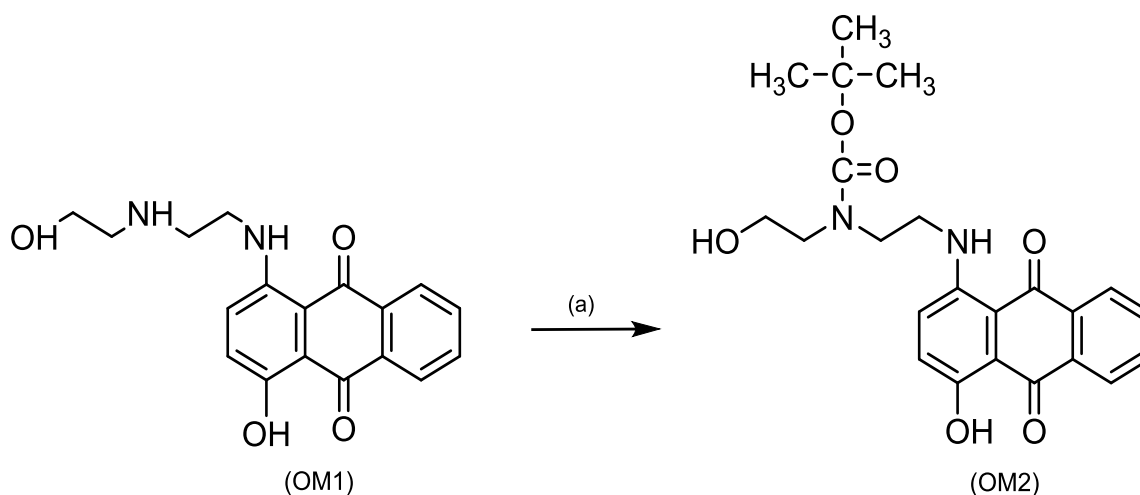


Figure 1.32: Reaction of OM1 with Boc₂O. (a) Boc₂O, methanol, 1 h

1.3.3.3 Synthesis of TPP-EAE-Boc-AQ-(4-OH) (OM22-Boc)

The ester bond to link the model compounds or active drug with mitochondrial vectors because the ester bond is the most common linkage in prodrug design, being easy to synthesize from compounds having a functional group such hydroxy and carboxyl acid group that are widely available in many drugs. As esterases are widely distributed in the body, after administration the ester bond can be hydrolyzed by esterases at the targeted site (Mahato *et al.*, 2011). Clearly, the ester bond requires a suitable half-life *in vivo* and should be stable enough to reach its target.

The TPP-conjugate TPP-EAE-Boc-AQ-(4-OH) (OM22-Boc) was synthesised by reaction of HO-EAE-Boc-AQ (4-OH) (OM2) (pre-dissolved in dichloromethane) with 4-(carboxybutyl-triphenylphosphonium bromide (TPP) (1.1 eq). The coupling agent, DCC (2.4 eq) and catalyst DMAP, were dissolved in dichloromethane with TPP and added to OM22-Boc and allowed to react for 1 hour. After 1 hour, the TLC showed that the starting compound OM2 was still in abundance, therefore a further half amount of TPP (0.55 eq) and coupling agents (DCC 1.2 eq) were added and allowed to react for another 1 hour and checked for purity by TLC, which demonstrated that only one compound was present in the mixture and all OM2 was reacted. After that, some white crystals of N,N'-dicyclohexylurea (DCU) were filtered off from the reaction solution. The rest of the reaction solution was extracted with water and chloroform. Chromatographic purification on silica gel using firstly dichloromethane as eluent to get rid of non-polar impurities and unreacted of TPP and DCC, then 9:1 dichloromethane: ethyl acetate with an increasing gradient of methanol (1-5%) were used to give the title compound (OM22 Boc) **Figure 1.33**. The structure of (OM22-Boc) was confirmed by its high resolution electrospray (+) mass spectrum which showed a clear signal at m/z 771.3177 for $[C_{46}H_{48}N_2O_7P]^+$ which corresponded to the expected molecular mass of the cation. Furthermore, there was a good correlation between the observed data and the theoretical isotope model for $C_{46}H_{48}N_2O_7P$ cation. This showed that TPP was successfully attached to OM2.

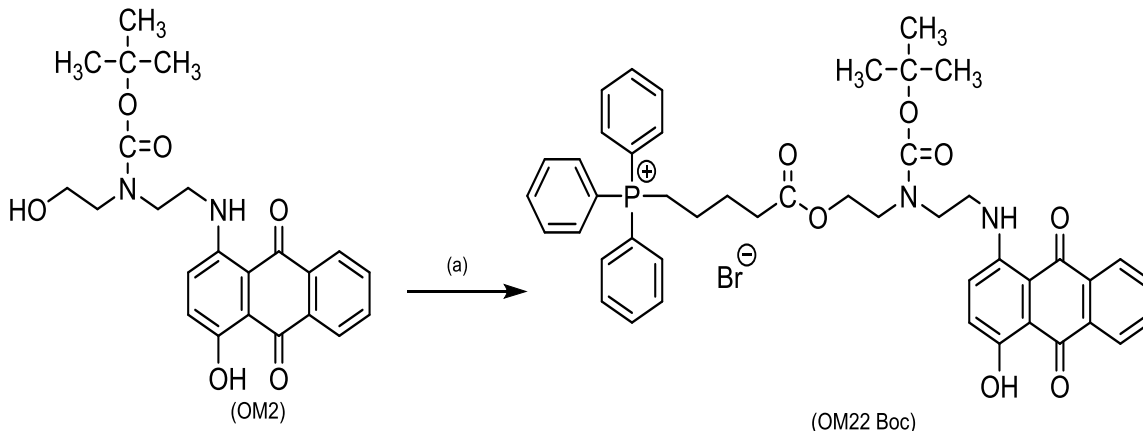


Figure 1.33: Reaction of OM2 with TPP. (a) TPP, DCC, DMAP, dichloromethane, 1 h

1.3.3.4 Synthesis of TPP-EAE-AQ(4-OH) (OM22 TFA)

Deprotection of the N-protected compound (OM22-Boc) was carried out by adding trifluoroacetic acid (TFA) for 30 minutes to OM22-Boc. A precipitate of the consequent salt (OM22 TFA) was obtained from an ether solution **Figure 1.34**. The structure of OM22 TFA was confirmed by high resolution mass spectrometry which showed a clear signal at m/z 671.2658 which corresponded to the expected molecular mass of the cation $[M - \text{TFA}]^+$. Furthermore, there was a good correlation between the observed data and the theoretical isotope model for $\text{C}_{41}\text{H}_{40}\text{N}_2\text{O}_5\text{P}$ $[M - \text{TFA}]^+$ **Figure 1.35**. This showed that the Boc group was successfully removed from OM22-BOC to form OM22 TFA.

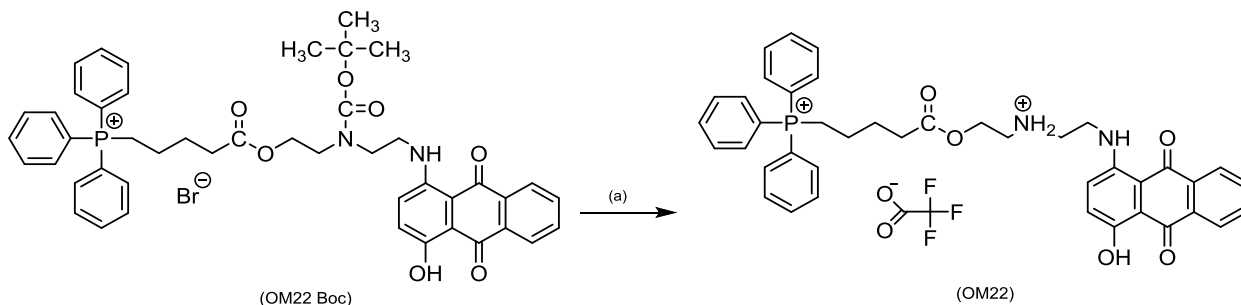


Figure 1.34: Reaction of OM22 Boc with (TFA). (a) TFA, room temperature, 30 min

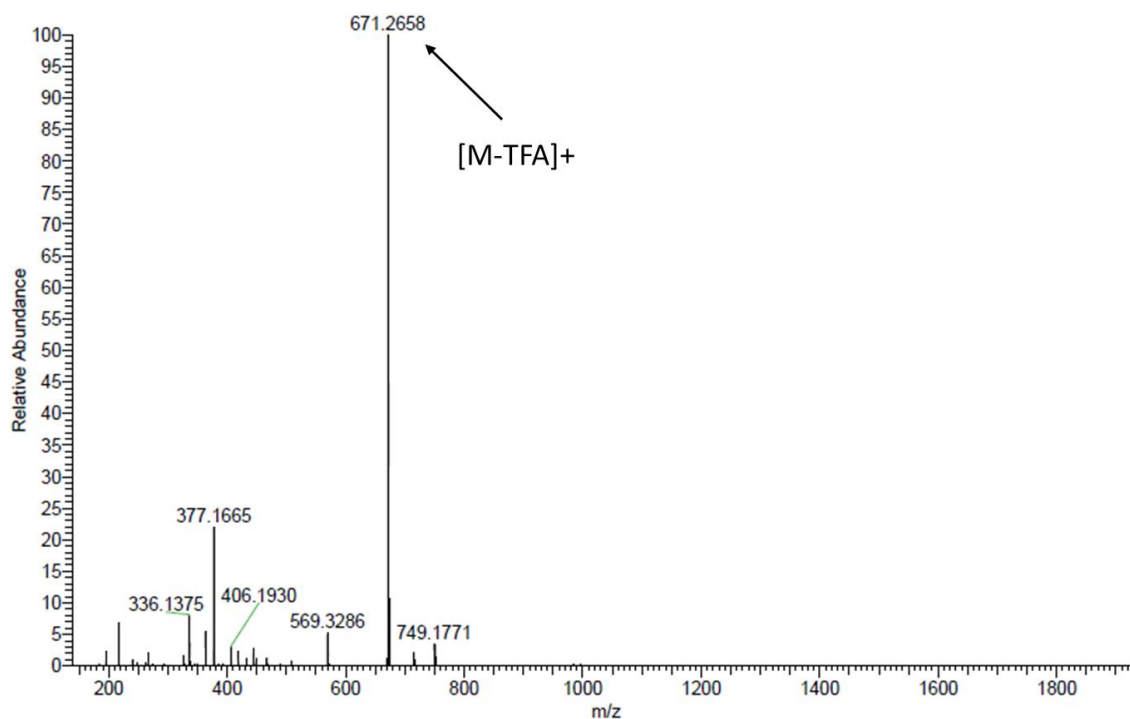


Figure 1.35: The ESI (+) mass spectrum of OM22 TFA

In addition, the structure of TPP-EAE-AQ(4-OH) OM22 TFA was characterized and confirmed by its ^1H NMR spectrum (in DMSO), which showed, a triplet signal at 10.20 ppm which was assigned to the amino proton at C-1 of the anthraquinone and a singlet signal at 13.54 ppm was assigned to the hydroxy proton at C-4 of the anthraquinone. The protons of the protonated amine of the anthraquinone spacer were found as a singlet signal at 9.03 ppm. Signals in the ^1H NMR spectrum between 1.51-1.81 ppm were assigned to the four protons of methylene spacer of TPP and another four protons of TPP spacer were found at 2.45 ppm (triplet) and 3.64 ppm (triplet). The methylene groups of anthraquinone spacer were found at 3.19-3.32 ppm, 3.82 ppm and 4.27 ppm (triplet). The fifteen aromatic protons of TPP and two of the anthraquinone were assigned between 7.73 ppm and 7.99 ppm. The signals at 7.39 ppm (doublet) and 7.61 ppm (doublet) were assigned to two anthraquinone protons at H-2 and H-3. The 2 protons for anthraquinone

H-5 and H-8 were assigned between 8.23-8.28 ppm **Figure 1.36** and **Figure 1.37**. These signals confirmed the successful synthesis of OM22 TFA.

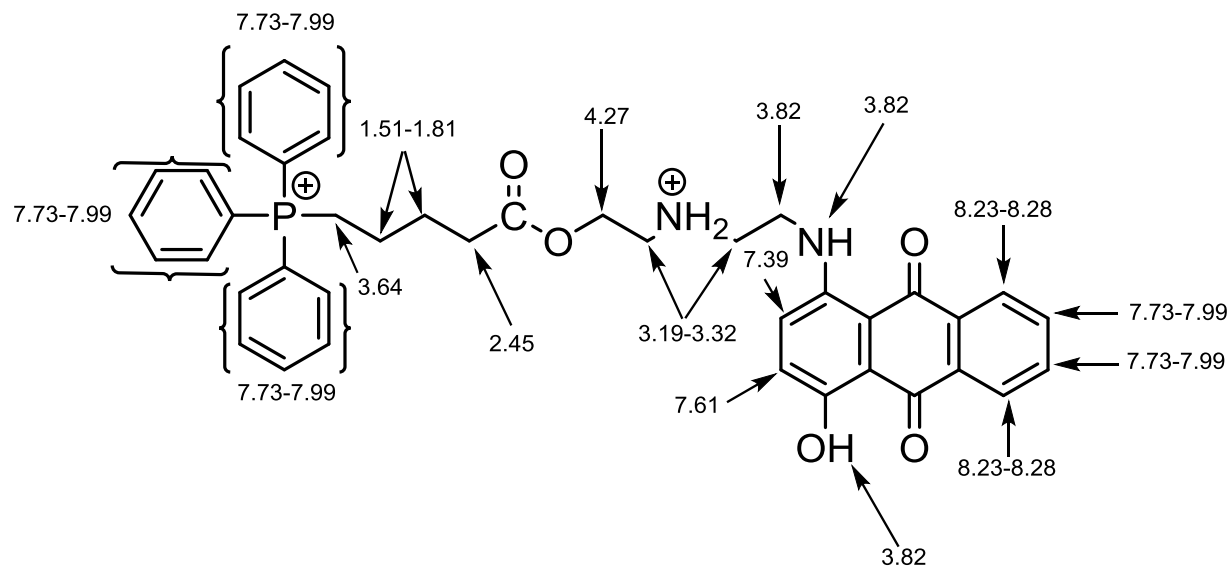


Figure 1.36: ¹H NMR signals (ppm) for OM22 TFA

1H 300.1MHz Job 68850 Napier MSc Student 272 DMSO 25.2 °C
OM 22 TFA



```

NAME: 68850
EXPNO: 1
PROCNO: 1
PROCPS: 2048
SOLVENT: DMSO
PROBHD: 5 mm QNP 1H/1
PULPROG: zgpg30
AQ: 0.7744
RG: 256.00
AQ2: 0.0000
SFOCUS: 200.00
TE: 300.2
DELTA: 6.00000000
DELTA2: 0.10000000
DELTA3: 0.10000000
DELTA4: 0.10000000
DELTA5: 0.10000000
DELTA6: 0.10000000
DELTA7: 0.10000000
DELTA8: 0.10000000
DELTA9: 0.10000000
DELTA10: 0.10000000
DELTA11: 0.10000000
DELTA12: 0.10000000
DELTA13: 0.10000000
DELTA14: 0.10000000
DELTA15: 0.10000000
DELTA16: 0.10000000
DELTA17: 0.10000000
DELTA18: 0.10000000
DELTA19: 0.10000000
DELTA20: 0.10000000
DELTA21: 0.10000000
DELTA22: 0.10000000
DELTA23: 0.10000000
DELTA24: 0.10000000
DELTA25: 0.10000000
DELTA26: 0.10000000
DELTA27: 0.10000000
DELTA28: 0.10000000
DELTA29: 0.10000000
DELTA30: 0.10000000
DELTA31: 0.10000000
DELTA32: 0.10000000
DELTA33: 0.10000000
DELTA34: 0.10000000
DELTA35: 0.10000000
DELTA36: 0.10000000
DELTA37: 0.10000000
DELTA38: 0.10000000
DELTA39: 0.10000000
DELTA40: 0.10000000
DELTA41: 0.10000000
DELTA42: 0.10000000
DELTA43: 0.10000000
DELTA44: 0.10000000
DELTA45: 0.10000000
DELTA46: 0.10000000
DELTA47: 0.10000000
DELTA48: 0.10000000
DELTA49: 0.10000000
DELTA50: 0.10000000
DELTA51: 0.10000000
DELTA52: 0.10000000
DELTA53: 0.10000000
DELTA54: 0.10000000
DELTA55: 0.10000000
DELTA56: 0.10000000
DELTA57: 0.10000000
DELTA58: 0.10000000
DELTA59: 0.10000000
DELTA60: 0.10000000
DELTA61: 0.10000000
DELTA62: 0.10000000
DELTA63: 0.10000000
DELTA64: 0.10000000
DELTA65: 0.10000000
DELTA66: 0.10000000
DELTA67: 0.10000000
DELTA68: 0.10000000
DELTA69: 0.10000000
DELTA70: 0.10000000
DELTA71: 0.10000000
DELTA72: 0.10000000
DELTA73: 0.10000000
DELTA74: 0.10000000
DELTA75: 0.10000000
DELTA76: 0.10000000
DELTA77: 0.10000000
DELTA78: 0.10000000
DELTA79: 0.10000000
DELTA80: 0.10000000
DELTA81: 0.10000000
DELTA82: 0.10000000
DELTA83: 0.10000000
DELTA84: 0.10000000
DELTA85: 0.10000000
DELTA86: 0.10000000
DELTA87: 0.10000000
DELTA88: 0.10000000
DELTA89: 0.10000000
DELTA90: 0.10000000
DELTA91: 0.10000000
DELTA92: 0.10000000
DELTA93: 0.10000000
DELTA94: 0.10000000
DELTA95: 0.10000000
DELTA96: 0.10000000
DELTA97: 0.10000000
DELTA98: 0.10000000
DELTA99: 0.10000000
DELTA100: 0.10000000
  
```

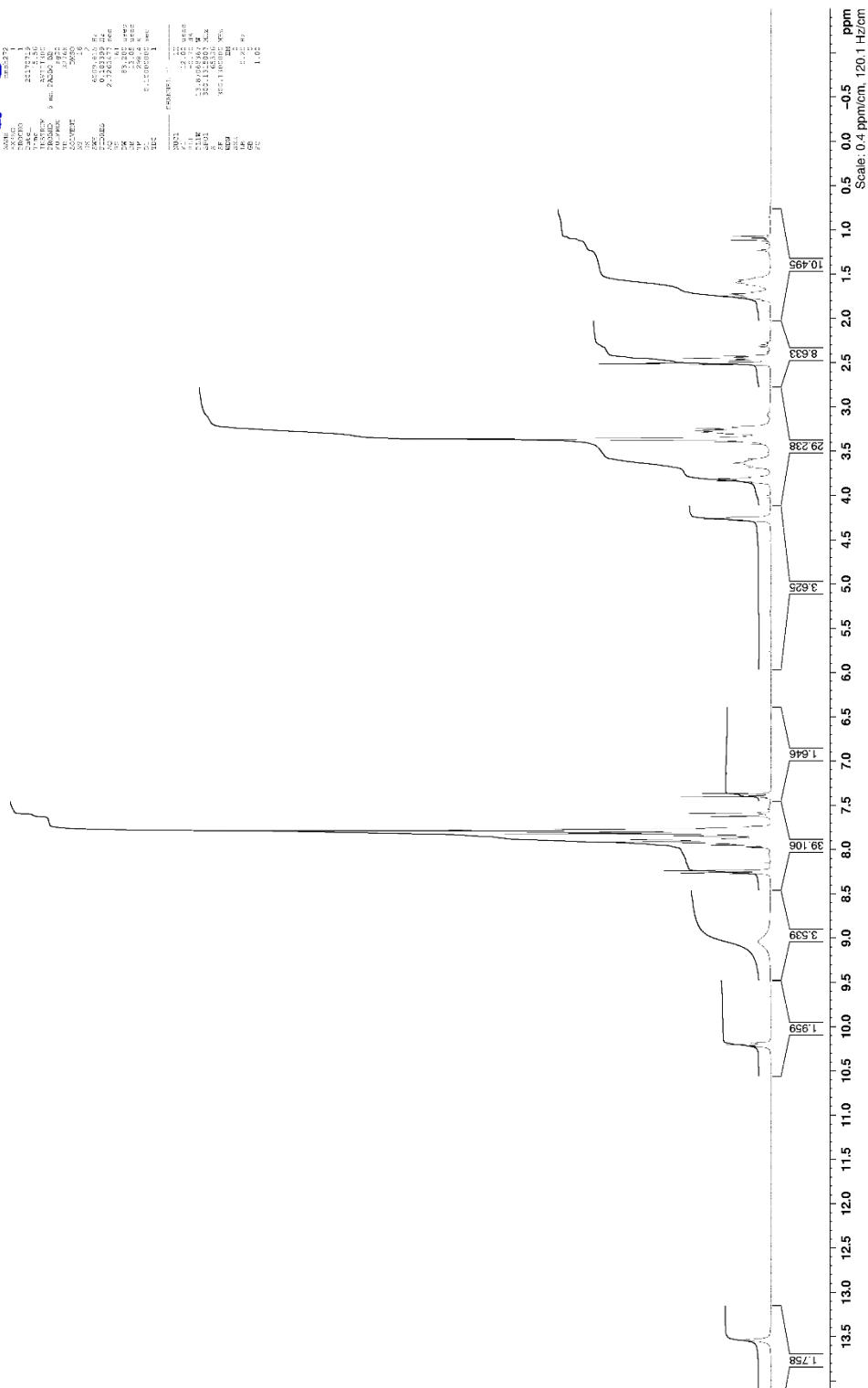


Figure 1.37: ¹H NMR spectrum (DMSO, 300 MHz) of OM22 TFA

The proton-decoupled, ^{13}C NMR spectrum showed signals for all carbon environments. A DEPT experiment differentiated the eight methylene CH_2 carbons, twenty one methine CH carbons (AQ_{TPP} and AQ_{AR}) and twelve quaternary carbons. Signals between 21.10 ppm and 59.41 ppm were assigned to eight methylene carbons. The two anthraquinone carbonyl groups and carbonyl group in the spacer were assigned at 172.30 ppm, 181.34 ppm and 186.96 ppm. Signals at 125.21-128.63 ppm, 133.28 ppm and 134.88 ppm were assigned to 6 methine CH carbons of the anthraquinone. Three aromatic methine carbon signals, corresponding to the ortho, meta and para carbon atoms of the TPP aromatic group were found in their expected positions at 130.14-130.31 ppm (meta), 133.47-133.61 pm (ortho) and 134.88 ppm (para) **Figure 1.38, Figure 1.39 and Figure 1.40**. Detection of all carbon atoms of OM22 TFA was possible confirming the successful synthesis of OM22 TFA.

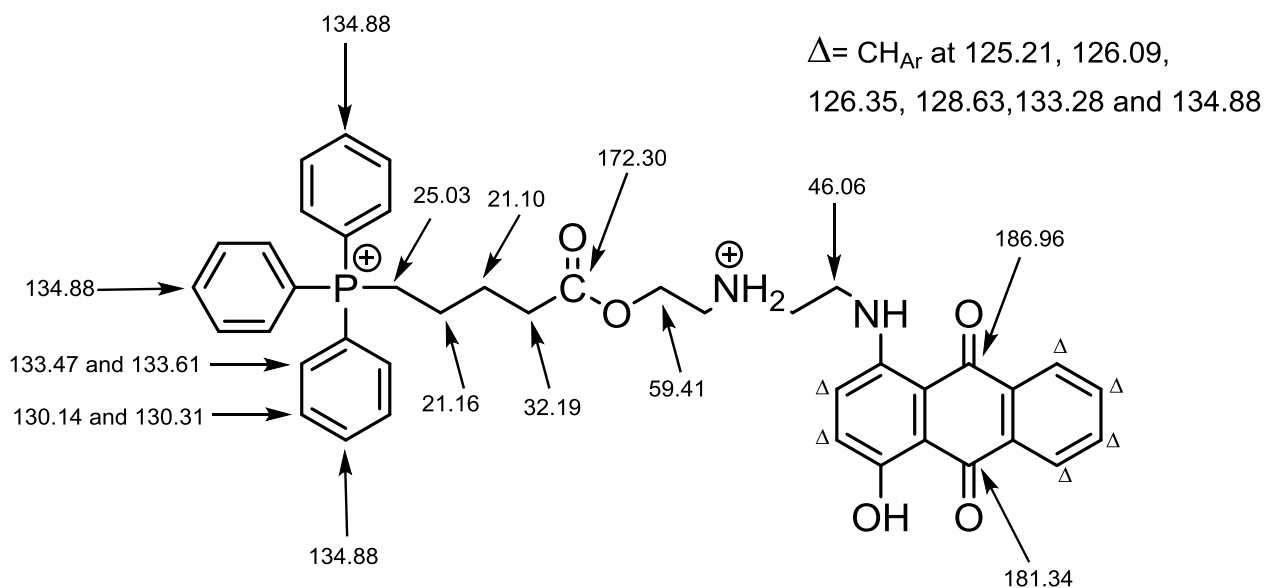


Figure 1.38: ^{13}C NMR signals (ppm) for OM22 TFA

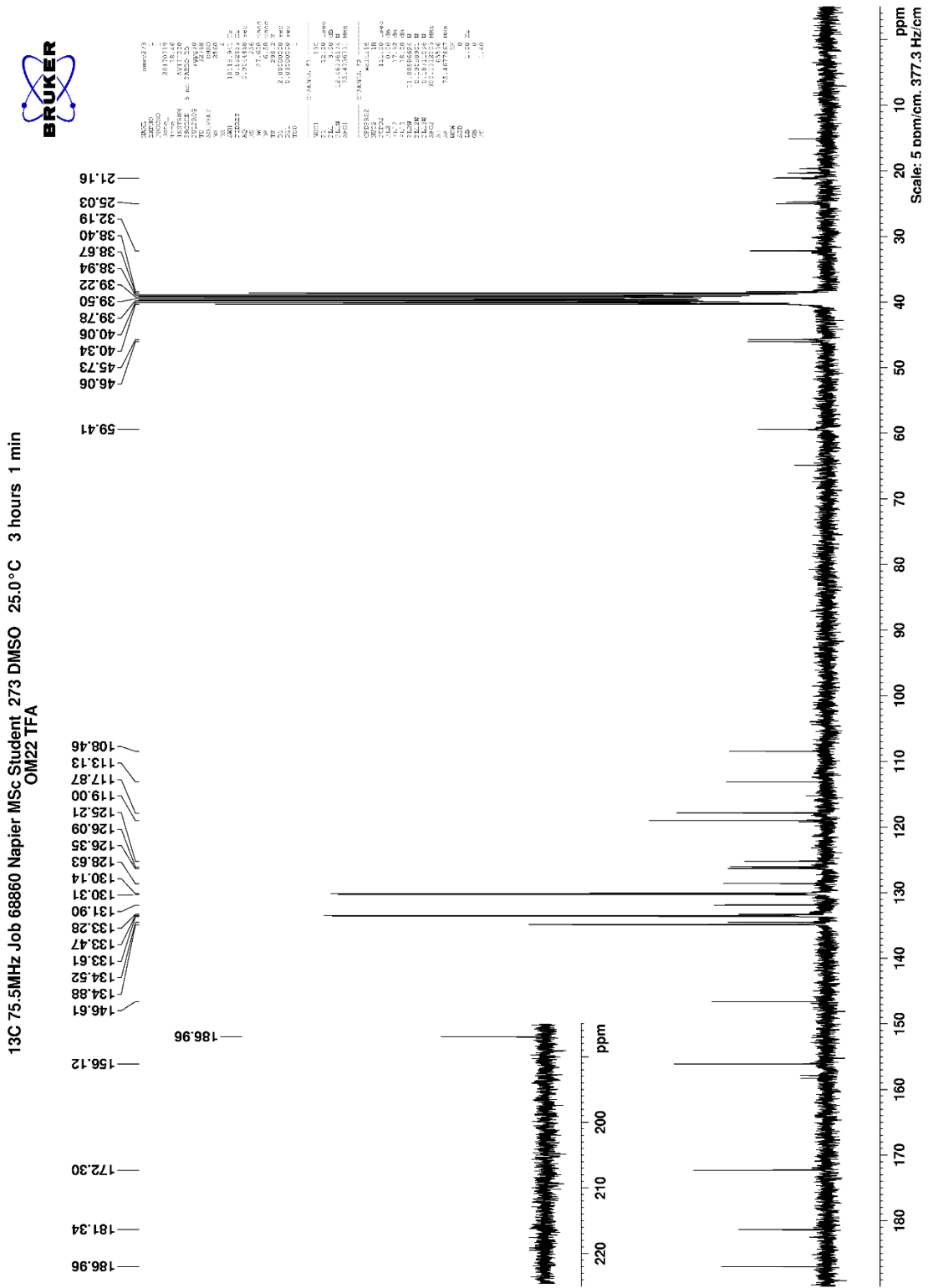


Figure 1.39: ¹³C NMR spectrum (DMSO, 75.5 MHz) of OM22 TFA

13C 75.5MHz Job 68860 Napier MSc Student 273 DMSO DEPT 25.0 °C
OM22 TFA

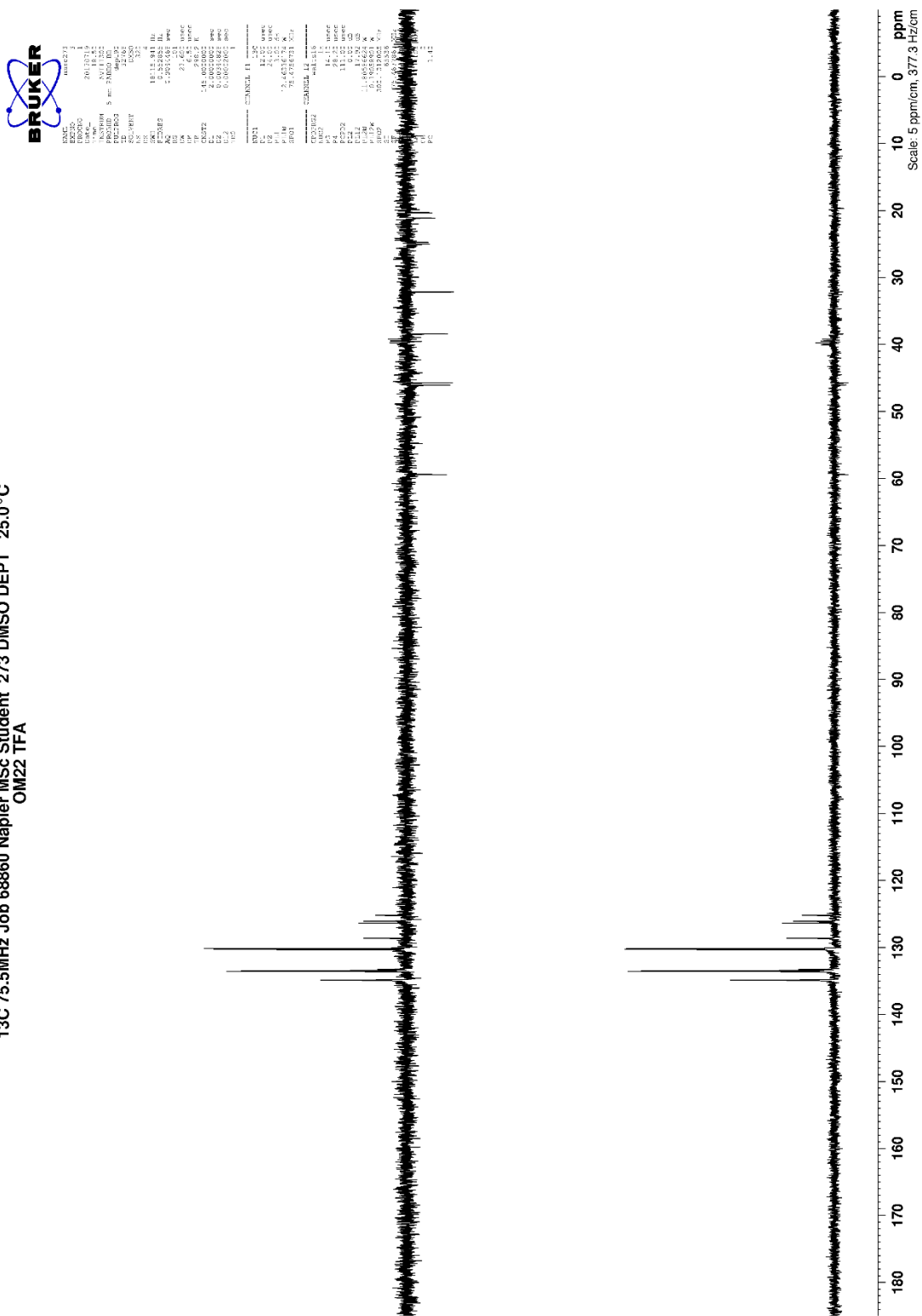


Figure 1.40: ¹³C NMR DEPT90 spectrum (DMSO, 75.5 MHz) of OM22 TFA

1.3.3.5 Synthesis of OH-Butyl-AQ (4-OH) (NU:UB 252)

OH-Butyl-AQ (4-OH) (NU:UB 252) was synthesised which shared similar anthraquinone structure with difference in the spacer length. NU:UB 252 has a butyl-spacer compared with OM22 which has ethylaminoethyl spacer. Also, NU:UB 252 lacks the secondary amino group in the spacer which is known for its role in the binding with DNA and stabilising the drug-DNA complex (Bailly *et al.*, 1996). Therefore, NU:UB 252 was synthesised and linked with TPP in order to evaluate the effect of structural changes on the localisation and toxicity of TPP conjugates.

To synthesise OH-Butyl-AQ (4-OH) (NU:UB 252), leucoquinizarin was reacted with 4-amino-1-butanol in dichloromethane, at reflux for 1 hour at 50°C (water bath). The product was then oxidized overnight by aeration with the addition of triethylamine (Et₃N) **Figure 1.41**. The progress of the reaction was monitored through TLC. Solvent extraction was carried out with chloroform/water. The crude product was purified by column chromatography, using firstly chloroform as eluent to remove nonpolar impurities. The polarity of the solvents was increased using chloroform + 2% ethyl acetate. The eluted fractions containing the pure product were filtered to remove silica and evaporated to dryness. Addition of diethyl ether gave a precipitate of NU:UB 252, which was filtered off and dried.

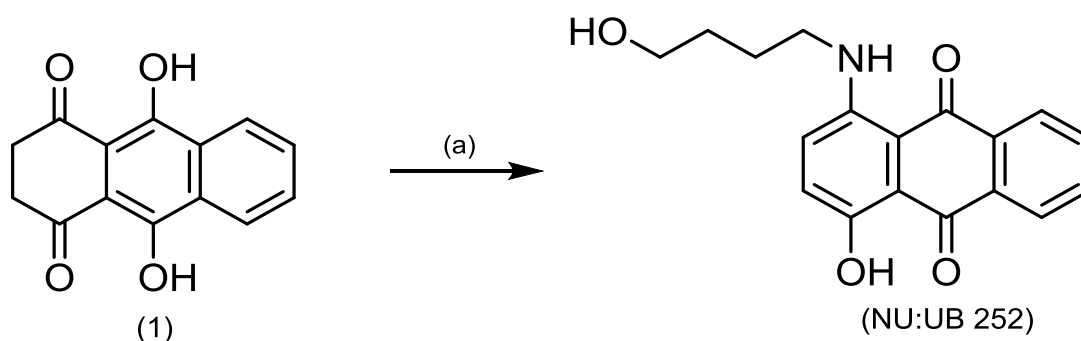


Figure 1.41: Synthesis of NU:UB 252 by reaction of Leucoquinizarin (1) with 4-amino-1-butanol. (a) 4-amino-1-butanol, dichloromethane, 50°C, 1 h, triethylamine, O₂, overnight.

The structure of NU:UB 252 was characterized and confirmed by its ^1H NMR spectrum (in DMSO), which showed, a singlet signal at 10.16 ppm and this was assigned to the amino proton at C-1 of the anthraquinone. Signals in the ^1H NMR spectrum between 1.50-1.73 ppm were assigned to four protons of the methylene spacer of the anthraquinone. The methylene closest to the amino group of the anthraquinone was found at 3.35 ppm, whereas, the methylene close to the hydroxyl group was found at 3.48 ppm (triplet). All aromatic protons of the anthraquinone were assigned; 7.21 ppm (1H, H-2, doublet), 7.35 (1H, H-3, doublet), 7.74-7.90 (2H, H-6 and H-7, multiplet) and 8.13 (2H, H-5 and H-8, multiplet). The signal for the aromatic hydroxyl was assigned at 13.57 ppm (1H, singlet) **Figure 1.42 and Figure 1.43.**

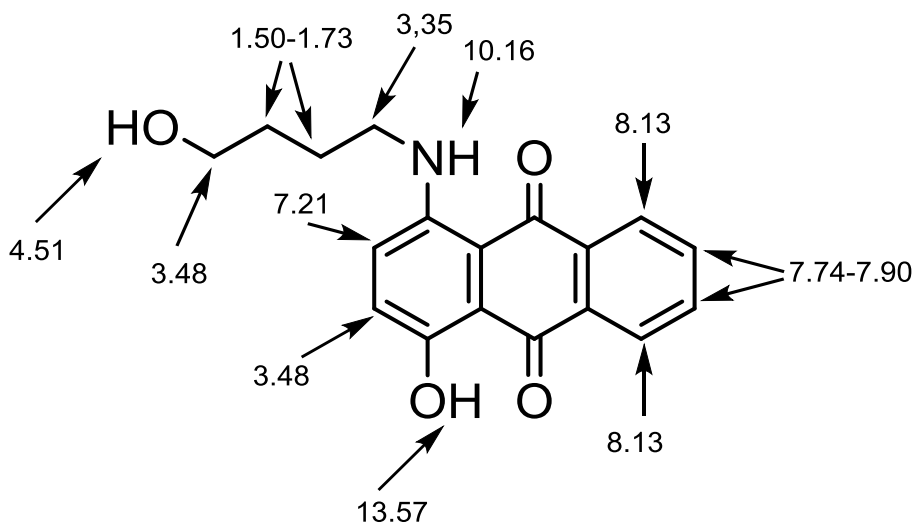


Figure 1.42: ^1H NMR signals (ppm) of NU:UB 252

1H 300.1MHz Job 61009 Napier MSc Student 234 DMSO 25.2 °C
NU:UB252

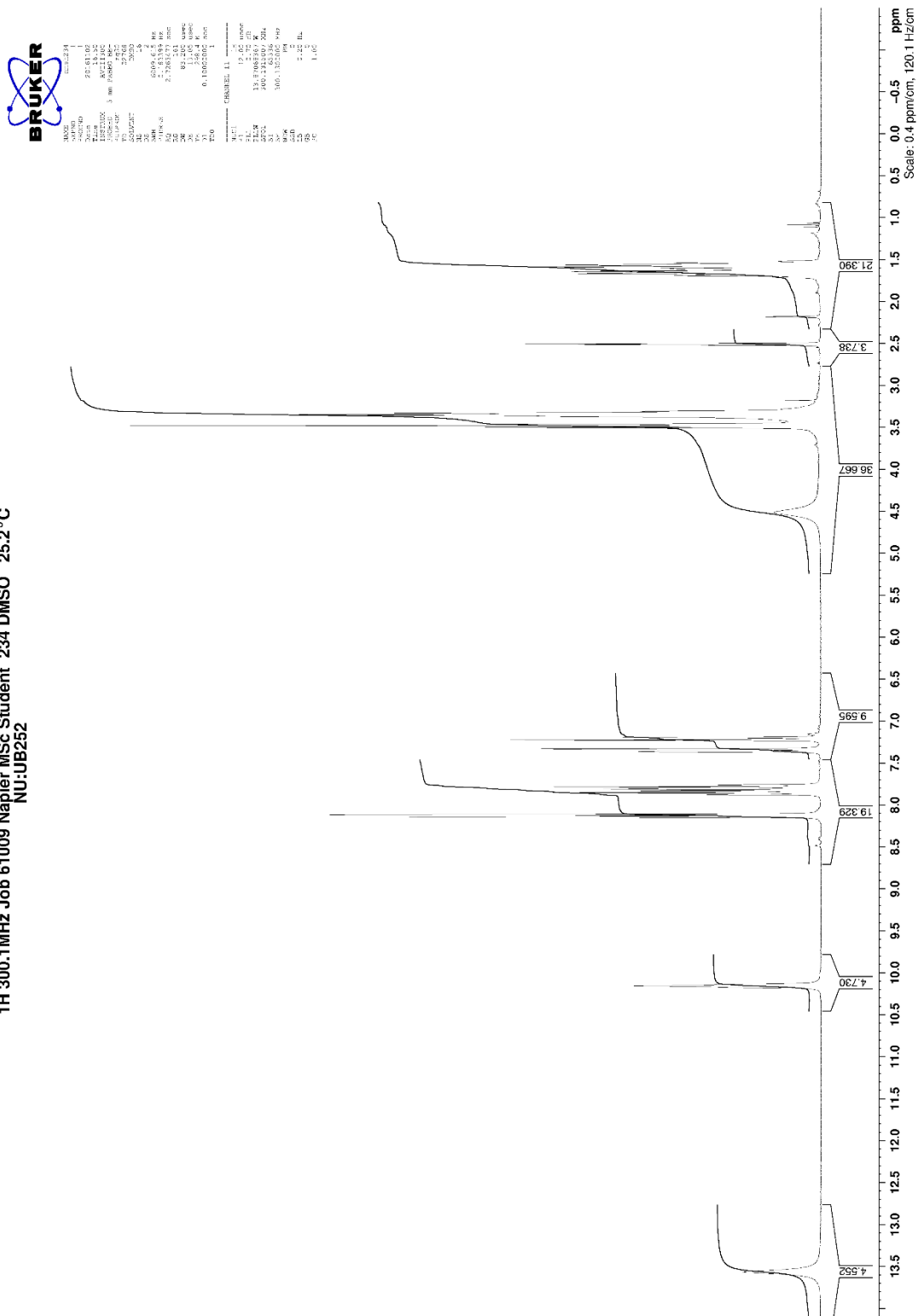


Figure 1.43: ¹H NMR spectrum (DMSO, 300 MHz) of NU:UB 252

The proton-decoupled ^{13}C NMR spectrum showed signals for all carbon environments. A DEPT experiment differentiated the four methylene CH_2 carbons, six methine CH carbons A_{QAR} and eight quaternary carbons. Signals between 25.67 ppm and 60.32 ppm were assigned to four methylene carbons. Signals at 125.22 ppm, 125.78 ppm, 126.15 ppm, 128.60 ppm, 132.67 ppm and 134.44 ppm were assigned to 6 methine CH carbons of the anthraquinone **Figure 1.44**, **Figure 1.45** and **Figure 1.46**.

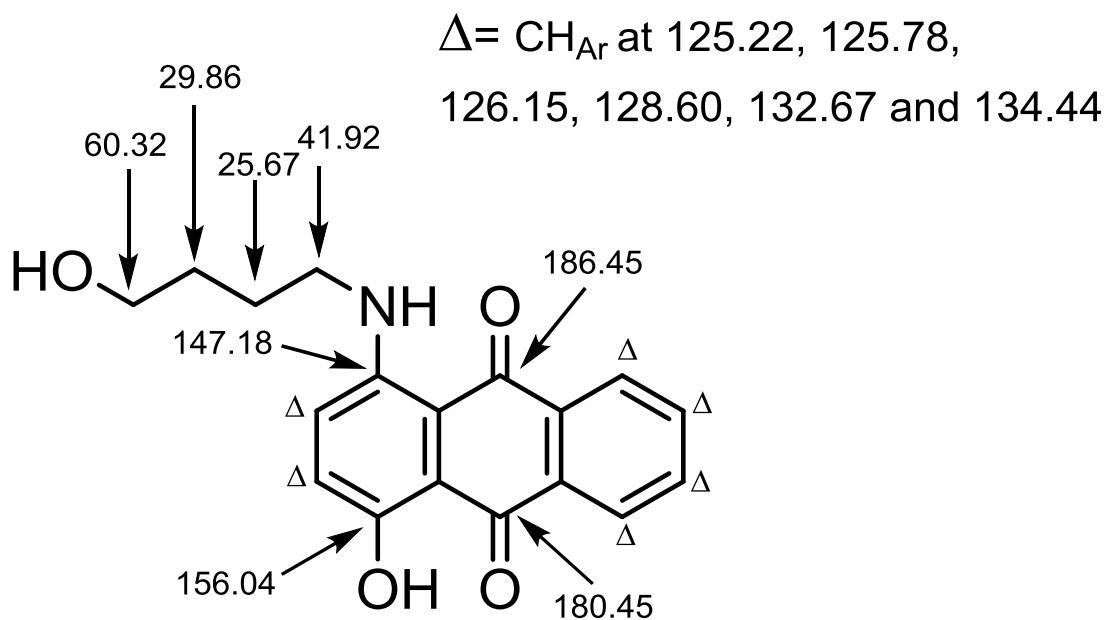


Figure 1.44: ^{13}C NMR signals (ppm) of NU:UB 252

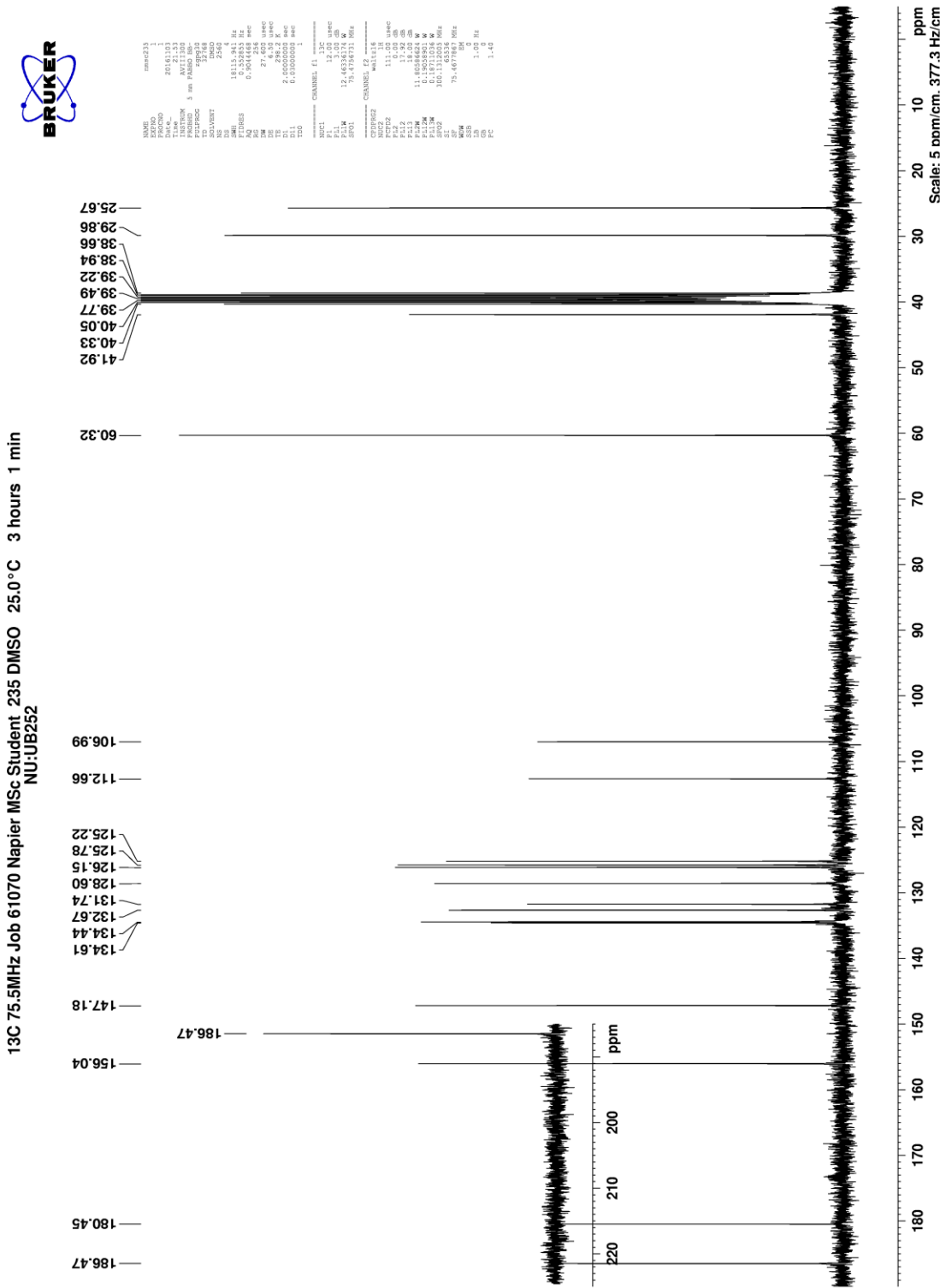


Figure 1.45: ¹³C NMR spectrum (DMSO, 75.5 MHz) of NU:UB 252

13C 75.5MHz Job 61070 Napier.MSc Student 235 DMSO DEPT 25.0 °C
 NU:UB252

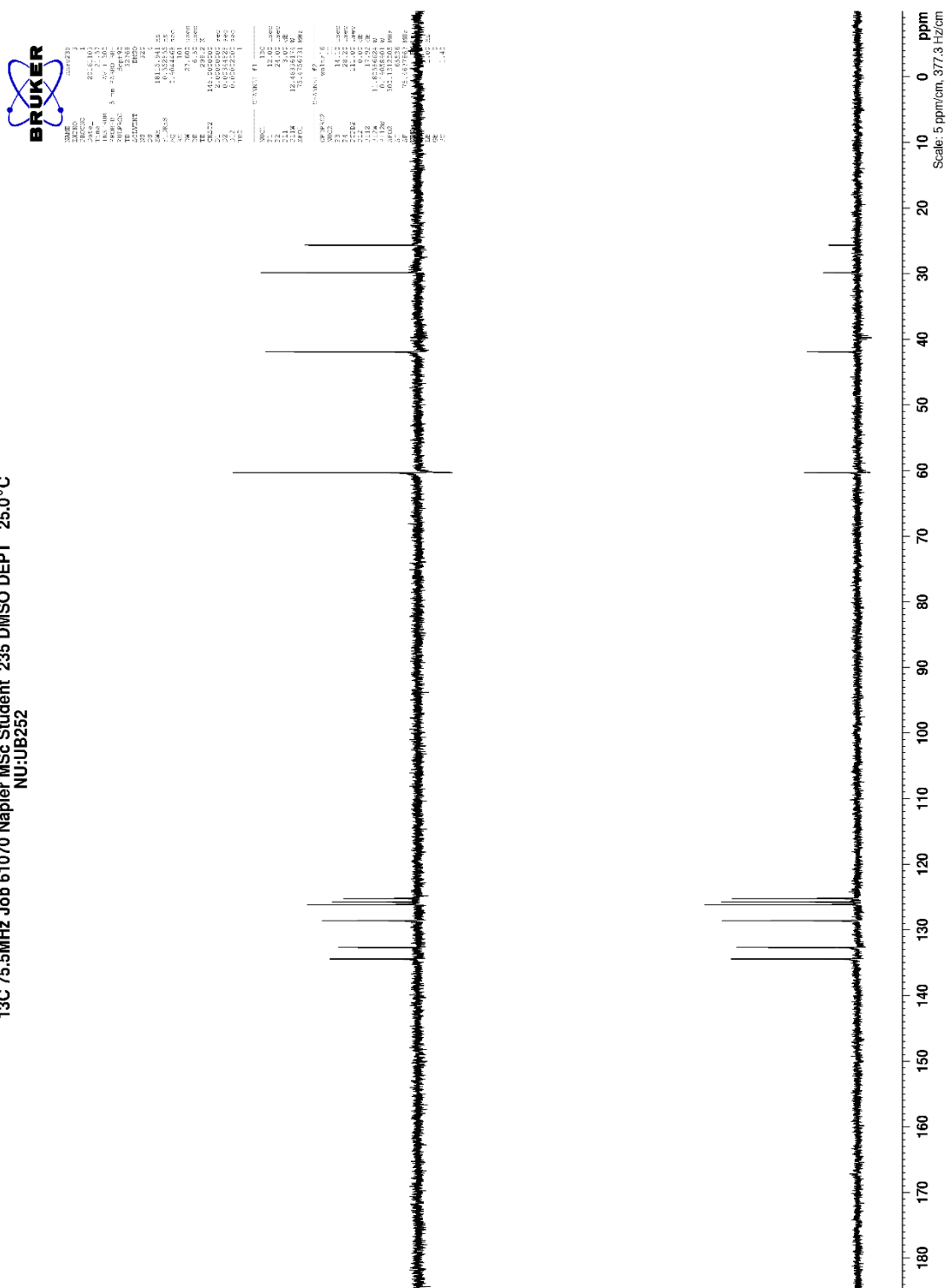


Figure 1.46: ¹³C NMR DEPT90 spectrum (DMSO, 75.5 MHz) of NU:UB 252

1.3.3.6 Synthesis of TPP-Butyl-AQ(4-OH) (OM30)

OH-Butyl-AQ (4-OH) (NU:UB 252) was reacted with TPP (1.5 eq) using the coupling agents DCC (3.6 eq) and DMAP to give TPP-Butyl-AQ(4-OH) (OM30). The reaction mixture was left to stir for 1 hour **Figure 1.47**. The reaction progress was monitored by TLC which showed after 1 hour that there was some of NU:UB 252 not reacted, therefore additional amounts of TPP (0.75 eq) and DCC (1,8 eq) were added. The white crystals of N,N'-dicyclohexylurea (DCU) were filtered off from the reaction solution, followed by solvent extraction with water and chloroform. However, there was an unknown pink compound in the reaction solution, therefore the reaction was left under water overnight to get rid of unknown pink impurity. The product was further purified by column chromatography using firstly chloroform as eluent to get rid of polar impurities and unreacted of TPP and DCC, then 9:1 dichloromethane: ethyl acetate with an increasing gradient of methanol to 3% were used to get the title compound OM30. The pure fractions from the chromatography were filtered off and dried and were precipitated under diethyl ether. The structure of OM30 was confirmed by its high resolution electrospray (+) mass spectrum which showed a clear signal at m/z 656.2546 which corresponded to the expected molecular mass of the 656.2546 Da $[M-Br]^+$ **Figure 1.48**. Furthermore, there was a good correlation between the observed data and the theoretical isotope model for $C_{41}H_{39}NO_5P$ $[M-Br]^+$.

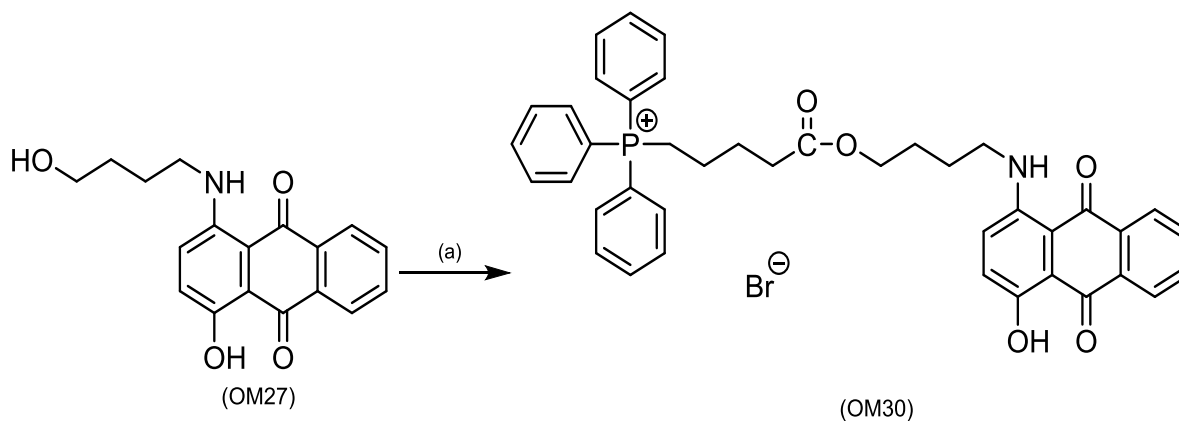


Figure 1.47: Synthesis of OM30 by of reaction of NU:UB 252 with TPP. (a) TPP, DCC, DMAP, dichloromethane, 1 h.

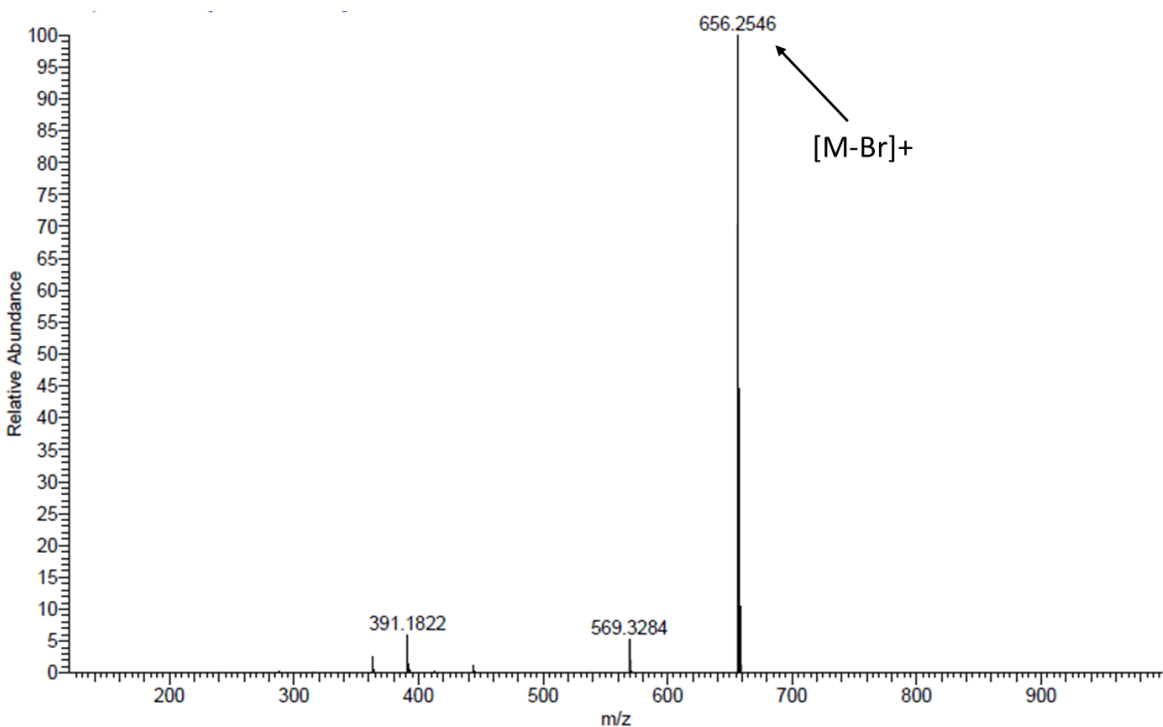


Figure 1.48: The ESI (+) mass spectrum of OM30

The structure of OM30 was characterized and confirmed by its ^1H NMR spectrum (in d_6 -DMSO), which showed, signals between 1.50-1.80 ppm which were assigned to eight protons of the methylene spacer of TPP and anthraquinone. The methylene close to carbonyl group in the spacer was found at 2.41 ppm (triplet) whereas, the methylene close to the amino group of the anthraquinone was found at 4.05 ppm. The methylene group close to the phosphonium group of TPP was found at 3.62 ppm (triplet). In addition, a signal at 4.05 ppm was assigned to the methylene group close to oxygen in the spacer. The fifteen aromatic protons of TPP and two of the anthraquinone were assigned between 7.71 ppm and 7.95 ppm. The signals at 7.33 ppm (doublet) and 7.48 ppm (doublet) were assigned to the anthraquinone protons of H-2 and H-3. The two protons for H-5 and H-8 were assigned between 8.17-8.25 ppm. At 10.25 ppm a signal was assigned to the amino proton at C-1 of the anthraquinone whereas, the hydroxyl proton of anthraquinone give a singlet signal at 13.63 ppm **Figure 1.49 and Figure 1.50.**

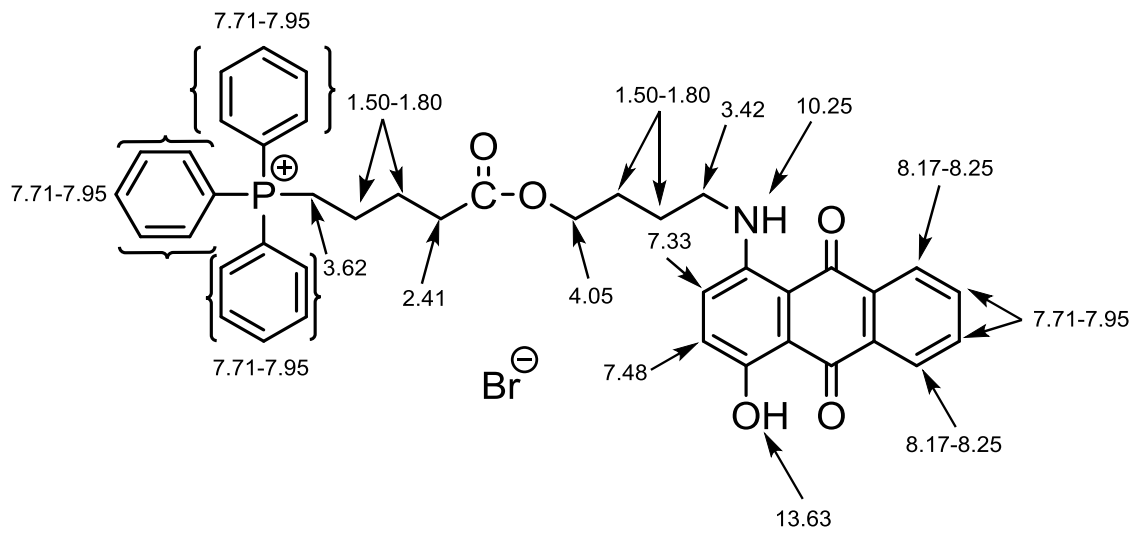


Figure 1.49: ^1H NMR signals (ppm) of OM30

The proton-decoupled ^{13}C NMR spectrum showed signals for all carbon environments. A DEPT experiment differentiated the eight methylene CH_2 carbons, twenty one methine CH carbons (AQ_{TPP} and AQ_{AR}) and twelve quaternary carbons. The eight methylene carbons gave signals between 20.25 ppm and 63.45 ppm. The two anthraquinone carbonyl groups were assigned at 180.74 ppm and 186.66 ppm. Signals at 125.46 ppm, 125.96 ppm, 126.25 ppm, 128.83 ppm, 132.94 ppm and 134.67 ppm were assigned to the six methine CH carbons of the anthraquinone. Three aromatic methine carbon signals, corresponding to the ortho, meta and para carbon atoms of the TPP aromatic group were found in their expected positions at 130.13-130.29 ppm (meta), 133.46-133.59 ppm (ortho) and 134.89 ppm (para) **Figure 1.51, Figure 1.52 and Figure 1.53.**

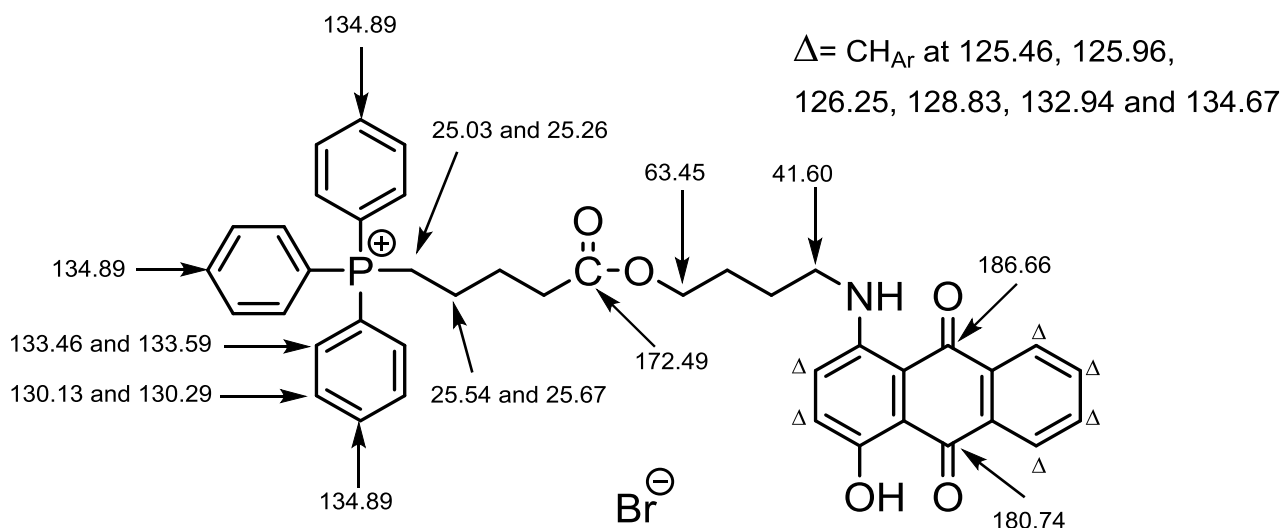


Figure 1.51: ^{13}C NMR signals (ppm) of OM30

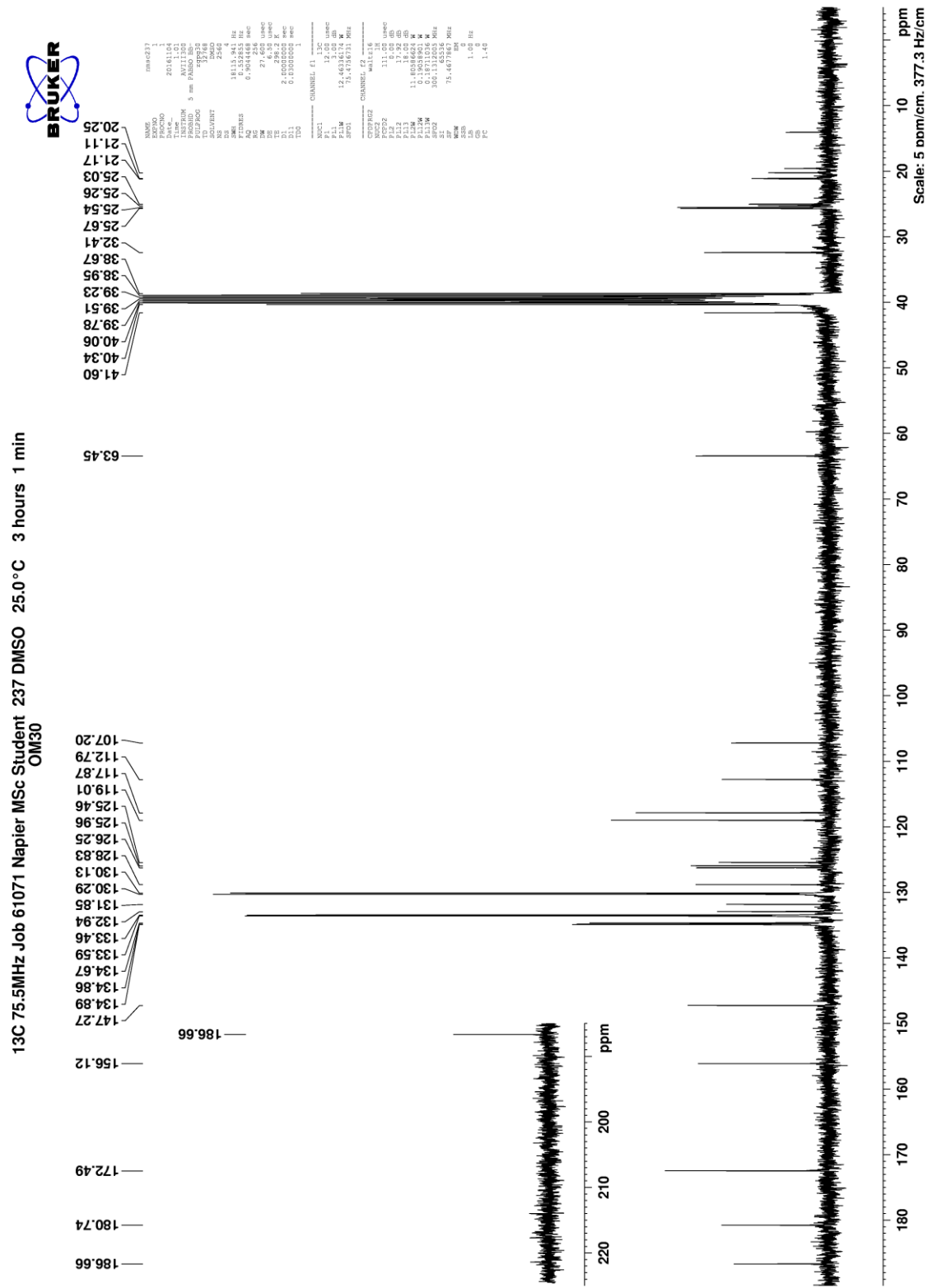


Figure 1.52: ¹³C NMR spectrum (DMSO, 75.5 MHz) of OM30

13C 75.5MHz Job 61071 Napier MSc Student 237 DMSO DEPT 25.0 °C
 OM30

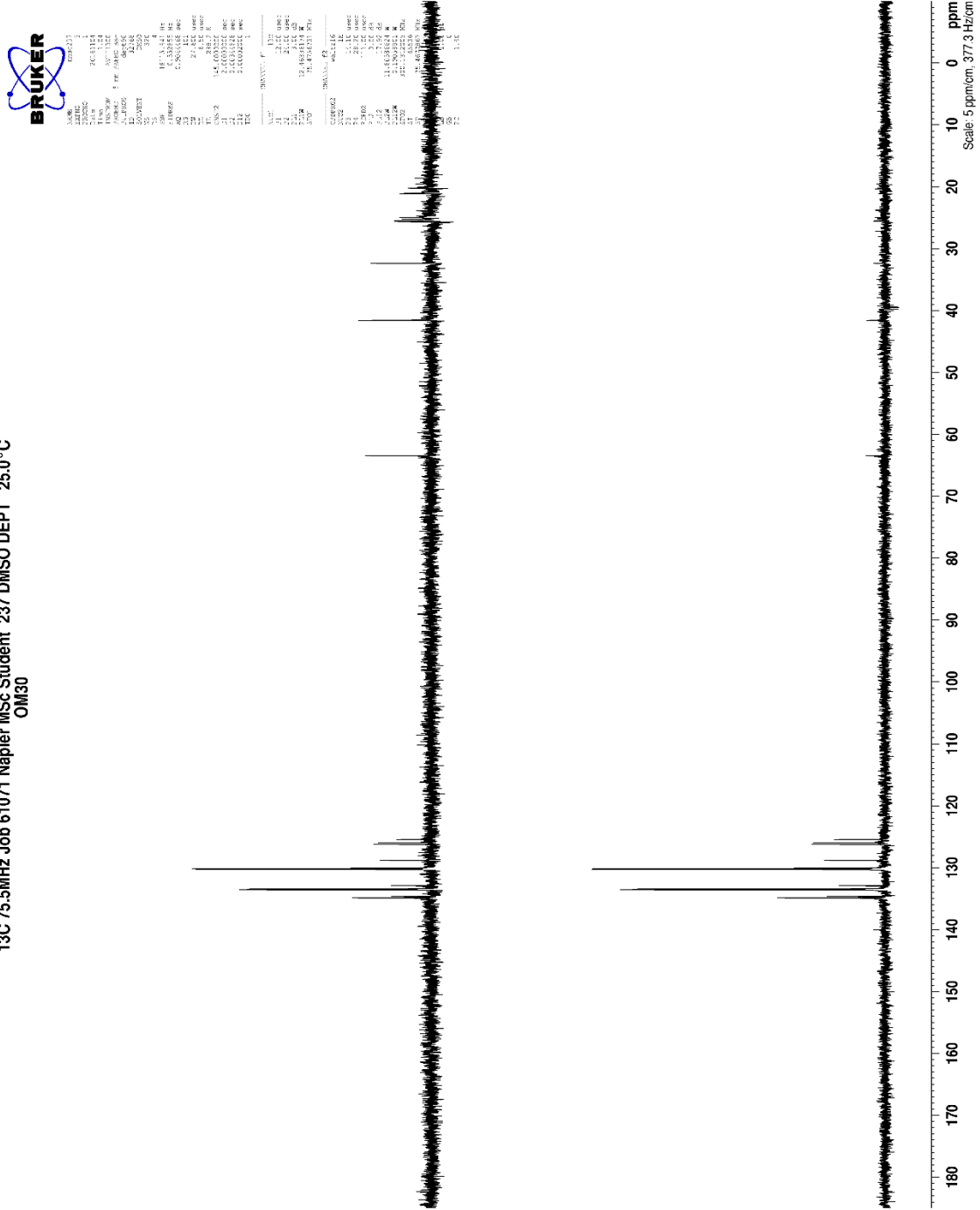


Figure 1.53: ¹³C NMR DEPT90 spectrum (DMSO, 75.5 MHz) of OM30

1.3.3.7 Synthesis of HO-pentyl-AQ(4-OH) (OM28)

HO-pentyl-AQ(4-OH) (OM28) was synthesised, which has the longer spacer (pentyl-spacer) compared with TPP-EAE-AQ(4-OH) (OM22) and TPP-Butyl-AQ(4-OH) (OM30). HO-pentyl-AQ(4-OH) (OM28) was synthesised to compare the cytotoxicity and localisation in comparison with previous compounds.

Leucoquinizarin was reacted with 5-amino-1-pentanol in dichloromethane. The reaction mixture was refluxed for 1 hour at 50°C over a water bath to give OM28. After 1 hour, the reaction mixture was oxidized overnight by aeration with the addition of triethylamine (Et₃N) **Figure 1.54**. The progress of the reaction was monitored through TLC. Solvent extraction was carried with chloroform/water. However, the organic layer was not separated well from the water during the extraction, therefore the water and the organic layer were evaporated and the reaction mixture was oxidized again. Solvent extraction was carried again with chloroform/water. The product was purified by column chromatography using chloroform first to get rid of polar impurities, then chloroform + 2% ethyl acetate were used to get the title compound OM28. The fractions were filtered off and dried. OM28 was precipitated under diethyl ether. The structure of OM28 was confirmed by its high resolution electrospray (+) mass spectrum which showed a clear signal at m/z 326.1389 [M + H]⁺ which corresponded to the expected molecular mass of the 326.1387 Da for the molecule. Furthermore, there was a good correlation between the observed data and the theoretical isotope model for [M + H]⁺.

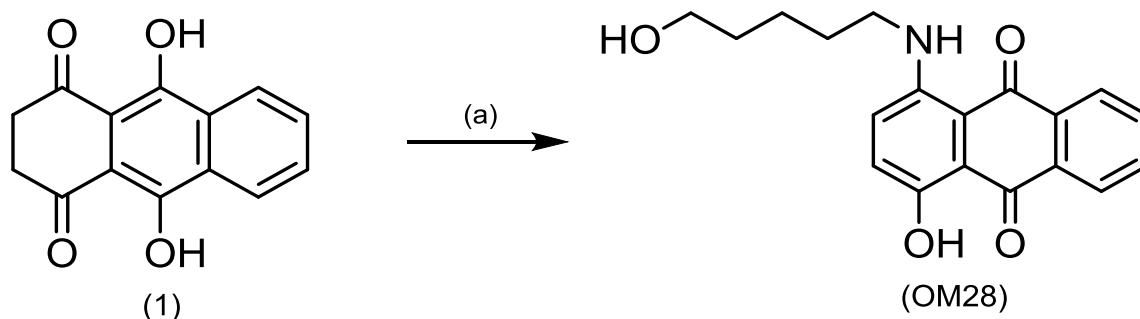


Figure 1.54: Synthesis of OM28 by reaction of Leucoquinizarin (1) with 5-amino-1-pentanol. (a) 5-amino-1-pentanol, dichloromethane, 50°C, 1 h, triethylamine, O₂, 4 h.

1.3.3.8 Synthesis of TPP-Pentyl-AQ(4-OH) (OM31)

OM31 was synthesized by the reaction of HO-pentyl-AQ(4-OH) (OM28) pre-dissolved in dichloromethane with TPP using DCC and DMAP as a coupling agent. The reaction mixture was left to stir over ice for 1 hour **Figure 1.55**. The reaction progress was monitored by TLC. The white crystals of N,N'-dicyclohexylurea (DCU) were filtered off from the reaction solution, followed by solvent extraction with water and chloroform. OM31 was purified by column chromatography using chloroform at the beginning followed by using more polar solvent systems, chloroform + 3% ethyl acetate, 9:1 chloroform: ethyl acetate; 4:1 chloroform: ethyl acetate, 4:1 chloroform: ethyl acetate + 5% methanol, chloroform + 5% methanol and 4:1 chloroform: methanol. The purest fractions of OM31 were collected, filtered and dried. Diethyl ether was added to precipitate the product and left overnight in cold place (4°C). However, there was also an unknown red compound which was collected for further determination. The structure of OM31 was confirmed by high resolution electrospray (+) mass spectrum which showed a clear signal at m/z 670.2698 which corresponded to the expected molecular mass of the 670.2698 Da cation **Figure 1.56**. Furthermore, there was a good correlation between the observed data and the theoretical isotope model for the C₄₂H₄₂NO₅P cation.

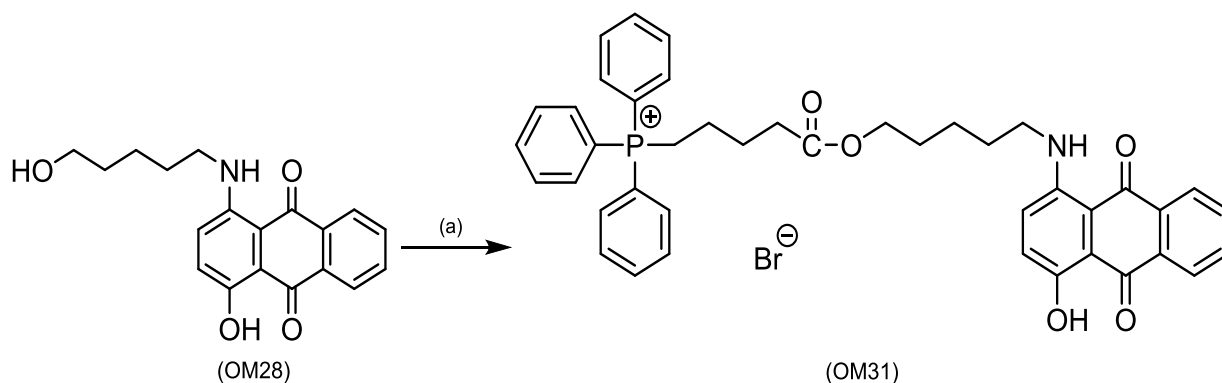


Figure 1.55: Synthesis of OM31 by reaction of OM28 with TPP. (a) TPP, DCC, DMAP, dichloromethane, 1 h

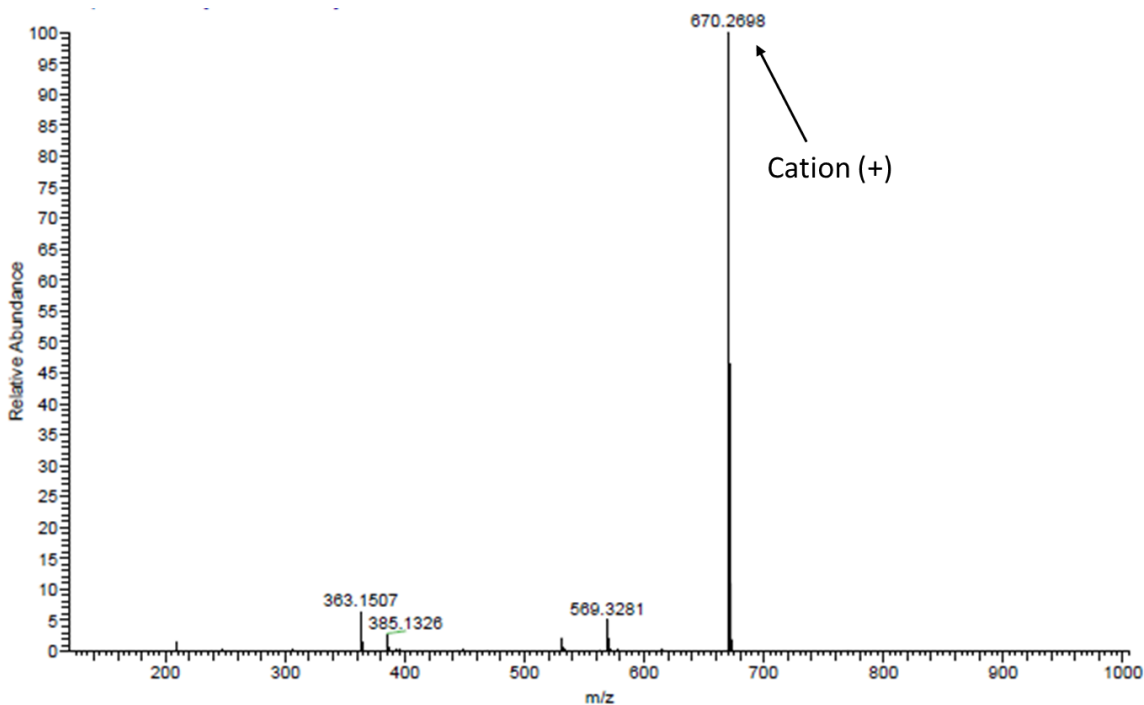


Figure 1.56: The ESI (+) mass spectrum of OM31

OM31 structure was characterized and confirmed by its ^1H NMR spectrum (in $\text{d}_6\text{-DMSO}$), which showed, a signal between 1.35-1.49 ppm which was assigned to the two protons of the methylene group in the middle of the spacer, whereas the eight protons of TPP and anthraquinone spacer were found between 1.5-1.81 ppm. The methylene closest to the carbonyl group in the spacer was found at 2.93 ppm (triplet) whereas, the methylene closest to the amino group of the anthraquinone was found at 3.42 ppm (quartet). The methylene group closest to the phosphonium group of TPP was found at 3.61 ppm (triplet). In addition, a signal at 4.01 ppm was assigned to the methylene group closest to oxygen in the spacer. The fifteen aromatic protons of TPP and two of the anthraquinone were assigned between 7.71 ppm and 7.95 ppm. The signals at 7.36 ppm (doublet) and 7.51 ppm (doublet) were assigned to the two anthraquinone protons, H-2 and H-3. The two protons for the anthraquinone, H-5 and H-8 were assigned at 8.24 ppm. At 10.3 ppm the signal was assigned to the amino proton at C-1 of the anthraquinone whereas, the hydroxyl proton of anthraquinone give a singlet signal at 13.67 ppm **Figure 1.57 and Figure 1.58**.

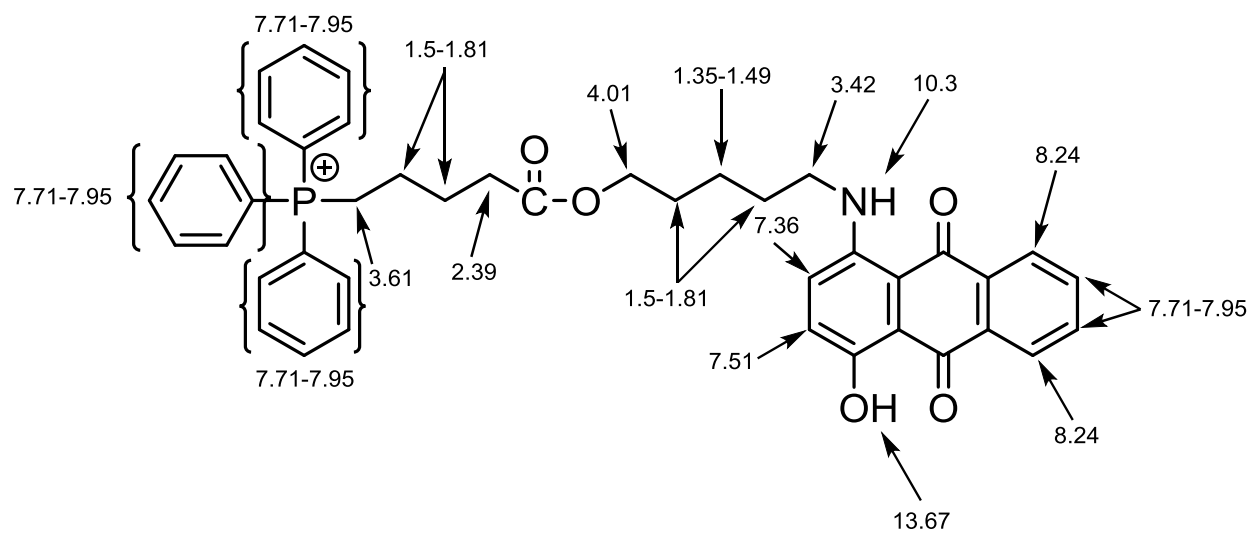


Figure 1.57: ^1H NMR signals (ppm) of OM31

1H 300.1MHz Job 64474 Napier MSc Student 256 DMSO 25.1 °C
OM 31

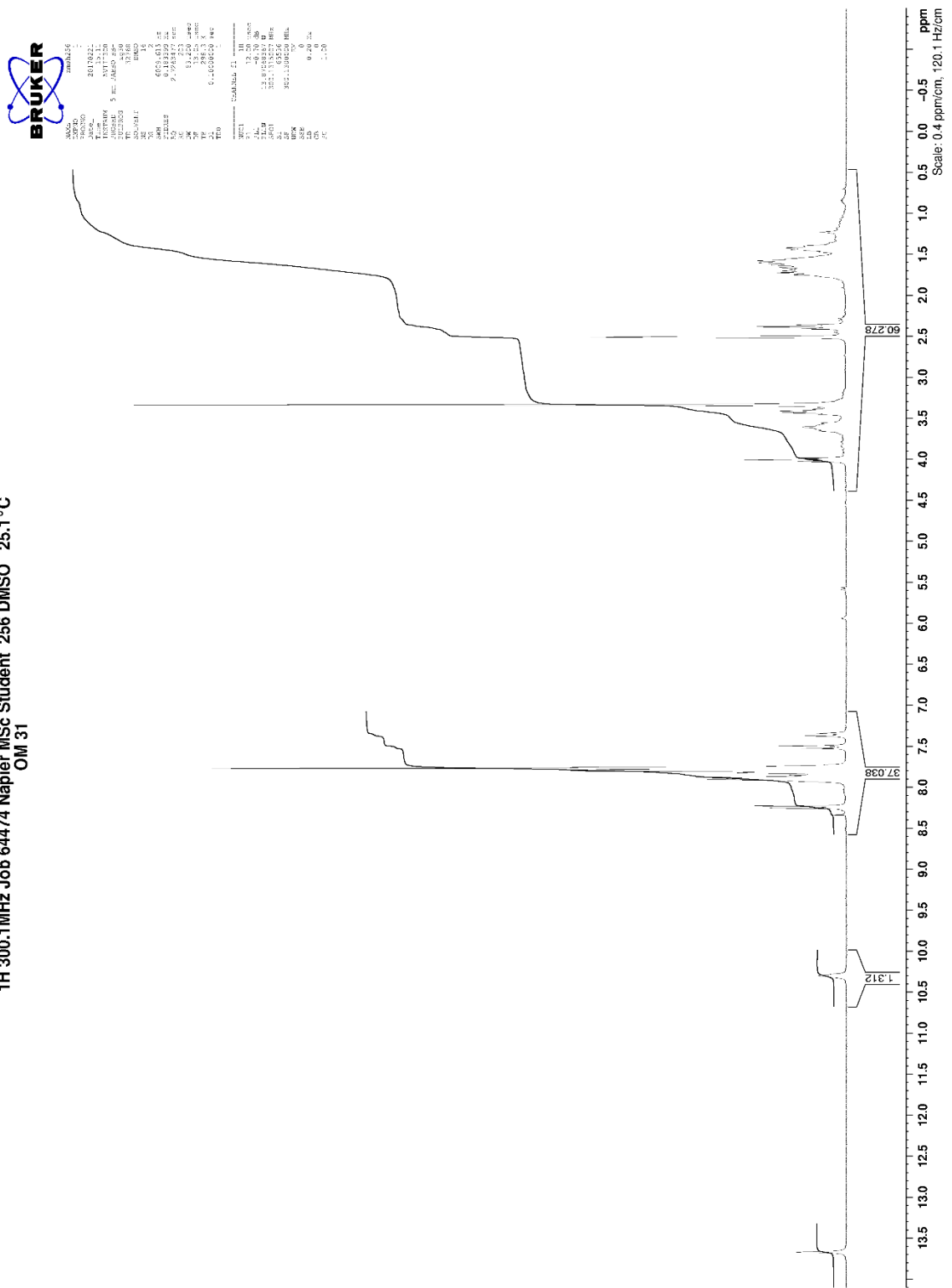


Figure 1.58: ¹H NMR spectrum (DMSO, 300 MHz) of OM31

The proton-decoupled ^{13}C NMR spectrum showed signals for all carbon environments. A DEPT experiment differentiated the nine methylene CH_2 carbons, twenty one methine CH carbons (AQ_{TPP} and AQ_{AR}) and twelve quaternary carbons. The nine methylene carbons gave signals between 20.22 ppm and 63.57 ppm. The two anthraquinone carbonyl groups were assigned at 180.72 ppm and 186.66 ppm. Signals at 125.58 ppm, 126.01 ppm, 126.27 ppm, 128.95 ppm, 132.94 ppm and 134.73 ppm were assigned to the six methine carbons of the anthraquinone. Three aromatic methine carbon signals, corresponding to the ortho, meta and para carbon atoms of the TPP aromatic group were found in their expected positions at 130.13-130.29 ppm (meta), 133.45-133.59 ppm (ortho) and 134.90 ppm (para) **Figure 1.59, Figure 1.60 and Figure 1.61.**

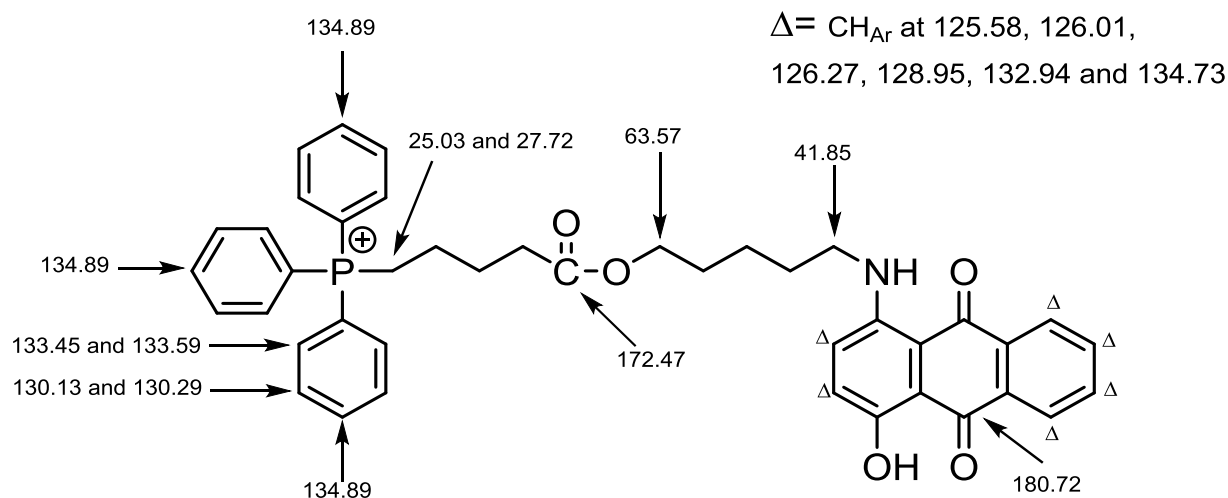


Figure 1.59: ^{13}C NMR signals (ppm) of OM31

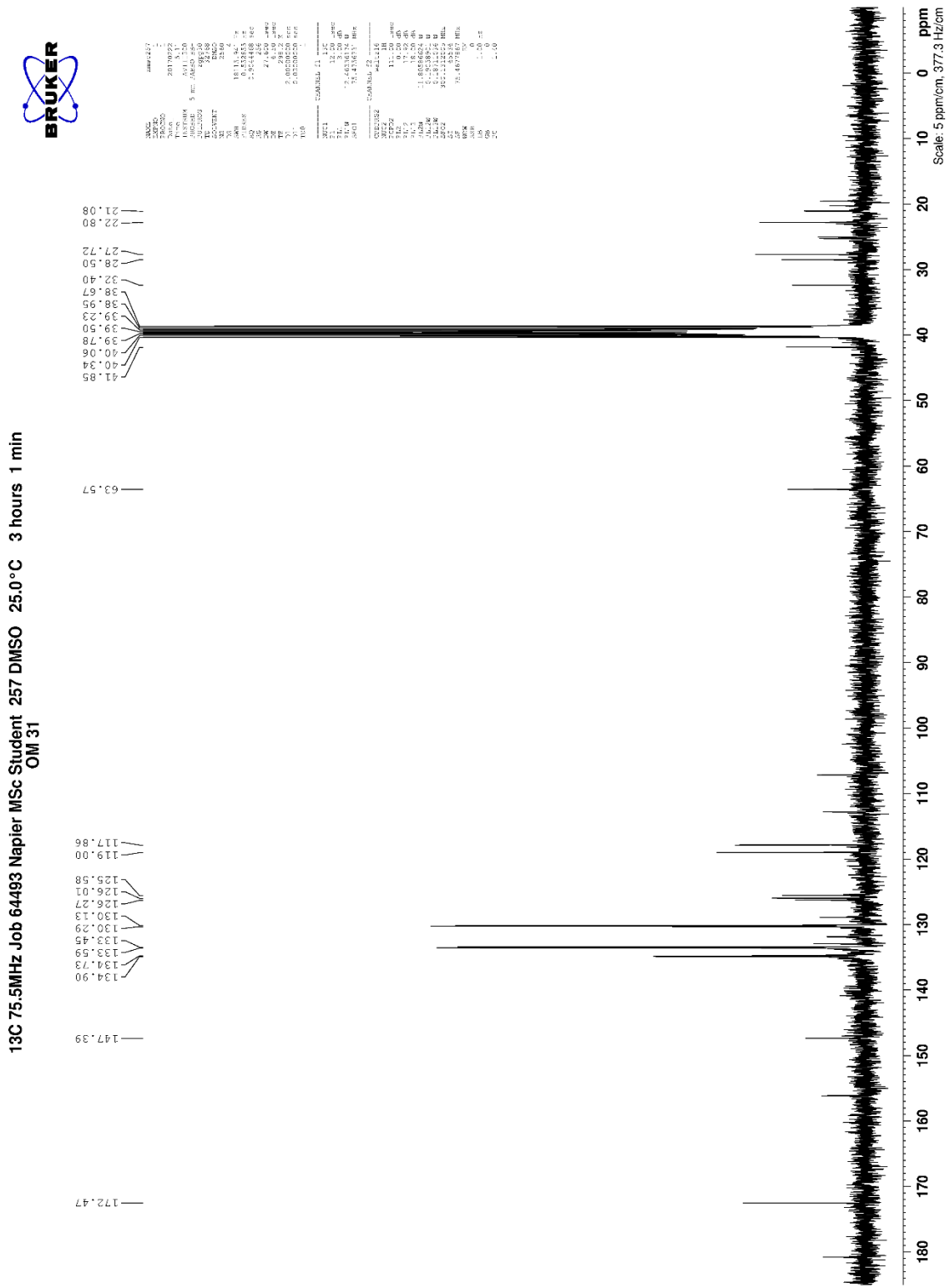


Figure 1.60: ¹³C NMR spectrum (DMSO, 75.5 MHz) of OM31

1.3.3.9 Synthesis of HO-EOE-AQ(4-OH) (OM29)

HO-EOE-AQ(4-OH) (OM29) was designed and developed specifically to study the effect of the oxygen group in the spacer on the cytotoxicity and localization of OM29 once attached with TPP in mitochondria or lysosomes and to compare the activity of this compound with previous synthesised compounds.

Leucoquinizarin was reacted with 2-(2-aminoethoxy)ethanol in dichloromethane. The reaction mixture was refluxed for 1 hour at 50°C over a water bath to give OM29. After 1 hour, the reaction mixture was oxidized overnight by aeration with the addition of triethylamine (Et₃N) **Figure 1.62**. The progress of the reaction was monitored through TLC. Solvent extraction was carried with chloroform/water. OM29 was purified by column chromatography using chloroform at the beginning followed by using chloroform with an increased percentage of methanol up to 6%. However, after the first purification, there were some impurities with OM29, therefore a second purification was performed using chloroform at the beginning then chloroform + 4% methanol to get the title compound OM29. The pure fractions were evaporated and dried. Diethyl ether was added to precipitate OM29. The structure of OM29 was confirmed by high resolution electrospray (+) mass spectrum which showed a clear signal at m/z 328.1181 [M + H]⁺ which corresponded to the expected molecular mass of the 327.1181. Furthermore, there was a good correlation between the observed data and the theoretical isotope model for C₁₈H₁₇NO₅ [M + H]⁺.

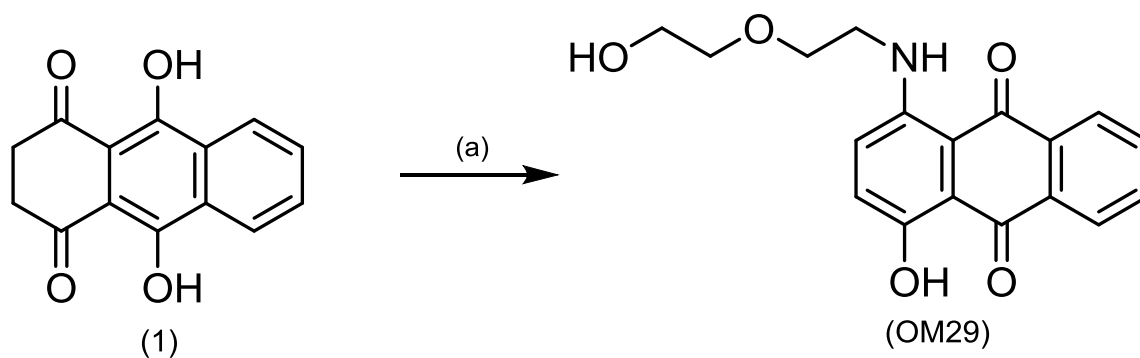


Figure 1.62: Synthesis of OM29 by reaction of Leucoquinizarin (1) with 2-(2-aminoethoxy)ethanol. (a) 2-(2-aminoethoxy)ethanol, dichloromethane, 50°C, 1 h, triethylamine, O₂, overnight.

1.3.3.10 Synthesis of TPP-EOE-AQ(4-OH) (OM32)

HO-EOE-AQ(4-OH) OM29 was reacted with TPP (1.2 eq) in dichloromethane using DCC (2.4 eq) and DMAP as a coupling agent. The reaction mixture was left to stir over ice for 1 hour **Figure 1.63**. The reaction progress was monitored by TLC. However, OM29 was not fully reacted with TPP, therefore additional amounts of TPP (0.6 eq) and DCC (1.2 eq) were added and allowed to react for 1 hour. The white crystals of N,N'-dicyclohexylurea (DCU) were filtered off from the reaction solution, followed by solvent extraction with water and chloroform. Column chromatography was performed using to chloroform first then more polar solvents were used, chloroform + 5% ethyl acetate, 9:1 chloroform: ethyl acetate, 4:1 chloroform: ethyl acetate: 4:1 chloroform: ethyl acetate + 5% methanol, chloroform + 5% methanol and 9:1 chloroform: methanol. The pure fractions were collected, filtered and dried. Diethyl ether was added to precipitate the product OM32. The structure of OM32 was confirmed by high resolution electrospray (+) mass spectrum which showed a clear signal at m/z 672.2501 which corresponded to the expected molecular mass of the 672.2501 Da cation **Figure 1.64**. Furthermore, there was a good correlation between the observed data and the theoretical isotope model for the $C_{41}H_{39}NO_6P$ cation.

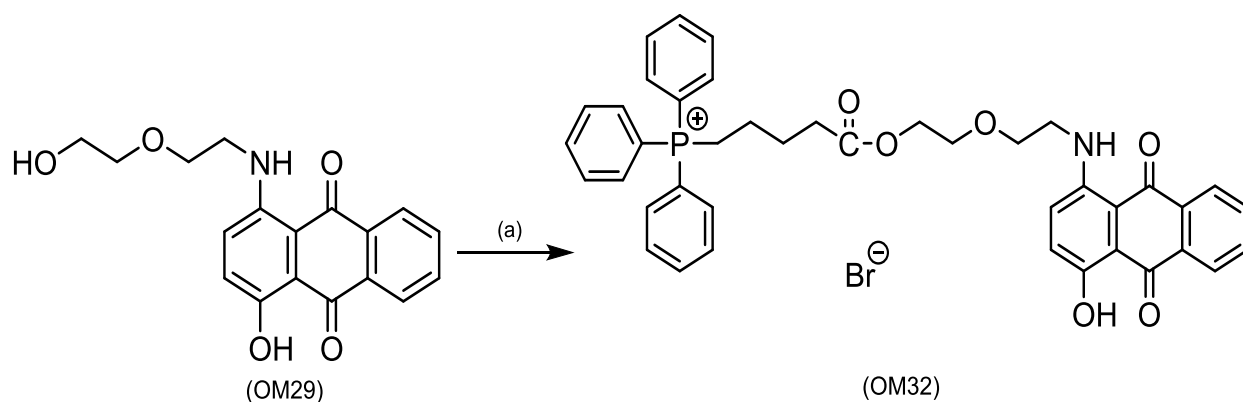


Figure 1.63: Synthesis of OM31 reaction of OM29 with TPP. (a) TPP, DCC, DMAP, dichloromethane, 1 h

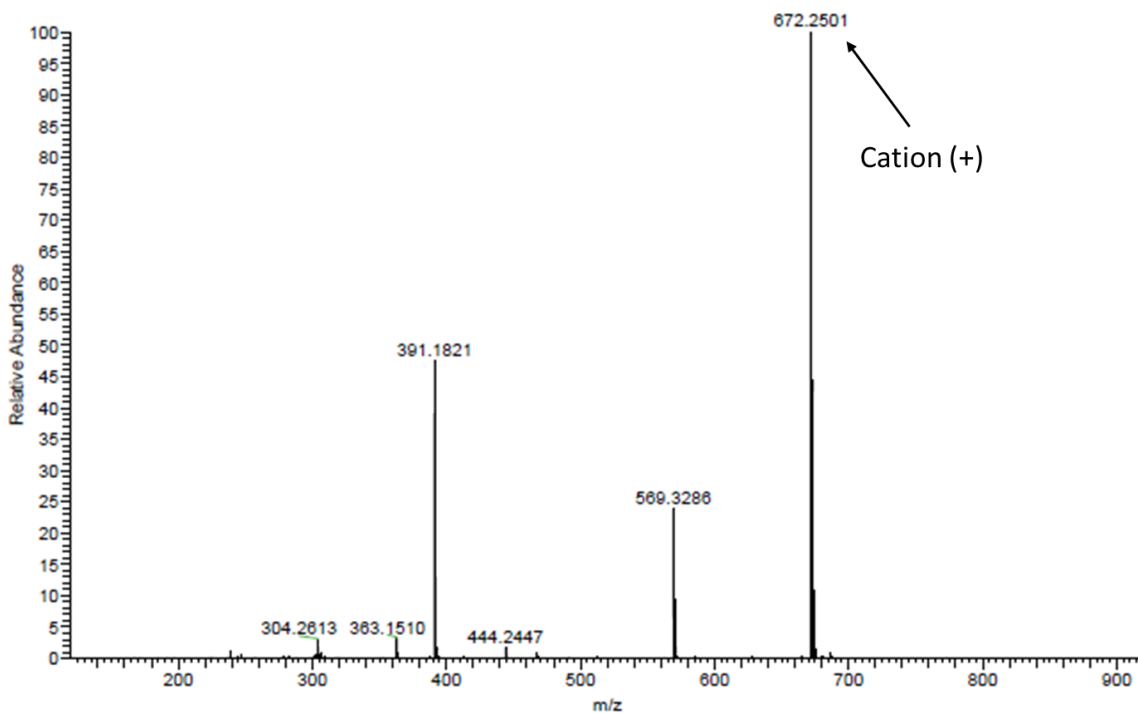


Figure 1.64: The ESI (+) mass spectrum of OM32

OM32 structure was characterized and confirmed by its ^1H NMR spectrum (in $\text{d}_6\text{-DMSO}$), which showed, signals between 1.47-1.79 ppm which were assigned to four protons of the methylene groups in the TPP spacer. The methylene closest to the carbonyl group in the spacer was found at 2.41 ppm whereas the methylene closest to the amino group of the anthraquinone was found at 3.34 ppm. Furthermore, the methylene protons around the oxygen atom in the spacer and the two protons of the methylene group closest to the phosphonium group of TPP were found between 3.5-3.73 ppm. In addition, a signal between 4.12-4.18 ppm was assigned to the methylene group closest to OH in the spacer. The fifteen aromatic protons of TPP and two anthraquinone protons were assigned between 7.71 ppm and 7.95 ppm. The signals at 7.37 ppm (doublet) and 7.55 ppm (doublet) were assigned to the anthraquinone protons of H-2 and H-3. The two protons for H-5 and H-8 were assigned between 8.20-8.27 ppm. At 10.37 ppm a triplet signal was assigned to the amino proton at C-1 of the anthraquinone whereas, the hydroxyl proton of anthraquinone give a singlet signal at 13.67 ppm **Figure 1.65** and **Figure 1.66**.

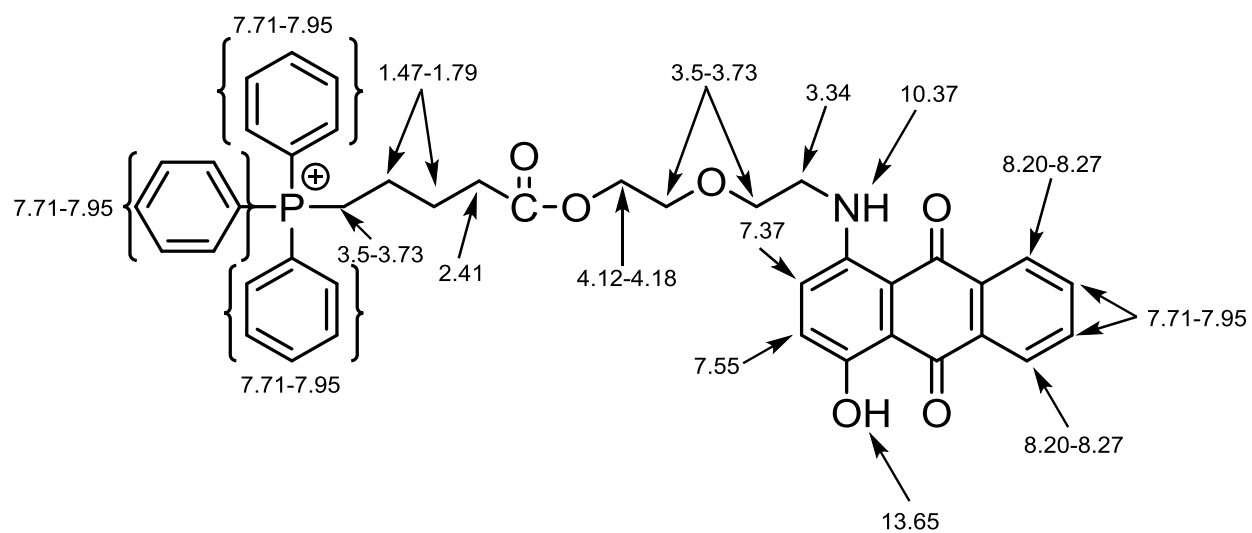


Figure 1.65: ^1H NMR signals (ppm) of OM32

The proton-decoupled, ^{13}C NMR spectrum showed signals for all carbon environments. A DEPT experiment differentiated the eight methylene CH_2 carbons, twenty one methine carbons and twelve quaternary carbons. Signals between 20.28 ppm and 68.12 ppm were assigned to the eight methylene carbons. The two anthraquinone carbonyl groups were assigned at 180.81 ppm and 186.78 ppm. Signals at 125.81 ppm, 126.02 ppm, 126.25 ppm, 128.71 ppm, 133.00 ppm and 133.61 ppm were assigned to six methine CH carbons of the anthraquinone. Three aromatic methine carbon signals, corresponding to the ortho, meta and para carbon atoms of the TPP aromatic group were found in their expected positions at 130.12-130.28 ppm (meta), 133.48-133.56 ppm (ortho) and 134.90 ppm (para) **Figure 1.67, Figure 1.68 and Figure 1.69.**

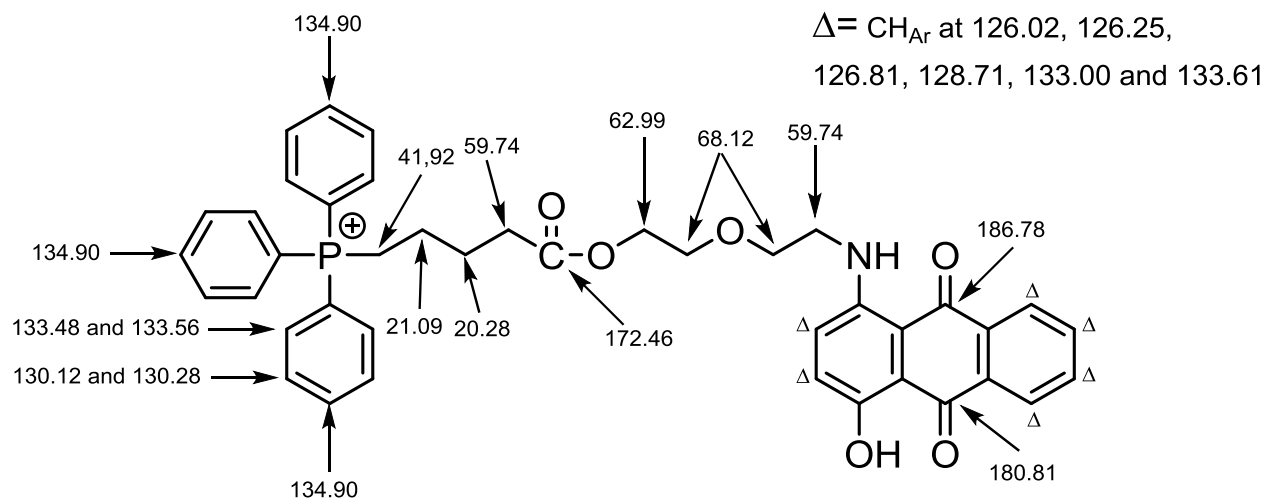


Figure 1.67: ^{13}C NMR signals (ppm) of OM32

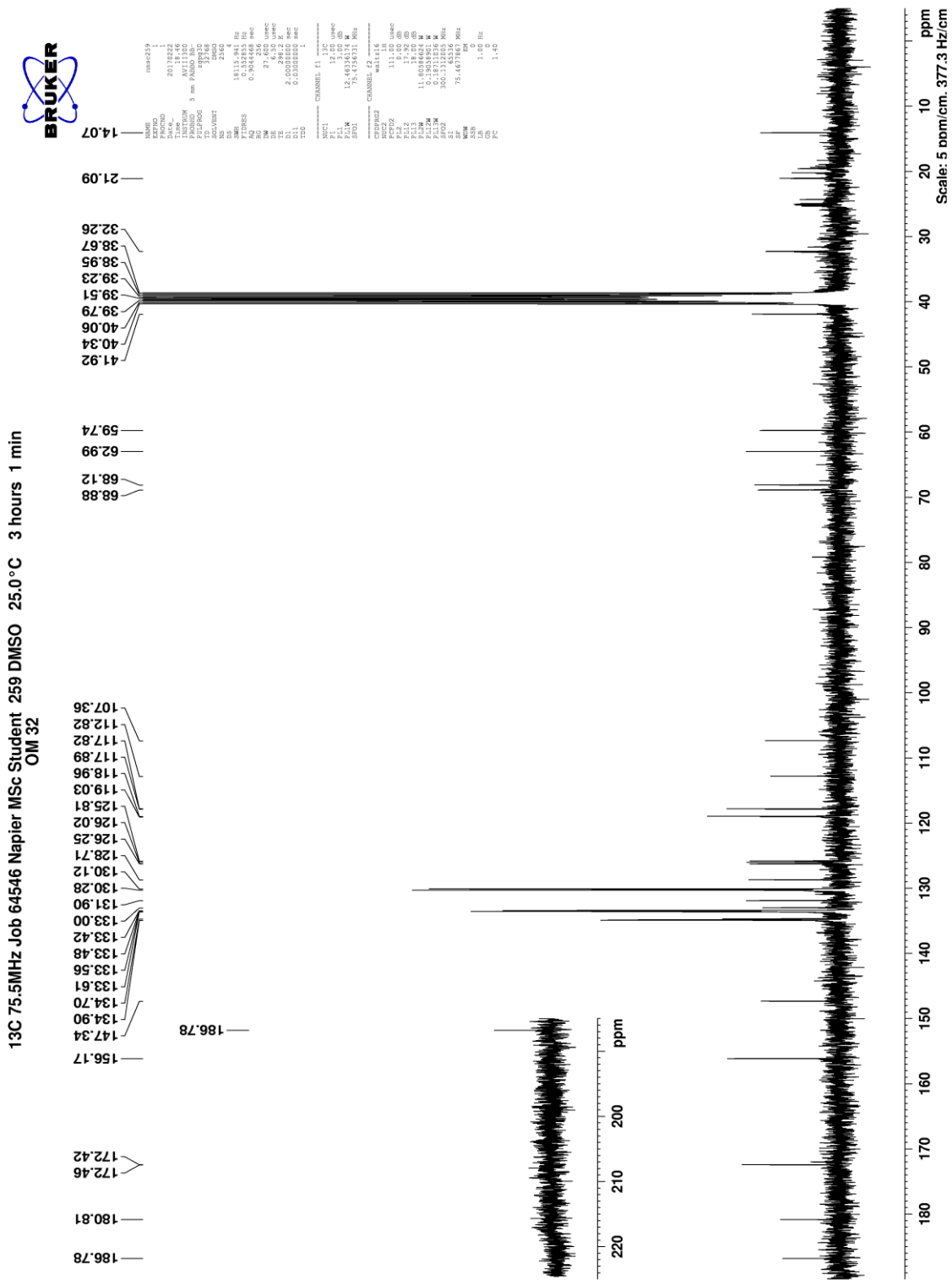


Figure 1.68: ¹³C NMR spectrum (DMSO, 75.5 MHz) of OM32

**¹³C 75.5MHz Job 64546 Napier MSc Student 259 DMSO DEPT 25.0°C
OM 32**

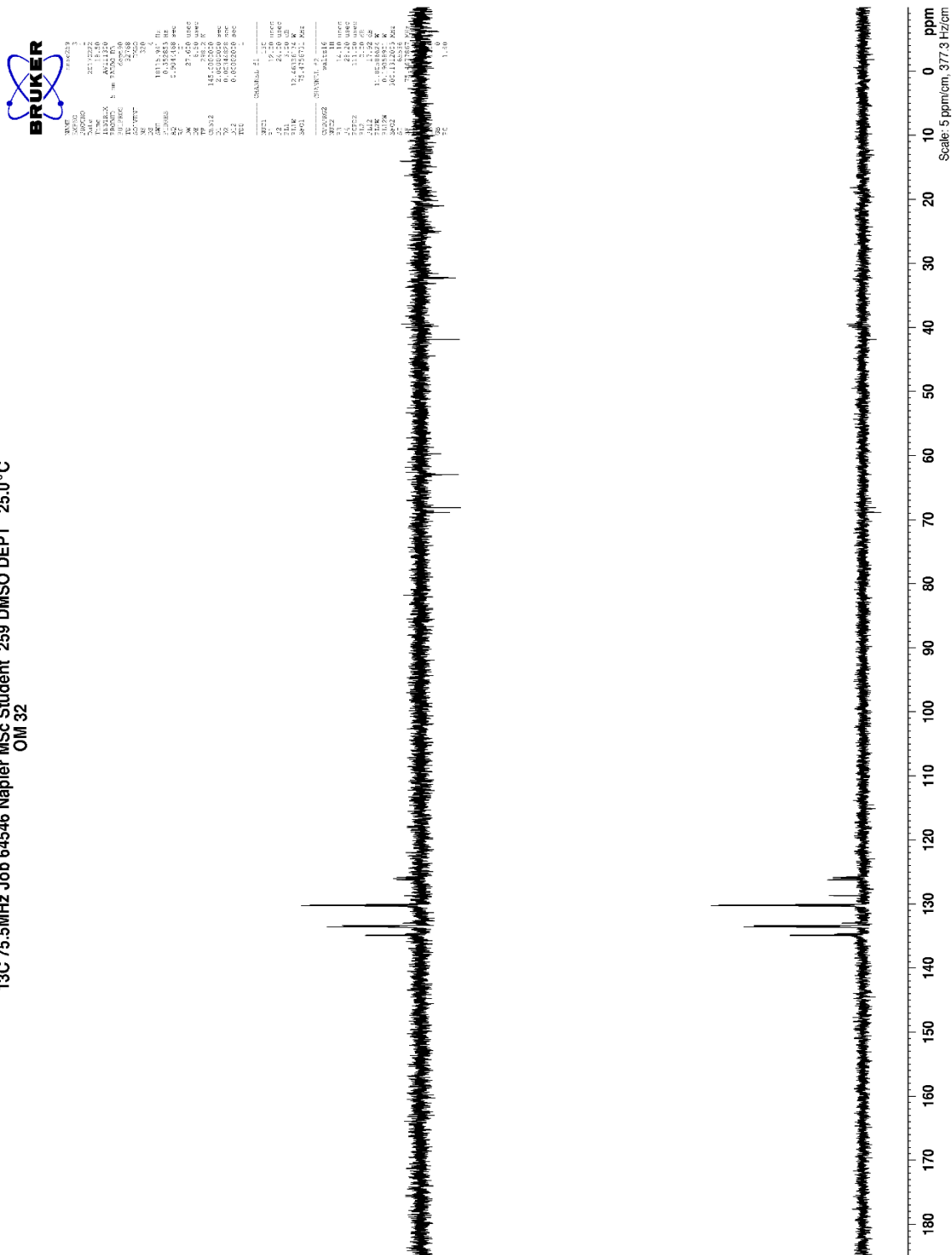


Figure 1.69: ¹³C NMR DEPT90 spectrum (DMSO, 75.5 MHz) of OM32

1.3.3.11 Synthesis of OH-butyl-AQ (NU:UB 238)

The reason behind the synthesis of NU:UB 238 was to evaluate the effect of (-OH) and (-NH₂), which present in TPP-EAE-AQ(4-OH) (OM22) and not in NU:UB 238 after attaching the TPP on the localization and if they still retained activity or were less active without the (-OH).

NU:UB 238 was synthesized by reaction of 1-chloroanthraquinone with 4-amino-1-butanol in DMSO, and then the reaction mixture was heated over a boiling water bath with a condenser for 30 minutes. The reaction solution was cooled and added to a large excess of water (500 mL) to give red solid precipitate which was filtered off, dried and used for subsequent reactions without further purification **Figure 1.70**. The structure of NU:UB 238 was confirmed by its high resolution electrospray (+) mass spectrum which showed a clear signal at m/z 296.1284 [M + H]⁺ which corresponded to the expected molecular mass of the compound. Furthermore, there was a good correlation between the observed data and the theoretical isotope model for C₁₈H₁₇O₃NH [M + H]⁺. This confirmed the correct structure of NU:UB 238.

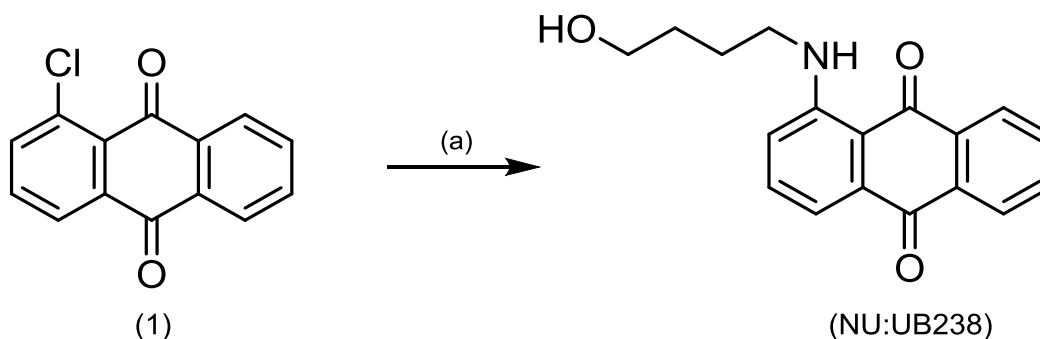


Figure 1.70: Synthesis of NU:UB 238 by reaction of 1-chloroanthraquinone (1) with 4-amino-1-butanol. (a) 4-amino-1-butanol, DMSO, 95°C, 30 min, water

1.3.3.12 Synthesis of (TPP-Butyl-AQ) (SH1)

SH1 was synthesized as it shares the same aminobutanol spacer as NU:UB 73 and NU:UB 76 (**Section 1.3.1**) but in SH1, the ester bond linking TPP to the spacer is likely to be more stable than the ester bond to L- and D- alanine in NU:UB 73 and NU:UB 76, respectively. Both NU:UB 73 and 76 were active *in vivo* once the AQ- aminobutanol spacer (NU:UB 238) was linked with L-alanine [NU:UB 73] and D-alanine [NU:UB 76], whereas the spacer alone was inactive both *in vitro* and *in vivo*.

SH1 (AQ- aminobutanol linked with TPP) was synthesized by the reaction of OH-butyl-AQ (NU:UB 238) pre-dissolved in dichloromethane with TPP using DCC and DMAP as a coupling agents. The reaction mixture was left to stir for 1 hour **Figure 1.71**. The reaction progress was monitored by TLC. The white crystals of *N,N'*-dicyclohexylurea (DCU) were filtered off from the reaction solution, followed by solvent extraction with water and chloroform. Column chromatography was performed using dichloromethane at the beginning followed by using more polar solvent systems, 9:1 dichloromethane: ethyl acetate; 9:1 dichloromethane: ethyl acetate + 1% methanol. The percentage of methanol was increased gradually to 7% until all SH1 was collected. However, the product of SH1 was difficult to precipitate by diethyl ether as it was very sticky, therefore column chromatography was performed for a second time to remove any impurities that prevented the precipitation of SH1. The solvents were evaporated and acetonitrile: diethyl ether solution was added and it was cooled (4°C) for 48 hours in order to precipitate SH1. The structure of NU:UB 238 was confirmed by its high resolution electrospray (+) mass spectrum which showed a clear signal at m/z 640.2594 which corresponded to the expected molecular mass of the cation. Also, there was a good correlation between the observed data and the theoretical isotope model for $[C_{41}H_{39}O_4NP]^+$ **Figure 1.72**. This confirmed the complete and successful addition of TPP to NU:UB 238.

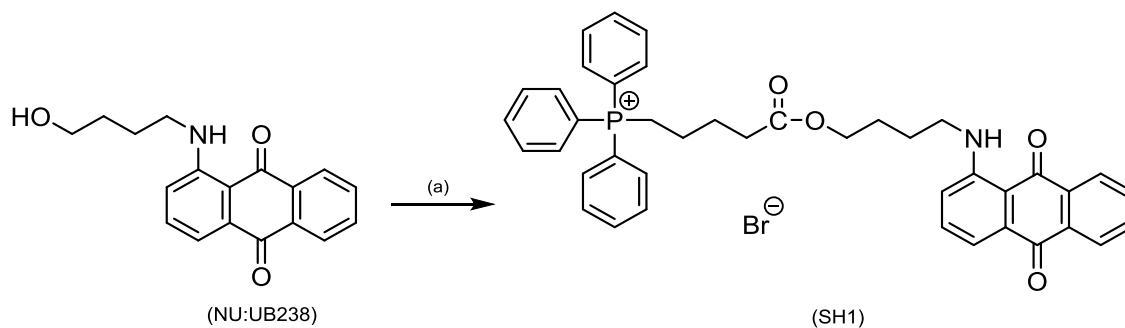


Figure 1.71: Synthesis of SH1 by reaction of NU:UB 238 with TPP. (a) TPP, DCC, DMAP, dichloromethane, 1 h.

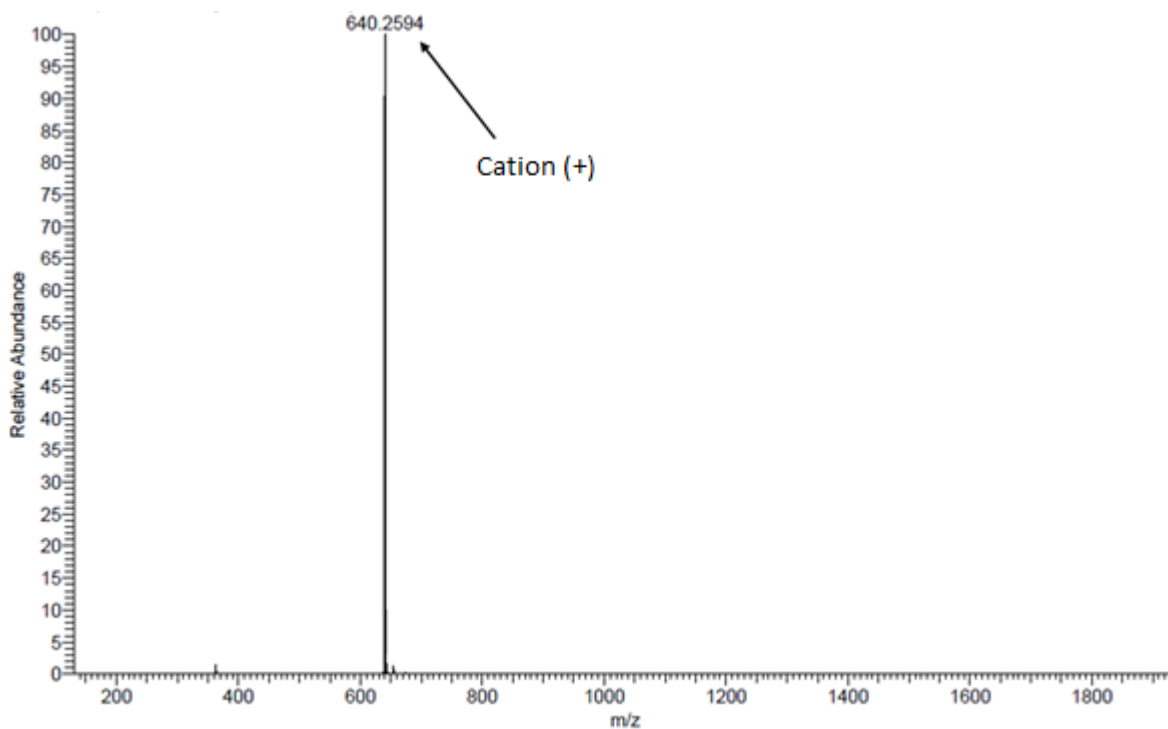


Figure 1.72: The ESI (+) mass spectrum of SH1

The structure of SH1 was characterized and confirmed by its ^1H NMR spectrum (in d_6 -DMSO), which showed, a triplet signal at 9.68 ppm which was assigned to the amino proton at position 1 of the anthraquinone. Signals between 1.50-1.80 ppm were assigned to the eight protons of the central methylene groups of TPP and the aminobutyl residue.

Another four protons of TPP were found at 3.62 ppm (triplet) and 4.06 ppm (triplet). The methylene closest to carbonyl group in the spacer was found at 2.41 ppm (triplet), whereas, the methylene group closest to the amino group of the anthraquinone was found at 4.06 ppm (singlet). The fifteen aromatic protons of TPP and two of the anthraquinone were assigned between 7.72 ppm and 7.94 ppm. The signals at 7.26 ppm, 7.43 ppm and 7.65 ppm were assigned to the anthraquinone protons of H-2, H-4 and H-3. The two protons for H-5 and H-8 of the anthraquinone were assigned between 8.10-8.21 ppm **Figure 1.73** and **Figure 1.74**. This confirmed the correct structure of SH1.

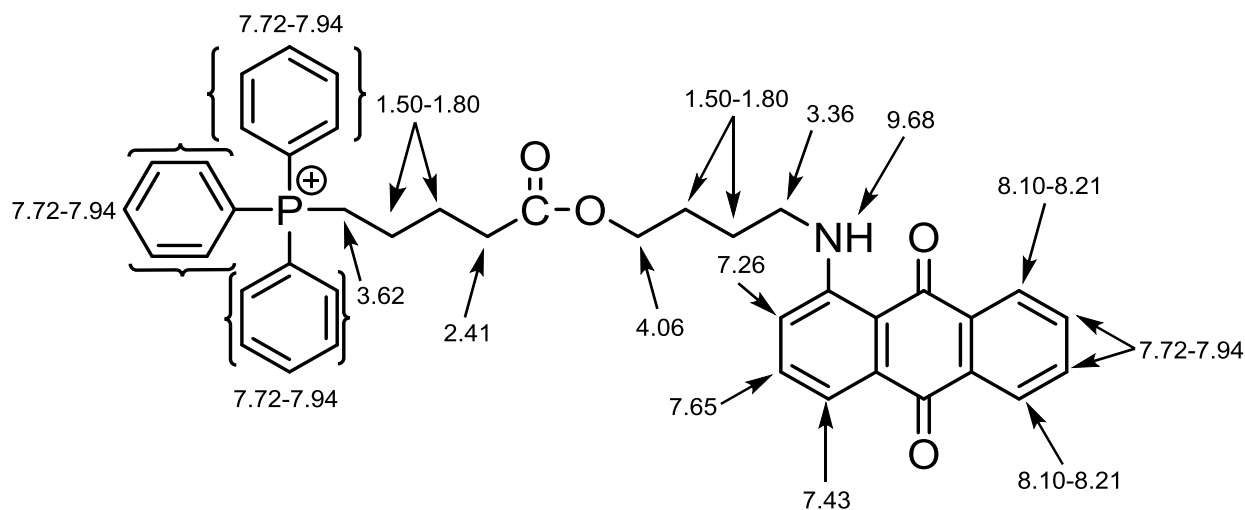


Figure 1.73: ¹H NMR signals (ppm) of SH1

1H 300.1MHz Job 59863 Napier MSc Student 196 DMSO 25.1 °C
SH1

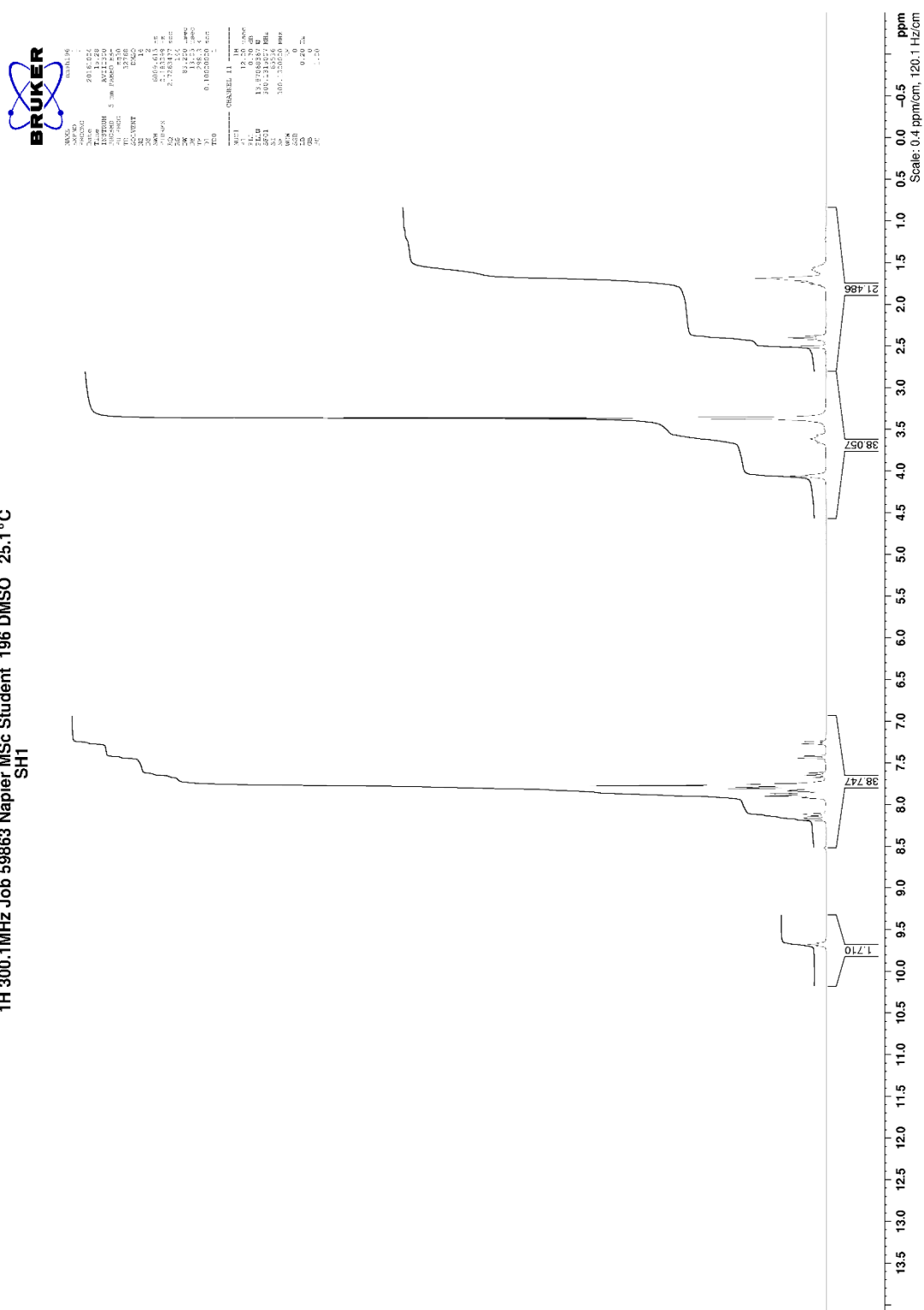


Figure 1.74: ^1H NMR spectrum (DMSO, 300 MHz) of SH1

The proton-decoupled ^{13}C NMR spectrum showed signals for all carbon environments. A DEPT experiment differentiated the eight methylene CH_2 carbons, twenty two methine CH carbons and eleven quaternary carbons. Signals between 20.25 ppm and 63.47 ppm were assigned to the eight methylene carbons. The two anthraquinone carbonyl groups were assigned at 184.00 ppm and 182.81 ppm. Signals at 115.02 ppm, 118.60 ppm, 126.25 ppm, 126.34 ppm, 134.49 ppm, 134.86 ppm, 135.65 ppm were assigned to the seven methine CH carbons of the anthraquinone. Three aromatic methine carbon signals, corresponding to the ortho, meta and para carbon atoms of the TPP aromatic group were found in their expected positions at 130.13-130.29 ppm (meta), 133.45-133.59 ppm (ortho) and 134.90 ppm (para) **Figure 1.75 and Figure 1.76 and Figure 1.77**. This confirmed the correct structure of SH1.

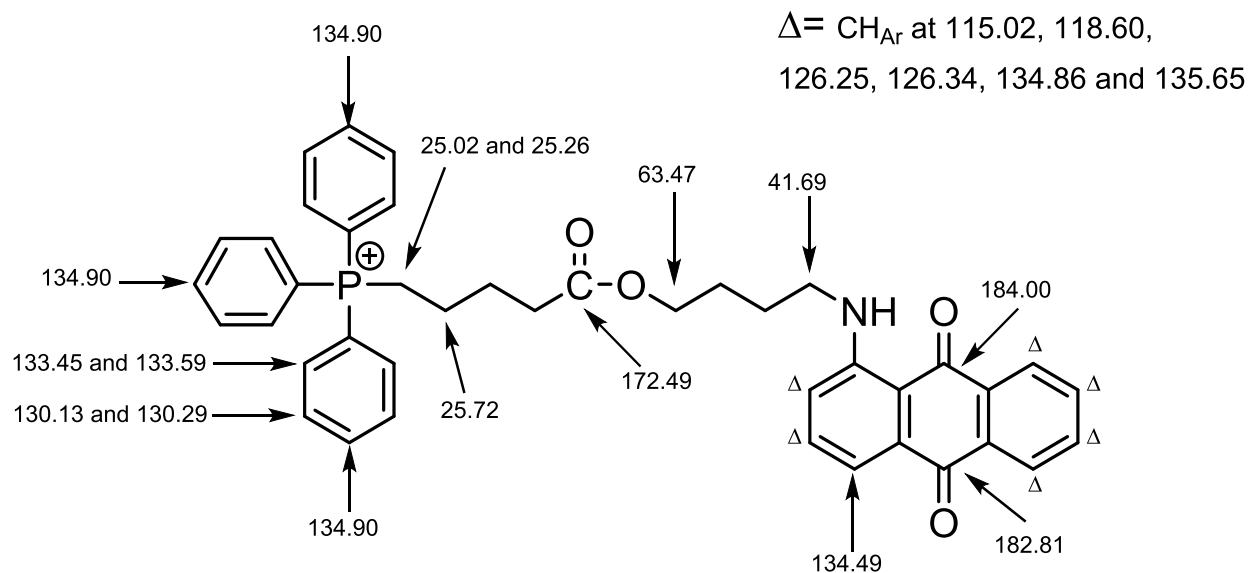


Figure 1.75: ^{13}C NMR signals (ppm) of SH1

13C 75.5MHz Job 59883 Napier MSc Student 197 DMSO 25.0°C 3 hours 1 min SH1

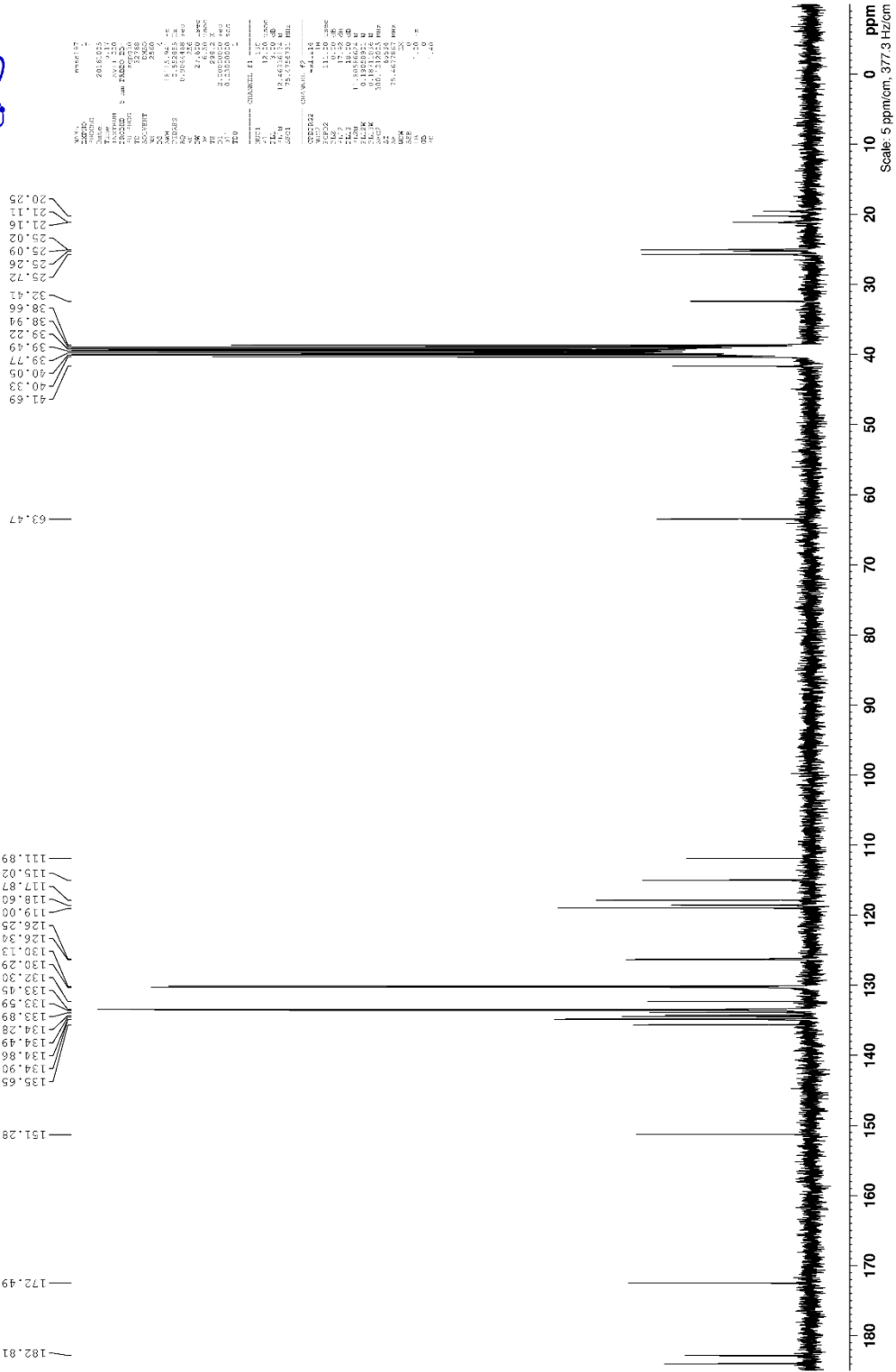


Figure 1.76: ¹³C NMR spectrum (DMSO, 75.5 MHz) of SH1

13C 75.5MHz Job 59883 Napier MSc Student 197 DMSO DEPT 25.0 °C
SH1

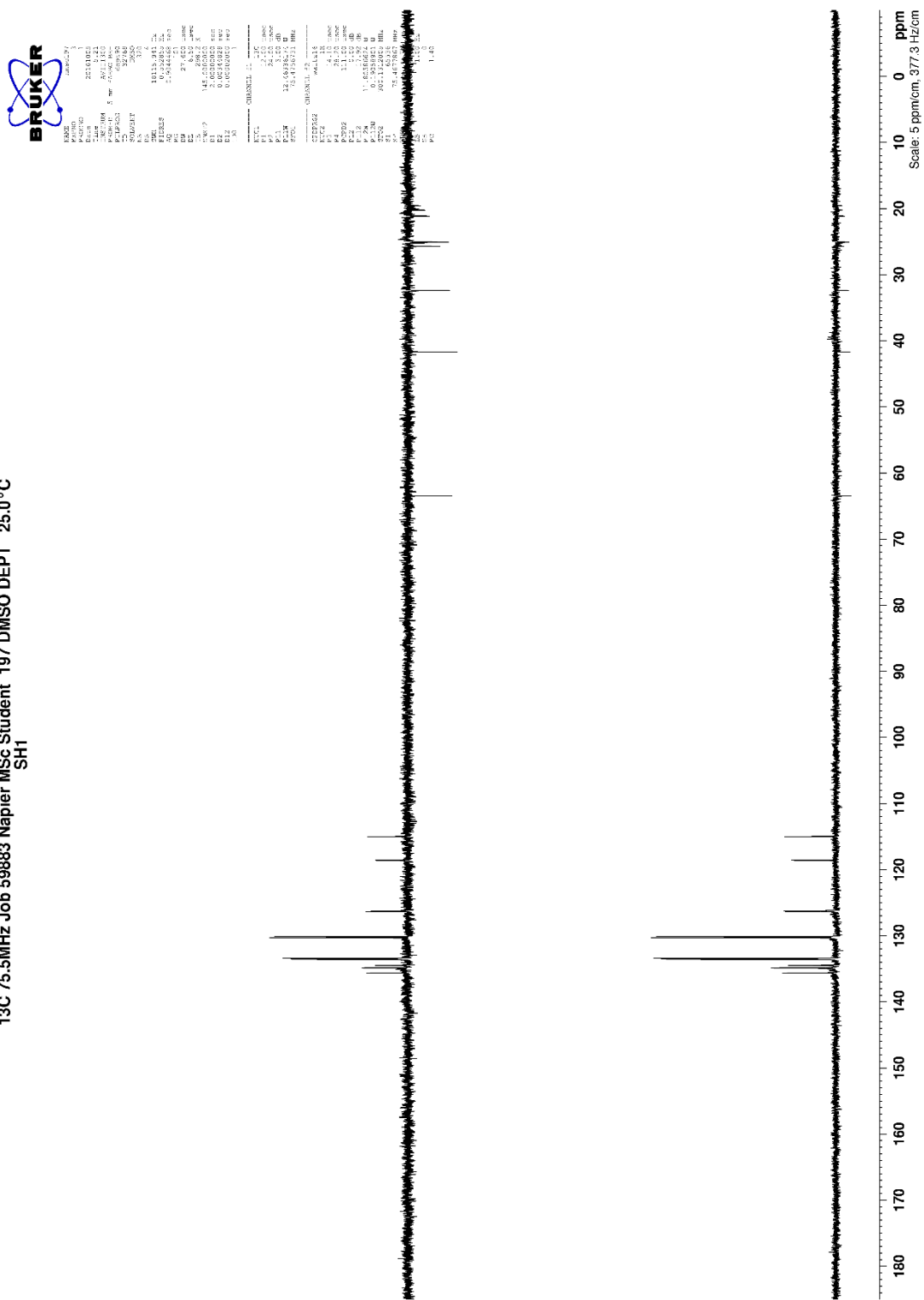


Figure 1.77: ¹³C NMR DEPT90 spectrum (DMSO, 75.5 MHz) of SH1

1.3.3.13 Synthesis of mono-TPP-NU:UB 65 (OM25)

NU:UB 65 is an aminoanthraquinone derivative that was developed and synthesized at the Anticancer Drug Design and Delivery Research Group at Napier University. NU:UB 65 has similar structural as mitoxantrone but it lacks the amino groups (-NH) in its side chains, which play an important role in the biological activity and DNA binding of mitoxantrone (Skladanowski and Konopa, 2000). Additionally, the absence of the two hydroxy groups (-OH) at positions C-5 and C-8 and poor solubility make NU:UB 65 inactive and lacking in anticancer activity. Therefore, it was hypothesized that attaching TPP to NU:UB 65 could modulate the activity of this compound. Herein, two TPP-NU:UB 65 derivatives were synthesized; first, the TPP was attached to one side chain of NU:UB 65. Secondly, TPP groups were attached to both side chains of NU:UB 65 and further investigation of the cytotoxicity effect and localization studies were performed. Additionally, the synthesis of OM25 and OM26, containing simple aminopentanol side chains without and any additional functional groups, was important as the methods developed during synthesis when controlling mono- or bis- attachment of TPP, could be used in later reactions when attaching TPP to ametantrone and mitoxantrone.

TPP-NU:UB 65 (OM25) was synthesized by reaction of NU:UB 65 (pre-dissolved in dichloromethane) with TPP. TPP and DCC were dissolved in dichloromethane and DMAP was added and allowed to react for 10 minutes. The mixture was added to NU:UB 65 and allowed to react for 1 hour **Figure 1.78**. The reaction was carried out in a very dilute solution and low equivalents of TPP and DCC (2 x 0.5 eq) were added twice to slow the reaction and make sure that TPP had been added on one side arm. The reaction progress was monitored by TLC. The reaction mixture was filtered to remove DCU. Solvent extraction was carried using dichloromethane and water followed by addition of sodium sulphate to remove any water residue in the reaction mixture. The solvents were evaporated to a lower volume before purification. OM25 was purified by column chromatography using solvent system 19:1 dichloromethane: methanol. The pure fractions were collected, filtered and evaporated to dryness. Diethyl ether was added to precipitate OM25 which was filtered and collected. The structure of OM25 was confirmed by its high resolution electrospray (+) mass spectrum which showed a clear signal at m/z

755.3590 which corresponded to the expected molecular mass of the cation. Also, there was a good correlation between the observed data and the theoretical isotope model for the $[C_{47}H_{52}N_2O_5P]^+$ cation.

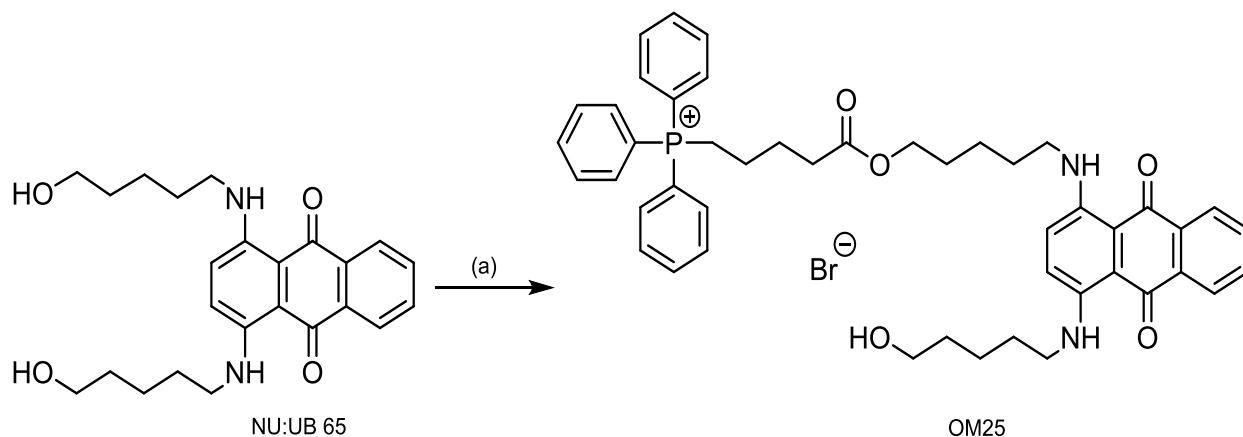


Figure 1.78: Reaction of NU:UB 65 with TPP. (a) TPP, DCC (2 x 0.5 eq) and DMAP in dilute solution of dichloromethane, 1 h.

1.3.3.14 Synthesis of bis-TPP-NU:UB 65 (OM26)

OM26 was synthesized by reaction of NU:UB 65 (pre-dissolved in dichloromethane) with TPP. TPP and DCC were dissolved in dichloromethane and DMAP was added and allowed to react for 10 minutes. The mixture was added to NU:UB 65 and allowed to react for 1 hour **Figure 1.79**. High equivalents of starting compounds and coupling agents (6 eq) were used in a concentrated solution to make sure that TPP added to both side chains of NU:UB 65. The reaction progress was monitored by TLC. The reaction mixture was filtered to remove DCU. Solvent extraction was carried out using dichloromethane and water followed by addition of sodium sulphate to remove any water residue in the reaction mixture. The solvents were evaporated to lower volume before purification. OM26 was purified by column chromatography using solvent system 19:1 dichloromethane: methanol. The pure fractions were collected, filtered and evaporated to dryness. Diethyl ether was added to precipitate OM26 which was filtered and collected. The structure of

OM26 was confirmed by its high resolution electrospray (+) mass spectrum which showed a clear signal at m/z 550.2491 at half mass for the doubly charged cation $[M-2Br]^{2+}$ **Figure 1.80**. Furthermore, there was a good correlation between the observed data and the theoretical isotope model for $[C_{70}H_{74}N_2O_6P_2]^{2+}$.

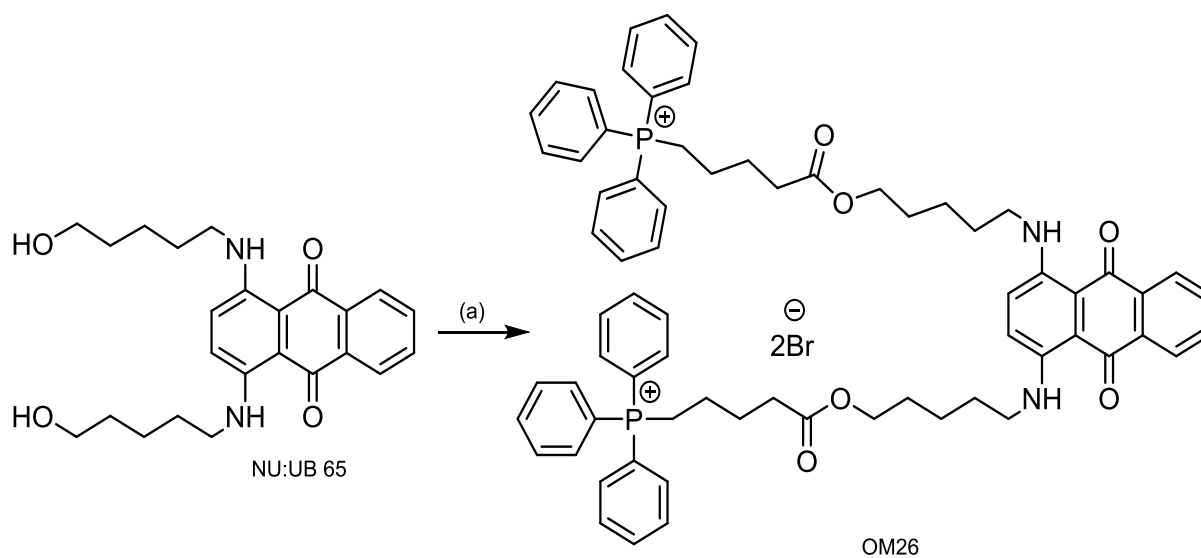
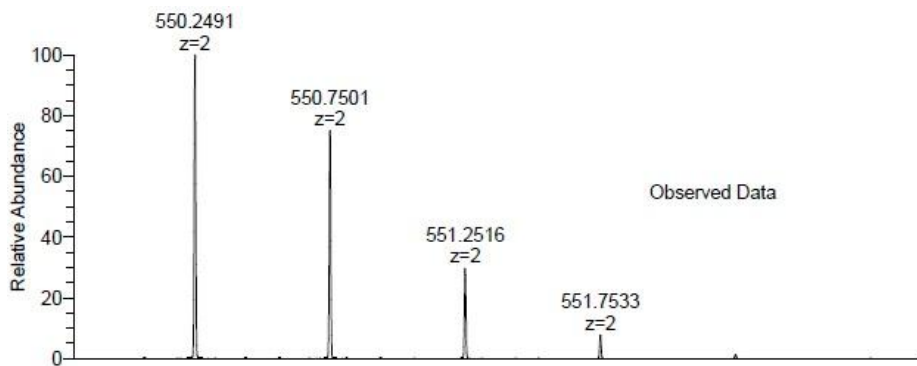
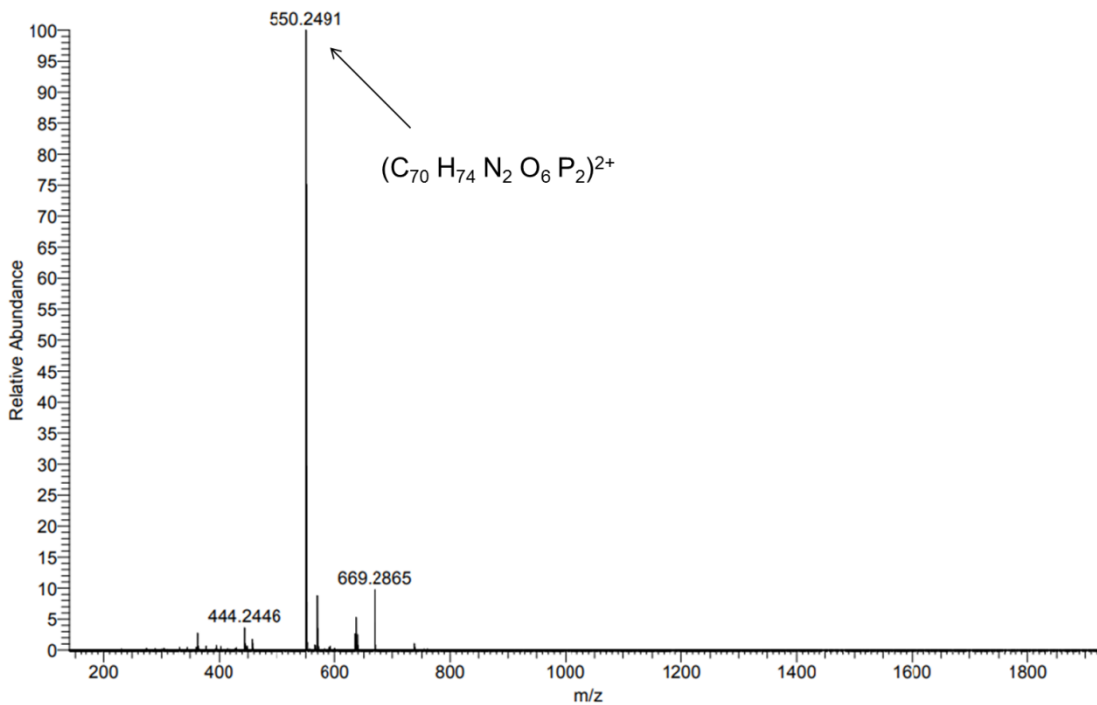
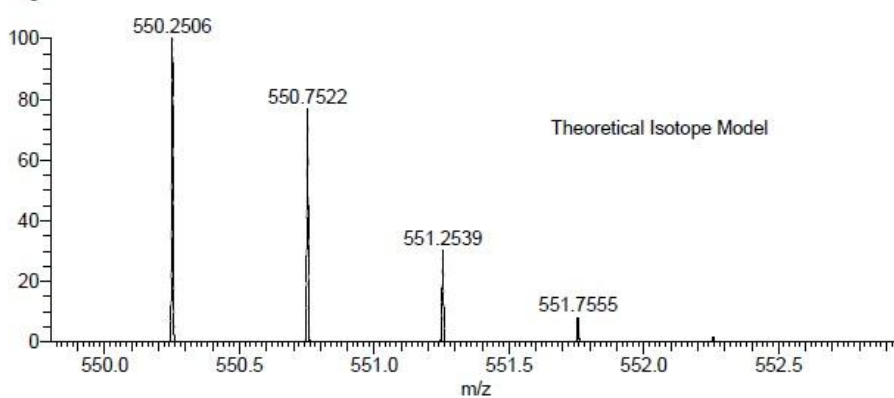


Figure 1.79: Reaction of NU:UB 65 with TPP. (a) high equivalent (6 eq) of TPP, DCC and DMAP in concentrated solution of dichloromethane, 1 h.



NL:
1.24E8
NAPMIN333-OA-HNESP#33-
46 RT: 0.72-1.05 AV: 13 T:
FTMS + p NSI Full ms
[140.00-1935.00]



NL:
1.07E4
C₇₀H₇₄N₂O₆P₂:
C₇₀H₇₄N₂O₆P₂
p (gss, s /p:40) Chrg 2
R: 100000 Res .Pwr . @FWHM

Figure 1.80: The ESI (+) mass spectrum of NU:UB 65

1.3.4 **Synthesis of mitoxantrone derivatives rhodamine B conjugates**

Rhodamine is the oldest, inexpensive and most popular dye used for different purposes such as fluorescent markers to study compounds structure under the microscope, laser dyes, photosensitizers (Meng *et al.*, 2007) and widely used in fluorescent probes (Wolfram *et al.*, 2018). Rhodamine has the ability to penetrate the cell more readily than fluoresceins due to the cationic charge of the rhodamine that can penetrate the negative plasma membrane potential within the cytoplasm of cells. Upon cell entry, rhodamine accumulates inside the mitochondria due to the lipophilic and cationic properties that allow it to pass through the high negative potential across mitochondrial inner membrane (Mottram *et al.*, 2012). In addition, rhodamine B can be used as a mitochondrial probe for determining the $\Delta\Psi_m$ of intact drug-resistant and drug-sensitive cells (Reungpatthanaphong *et al.*, 2003). Reungpatthanaphong *et al.*, (2003), designed a non-invasive method to determine and monitor the mitochondrial membrane potential $\Delta\Psi_m$. They found that rhodamine B accumulated in the matrix of mitochondria which was determined by the decrease of rhodamine B fluorescence in the presence of formazan, which acts as a quencher for rhodamine B (Reungpatthanaphong *et al.*, 2003). (Muli *et al.*, 2014) designed and synthesised asymmetric zinc phthalocyanine ZnPc-Rho B conjugates in which ZnPc-OH chromophores were linked with rhodamine B via a DIC-activated ester. ZnPc-Rho B were found to be more lipophilic than the unconjugated ZnPc precursors and attaching the rhodamine B moiety increased the phototoxicity of the dyes and the mitochondrial uptake compared with the unconjugated ZnPc (Muli *et al.*, 2014).

Based on this demonstrated mitochondrial cellular targeting of rhodamine B, in this research programme, rhodamine B conjugates were synthesised in which rhodamine B was linked with piperazine-succinate to form tertiary amide bond and lock the rhodamine B in the open-ring (fluorescent) form (Nguyen and Francis, 2003). Rhodamine B was also amide linked to β -alanine to conjugates that could ring open or ring close, depending upon pH (Beija *et al.*, 2009). These novel compounds were synthesised to compare the synthesis and purification differences between these conjugates and TPP-conjugates and the percentage yield obtained from the synthesis of each conjugates.

1.3.4.1 Synthesis of Rho- β -ala-O^tBu (OM6) and Rho- β -ala-OH (OM7)

OM6 was synthesized by reaction of rhodamine B with β -ala-O^tBu (1.1 eq) in DMF using PyBoP (1.5 eq) and DIPEA (4.6 eq) as a coupling conditions with stirring for 2 hours **Figure 1.81**. The reaction progress was monitored by TLC which showed that there was still unreacted rhodamine B, therefore additional amounts of β -ala-O^tBu (0.55 eq), PyBOP (0.75 eq) and DIPEA (2.3 eq) were added and stirring continued for another two hours. Solvent extraction was performed with water and chloroform. Sodium sulfate was added to remove any water followed by filtration and solvent evaporation. OM6 was purified by column chromatography using chloroform at the beginning then, more polar solvent was used, 9:1 chloroform: methanol + 1% pyridine. However, there were some impurities, therefore some fractions were purified again using the same solvent system. The pure fractions were filtered and evaporated to dryness followed by addition of water to solidify the product (OM6) and left overnight (4°C). The structure of OM6 was confirmed by high resolution electrospray (+) mass spectrum which showed a clear signal at m/z 570.3316 which corresponded to the expected molecular mass of the cation. Furthermore, there was good correlation between the observed data and the theoretical isotope model for $[C_{35}H_{43}N_3O_4]^+$.

Trifluoroacetic acid (TFA) was added and left overnight to remove O^tBu group **Figure 1.81**. TFA was evaporated and diethyl ether was added and left overnight with cooling (4°C) to precipitate the product OM7 which then was filtered and collected. The structure of OM7 was confirmed by high resolution electrospray (+) mass spectrum which showed a clear signal at m/z 514.2687 which corresponded to the expected molecular mass of the cation. Furthermore, there was a good correlation between the observed data and the theoretical isotope model for $[C_{31}H_{36}N_3O_4]^+$.

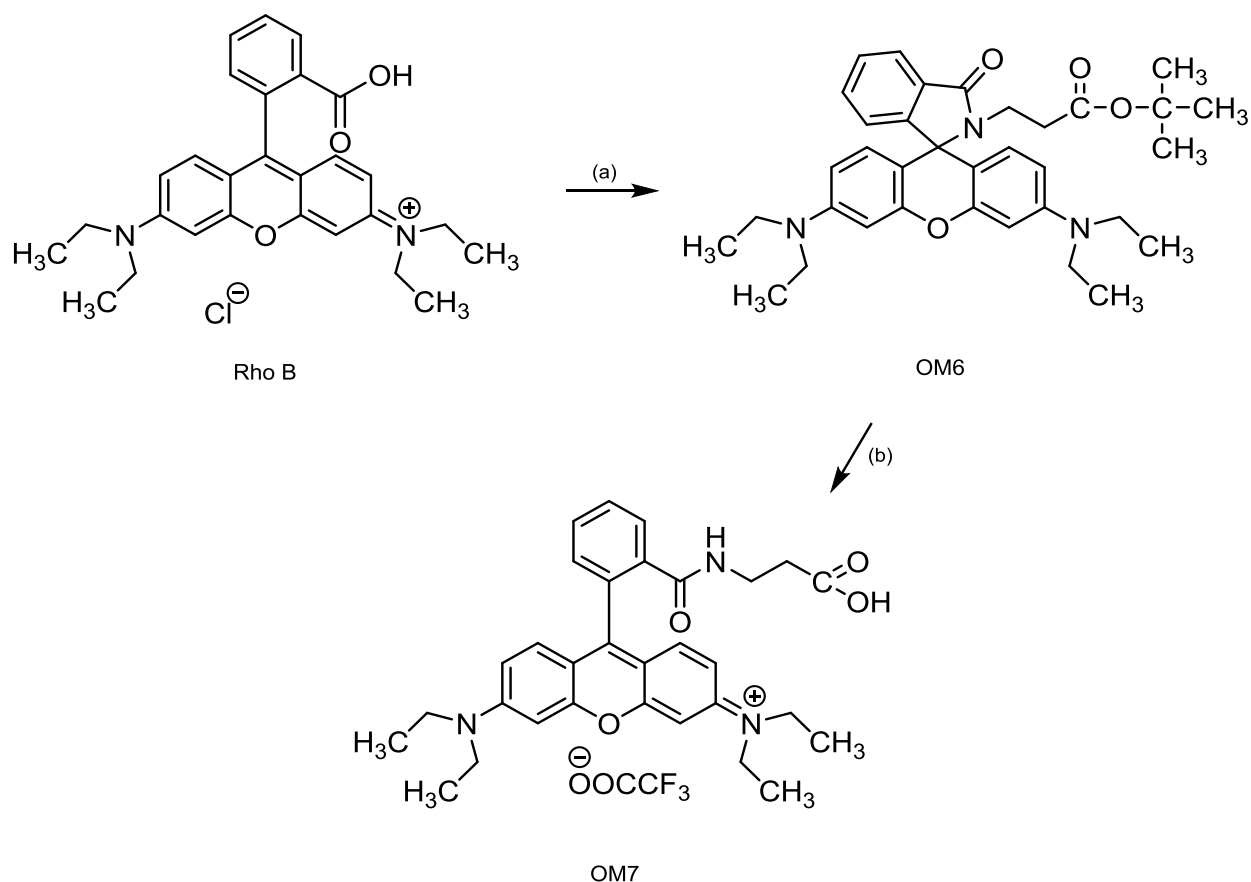


Figure 1.81: synthesis of OM6 and OM7. (a) HN- β -ala-O^tBu, PyBop, DIPEA, DMF, 2 h. (b) TFA, overnight.

1.3.4.2 Synthesis of Rho- β -ala-EAE-Boc-AQ (4-OH) (OM17) and Rho- β -ala-EAE-AQ (4-OH) (OM18)

OM17 was synthesized by the reaction of OM7 (1.1 eq) with pre-dissolved of HO-EAE-Boc-AQ (4-OH) (OM2) in dichloromethane using DCC (2.4 eq) and DMAP as a coupling agent **Figure 1.82**. The reaction was carried out over ice with stirring. However, OM7 did not completely dissolve in dichloromethane therefore a few drops of acetonitrile and DIPEA were added. The reaction progress was monitored by TLC, which showed after one hour that there was some of OM2 not reacted therefore, additional amounts of OM7 (0.55 eq) and DCC (1.2 eq) were added. The reaction mixture was filtered to remove DCU and extracted using dichloromethane and water. OM17 was purified by column chromatography using firstly dichloromethane alone to remove all rhodamine impurities

then the polarity of solvent was increased using 9:1 dichloromethane: ethyl acetate then 9:1 dichloromethane: ethyl acetate + 5% methanol. The impurities of fractions were monitored by TLC which showed that some fractions were not pure, therefore column chromatography was run again using firstly dichloromethane then dichloromethane + 5% ethyl acetate to remove all rhodamine impurities and finally, 9:1 dichloromethane: ethyl acetate was used to get pure OM17. The pure fractions were filtered and solvents were evaporated.

Trifluoroacetic acid (TFA) was added and left for 30 minutes to remove the Boc group **Figure 1.82**. TFA was evaporated and ethanol was added to lower the boiling point of TFA before adding diethyl ether to solidify the product. However, Rho- β -ala-EAE-AQ (4-OH) OM18 was not precipitated with diethyl ether therefore, hexane was used with few drops of 1,4-dioxane and cooled (4°C) overnight. OM18 was collected by centrifugation. The structure of OM18 was confirmed by high resolution electrospray (+) mass spectrum which showed a clear signal at m/z 822.3857 which corresponded to the expected molecular mass of the cation. Furthermore, there was a good correlation between the observed data and the theoretical isotope model for $[C_{49}H_{53}N_5O_7]^{2+}$.

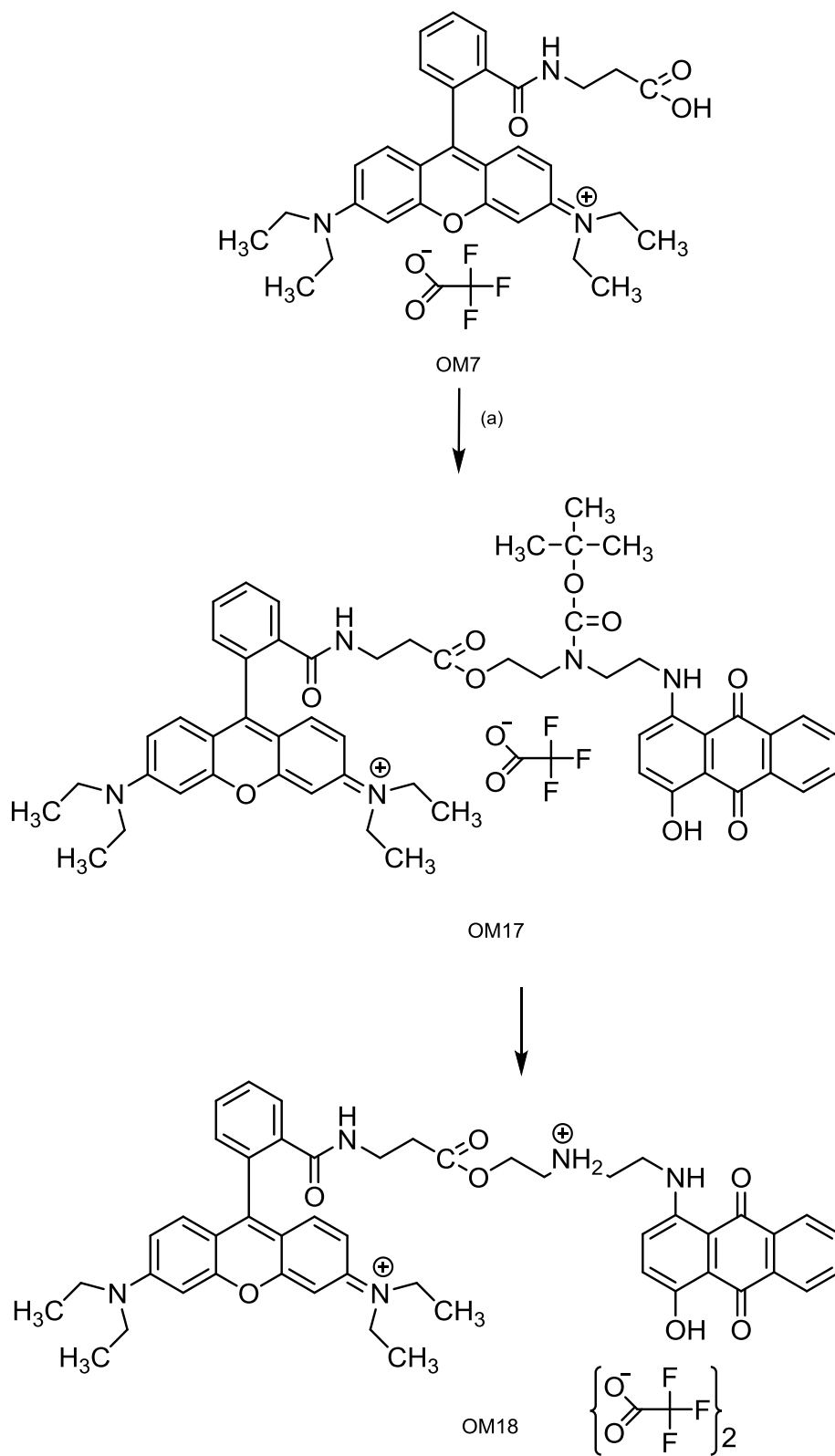


Figure 1.82: Reaction of OM2 with OM7 followed by reaction of OM17 with TFA. (a) OM2, DCC, DMAP, dichloromethane, overnight. (b) TFA, 30 min.

1.3.4.3 Synthesis of Rho-pip-Boc (OM4) and Rho-piperazine TFA (OM4 TFA)

Rhodamine B was dissolved in 2:1 dichloromethane: DMF and HATU was added as a coupling agent with triethylamine and allowed to activate for 10 minutes. Boc-piperazine was dissolved in 2:1 dichloromethane: DMF then added to activated rhodamine B. The reaction mixture was stirred at room temperature and was left overnight **Figure 1.83**. The reaction progress was monitored by TLC. Solvent extraction was with dichloromethane and water followed by addition of sodium sulphate to remove any water. The reaction mixture was filtered and solvents were evaporated to a lower volume before purification. OM4 was purified by column chromatography using 19:1 dichloromethane: methanol. The pure fractions were filtered and solvents were evaporated to dryness. Trifluoroacetic acid (TFA) was added and left overnight to remove the Boc group **Figure 1.83**. TFA was evaporated and 1,4-dioxane was added followed by the addition of diethyl ether to precipitate the product OM4 TFA which was filtered off and collected. The structure of OM4 TFA was confirmed by its high resolution electrospray (+) mass spectrum which showed a clear signal at m/z 511.3054 which corresponded to the expected molecular mass of the cation $[M-TFA]^+$. Furthermore, there was a good correlation between the observed data and the theoretical isotope model for $[C_{32}H_{39}N_4O_2]^+$.

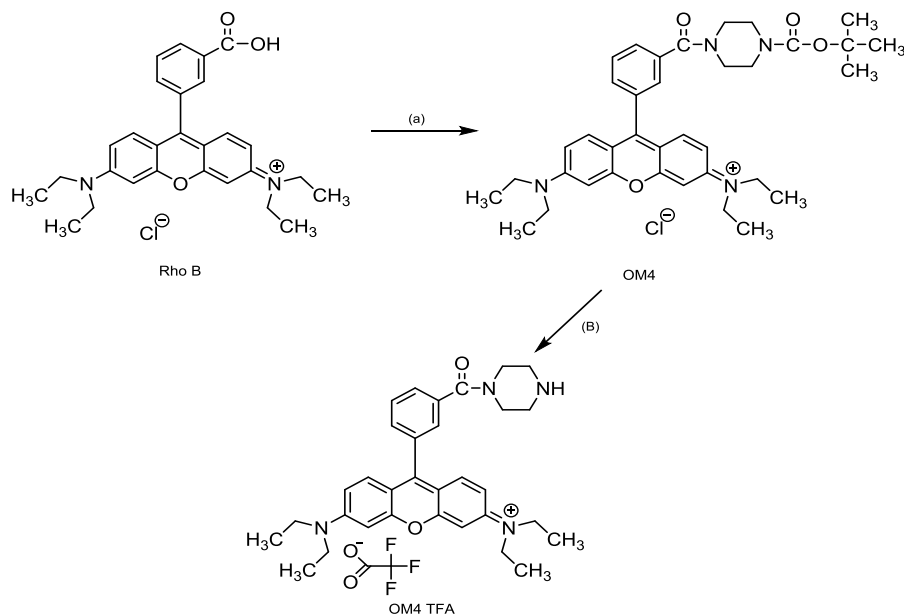


Figure 1.83: Reaction of Rho B with Boc-piperazine (a) Boc-piperazine, HATU, DIPEA, DMF/dichloromethane, overnight. (b) TFA, overnight.

1.3.4.4 Synthesis of Rho-pip-succinate (OM5)

OM5 was synthesized by reaction of Rho-piperazine-TFA (OM4 TFA) with succinic anhydride in DMF using DIPEA as a base **Figure 1.84**. The reaction progress was monitored by TLC. The reaction mixture was extracted using dichloromethane and water. However, during the extraction progress it was very difficult to see clear separation, therefore a small amount of reaction mixture was extracted every time while carefully collecting the organic layer to avoid any water contamination. The solvents were evaporated overnight at room temperature to get rid of all DMF. Diethyl ether was added to precipitate the product OM5 which was filtered off and collected.

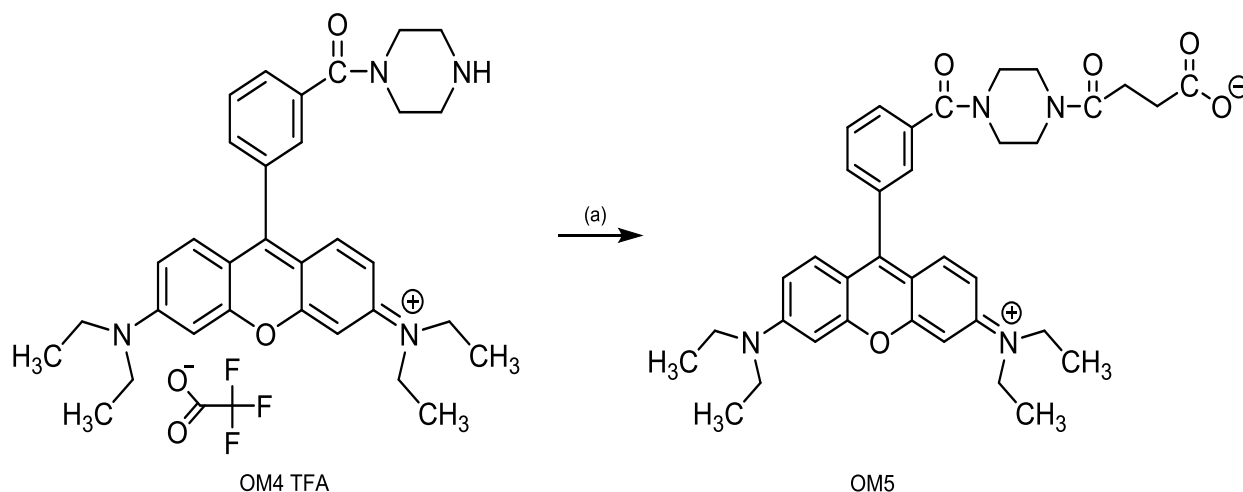


Figure 1.84: Reaction of OM4 with succinic anhydride to give OM5, (a) succinic anhydride, DIPEA, DMF, 1 h.

1.3.4.5 Synthesis of Rho-pip-succ-EAE-Boc-AQ(4-OH) (OM15) and Rho-pip-succ-EAE-AQ(4-OH) (OM16)

Rho-pip-succinate (OM5) and HO-EAE-Boc-AQ(4-OH) (OM2) were dissolved in dichloromethane and cooled over ice with stirring. The coupling agent DCC was dissolved in dichloromethane and DMAP was added as a catalytic base which then was added dropwise to the cooled mixture and allowed to react for 12 hours **Figure 1.85**. The reaction mixture was monitored by TLC. The reaction mixture was filtered off to remove DCU followed by solvent extraction with dichloromethane and water. The solvents were evaporated to a lower volume prior to purification. OM15 was purified by column

chromatography using firstly 9:1 dichloromethane: methanol which was too polar to start with because all the mixture ran through the column too quickly. Therefore, the solvent was switched to chloroform alone at the beginning and then the polarity of the solvents was increased slowly, 9:1 chloroform: ethyl acetate and 9:1 chloroform: methanol. The pure fractions were filtered off and solvents were evaporated to dryness. The structure of OM15 was confirmed by high resolution electrospray (+) mass spectrum which showed a clear signal at m/z 1019.4914 which corresponded to the expected molecular mass of the cation. Furthermore, there was a good correlation between the observed data and the theoretical isotope model for $[C_{59}H_{67}N_6O_{10}]^+$.

Trifluoroacetic acid (TFA) was added and left for 30 minutes to remove the Boc group **Figure 1.85**. TFA was evaporated and few drops of ethanol was added to lower the boiling point of TFA. Once the product was completely dry, diethyl ether was added to precipitate the product OM16 which was filtered off and collected. The structure of OM16 was confirmed by high resolution electrospray (+) mass spectrum which showed a clear signal at m/z 919.4388 which corresponded to the expected molecular mass of the cation $[M - TFA]^+$. Furthermore, there was good correlation between the observed data and the theoretical isotope model for $[C_{54}H_{60}N_6O_8]^+$.

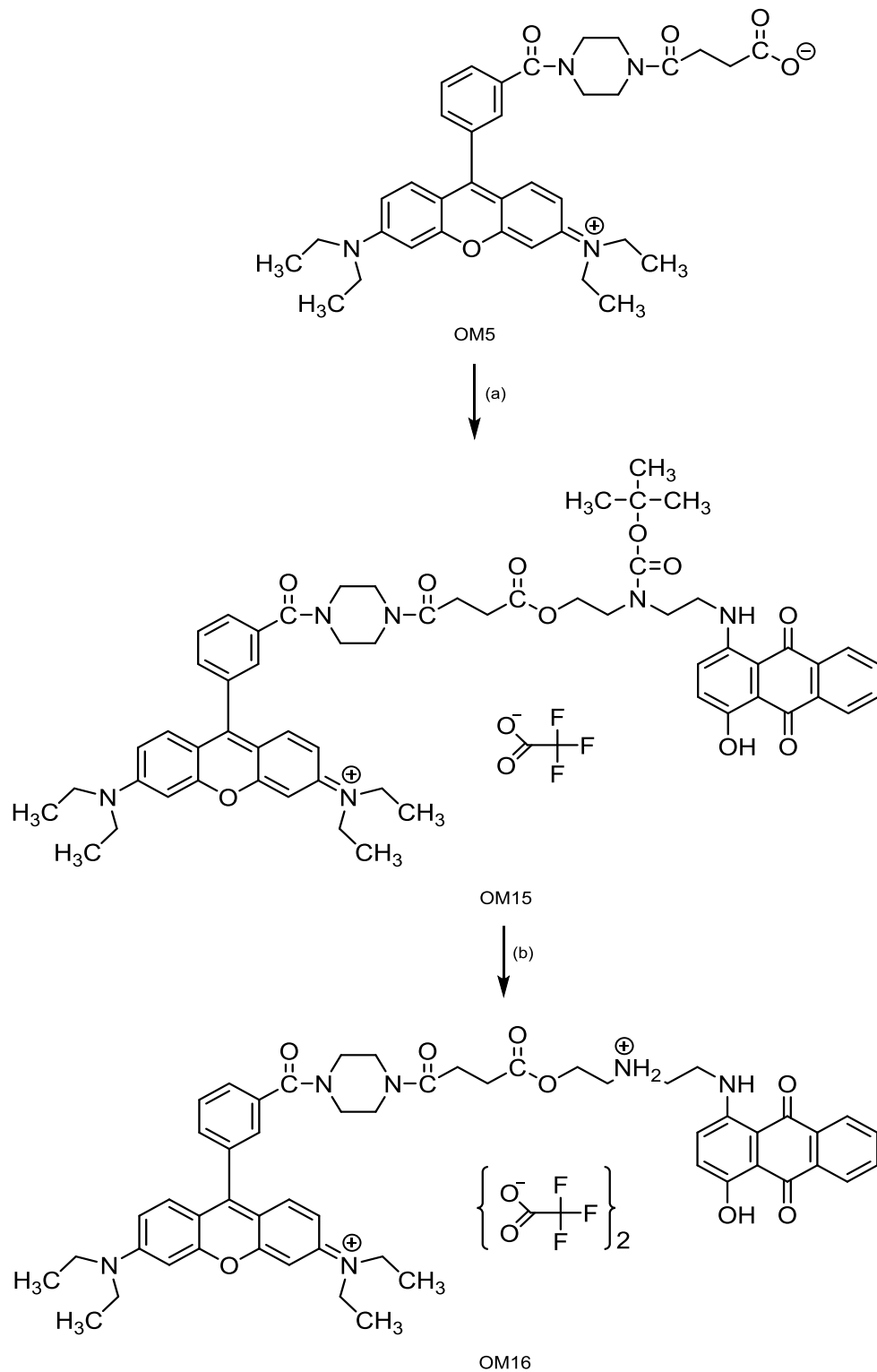


Figure 1.85: Reaction of OM2 with OM5 to give OM15 followed by deprotection of OM15 to give OM16. (a) OM2, DCC, DMAP, dichloromethane, 12 h. (b) TFA, 30 min.

1.3.5 **Synthesis of mitoxantrone and ametantrone-linked conjugate**

Mitoxantrone is an anticancer drug that was synthesized to reduce the cardiotoxic side effects associated with doxorubicin and daunomycin (Parker *et al.*, 2004). Mitoxantrone is used mainly in the treatment of prostate and breast cancer, lymphoma, acute leukemia and also multiple sclerosis (Rossato *et al.*, 2014). It has been reported that mitoxantrone accumulates inside the cell including the nucleus where it functions as a topoisomerase II inhibitor (Parker *et al.*, 2004). However, mitoxantrone is also a hydrophobic weak base and is trapped in acidic lysosomes and is highly accumulated in the lysosome (Zhitomirsky and Assaraf, 2015). The planar structure and the presence of nitrogen-containing side chains allow mitoxantrone to intercalate between DNA base pairs and bind with the phosphate backbone of DNA (Li *et al.*, 2005). Therefore, taking advantage of the unique structural features of mitoxantrone in binding to DNA and to reduce the side effects by altering the targeting and localization of mitoxantrone in mitochondria, mitochondrial targeted vectors were ester linked with mitoxantrone to increase the therapeutic index and reduce side effects. Additionally, the amino groups present in the side chains of the mitoxantrone were protected with a Boc group to prevent any side reaction that could happen during the attachment of TPP with mitoxantrone. The Boc group was then removed by TFA to afford the final product.

Ametantrone has a similar structure to mitoxantrone but without the two hydroxy groups at positions C-5 and C-8. Although mitoxantrone is 100-fold more potent than ametantrone due to the absence of the hydroxy groups at these positions (Kapusinski and Darzynkiewicz, 1986). Also, it has been reported that ametantrone has lower efficacy on tumour cells of breast cancer, ovarian cancer, melanomas and small cells lung cancer. Therefore, further development of ametantrone was stopped (Piccart *et al.*, 1981; Rozenzweig *et al.*, 1985). Herein, a novel ametantrone-TPP conjugate was developed and synthesized to evaluate the effect of attaching a TPP carrier to study the changes in physiochemical properties as a result

1.3.5.1 Synthesis of Mitoxantrone-Boc (OM19)

Mitoxantrone was dissolved in methanol and was stirred and cooled with addition of DIPEA, Boc₂O (4 eq) dissolved in methanol added dropwise to the solution and left to react for 1 hour **Figure 1.86**. The reaction progress was monitored by TLC which showed there was some unreacted mitoxantrone, therefore a further half equivalent of Boc₂O was added and allowed to react overnight. The reaction mixture was filtered to remove any unreacted Boc₂O and was extracted using dichloromethane and water. OM19 was purified by column chromatography using dichloromethane alone at the beginning to remove any unreacted Boc₂O and other impurities, then a more polar solvent system was used; 9:1 dichloromethane: methanol. After purification, iodine was used to check if there were any invisible impurities that could not be detected by UV or visible light because iodine reacts with any hydrocarbon to give a brown color. The TLC of OM19 was left in an iodine chamber for 5 minutes and after the plate was removed there was no color indicating that the product was free from organic impurities. The pure fractions were collected and solvents were evaporated followed by addition of diethyl ether to precipitate the product OM19. However, OM19 did not precipitate easily with diethyl ether therefore, an empty round bottom flask was weighed and the product was transferred; then the solvents were completely evaporated to dryness.

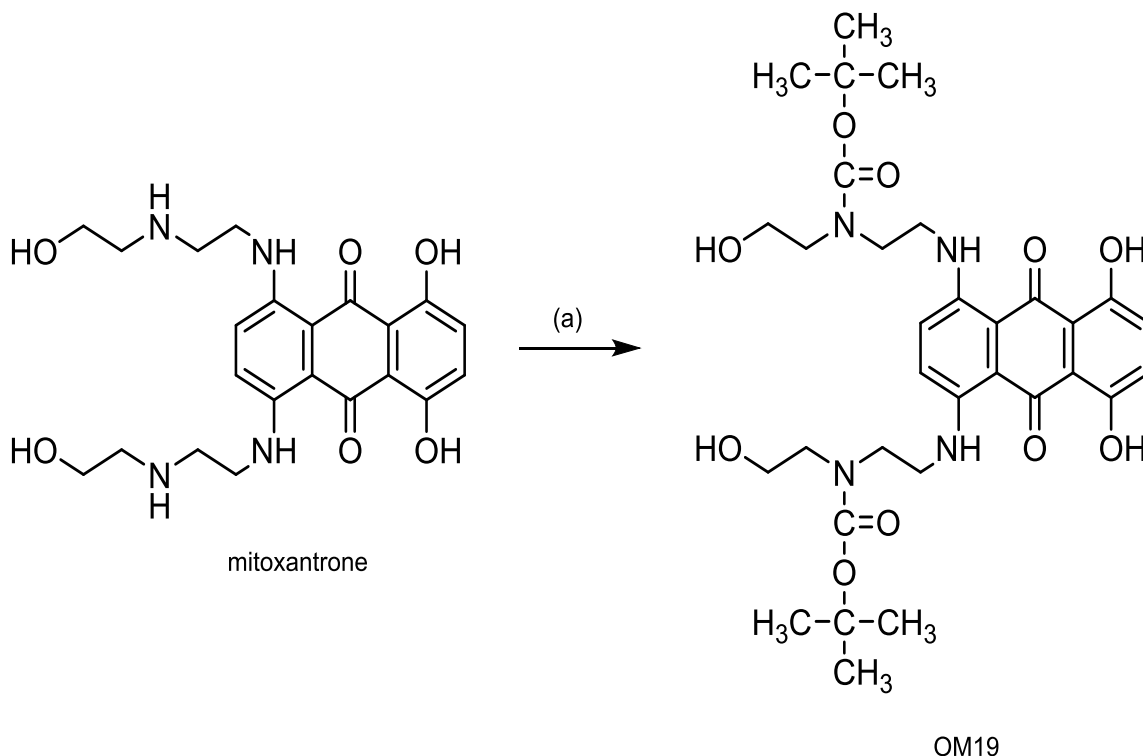


Figure 1.86: Reaction of mitoxantrone with Boc_2O . (a) Boc_2O , DIPEA, methanol, 1 h.

1.3.5.2 Attempted synthesis of Rho-pip-succ-mitoxantrone-Boc (OM20) and Rho-pip-succ-mitoxantrone (OM21)

Mitoxantrone-Boc (OM19) and OM5 (1.1 eq) were dissolved in dichloromethane and stirred with cooling. The coupling agent DCC (2.4 eq) was dissolved in dichloromethane and DMAP was added and the mixture was cooled and added dropwise to OM19 and OM5 and allowed to react for 1 hour **Figure 1.87**. The reaction progress was monitored by TLC which showed that some OM19 did not react with OM5 therefore, a half equivalent of the original amount of DCC (1.2 eq) was added and allowed to react overnight. After the end of the reaction, the TLC showed that there were two new products. The reaction mixture was filtered to remove DCU followed by solvent extraction with dichloromethane and water. The solvents were evaporated to a lower volume before purification. OM20 was purified by column chromatography using dichloromethane alone first followed by using more polar solvents, 9:1 dichloromethane: ethyl acetate, 4:1 dichloromethane: ethyl acetate + 5% methanol and 4:1 dichloromethane: methanol. However, a very polar

product could not be eluted from the column so methanol was used and the product was left under methanol to elute from silica. The impure fractions were purified again using the same solvents system as previously. The pure fractions were collected, filtered and evaporated to dryness. The structure of OM20 was characterized by its high resolution electrospray (+) mass spectrum which showed two main signals at m/z 1351.6486 and 687.3192 which did not correspond to the expected molecular mass of the cation at 1826.1211, this indicated unsuccessful synthesis of OM20.

Trifluoroacetic acid (TFA) was added and left for 30 min to remove Boc₂O group **Figure 1.88**. TFA was evaporated and ether was added to precipitate the product OM21 which was filtered and collected. The structure of OM20 was tested by high resolution electrospray (+) mass spectrum which showed three main signals at m/z 460.2225, 919.4388 and 969.1782 which did not correspond to the expected molecular mass of the cation at 919.4388 and this also indicated the unsuccessful synthesis of OM21.

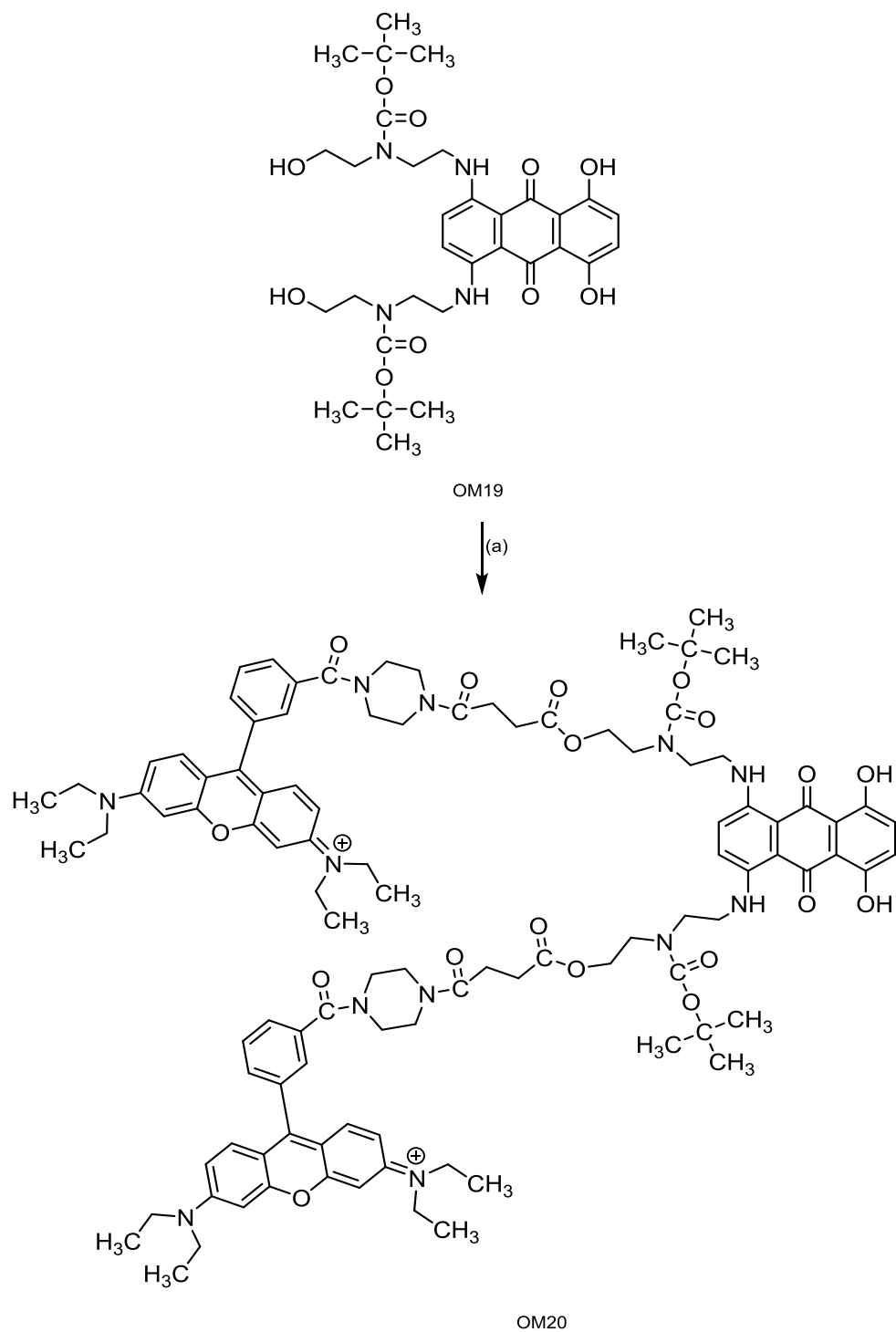


Figure 1.87: Reaction of OM19 with Rho-pip-succinate. (a) Rho-pip-succinate, DCC, DMAP, dichloromethane, 1 h.

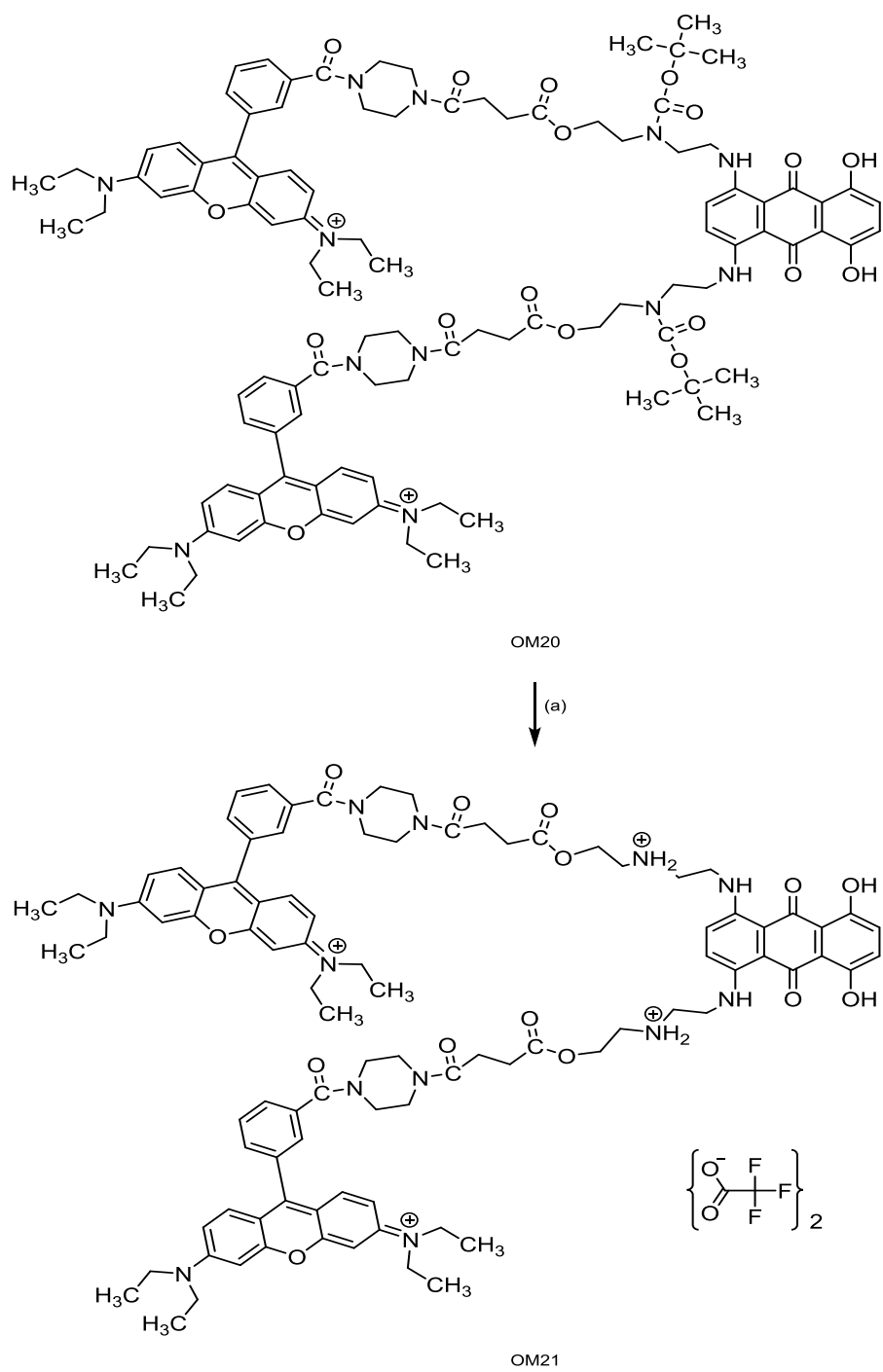


Figure 1.88: Reaction of OM20 with TFA. (a) TFA, 30 min

1.3.5.3 Attempted synthesis of TPP-mitoxantrone-Boc (OM23) and bis-TPP-mitoxantrone-Boc (OM24)

Mitoxantrone-Boc (OM19) was dissolved in dichloromethane and was stirred with cooling. TPP and DCC were dissolved in dichloromethane and DMAP was added and allowed to activate for 10 minutes. The mixture was added to OM19 and allowed to react for 1 hour **Figure 1.89**. TPP and DCC were added 3 times with small equivalents in a very dilute solution to give the mono-TPP compound (OM23). The equivalents of TPP and DCC were increased an additional three times to give the bis-TPP compound (OM24). The reaction progress was monitored by TLC. The reaction was extracted with dichloromethane and water. The products were purified by column chromatography using dichloromethane first then more polar solvents were used, 19:1 dichloromethane: methanol to get OM23 then, the solvents system was changed to 9:1 dichloromethane: methanol and 4:1 dichloromethane: methanol to get OM24. However, there was an unknown compound not moving with these solvents, therefore methanol was added and left overnight to get the compound from the silica. The pure fractions were collected and solvents were evaporated followed by addition of diethyl ether to precipitate OM23 and OM24. The structure of OM24 was tested by high resolution electrospray (+) mass spectrum which showed the main signal at m/z 580.2807 which did not correspond to the expected molecular mass of the cation (2^+) at 667.2919 and this indicated unsuccessful synthesis of OM24.

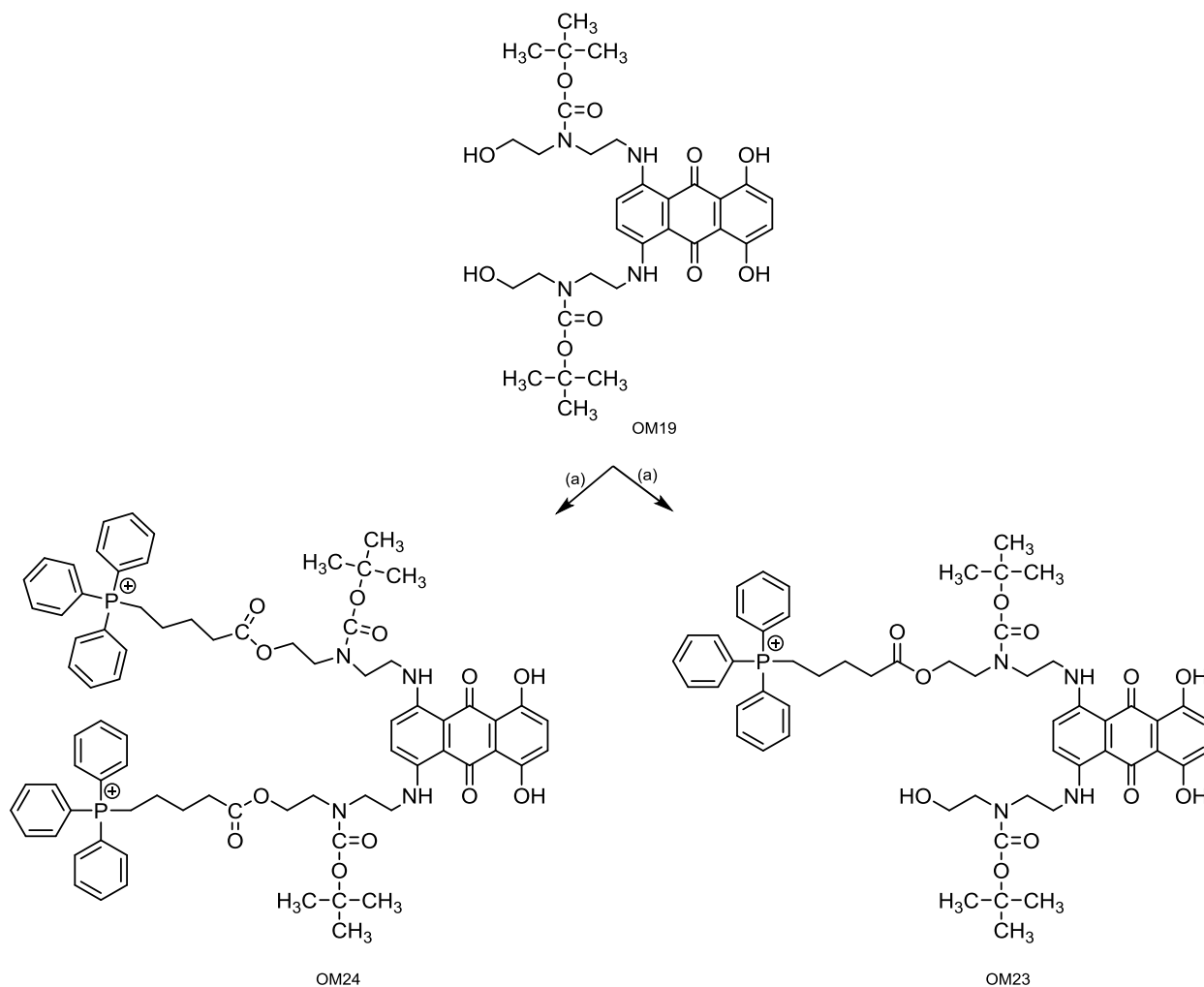


Figure 1.89: Reaction of OM19 with TPP. (a) high equivalent of TPP, DCC and DMAP. dichloromethane, 1 h.

Therefore, the synthesis of mitoxantrone-linked prodrugs was unsuccessful as unknown products were obtained. However, further identification of these products is required to identify the reason behind the failure of the synthesis. In addition, new method should be developed to synthesis the mitoxantrone-linked prodrugs and this will be in a future study.

1.3.5.4 Synthesis of ametantrone (NK1)

NK1 was produced by the reaction of leucoquinizarin with a large excess of *N*-(2-hydroxyethyl)ethylenediamine. The reaction mixture was heated in dichloromethane over a water bath for one hour until the colour of the mixture became greenish blue. The intermediate was oxidized with O₂ with the addition of few drops of triethylamine and the color changed to deep blue over one hour **Figure 1.90**. The oxidation progress was monitored by TLC which shows there were still some unoxidized leuco-products therefore, more triethylamine was added and the air oxidation was continued for another 3.5 hours. NK1 was separated from some impurities by dissolving the reaction mixture in ethanol and heating over a boiling water bath (with a water condenser) for 2 hours, followed by the cooling. A blue solid was precipitated and then separated from the green solvent. NK1 was filtered and more ethanol was added to remove any remaining impurities. The TLC was checked and showed that the ethanol residual solvent contained more ametantrone and less impurities whereas the solid from partial separation still contained the impurities from the ametantrone initial reaction, therefore this method was unable to completely separate the NK1 from the impurities and was decided the subsequent reaction would be continued without separating ametantrone from the impurities.

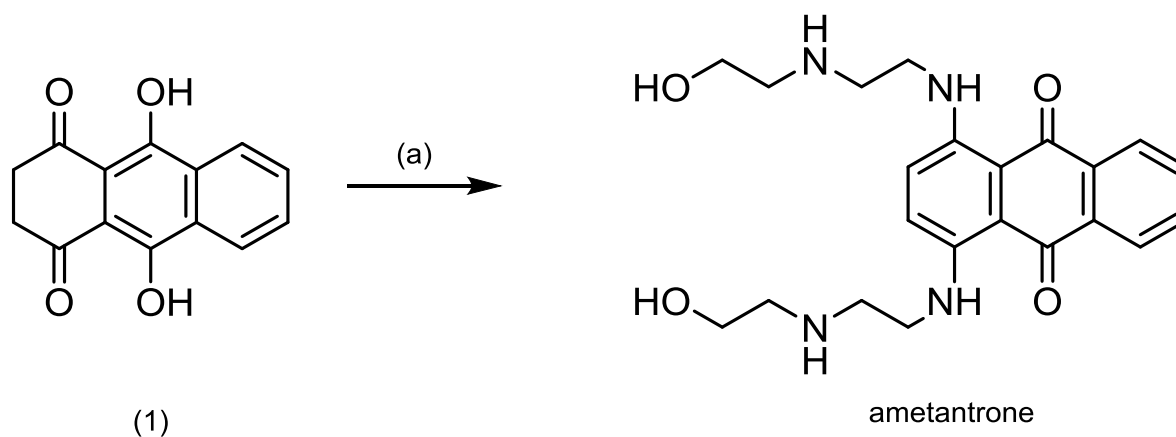


Figure 1.90: Reaction of leucoquinizarin with *N*-(2-hydroxyethyl)ethylenediamine. (a) *N*-(2-hydroxyethyl)ethylenediamine, dichloromethane, 50°C, condensation, 1 h. (b) triethylamine, O₂, 4.5 h.

1.3.5.5 Synthesis of Ametantrone-Boc (NK4)

Ametantrone (NK1) was dissolved in methanol and stirred over ice. Boc_2O in cold methanol was added dropwise to the solution to let the reaction occur slowly. The solution was left over ice and allowed to react for 1 hour **Figure 1.91**. The reaction progress was monitored by TLC. Solvent extraction was carried out using chloroform and water to destroy the unreacted Boc_2O with water. Sodium sulfate was added to the organic layer to remove excess water in the solution by forming sodium sulfate hydrate. The mixture was filtered and dried before purification. NK4 was purified by column chromatography using chloroform alone at the beginning followed by using more polar solvents, chloroform : ethyl acetate (19:1), chloroform: ethyl acetate (19:1) + methanol 2%, chloroform : ethyl acetate (9:1) + methanol 2%, chloroform : ethyl acetate (9:1) + methanol 4%, and chloroform : ethyl acetate (9:1) + methanol 6% until all NK4 was removed from the column.

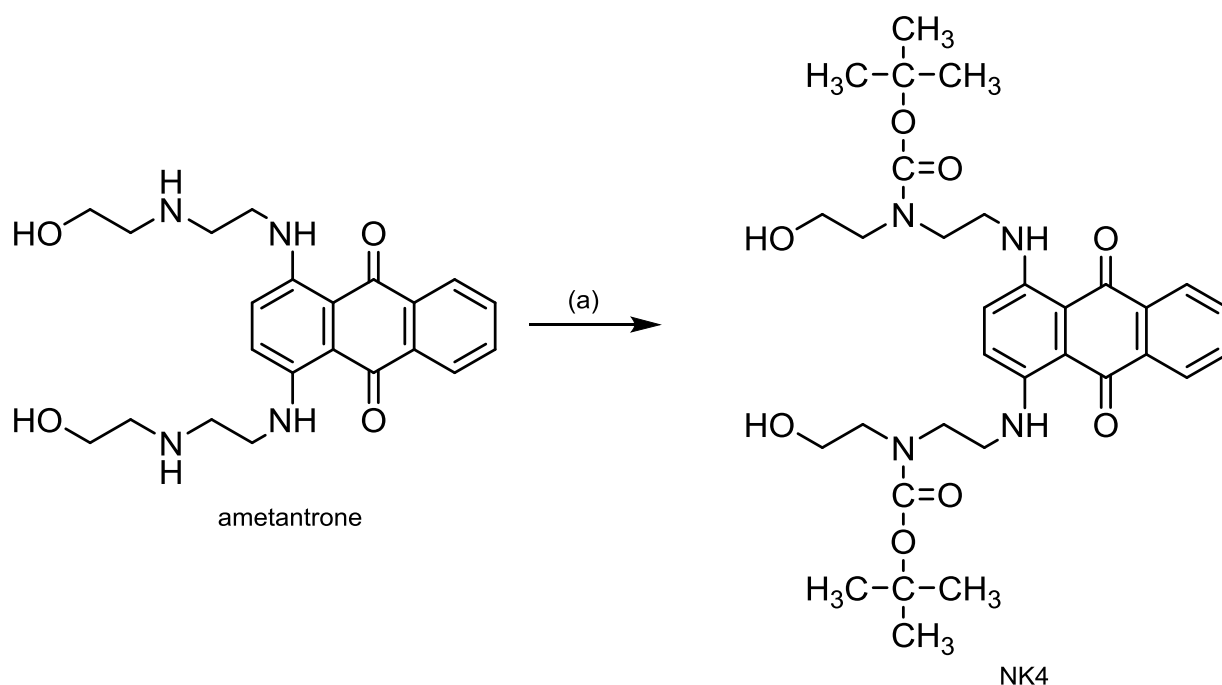


Figure 1.91: Reaction of ametantrone (NK1) with Boc_2O . (a) Boc_2O , methanol, 1 h.

1.3.5.6 Synthesis of TPP-ametantrone-Boc (NK6) and TPP-ametantrone-TFA (NK8)

NK6 was synthesized by dissolving ametantrone-Boc (NK4) in DMF and TPP was dissolved in DMF with the coupling agent HATU and 4-methylmorpholine to activate TPP carboxylic acid, which were added to NK4 in DMF. The mixture was left to react for 1 hour with stirring **Figure 1.92**. The reaction progress was monitored by TLC which showed that NK4 and TPP still in abundance and only a little of NK4 was formed therefore, the reaction was continued by heating (water bath 40°C) without stirring for another 1.5 hours. After 1.5 hours, the TLC showed that more NK4 was formed and TPP was barely visible therefore, it was decided that the reaction was continued for another hour without addition of more coupling agents. After twenty hours, TLC showed that NK6 had formed although the reaction was not complete. Solvent extraction was performed with chloroform and water. The organic layer was collected and dried before purification. NK6 was purified by column chromatography using chloroform initially and then more polar solvent chloroform: ethyl acetate (19:1), chloroform: ethyl acetate (19:1) + methanol 1%, chloroform: ethyl acetate (19:1) + methanol 2% were used. The pure fractions were collected and dried. The structure of NK6 was confirmed by high resolution electrospray (+) mass spectrum which showed main signal at m/z 651.2971 which corresponded to the expected molecular mass of the doubly charged cation. Furthermore, there was a good correlation between the observed data and the theoretical isotope model for $[C_{78}H_{88}N_4O_{10}P_2]^{2+}$, which indicated successful synthesis of NK6.

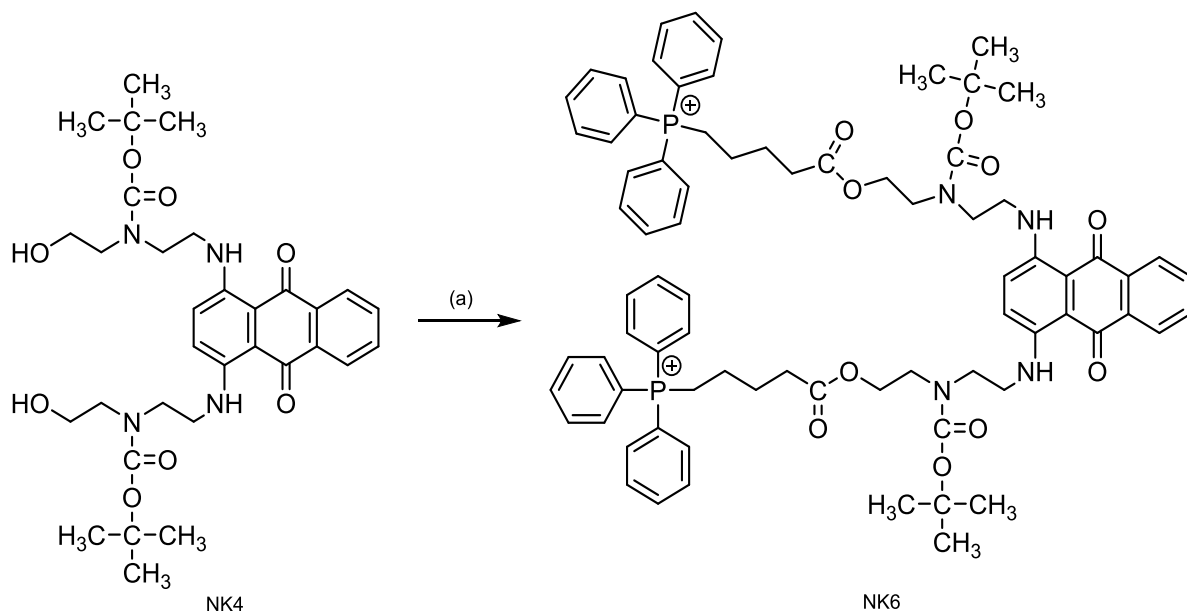


Figure 1.92: Reaction of TPP with NK4. (a) TPP, HATU, 4-methylmorpholine, DMF, room temperature for 1 h, 40°C for 1.5 h, room temperature for 18 h.

Trifluoroacetic acid (TFA) was added and left for 30 minutes to react with TPP-ametantrone-Boc (NK6) to remove the Boc group **Figure 1.93**. TFA was evaporated and a few drops of ethanol were added to lower the boiling point of TFA. Once the product was completely dry, diethyl ether was added to precipitate the product NK8 which was filtered off and collected. The structure of NK8 was confirmed by high resolution electrospray (+) mass spectrum which showed the main signal at m/z 551.2442 for the doubly charged cation and this corresponded to the expected molecular mass of the compound and indicated the successful synthesis of NK8 **Figure 1.94**.

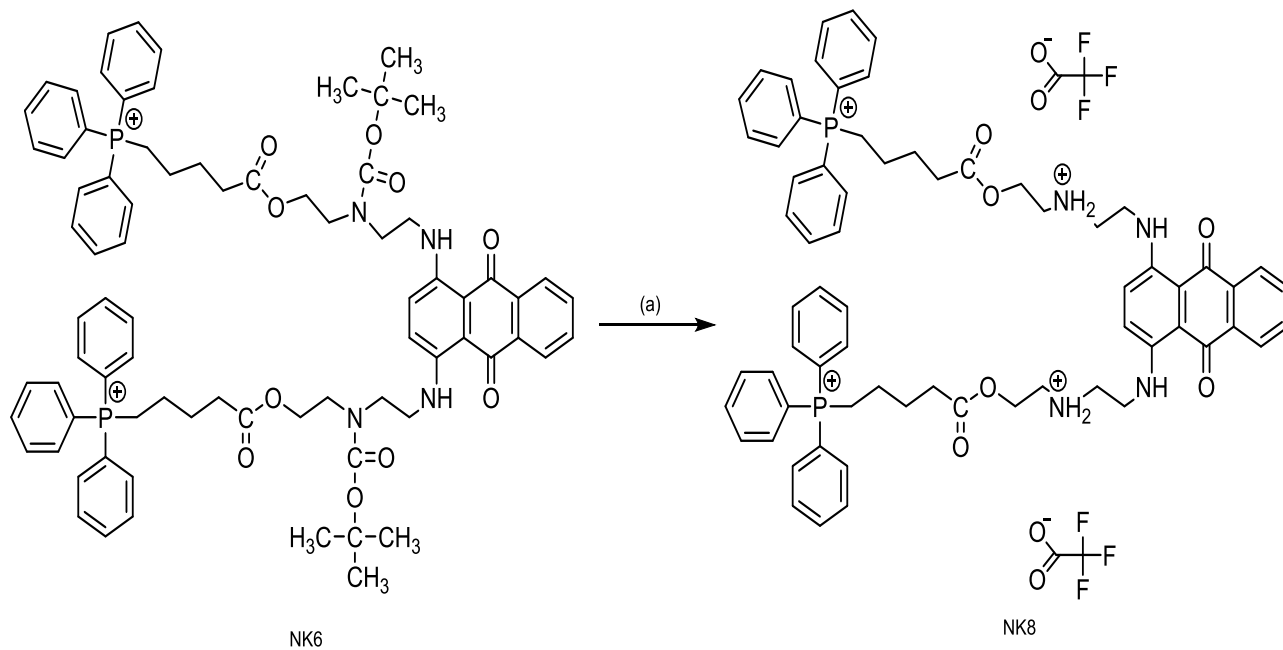


Figure 1.93: Reaction of NK6 with TFA. (a) TFA, 30 min

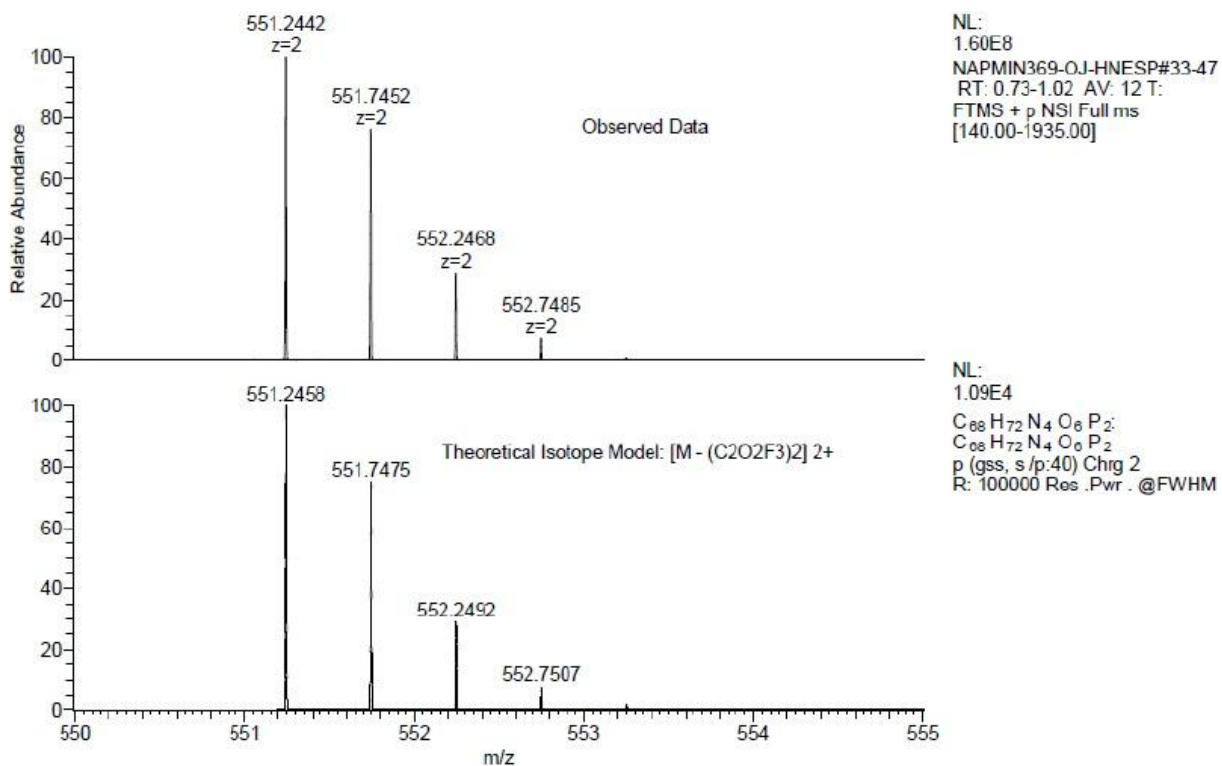
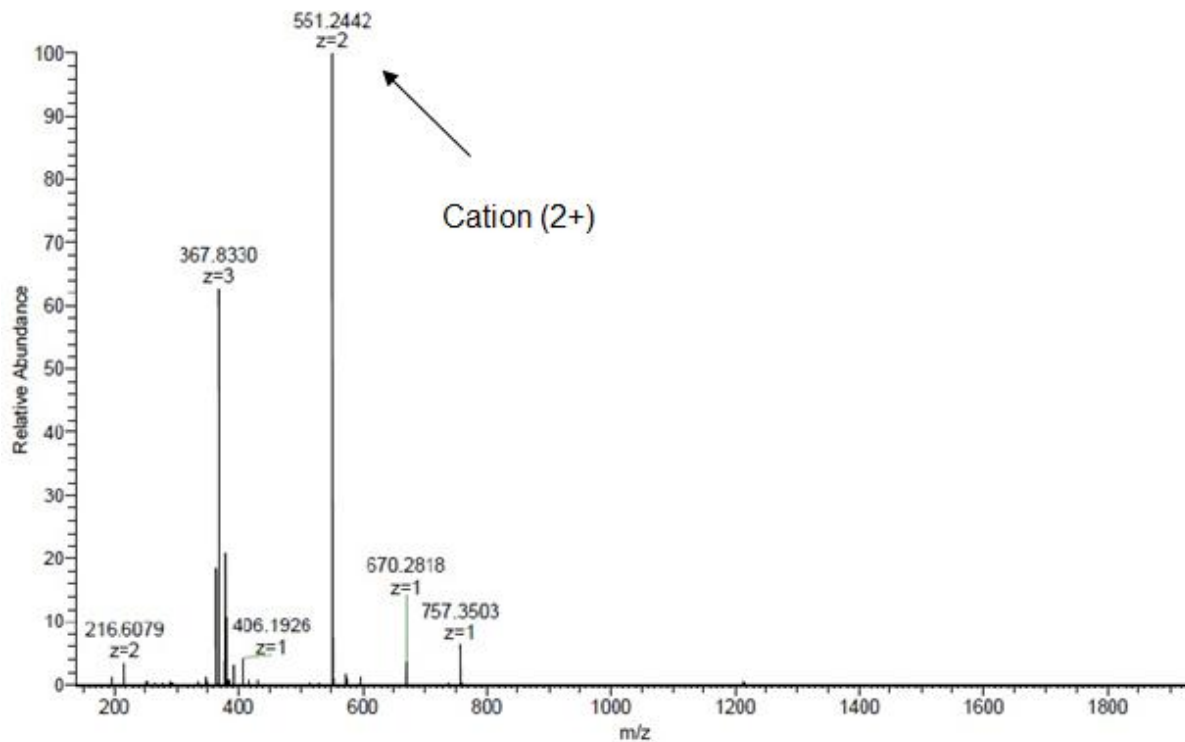


Figure 1.94: The ESI (+) mass spectrum of NK8

In conclusion, the synthesis of a series of TPP-conjugated compounds was successful and the compounds were characterized by their high resolution electrospray (+) mass spectra and ^1H NMR and ^{13}C NMR. However, the synthesis of OM23 and OM24 (mitoxantrone-TPP) was unsuccessful. *In vitro* assays such as DNA binding, distribution coefficient, cytotoxicity (MTT), confocal microscopy imaging and morphology studies were then performed for selected compounds as described in the following sections. Although, rhodamine B-conjugated compounds were also successfully synthesized, the synthesis and purification of these compounds were more complicated due to the presence of rhodamine B in compared with the TPP-conjugated compounds which the synthesis and purification was easier. In addition, the yield obtained from the reaction of TPP with mitoxantrone derivatives was much higher than the yield obtained from the reaction of rhodamine B with mitoxantrone derivatives. Therefore, it was decided to focus on the TPP conjugate compounds for further evaluations and *in vitro* assays.

1.3.6 **DNA binding assay**

Development of new chemotherapeutic agents has been a main subject of interest for many years (Al-otaibi *et al.*, 2017). Large percentages of these anticancer drugs are designed to target the DNA by interacting with DNA directly or by preventing the relaxation of DNA, through the inhibition of topoisomerases (Palchaudhuri and Hergenrother, 2007). The unique structure of the double helix of DNA, that contains two sugar-phosphate polyelectrolyte strands that bond with each other through a hydrogen bond between nucleotide bases, makes the DNA an attractive molecule inside the cell to be targeted to inhibit DNA replication, transcription and gene expression. Anticancer drugs interact with DNA by two main mechanisms; covalent interaction and non-covalent interactions are classified into intercalation and groove binding (Adhikari and Mahar, 2016). In the intercalation process, a planar aromatic molecule binds with DNA by insertion of the planar aromatic rings between the DNA base pairs which results in decrease the DNA length and DNA helical twist. The stability of the intercalation complex is established by hydrogen bonding, van der Waals and electrostatic forces. In addition, the presence of

electrophilic, cationic and basic functional groups are important factors for the genotoxicity of the intercalators (Palchaudhuri and Hergenrother, 2007). Among all these properties, anthraquinones, which have aromatic planar structures, are an important class of anticancer drug, known to intercalate with DNA between the base pairs of the DNA double helix resulting in significant changes in DNA which in turn inhibit the DNA replication, inhibition of topoisomerase II and leading to irreversible DNA damage (Alotaibi *et al.*, 2017). In addition, mitoxantrone is the leader of the anthraquinone compounds that bind with DNA and used in the treatment of breast cancers, ovarian cancers and haematological malignancies has a significant cytotoxic activity (Kamal *et al.*, 2007).

However, *in vitro* experiments can be performed to study the binding of the anticancer drugs with DNA. The most popular method to measure the binding affinity of anticancer drugs with DNA, is using a fluorometric monitoring of the reaction between the DNA and a fluorescent compound that has the ability to bind with DNA and its fluorescence emission can increase upon binding with DNA. The most popular fluorescent compound that has the ability to bind with DNA is ethidium bromide (EtdBr) (Alonso *et al.*, 2006).

Therefore, in this research programme, a DNA binding assay was carried out to study the binding affinity of the novel compounds with calf thymus DNA (CT DNA) by displacing ethidium bromide from the fluorescent DNA-ethidium bromide complex. Ethidium bromide (EtdBr) [(3,8-diamino-5-ethyl-6-phenyl phenanthridinium bromide)] **Figure 1.95** has the ability to intercalate between base pairs in both double stranded DNA and RNA and enhances the fluorescence intensity of ligand-DNA and ligand-RNA complexes. Therefore, this method was used to study the binding of DNA with EtdBr and other compounds that noncompetitively or competitively inhibit the binding between DNA and EtdBr (Alonso *et al.*, 2006). When EtdBr binds with DNA, the fluorescence of EtdBr can increase by 24-fold. However, when EtdBr is displaced from its intercalated site, its fluorescence can decrease by 24-fold and its excitation spectrum will be shifted (Palchaudhuri and Hergenrother, 2007).

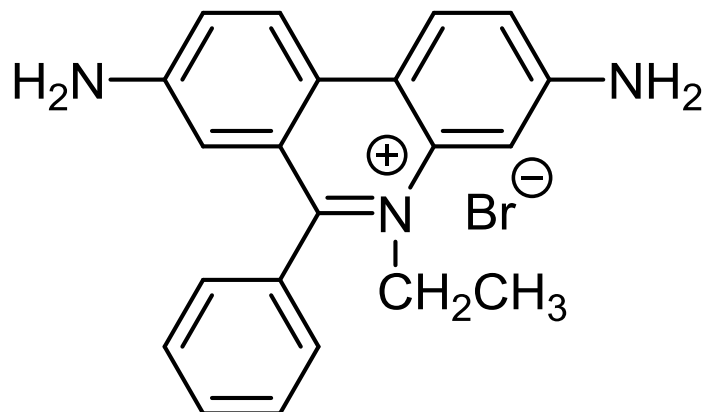


Figure 1.95: Chemical structure of ethidium bromide (EtdBr)

During the addition of active agent, aliquots of compounds were used and the concentration of each compound was increased each time until a decrease by 50% in the fluorescence intensity (of the ethidium-CT DNA complex) was achieved. QE_{50} values were calculated by plotting the fluorescence intensity against compound concentration and were calculated from the mean value ($n = 3$). The QE_{50} value is the mean concentration of the test compound required to reduce the initial fluorescence of the starting DNA-bound ethidium complex by 50%. The apparent binding constant (K_{app}) was calculated from the equation $K_{app} = (KEB[EB])/[Drug]$, where the binding constant for the CT DNA-ethidium complex was taken from the literature value for mitoxantrone as reported by (Kundu *et al.*, 2011), therefore, the smaller the QE_{50} value, the greater binding affinity of the compound with CT DNA.

1.3.6.1 Mitoxantrone 2HCl DNA binding

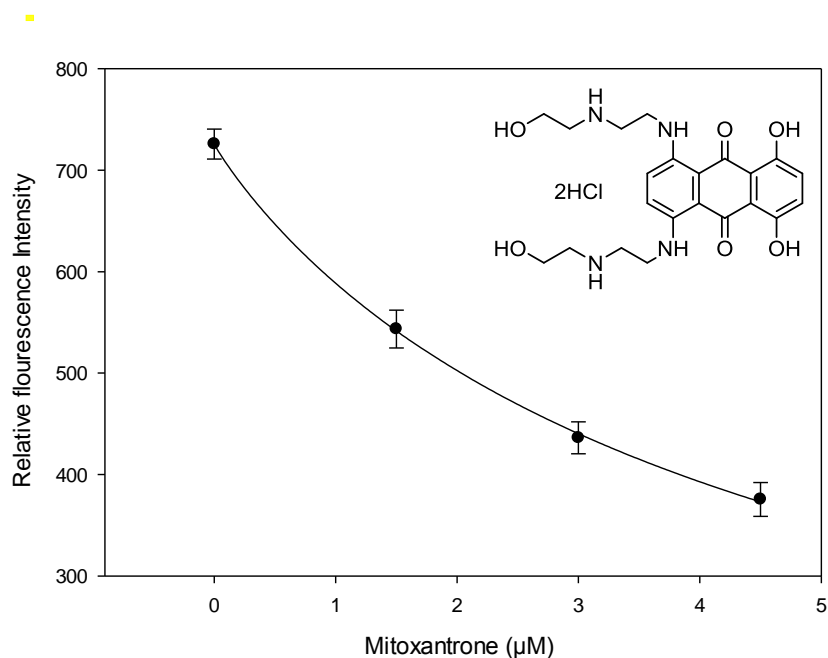


Figure 1.96: Variation of relative fluorescence intensity of CT-DNA (60 μM) with pre-bound EtdBr (30 μM) when treated with different concentrations of mitoxantrone in PBS buffer. λ_{ex} 480 nm; λ_{em} 610 nm (n = 3).

	Coefficient	Std. Error	t	p
Min	-0.0000	0.0000	(+inf)	<0.0001
Max	725.98	5.16	140.52	<0.0001
QE₅₀	4.77	0.15	31.04	<0.0001

The concentration of mitoxantrone 2HCl when the relative fluorescence intensity reached 50% was $4.77 \pm 0.15 \mu\text{M}$. Therefore, the binding constant for mitoxantrone was $6.2 \times 10^7 \text{M}^{-1}$.

1.3.6.2 OM2 [AQ-EAE-OH (4-OH)] TFA DNA binding

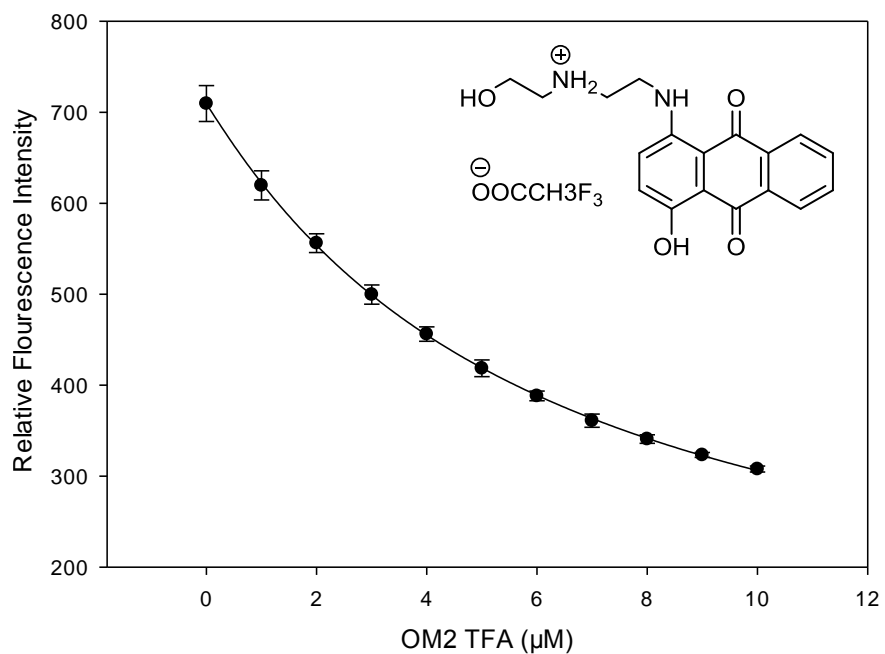


Figure 1.97: : Variation of relative fluorescence intensity of CT-DNA (60 μM) with pre-bound EtdBr (30 μM) when treated with different concentrations of OM2 TFA in PBS buffer. (n = 3). λ_{ex} 480 nm; λ_{em} 610 nm.

	Coefficient	Std. Error	t	p
Min	-0.0000	0.0000	(+inf)	<0.0001
Max	710.44	2.50	283.34	<0.0001
QE₅₀	7.37	0.06	105.53	<0.0001

The concentration of OM2 [AQ-EAE-OH (4-OH)] TFA when the relative fluorescence intensity reached 50% was $7.37 \pm 0.06 \mu\text{M}$. Therefore, the binding constant for OM2 TFA was $4.06 \times 10^7 \text{M}^{-1}$.

1.3.6.3

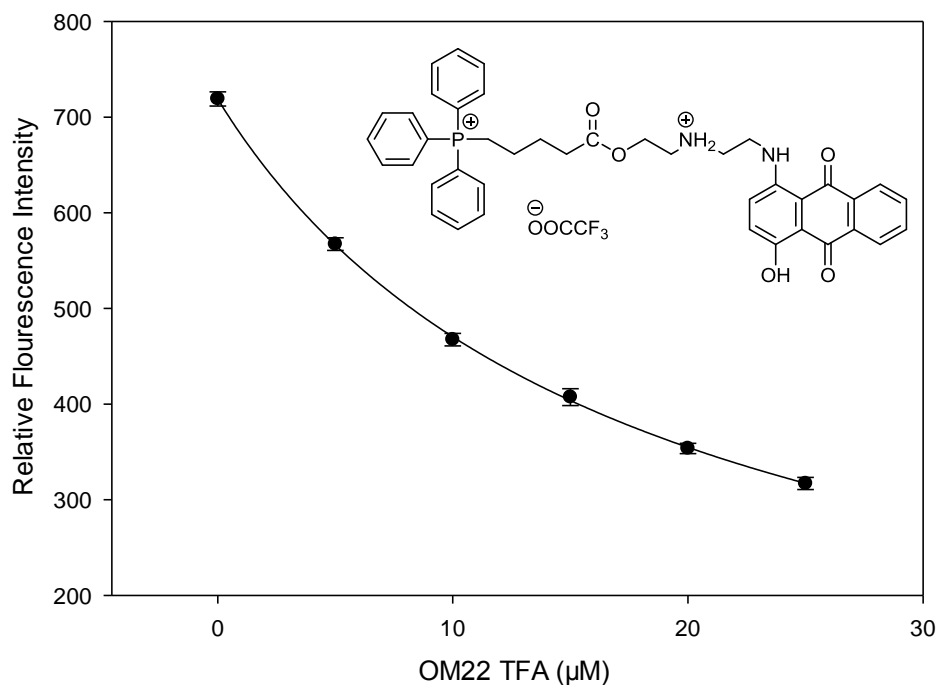
OM22 [AQ-EAE-TPP(4-OH)] TFA DNA binding

Figure 1.98: Variation of relative fluorescence intensity of CT-DNA (60 μM) with pre-bound EtdBr (30 μM) when treated with different concentrations of OM22 TFA in PBS buffer. (n = 3) λ_{ex} 480 nm; λ_{em} 610 nm.

	Coefficient	Std. Error	t	p
Min	-0.0000	0.0000	(+inf)	<0.0001
Max	719.28	2.86	251.38	<0.0001
QE₅₀	19.45	0.24	80.19	<0.0001

The concentration of OM22 [AQ-EAE-TPP(4-OH)] TFA when the relative fluorescence intensity reached 50% was $19.45 \pm 0.2 \mu\text{M}$. Therefore, the binding constant for OM22 TFA was $1.5 \times 10^7 \text{M}^{-1}$.

1.3.6.4 OM30 [AQ-Butyl-TPP(4-OH)] DNA binding

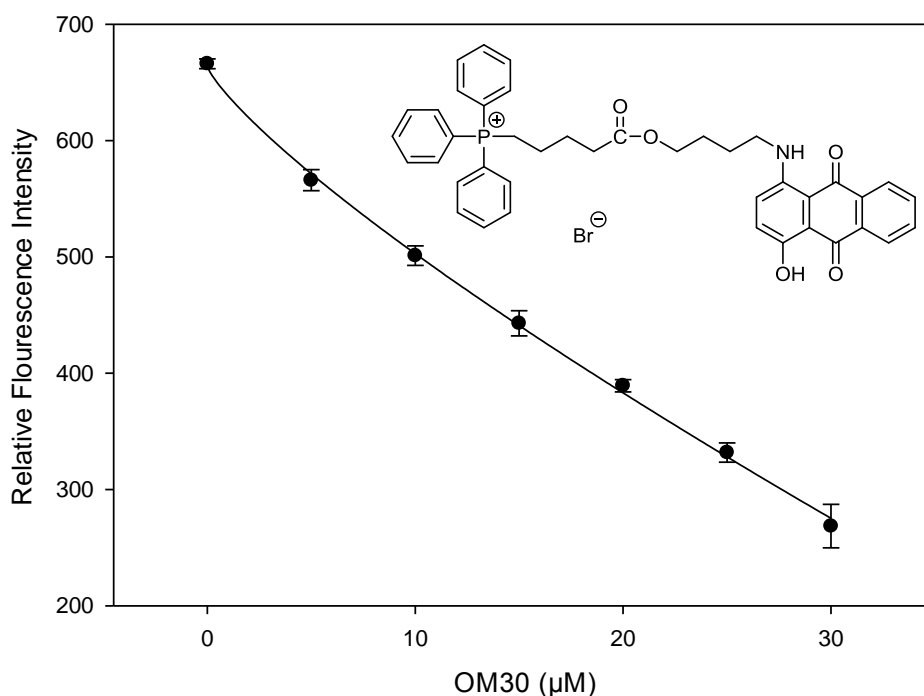


Figure 1.99: Variation of relative fluorescence intensity of CT-DNA (60 μM) with pre-bound EtdBr (30 μM) when treated with different concentrations of OM30 in PBS buffer. (n = 3). λ_{ex} 480 nm; λ_{em} 610 nm.

	Coefficient	Std. Error	t	p
Min	-0.0000	0.0000	(+inf)	<0.0001
Max	658.16	16.35	40.23	<0.0001
QE₅₀	24.83	1.44	17.23	0.05

The concentration of OM30 [AQ-Butyl-TPP(4-OH)] when the relative fluorescence intensity reached 50% was $24.83 \pm 1.4 \mu\text{M}$. Therefore, the binding constant for OM30 was $1.2 \times 10^7 \text{M}^{-1}$.

1.3.6.5 OM31 [AQ-Pentyl-TPP(4-OH)] DNA binding

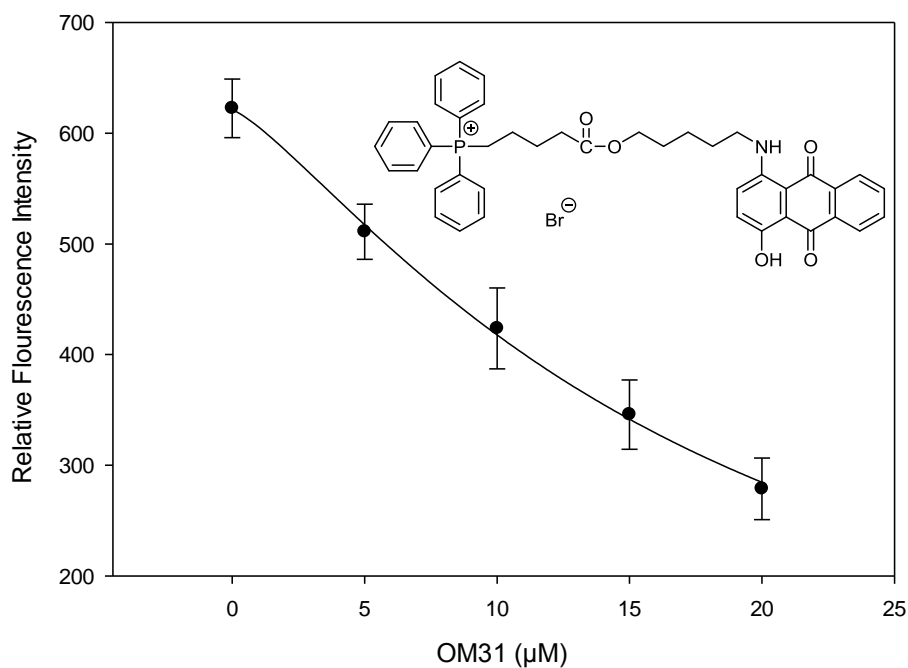


Figure 1.100: Variation of relative fluorescence intensity of CT-DNA (60 μM) with pre-bound EtdBr (30 μM) when treated with different concentrations of OM31 in PBS buffer. (n = 3). λ_{ex} 480 nm; λ_{em} 610 nm.

	Coefficient	Std. Error	t	p
Min	-0.0000	0.0000	(+inf)	<0.0001
Max	620.90	7.93	78.28	0.0002
QE₅₀	17.55	0.59	29.63	0.0011

The concentration of OM31 [AQ-Pentyl-TPP(4-OH)] when the relative fluorescence intensity reached 50% was 17.55 ± 0.5 μM. Therefore, the binding constant for OM31 was **1.7×10⁷M⁻¹**.

1.3.6.6 OM32 [AQ-EOE-TPP(4-OH)] DNA binding

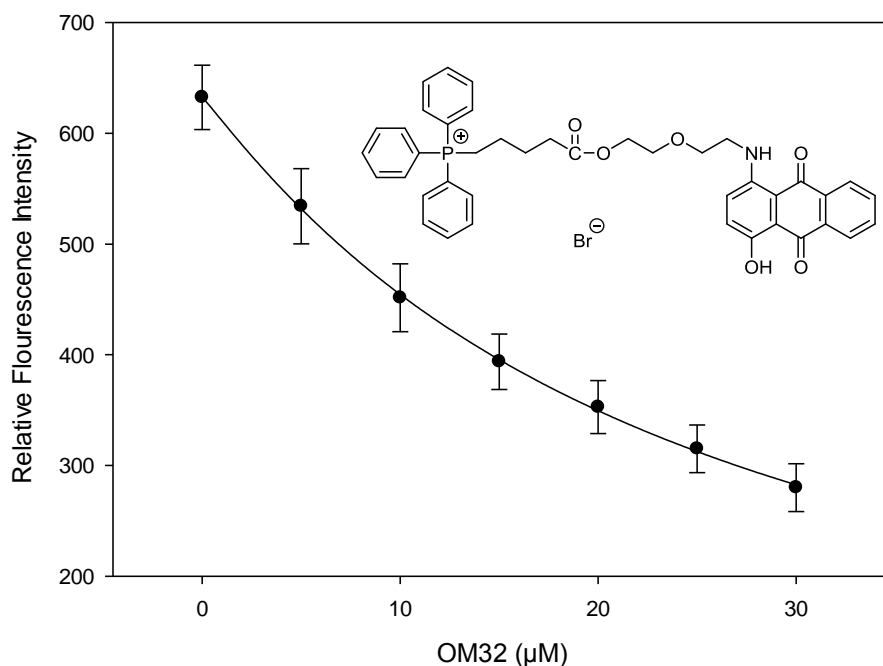


Figure 1.101: Variation of relative fluorescence intensity of CT-DNA (60 μM) with pre-bound EtdBr (30 μM) when treated with different concentrations of OM32 in PBS buffer. (n=3). λ_{ex} 480 nm; λ_{em} 610 nm.

	Coefficient	Std. Error	t	p
Min	-0.0000	0.0000	(+inf)	<0.0001
Max	632.78	3.15	200.51	<0.0001
QE₅₀	24.43	0.34	71.57	<0.0001

The concentration of OM32 [AQ-EOE-TPP(4-OH)] when the relative fluorescence intensity reached 50% was $24.43 \pm 0.3 \mu\text{M}$. Therefore, the binding constant for OM32 was $1.22 \times 10^7 \text{M}^{-1}$.

1.3.6.7 SH1 (AQ-Butyl-TPP) DNA binding

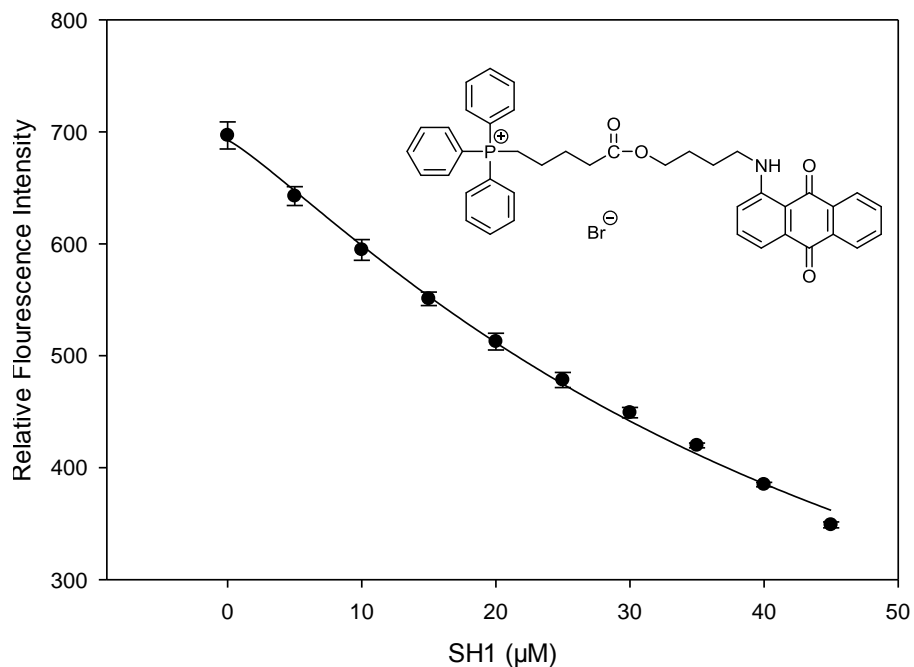


Figure 1.102: Variation of relative fluorescence intensity of CT-DNA (60 μM) with pre-bound EtdBr (30 μM) when treated with different concentrations of SH1 in PBS buffer. (n = 3). to λ_{ex} 480 nm; λ_{em} 610 nm.

	Coefficient	Std. Error	t	p
Min	-0.0000	0.0000	(+inf)	<0.0001
Max	692.45	6.60	104.91	<0.0001
QE₅₀	48.62	1.23	39.33	<0.0001

The concentration of SH1 (AQ-Butyl-TPP) when the relative fluorescence intensity reached 50% was $48.62 \pm 1.2 \mu\text{M}$. Therefore, the binding constant for SH1 was $0.616 \times 10^7 \text{M}^{-1}$.

1.3.6.8 OM26 (bis-TPP-NU:UB 65) DNA binding

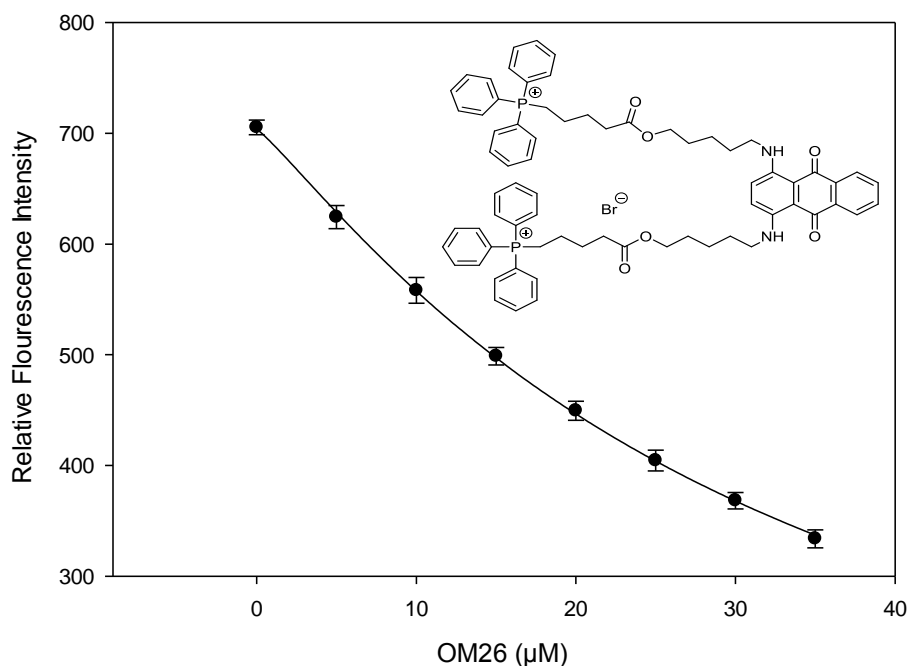


Figure 1.103: Variation of relative fluorescence intensity of CT-DNA (60 μM) with pre-bound EtdBr (30 μM) when treated with different concentrations of OM26 in PBS buffer. (n = 3). λ_{ex} 480 nm; λ_{em} 610 nm.

	Coefficient	Std. Error	t	p
Min	-0.0000	0.0000	(+inf)	<0.0001
Max	703.62	2.85	246.18	<0.0001
QE₅₀	32.51	0.34	93.56	<0.0001

The concentration of OM26 (NU:UB 65-bis-TPP) when the relative fluorescence intensity reached 50% was $32.51 \pm 0.3 \mu\text{M}$. Therefore, the binding constant for OM26 was $0.92 \times 10^7 \text{M}^{-1}$.

1.3.6.9 Ametantrone DNA binding

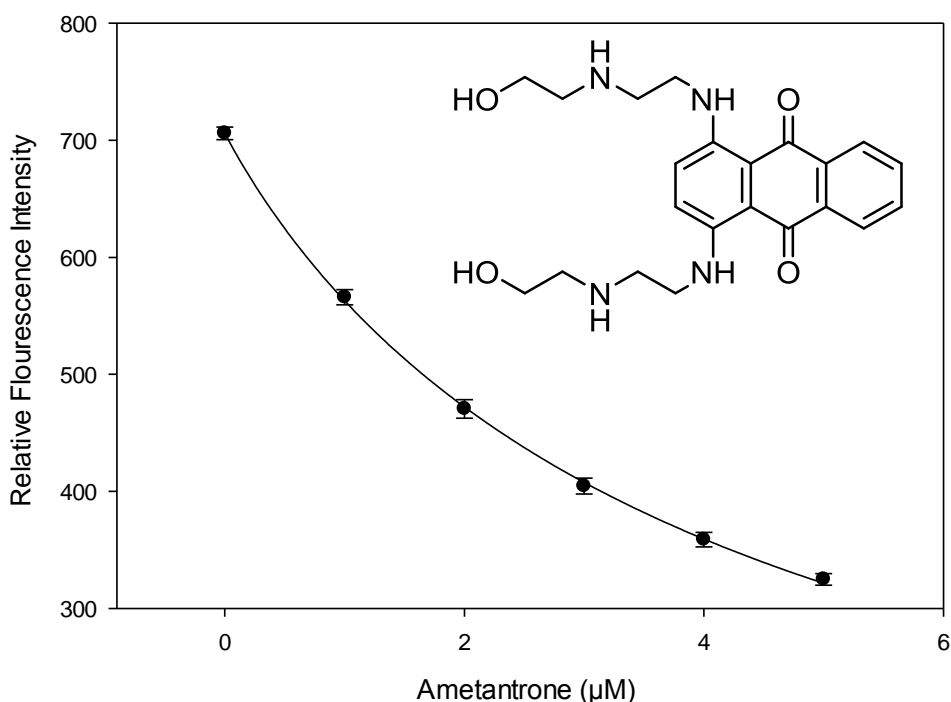


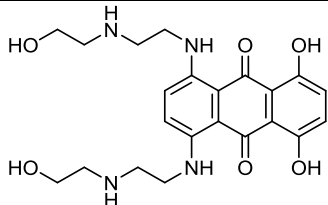
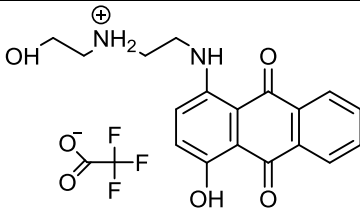
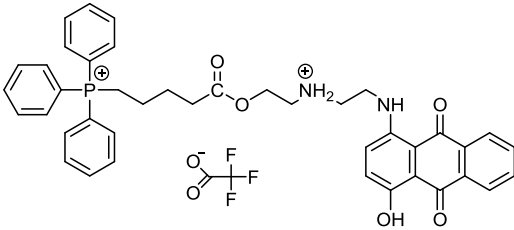
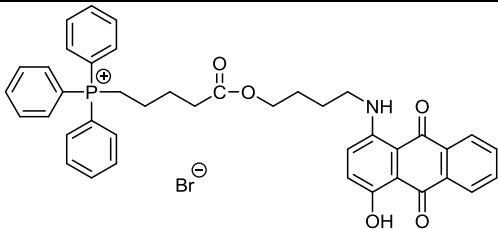
Figure 1.104: Variation of relative fluorescence intensity of CT-DNA (60 μM) with pre-bound EtdBr (30 μM) when treated with different concentrations of ametantrone in PBS buffer. (n = 3). λ_{ex} 480 nm; λ_{em} 610 nm.

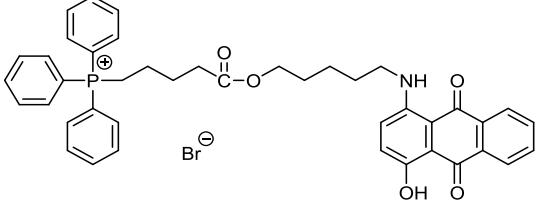
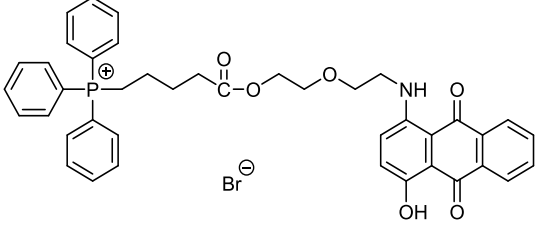
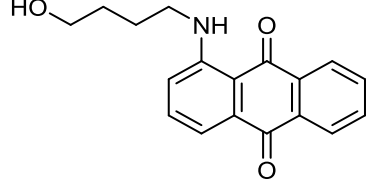
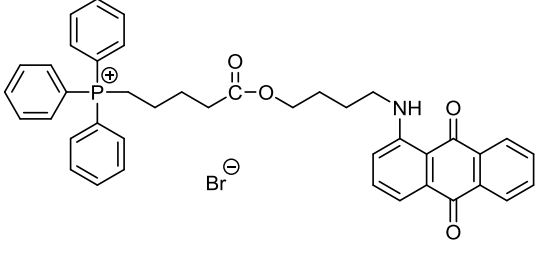
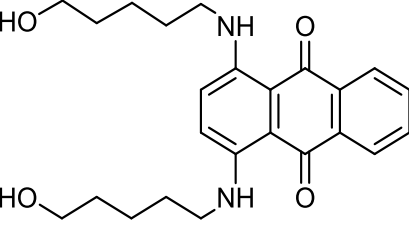
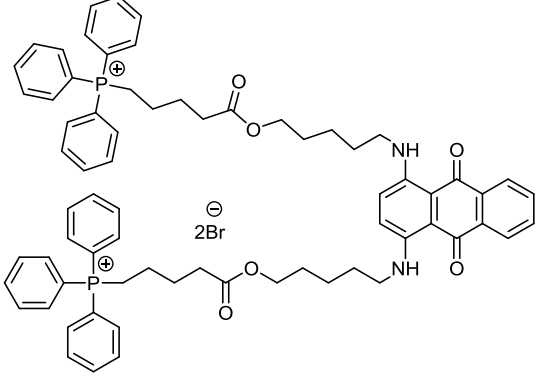
	Coefficient	Std. Error	t	p
Min	-0.0000	0.0000	(+inf)	<0.0001
Max	706.50	3.29	214.37	<0.0001
QE₅₀	4.14	0.06	66.89	<0.0001

The concentration of ametantrone when the relative fluorescence intensity reached 50% was $4.14 \pm 0.06 \mu\text{M}$. Therefore, the binding constant for ametantrone was $7.3 \times 10^7 \text{M}^{-1}$.

The novel compounds that have been tested in competitive ethidium displacement assay are all structurally related to mitoxantrone and to each other, with all having an anthraquinone core and amine groups at the C1 position linked with a spacer. The length

and composition of the spacer, which may have amino groups in addition to a hydroxyl group, could affect DNA binding constant (K_{app}). Also, the number of hydroxyl groups on the anthraquinone core structure specially at the C4 and/or C8 position would affect the K_{app} value. However, with TPP conjugated compounds, the K_{app} value might be lower when compared with its unconjugated precursor, due to the presence of the bulky TPP group adversely binding due to steric factors. These important factors that affect the K_{app} will be discussed below.

Name	Structure	QE ₅₀	K _{app}
Mitoxantrone		4.77 ± 0.15 μM	6.2×10 ⁷ M ⁻¹
OM2 TFA		7.37 ± 0.06 μM	4.0×10 ⁷ M ⁻¹
OM22 TFA		19.45 ± 0.2 μM	1.5×10 ⁷ M ⁻¹
OM30		24.83 ± 1.4 μM	1.2×10 ⁷ M ⁻¹

OM31		17.55 ± 0.5 μM	1.7×10 ⁷ M ⁻¹
OM32		24.43 ± 0.3 μM	1.2×10 ⁷ M ⁻¹
NU:UB 283		#ND	#ND
SH1		48.62 ± 1.2 μM	0.1×10 ⁷ M ⁻¹
NU:UB 65		#ND	#ND
OM26		32.51 ± 0.3 μM	0.9×10 ⁷ M ⁻¹

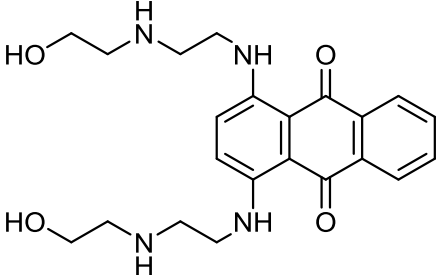
<p>Ametantrone</p>		<p>$4.14 \pm 0.06 \mu\text{M}$</p>	<p>$7.3 \times 10^7 \text{M}^{-1}$</p>
---------------------------	---	---	---

Table 1.1: Summary of QE_{50} and K_{app} values for tested compounds. #ND (not determined)

According to the data obtained from **Table 1.1**, mitoxantrone has a high DNA binding affinity with K_{app} $6.2 \times 10^7 \text{M}^{-1}$ and low QE_{50} $4.77 \pm 0.15 \mu\text{M}$. This is due to the fact that mitoxantrone has two nitrogen-containing side chains that allow electrostatic binding with the negatively charged phosphate backbone of DNA and it also has a planar anthraquinone ring system that can intercalate between DNA base pairs (Li *et al.*, 2005). Furthermore, ametantrone also binds with DNA with high affinity, K_{app} $7.3 \times 10^7 \text{M}^{-1}$, although ametantrone has a similar structure to mitoxantrone but with no hydroxyl group at positions 5 and 8. Bailly *et al.*, (1996) reported that in addition of the important role of 5,8-(OH) groups in intercalation with DNA, there is an additional role in that these groups stabilize the drug-DNA complex, hence mitoxantrone dissociates more slowly from DNA when compared with ametantrone because there are no hydroxyl groups at positions 5 and 8 in ametantrone yet both drugs unwind the DNA double helix with equal efficacy (Bailly *et al.*, 1996).

The compound AQ-EAE-OH (4-OH) (OM2) TFA binds to DNA with 1.5-fold less affinity than mitoxantrone possibly because the removal of one hydroxyethylaminoalkyl side chain as well as the hydroxyl groups at positions 5 and 8 present in mitoxantrone, results in decreased intercalation with DNA. However, by attaching triphenylphosphonium (TPP) to OM2 TFA to give AQ-EAE-TPP(4-OH) (OM22) TFA, the binding constant K_{app} decreased by 2.5-fold ($1.5 \times 10^7 \text{M}^{-1}$) this decrease in K_{app} may be due to the bulky nature of TPP that surrounds the positive charge on the phosphorus atom, which leads to a

decrease in the contact with the DNA backbone phosphate groups or prevents intercalation.

In addition, as predicted, the anthraquinone spacers NU:UB 238 and NU:UB 65 did not bind with DNA because they lack the amino group in the side chain and also the hydroxyl groups at positions 5 and 8. However, attaching TPP to these compounds, to afford AQ-Butyl-TPP (SH1) and bis-TPP-NU:UB 65 (OM26), gave compounds which did bind to DNA. From the data shown in **Table 1.1** OM26 has a higher binding constant ($0.9 \times 10^7 \text{M}^{-1}$) than SH1 ($0.1 \times 10^7 \text{M}^{-1}$) because OM26 has two TPP groups attached to its two side arms. Therefore, this presumably indicates that increasing the number of TPP groups increases DNA affinity.

Table 1.1 showed that the DNA binding constant K_{app} for OM22 TFA is almost 15-fold greater than the constant K_{app} of SH1, which both have TPP attached to the side chain, because OM22 TFA has an amino group in the side chain and hydroxyl group at C4 position of the anthraquinone which is absent in the SH1. So, removing the amino group from the side chain and the hydroxyl group from the anthraquinone structure leads to a dramatic decrease in the DNA binding affinity.

However, the binding constant K_{app} for the TPP conjugates AQ-Butyl-TPP(4-OH) (OM30), AQ-Pentyl-TPP(4-OH) (OM31) and AQ-EOE-TPP(4-OH) (OM32) is nearly equal to the binding constant K_{app} for OM22 TFA. Although these compounds lack the amino group present in the side chain of the TPP conjugate OM22 TFA, they retain the hydroxyl group at position C4, clearly showing the importance of the hydroxyl group at position C4 in the DNA binding of this series of TPP conjugates.

Furthermore, when comparing the results for the TPP conjugates SH1 and OM30, which differ only in the presence of the hydroxyl group at position C4 in OM30, the binding constant K_{app} for OM30 was almost 12-fold higher than the binding constant K_{app} for SH1. This indicated the importance of a hydroxyl group at position C4 of the anthraquinone that makes the compounds bind with DNA with high affinity compared with compounds that lack the hydroxyl groups at positions C4, C5 or C8.

OM30 and OM31 have similar structures. However, in OM31, the pentane spacer structure has one additional CH₂ compared with the butane spacer in OM30. Thus, the K_{app} value for OM31 was slightly higher than the K_{app} value for OM30. This may suggest the compound with a longer spacer binds DNA with higher affinity.

Interestingly, OM31 and OM32 have similar structure with the same spacer length, but with the addition of oxygen atom in the middle of the spacer of OM32. As shown in **Table 1.1**. The DNA binding constant K_{app} for these two compounds was similar and both compounds have similar QE₅₀. This shows clearly that the oxygen atom which was added to the spacer has no effect on DNA binding.

In conclusion, mitoxantrone and ametantrone have high binding constants which indicates that these two compounds have high affinity for the base pairs of DNA. These results are in agreement with previous studies reported in the literature on binding of mitoxantrone and its intercalation into the DNA duplex and where it was reported that the electrostatic attraction between the DNA phosphates and cationic charge on mitoxantrone and ametantrone might improve the DNA binding affinity (Varadwaj *et al.*, 2010). The results of the DNA binding studies of the novel compounds clearly showed that attaching TPP makes the compounds bind with DNA when compared to their unconjugated precursors. Also, it was clear that where compounds share the same anthraquinone base structure, the DNA binding constant would increase if there were more hydroxyl groups attached to the anthraquinone chromophore, regardless of the composition of the side chains. Also, the amino group in the side chain plays an important role in the DNA binding strength, probably through electrostatic binding with the negatively charged of DNA phosphate backbone that sometimes leads to a higher DNA binding value, than the compounds that do not have amino group in its spacer (Mcknight *et al.*, 2004).

1.3.7 **Distribution Coefficient**

Distribution coefficient assays were performed in this research programme to determine the physicochemical properties (lipophilicity) of the novel compounds. Lipophilicity is an important physicochemical property in drug development and the discovery of novel drugs

(Rutkowska *et al.*, 2013). Lipophilicity is usually expressed by the logarithm of a compound's octanol/buffer distribution coefficient (log D) at specific pH (unionized and ionized compound). Distribution coefficients often indicate the logarithmic ratio of the concentration of the compounds in two different solvent (immiscible solvents) at equilibrium (Stéen *et al.*, 2017). In addition, lipophilicity has a significant role in drug action processes that are related with the solubility and permeability of a drug, therefore lipophilicity determination during the early stage of drug discovery and development is very important and has a crucial role in the further studies of novel drugs (Rudraraju *et al.*, 2014).

Herein, OM2 [HO-EAE-AQ(4-OH)], OM22 [TPP-EAE-AQ(4-OH)], NU:UB 252 [OH-Butyl-AQ (4-OH)], OM30 [TPP-Butyl-AQ(4-OH)], SH1 (TPP-Butyl-AQ), NU:UB 238 (OH-butyl-AQ) and OM16 [Rho-pip-succ-EAE-AQ(4-OH)] were studied to determine the distribution coefficient (lipophilicity) by using the shake-flask method, using mitoxantrone as a comparator. In this assay, octanol was used as the organic solvent as it has a chemical structure similar to that of the hydrophobic fatty molecules present in the cell membrane (Rutkowska *et al.*, 2013). In measuring the distribution coefficient, phosphate buffered saline (PBS) at pH 7.4 was used as the aqueous phase, allowing for contributions from both ionised and un-ionised species, in contrast to the partition coefficient which uses water as the aqueous phase (Leo *et al.*, 1971). The distribution coefficient (Log D) assay measures whether the compound is hydrophilic or lipophilic, which is important to know as it predicts whether the compound will move across the cells phospholipid bilayer and can be taken up by the cell. The more lipophilic the compound, the more readily it will cross into the cell (Murphy, 2008).

To obtain log D results, firstly, UV/VIS absorbance calibration curves for tested compounds at different concentrations were created in order to quantify the concentration of the compound in the organic and aqueous phases. Absorbance measurements were recorded using a range of known concentrations of OM2, OM22, NU:UB 252, OM30, SH1, NU:UB 238 and OM16 in both PBS buffer pH 7.4 and in octanol. The absorbance at a single strongly absorbing wavelength was used for preparation of each calibration curve.

The shake flask octanol-water partition coefficient method was used by dissolving the tested compound in PBS (saturated in octanol) and octanol (saturated in PBS) and shaken for 24 hours at room temperature allowing the compounds to dissolve and move into the desired layer. After 24 hours, the compounds with TPP were almost completely partitioned into the octanol layer, whereas some of the compounds without TPP distributed between both layers, visually confirming that TPP increases the lipophilicity of the compounds in comparison with compounds without TPP.

To calculate the log D (octanol/PBS), the compound concentrations were determined using the absorbance reading from each layer in the Eppendorf tube. A known aliquot from each sample was taken from both octanol and PBS layers and diluted to give a known final volume in the cuvettes. The absorbance was measured at the wavelength of maximum absorbance used to prepare the calibration curves and the linear calibration curve graph equation used to calculate the corresponding concentration of each sample. Then the log D value was calculated for each compound and a mean log D value for each compound was obtained from a minimum of three separate experiments **Table 1.2**. Negative log D values indicate that the compound is hydrophilic whereas positive values indicate that the compound is lipophilic. From the results shown in **Table 1.2** and **Figure 1.105**, OM22 [TPP-EAE-AQ(4-OH)] and SH1 (TPP-Butyl-AQ), which are TPP conjugates, have greater log D values, 1.69 ± 0.06 and 2.68 ± 0.04 , respectively, in comparison with their unconjugated precursors, OM2 [HO-EAE-AQ(4-OH)] (0.69 ± 0.09) and NU:UB 238 [OH-butyl-AQ] (1.97 ± 0.12), respectively. This indicated that attaching TPP makes the compounds more lipophilic when compared with the compounds without TPP which in turn should increase the ability of TPP compounds to cross the phospholipid bilayer and be taken into the mitochondrial matrix (Bielski *et al.*, 2015).

On the other hand, OM16 [Rho-pip-succ-EAE-AQ(4-OH)] had a negative value (-0.16 ± 0.05) this is due to OM16 having rhodamine B-pip-succ attached on its side chain (EAE) instead of TPP which makes the compound hydrophilic in comparison with OM22 which has the same side chain attached with TPP and it is lipophilic (1.69 ± 0.06). These results suggest that the attachment of TPP increases the lipophilic properties of compounds,

potentially allowing the drug to pass through cell membranes and accumulate in the mitochondria.

Tube	solvent	Conc. In Eppendorf μM	Log D	Log D mean \pm SD	
Mitoxantrone (1)	PBS	3432	-1.699	-1.665 \pm 0.02	
	Octanol	68.722			
Mitoxantrone (2)	PBS	2922.95	-1.658		
	Octanol	65.114			
Mitoxantrone (3)	PBS	2826.94	-1.638		
	Octanol	65.256			
OM2 (1)	PBS	184.99	0.8		
	Octanol	1172.49			
OM2 (2)	PBS	320.49	0.7		0.69 \pm 0.09
	Octanol	1606.65			
OM2 (3)	PBS	138	0.57		
	Octanol	513.33			
OM22 (1)	PBS	13.33	1.668		
	Octanol	621.6			
OM22 (2)	PBS	13.96	1.640	1.69 \pm 0.06	
	Octanol	609.6			
OM22 (3)	PBS	13.22	1.780		
	Octanol	797.4			
NU:UB 252 (1)	PBS	3.94	3.00		3.05 \pm 0.14
	Octanol	3945.60			
NU:UB 252 (2)	PBS	4.36	2.95		
	Octanol	3891.60			

NU:UB 252 (3)	PBS	2.24	3.21	
	Octanol	3658.20		
OM30(1)	PBS	1.78	2.93	2.97 ± 0.4
	Octanol	1506.06		
OM30 (2)	PBS	1.77	3.00	
	Octanol	1768.09		
OM30 (3)	PBS	1.66	2.97	
	Octanol	1544.04		
SH1 (1)	PBS	3.75	2.68	2.68 ± 0.04
	Octanol	1821.32		
SH1 (2)	PBS	3.47	2.75	
	Octanol	1952.10		
SH1 (3)	PBS	3.71	2.63	
	Octanol	1586.16		
NU:UB 238 (1)	PBS	15.28	1.96	1.97 ± 0.12
	Octanol	1421.84		
NU:UB 238 (2)	PBS	15.23	1.83	
	Octanol	1024.03		
NU:UB 238 (3)	PBS	16.18	2.12	
	Octanol	2153.09		
OM16 (1)	PBS	3.97	-0.13	-0.16 ± 0.05
	Octanol	2.89		
OM16 (2)	PBS	3.06	-0.12	
	Octanol	2.30		

OM16 (3)	PBS	7.29	-0.25	
	Octanol	4.05		

Table 1.2: LOG D values for tested compound in PBS buffer 7.4 and saturated octanol

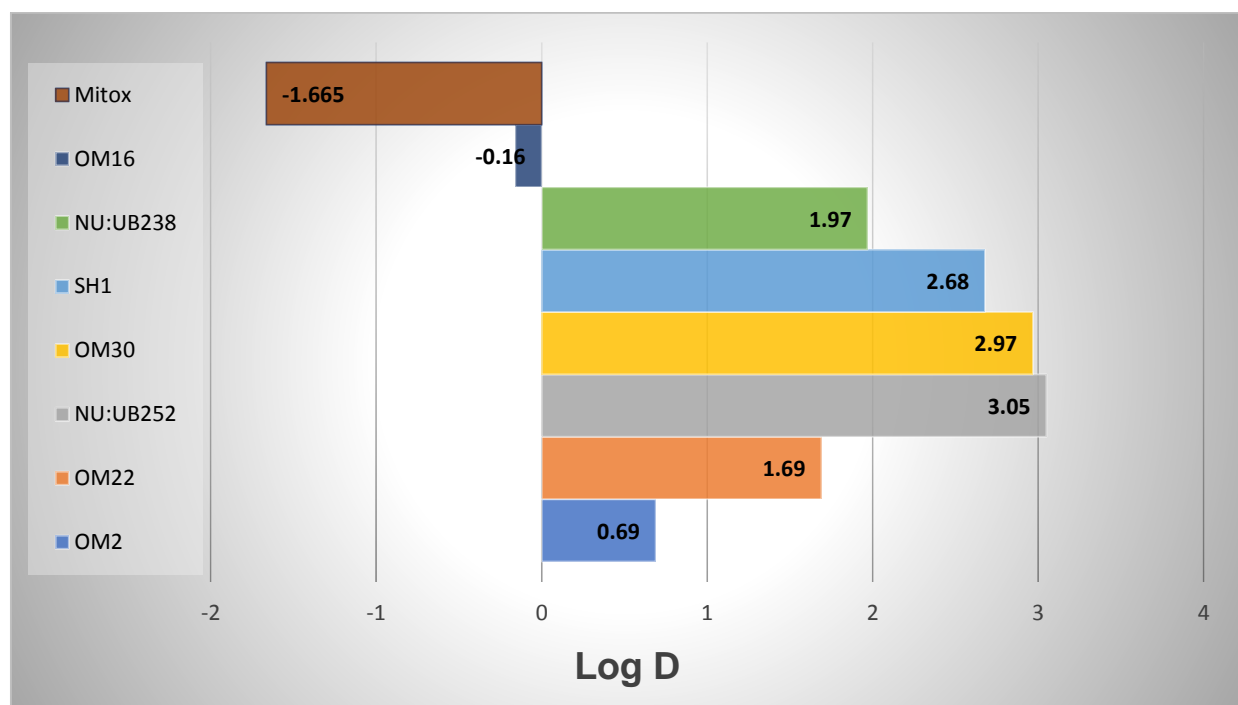


Figure 1.105: Relative lipophilicity/ hydrophobicity of OM2, OM22, NU:UB 252, OM30, SH1, NU:UB 238, OM16 and mitoxantrone.

Therefore, attaching TPP to mitoxantrone derivatives makes them more lipophilic. As predicted, which is an important factor to pass easily through lipid bilayers. It has been reported that lipophilic cations such as TPP has a unique property of being lipid soluble in addition to its net positive charge that they can easily pass through phospholipid bilayers into mitochondria (Ketterer *et al.*, 1971; Murphy, 1997). While the hydrophilic cations such as Na^+ can only cross the biological membrane when it transported by ionophores or carrier proteins. In addition, the impermeability of biological membranes to hydrophilic cations is due to the fact that moving the ion from aqueous environment to the nonpolar interior lipid of membrane required higher activation energy for movement of this ions through the hydrophobic core of the membrane, in contrast with the lipophilic cations

which required low activation energy, allowing it to pass through the biological membrane (Ketterer *et al.*, 1971; Ross *et al.*, 2005). Therefore, it was extremely important to measure the lipophilic properties of the novel compounds synthesised in this research programme as a predictor of the ability of these compounds to pass through the biological membrane and accumulate inside the mitochondria.

1.3.8 **MTT Assay**

The MTT [(3-[4,5-dimethylthiazol-2-yl]-2,5-diphenyltetrazolium bromide)] assay is generally used as a method to determine the number of viable cells after exposure to several drugs at different concentrations (Meerloo *et al.*, 2011). This assay was first developed by Mosmann (1983) and was further modified by Denizot and Lang (1986) to increase the sensitivity and reliability of the *in vitro* tumour cells chemosensitivity (Mosmann, 1983; Denizot and Lang, 1986) The principle of the MTT assay is that succinate dehydrogenase within the mitochondria converts tetrazolium salt (MTT), which is water soluble, into water insoluble dark purple formazan crystals **Figure 1.106**. Formazan accumulates in viable cells thereby measuring mitochondrial activity (Fotakis and Timbrell, 2006), by measuring the concentration of formazan using a microplate reader, any increase or decrease in viable cell number can be detected.

Hence, drug toxicity can be measured by MTT assay as a decrease in the number of cells indicates cell growth inhibition, therefore, drug potency is usually determined by the concentration of the drug required to produce 50% growth inhibition in comparison with the growth of untreated control cells (IC_{50}) (Meerloo *et al.*, 2011).

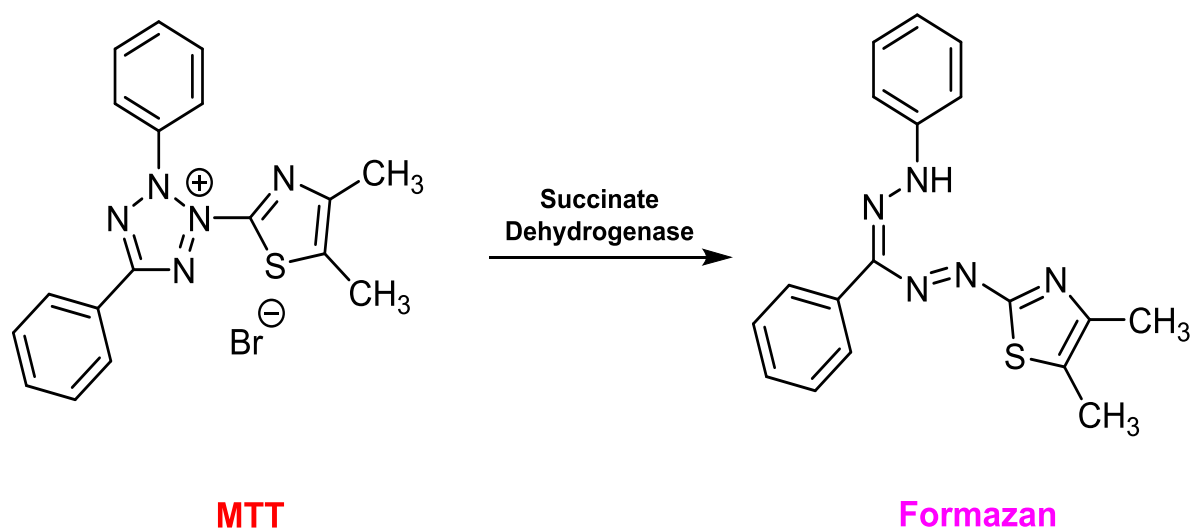


Figure 1.106: Conversion of MTT to formazan (the basis of the colourimetric method)

In this research programme, the MTT assay was used to determine the cell viability after treatment with novel compounds. The assay was carried out in two different cell lines; MCF-7 breast carcinoma cell line and HCT-15 colon carcinoma cell line. The advantage of using these cell lines is that they are part of the NCI 60 cell line screen, and have been well characterized by the Developmental Therapeutics Program in collaboration with various investigators who have measured mutation status, protein levels, RNA measurements, and enzyme activity levels in 60 human tumour cell lines (<https://dtp.cancer.gov/default.htm>). They measured *Mdr1* levels relative to actin RNA by RT-PCR RNA [Experiment Id: 20103 Pattern Id: MT1614] and detected that the level for HCT-15 was 17-fold higher in HCT-15 than MCF-7. Therefore, these cell lines can be used to screen for compounds that have the potential to circumvent P-gp drug resistance. Ideally, matched wild type and MDR cell lines would have been used, but MCF-7 and HCT-15 were chosen as an initial screen. Thus, comparison of the IC_{50} values was made to determine whether the compounds could potentially circumvent multidrug resistance by evading the P-gp pumps after attachment with TPP.

In vitro cytotoxicity of OM2 [HO-EAE-AQ(4-OH)], OM22 [TPP-EAE-AQ(4-OH)], NU:UB 238 (OH-butyl-AQ), SH1 (TPP-Butyl-AQ), NU:UB 65 and OM26 (TPP-bis-NU:UB 65) were measured after 48 hours and mitoxantrone, OM30 [TPP-Butyl-AQ(4-OH)], OM31

[(TPP-Pentyl-AQ(4-OH))] and OM32 [(TPP-EOE-AQ(4-OH))], were measured after 96 hours incubation by MTT assay. HCT-15 and MCF-7 cells growth curves against different concentrations of tested compound are shown in **Figure 1.107**, **Figure 1.108** and **Figure 1.109**.

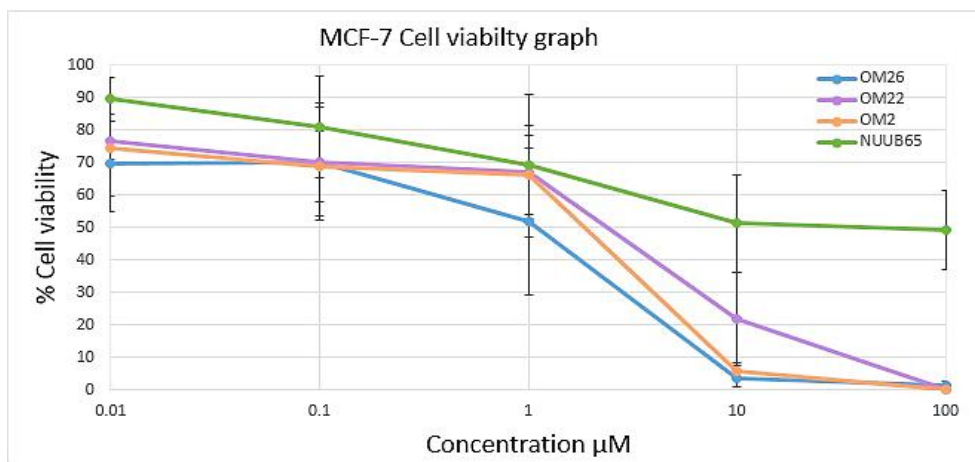


Figure 1.107: Survival rate of MCF-7 breast cancer cells treated with OM2, OM22, NU:UB 65 and OM26 for 48 h (n = 8) in comparison with untreated cells.

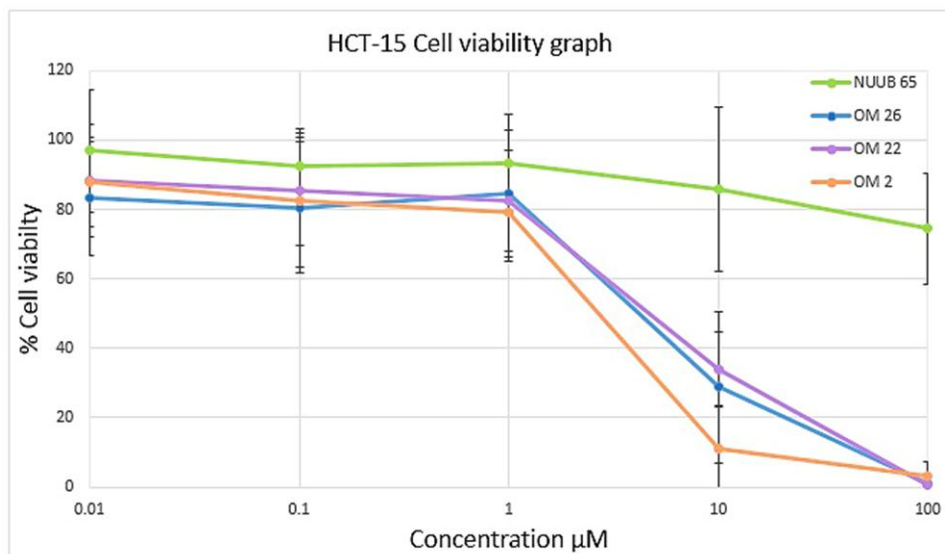


Figure 1.108: Survival rate of HCT-15 colon carcinoma cell lines treated with OM2, OM22, NU:UB 65 and OM26 for 48 h (n = 8) in comparison with untreated cells.

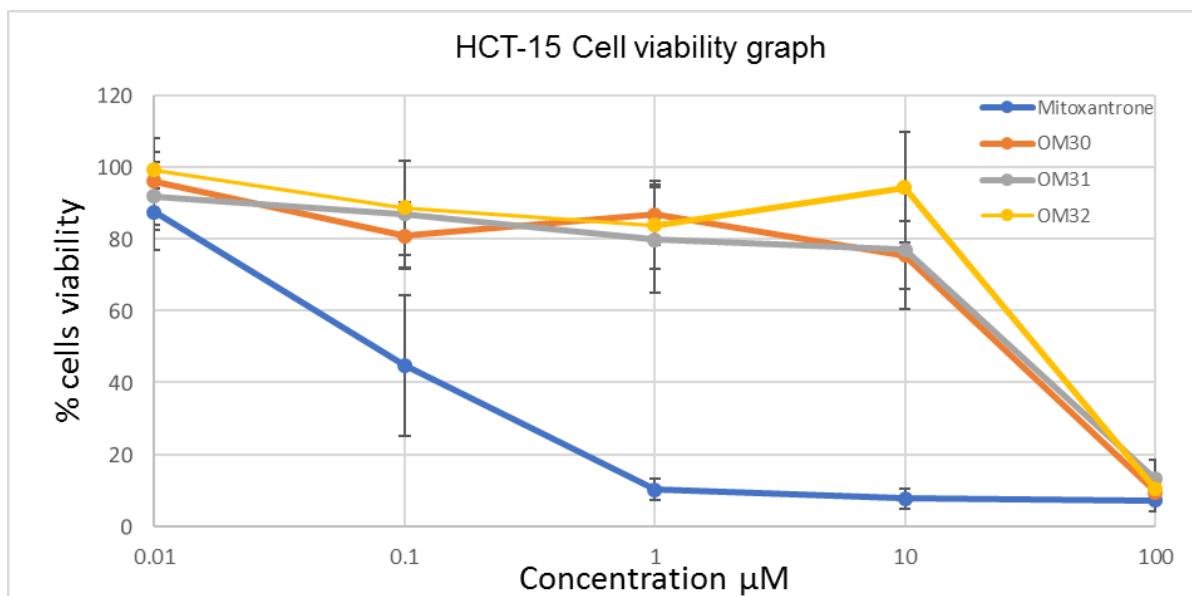


Figure 1.109: Survival rate of HCT-15 colon carcinoma cell lines treated with Mitoxantrone, OM30, OM31 and OM32 for 96 h (n = 8) in comparison with untreated cells.

According to the results presented in **Table 1.3**, **Figure 1.107**, **Figure 1.108** and **Figure 1.109**, the IC_{50} values of OM2 (3.39 μ M in MCF-7 and 3.07 μ M in HCT-15) and SH1 (9.69 μ M in MCF-7 and 9.48 μ M in HCT-15) suggest that these compounds retained activity in both cell lines which indicates that OM2, despite not having a TPP targeting group attached, might not be a P-gp substrate and may have the same mechanism of action in both cell lines as they both have similar values in MCF-7 and HCT-15, which have a higher level of P-gp pumps in comparison with MCF-7. Therefore, this suggests that OM2 and SH1 might possibly evade the P-gp pumps. Therefore, 48 hours treatment period may be too short for the active drug to be completely released. Additionally, OM22 is a lipophilic weak base and once entered into acidic lysosomes it may become protonated and trapped by the lysosomes and then prevented from reaching its target (Zhitomirsky and Assaraf, 2015).

Compounds	MCF-7	HCT-15
Mitoxantrone	#ND	0.082 ± 0.02
OM2	3.39 ± 0.84	3.07 ± 0.96
OM22	5.78 ± 2.91	8.15 ± 0.80
OM30	N.D.	21.43 ± 10.11
OM31	N.D.	23.22 ± 11.97
OM32	N.D.	36.42 ± 19.28
NU:UB 238	>100	>100
SH1	9.69 ± 3.35	9.48 ± 0.32
NU:UB 256	>100	>100
OM26	1.8 ± 0.98	7.45 ± 2.80

Table 1.3: The mean IC₅₀ values for different compounds (µM) in MCF-7 and HCT-16 cell lines, after 48 h and 96 h incubation. #ND (not determined)

In addition, mitoxantrone has a very low IC₅₀ value (0.082 µM) against HCT15 in comparison with all tested compounds; this is likely due to the high binding affinity of mitoxantrone with DNA and that it has OH groups at positions C4, C5 and C8, as well as amino groups at the side chains which also play an important role in the DNA binding and increase the toxicity of the drug. Furthermore, the IC₅₀ value of OM2 [HO-EAE-AQ(4-OH)] (3.07 µM) was the lowest amongst the OM series against HCT15 which may be related to sharing a similar structure with mitoxantrone having a protonated amine group, an OH group at position C4 but lacking the OH groups at positions C5 and C8.

The data in **Table 1.3** illustrates that the more hydroxy groups in the anthraquinone basic structure, the more potent and cytotoxic the drug will be, such as in mitoxantrone and OM2. Also, having the protonated amine group in the side chain plays a crucial role in DNA binding which in turn can increase the cytotoxicity. This is because the planar anthraquinone ring intercalates between DNA base pairs and the amino group in the side

chain binds with the negatively charged phosphate group of DNA which in turn causes DNA condensation and inhibits the DNA replication. Also mitoxantrone inhibits topoisomerase II which plays a role in DNA strand repair, which leads to cell death (Hajihassan and Rabbani-Chadegani, 2009). In addition, the OH groups at positions C5 and C8 of the anthraquinone chromophore play a role in the toxicity of the compounds as these groups participate in the DNA intercalation – it is known mitoxantrone dissociates more slowly from the DNA than ametantrone that lack these groups (Bailly *et al.*, 1996).

Furthermore, Hong *et al.*, (2017), synthesized drugs targeted to mitochondria using TPP-conjugated superoxide dismutase mimetic carboxypropyl (Mito-CP) and TPP-conjugated ubiquinone (Mito-Q). They studied the cytotoxicity of these compounds by MTT assay and they found that Mito-CP decreased the viability of all cell lines at concentrations ranging from 0.01-10 μM within 48 hours and the IC_{50} values were calculated at 0.84 μM for RPMI-7951, 0.30 μM for A375 and 0.28 μM for SK-MEL28 cells. However, the same concentrations for CP were used and no significant decrease in cell growth was observed. The same results were obtained with Mito-Q, which effectively decreased the growth of all cell lines with no decrease in cells growth for CoQ10. Hong *et al.*, (2017) further investigated the toxicity of TPP to indicate whether the toxicity of TPP conjugates was from TPP itself or from the conjugates. They revealed that TPP alone caused very little decrease in cell viability even at higher dose (Hong *et al.*, 2017).

Han *et al.*, (2014) linked a TPP carrier with doxorubicin to deliver the drug to mitochondria. the cytotoxicity of TPP-doxorubicin was studied by MTT assay using MDA-MB-435/WT and MDA-MB-435/DOX cell lines with incubation times 24, 48, and 72 hours. They found that TPP alone did not show any significant toxicity in both cell lines. The results revealed that the free doxorubicin has a better cytotoxicity than TPP-doxorubicin after 24 hours in MDA-MB-435/WT cells. However, the cytotoxicity of TPP-doxorubicin increased with the time and reached the cytotoxicity of free doxorubicin after 48 hours and exceeded it after 72 hours. The reason behind increasing the cytotoxicity of TPP-doxorubicin with time is the differences in mechanism of action of TPP-doxorubicin and free doxorubicin and/or the intracellular escaping of TPP conjugates to reach the target site (Han *et al.*, 2014). Therefore, this is might be the reason behind a high IC_{50} for some TPP conjugates

compounds such as OM22, OM30, OM31 and OM32 as they required more time to reach the target site and produce cytotoxicity at the targeted site.

In conclusion, according to the results obtained from MTT assay in this project and along with the results from the literature, it clearly shows that attaching a TPP carrier to anticancer drugs, significantly increases the cytotoxicity even after a long period of time. Also, the free NU:UB 252 and NU:UB 238 showed no cytotoxicity and they were inactive and upon attaching the TPP carrier, these compounds showed significant increase in toxicity. Notably, two compounds retained activity in both the sensitive MCF7 cell line and resistant HCT15 cell line. TPP-conjugate SH1 was equipotent in each of these cell lines, which suggests it may be able to circumvent multidrug resistance. In addition, when comparing the obtained results from DNA binding assay and MTT assay, it seems that the stronger DNA binding affinity a compound shows, the more cytotoxic potency a compound will show, as it appeared that there is a direct correlation between DNA binding and cytotoxicity. This illustrates that there is a good connection between drug-DNA binding affinity and the drug inhibition of cancer cell growth.

1.3.9 **Cellular uptake and localization**

The main problem with most chemotherapy treatments is limited by lack of tumour cell specific selectivity, systemic toxicity and drug resistance. Several methods and strategies have been developed to increase the selectivity of anticancer drugs and reduce side effects and avoid drug resistance. Now-a-days, a most notable and interesting method to increase the efficiency of anticancer drug is by specific delivery of anticancer drug to mitochondria. Mitochondria are vital organelles in eukaryotic cells known as a powerhouse by playing a central role in energy generating processes (adenosine triphosphate, ATP) via oxidative phosphorylation. Mitochondria also have crucial roles in other complex processes such as metabolism, apoptosis and intracellular signaling (Via *et al.*, 2014). Therefore, as the mitochondria play an essential role in cell death, mitochondrial targeting could be a promising strategy for cancer therapy (Biswas *et al.*, 2012). In addition, the membrane potential ($\Delta\Psi_m$) of mitochondria in a cancer cell is

higher than in that of normal cells. Thus, lipophilic cations that have a delocalized positive charge pass through the hydrophobic barrier of plasma and mitochondrial membranes and accumulate in the mitochondrial matrix in response to the negative charge inside the mitochondria (Modica-Napolitano and Aprile, 2001). Mitochondrial membrane potential can uptake the cationic compounds to give concentration 100-1000 higher than in the cytoplasm (Murphy, 1997). Therefore, specific targeting of anticancer drug to mitochondria using lipophilic cations such as triphenylphosphonium (TPP), could drive the uptake of the anticancer drug by mitochondria and increase the accumulation inside the mitochondria which in turn reduce side effects, avoid drug resistance and increase drug efficiency.

Diffusion of anticancer drugs across the lysosomal membrane and mitochondrial membrane depends on the physicochemical properties (lipophilicity) of these drugs. As shown in **(section 1.3.6.10)**, attaching TPP to the novel compounds makes the compounds lipophilic as they have positive Log D value. It is well known from the literature that the main localization site of mitoxantrone is inside the nucleus (Panousis and Phillips, 1994), while Smith *et al.*, (1992) indicated the subcellular distribution of mitoxantrone in nucleus and cytoplasm (Smith *et al.*, 1992). Additionally, Shaul *et al.*, (2013) showed that anthracycline based derivatives are localized in lysosomes (Shaul *et al.*, 2013). Therefore, it was hypothesized that attaching the TPP could alter the subcellular localization of anticancer drugs such as mitoxantrone and doxorubicin from lysosome or nucleus to mitochondria. Furthermore, it has been reported that attaching TPP to an anticancer drug, increases the accumulation of this drug inside the mitochondria (Smith *et al.*, 2003; Theodossiou *et al.*, 2013; Bielski *et al.*, 2015). Han *et al.*, (2014) altered the localization of doxorubicin by attaching TPP to its side chain from lysosome to the mitochondria due to the cationic and lipophilic properties of TPP that take the compound to the mitochondria (Han *et al.*, 2014). This supports the concept that mitoxantrone derivatives that have been synthesized in this project, which have anthracycline-based structures, can be targeted to mitochondria by attaching TPP.

Therefore, confocal imaging was performed in this project to analyse the cellular uptake, and localization of novel compounds which showed a promising result in MTT and DNA

binding assays. Three cell lines were used; (live) prostate cancer cells (PC-3), (live) colon carcinoma cells (HCT-15) and (live) colon carcinoma cells (HCT-116) in the presence of MitoTracker green FM (fluorescent mitochondrial) and LysoTracker green DND26 for the mitochondria and lysosomes, respectively. However, the focus was on HCT-116 due to the growth rate and the shape of the cells under the microscope was better than HCT-15 and PC-3.

MitoTracker green was used in this test because it is good and suitable for live cells (Invitrogen Ltd.) and to distinguish the green colour from the red colour of tested compounds. To stain mitochondria, the cells were incubated with MitoTracker green FM probes, which then passively diffuse across the plasma membrane and accumulate in active mitochondria (according to Invitrogen Ltd.). LysoTracker green DND26 was used to stained lysosomes due to its ability to penetrate the cell membrane and it contains fluorophore which is attached to a weak base that helps in staining acidic compartments (lysosomes) in live cells.

Taking the advantage of anthraquinone natural fluorescence, the subcellular localization of mitoxantrone derivatives was studied and determined. Herein, cell lines were treated with a co-stain solution tested compounds and MitoTracker Green FM (50 nM) and the solution was applied to the cell culture medium and incubated as 37°C for 15 minutes prior to imaging. Also, cell culture medium was treated with LysoTracker Green DND 26 (60 nm) and tested compound solution and incubated at 37°C for 30 minutes. **Figure 1.110** shows the cellular uptake of SH1 (TPP-Butyl-AQ) after 90 minutes of live cell imaging. The results confirmed that SH1 was detected in mitochondria, but not in the lysosome and nucleus. SH1 showed a clear staining in HCT-116 cells (**panel A**) and a clear yellow dot indicating the localization of SH1 in mitochondria (**panel C ii**). **Panel C** is the merged image for panel **A** (SH1) and panel **B** (MitoTracker Green FM or LysoTracker green DND26). The yellow dots (**panel C ii**) confirming the colocalization of SH1 with mitochondria. The cellular uptake of SH1 was due to its cationic and lipophilic properties (Log D: 2.68 ± 0.04). To indicate that SH1 staining was specific to mitochondria, HCT-116 cells were stained with an alternative marker for lysosomes (LysoTracker green DND26). **Figure 1.110 (i)** shows the lack of co-localization of SH1 with lysosomes and

the nucleus. The co-localization of SH1 with MitoTracker Green FM, instead of LysoTracker Green DND26, suggested that SH1 displayed a better selectivity for mitochondria as compared to lysosomes in HCT-116 live cells, this is consistent with mitochondria in cancer cells that have a high membrane potential ($\Delta\Psi_m$) compared with plasma membrane and mitochondria in healthy cells, which in turn increases the mitochondrial penetration of cationic drugs (SH1), consequently increasing the accumulation of cationic drug inside mitochondria (Constance and Lim, 2012). This result aligns with literature reporting that attaching TPP to anticancer drugs make it more lipophilic and increase the cationic properties of the anticancer drug, which allow it to accumulate in mitochondria.

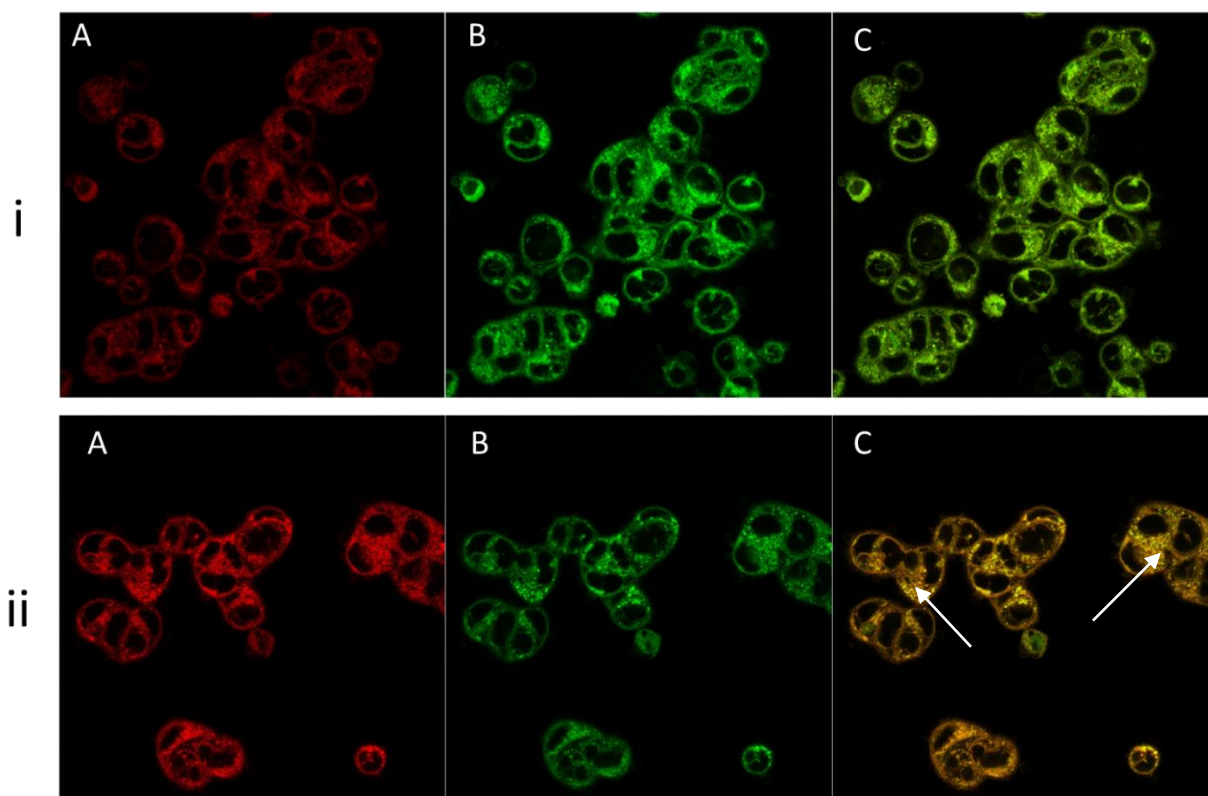


Figure 1.110: Localisation of SH1 in HCT-116 cells. SH1 (2 μM) localised to the mitochondria within 90 min as measured by live cell imaging. (i) SH1 stained with LysoTracker Green DND26, (A) SH1, (B) LysoTracker and (C) merged image. (ii) SH1 stained with MitoTracker Green FM, (A) SH1, (B) MitoTracker and (C) merged image. Images were captured as 63 x magnification.

In addition, the co-localization study was also performed for OM22 [TPP-EAE-AQ(4-OH)] compound, which has a structure related to SH1 with addition of an amino group in its side chain and a hydroxyl group at position C4 in the anthraquinone base structure. The cellular uptake of OM22 showed that OM22 co-localized with lysosomes observed after 90 minutes of live cell imaging as shown in **Figure 1.111 (i)**. OM22 showed a clear staining of HCT-116 cells (**panel A**) and a clear yellow dot indicating the localization of OM22 in lysosomes (**C i**), **Panel C** is the merged image for panel **A** (OM22) and panel **B** (MitoTracker Green FM or LysoTracker green DND26). The yellow dots (**panel C i**) confirmed the colocalization of OM22 with lysosome and not with mitochondria. However, the lipophilicity of OM22 ($\text{Log D: } 1.69 \pm 0.06$) and the cationic properties should allow the compound to penetrate the mitochondrial membrane and accumulate inside the mitochondria, but OM22 is a lipophilic amine drug. The localization of lipophilic amine drugs in the lysosome known as lysosomal sequestration or lysosomal trapping in which the weak base (OM22) will sequester or trap inside the acidic lysosomes (Ndolo *et al.*, 2012). It is well known from the literature that lipophilic weak amine base drugs diffuse through cell membranes at physiological pH via passive diffusion, once it is inside the lysosomes, they become protonated, therefore sequestered in lysosomes in their cationic state (Zhitomirsky and Assaraf, 2015). This is likely the reason behind the localization of OM22 in the lysosome. However, to demonstrate that OM22 staining was specific for lysosomes, HCT-116 cells were stained with an alternative marker for mitochondria (MitoTracker Green FM). **Figure 1.111 (ii)**, shows a lack of co-localization of OM22 with mitochondria and nucleus after 90 minutes of live cell imaging. Therefore, the localization of OM22 with LysoTracher Green DND26, not with MitoTracker Green FM, suggested that OM22 was trapped in acidic lysosomes which prevented it from reaching to its targeting site of mitochondria. This result is consistent with literature reporting that the lipophilic amine weak base drugs become trapped or sequestered in the acidic lysosomes.

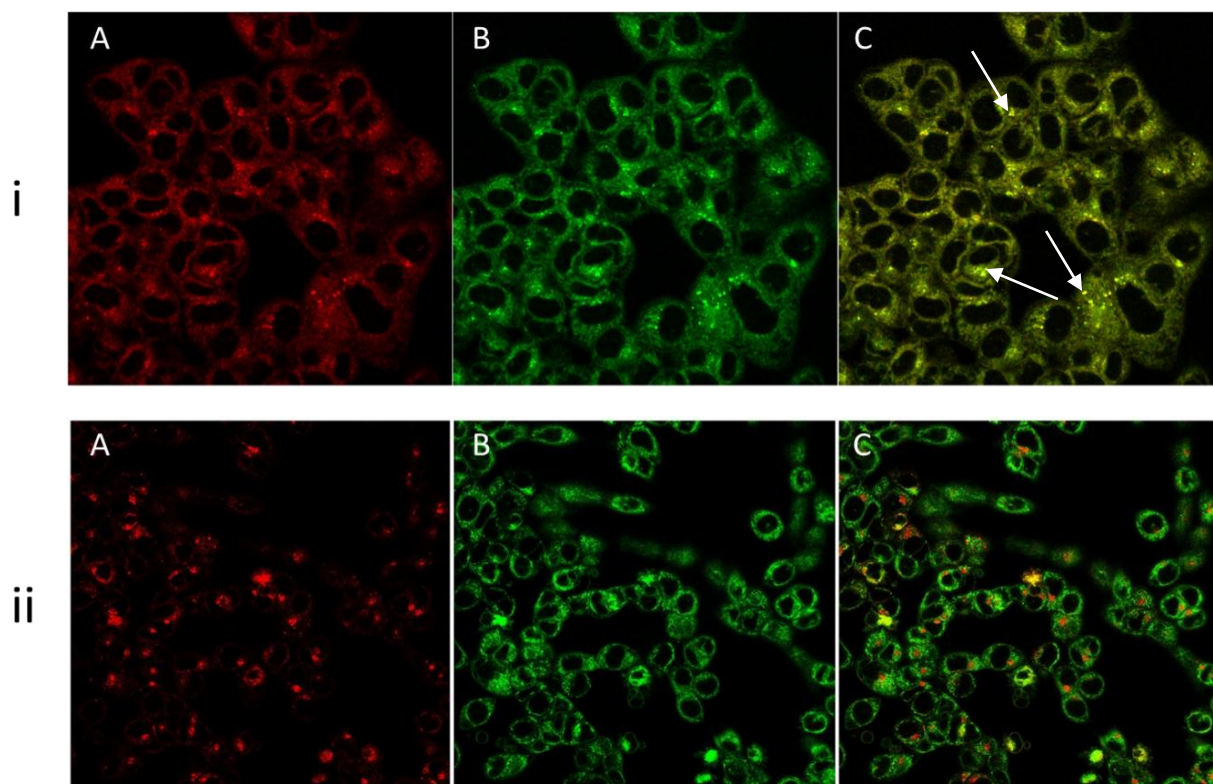


Figure 1.111: Localisation of OM22 in the HCT-116 cells. OM22 (2 μ M) localised to the lysosome within 90 min as measured by live cell imaging. (i) OM22 stained with LysoTracker Green DND26, (A) OM22, (B) LysoTracker and (C) merged image. (ii) OM22 stained with MitoTracker Green FM, (A) OM22, (B) MitoTracker and (C) merged image. Images were captured as 63 x magnification.

To further investigate the effect of anticancer drug structure on the localization inside the cells, OM30 [(TPP-Butyl-AQ(4-OH)], OM31 [(TPP-Pentyl-AQ(4-OH)] and OM32 [(TPP-EOE-AQ(4-OH))] were synthesised. These compounds are structurally related to SH1 and OM22; OM30 has an extra hydroxyl group at the C4 position in the anthraquinone base structure and no amino group in the side chain, OM31 has a longer side chain compared with SH1, OM22 and OM30 and no amino group in the side chain and OM32 has a similar structure to OM22 and OM30 with the addition of oxygen atom at the side chain. These compounds showed a promising results in the DNA binding assay and MTT assay. The cellular uptake of these compounds was studied using the HCT-116 cells and the localisation was observed after 90 minutes by live cell imaging. **Figure 1.112** shows a clear staining of these compounds to HCT-116 (**panel A**) and a clear yellow dot indicating the localization of these compounds in mitochondria (**panel C**), which is the

merged image for panel **A** and panel **B** (MitoTracker Green FM), confirming the colocalization of these compounds in the mitochondria. To further investigate the localization of these compounds with lysosomes, HCT-116 cells were stained with an alternative marker for lysosomes (LysoTracker green DND26), we found that these compounds lacked the localization with lysosomes and nucleus after 90 minutes of live cell imaging (image not shown). This indicated that changing the structure of the targeted compounds for example, by replacing the amino group in the side chain of OM22 with an oxygen atom in OM32, altered the basic properties of OM22 and changed localization of this compound from lysosome to mitochondria by successfully escaping the acidic lysosome and co-localized in the mitochondria.

Furthermore, the effect of the structure on the localisation of anticancer drugs was further studied for mitoxantrone and ametantrone, which are clinically approved anticancer drugs and they are structurally related to each other. **Figure 1.113** shows the cellular uptake of mitoxantrone which is clearly co-localized with lysosomes **Figure 1.113 C**, this is due to the two amino groups present at the side chains of mitoxantrone. These amino groups make the compounds weak bases, and suggesting that mitoxantrone was trapped in the acidic lysosomes (same as OM22) (Ndolo *et al.*, 2012). However, for ametantrone which has no hydroxyl groups at position C5 and C8 of the anthraquinone base structure compared with mitoxantrone, as shown in the confocal imaging, **Figure 1.114**, showed that ametantrone was co-localized in the nucleus of the cells not in the lysosomes or mitochondria. These results, indicated that even small alterations in the structure of the molecule could effect its localization inside the cells. Also it was necessary to evaluate several features including lipophilicity, to better understand which aspect of the molecule prevented ametantrone entry to the lysosome and targeted the nucleus.

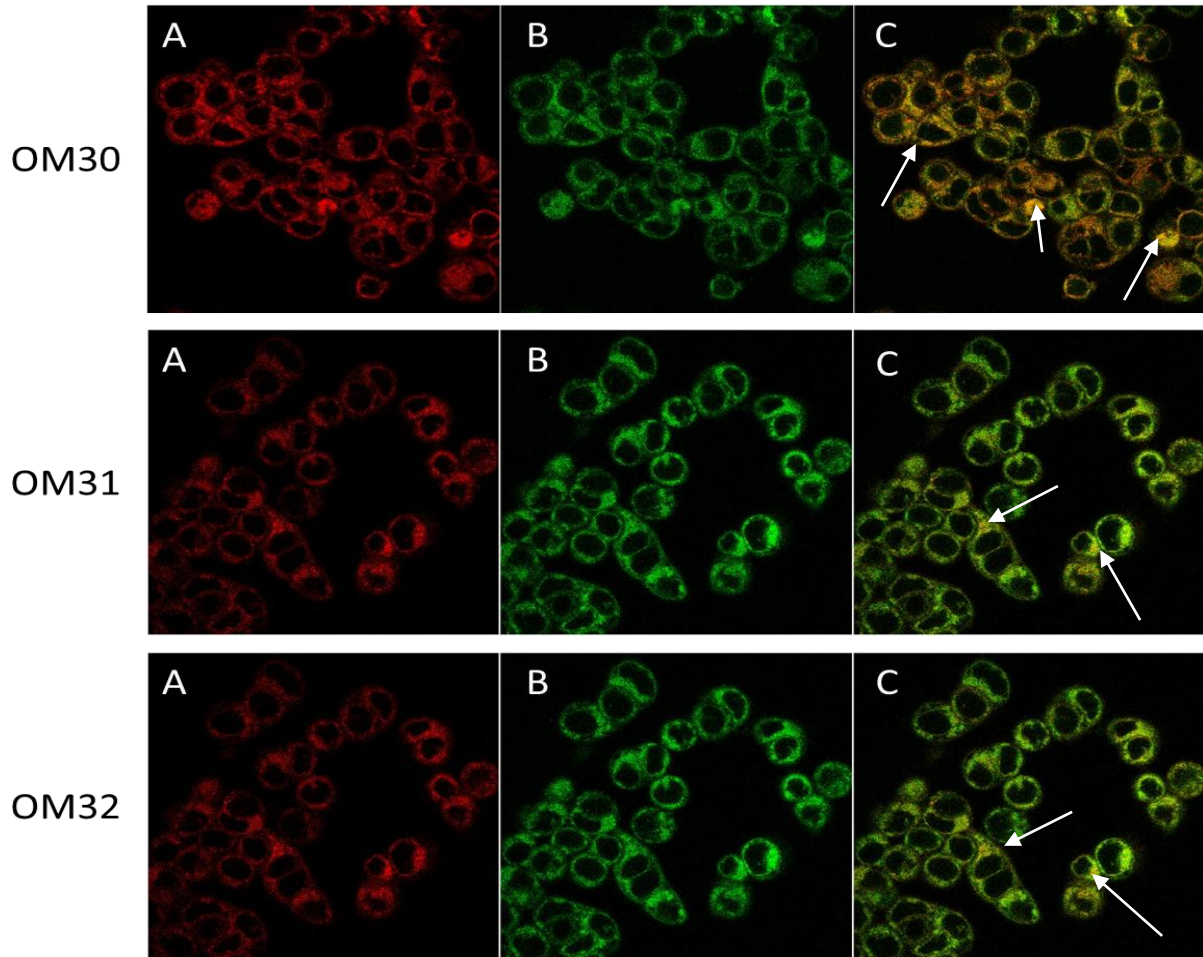


Figure 1.112: Localization of OM30 (2 μM), OM31 (2 μM) and OM32 (2 μM) with mitochondria in HCT-116 cells within 90 min as measured by live cell imaging. (A) OM30, OM31 and OM32, (B) MitoTracker and (C) merged images. Images were captured as 63 x magnification.

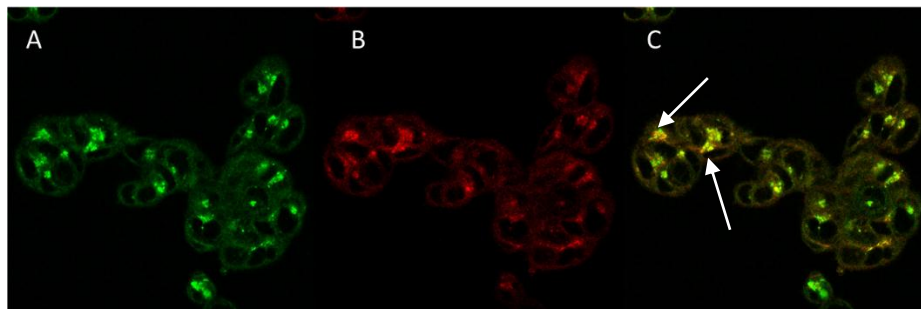
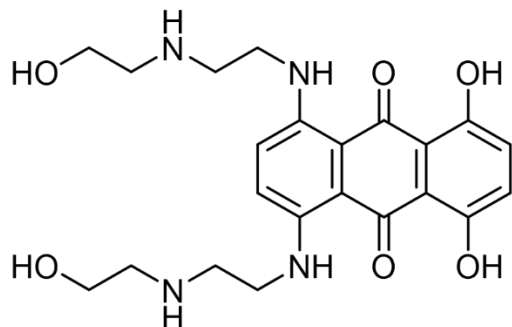


Figure 1.113: Structure and localization of mitoxantrone (1 μ M) with lysosome in HCT-116 cells within 90 min of live cell imaging. (A) mitoxantrone, (B) LysoTracker and (C) merged images. Images were captured as 63 x magnification.

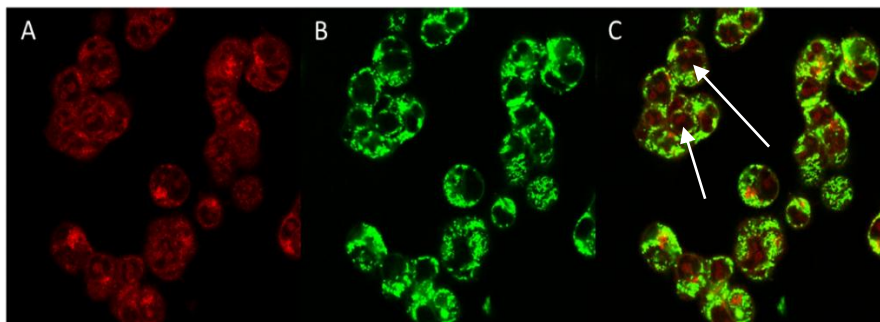
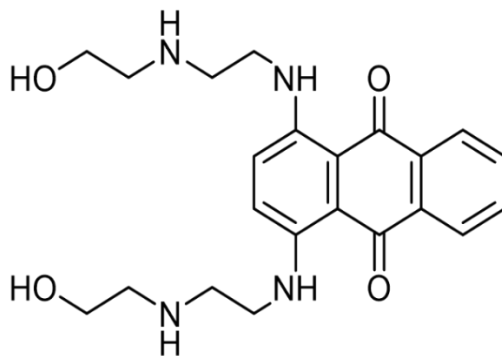


Figure 1.114: Structure and localization of ametantrone with nucleus in stained HCT-116 cell line with MitoTracker Green FM within 90 min of live cell imaging. (A) ametantrone, (B) MitoTracker and (C) merged images. Images were captured as 63 x magnification.

All in all, from the above images obtained from live cell imaging it clearly indicates the role of triphenylphosphonium (TPP) in the co-localisation of anticancer drugs in the mitochondria as it will increase the lipophilic and cationic properties of these drugs, which in turn increases the accumulation of the anticancer drug inside the mitochondria, which could avoid drug resistance, reduce side effects and increase drug activity. However, in addition to the role of TPP in the localization of anticancer drugs inside the mitochondria, it was clearly observed that changing the structure, even in the presence of the lipophilic and cationic vector (TPP), may alter the localization of compounds from the mitochondria to the lysosomes as seen in TPP conjugate drug OM22. Therefore, these results demonstrated that even small structural changes and differences between members of the this anthraquinone family, studied by confocal live cell imaging, have a significant effect on their subcellular distribution and co-localization inside the cells.

1.3.10 **Morphological evaluation**

Cell death is an essential part and occur frequently in complex organism (multicellular organism) to maintain tissue homeostasis and killing of infected cells by immune system (Ziegler and Groscurth, 2004). Different expressions have been formulated to describe cell death such as necrosis and apoptosis. Necrosis describes the sudden or premature form of cell death and characterized by comparatively slow disintegration (by autolysis) of the cell and often applies to describe cell death *in vivo*. On the other hand, apoptosis describes the morphology and the mechanism of cell active processes in which specific signaling pathways are active to kill the cell and regulating its disposal (Majno and Joris, 1995). In addition, cells dying by apoptosis usually show similar manner of morphological changes regardless of which agent is used to induce apoptosis (programmed cell death). However, *in vitro*, a cell line can show a full apoptosis when treated with one initiator and can show only a few morphological changes when treated with another initiator suggesting that cell death is initiated by different cell death mechanisms or by a part of the apoptotic pathway only (Hacker, 2000).

Different morphological studies describe the visible changes in cells during death *in vivo*

and *in vitro* but Kerr *et al.*, (1972) were the first who coined the term of apoptosis by describing a specific morphological part of cell death and this description remains a morphological description (Doonan and Cotter, 2008) and found wide acceptance (Hacker, 2000). The beginning of the apoptosis is characterised by shrinkage of the cells, contraction of the nucleus and condensation of nuclear chromatin. As cells shrink they detach and lose contact with surrounding cells (Saraste and Pulkki, 2000) or extracellular matrix, then the cells become more rounded in morphology (Doonan and Cotter, 2008). This is followed by formation of irreversible blebs at the cell surface (plasma membrane); this process called plasma membrane blebbing (Elmore, 2007) is due to the separation of the cell from the cytoskeleton (Doonan and Cotter, 2008). After blebbing, the cell dissociates into apoptotic bodies which consist of cytoplasm with tightly packed cell organelles or any other part of cellular materials. Finally, apoptotic bodies are taken up by macrophages or other cells and degraded by lysosomal pathways (Hacker, 2000)

Figure 1.115.

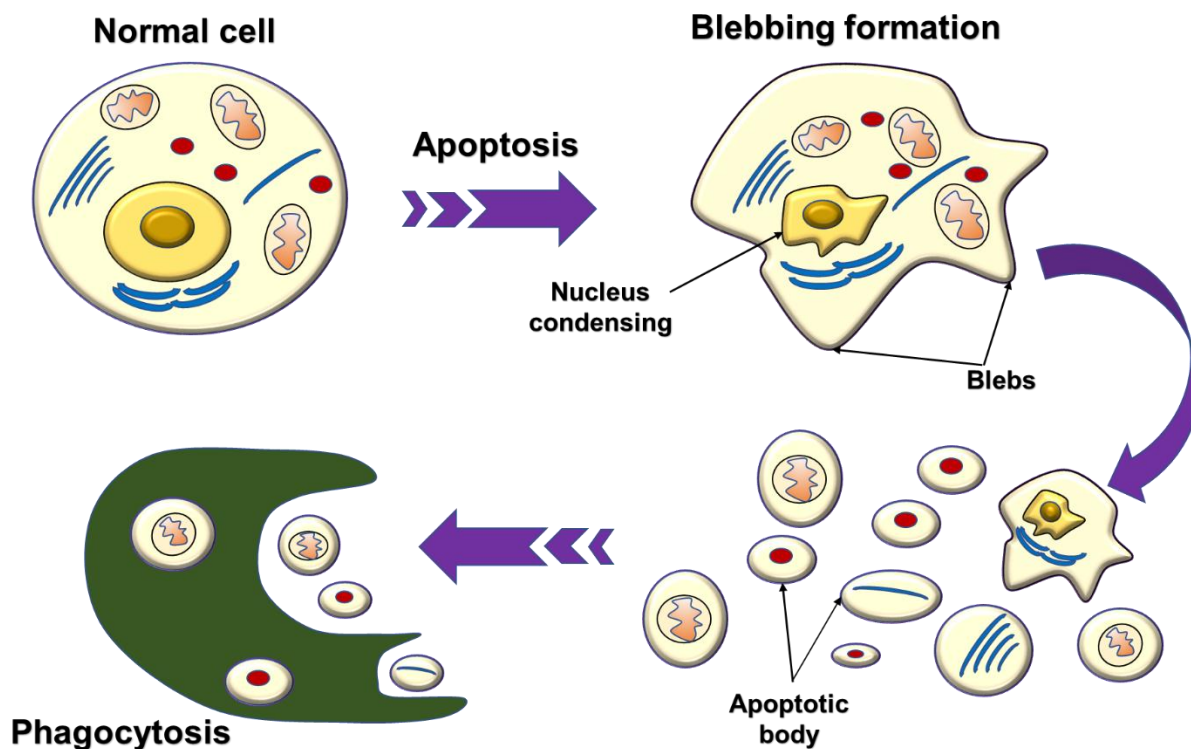


Figure 1.115: Schematic representation of the morphological changes during apoptosis

Therefore, in this experiment, a more in-depth evaluation using a bright field microscope has been carried out to determine the effect of SH1 (TPP-Butyl-AQ) and OM22 [TPP-EAE-AQ(4-OH)] on the morphological characteristics of HCT-116 colon cancer cells as an indication that these conjugates were inducing apoptosis. Apoptotic cells were characterised by suggesting that the cells get smaller in size, round shape, shrinkage and floating in the medium solution (Hacker, 2000), as HCT-116 cells when metabolically active should adhere to the flask surface.

Different concentrations of OM22 and SH1 at different time points with HCT-116 cells were tested (1 μ M, 5 μ M, 10 μ M; 2, 4, 6, 24 hours) and compared with untreated control cells, DMSO treated cells (vehicle control) and mitoxantrone (1 μ M; positive control). **Figure 1.116-1.119** shows the effect of SH1 on HCT-116 after treating with different concentrations and period of time. At 10 μ M, SH1 exhibited prominent growth inhibition of HCT-116 and cells were shrunken and floating indicating that the cells were dead at all tested time points compared to untreated cells and other concentrations. However, SH1 has a lower and slower effect on the cell morphology at concentrations of 1 μ M and 5 μ M compared with 10 μ M. After 2 hours, SH1 at 1 μ M and 5 μ M had no effect on the HCT-116 cells **Figure 1.116-1.117**, whereas the effect at 1 μ M and 5 μ M was noticed after 4 hours and 6 hours, when there was some cell shrinkage and changes in the cell morphology **Figure 1.116-1.119**. After 24 hours, most of the cells were shrunken and floating indicating the cell death at all concentrations but with less effect compared with the 10 μ M concentration **Figure 1.119**. This is in line with results from the MTT assay which showed that SH1 is a cytotoxic compound and induced toxicity at IC₅₀ values of 9.69 μ M in MCF-7 cell line and 9.48 μ M in HCT-15 cell line. Although there was no significant change in the cell morphology noticed at all time points of culture in the untreated HCT-116 cells and in the presence of DMSO. There were significant changes observed after 24 hours of culture in the presence of SH1 at all concentrations with different apoptotic ratio for each concentration, lower apoptosis at 1 μ M and higher apoptosis at 10 μ M. In addition, there were no significant changes in cell morphology in the presence of mitoxantrone at all concentrations, this was most likely due to the 24 hours incubation time not being long enough for mitoxantrone to induce toxicity as it was shown in the MTT assay results that mitoxantrone induced toxicity after 48 hours. This

was also confirmed by Bellosillo *et al.*, (1998) when they studied the effect of mitoxantrone on B-CLL cells, they found that mitoxantrone induced decrease in cells viability after 48 hours when treating the B-CLL cells with mitoxantrone (0.5 $\mu\text{g}/\text{ml}$) (Bellosillo *et al.*, 1998).

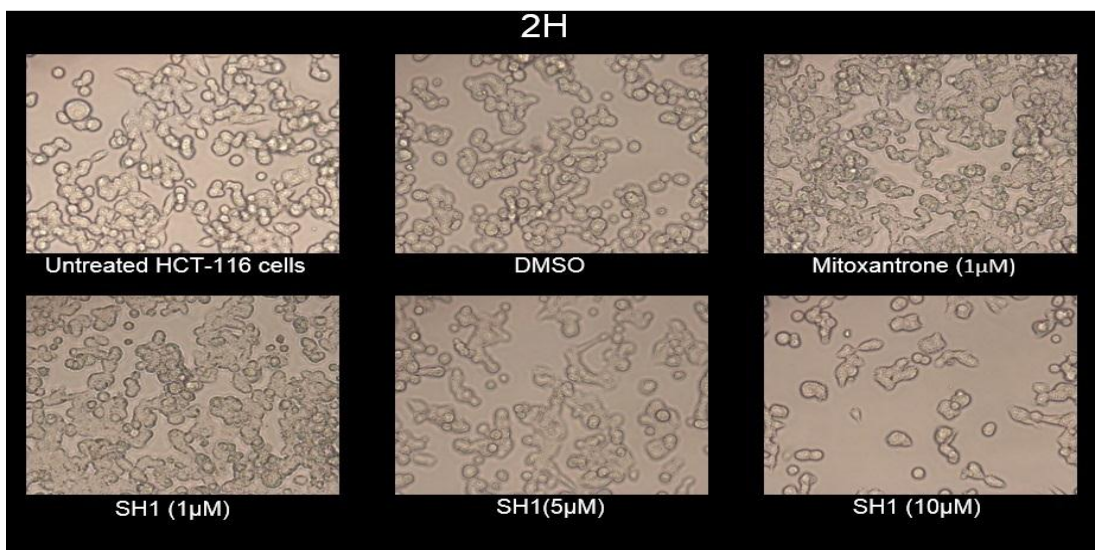


Figure 1.116: Cytotoxic effects of SH1 on HCT-116 cells. Bright field microscopy changes in cell morphology after 2 h post-treatment with SH1 at 10 μM with no changes at other concentrations and control cells.

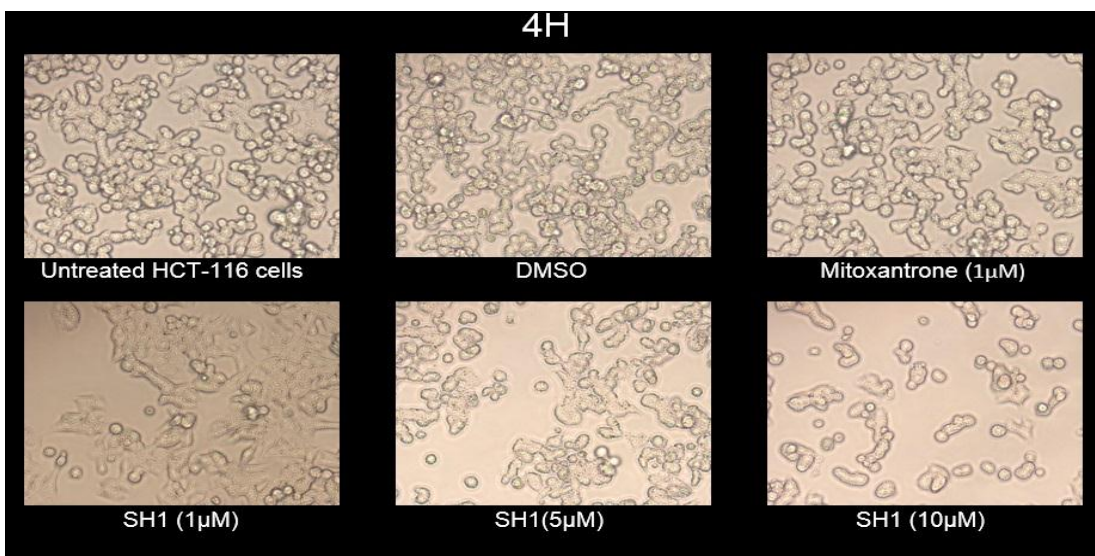


Figure 1.117: Cytotoxic effects of SH1 on HCT-116 cells. Bright field microscopy changes in cell morphology after 4 h post-treatment with SH1 at 5 μM and 10 μM with no changes at other concentration and control cells.

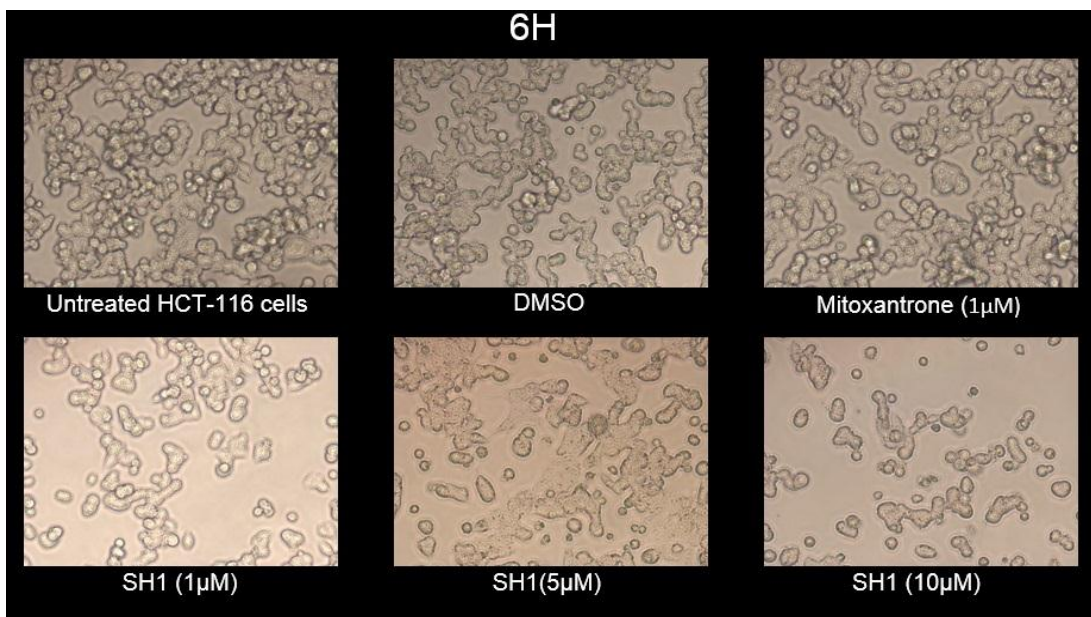


Figure 1.118: Cytotoxic effects of SH1 on HCT-116 cells. Bright field microscopy changes in cell morphology after 6 h post-treatment with SH1 at 1 μ M, 5 μ M and 10 μ M with no changes in control cells.

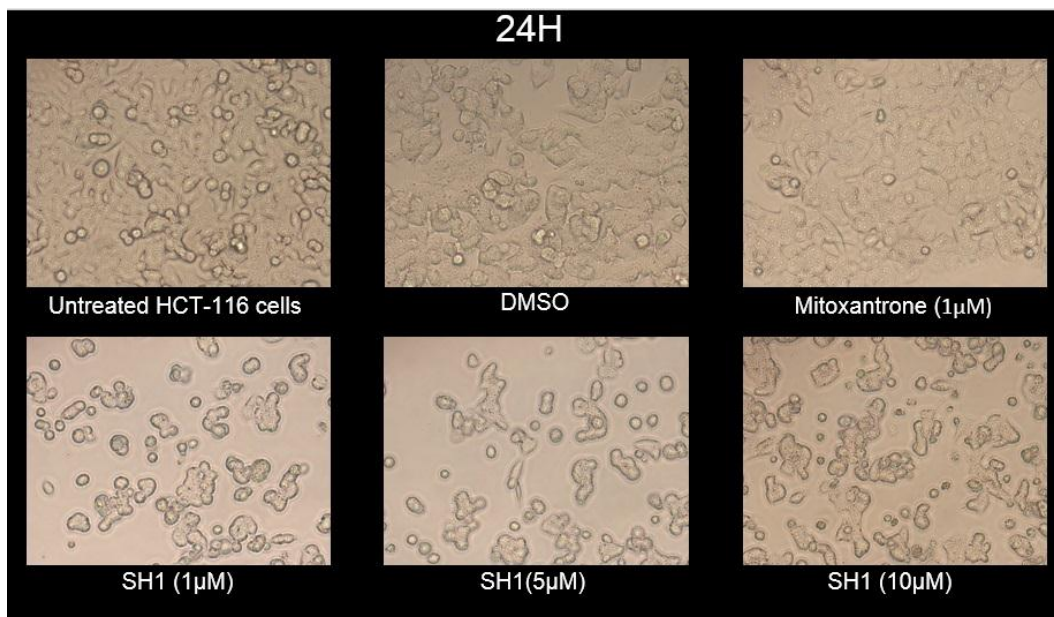


Figure 1.119: Cytotoxic effects of SH1 on HCT-116 cells. Bright field microscopy changes in cell morphology after 24 h post-treatment with SH1 at 1 μ M, 5 μ M and 10 μ M with no changes in control cells.

Figure 1.120-1.123 show the morphological changes of HCT-116 induced by OM22 at different concentrations and time. OM22 exhibited prominent growth inhibition and cell

shrinkage at a concentration of 5 μM after 4, 6 and 24 hours of incubation compared with SH1 in which there was less growth inhibition and apoptosis at this concentration and period of time **Figure 1.121-1.23**. This was due to OM22 having a lower IC_{50} (5.78 μM in MCF-7 cell line and 8.15 μM in HCT-15) than SH1, suggesting that OM22 is more toxic and changes the cell morphology at lower concentrations than SH1. However, at high concentration 10 μM , OM22 induced apoptosis and growth inhibition for duration 2 - 24 hours **Figure 1.120-1.123**. At 1 μM , there were no significant morphological changes at 2, 4 and 6 hours with less morphological changes at 24 hours compared with cells treated with 5 μM and 10 μM . In addition, there were no morphological changes noticed after 24 hours of culture in the untreated cells or in the presence of DMSO or in the presence of mitoxantrone, but there were significant changes observed after 24 hours of cell culture treated with OM22 at all concentrations.

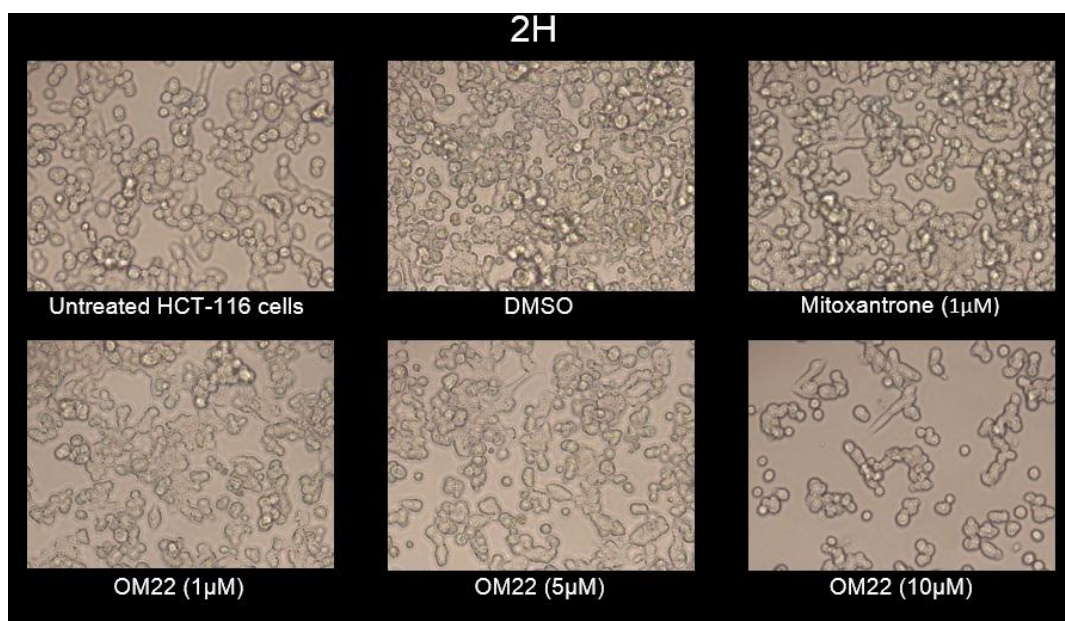


Figure 1.120: Cytotoxic effects of SH1 on HCT-116 cells. Bright field microscopy changes in cell morphology after 2 h post-treatment with OM22 at 10 μM with no changes at other concentrations and control cells.

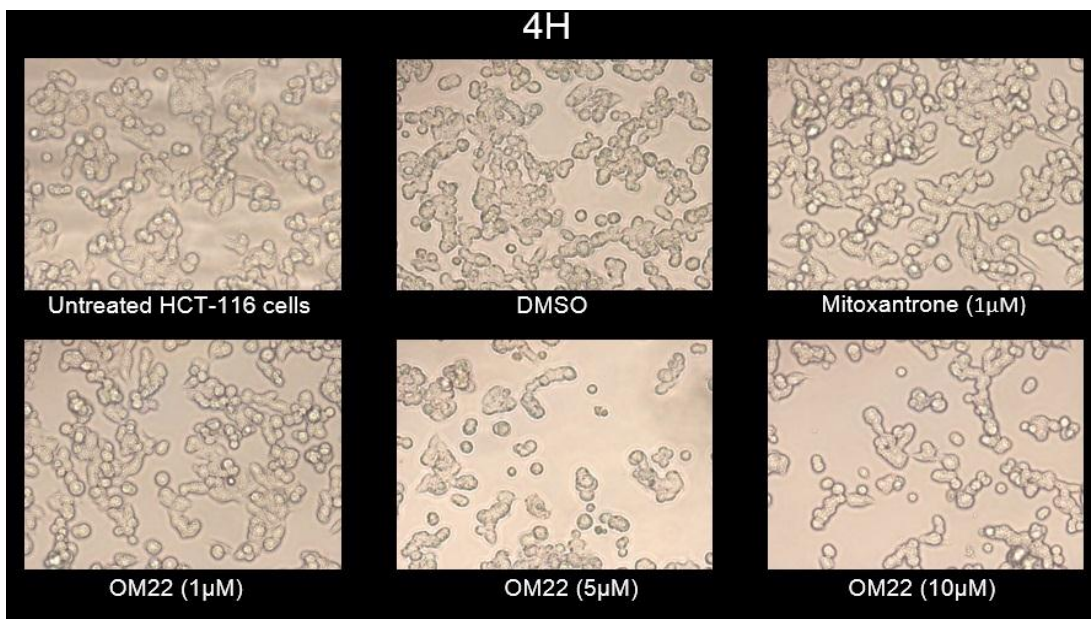


Figure 1.121: Cytotoxic effects of SH1 on HCT-116 cells. Bright field microscopy changes in cell morphology after 4 h post-treatment with OM22 at 5 µM and 10 µM with no changes at other concentrations and control cells.

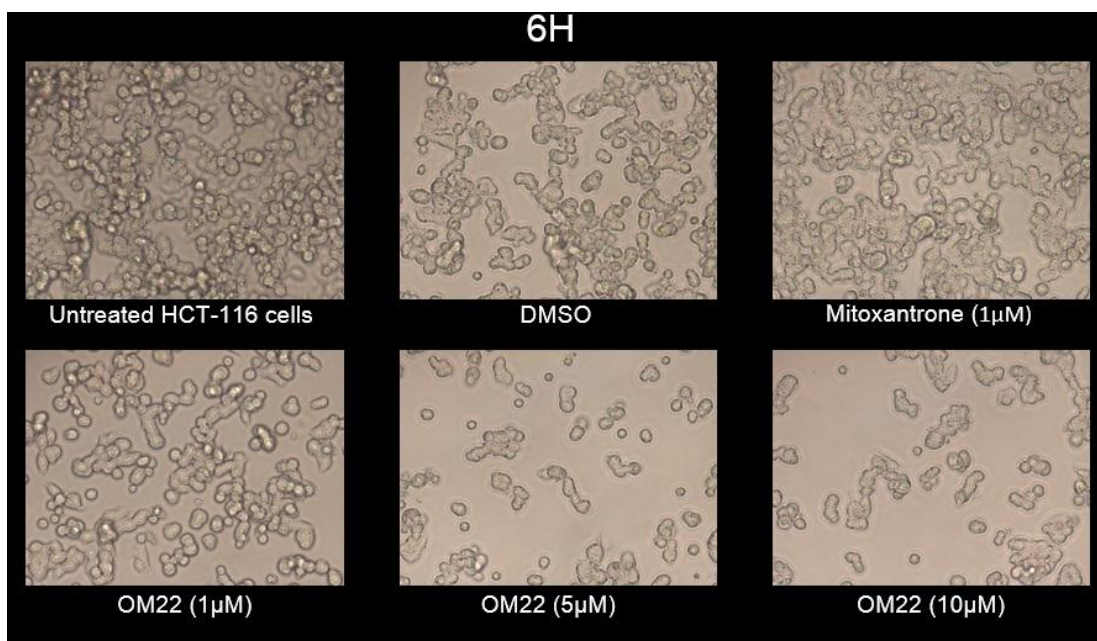


Figure 1.122: Cytotoxic effects of SH1 on HCT-116 cells. Bright field microscopy changes in cell morphology after 6 h post-treatment with OM22 at 1 µM, 5 µM and 10 µM with no changes in control cells.

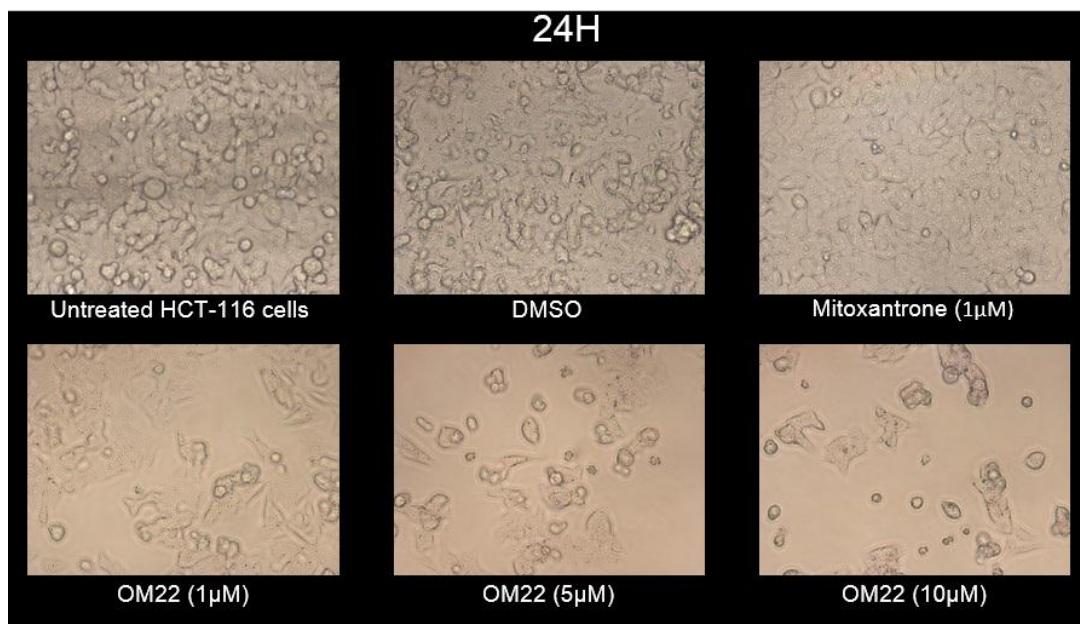


Figure 1.123: Cytotoxic effects of SH1 on HCT-116 cells. Bright field microscopy changes in cell morphology after 24 h post-treatment with OM22 at 1 µM, 5 µM and 10 µM with no changes in control cells.

In conclusion, cell morphological changes characteristic of apoptosis such as round shape of the cell, cell shrinkage, nucleus condensation, plasma membrane blebbing and formation of apoptotic bodies (Hacker, 2000) were confirmed under bright field microscopy. According to Doonan and Cotter (2008), using bright field microscopy to determine the morphological features remains the best and easiest way and these special morphological changes form the basis of a widely used technique for the definition of cell apoptosis (Doonan and Cotter, 2008). Thus, the morphological changes induced by SH1 and OM22 indicated that these novel compounds induced cell apoptosis. The percentage of apoptotic cells treated with SH1 and OM22 increased with time at all tested concentrations in contrast with untreated cells, DMSO treated cells and cells treated with mitoxantrone which there were no morphological changes observed in cell culture at all time points.

1.3.11 **Conclusion**

Many anticancer drugs experience limitations from high side effects on normal cells, poor selectivity to target cells and resistance of cancer cells which leads to a decrease in the accumulations of the anticancer drugs inside the targeted cells. Therefore, a series of novel prodrugs and experimental mitoxantrone-related anthraquinone derivatives were synthesized and ester-linked with TPP or rhodamine B. The prodrugs were designed in order to evade P-glycoprotein (P-gp) efflux pumps and thus potentially circumvent multidrug resistance. The TPP and rhodamine B conjugate compounds were successfully synthesized in this research programme and the structures of these novel compounds were confirmed by high resolution electrospray (+) mass spectrometry, ¹H NMR and ¹³C NMR spectroscopy. However, the synthesis of mitoxantrone conjugates was unsuccessful and compounds of unconfirmed structure were obtained from the reactions of TPP or rhodamine B with mitoxantrone. During *in vitro* assays, the distribution coefficient assay revealed that attaching TPP to the target compounds increased the lipophilic properties of these compounds which meant that they will be easily taken up by the cells. In addition to the lipophilic characteristic, the cationic charge also plays a significant role in the localisation of TPP conjugates inside the mitochondria as shown by confocal microscopy. The results from the cellular uptake also indicated that even small structural changes could alter the localisation of the targeting compound as in OM22 [TPP-EAE-AQ(4-OH)] which has a secondary amine in its side chain and make it weakly basic and localised in the lysosome. From DNA binding studies, the results showed that the novel TPP conjugated compounds bind with DNA with high affinity compared with unconjugated compounds. The DNA binding for TPP conjugates were also compared with mitoxantrone, which is known to bind with DNA with high affinity, in order to determine the factors that could affect the drug-DNA binding affinity. In general, the more hydroxy groups in the anthraquinone chromophore, the greater the DNA binding affinity a compound possesses. Also, the presence of the amino groups in the side chains has a crucial effect on the DNA binding affinity. These results are in line with the results obtained from the MTT assay and the morphology study, which showed that attaching TPP makes the compound more cytotoxic in comparison with unconjugated compounds in tested cells lines. This suggests that the greater DNA binding affinity the compounds have, the more

cytotoxic potency they will possess. Additionally, The TPP conjugated compounds showed effective morphological changes such as cell shrinkage, floating and change in cell size indicating that these compounds effectively induced apoptosis in HCT-116 colon cancer cells. Therefore, this shows the great potential of the novel compounds that have been synthesised in this research project as promising mitochondrial targeting agents in cancer cells with high efficacy and could potentially reduce the side effects on normal cells.

Chapter 1

Experimental

1.4 Experimental

1.4.1 Analytical methods

1.4.1.1 Instruments

UV-visible absorbance spectra were obtained on a Beckman Coulter DU800 spectrophotometer and fluorescence experiments were obtained on a Perkin Elmer LS55 spectrophotometer.

1.4.1.2 Thin layer chromatography (TLC)

Thin layer chromatography was carried out on Kieselgel 60 F₂₅₄ pre-coated aluminium plates (Merck). Most compounds synthesised absorbed in the visible region, additional visualisation where required was by UV light (254 and 365 nm). Solvent systems used for TLC were A) chloroform: methanol 4:1; B) chloroform: methanol 9:1; and C) butanol: glacial acetic acid: water 4:5:1.

1.4.1.3 Column chromatography

Kieselgel 60 (0.063-0.0200 mm, Merck) silica gel was used in column chromatography.

1.4.1.4 Mass spectrometry

High and low resolution (nano) electrospray mass spectra were recorded on a Thermofisher LTQ Orbitrap XL and Waters ZQ4000 instruments (EPSRC National Mass Spectrometry Facility, Swansea).

1.4.1.5 High performance liquid chromatography (HPLC)

Reverse-phase HPLC was performed on Phenomenex Synergi POLAR column [4 µM (30 mm x 4.6 mm), flow rate 2 mL/min] using mobile phase 100% ACN + 0.1% TFA (A) and 100% water + 0.08% TFA (B).

1.4.1.6 Proton and carbon nuclear magnetic resonance (¹H and ¹³C NMR)

¹H and ¹³C NMR spectra were recorded on either a Bruker AC300 NMR spectrometer at 25°C at 300.1 MHz and 75.5 MHz, the samples were dissolved either in deuterated DMSO or deuterated chloroform and transferred to standard NMR testing tubes with a solution height range between 5 and 5.5cm.

1.4.2 General method A: For dichloromethane or chloroform / water solvent extraction

The reaction mixture was partitioned between chloroform and water (1:1, 200 mL, total volume), the chloroform layer was washed with water (3x100 mL), dried (anhydrous sodium sulfate), filtered and evaporated to dryness.

1.4.3 Synthesis of the mitoxantrone derivative-TPP conjugates

1.4.3.1 Synthesis of 1-hydroxy-4-((2-((2-hydroxyethyl)amino)ethyl)amino)anthracene-9,10-dione (HO-EAE-AQ(4-OH) (OM1))

Leucoquinizarin (1 g, 4.13 mmol) was dissolved in CH₂Cl₂ (50 mL) and N-(2-hydroxyethyl)ethylenediamine (1.3 mL, 12.5 mmol) was added and heated at 400°C for 1 h. The product was then oxidized by aeration with the addition of triethylamine (Et₃N, 0.5 mL). The product OM1 (R_f 0.43) was then isolated by CH₂Cl₂/water solvent extraction [general method A] and the organic extracts were left overnight to dry. The crude product was then used for further reaction without further purification.

TLC of the crude mixture (chloroform: methanol, 4:1): R_f 0.43 (purple) OM1, 0.88 (orange) oxidized form of leucoquinizarin.

1.4.3.2 Synthesis of tert-butyl (2-((4-hydroxy-9,10-dioxo-9,10-dihydroanthracen-1-yl)amino)ethyl)(2-hydroxyethyl)carbamate (HO-EAE-Boc-AQ (4-OH) (OM2)

Crude OM1 (2 g, 6.15 mmol) was suspended in methanol (50 mL) and cooled over ice (0°C). Di-tert-butyl dicarbonate (Boc₂O) (2.6 g, 12 mmol) was dissolved in methanol and was added to OM1 dropwise with stirring and allowed to react over ice for 60 min. The product OM2 was extracted into chloroform using chloroform/water solvent extraction [general method A]. The product was filtered and applied to a silica gel chromatography column initially using neat chloroform and then the polarity of the solvent was increased by using chloroform: ethyl acetate + 6% methanol. Fractions containing OM2 were filtered and evaporated to dryness in vacuo.

TLC of OM2 (chloroform: methanol, 4:1) R_f 0.7 (purple) (OM2).

ESMS (+) m/z: 427.1864 (100%) [M+H]⁺, 449.1681 (37%) [M+Na]⁺, 875.3477 (51%) [2M+Na]⁺.

1.4.3.3 Synthesis of (5-(2-((tert-butoxycarbonyl)(2-((4-hydroxy-9,10-dioxo-9,10-dihydroanthracen-1-yl)amino)ethyl)amino)ethoxy)-5-oxopentyl)triphenylphosphonium (TPP-EAE-Boc-AQ-(4-OH)) (OM22-Boc)

4-Carboxybutyl)triphenylphosphonium bromide (TPP) (0.24 g, 0.54 mmol), DCC (0.24 g, 1.18 mmol) and DMAP (5-10 mg) were dissolved in CH₂Cl₂ (10 mL) and allowed to react for 15 min then added to OM2 (0.21 g, 0.49 mmol) in CH₂Cl₂ (5 mL) and left over ice with stirring for 1 h. After 1 h, additional half amounts of TPP and DCC were added and allowed to react for another 1 h. The product was washed with water and filtered. OM22-Boc was applied to a silica gel chromatography column using neat CH₂Cl₂ initially and then more polar solvents CH₂Cl₂: ethyl acetate and then CH₂Cl₂: ethyl acetate + 2% methanol were used. OM22-Boc was filtered and evaporated to dryness in vacuo. Ethyl acetate was added then cooled for 30 min. The product was isolated by filtration and evaporation to dryness in vacuo.

TLC of OM22 BOC (dichloromethane: methanol, 9:1) R_f 0.4 (purple) (OM22 BOC).

HRMS (ESI) (+) m/z : 771.3177 (100%) $[M]^+$. Calculated for $[C_{46}H_{48}N_2O_7P]^+$ 771.3177; Found 771.3177.

1.4.3.4 Synthesis of (5-(2-((2-((4-hydroxy-9,10-dioxo-9,10-dihydroanthracen-1-yl)amino)ethyl)ammonio)ethoxy)-5-oxopentyl)triphenylphosphonium TPP-EAE-AQ(4-OH) (OM22)

Trifluoroacetic acid (TFA) (1 mL) was added for 30 min. The solvent was evaporated and addition of diethyl ether (20 mL) gave a precipitate of OM22, which was filtered off and dried. Yield 47%, 0.24 g.

TLC of OM22 (dichloromethane: methanol, 9:1) R_f 0.32 (purple) (OM22).

HRMS (ESI) (+) m/z : 671.2658 (100%) $[M-TFA]^+$. Calculated for $[C_{41}H_{40}N_2O_5P]^+$ 671.2669; Found 671.2658.

1H NMR (DMSO- d_6 , 300 MHz): δ (ppm) 1.51-1.81 (m, 4H, $CH_2CH_2CH_2CH_2P$), 2.45 (t, 2H, $CH_2-C=O$, J 12 Hz), 3.19-3.32 (m, 4H, $CH_2-NH-CH_2$), 3.64 (t, 2H, CH_2-P , J 21 Hz) 3.82 (m, 2H, AQ-NH- CH_2), 4.27 (t, 2H, CH_2O , J 12 Hz), 7.39 (d, 1H, AQ-H2, J 15 Hz), 7.61 (d, 1H, AQ-H3, J 15 Hz), 7.73-7.99 (m, 17H, H_{AR} of AQ and TPP), 8.23-8.28 (m, 2H, AQ-H5 and H8), 9.03 (s, 2H, NH_2), 10.20 (t, 1H, AQ-NH, J 12 Hz), 13.54 (s, 1H, AQ-OH).

^{13}C NMR (DMSO- d_6 , 75.5 MHz): δ (ppm) 21.10 (-ve, CH_2), 21.16 (-ve, CH_2), 25.03 (-ve, CH_2-P), 32.19 (-ve, CH_2), 38.40 (-ve, CH_2-NH), 45.73 (-ve, CH_2-NH_2), 46.06 (-ve, NH_2-CH_2), 59.41 (-ve, CH_2-O), 108.46 (ab, q, C_{AR-AQ}), 113.13 (ab, q, C_{AR-AQ}), 117.87 and 119.00 (d, ab, C_{AR-TPP}), 125.21 (+ve, C_{AR-AQ}), 126.09 (+ve, C_{AR-AQ}), 126.35 (+ve, C_{AR-AQ}), 128.63 (+ve, C_{AR-AQ}), 130.14 and 130.31 (+ve, C_{AR-TPP} meta), 131.90 (ab, q, C_{AR-AQ}), 133.28 (+ve, C_{AR-AQ}), 133.47 and 133.61 (+ve, C_{AR-TPP} ortho), 134.52 (+ve, C_{AR-AQ}), 134.88 (+ve, C_{AR-AQ} and C_{AR-TPP} para), 146.61 (ab, q, C_{AR-AQ}), 156.12 (ab, q, C_{AR}), 172.30 (ab, q, $C=O$), 181.34 (ab, q, $C=O$), 186.96 (ab, q, $C=O$).

1.4.3.5 Synthesis of 1-hydroxy-4-((4-hydroxybutyl)amino)anthracene-9,10-dione (OH-Butyl-AQ (4-OH) (NU:UB 252))

Leucoquinizarin (1 g, 4.13 mmol) was dissolved in CH₂Cl₂ (50 mL) and 4-amino-1-butanol (1.901 mL, 20.65 mmol) was added and heated at 40°C for 1 h. The product was then oxidized by aeration with the addition of triethylamine (Et₃N, 0.5 mL). The product was then isolated by CH₂Cl₂/water solvent extraction [general method A] and the organic extracts were evaporated. The product was purified by using silica gel chromatography column initially using neat chloroform then chloroform: ethyl acetate was used. The solvent was evaporated and addition of diethyl ether (20 mL) gave a precipitate of NU:UB 252, which was filtered off and dried. Yield 22%, 0.28 g

TLC of the crude mixture (chloroform: methanol, 9:1): R_f 0.51 (purple) NU:UB 252, 0.42 (blue) 1,4-bis substituted compound, 0.8 (orange) oxidized form of leucoquinizarin.

¹H NMR (DMSO-_d6, 300MHz): δ (ppm) 1.50-1.73 (m, 4H, NHCH₂CH₂CH₂CH₂OH), 3.35 (m, 2H, AQ-NH-CH₂), 3.48 (t, 2H, CH₂OH, J 6 Hz), 4.51 (s, 1H, OH), 7.21 (d, 1H, AQ-H2, J 9 Hz), 7.35 (d, 1H, AQ-H3, J 9 Hz), 7.74-7.90 (m, 2H, AQ-H6 and H7), 8.13 (m, 2H, AQ-H5 and H8), 10.16 (s, 1H, AQ-NH), 13.57 (s, 1H, AQ-OH).

¹³C NMR (DMSO-_d6, 75.5 MHz): δ (ppm) 25.67 (-ve, CH₂), 29.86 (-ve, CH₂), 41.92 (-ve, CH₂-NH), 60.32 (-ve, CH₂-O), 106.99 (ab, q, C_{AR}-AQ), 112.66 (ab, q, C_{AR}-AQ), 125.22 (+ve, C_{AR}-AQ), 125.78 (+ve, C_{AR}-AQ), 126.15 (+ve, C_{AR}-AQ), 128.60 (+ve, C_{AR}-AQ), 131.74 (ab, q, C_{AR}-AQ), 132.67 (+ve, C_{AR}-AQ), 134.44 (+ve, C_{AR}-AQ), 134.61 (ab, q, C_{AR}-AQ), 147.18 (ab, q, C_{AR}-AQ), 156.04 (ab, q, C_{AR}-AQ), 180.45 (ab, q, C=O), 186.47 (ab, q, C=O).

1.4.3.6 Synthesis of (5-(4-((4-hydroxy-9,10-dioxo-9,10-dihydroanthracen-1-yl)amino)butoxy)-5-oxopentyl)triphenylphosphonium (TPP-Butyl-AQ(4-OH) (OM30))

(4-Carboxybutyl)triphenylphosphonium bromide (TPP) (0.42 g, 0.94 mmol), DCC (0.46 g, 2.23 mmol) and DMAP (5-10 mg) were dissolved in CH₂Cl₂ (10 mL) and allowed to react for 15 min then added to NU:UB 252 (0.2 g, 0.64 mmol) in dichloromethane (5 mL) and

left over ice with stirring for 1 h. After 1 h, additional half amounts of TPP and DCC were added and allowed to react for another 1 h. The product OM30 was extracted using chloroform/water solvent extraction [general method A]. The product was filtered and applied to a silica gel chromatography column using neat chloroform initially and then 9:1 chloroform: ethyl acetate and chloroform: ethyl acetate + 3% methanol were used. The solvent was evaporated and addition of diethyl ether (20 mL) gave a precipitate of OM30, which was filtered off and dried. Yield 42%, 0.26 g.

TLC of OM30 (chloroform: methanol, 9:1) R_f 0.4 (purple) (OM30).

HRMS (ESI) (+) m/z : 656.2546 (100%) $[M-Br]^+$. Calculated for $[C_{41}H_{39}NO_5P]^+$ 656.2560; Found 656.2546.

1H NMR (DMSO- d_6 , 300MHz): δ (ppm) 1.50 – 1.80 (m, 8H, $NHCH_2CH_2CH_2CH_2O$ and $OCOCH_2CH_2CH_2CH_2P$), 2.41 (t, 2H, $CH_2-C=O$, J 6 Hz), 3.42 (m, 2H, AQ-NH- CH_2), 3.62 (t, 2H, CH_2P , J 12 Hz), 4.05 (m, 2H, CH_2O), 7.33 (d, 1H, AQ-H2, J 9 Hz), 7.48 (d, 1H, AQ-H3, J 9 Hz), 7.71 – 7.95 (m, 17H, H_{AR} of AQ and TPP), 8.17 – 8.25 (m, 2H, AQ-H5 and H8); 10.25 (s, 1H, AQ-NH), 13.63 (s, 1H, AQ-OH).

^{13}C NMR (DMSO- d_6 , 75.5 MHz): δ (ppm) 20.25 (-ve, CH_2), 21.11 (-ve, CH_2), 21.17 (-ve, CH_2), 25.03 and 25.26 (-ve, CH_2-P), 25.54-25.67 (-ve, CH_2CH_2-P), 32.41 (-ve, CH_2), 41.60 (-ve, CH_2-NH), 63.45 (-ve, CH_2-O), 107.20 (ab, q, C_{AR_AQ}), 112.79 (ab, q, C_{AR0-AQ}), 117.87 and 119.01 (d, ab, C_{AR-TPP}), 125.46 (+ve, C_{AR-AQ}), 125.96 (+ve, C_{AR-AQ}), 126.25 (+ve, C_{AR-AQ}), 128.83 (+ve, C_{AR-AQ}), 130.13 and 130.29 (+ve, C_{AR-TPP} meta), 131.85 (ab, q, C_{AR-AQ}), 132.94 (+ve, C_{AR-AQ}), 133.46 and 133.59 (+ve, C_{AR-TPP} ortho), 134.67 (+ve, C_{AR-AQ}), 134.86 (ab, q, C_{AR-AQ}) 134.89 (+ve, C_{AR-TPP} para), 147.27 (ab, q, C_{AR-AQ}), 156.12 (ab, q, C_{AR-AQ}), 172.49 (ab, q, $C=O$), 180.74 (ab, q, $C=O$), 186.66 (ab, q, $C=O$).

1.4.3.7 Synthesis of 1-hydroxy-4-((5-hydroxypentyl)amino)anthracene-9,10-dione (HO-pentyl-AQ(4-OH) (OM28)

Leucoquinizarin (1 g, 4.13 mmol) was dissolved in CH_2Cl_2 (50 mL) and 5-amino-1-pentanol (2.12g, 20.58 mmol) was added and heated at 40°C for 1 h. The product was

oxidized by aeration with the addition of triethylamine (Et₃N, 0.5 mL). The product was isolated by CH₂Cl₂/water solvent extraction [general method A] and the organic extracts were evaporated. The product was purified by using silica gel chromatography column using neat chloroform initially then, chloroform + 2% ethyl acetate was used. The solvents were evaporated in vacuo to dryness and addition of diethyl ether (20 mL) gave a precipitate of the AQ-aminopentanol compound (OM28), which was filtered off and dried. Yield 21%, 0.28 g.

TLC of the crude mixture (chloroform: methanol, 9:1): R_f 0.51 (purple) OM28, 0.5 (blue) bis-substituted compound, 0.83 (orange) oxidized form of leucoquinizarin.

HRMS (ESI) (+) m/z: 326.1389 (100%) [M+H]⁺. Calculated for [C₁₉H₁₉O₄NH]⁺ 326.1387; Found 326.1389.

1.4.3.8 Synthesis (5-((5-((4-hydroxy-9,10-dioxo-9,10-dihydroanthracen-1-yl)amino)pentyl)oxy)-5-oxopentyl)triphenylphosphonium (TPP-Pentyl-AQ(4-OH) (OM31)

4-Carboxybutyl)triphenylphosphonium bromide (TPP) (0.4 g, 0.9 mmol), DCC (0.45 g, 2.18 mmol) and DMAP (5-10 mg) were dissolved in CH₂Cl₂ (10 mL) and allowed to react for 15 min then added to OM28 (0.2 g, 0.61 mmol, 1 eq) in CH₂Cl₂ (5 mL) and left over ice with stirring for 1 h. The product OM31 was extracted using chloroform/water solvent extraction [general method A]. The product was filtered and applied to a silica gel chromatography column using neat chloroform initially and then the polarity of the solvents was increased as follows; chloroform + 3% ethyl acetate, 9:1 chloroform: ethyl acetate, 4:1 chloroform: ethyl acetate, 4:1 chloroform: ethyl acetate + 5% methanol and 9:1 chloroform: methanol. The solvents were evaporated in vacuo to dryness and addition of diethyl ether (20 mL) gave a precipitate of OM30, which was filtered off and dried. Yield 39%, 0.16 g.

TLC of OM31 (chloroform: methanol, 9:1) R_f 0.28 (purple) OM31, 0.38 (red) unknown red compound.

HRMS (ESI) (+) m/z: 670.2698 (100%) cation (+). Calculated for [C₄₂H₄₁NO₅P]⁺ 670.2717; Found 670.2698.

¹H NMR (DMSO, 300MHz): δ (ppm) 1.35-1.49 (m, 2H, NH-CH₂CH₂CH₂CH₂CH₂-O), 1.5-1.81 (m, 8H, NH-CH₂CH₂CH₂CH₂CH₂-O and CH₂CH₂CH₂-P) 2.39 (t, 2H, CH₂-C=O, J 9 Hz), 3.42 (q, 2H, AQ-NH-CH₂), 3.61 (t, 2H, CH₂-P, J 15 Hz), 4.01 (t, 2H, CH₂-O, J 6 Hz), 7.36 (d, 1H, AQ-H₂, J 9 Hz), 7.51 (d, 1H, AQ-H₃, J 9 Hz), 7.71-7.95 (m, 17H, H_{AR} of AQ and TPP), 8.24 (m, 2H, AQ-H₅ and H₈), 10.3 (s, 1H, AQ-NH), 13.67 (s, 1H, AQ-OH).

¹³C NMR (DMSO-d₆, 75.5 MHz): δ (ppm) 20.22 (-ve, CH₂), 21.08 (-ve, CH₂), 22.80 (-ve, CH₂), 25.00 (-ve, CH₂-P), 27.72 (-ve, CH₂), 32.40 (-ve, CH₂), 38.67 (-ve, CH₂), 41.85 (-ve, CH₂-NH), 63.57 (-ve, CH₂-O), 107.19 (ab, q, C_{AR}-AQ), 113.78 (ab, q, C_{AR}-AQ), 117.86 and 119.0 (d, ab, C_{AR}-TPP), 125.58 (+ve, C_{AR}-AQ), 126.01 (+ve, C_{AR}-AQ), 126.27 (+ve, C_{AR}-AQ), 128.95 (+ve, C_{AR}-AQ), 130.13 and 130.29 (+ve, C_{AR}-TPP meta), 131.97 (ab, q, C_{AR}-AQ), 132.94 (+ve, C_{AR}-AQ), 133.45 and 133.59 (+ve, C_{AR}-TPP ortho), 134.73 (+ve, C_{AR}-AQ), 134.82 (ab, q, C_{AR}-AQ) 134.90 (+ve, C_{AR}-TPP para), 147.39 (ab, q, C_{AR}-AQ), 156.24 (ab, q, C_{AR}-AQ), 172.47 (ab, q, C=O), 180.72 (ab, q, C=O).

1.4.3.9 Synthesis of 1-hydroxy-4-((2-(2-hydroxyethoxy)ethyl)amino)anthracene-9,10-dione (HO-EOE-AQ(4-OH) (OM29)

Leucoquinizarin (1 g, 4.13 mmol) was dissolved in CH₂Cl₂ (50 mL) and 2-(2-aminoethoxy)ethanol (2.16g, 20.57 mmol) was added and heated at 40°C for 1 h. The product was then oxidized by aeration with the addition of triethylamine (Et₃N, 0.5 mL). The product was then isolated by CH₂Cl₂/water solvent extraction [general method A] and the organic extracts were evaporated in vacuo to a low volume. The product was purified by using silica gel chromatography column using neat chloroform at the beginning then chloroform + 4% methanol followed by chloroform + 6% methanol. Yield 39%, 0.52 g.

TLC of the crude mixture (chloroform: methanol, 9:1): R_f 0.58 (purple) OM29, 0.51 (blue) two arm compound, 0.84 (orange) oxidized form of leucoquinizarin.

HRMS (ESI) (+) m/z: 328.1181 (100%) [M+H]⁺. Calculated for [C₁₈H₁₇O₅NH]⁺ 328.1179; Found 328.1181.

1.4.3.10 Synthesis of (5-(2-(2-((4-hydroxy-9,10-dioxo-9,10-dihydroanthracen-1-yl)amino)ethoxy)ethoxy)-5-oxopentyl)triphenylphosphonium (TPP-EOE-AQ(4-OH) (OM32)

(4-Carboxybutyl)triphenylphosphonium bromide (TPP) (0.4 g, 0.9 mmol), DCC (0.37 g, 1.79 mmol) and DMAP (5-10 mg) were dissolved in CH₂Cl₂ (10 mL) and allowed to react for 15 min then added to OM29 (0.25 g, 0.76 mmol, 1 eq) in CH₂Cl₂ (5 mL) and left over ice with stirring for 1 h. After 1 h, additional half amounts of TPP and DCC were added and allowed to react for another 1 h. The product OM32 was extracted using chloroform/water solvent extraction [general method A]. The product was filtered and solvents were evaporated in vacuo to lower volume and applied to a silica gel chromatography column using neat chloroform initially and then the polarity of the solvents were increased as follows ; chloroform + 3% ethyl acetate, 9:1 chloroform: ethyl acetate, 4:1 chloroform: ethyl acetate, 4:1 chloroform: ethyl acetate + 5% methanol and 9:1 chloroform: methanol. The solvents were evaporated in vacuo to dryness and addition of diethyl ether (20 mL) gave a precipitate of OM32, which was filtered off and dried. Yield 47%, 0.24 g.

TLC of OM32 (chloroform: methanol, 9:1) R_F 0.12 (purple) OM32, 0.28 (red) unknown compound.

HRMS (ESI) (+) m/z: 672.2501 (100%) cation (+). Calculated for [C₄₁H₃₉NO₆P]⁺ 672.2510; Found 672.2501.

¹H NMR (DMSO-d₆, 300 MHz): δ (ppm) 1.47-1.79 (m, 4H, CH₂CH₂CH₂CH₂P), 2.41 (m, 2H, CH₂-C=O), 3.34 (m, 2H, AQ-NH-CH₂), 3.5-3.73 (m, 6H, NHCH₂CH₂-O-CH₂CH₂O and CH₂-P) 4.12-4.18 (m, 2H, NHCH₂CH₂-O-CH₂CH₂O), 7.37 (d, 1H, AQ-H₂, J 15 Hz), 7.55 (d, 1H, AQ-H₃, J 15) Hz, 7.71-7.95 (m, 17H, H_{AR} of AQ and TPP), 8.20-8.27 (m, 2H, AQ-H₅ and H₈), 10.37 (t, 1H, AQ-NH), 13.65 (s, 1H, AQ-OH).

^{13}C NMR (DMSO- d_6 , 75.5 MHz): δ (ppm) 20.28 (-ve, CH_2), 21.09 (-ve, CH_2), 32.26 (-ve, $\text{CH}_2\text{-P}$), 41.92 (-ve, NHCH_2), 59.74 (-ve, CH_2), 62.99 (-ve, CH_2O), 68.12 (-ve, OCH_2), 68.88 (-ve, CH_2O), 107.36 (ab, q, $\text{C}_{\text{AR-AQ}}$), 112.82 (ab, q, $\text{C}_{\text{AR-AQ}}$), 117.82 and 117.89 (d, ab, $\text{C}_{\text{AR-TPP}}$), 118.96 and 119.03 (d, ab, $\text{C}_{\text{AR-TPP}}$), 125.81 (+ve, $\text{C}_{\text{AR-AQ}}$), 126.02 (+ve, $\text{C}_{\text{AR-AQ}}$), 126.25 (+ve, $\text{C}_{\text{AR-AQ}}$), 128.71 (+ve, $\text{C}_{\text{AR-AQ}}$), 130.12 and 130.28 (+ve, $\text{C}_{\text{AR-TPP}}$ meta), 131.90 (ab, q, $\text{C}_{\text{AR-AQ}}$), 133.00 (+ve, $\text{C}_{\text{AR-AQ}}$), 133.48 and 133.56 (+ve, $\text{C}_{\text{AR-TPP}}$ ortho), 133.61 (+ve, $\text{C}_{\text{AR-AQ}}$), 134.70 (ab, q, $\text{C}_{\text{AR-AQ}}$), 134.90 (+ve, $\text{C}_{\text{AR-TPP}}$ para), 147.34 (ab, q, $\text{C}_{\text{AR-AQ}}$), 156.17 (ab, q, $\text{C}_{\text{AR-AQ}}$), 172.46 (ab, q, $\text{C}=\text{O}$), 180.81 (ab, q, $\text{C}=\text{O}$), 186.78 (ab, q, $\text{C}=\text{O}$).

1.4.3.11 Synthesis of 1-((4-hydroxybutyl)amino)anthracene-9,10-dione (OH-butyl-AQ) (NU:UB 238)

1-Chloroanthraquinone (40 mmol) was suspended in DMSO (15 mL) and 4-amino-1-butanol (5.0 g, 56 mmol) was added and the mixture was heated for 30 min over a boiling water bath. The solution was cooled and added to a large excess of water (500 mL). The red precipitated solid was filtered off, dried and used for subsequent reactions without further purification.

TLC of the crude mixture (dichloromethane: methanol, 9:1): R_f 0.1 (red) NU:UB 238, 0.9 (yellow) 1-chloroanthraquinone.

HRMS (ESI) (+) m/z : 296.1284 (100%) $[\text{M}+\text{H}]^+$. Calculated for $[\text{C}_{18}\text{H}_{17}\text{O}_3\text{NH}]^+$ 296.1281; Found 296.1284.

1.4.3.12 Synthesis of (5-(4-((9,10-dioxo-9,10-dihydroanthracen-1-yl)amino)butoxy)-5-oxopentyl)triphenylphosphonium (TPP-Butyl-AQ) (SH1)

(4-Carboxybutyl)triphenylphosphonium bromide (TPP) (0.49 g, 1.10 mmol), DCC (0.49 g, 2.37 mmol) and DMAP (5-10 mg) were dissolved in CH_2Cl_2 (10 mL) and allowed to react for 15 min then added to 1-[(4-hydroxybutyl)amino]anthraquinone NU:UB 238, (0.25 g,

0.84 mmol) in CH₂Cl₂ (5 mL) and stirred for 1 h. The product SH1 was extracted using chloroform/water solvent extraction [general method A]. The product was filtered and applied to a silica gel chromatography column using neat CH₂Cl₂ initially and then CH₂Cl₂: ethyl acetate and then CH₂Cl₂: ethyl acetate + 2% - 7% methanol. SH1 was filtered and evaporated to dryness in vacuo. The compound was sticky, so second column chromatography was performed. The crude product was filtered and evaporated to dryness under vacuo and acetonitrile: diethyl ether solution was added to solidify SH1. Yield 46%, 0.11 g.

TLC of SH1 (chloroform: methanol, 9:1) R_f 0.34 (red) (SH1).

HRMS (ESI) (+) m/z: 640.2594 (100%) [M]⁺. Calculated for [C₄₁H₃₉NO₄P]⁺ 640.2611; Found 640.2594.

¹H NMR (DMSO-*d*₆, 300MHz): δ (ppm) 1.50 – 1.80 (m, 8H, NHCH₂CH₂CH₂CH₂O and OCOCH₂CH₂CH₂CH₂P), 2.41 (t, 2H, CH₂-C=O, J 15 Hz), 3.36 (m, 2H, AQ-NH-CH₂), 3.62 (t, 2H, CH₂P, J 30 Hz), 4.06 (s, 2H, CH₂O), 7.26 (d, 1H, AQ-H₂, J 18 Hz), 7.43 (d, 1H, AQ-H₄, J 15 Hz), 7.65 (d, 1H, AQ-H₃, J 15 Hz), 7.72 – 7.94 (m, 17H, H_{AR} of AQ and TPP), 8.10 – 8.21 (m, 2H, AQ-H₅ and H₈); 9.68 (t, 1H, AQ-NH, J 9 Hz).

¹³C NMR (DMSO-*d*₆, 75.5 MHz): δ (ppm) 20.25 (-ve, CH₂), 21.11 (-ve, CH₂), 21.16 (-ve, CH₂), 25.02 and 25.09 (-ve, CH₂-P), 25.54-25.67 (-ve, CH₂CH₂-P), 32.41 (-ve, CH₂), 41.69 (-ve, CH₂-NH), 63.47 (-ve, CH₂-O), 111.89 (ab, q, C_{AR}-AQ), 115.02 (+ve, C_{AR}-AQ), 117.87 and 119.00 (d, ab, C_{AR}-TPP), 126.25 (+ve, C_{AR}-AQ), 126.34 (+ve, C_{AR}-aq), 130.13 and 130.29 (+ve, C_{AR}-TPP meta), 132.30 (ab, q, C_{AR}-AQ), 133.45 and 133.59 (+ve, C_{AR}-TPP ortho), 133.89 (ab, q, C_{AR}-AQ), 134.28 (ab, q, C_{AR}-AQ) 134.49 (+ve, C_{AR}-AQ), 134.86 (+ve, C_{AR}-AQ), 134.90 (+ve, C_{AR}-TPP para), 135.65 (+ve, C_{AR}-AQ), 151.28 (ab, C_{AR}-AQ), 172.49 (ab, q, C=O), 182.81 (ab, q, C=O), 184.00 (ab, q, C=O).

1.4.3.13 Synthesis of (5-((5-((4-((5-hydroxypentyl)amino)-9,10-dioxo-9,10-dihydroanthracen-1-yl)amino)pentyl)oxy)-5-oxopentyl)triphenylphosphonium TPP-NU:UB 65 (OM25)

NU:UB 65 (0.1 g, 0.24 mmol) was dissolved in CH₂Cl₂. TPP (0.05 g, 0.121 mmol), DCC (0.025 g, 0.121 mmol) and DMAP (5-10 mg) were dissolved in CH₂Cl₂ and allowed to react for 10 min then was added to NU:UB 65 in CH₂Cl₂ and allowed to react at rt for 1 h. The reaction was filtered and was extracted using CH₂Cl₂/ water solvent extraction [general method A]. OM25 was purified by column chromatography using CH₂Cl₂: methanol (19:1). The solvents were evaporated and diethyl ether was added to solidify OM25, which was filtered and dried. Yield 33%, 0.06 g.

TLC for OM25 (dichloromethane: methanol, 9:1) R_f 0.35 (purple) (OM25).

HRMS (ESI) (+) m/z: 755.3590 (100%) cation (+). Calculated for [C₄₇H₅₂N₂O₅P]⁺ 755.3608; Found 755.3590.

1.4.3.14 Synthesis of (((((9,10-dioxo-9,10-dihydroanthracene-1,4-diyl)bis(azanediy))bis(pentane-5,1-diyl))bis(oxy))bis(5-oxopentane-5,1-diyl))bis(triphenylphosphonium) bis-TPP-NU:UB 65 (OM26)

NU:UB 65 (0.1 g, 0.24 mmol) was dissolved in CH₂Cl₂. TPP (0.64 g, 1.46 mmol), DCC (0.3 g, 1.46 mmol) and DMAP (5-10 mg) were dissolved in CH₂Cl₂ and allowed to react for 10 min then added to NU:UB 65 in CH₂Cl₂ and allowed to react at rt for 1 h. The reaction was filtered to remove DCU and was extracted using CH₂Cl₂/ water solvent extraction [general method A]. Ethyl acetate was added to remove DCU and it was filtered and dried. OM26 was applied to a silica gel chromatography column using CH₂Cl₂: methanol (19:1). The solvents were evaporated and diethyl ether was added and cooled overnight to solidify OM26, which was filtered and dried. Yield 69%, 0.18 g.

TLC for OM26 (dichloromethane: methanol, 9:1) R_f 0.17 (purple) (OM26).

HRMS (ESI) (+) m/z: 550.2491 (100%) [cation]²⁺. Calculated for [C₇₀H₇₄N₂O₆P₂]²⁺ 550.2506; Found 550.2491.

1.4.4 Synthesis of mitoxantrone derivatives rhodamine B conjugates

1.4.4.1 Synthesis of tert-butyl 3-(3',6'-bis(diethylamino)-3-oxospiro[isoinoline-1,9'-xanthen]-2-yl)propanoate (Rho- β -ala-O^tBu) (OM6)

Rhodamine B (0.6 g, 1.25 mmol), PyBOP (0.98 g, 1.87 mmol) were dissolved in DMF (5 mL) and DIPEA (0.99 mL, 5.76 mmol) was added and allowed to react for 15 min. The mixture was added to HN- β -ala-O^tBu.HCl (0.25 g, 1.37 mmol) pre-dissolved in DMF (5 mL) and DIPEA (0.25 mL) and was left at rt with stirring to react for 2 h. Additional amount of HN- β -ala-O^tBu (0.25 g, 1.37 mmol) and PyBop (0.98 g, 1.87 mmol) were Rho B and allowed to react for another 2 h. The product was separated from DMF using chloroform/water solvent extraction [general method A]. OM6 was purified by using silica gel chromatography column using neat chloroform initially then chloroform: methanol + 1% pyridine was used. OM6 was filtered and evaporated to dryness in vacuo. Water was added (100 mL) and precipitated OM6 was filtered and dried. Yield 44%, 0.52 g.

TLC of OM13 (dichloromethane: methanol, 9:1 + 1% pyridine) R_f 0.73 (pink) OM6, 0.43 (pink) rhodamine B.

HRMS (ESI) (+) m/z: 570.3316 (100%) [M]⁺. Calculated for [C₃₅H₄₄N₃O₄]⁺ 570.3326; Found 570.3316.

1.4.4.2 Synthesis of N-(9-(2-((2-carboxyethyl)carbamoyl)phenyl)-6-(diethylamino)-3H-xanthen-3-ylidene)-N-ethylethanaminium (Rho- β -ala-OH) (OM7)

Trifluoroacetic acid (TFA) (1 mL) was added and left overnight. The solvent was evaporated and addition of diethyl ether (20 mL) gave a precipitate of OM7, which was filtered off and dried. Yield 97%, 0.14 g.

TLC for OM7 (butanol: acetic acid: water, 4:5:1) R_f 0.54 (pink) (OM7).

HRMS (ESI) (+) m/z: 514.2687 (100%) [M]⁺. Calculated for [C₃₁H₃₆N₃O₄]⁺ 514.2700; Found 514.2687.

1.4.4.3 Synthesis of N-(9-(2-((3-(2-((tert-butoxycarbonyl)(2-((4-hydroxy-9,10-dioxo-9,10-dihydroanthracen-1-yl)amino)ethyl)amino)ethoxy)-3-oxopropyl)carbonyl)phenyl)-6-(diethylamino)-3H-xanthen-3-ylidene)-N-ethylethanaminium Rho-β-ala-EAE-Boc-AQ(4-OH) (OM17)

Rho-β-ala-OH (OM7) (0.12 g, 0.413 mmol) was dissolved in CH₂Cl₂ with few drops of acetonitrile and DIPEA. DCC (0.126 g, 0.901 mmol) and DMAP (5-10 mg) were dissolved in CH₂Cl₂ (10 mL) and were added to pre-dissolved OM7 and allowed to react for 15 min then added to OM2 (0.16 g, 0.37 mmol) in CH₂Cl₂ (5 mL) and was left over ice with stirring for 1 h. After 1 h, additional amounts of OM7 (0.12 g, 0.413 mmol) and DCC (0.126 g, 0.901 mmol) were added and allowed to react overnight. The product was filtered and was extracted using CH₂Cl₂/ water solvent extraction [general method A]. OM17 was applied to a silica gel chromatography column using neat CH₂Cl₂ initially then a more polar solvent CH₂Cl₂: ethyl acetate was used and 5 mL of methanol was added at the end to elute all the product from the column. Column chromatography was repeated using neat CH₂Cl₂ at the beginning and the solvent system was changed by adding 5% ethyl acetate to CH₂Cl₂ to remove all rhodamine B impurity from the product. OM17 was filtered and evaporated to dryness in vacuo.

TLC for OM17 (chloroform: ethylacetate: methanol, 40:9:1) R_f 0.87 (purple) OM17, 0.59 (purple) AQ-SP.

HRMS (ESI) (+) m/z: 938.4338 (100%) [M]⁺. Calculated for [C₅₄H₆₀N₅O₉]⁺ 922.4386; Found 922.4393.

1.4.4.4 Synthesis of 2-((3-(2-(6-(diethylamino)-3-(diethyliminio)-3H-xanthen-9-yl)benzamido)propanoyl)oxy)-N-(2-((4-hydroxy-9,10-dioxo-9,10-dihydroanthracen-1-yl)amino)ethyl)ethan-1-aminium (Rho-β-ala-EAE-AQ(4-OH) (OM18)

Trifluoroacetic acid (TFA) (1 mL) was added for 30 min. TFA was evaporated and 1, 4-dioxane (0.5 mL) and hexane was used to solidify OM18, which was centrifuged and dried. Yield 17%, 0.051 g

TLC for OM18 (dichloromethane: methanol, 9:1 +2 drops of acetic acid) R_f 0.68 (purple) (OM18).

HRMS (ESI) (+) m/z: 822.3857 (100%) [M-TFA]⁺. Calculated for [C₄₉H₅₂N₅O₇]⁺ 822.3861; Found 822.3857.

1.4.4.5 Synthesis of N-(9-(3-(4-(tert-butoxycarbonyl)piperazine-1-carbonyl)phenyl)-6-(diethylamino)-3H-xanthen-3-ylidene)-N-ethylethanaminium (Rho-pip-Boc) (OM4)

Rhodamine B (1 g, 2.08 mmol) and HATU (1.19 g, 3.13 mmol) were dissolved in CH₂Cl₂/DMF (1:2). Triethylamine (1.45 mL, 8.35 mmol) was added and allowed to react for 10 min. Boc-piperazine in CH₂Cl₂/DMF (1:2) was added to the mixture and allowed to react at rt with stirring overnight. The reaction was extracted using CH₂Cl₂/ water solvent extraction [general method A]. The product OM4 was purified by column chromatography using 19:1 CH₂Cl₂: methanol. Rho-pip-Boc was filtered and evaporated to dryness in vacuo.

TLC for OM4 (dichloromethane: methanol, 9:1) R_f 0.47 (pink) (OM4).

1.4.4.6 Synthesis of N-(6-(diethylamino)-9-(3-(piperazine-1-carbonyl)phenyl)-3H-xanthen-3-ylidene)-N-ethylethanaminium (Rho-piperazine TFA) (OM4 TFA)

TFA (1 mL) was added for 30 min. TFA was evaporated and 1, 4-dioxane (0.5 mL) was added. Diethyl ether was used to precipitate the product, which was filtered and dried. Yield 79%, 0.84 g.

TLC for OM4 TFA (dichloromethane: methanol, 9:1) R_f 0.105 (pink) (OM4 TFA).

HRMS (ESI) (+) m/z : 511.3054 (100%) $[M-TFA]^+$. Calculated for $[C_{32}H_{39}N_4O_2]^+$ 511.3068; Found 511.3054.

1.4.4.7 Synthesis of 4-(4-(3-(6-(diethylamino)-3-(diethyliminio)-3H-xanthen-9-yl)benzoyl)piperazin-1-yl)-4-oxobutanoate (Rho-pip-succinate) (OM5)

Succinic anhydride (0.192 g, 1.92 mmol) was dissolved in DMF (5 mL) and DIPEA (0.334 mL, 1.92 mmol) was added and allowed to react for 10 min then was added to OM4 TFA (0.6 g, 0.96 mmol) in DMF and allowed to react at rt with stirring for 1 h. The reaction was extracted using CH_2Cl_2 /water solvent extraction [general method A]. The solvents were evaporated and diethyl ether was added to solidify the product, which was filtered and dried. Yield 77%, 0.55 g.

TLC for OM5 (butanol: acetic acid: water, 4:5:1) R_f 0.608 (pink) (OM5).

1.4.4.8 Synthesis of N-(9-(3-(4-(4-(2-((tert-butoxycarbonyl)(2-((4-hydroxy-9,10-dioxo-9,10-dihydroanthracen-1-yl)amino)ethyl)amino)ethoxy)-4-oxobutanoyl)piperazine-1-carbonyl)phenyl)-6-(diethylamino)-3H-xanthen-3-ylidene)-N-ethylethanaminium (Rho-pip-succ-EAE-Boc-AQ(4-OH) (OM15)

OM2 (0.12 g, 0.28 mmol) was dissolved in CH_2Cl_2 , cooled and stirred. OM5 (0.16 g, 0.25 mmol), DCC (0.063 g, 0.306 mmol) and DMAP (5-10 mg) were dissolved in CH_2Cl_2 and

allowed to react for 10 min then added dropwise to OM2 in CH₂Cl₂ and allowed to react for 12 h. The reaction was filtered and extracted using CH₂Cl₂/water solvent extraction [general method A]. OM15 was applied to a silica gel chromatography column using neat chloroform initially then more polar solvents chloroform: ethyl acetate then chloroform: methanol were used. Column chromatography was repeated a further three times to obtain the product in a homogenous form on TLC.

TLC for OM15 (dichloromethane: methanol, 9:1) R_f 0.35 (purple) OM15, 0.1 (pink) rhodamine B.

HRMS (ESI) (+) m/z: 1019.4914 (100%) [M]⁺. Calculated for [C₅₉H₆₇N₆O₁₀]⁺ 1019.4913; Found 1019.4914.

1.4.4.9 Synthesis of 2-((4-(4-(3-(6-(diethylamino)-3-(diethyliminio)-3H-xanthen-9-yl)benzoyl)piperazin-1-yl)-4-oxobutanoyl)oxy)-N-(2-((4-hydroxy-9,10-dioxo-9,10-dihydroanthracen-1-yl)amino)ethyl)ethan-1-aminium (Rho-pip-succ-EAE-AQ(4-OH) (OM16)

TFA (1 mL) was added for 20 min then it was evaporated to dryness under vacuum. Ethanol was added then diethyl ether was added to precipitate OM16, which was filtered and dried. Yield 91%, 0.21 g

TLC for OM16 (chloroform: methanol, 4:1) R_f 0.38 (purple) (OM16).

HRMS (ESI) (+) m/z: 919.4388 (86%) [M-TFA]⁺. Calculated for [C₅₄H₅₉N₆O₈]⁺ 919.4389; Found 919.4388.

1.4.5 Synthesis of mitoxantrone and ametantrone-linked prodrugs

1.4.5.1 Synthesis of di-tert-butyl (((5,8-dihydroxy-9,10-dioxo-9,10-dihydroanthracene-1,4-diyl)bis(azanediyl))bis(ethane-2,1-diyl))bis((2-hydroxyethyl)carbamate) (Mitoxantrone-Boc) (OM19)

Mitoxantrone (0.03 g, 0.058 mmol) was dissolved in methanol (10 mL) and cooled down with stirring. Boc₂O (0.05 g, 0.23 mmol) was dissolved in methanol and DIPEA (0.025 ml, 0.14 mmol) was added then the mixture was added to activated mitoxantrone dropwise and allowed to react for 1 h. A further half amount of Boc₂O was added. The reaction was filtered and extracted using CH₂Cl₂/ water solvent extraction [general method A]. OM19 was applied to a silica gel chromatography column using neat CH₂Cl₂ at the beginning then the polarity of the solvent system was increased by using CH₂Cl₂: methanol. OM19 was filtered and evaporated to dryness under vacuum. The crude product was then used for further reaction without precipitation.

TLC for OM19 (dichloromethane: methanol, 9:1) R_f 0.47 (blue) (OM19).

HRMS (ESI) (+) m/z: 645.3128 (100%) [cation]²⁺. Calculated for [C₃₂H₄₂N₄O₁₀H]⁺ 643.2974; Found 645.3130.

1.4.5.2 Attempted synthesis of Rho-pip-succ-mitoxantrone-Boc (OM20)

OM19 (0.12 g, 0.18 mmol) was dissolved in CH₂Cl₂ and it was cooled in ice with stirring. OM5 (0.125 g, 0.204 mmol), DCC (0.092 g, 0.186 mmol) and DMAP (5-10 mg) were dissolved in CH₂Cl₂ and allowed to react for 10 min then added dropwise to Mitoxantrone-Boc in dichloromethane and allowed to react for 1 h. The reaction was filtered and extracted using CH₂Cl₂/water solvent extraction [general method A]. OM20 was applied to a silica gel chromatography column using neat CH₂Cl₂ initially then more polar solvents CH₂Cl₂: ethyl acetate, CH₂Cl₂: ethyl acetate + 4% methanol and dichloromethane:

methanol were used. Column chromatography was performed twice to obtain a product homogenous on TLC.

TLC for OM20 (dichloromethane: methanol, 9:1) R_f 0.40 (purple) 1 arm product, 0.14 (purple) 2 arm product, 0.03 (pink) rhodamine B.

HRMS (ESI) (+) m/z : 1351.6486 (100%) $[M+H]^+$. Calculated for $[C_{104}H_{126}N_{12}O_{18}]^+$, not match with Theoretical Isotope Model 1832.9417 and Observed Data 1826.1211.

1.4.5.3 Attempted synthesis of 2,2'-((5,8-dihydroxy-9,10-dioxo-9,10-dihydroanthracene-1,4-diyl)bis(azanediyl))bis(N-(2-((4-(4-(3-(6-(diethylamino)-3-(diethyliminio)-3H-xanthen-9-yl)benzoyl)piperazin-1-yl)-4-oxobutanoyl)oxy)ethyl)ethan-1-aminium) (Rho-pip-succ-mitoxantrone) (OM21)

TFA (1 mL) was added for 30 min then it was evaporated to dryness. Diethyl ether was added to precipitate OM21, which was filtered and dried. Yield 20%, 0.06 g

TLC for OM21 (dichloromethane: methanol, 9:1) R_f 0.44 (purple) (OM21)

HRMS (ESI) (+) m/z : 576.2742 (100%) $[M+H]^{2+}$. Calculated for $[C_{94}H_{110}N_{12}O_{14}]^+$, the data did not match with the Theoretical Isotope Model 1632.8369 and the Observed Data 1684.2618.

1.4.5.4 Attempted synthesis of TPP-mitoxantrone-Boc (one arm) (OM23) and TPP-mitoxantrone (two arm) (OM24)

OM19 (0.06 g, 0.093 mmol) was dissolved in CH_2Cl_2 and cooled in ice with stirring. TPP (0.02 g, 0.046 mmol), DCC (0.03 g, 0.186 mmol) and DMAP (5-10 mg) were dissolved in CH_2Cl_2 and allowed to react for 10 min then added dropwise to OM19 in CH_2Cl_2 and allowed to react for 1 h. The reaction was filtered and extracted using CH_2Cl_2 /water solvent extraction [general method A]. OM23 and OM24 were purified by column chromatography using neat CH_2Cl_2 at the beginning then more polar solvents system

CH₂Cl₂: methanol (19:1), CH₂Cl₂: methanol (9:1) and CH₂Cl₂: methanol (4:1) were used to get one arm and two arms products respectively. The solvents were evaporated and diethyl ether was added to precipitate OM23 and OM24, which were filtered and dried. Yield 67%, 0.06 g and 23%, 0.03 g.

TLC for OM23 and OM24 (chloroform: methanol, 4:1) R_f 0.29 (blue) (OM!) one arm product, 0.58 (blue) (OM!) 2 arm product.

HRMS (ESI) (+) m/z: 667.2919 (22%) [cation]²⁺. Calculated for [C₇₈H₈₈N₄O₁₂P₂]⁺ 667.2932; Found 667.2919.

1.4.5.5 Synthesis of ametantrone (NK1)

Leucoquinizarin (1 g, 4.13 mmol, 1 eq) was dissolved in CH₂Cl₂ (50 mL) and N-(2-hydroxyethyl)ethylenediamine (8.59 g, 82.60 mmol, 20 eq) was added and heated at 50°C for 1 h. The product was then oxidized by aeration with the addition of triethylamine (Et₃N, 1 mL) for 4.5 h and the solution colour became blue. The solid was precipitated and filtered under vacuum. The solid was washed with CH₂Cl₂ (20 mL) and dried (rotary evaporation). The sticky blue solid was precipitated using diethyl ether (5 mL) and was filtered and evaporated to dryness in vacuo. Yield: 71%, 1.2 g.

TLC of the anthraquinone crude product (butanol : acetic acid : water, 4:5:1): R_f 0.08 [blue, ametantrone (NK1)], 0.29 (purple, single armed anthraquinone derivative), 0.56 (pink).

1.4.5.6 Synthesis of di-tert-butyl (((9,10-dioxo-9,10-dihydroanthracene-1,4-diyl)bis(azanediyl))bis(ethane-2,1-diyl))bis((2-hydroxyethyl)carbamate) (ametantrone-Boc) (NK4)

NK1 (0.7 g, 2.03 mmol, 1 eq) was dissolved in methanol (20 mL) and cooled over ice (0°C). Boc₂O (1.77 g, 8.12 mmol, 4 eq) was dissolved in methanol (30 mL) and was added to NK1 dropwise and allowed to react over ice for 60 min. The product NK4 was extracted using chloroform/water solvent extraction [general method A]. The product was filtered and evaporated to low volume and applied to a silica gel chromatography column using

neat chloroform at the beginning and then the polarity of the solvent was increased by using chloroform : ethyl acetate (19:1), chloroform: ethyl acetate (19:1) + methanol 2%, chloroform : ethyl acetate (9:1) + methanol 2%, chloroform : ethyl acetate (9:1) + methanol 4%, and chloroform : ethyl acetate (9:1) + methanol 6%. NK4 was filtered and evaporated to dryness in vacuo. Addition of diethyl ether (20 mL) gave a precipitate of NK4, which was filtered off and dried. Yield: 68%, 0.86 g.

TLC of NK3 and NK4 (chloroform: methanol, 9:1): R_f 0.54 (purple) OM2, 0.57 (blue) NK4.

1.4.5.7 Synthesis of ((((((9,10-dioxo-9,10-dihydroanthracene-1,4-diyl)bis(azanediyl))bis(ethane-2,1-diyl))bis((tert-butoxycarbonyl)azanediyl))bis(ethane-2,1-diyl))bis(oxy))bis(5-oxopentane-5,1-diyl))bis(triphenylphosphonium) (TPP-ametantrone-Boc) (NK6)

4-Carboxybutyl)triphenylphosphonium bromide (TPP) (0.45 g, 1.02 mmol, 6 eq) and HATU (0.46 g, 1.19 mmol, 7 eq) were dissolved in DMF (2.25 mL), and added with 4-methylmorpholine (242 μ L, 2.21 mmol) and allowed to react for 30 min then added to pre-dissolved NK4 (0.1 g, 0.17 mmol, 1 eq) in DMF (2.75 mL) The mixture was stirred using magnetic stirrer for 1 h, heated over water bath at 40°C (without stirring) for 1.5 h, and left to react overnight at rt. The product NK6 was extracted using chloroform/water solvent extraction [general method A]. NK6 was applied to a silica gel chromatography column using neat chloroform initially and then more polar solvent chloroform: ethyl acetate (19:1), chloroform: ethyl acetate (19:1) + methanol 1%, chloroform: ethyl acetate (19:1) + methanol 2% were used. NK6 was filtered and evaporated to dryness in vacuo. Addition of diethyl ether (3 mL) gave a precipitate of NK6, which was filtered and evaporated to dryness in vacuo. Yield: 50%, 0.10 g.

TLC of NK6 (chloroform: methanol, 9:1): R_f 0.53 (blue) (NK6).

HRMS (ESI) (+) m/z: 651.2971 (100%) [M-Br₂]⁺. Calculated for [C₇₈H₈₈N₄O₁₀P₂]⁺ 651.2982; Found 651.2971.

1.4.5.8 Synthesis of ((((((9,10-dioxo-9,10-dihydroanthracene-1,4-diyl)bis(azanediyl))bis(ethane-2,1-diyl))bis(ammoniumdiyl))bis(ethane-2,1-diyl))bis(oxy))bis(5-oxopentane-5,1-diyl))bis(triphenylphosphonium) (TPP-ametantrone tfa) (NK8)

Boc-Ametantrone-bis-TPP (0.07 g) was dissolved in TFA (1 mL) for 30 min. Ethanol (0.3 mL) was added and the solvent was evaporated, to give (NK8) which was precipitated with diethyl ether (2 mL). Yield: 71%, 0.05 g.

TLC of NK8 (butanol: acetic acid: water, 4:5:1): R_f 0.03 (blue) (NK8).

HRMS (ESI) (+) m/z: 551.2442 (100%) [M-(TFA)₂]⁺. Calculated for [C₆₈H₇₂N₄O₆P₂]⁺ 551.2458; Found 551.2442.

1.4.6 DNA binding assay

1.4.6.1 Materials

PBS buffer was made by dissolving one phosphate tablet (Sigma) in 200 mL of distilled water to obtain 0.01 M phosphate buffer, 0.0027 M potassium chloride, 0.137 M sodium chloride, pH 7.4 at 25°C. Ethidium bromide 10 mg/mL (300 μM) of stock solution in deionized water was prepared and protected from light and kept at 4°C, which was further diluted to 30 μM (final concentration). One centimeter portion (approximately) of Calf Thymus DNA (Sigma) was dissolved slowly in 5 mL of PBS buffer at 4°C for 24 h. Undissolved Calf Thymus DNA residue was filtered off and the concentration of Calf Thymus DNA stock solution was determined by using Beckman DU800 UV/Vis spectrophotometer at 260 nm using a molar extinction coefficient of 6600 M⁻¹cm⁻¹. Drug test solutions were prepared and by making a stock solution of 1 mg/mL or 10 mg/mL in DMSO, then further diluted to give a final concentration in the cuvette of 1~10 μM as required. Measurements were performed using a Perkin Elmer Luminescence Spectrometer LS50B,

1.4.6.2 DNA quantification

DNA stock solution (100~300 μL) was transferred into the cuvette and diluted with PBS buffer to give a final volume of 3 mL. 3 mL of PBS was added to a cuvette and was used as a blank. The analytical wavelength for the spectrophotometer was set at 260 nm. According to the linearity range of the Beer-Lambert Law, the ideal absorbance should fall between 0.5 and 0.7. The experiments were performed in triplicate. The mean value was then used to determine the concentration of this DNA stock solution using the equation below:

Absorbance (A) = Concentration (C) \times Cell length (L) \times Molar extinction coefficient (Σ)

(The units are: mol/L for C, cm for L, $\text{mol}^{-1}\text{dm}^3\text{cm}^{-1}$ for Σ)

the concentration of the original DNA stock solution were determined by using equation $C_1 V_1 = C_2 V_2$.

1.4.6.3 Method

Excitation and emission wavelengths were set at 480 nm and 550-750 nm, respectively to measure the fluorescence intensity. Solutions (3 mL) were added to the fluorescence cuvette in the following order: 1) DNA (final conc. 60 μM), 2) ethidium bromide (final conc. 30 μM) 3) buffer to complete the volume to 3 mL. The fluorescence intensity of this mixture was recorded after it came to equilibrium. Drugs solutions in DMSO (stock solution) were further diluted to give a final concentration in cuvette 1~10 μM as required, then the solution was mixed well and allowed to reach equilibrium for 5 min each time. Aliquots of drug solution were added into the cuvette until the fluorescence intensity reach below half the fluorescence intensity of the original DNA-drug free solution. The apparent DNA binding constant K_{app} were calculated from the plot of relative fluorescence intensity against DNA binding ligand concentration, using the equation: $K_{\text{EB}}[\text{EB}] = K_{\text{app}}[\text{DNA binding ligand}]$ where ($K_{\text{EB}} = 1.0 \times 10^7 \text{M}^{-1}$, EB ethidium bromide concentration and DNA binding ligand is the concentration that caused a 50% decrease of the relative fluorescence intensity of DNA-bound ethidium bromide. The DNA binding $Q_{\text{E}50}$ values for each drug were analyzed by SigmaPlot 12.

1.4.7 Distribution Coefficient Assay

1.4.7.1 Materials

Beckman DU800 spectrophotometer; octanol; PBS buffer (Sigma-Aldrich Phosphate buffered saline. One tablet dissolved in 200 mL of deionized water yields 0.01 M phosphate buffer, 0.0027 M potassium chloride and 0.137 M sodium chloride, pH 7.4, at 25 °C.); 3 mL quartz cuvette; test compounds: [HO-EAE-AQ (4-OH)] OM2 TFA, [TPP-EAE-AQ(4-OH)] OM22, [(OH-Butyl-AQ (4-OH)] NU:UB 252, [(TPP-Butyl-AQ(4-OH)] OM30, (OH-butyl-AQ) NU:UB 238, (TPP-Butyl-AQ) SH1 and [(Rho-pip-succ-EAE-AQ(4-OH)] OM16.

1.4.7.2 Calibration curve methods

PBS buffer solution was made by dissolving a PBS tablet in (100 mL) of deionized water and was used in the measurement of standard calibration curve. Saturating buffer was made by using PBS buffer (100 mL) and octanol (100 mL) and shaken for 24 h on vortex. Each phase layer of phosphate and octanol were separated using a separating funnel. 1mg/mL of stock solution samples (OM2 TFA, OM22, NU:UB 252, OM30, NU:UB 238, SH1 and OM16) in dimethyl sulfoxide (DMSO) was taken and diluted with PBS (octanol saturated) or octanol (PBS saturated) in cuvettes to give a series of different concentrations of the test compounds. Scan speed was set as 1200 nm/min and wavelength range was set as 400 to 700 nm and the maximum absorbance was plotted into a regression graph to obtain the $y = mx + c$ equation. The experiments were performed in triplicate.

1.4.7.3 Distribution coefficient

Compounds (OM2 TFA, OM22, NU:UB 252. OM30, NU:UB 238, SH1 and OM16) 1 mg were dissolved in 900 μ L of octanol (PBS saturated) and 900 μ L of PBS 7.4 (octanol saturated) in a 2000 μ L Eppendorf tube. This was prepared in triplicate for each

compound. The tubes were shaken for 24 h at rt. For the experiment, for example; 50 μ L of OM2 TFA in PBS and 400 μ L of OM22 were taken out and transferred into cuvette and diluted with PBS to give a final volume of 800 μ L. 100 μ L of OM2 TFA in octanol and 200 μ L of OM22 in octanol were taken out and transferred into cuvette and diluted with octanol to give a final volume of 3000 μ L. The absorbance in both layers was measured. Finally, the concentrations of samples in each phase were determined from standard curves made by plotting absorbance against concentration. Log D values were calculated from the calibration curves equation by dividing the concentration in the octanol by the concentration in PBS phase.

1.4.8 **MTT assay**

1.4.8.1 **Materials**

HCT-15 (Human colon carcinoma cells), MCF-7 (human breast cancer cells), RPMI 1640 medium containing phenol red (sigma), 10% foetal bovine serum, FBS, 1% L-glutamine, 1% penicillin and streptomycin, sodium chloride (NaCl), 0.5% trypsin, PBS buffer, 3-(4,5-dimethylthiazole-2-yl)-2,5-diphenyltetrazolium bromide (MTT), test compounds: OM2 [HO-EAE-AQ(4-OH)], OM22 [TPP-EAE-AQ(4-OH)], NU:UB 238 (OH-butyl-AQ), SH1 (TPP-Butyl-AQ), NU:UB 65 and OM26 (TPP-bis-NU:UB 65), mitoxantrone, OM30 [TPP-Butyl-AQ(4-OH)], OM31 [(TPP-Pentyl-AQ(4-OH))] and OM32 [(TPP-EOE-AQ(4-OH))].

1.4.8.2 **Cell culture method**

HCT-15 and MCF-7 cells line were used for cytotoxicity assay. The cells were grown in RPMI media replenished with 10% foetal bovine serum, FBS, 1% L-glutamine, 1% penicillin and streptomycin in T-75 tissue culture flasks at 37°C in 5% CO₂ in air. The media was removed and cells were washed with NaCl (10 mL; 2x) and the flask was gently shaken without disturbing the layer of the cells to wash off any remaining foetal bovine serum. Trypsin (2 mL) was added to cells and incubated (5 min, 37°C, 5% CO₂).

After 5 min, the cells were removed from the incubator and observed under the microscope if the cells were detached. Then 8 mL of fresh RPMI 1640 media was added to the flask (to de-activate the action of trypsin) and wash all the cells to the bottom and the mixture was centrifuged (2 min, 2000 rpm). The supernatant was poured off and the cell pellet was re-suspended in RPMI 1640 media according to passage split (1/2, 1/4, 1/8, 1/10) in mLs and 1 mL of this was transferred to a fresh flask. Cell count and MTT assay were performed using the remainder of the cells.

1.4.8.3 MTT assay method

HCT-15 and MCF-7 cells were seeded in 96 well plates at a cell density 5×10^4 cells/well for 24 h at 37°C. Each cell line was plated on separate plates. Row A1-A3 contained RPMI media only (blank); row B1-B3 contained media and cells (positive control); row C1-C3 contained media and cells (negative control); row D-H contained cells and media, which treated with test compounds. After 24 h of incubation, all media was removed and replaced with test compounds (50 µM, 0.01 µM, 0.1 µM, 1 µM, 10 µM and 100 µM) in triplicate and incubated for 48 h. after 48 h, all medium was removed from wells C1-C3 and replaced with Triton X (0.5%, 70 µL) to kill the cells. The medium from the rest of the well was removed and replaced with fresh media RPMI (70 µL). C1-C3 were then also replaced with fresh media RPMI (70 µL). MTT solution (5mg/mL) was prepared by adding 10 mg MTT to 2 mL PBS. 50 µL of MTT solution was then added to each well and incubated 4 h at 37°C. after 4 h, all medium was removed and replaced with DMSO (150 µL) and mixed vigorously and left in dark place for 30 min at 37°C. the absorbance was measured at 550 nm with a microplate reader and the IC₅₀ was recorded for each test compound using Sigma Plot 12.

1.4.9 Confocal microscopy

1.4.9.1 Materials

HCT-15 (Human colon carcinoma cells, HCT-116 (Human colon carcinoma) and PC3 (prostate cancer cells); RPMI 1640 medium containing phenol red; sterile NaCl; 35 mm glass bottomed micro well dish (Ibidi/Thistle Scientific); compounds: [HO-EAE-AQ(4-OH)] OM2 TFA, [TPP-EAE-AQ(4-OH)] OM22, OM30 [TPP-Butyl-AQ(4-OH)], OM31 [(TPP-Pentyl-AQ(4-OH)], OM32 [(TPP-EOE-AQ(4-OH)], (TPP-Butyl-AQ) SH1, ametantrone, mitoxantrone. LysoTracker Green DND 26 probe and MitoTracker Green FM probe. Live cell imaging was performed using Zeiss LSM800 confocal laser scanning microscope with HCX PL APO lambda blue (63.0 x 1.4 oil objective). Lasers used were: diode (405nm), Argon (458 nm, 488 nm and 514 nm), HeNe (543 nm), HeNe (543 nm), HeNe (594 nm) and HeNe (633 nm).

1.4.9.2 Method

Stock solutions of tested compounds (1 mg/mL) were prepared in DMSO. PC-3 cells (1.5×10^5), HCT-15 (2.5×10^5) and HCT-116 (2×10^5) were seeded in 35 mm glass bottomed micro well dish and incubated for 24 h. Cells were washed with PBS x3. For the LysoTracker Green DND 26, a solution of dye (60 nM) was added to the cell culture medium and incubated at 37°C for 20 m. After 20 min the medium was removed and the cells were washed with sterile NaCl. Then tested compound solution was applied to cell culture medium and were imaged live using a Zeiss LSM800 confocal laser scanning microscope. For MitoTracker Green FM, a solution of dye (50 nM) was added to the cell culture medium and incubated at 37°C for 20 min. After 20 min the medium was removed and the cells were washed with sterile NaCl. Then tested compound solution was applied to cell culture medium and were imaged live using a Zeiss LSM800 confocal laser scanning microscope. Lens used was a 63.0 x 1.4 oil-immersion objective. Image analysis (field of view) was performed using Image J software

1.4.10 **Morphology studies**

1.4.10.1 **Materials**

HCT-116 (Human colon carcinoma), RPMI 1640 medium containing phenol red; sterile NaCl; 35 mm glass bottom micro 6-well dish; compounds: [TPP-EAE-AQ(4-OH)] OM22 and (TPP-Butyl-AQ) SH1 (1 mg/mL) and mitoxantrone (1 mg/mL) were prepared in DMSO. Morphological studies were performed using a Zeiss microscope (HBO100; 20 x magnification).

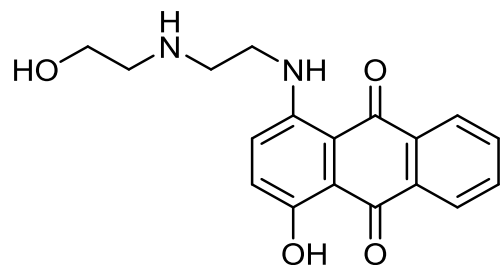
1.4.10.2 **Method**

HCT-116 cells (2×10^5) were seeded in a 6 well plate and incubated for 24 h. Cells were washed with NaCl x3. Cells were left untreated (negative control) or cultured with DMSO (0.1% vehicle control), mitoxantrone (1 μ M positive control), OM22 (1 μ M, 5 μ M, 10 μ M), SH1 (1 μ M, 5 μ M, 10 μ M). Morphological characteristics of HCT-116 cells were tested using bright field microscopy after 2, 6, 8 and 24 h.

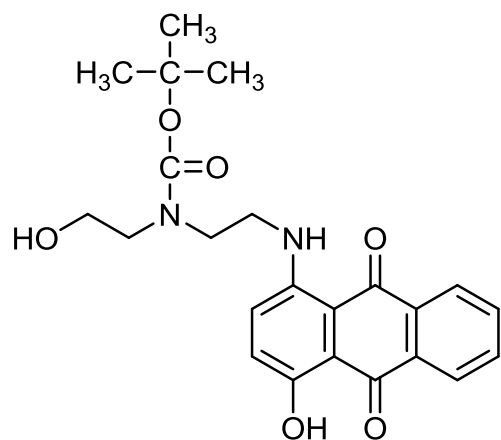
Chapter 1

Structure Library

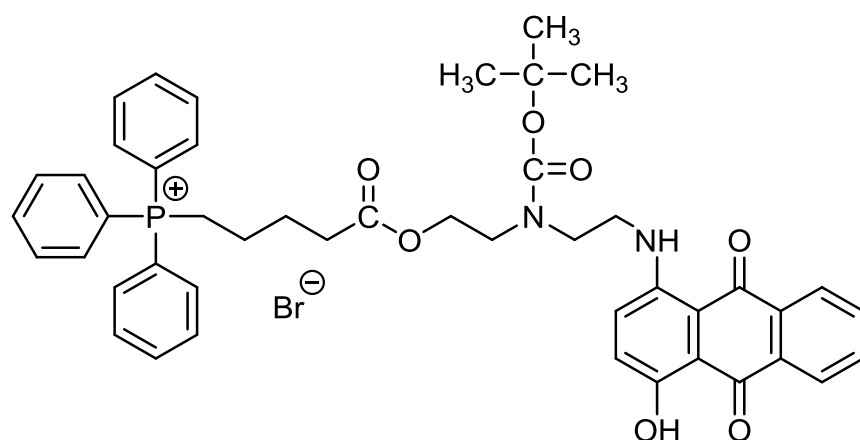
1.5 Structure library



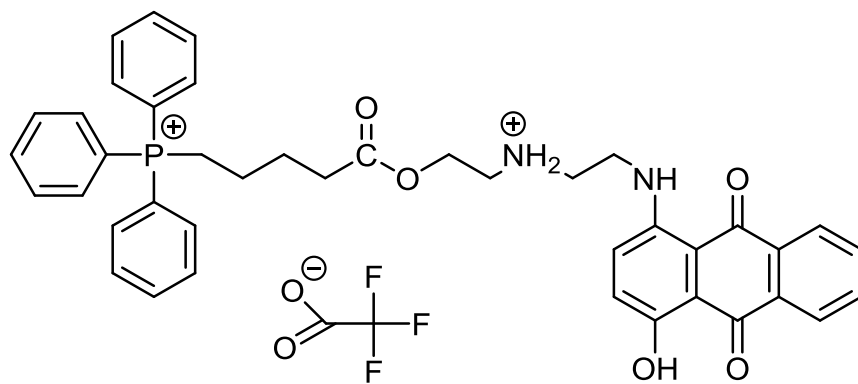
HO-EAE-AQ(4-OH) (OM1)



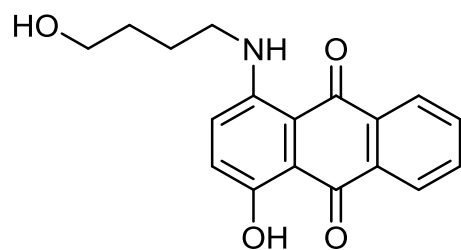
HO-EAE-Boc-AQ (4-OH) (OM2)



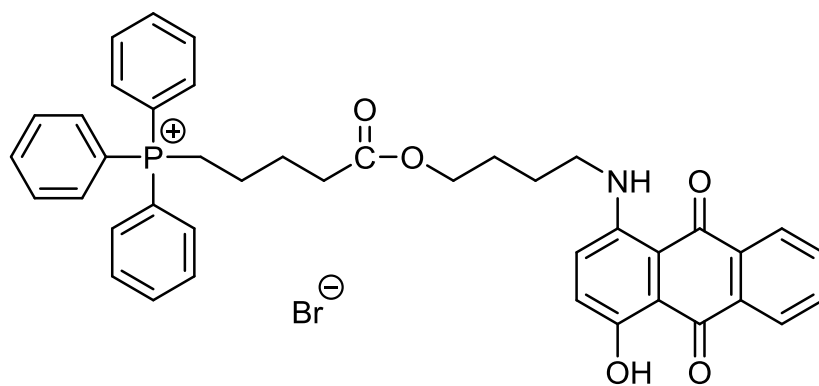
TPP-EAE-Boc-AQ-(4-OH) (OM22-Boc)



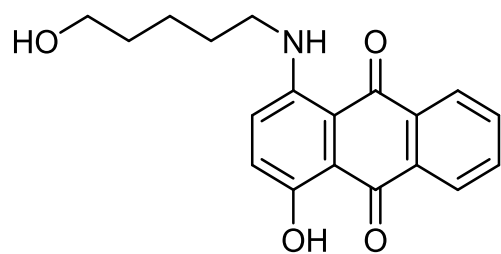
TPP-EAE-AQ(4-OH) (OM22)



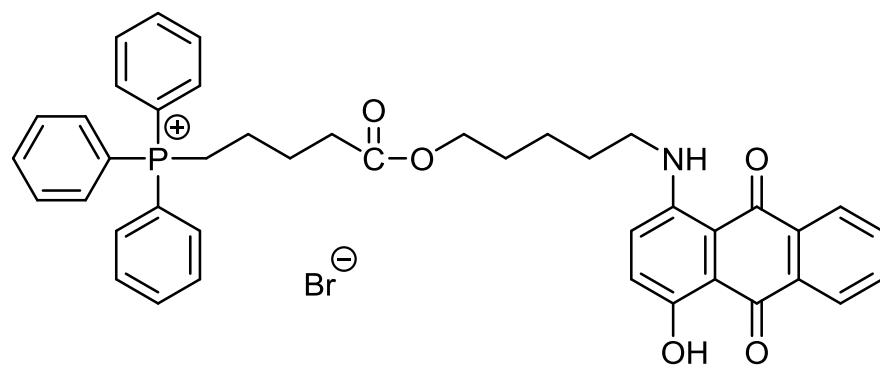
OH-Butyl-AQ (4-OH) (NU:UB 252)



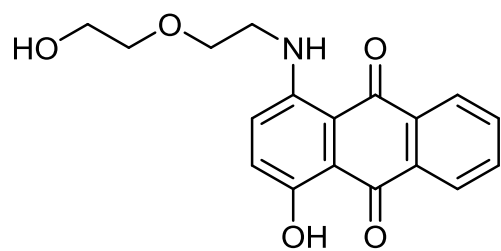
TPP-Butyl-AQ(4-OH) (OM30)



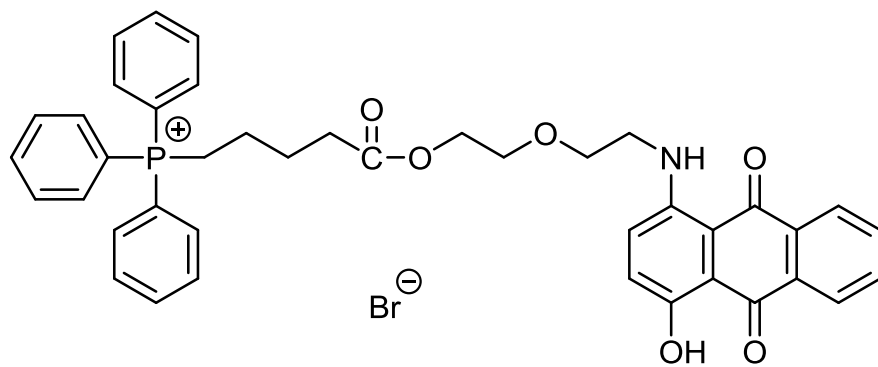
HO-pentyl-AQ(4-OH) (OM28)



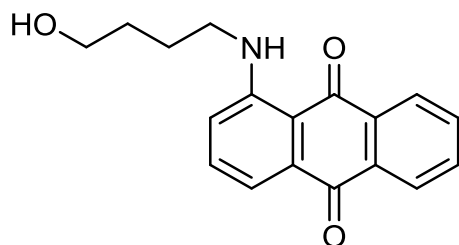
TPP-Pentyl-AQ(4-OH) (OM31)



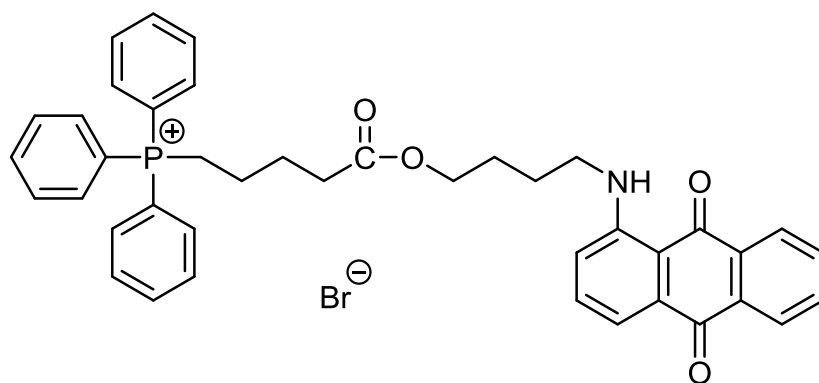
HO-EOE-AQ(4-OH) (OM29)



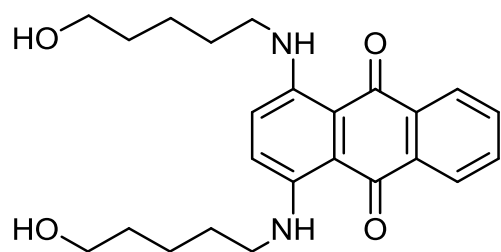
TPP-EOE-AQ(4-OH) (OM32)



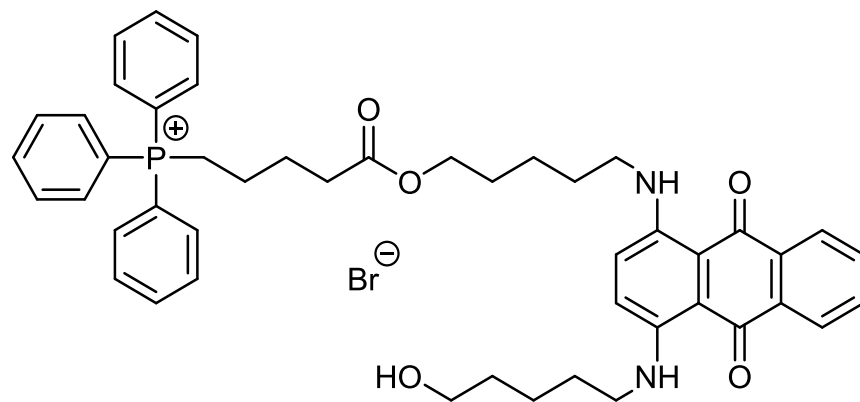
OH-butyl-AQ (NU:UB 238)



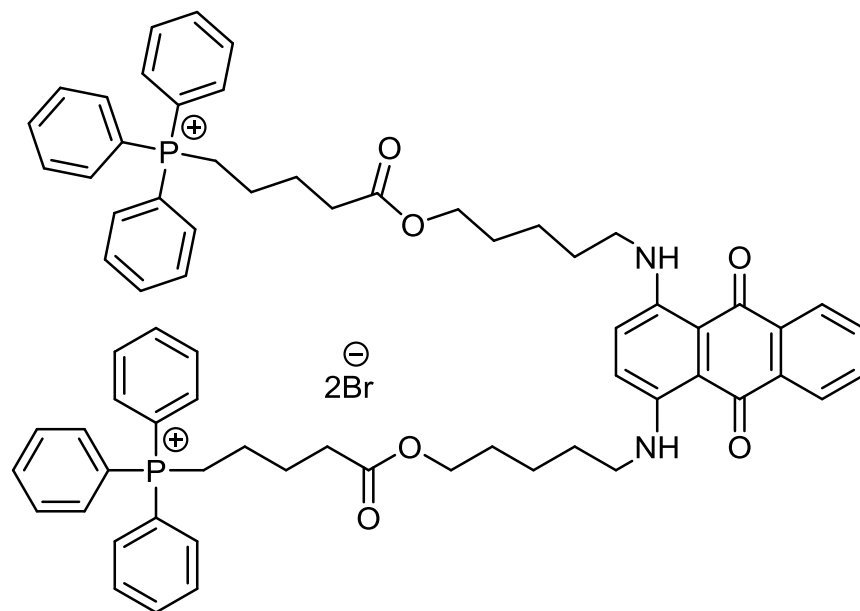
TPP-Butyl-AQ (SH1)



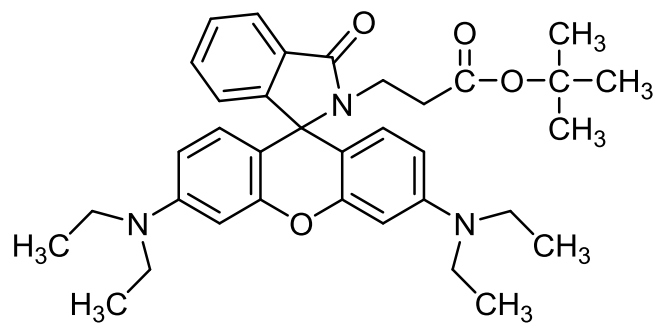
bis-(OH-pentyl-AQ) (NU:UB 65)



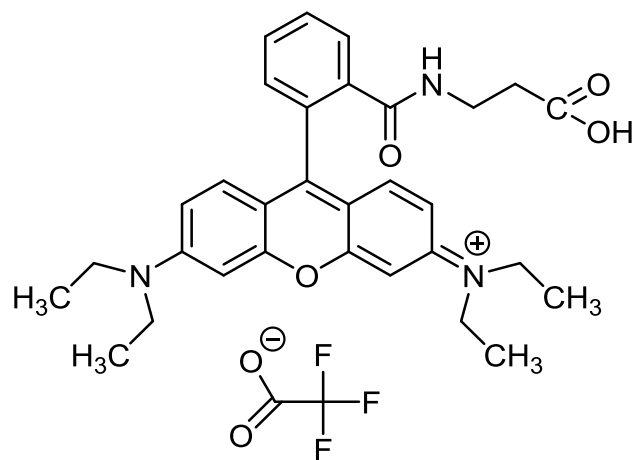
TPP-NU:UB 65 (OM25)



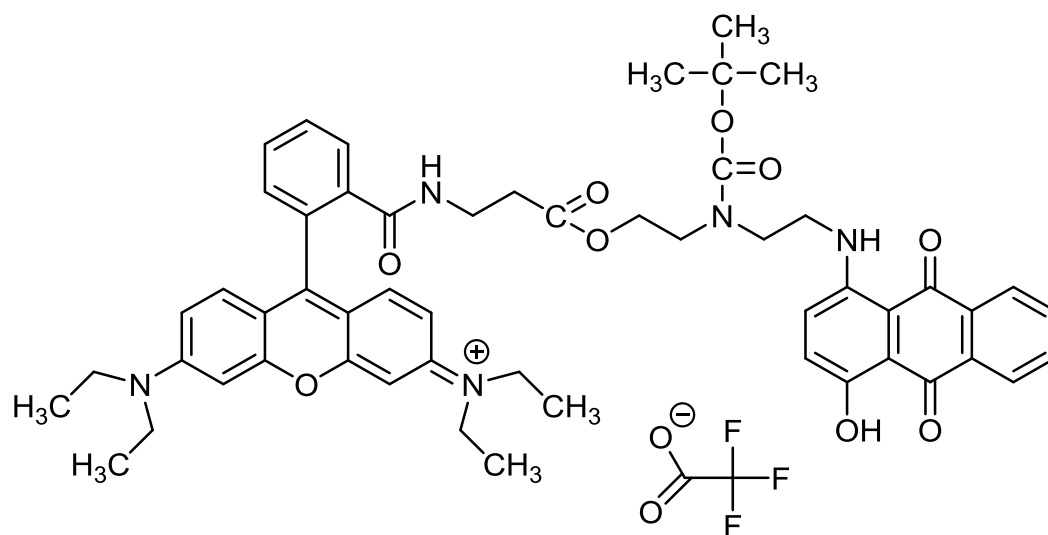
Bis-TPP-NU:UB 65 (OM26)



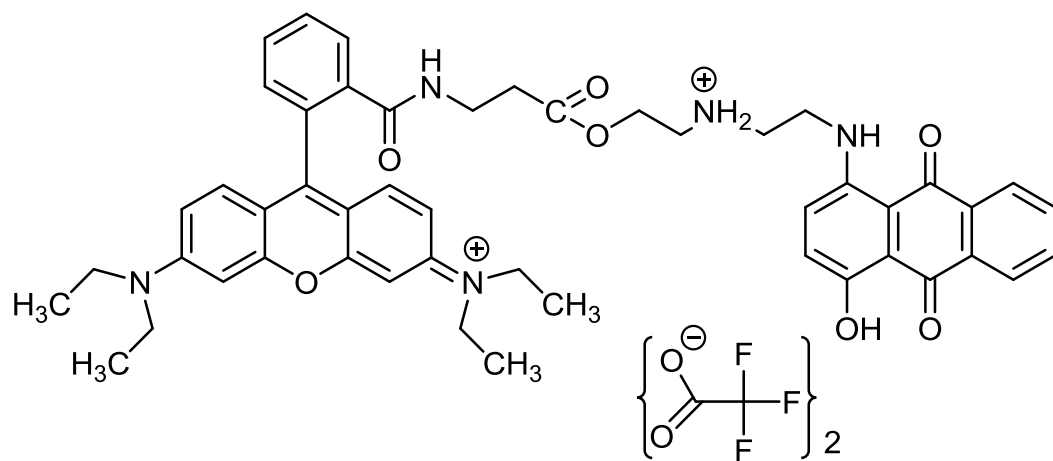
Rho- β -ala-O^tBu (OM6)



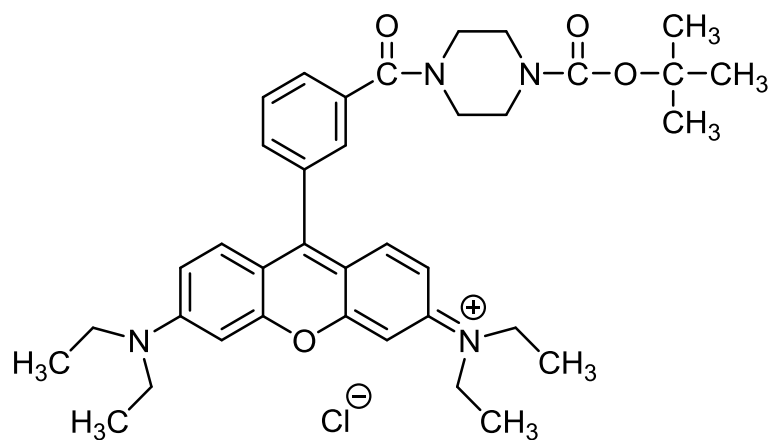
Rho- β -ala-OH (OM7)



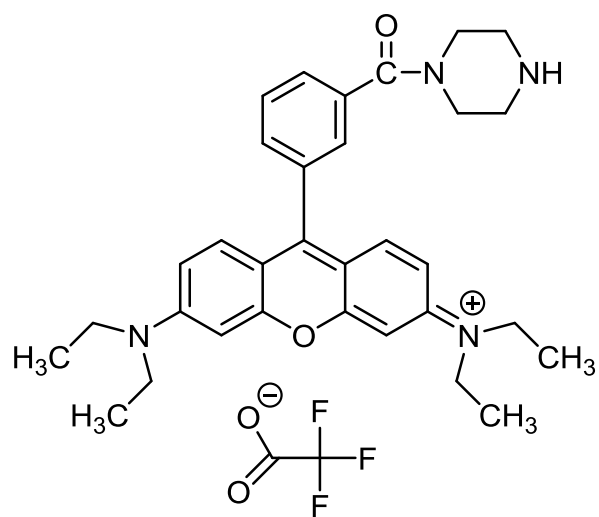
Rho- β -ala-EAE-Boc-AQ(4-OH) (OM17)



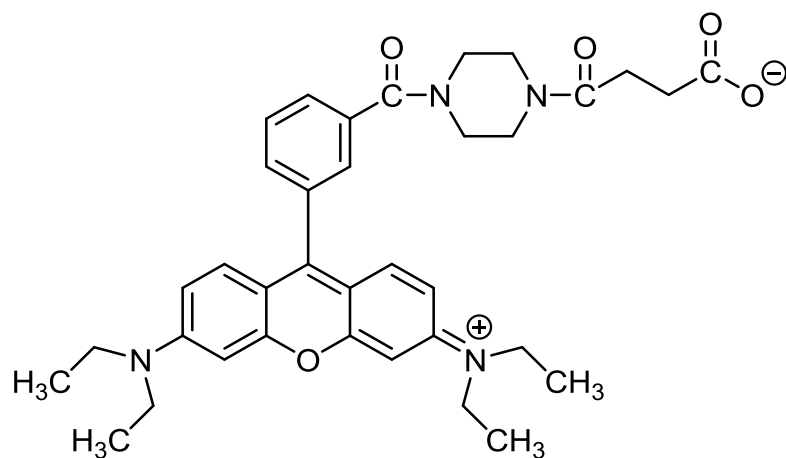
Rho-β-ala-EAE-AQ(4-OH) (OM18)



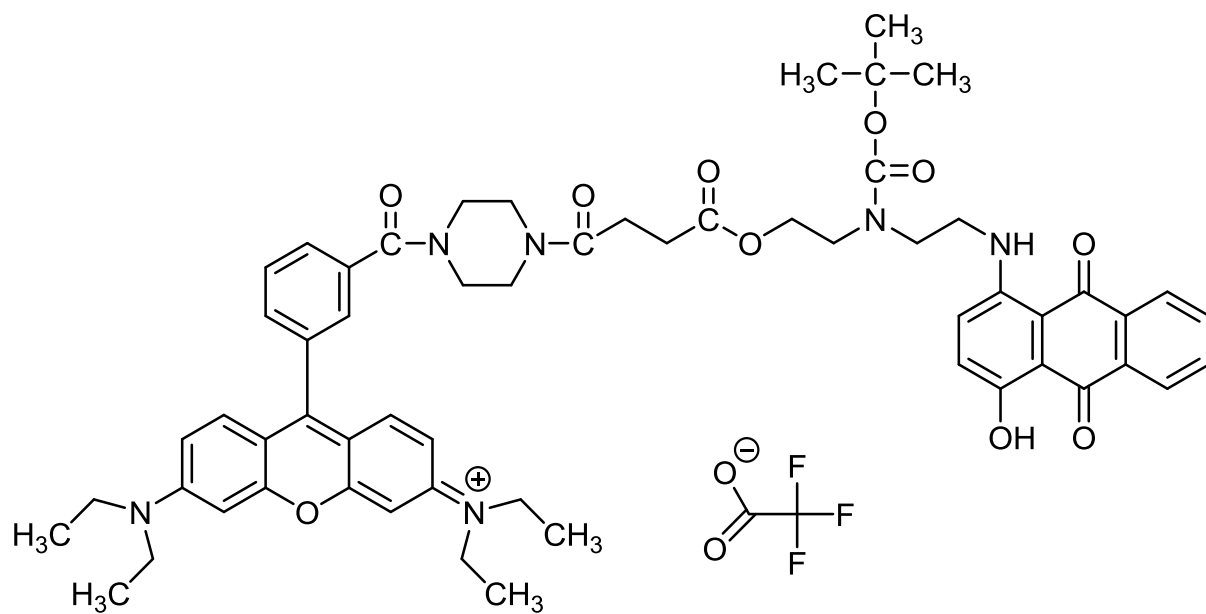
Rho-pip-Boc (OM4)



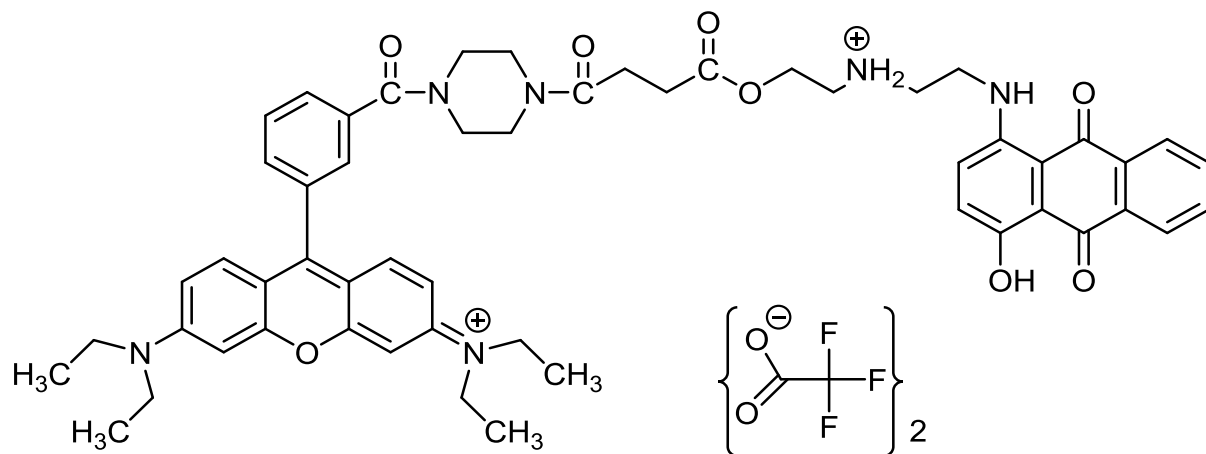
Rho-piperazine TFA (OM4 TFA)



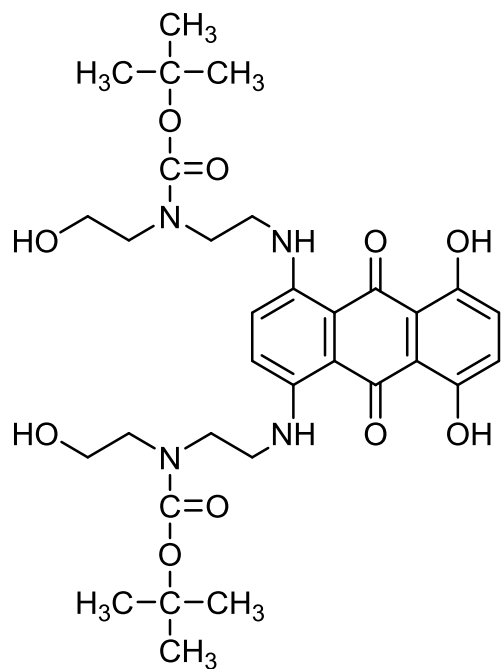
Rho-pip-succinate (OM5)



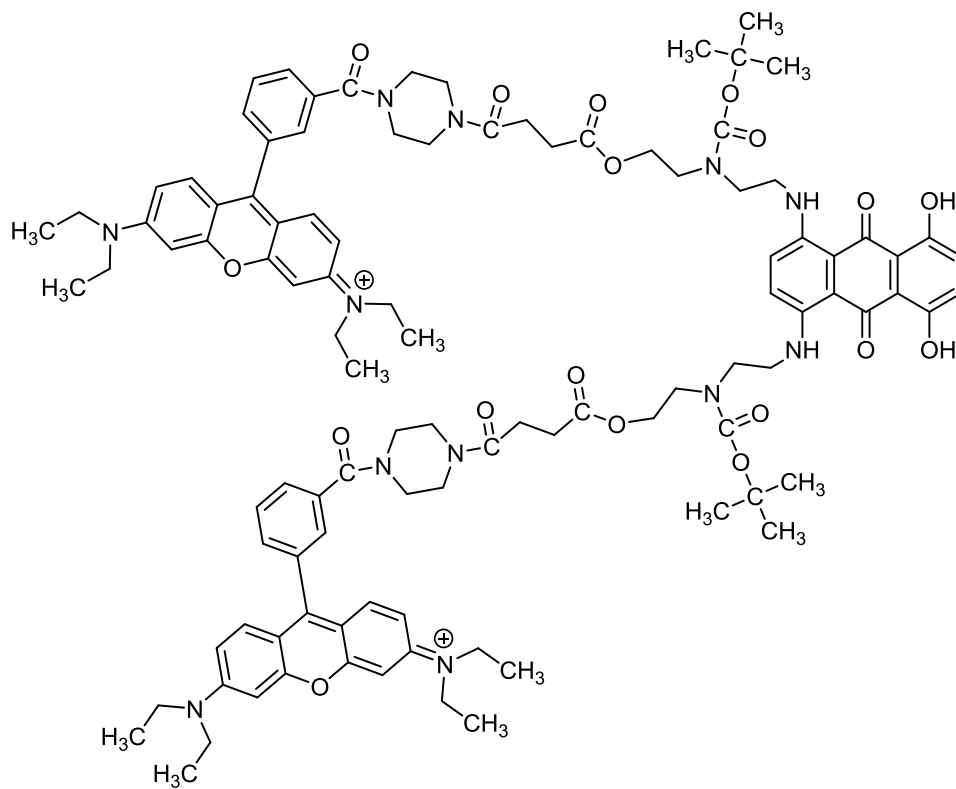
Rho-pip-succ-EAE-Boc-AQ(4-OH) (OM15)



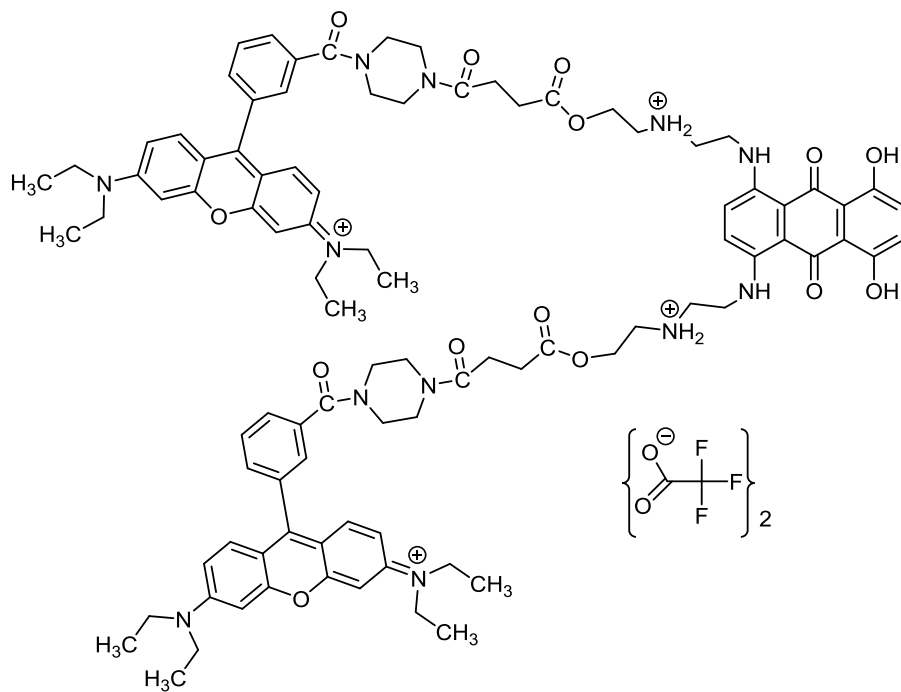
Rho-pip-succ-EAE-AQ(4-OH) (OM16)



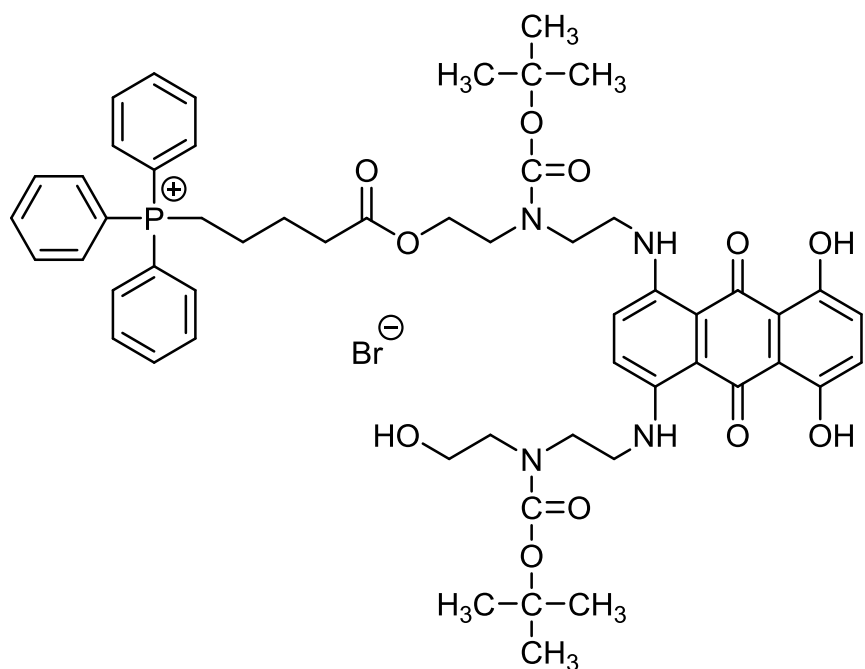
Mitoxantrone-Boc (OM19)



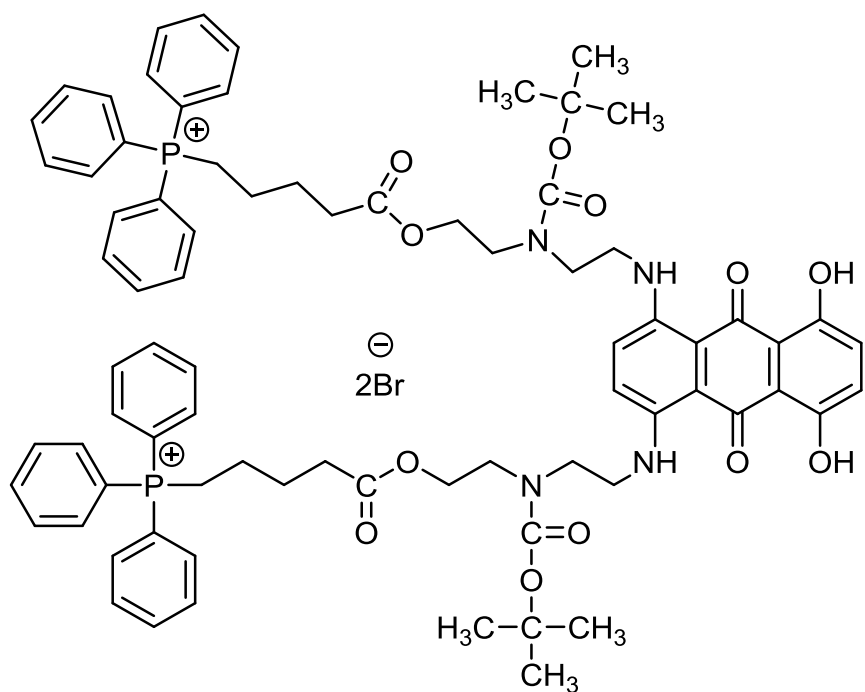
Rho-pip-succ-mitoxantrone-Boc (OM20)



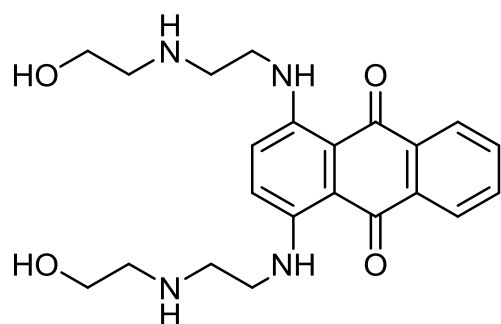
Rho-pip-succ-mitoxantrone (OM21)



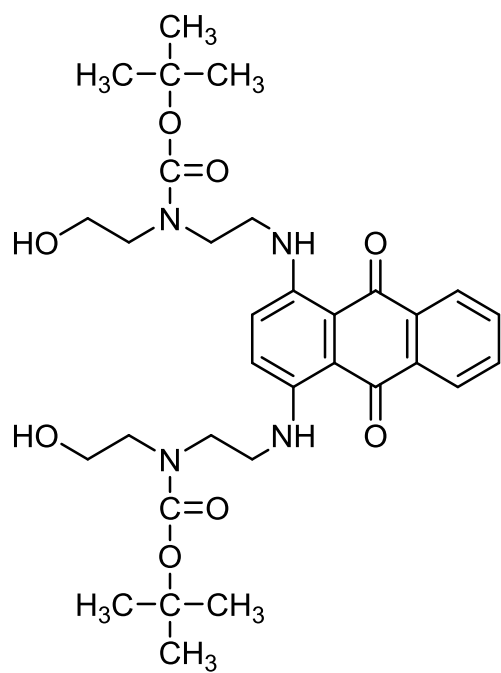
TPP-mitoxantrone-Boc (OM23)



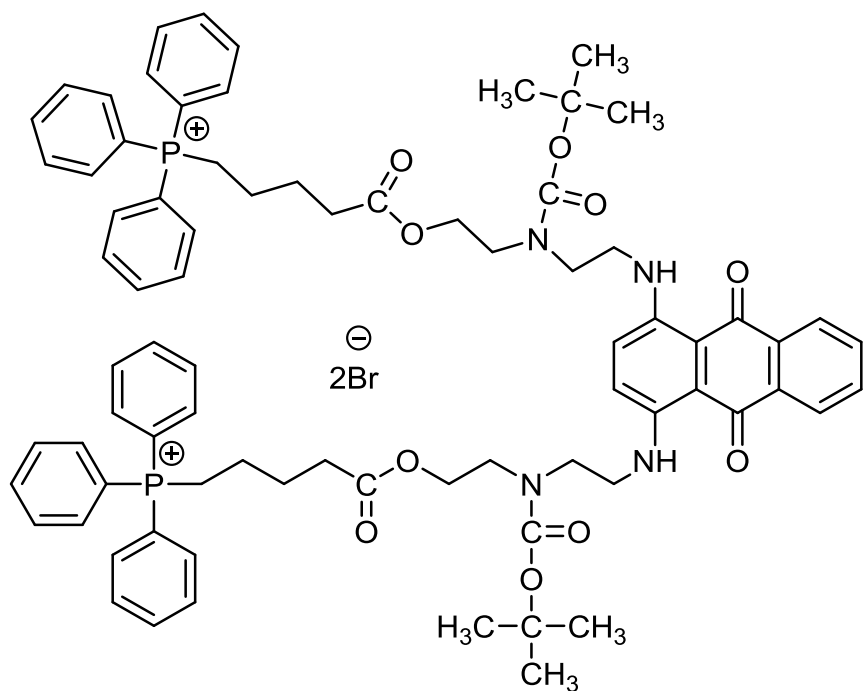
bis-TPP-mitoxantrone (OM24)



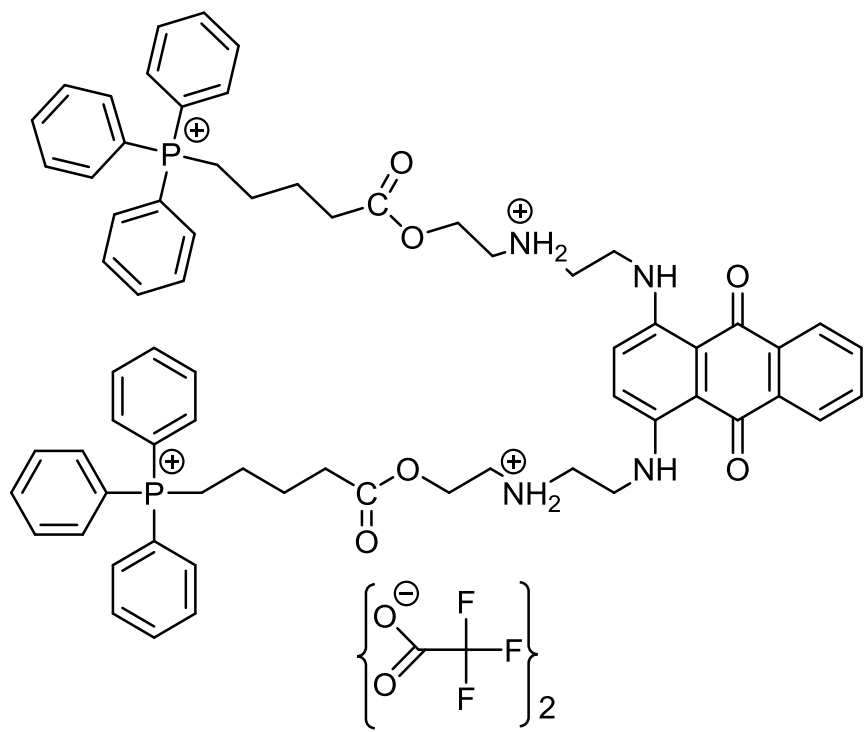
ametantrone (NK1)



ametantrone-Boc (NK4)



bis-TPP-ametantone-Boc (NK6)



bis-TPP-ametantone (NK8)

1.6 References

Adhikari, A. and Mahar, K. S. (2016) 'DNA targeted anthraquinone derivatives: An important anticancer agents', *International Journal of Pharmacy and Pharmaceutical Sciences*, **8**(6), pp. 17–25.

Aftab, S., Shah, A., Nadhman, A., Kurbanoglu, S., Aysil Ozkan, S., Dionysiou, D. D., Shukla, S. S. and Aminabhavi, T. M. (2018) 'Nanomedicine: An effective tool in cancer therapy', *International Journal of Pharmaceutics*, **540**(1–2), pp. 132–149. doi: 10.1016/j.ijpharm.2018.02.007.

Agostinis, P., Berg, K., Cengel, K. a, Foster, T. H., Girotti, A. W., Gollnick, S. O., Hahn, S. M., Hamblin, M. R., Juzeniene, A., Kessel, D., Korbelik, M., Moan, J., Mroz, P., Nowiz, D., Piette, J., Willson, B. C. and Golab, J. (2011) 'Photodynamic Therapy of Cancer : An Update', *American Cancer Society*, **61**, pp. 250–281. doi: 10.3322/caac.20114.Available.

Al-Otaibi, J. S., Teesdale Spittle, P. and El Gogary, T. M. (2017) 'Interaction of anthraquinone anti-cancer drugs with DNA:Experimental and computational quantum chemical study', *Journal of Molecular Structure*, **1127**, pp. 751–760. doi: 10.1016/j.molstruc.2016.08.007.

Albericio, F. (2008) 'PyClock, the phosphonium salt derived from 6-Cl-HOBt', *Chimica Oggi*, **26**(4), pp. 10–12.

Alonso, A., Almendral, M. J., Curto, Y., Criado, J. J., Rodríguez, E. and Manzano, J. L. (2006) 'Determination of the DNA-binding characteristics of ethidium bromide, proflavine, and cisplatin by flow injection analysis: Usefulness in studies on antitumor drugs', *Analytical Biochemistry*, **355**(2), pp. 157–164. doi: 10.1016/j.ab.2006.06.004.

Ambudkar, S. V, Dey, S., Hrycyna, C. A., Ramachandra, M., Pastan, I. and Gottesman, M. M. (1999) 'Biochemical, cellular, and pharmacological aspects of the multidrug transporter', *Annual Review of Pharmacology and Toxicology*, **39**(1), pp. 361–398. doi: 10.1146/annurev.pharmtox.39.1.361.

Ammirati, E. and Fogacci, F. (2017) 'Clinical relevance of biomarkers for the identification of patients with carotid atherosclerotic plaque: Potential role and limitations of cysteine protease legumain', *Atherosclerosis*, **257**, pp. 248–249. doi: 10.1016/j.atherosclerosis.2017.01.003.

Anderson, S., Bankier, A. T., Barrell, B. G., de Bruijn, M. H. L., Coulson, A. R., Drouin, J., Eperon, I. C., Nierlich, D. P., Roe, B. A., Sanger, F., Schreier, P. H., Smith, A. J. H., Staden, R. and Young, I. G. (1981) 'Sequence and organization of the human mitochondrial genome', *Nature*, **290**(5806), pp. 457–465. doi: 10.1038/290457a0.

Apostolova, N. and Victor, V. M. (2015) 'Molecular Strategies for Targeting Antioxidants to Mitochondria: Therapeutic Implications', *Antioxidants & Redox Signaling*, **22**(8), pp. 686–729. doi: 10.1089/ars.2014.5952.

Arroyo-crespo, J. J., Armiñán, A., Charbonnier, D., Balzano-nogueira, L., Huertas-lópez, F., Martí, C., Tarazona, S., Forteza, J., Conesa, A. and Vicent, M. J. (2018) 'Tumor microenvironment-targeted poly-L-glutamic acid-based combination conjugate for enhanced triple negative breast cancer treatment', *Biomaterials*, **186**, pp. 8–21. doi: 10.1016/j.biomaterials.2018.09.023.

Bailly, C., Routier, S., Bernier, J. L. and Waring, M. J. (1996) 'DNA recognition by two mitoxantrone analogues: Influence of the hydroxyl groups', *FEBS Letters*, **379**(3), pp. 269–272. doi: 10.1016/0014-5793(95)01528-0.

Bajjuri, K. M., Liu, Y., Liu, C. and Sinha, S. C. (2011) 'The Legumain Protease-Activated Auristatin Prodrugs Suppress Tumor Growth and Metastasis without Toxicity', *ChemMedChem.*, **6**(1), pp. 54–59. doi: 10.1002/cmdc.201000478.The.

Behrendt, R., White, P. and Offer, J. (2016) 'Advances in Fmoc solid-phase peptide synthesis', *Journal of Peptide Science*, **22**(1), pp. 4–27. doi: 10.1002/psc.2836.

Beija, M., Afonso, C. A. M. and Martinho, J. M. G. (2009) 'Synthesis and applications of Rhodamine derivatives as fluorescent probes', *Chemical Society Reviews*, **38**, p. 2410. doi: 10.1039/b901612k.

Bellosillo, B., Colomer, D., Pons, G. and Gil, J. (1998) 'Mitoxantrone, a topoisomerase II inhibitor, induces apoptosis of B- chronic lymphocytic leukaemia cells', *British Journal of Haematology*, **100**(1), pp. 142–146. doi: 10.1046/j.1365-2141.1998.00520.x.

Bhuniya, S., Maiti, S., Kim, E.-J., Lee, H., Sessler, J. L., Hong, K. S. and Kim, J. S. (2014) 'An Activatable Theranostic for Targeted Cancer Therapy and Imaging', *Angewandte Chemie International Edition*, **53**(17), pp. 4469–4474. doi: 10.1002/anie.201311133.

Bielski, E. R., Zhong, Q., Brown, M. and Da Rocha, S. R. P. (2015) 'Effect of the Conjugation Density of Triphenylphosphonium Cation on the Mitochondrial Targeting of Poly(amidoamine) Dendrimers', *Molecular Pharmaceutics*, **12**(8), pp. 3043–3053. doi: 10.1021/acs.molpharmaceut.5b00320.

Birtalan, E., Rudat, B., Kolmel, D. K., Fritz, D., Vollrath, S. B. L., Schepers, U. and Brase, S. (2011) 'Investigating rhodamine B-labeled peptoids: Scopes and limitations of its applications', *Biopolymers*, **96**(5), pp. 694–701. doi: 10.1002/bip.21617.

Biswas, S., Dodwadkar, N. S., Deshpande, P. P. and Torchilin, V. P. (2012) 'Liposomes Loaded with Paclitaxel and Modified with Novel Triphenylphosphonium-PEG-PE Conjugate Possess Low Toxicity, Target Mitochondria and Demonstrate Enhanced Antitumor Effects In Vitro and In Vivo', *Journal of Controlled Release*, **159**(3), pp. 393–402. doi: 10.1016/j.jconrel.2012.01.009.Liposomes.

Bogman, K., Peyer, A. K., Török, M., Küsters, E. and Drewe, J. (2001) 'HMG-CoA reductase inhibitors and P-glycoprotein modulation', *British Journal of Pharmacology*, **132**(6), pp. 1183–1192. doi: 10.1038/sj.bjp.0703920.

Boya, P. (2012) 'Lysosomal Function and Dysfunction: Mechanism and Disease', *Antioxidants & Redox Signaling*, **17**(5), pp. 766–774. doi: 10.1089/ars.2011.4405.

Callaghan, R., Luk, F. and Bebawy, M. (2014) 'Inhibition of the multidrug resistance P-glycoprotein: Time for a change of strategy?', *Drug Metabolism and Disposition*, **42**(4), pp. 623–631. doi: 10.1124/dmd.113.056176.

Carpino, L. A. (1987) 'The 9-Fluorenylmethyloxycarbonyl Family of Base-Sensitive Amino-Protecting Groups', *Accounts of Chemical Research*, **20**(11), pp. 401–407. doi: 10.1021/ar00143a003.

Chakraborty, A. and Jana, N. R. (2015) 'Design and synthesis of triphenylphosphonium functionalized nanoparticle probe for mitochondria targeting and imaging', *Journal of Physical Chemistry C*, **119**(5), pp. 2888–2895. doi: 10.1021/jp511870e.

Chang, E., Miller, J. S., Sun, J., Yu, W. W., Colvin, V. L., Drezek, R. and West, J. L. (2005) 'Protease-activated quantum dot probes', *Biochemical and Biophysical Research Communications*, **334**, pp. 1317–1321. doi: 10.1016/j.bbrc.2005.07.028.

Chatterjee, A., Mambo, E. and Sidransky, D. (2006) 'Mitochondrial DNA mutations in human cancer', *Oncogene*, **25**(34), pp. 4663–4674. doi: 10.1038/sj.onc.1209604.

Chen, H., Liu, X., Clayman, E. S., Shao, F., Xiao, M., Tian, X., Fu, W., Zhang, C., Ruan, B., Zhou, P., Liu, Z., Wang, Y. and Rui, W. (2015) 'Synthesis and Evaluation of a CBZ-AAN-Dox Prodrug and its in vitro Effects on SiHa Cervical Cancer Cells under Hypoxic Conditions', *Chemical Biology and Drug Design*, **86**, pp. 589–598. doi: 10.1111/cbdd.12525.

Chen, J.-M., Watts, C., Dando, P. M., Rawlings, N. D., Hewitt, E., Brown, M. A., Barrett, A. J., Stevens, R. A. and Young, N. E. (1997) 'Cloning, Isolation, and Characterization of Mammalian Legumain, an Asparaginyl Endopeptidase', *Journal of Biological Chemistry*, **272**(12), pp. 8090–8098. doi: 10.1074/jbc.272.12.8090.

Choe, Y., Leonetti, F., Greenbaum, D. C., Lecaille, F., Bogyo, M., Bromme, D., Ellman, J. A. and Craik, C. S. (2006) 'Substrate Profiling of Cysteine Proteases Using a Combinatorial Peptide Library Identifies Functionally Unique Specificities', *Journal of Biological Chemistry*, **281**(18), pp. 12824–12832. doi: 10.1074/jbc.m513331200.

Choi, C.-H. (2005) 'ABC transporters as multidrug resistance mechanisms and the development of chemosensitizers for their reversal.', *Cancer Cell International*, **5**, pp. 1–13. doi: 10.1186/1475-2867-5-30.

Choi, K. Y., Swierczewska, M., Lee, S. and Chen, X. (2012) 'Protease-Activated Drug Development', *Theranostics*, **2**(2). doi: 10.7150/thno.4068.

Cole, S. P. C. (2014) 'Targeting Multidrug Resistance Protein 1 (MRP1, *ABCC1*): Past, Present, and Future', *Annual Review of Pharmacology and Toxicology*, **54**(1), pp. 95–117. doi: 10.1146/annurev-pharmtox-011613-135959.

Constance, J. E. and Lim, C. S. (2012) 'Targeting malignant mitochondria with therapeutic peptides.', *Therapeutic delivery*, **3**(8), pp. 961–79. doi: 10.4155/tde.12.75.

Cornbleet, M. A., Stuart-Harris, R. C., Smith, I. E., Coleman, R. E., Rubens, R. D., McDonald, M., Mouridsen, H. T., Rainer, H., Van Oosterom, A. T. and Smyth, J. F. (1984) 'Mitoxantrone for the treatment of advanced breast cancer: Single-agent therapy in previously untreated patients', *European Journal of Cancer*, **20**(9), pp. 1141–1146. doi: 10.1016/0277-5379(84)90122-6.

Cummings, J., Macpherson, J. S., Meikle, I. and Smyth, J. F. (1996) 'Development of anthracenyl-amino acid conjugates as topoisomerase I and II inhibitors that circumvent drug resistance', *Biochemical Pharmacology*, **52**(7), pp. 979–990. doi: 10.1016/0006-2952(96)00301-2.

Dean, M., Hamon, Y. and Chimini, G. (2001) 'The Human ATP-Binding Cassette transporter superfamily', *Journal of Lipid Research*, **42**, pp. 1007–1017. doi: 10.1101/gr.184901.The.

Denizot, F. and Lang, R. (1986) 'Rapid colorimetric assay for cell growth and survival Modifications to the tetrazolium dye procedure giving improved sensitivity and reliability', *J Immunol Methods*, **89**, pp. 271–277.

Detmer, S. A. and Chan, D. C. (2007) 'Functions and dysfunctions of mitochondrial dynamics', *Nature Reviews Molecular Cell Biology*, **8**(11), pp. 870–879. doi: 10.1038/nrm2275.

Diehn, M., Cho, R. W., Lobo, N. A., Kalisky, T., Jo, M., Kulp, A. N., Qian, D., Lam, J. S., Ailles, L. E., Wong, M., Joshua, B., Kaplan, M. J., Wapnir, I., Dirbas, F., Somlo, G., Paz, B., Shen, J., Lau, S. K., Quake, S. R., Martin, J., Weissman, I. L. and Clarke, M. F. (2009)

'Association of Reactive Oxygen Species Levels and Radioresistance in Cancer Stem Cells', *Nature*, **458**(7239), pp. 780–783. doi: 10.1038/nature07733.Association.

Doonan, F. and Cotter, T. G. (2008) 'Morphological assessment of apoptosis', *Methods*, **44**(3), pp. 200–204. doi: 10.1016/j.ymeth.2007.11.006.

Duchen, M. R. (2004) 'Mitochondria in health and disease: Perspectives on a new mitochondrial biology', *Molecular Aspects of Medicine*, **25**(4), pp. 365–451. doi: 10.1016/j.mam.2004.03.001.

Edgington, L. E., Verdoes, M. and Bogyo, M. (2011) 'Functional imaging of proteases : recent advances in the design and application of substrate-based and activity-based probes', *Current Opinion in Chemical Biology*, **15**(6), pp. 798–805. doi: 10.1016/j.cbpa.2011.10.012.

Ehninger, G., Schuler, U., Proksch, B., Zeller, K. P. and Blanz, J. (1990) 'Pharmacokinetics and metabolism of mitoxantrone. A review.', *Clinical pharmacokinetics*, **18**(5), pp. 365–380.

Elmore, S. (2007) 'Apoptosis: A Review of Programmed Cell Death', *Toxicologic Pathology*, **35**(4), pp. 495–516. doi: 10.1080/01926230701320337.

Enache, M., Ionescu, S. and Volanschi, E. (2015) 'Studies on the anticancer drug mitoxantrone-DNA-sodium dodecyl sulfate system', *Journal of Molecular Liquids*, **208**, pp. 333–341. doi: 10.1016/j.molliq.2015.05.006.

Endo, T. and Yamano, K. (2010) 'Transport of proteins across or into the mitochondrial outer membrane', *Biochimica et Biophysica Acta - Molecular Cell Research*, **1803**(6), pp. 706–714. doi: 10.1016/j.bbamcr.2009.11.007.

Feofanov, A., Sharonov, S., Fleury, F., Kudelina, I. and Nabiev, I. (1997) 'Quantitative confocal spectral imaging analysis of mitoxantrone within living K562 cells: Intracellular accumulation and distribution of monomers, aggregates, naphthoquinoline metabolite, and drug-target complexes', *Biophysical Journal*, **73**(6), pp. 3328–3336. doi: 10.1016/S0006-3495(97)78357-7.

Ferreira, J. A. B. and Costa, S. M. B. (2006) 'Activationless nonradiative decay in

rhodamines: Role of NH and lower frequency vibrations in solvent kinetic isotope effects', *Chemical Physics*, **321**, pp. 197–208. doi: 10.1016/j.chemphys.2005.08.069.

Fields, G. B. (1994) 'Methods for Removing the Fmoc Group', *Methods in Molecular Biology*, **35**. doi: 10.1385/0-89603-273-6.

Filion, M. C. and Phillips, N. C. (1998) 'Major limitations in the use of cationic liposomes for DNA delivery', *International Journal of Pharmaceutics*, **162**(1), pp. 159–170. doi: [https://doi.org/10.1016/S0378-5173\(97\)00423-7](https://doi.org/10.1016/S0378-5173(97)00423-7).

Forster, T. (1948) 'Zwischenmolekulare Energiewanderung und Fluoreszenz', *Die Naturwissenschaften*, **33**(6), pp. 166–175. doi: 10.1007/BF00585226.

Fotakis, G. and Timbrell, J. A. (2006) 'In vitro cytotoxicity assays: Comparison of LDH, neutral red, MTT and protein assay in hepatoma cell lines following exposure to cadmium chloride', *Toxicology Letters*, **160**(2), pp. 171–177. doi: 10.1016/j.toxlet.2005.07.001.

Fulda, S., Galluzzi, L. and Kroemer, G. (2010) 'Targeting mitochondria for cancer therapy', *Drug Discovery*, **9**(5), pp. 476–489. doi: 10.1002/em.20552.

Galluzzi, L. and Kroemer, G. (2008) 'Necroptosis: A Specialized Pathway of Programmed Necrosis', *Cell*, **135**(7), pp. 1161–1163. doi: 10.1016/j.cell.2008.12.004.

Galluzzi, L., Morselli, E., Kepp, O., Vitale, I., Rigoni, A., Vacchelli, E., Michaud, M., Zischka, H., Castedo, M. and Kroemer, G. (2010) 'Mitochondrial gateways to cancer', *Molecular Aspects of Medicine*, **31**(1), pp. 1–20. doi: 10.1016/j.mam.2009.08.002.

Gewirtz, D. A. (1999) 'A critical evaluation of the mechanisms of action proposed for the antitumor effects of the anthracycline antibiotics adriamycin and daunorubicin', *Biochemical Pharmacology*, **57**(7), pp. 727–741. doi: 10.1016/S0006-2952(98)00307-4.

Goffart, S., Hangan, A. and Pohjoismäki, J. L. O. (2019) 'Twist and turn—topoisomerase functions in mitochondrial DNA maintenance', *International Journal of Molecular Sciences*, **20**(8). doi: 10.3390/ijms20082041.

Goldstein, L. J., Galski, H., Fojo, A., Willingham, M., Lai, S.-L., Gazdar, A., Pirker, R., Green, A., Crist, W., Brodeur, G. M., Lieber, M., Cossman, J., Gottesman, M. M. and

Pastan, I. (1989) 'Expression of Multidrug Resistance Gene in Human Cancers', *Journal of the National Cancer Institute*, **81**(2), pp. 116–124. Available at: <http://dx.doi.org/10.1093/jnci/81.2.116>.

Gotink, K. J., Broxterman, H. J., Labots, M., De Haas, R. R., Dekker, H., Honeywell, R. J., Rudek, M. A., Beerepoot, L. V., Musters, R. J., Jansen, G., Griffioen, A. W., Assaraf, Y. G., Pili, R., Peters, G. J. and Verheul, H. M. W. (2011) 'Lysosomal sequestration of sunitinib: A novel mechanism of drug resistance', *Clinical Cancer Research*, **17**(23), pp. 7337–7346. doi: 10.1158/1078-0432.CCR-11-1667.

Gottesman, M. M. (2002) Mechanisms of cancer drug resistance ", *Annual Review of Medicine*, **53**, pp. 615–627.

Green, D. R. and Kroemer, G. (2004) 'The Pathology of Mitochondrial Cell Death', *Science*, **305**(2004), pp. 626–629. doi: 10.1126/science.1099320.

Guo, P., Zhu, Z., Sun, Z., Wang, Z., Zheng, X. and Xu, H. (2013) 'Expression of legumain correlates with prognosis and metastasis in gastric carcinoma.', *Plos one*, **8**(9). doi: 10.1371/journal.pone.0073090.

Guzman-villanueva, D., Mendiola, M. R., Nguyen, H. X. and Weissig, V. (2015) 'Influence of Triphenylphosphonium (TPP) Cation Hydrophobization with Phospholipids on Cellular Toxicity and Mitochondrial Selectivity', *SOJ Pharm Pharm Sci*, **2**(1), pp. 1–9.

Hacker, G. (2000) 'The morphology of apoptosis', *Cell and Tissue Research*, **301**, pp. 5–17. doi: 10.1007/s004410000193.

Hajihassan, Z. and Rabbani-Chadegani, A. (2009) 'Studies on the binding affinity of anticancer drug mitoxantrone to chromatin, DNA and histone proteins', *Journal of Biomedical Science*, **16**(1), pp. 1–7. doi: 10.1186/1423-0127-16-31.

Halaby, R. (2015) 'Role of lysosomes in cancer therapy', *Research and Reports in Biology*, **6**, pp. 147–155. doi: dx.doi.org/10.2147/RRB.S83999.

Han, M., Vakili, M. R., Abyaneh, H. S., Molavi, O., Lai, R. and Lavasanifar, A. (2014) 'Mitochondrial Delivery of Doxorubicin via Triphenylphosphine Modification for Overcoming Drug Resistance in MDA-MB-435/DOX Cells', *Molecular pharmaceuticals*, **11**,

pp. 2640–2649.

Haugen, M. H., Boye, K., Nesland, J. M., Pettersen, S. J., Egeland, E. V., Tamhane, T., Brix, K., Maelandsmo, G. M. and Flatmark, K. (2015) 'High expression of the cysteine proteinase legumain in colorectal cancer - Implications for therapeutic targeting', *European Journal of Cancer*, **51**(1), pp. 9–17. doi: 10.1016/j.ejca.2014.10.020.

Haugen, M. H., Johansen, H. T., Pettersen, S. J., Solberg, R., Brix, K., Flatmark, K. and Maelandsmo, G. M. (2013) 'Nuclear Legumain Activity in Colorectal Cancer', *Plos One*, **8**(1). doi: 10.1371/journal.pone.0052980.

Heerdt, B. G., Houston, M. A. and Augenlicht, L. H. (2005) 'The intrinsic mitochondrial membrane potential of colonic carcinoma cells is linked to the probability of tumor progression', *Cancer Research*, **65**(21), pp. 9861–9867. doi: 10.1158/0008-5472.CAN-05-2444.

Higgs, H. N. and Peterson, K. J. (2005) 'Phylogenetic analysis of the formin homology 2 domain.', *Molecular biology of the cell*, **16**(1), pp. 1–13. doi: 10.1091/mbc.E04.

Hong, S. K., Starenki, D., Wu, P. K. and Park, J. I. (2017) 'Suppression of B-Raf V600E melanoma cell survival by targeting mitochondria using triphenyl-phosphonium-conjugated nitroxide or ubiquinone', *Cancer Biology and Therapy*. Taylor & Francis, **18**(2), pp. 106–114. doi: 10.1080/15384047.2016.1250987.

Horobin, R. W., Trapp, S. and Weissig, V. (2007) 'Mitochondriotropics: A review of their mode of action, and their applications for drug and DNA delivery to mammalian mitochondria', *Journal of Controlled Release*, **121**(3), pp. 125–136. doi: 10.1016/j.jconrel.2007.05.040.

Horton, K. L., Stewart, K. M., Fonseca, S. B., Guo, Q. and Kelley, S. O. (2008) 'Mitochondria-Penetrating Peptides', *Chemistry and Biology*, **15**(4), pp. 375–382. doi: 10.1016/j.chembiol.2008.03.015.

Hosoya, N. and Miyagawa, K. (2014) 'Targeting DNA damage response in cancer therapy', *Cancer Science*, **105**(4), pp. 370–388. doi: 10.1111/cas.12366.

Hoye, A. T., Davoren, J. E., Wipf, P., Fink, M. P. and Kagan, V. E. (2008) 'Targeting

Mitochondria', *Accounts of Chemical Research*, **41**(1), pp. 87–97. doi: 10.1021/ar700135m.

Hu, Z., Sim, Y., Kon, O. L., Ng, W. H., Ribeiro, A. J. M., Ramos, M. J., Fernandes, P. A., Ganguly, R., Xing, B., García, F. and Yeow, E. K. L. (2017) 'Unique Triphenylphosphonium Derivatives for Enhanced Mitochondrial Uptake and Photodynamic Therapy', *Bioconjugate Chemistry*, **28**(2), pp. 590–599. doi: 10.1021/acs.bioconjchem.6b00682.

Isidro-Liobet, A., Alvarez, M. and Albericio, F. (2009) 'Amino acid-protecting groups', *Chemical Reviews*, **109**(6), pp. 2455–2504. doi: 10.1021/cr800323s.

Jares-Erijman, E. A. and Jovin, T. M. (2003) 'FRET imaging', *Nature Biotechnology*, **21**(11), pp. 1387–1395. doi: 10.1038/nbt896.

Kamal, A., Ramu, R., Tekumalla, V., Khanna, G. B. R., Barkume, M. S., Juvekar, A. S. and Zingde, S. M. (2007) 'Synthesis, DNA binding, and cytotoxicity studies of pyrrolo[2,1-c][1,4]benzodiazepine-anthraquinone conjugates', *Bioorganic and Medicinal Chemistry*, **15**(22), pp. 6868–6875. doi: 10.1016/j.bmc.2007.08.026.

Kang, B. H., Plescia, J., Song, H. Y., Meli, M., Colombo, G., Beebe, K., Scroggins, B., Neckers, L. and Altieri, D. C. (2009) 'Combinatorial drug design targeting multiple cancer signaling networks controlled by mitochondrial Hsp90', *The Journal of Clinical Investigation*, **119**(3), pp. 454–464. doi: 10.1172/JCI37613DS1.

Kapuscinski, J. and Darzynkiewicz, Z. (1986) 'Relationship between the pharmacological activity of antitumor drugs Ametantrone and mitoxantrone (Novatrone) and their ability to condense nucleic acids.', *Proceedings of the National Academy of Sciences*, **83**(17), pp. 6302–6306. doi: 10.1073/pnas.83.17.6302.

Kapuscinski, J., Darzynkiewicz, Z., Traganos, F. and Melamed, M. R. (1981) 'Interactions of a new antitumor agent, 1,4-dihydroxy-5,8-bis[[2-[(2-hydroxyethyl)amino]-ethyl]amino]-9,10-anthracenedione, with nucleic acids', *Biochemical Pharmacology*, **30**(3), pp. 231–240. doi: [https://doi.org/10.1016/0006-2952\(81\)90083-6](https://doi.org/10.1016/0006-2952(81)90083-6).

Karpiuk, J., Grabowski, Z. R. and De Schryver, F. C. (1994) 'Photophysics of the lactone

form of rhodamine 101', *Journal of Physical Chemistry*, **98**, pp. 3247–3256. doi: 10.1021/j100064a001.

Katayama, K., Noguchi, K. and Sugimoto, Y. (2014) 'Regulations of P-glycoprotein/ABCB1/MDR1 in Human Cancer Cells', *New Journal of Science*, **2014**, pp. 1–10. doi: 10.1155/2014/476974.

Kelley, S. O., Stewart, K. M. and Mourtada, R. (2011) 'Development of novel peptides for mitochondrial drug delivery: Amino acids featuring delocalized lipophilic cations', *Pharmaceutical Research*, **28**(11), pp. 2808–2819. doi: 10.1007/s11095-011-0530-6.

Kent, S. B. H. (2008) 'Total chemical synthesis of proteins', *Chemical Society Reviews*, **38**(2), pp. 338–351. doi: 10.1039/B700141J.

KERR, J. F. R., WYLLIE, A. H. and CURRIE, A. R. (1972) 'Apoptosis: a basic biological phenomenon with wide-ranging implications in tissue kinetics', *British Journal of Cancer*, **26**, pp. 239–257. doi: 10.1111/j.1365-2796.2005.01570.x.

Ketterer, B., Neumcke, B. and Lauger, P. (1971) 'Transport mechanism of hydrophobic ions through lipid bilayer membranes', *The Journal of Membrane Biology*, **5**(3), pp. 225–245. doi: 10.1007/BF01870551.

Khiati, S., Rosa, I. D., Sourbier, C., Ma, X., Rao, V. A., Neckers, L. M., Zhang, H. and Pommier, Y. (2014) 'Mitochondrial topoisomerase i (Top1mt) is a novel limiting factor of doxorubicin cardiotoxicity', *Clinical Cancer Research*, **20**(18), pp. 4873–4881. doi: 10.1158/1078-0432.CCR-13-3373.

Kikuchi, M., Yamagishi, T. and Hida, M. (1982) 'Kinetic studies on the amination of leucoquinizarin', *Bulletin of the Chemical Society of Japan*, pp. 1209–1212. doi: 10.1246/bcsj.55.1209.

Kim, E. J., Bhuniya, S., Lee, H., Kim, H. M., Cheong, C., Maiti, S., Hong, K. S. and Kim, J. S. (2014) 'An activatable prodrug for the treatment of metastatic tumors', *Journal of the American Chemical Society*, **136**(39), pp. 13888–13894. doi: 10.1021/ja5077684.

Kim, G. B. and Kim, Y. P. (2012) 'Analysis of protease activity using quantum dots and resonance energy transfer', *Theranostics*, **2**(2), pp. 127–138. doi: 10.7150/thno.3476.

- Kircher, M. F., Weissleder, R. and Josephson, L. (2004) 'A Dual Fluorochrome Probe for Imaging Proteases', *Bioconjugate Chemistry*, **15**, pp. 242–248. doi: 10.1021/bc034151d.
- Kodama, S., Asano, S., Moriguchi, T., Sawai, H. and Shinozuka, K. (2006) 'Novel fluorescent oligoDNA probe bearing a multi-conjugated nucleoside with a fluorophore and a non-fluorescent intercalator as a', *Bioorganic and Medicinal Chemistry Letters*, **16**(10), pp. 2685–2688. doi: 10.1016/j.bmcl.2006.02.016.
- Kroemer, G. (2006) 'Mitochondria in cancer', *Oncogene*, **25**(34), pp. 4630–4632. doi: 10.1038/sj.onc.1209589.
- Kühlbrandt, W. (2015) 'Structure and function of mitochondrial membrane protein complexes', *BMC Biology*, **13**(1), pp. 1–11. doi: 10.1186/s12915-015-0201-x.
- Kundu, S., Maity, S., Bhadra, R. and Ghosh, P. (2011) 'Trans-dichlorobis(N-p-tolylpyridin-2-amine)palladium(II): Synthesis, structure, fluorescence features and DNA binding', *Indian Journal of Chemistry*, **50**, pp. 1443–1449.
- Lampidis, T. J., Kolonias, D., Podona, T., Israel, M., Safa, A. R., Lothstein, L., Savaraj, N., Tapiero, H. and Priebe, W. (1997) 'Circumvention of P-GP MDR as a Function of Anthracycline Lipophilicity and Charge', *Biochemistry. American Chemical Society*, **36**(9), pp. 2679–2685. doi: 10.1021/bi9614489.
- Lavis, L. D. and Raines, R. T. (2008) 'Bright ideas for chemical biology', *ACS chemical biology*, **3**(3), pp. 142–55. doi: 10.1021/cb700248m.
- Leo, A., Hansch, C. and Elkins, D. (1971) 'Partition coefficients and their uses', *Chemical Reviews*, **71**(6), pp. 525–616. doi: 10.1021/cr60274a001.
- Li, J., Wang, Y., Zhu, Y. and Oupický, D. (2013) 'Recent advances in delivery of drug–nucleic acid combinations for cancer treatment', *Journal of Controlled Release*, **172**(2), pp. 589–600. doi: <https://doi.org/10.1016/j.jconrel.2013.04.010>.
- Li, N., Ma, Y., Yang, C., Guo, L. and Yang, X. (2005a) 'Interaction of anticancer drug mitoxantrone with DNA analyzed by electrochemical and spectroscopic methods', *Biophysical Chemistry*, **116**(3), pp. 199–205. doi: 10.1016/j.bpc.2005.04.009.

Liscovitch, M. and Lavie, Y. (2002) 'Cancer multidrug resistance: a review of recent drug discovery research.', *IDrugs*, **5**(4), pp. 349–355.

Liu, C., Sun, C. and Huang, H. (2003) 'Overexpression of Legumain in Tumors Is Significant for Invasion / Metastasis and a Candidate Enzymatic Target for Prodrug Therapy.', *Cancer Research*, **63**, pp. 2957–2964.

Liu, Y., Bajjuri, K. M., Liu, C. and Sinha, S. C. (2012) 'Targeting cell surface alpha(v)beta(3) integrin increases therapeutic efficacies of a legumain protease-activated Auristatin Prodrug', *Molecular Pharmaceutics*, **9**, pp. 168–175. doi: 10.1021/mp200434n.

Longmire, M. R., Ogawa, M., Hama, Y., Kosaka, N., Regino, C. A. S., Choyke, P. L. and Kobayashi, H. (2008) 'Determination of Optimal Rhodamine Fluorophore for in Vivo Optical Imaging', *Bioconjugate Chemistry*, **19**(8), pp. 1735–1742. doi: 10.1021/bc800140c.

Longo-Sorbello, G. and Bertino, J. R. (2001) 'Current understanding of methotrexate pharmacology and efficacy in acute leukemias. Use of newer antifolates in clinical trials', *haematologica*, **86**, pp. 121–127.

López-Otín, C. and Hunter, T. (2010) 'The regulatory crosstalk between kinases and proteases in cancer', *Nature Reviews Cancer*, **10**(4), pp. 278–292. Available at: <https://doi.org/10.1038/nrc2823>.

Løvsletten, R., Alexander, O., Åstrand, H., Minh, L., Elvestrand, T., Hagelin, G., Solberg, R., Thidemann, H. and Rongved, P. (2014) 'Synthesis of a novel legumain-cleavable colchicine prodrug with cell-specific toxicity', *Bioorganic & Medicinal Chemistry*, **22**(13), pp. 3309–3315. doi: 10.1016/j.bmc.2014.04.056.

Mahato, R., Tai, W. and Cheng, K. (2011) 'Prodrugs for Improving Tumor Targetability and Efficiency', *Advanced Drug Delivery Reviews*, **63**(8), pp. 659–670. doi: 10.1111/j.1743-6109.2008.01122.x.Endothelial.

Majno, G. and Joris, I. (1995) 'Apoptosis, oncosis, and necrosis', *The American journal of pathology*, **146**(1), pp. 3–15. doi: 7856735.

Mansour, O. C., Evison, B. J., Sleebs, B. E., Watson, K. G., Nudelman, A., Rephaeli, A.,

Buck, D. P., Collins, J. G., Bilardi, R. A., Phillips, D. R. and Cutts, S. M. (2010) 'New anthracenedione derivatives with improved biological activity by virtue of stable drug-DNA adduct formation', *Journal of Medicinal Chemistry*, **53**(19), pp. 6851–6866. doi: 10.1021/jm901894c.

May, J. P., Brown, L. J., Van Delft, I., Thelwell, N., Harley, K. and Brown, T. (2005) 'Synthesis and evaluation of a new non-fluorescent quencher in fluorogenic oligonucleotide probes for real-time PCR', *Organic and Biomolecular Chemistry*, **3**(14), pp. 2534–2542. doi: 10.1039/b504759e.

McKnight, R. E., Zhang, J. and Dixon, D. W. (2004) 'Binding of a homologous series of anthraquinones to DNA', *Bioorganic and Medicinal Chemistry Letters*, **14**(2), pp. 401–404. doi: 10.1016/j.bmcl.2003.10.054.

Meerlo, J. van, Kaspers, G. J. L. and Cloos, J. (2011) 'Cell Sensitivity Assays: The MTT Assay', *Cancer Cell Culture*, **731**, pp. 237–245. doi: 10.1385/1592594069.

Meng, Q., Yu, M., Zhang, H., Ren, J. and Huang, D. (2007) 'Synthesis and application of N-hydroxysuccinimidyl rhodamine B ester as an amine-reactive fluorescent probe', *Dyes and Pigments*, **73**(2), pp. 254–260. doi: 10.1016/j.dyepig.2005.12.008.

Merrifield, R. B. (1963) 'Solid Phase Peptide Synthesis. I. The Synthesis of a Tetrapeptide', *Journal of the American Chemical Society*, **85**(14), pp. 2149–2154. doi: 10.1021/ja00897a025.

Mincher, DJ. (1999). 'Anthracene derivatives for use as anticancer agents', Publ.

Modica-Napolitano, J. S. and Aprille, J. R. (2001) 'Delocalized lipophilic cations selectively target the mitochondria of carcinoma cells', *Advanced Drug Delivery Reviews*, **49**(1–2), pp. 63–70. doi: 10.1016/S0169-409X(01)00125-9.

Montalbetti, C. A. G. N. and Falque, V. (2005) 'Amide bond formation and peptide coupling', *Tetrahedron*, **61**(46), pp. 10827–10852. doi: 10.1016/j.tet.2005.08.031.

Mordente, A., Meucci, E., Silvestrini, A., Martorana, G. E. and Giardina, B. (2012) 'Anthracyclines and Mitochondria', in Scatena, R., Bottoni, P., and Giardina, B. (eds) *Advances in Mitochondrial Medicine*, pp. 385–419. doi: 10.1007/978-94-007-2869-1_18.

Morris, G. A., Mullah, K. B. and Sutherland, J. K. (1986) 'Some experiments with aminodihydroxyanthraquinones', *Tetrahedron*, **42**(12), pp. 3303–3309. doi: [https://doi.org/10.1016/S0040-4020\(01\)87394-4](https://doi.org/10.1016/S0040-4020(01)87394-4).

Mosmann, T. (1983) 'Rapid Colorimetric Assay for Cellular Growth and Survival: Application to Proliferation and Cytotoxicity Assays', *Journal of Immunological Methods*, **65**, pp. 55–63.

Mottram, L. F., Forbes, S., Ackley, B. D. and Peterson, B. R. (2012) 'Hydrophobic analogues of rhodamine B and rhodamine 101: Potent fluorescent probes of mitochondria in living *C. elegans*', *Beilstein Journal of Organic Chemistry*, **8**, pp. 2156–2165. doi: [10.3762/bjoc.8.243](https://doi.org/10.3762/bjoc.8.243).

Mrschik, M. and Ryan, K. M. (2015) 'Lysosomal proteins in cell death and autophagy', *FEBS Journal*, **282**(10), pp. 1858–1870. doi: [10.1111/febs.13253](https://doi.org/10.1111/febs.13253).

Muli, D. K., Rajaputra, P., You, Y. and McGrath, D. V. (2014) 'Asymmetric ZnPc-rhodamine B conjugates for mitochondrial targeted photodynamic therapy', *Bioorganic and Medicinal Chemistry Letters*, **24**(18), pp. 4496–4500. doi: [10.1016/j.bmcl.2014.07.082](https://doi.org/10.1016/j.bmcl.2014.07.082).

Murphy, M. P. (1997) 'Selective targeting of bioactive compounds to mitochondria', *Trends in Biotechnology*, **15**, pp. 326–330.

Murphy, M. P. (2008) 'Targeting lipophilic cations to mitochondria', *Biochimica et Biophysica Acta*, **1777**(7–8), pp. 1028–1031. doi: [10.1016/j.bbabi.2008.03.029](https://doi.org/10.1016/j.bbabi.2008.03.029).

Nass, M. M. K. and Nass, S. (1963) 'Fibers with DNA characteristics I. Fixation and electron staining reactions', *The Journal of Cell Biology*, **19**, pp. 593–611.

Ndolo, R. A., Luan, Y., Duan, S., Forrest, M. L. and Krise, J. P. (2012) 'Lysosomotropic Properties of Weakly Basic Anticancer Agents Promote Cancer Cell Selectivity In Vitro', *Plos One*, **7**(11), pp. 1–9. doi: [10.1371/journal.pone.0049366](https://doi.org/10.1371/journal.pone.0049366).

Neises, B. and Steglich, W. (1978) 'Simple Method for the Esterification of Carboxylic Acids', *Angewandte Chemie International Edition in English*, **17**(7), pp. 522–524. doi: [10.1002/anie.197805221](https://doi.org/10.1002/anie.197805221).

- Ngen, E. J., Rajaputra, P. and You, Y. (2009) 'Evaluation of delocalized lipophilic cationic dyes as delivery vehicles for photosensitizers to mitochondria', *Bioorganic and Medicinal Chemistry*, **17**(18), pp. 6631–6640. doi: 10.1016/j.bmc.2009.07.074.
- Nguyen, T. and Francis, M. B. (2003) 'Practical synthetic route to functionalized rhodamine dyes', *Organic Letters*, **5**(18), pp. 3245–3248. doi: 10.1021/ol035135z.
- Nitiss, J. (2009) 'Targeting DNA topoisomerase II in cancer chemotherapy', *Nature Reviews Cancer*, **9**(5), pp. 338–350. doi: 10.1038/nrc2607.Targeting.
- Nurgali, K., Jagoe, R. T. and Abalo, R. (2018) 'Editorial: Adverse Effects of Cancer Chemotherapy: Anything New to Improve Tolerance and Reduce Sequelae?', *Frontiers in Pharmacology*, **9**, pp. 1–3. doi: 10.3389/fphar.2018.00245.
- Ohno, Y., Nakashima, J., Izumi, M., Ohori, M., Hashimoto, T. and Tachibana, M. (2013) 'Association of legumain expression pattern with prostate cancer invasiveness and aggressiveness', *World Journal of Urology*, **31**, pp. 359–364. doi: 10.1007/s00345-012-0977-z.
- van Oven, M. and Kayser, M. (2009) 'Updated comprehensive phylogenetic tree of global human mitochondrial DNA variation.', *Human mutation*, **30**(2). doi: 10.1002/humu.20921.
- Ozben, T. (2006) 'Mechanisms and strategies to overcome multiple drug resistance in cancer', *FEBS Letters*, **580**(12), pp. 2903–2909. doi: 10.1016/j.febslet.2006.02.020.
- Palchaudhuri, R. and Hergenrother, P. J. (2007) 'DNA as a target for anticancer compounds: methods to determine the mode of binding and the mechanism of action', *Current Opinion in Biotechnology*, **18**(6), pp. 497–503. doi: 10.1016/j.copbio.2007.09.006.
- Panousis, C. and Phillips, D. R. (1994) 'DNA sequence specificity of mitoxantrone.', *Nucleic acids research*, **22**(8), pp. 1342–1345. doi: 10.1093/nar/22.8.1342.
- Parker, B. S., Buley, T., Evison, B. J., Cutts, S. M., Neumann, G. M., Iskander, M. N. and Phillips, D. R. (2004) 'A molecular understanding of mitoxantrone-DNA adduct formation: Effect of cytosine methylation and flanking sequences', *Journal of Biological Chemistry*, **279**(18), pp. 18814–18823. doi: 10.1074/jbc.M400931200.

Paterson, J. K. and Gottesman, M. M. (2007) 'P-Glycoprotein is not present in mitochondrial membranes', *Experimental Cell Research*, **313**(14), pp. 3100–3105. doi: 10.1016/j.yexcr.2007.04.019.

Pathania, D., Millard, M. and Neamati, N. (2009) 'Opportunities in discovery and delivery of anticancer drugs targeting mitochondria and cancer cell metabolism', *Advanced Drug Delivery Reviews*, **61**(14), pp. 1250–1275. doi: 10.1016/j.addr.2009.05.010.

Paumard, P. (2002) 'The ATP synthase is involved in generating mitochondrial cristae morphology', *EMBO Journal*, **21**(3), pp. 221–230. doi: 10.1093/emboj/21.3.221.

Pelicano, H., Martin, D. S., Xu, R. H. and Huang, P. (2006) 'Glycolysis inhibition for anticancer treatment', *Oncogene*, **25**(34), pp. 4633–4646. doi: 10.1038/sj.onc.1209597.

Petersen, N. H. T., Olsen, O. D., Groth-pedersen, L., Ellegaard, A., Bilgin, M., Redmer, S., Ostenfeld, M. S., Ulanet, D., Dovmark, T. H., Lønborg, A., Vindeløv, S. D., Hanahan, D., Arenz, C., Ejsing, C. S., Kirkegaard, T., Rohde, M. and Nylandsted, J. (2013) 'Transformation-Associated Changes in Sphingolipid Metabolism Sensitize Cells to Lysosomal Cell Death Induced by Inhibitors of Acid Sphingomyelinase', *Cancer Cell*, **24**, pp. 379–393. doi: 10.1016/j.ccr.2013.08.003.

Pham, W., Choi, Y., Weissleder, R. and Tung, C. H. (2004) 'Developing a peptide-based near-infrared molecular probe for protease sensing', *Bioconjugate Chemistry*, **15**(6), pp. 1403–1407. doi: 10.1021/bc049924s.

Piccart, M., Rozenzweig, M., Abele, R., Cumps, E., Dodion, P., Dupont, D., Kisner, D. and Kenis, Y. (1981) 'Phase I clinical trial with ametantrone (NSC-287513)', *European Journal of Cancer and Clinical Oncology*, **17**(7), pp. 775–779. doi: [https://doi.org/10.1016/0014-2964\(81\)90233-4](https://doi.org/10.1016/0014-2964(81)90233-4).

Piddock, L. J. V (2006) 'Multidrug - resistance efflux pumps — not just for resistance', *Nature Reviews Microbiology*, **4**, pp. 629–636. doi: 10.1038/nrmicro1464.

Pluen, A., Boucher, Y., Ramanujan, S., McKee, T. D., Gohongi, T., di Tomaso, E., Brown, E. B., Izumi, Y., Campbell, R. B., Berk, D. A. and Jain, R. K. (2001) 'Role of tumor-host interactions in interstitial diffusion of macromolecules: Cranial vs. subcutaneous tumors',

Proceedings of the National Academy of Sciences, **98**(8), pp. 4628–4633. doi: 10.1073/pnas.081626898.

Pommier, Y., Leo, E., Zhang, H. and Marchand, C. (2010) 'DNA topoisomerases and their poisoning by anticancer and antibacterial drugs', *Chemistry and Biology*, **17**(5), pp. 421–433. doi: 10.1016/j.chembiol.2010.04.012.

Rautio, J., Kumpulainen, H., Heimbach, T., Oliyai, R., Oh, D., Järvinen, T. and Savolainen, J. (2008) 'Prodrugs: design and clinical applications', *Nature Reviews Drug Discovery*, **7**(3), pp. 255–270. doi: 10.1038/nrd2468.

Reily, C., Mitchell, T., Chacko, B. K., Benavides, G. A., Murphy, M. P. and Darley-Usmar, V. M. (2013) 'Mitochondrially targeted compounds and their impact on cellular bioenergetics', *Redox Biology*, **1**(1), pp. 86–93. doi: 10.1016/j.redox.2012.11.009.

Reungpatthanaphong, P., Dechsupa, S., Meesungnoen, J., Loetchutinat, C. and Mankhetkorn, S. (2003) 'Rhodamine B as a mitochondrial probe for measurement and monitoring of mitochondrial membrane potential in drug-sensitive and -resistant cells', *Journal of Biochemical and Biophysical Methods*, **57**, pp. 1–16. doi: 10.1016/S0165-022X(03)00032-0.

Riganti, C., Rolando, B., Kopecka, J., Campia, I., Chegaev, K., Lazzarato, L., Federico, A., Fruttero, R. and Ghigo, D. (2013) 'Mitochondrial-targeting nitrooxy-doxorubicin: A new approach to overcome drug resistance', *Molecular Pharmaceutics*, **10**(1), pp. 161–174. doi: 10.1021/mp300311b.

Rin Jean, S., Tulumello, D. V., Wisnovsky, S. P., Lei, E. K., Pereira, M. P. and Kelley, S. O. (2014) 'Molecular vehicles for mitochondrial chemical biology and drug delivery', *ACS Chemical Biology*, **9**(2), pp. 323–333. doi: 10.1021/cb400821p.

Ross, M. F., Kelso, G. F., Blaikie, F. H., James, A. M., Cochemé, H. M., Filipovska, A., Ros, T. Da, Hurd, T. R., Smith, R. A. J. and Murphy, M. P. (2005) 'Lipophilic triphenylphosphonium cations as tools in mitochondrial bioenergetics and free ... Lipophilic Triphenylphosphonium Cations as Tools in Mitochondrial Bioenergetics and Free Radical Biology', *Biochemistry*, **70**(2), pp. 222–230. doi: 10.1007/s10541-005-0104-

5.

Ross, M. F., Prime, T. A., Abakumova, I., James, A. M., Porteous, C. M., Smith, R. A. J. and Murphy, M. P. (2008) 'Rapid and extensive uptake and activation of hydrophobic triphenylphosphonium cations within cells', *Biochemical Journal*, **411**(3), pp. 633–645. Available at: <http://www.biochemj.org/content/411/3/633.abstract>.

Rossato, L. G., Costa, V. M., Dallegrave, E., Arbo, M., Silva, R., Ferreira, R., Amado, F., Dinis-Oliveira, R. J., Duarte, J. A., De Lourdes Bastos, M., Palmeira, C. and Remião, F. (2014) 'Mitochondrial cumulative damage induced by mitoxantrone: Late onset cardiac energetic impairment', *Cardiovascular Toxicology*, **14**(1), pp. 30–40. doi: 10.1007/s12012-013-9230-2.

Rozenzweig, M., Sanders, C., Rombaut, W., Crespeigne, N., Kenis, Y. and Klastersky, J. (1985) 'Phase II study of ametantrone in a human tumor cloning assay', *European Journal of Cancer and Clinical Oncology*, **21**(2), pp. 195–198. doi: [https://doi.org/10.1016/0277-5379\(85\)90173-7](https://doi.org/10.1016/0277-5379(85)90173-7).

Rudraraju, A. V., Amoyaw, P. N. A., Hubin, T. J. and Khan, M. O. F. (2014) 'Determination of log P values of new cyclen based antimalarial drug leads using RP-HPLC', *Pharmazie*, **69**(9), pp. 655–662. doi: 10.1691/ph.2014.4019.

Rutkowska, E., Pająk, K. and Józwiak, K. (2013) 'Lipophilicity - Methods of determination and its role in medicinal chemistry', *Acta Poloniae Pharmaceutica - Drug Research*, **70**(1), pp. 3–18. doi: 10.1097/00005392-199608001-00059.

Saraste, A. and Pulkki, K. (2000) 'Morphologic and biochemical hallmarks of apoptosis', *Cardiovascular Research*, **45**(3), pp. 528–537. doi: 10.1016/s0008-6363(99)00384-3.

Sauna, Z. E., Smith, M. M., Müller, M., Kerr, K. M. and Ambudkar, S. V. (2001) 'The Mechanism of Action of Multidrug-Resistance-Linked P-Glycoprotein', *Clinical and Experimental Dermatology*, **33**(6), pp. 481–491. Available at: <http://www.ncbi.nlm.nih.gov/pubmed/2689019>.

Seiter, K. (2005) *Toxicity of the topoisomerase II inhibitors*, *Expert opinion on drug safety*, **4**(2), pp. 219-234. doi: 10.1517/14740338.4.2.219.

Settanni, G., Zhou, J., Suo, T., Schöttler, S., Landfester, K., Schmid, F. and Mailänder, V. (2012) 'Design and Synthesis of a Mitochondria-Targeting Carrier for Small Molecule Drugs', *The Royal Society of Chemistry*. doi: 10.1039/x0xx00000x.

Shaul, P., Frenkel, M., Goldstein, E. B., Mittelman, L., Grunwald, A., Ebenstein, Y., Tsarfaty, I. and Fridman, M. (2013) 'The Structure of Anthracycline Derivatives Determines Their Subcellular Localization and Cytotoxic Activity', *American Chemical Society*, **4**, pp. 323–328. doi: 10.1021/ml3002852.

Shen, D.-W., Goldenberg, S., Pastan, I. and Gottesman, M. M. (2000) 'Decreased accumulation of [14c]carboplatin in human cisplatin-resistant cells results from reduced energy-dependent uptake', *Journal of Cellular Physiology*, **183**(1), pp. 108–116. doi: 10.1002/(SICI)1097-4652(200004)183:1<108::AID-JCP13>3.0.CO;2-4.

Shen, Y., Chu, Y., Yang, Y. and Wang, Z. (2012) 'Mitochondrial localization of P-glycoprotein in the human breast cancer cell line MCF-7/ADM and its functional characterization', *Oncology Reports*, **27**(5), pp. 1535–1540. doi: 10.3892/or.2012.1671.

Sheppard, R. (2003) 'The fluorenylmethoxycarbonyl group in solid phase synthesis', *Journal of Peptide Science*, **9**(9), pp. 545–552. doi: 10.1002/psc.479.

Shirahama-Noda, K., Yamamoto, A., Sugihara, K., Hashimoto, N., Asano, M., Nishimura, M. and Hara-Nishimura, I. (2003) 'Biosynthetic Processing of Cathepsins and Lysosomal Degradation Are Abolished in Asparaginyl Endopeptidase-deficient Mice', *Journal of Biological Chemistry*, **278**(35), pp. 33194–33199. doi: 10.1074/jbc.m302742200.

Skladanowski, A. and Konopa, J. (2000) 'Mitoxantrone and ametantrone induce interstrand cross-links in DNA of tumour cells', *British Journal of Cancer*, **82**(7), pp. 1300–1304. doi: 10.1054/bjoc.1999.1095.

Smith, P. J., Morgan, S. A., Fox, M. E. and Watson, J. V (1990) 'Mitoxantrone-DNA binding and the induction of topoisomerase II associated DNA damage in multi-drug resistant small cell lung cancer cells', *Biochemical Pharmacology*, **40**(9), pp. 2069–2078. doi: [https://doi.org/10.1016/0006-2952\(90\)90237-F](https://doi.org/10.1016/0006-2952(90)90237-F).

Smith, P. J., Sykes, H. R., Fox, M. E. and Furlong, I. J. (1992) 'Subcellular Distribution of

the Anticancer Drug Mitoxantrone in Human and Drug-resistant Murine Cells Analyzed by Flow Cytometry and Confocal Microscopy and Its Relationship to the Induction of DNA Damage¹, *Cancer Research*, **52**, pp. 4000–4008.

Smith, R. a J., Porteous, C. M., Gane, A. M. and Murphy, M. P. (2003) 'Delivery of bioactive molecules to mitochondria in vivo.', *Proceedings of the National Academy of Sciences of the United States of America*, **100**(9), pp. 5407–5412. doi: 10.1073/pnas.0931245100.

Smith, R., Hartley, R. and P Murphy, M. (2011) *Mitochondria-Targeted Small Molecule Therapeutics and Probes, Antioxidants & redox signaling*, **15**(12). doi: 10.1089/ars.2011.3969.

Smith, R., Johansen, H. T., Nilsen, H., Haugen, M. H., Pettersen, S. J., Mælandsmo, G. M., Abrahamson, M. and Solberg, R. (2012) 'Intra- and extracellular regulation of activity and processing of legumain by cystatin E/M', *Biochimie*, **94**, pp. 2590–2599. doi: 10.1016/j.biochi.2012.07.026.

Stéen, E. J. L., Nyberg, N., Lehel, S., Andersen, V. L., Di Pilato, P., Knudsen, G. M., Kristensen, J. L. and Herth, M. M. (2017) 'Development of a simple proton nuclear magnetic resonance-based procedure to estimate the approximate distribution coefficient at physiological pH (log D_{7.4}): Evaluation and comparison to existing practices', *Bioorganic and Medicinal Chemistry Letters*, **27**(2), pp. 319–322. doi: 10.1016/j.bmcl.2016.11.048.

Stern, L., Perry, R., Ofek, P., Many, A., Shabat, D. and Satchi-Fainaro, R. (2009a) 'A novel antitumor prodrug platform designed to be cleaved by the endoprotease legumain', *Bioconjugate Chemistry*, **20**(3), pp. 500–510. doi: 10.1021/bc800448u.

Stockholm, D., Bartoli, M., Sillon, G., Bourg, N., Davoust, J. and Richard, I. (2005) 'Imaging Calpain Protease Activity by Multiphoton FRET in Living Mice', *Journal of Molecular Biology*, **346**, pp. 215–222. doi: 10.1016/j.jmb.2004.11.039.

Sukhai, M. A., Prabha, S., Hurren, R., Rutledge, A. C., Lee, A. Y., Sriskanthadevan, S., Sun, H., Wang, X., Skrtic, M., Seneviratne, A., Cusimano, M., Jhas, B., Gronda, M.,

MacLean, N., Cho, E. E., Spagnuolo, P. A., Sharmeen, S., Gebbia, M., Urbanus, M., Eppert, K., Dissanayake, D., Jonet, A., Dassonville-Klimpt, A., Li, X., Datti, A., Ohashi, P. S., Wrana, J., Rogers, I., Sonnet, P., Ellis, W. Y., Corey, S. J., Eaves, C., Minden, M. D., Wang, J. C. Y., Dick, J. E., Nislow, C., Giaever, G. and Schimmer, A. D. (2013) 'Lysosomal disruption preferentially targets acute myeloid leukemia cells and progenitors', *The Journal of Clinical Investigation*, **123**(1), pp. 315–328. doi: 10.1172/JCI64180DS1.

Swift, L. P., Rephaeli, A., Nudelman, A., Phillips, D. R. and Cutts, S. M. (2006) 'Doxorubicin-DNA adducts induce a non-topoisomerase II-mediated form of cell death', *Cancer Research*, **66**(9), pp. 4863–4871. doi: 10.1158/0008-5472.CAN-05-3410.

Tanabe, M., Ieiri, I., Nagata, N., Inoue, K., Ito, S., Kanamori, Y., Takahashi, M., Kurata, Y., Kigawa, J., Higuchi, S., Terakawa, N. and Otsubo, K. (2001) 'Expression of P-glycoprotein in human placenta: relation to genetic polymorphism of the multidrug resistance (MDR)-1 gene.', *The Journal of pharmacology and experimental therapeutics*, **297**(3), pp. 1137–1143.

Taya, P., Maiti, B., Kumar, V., De, P. and Satapathi, S. (2018) 'Design of a novel FRET based fluorescent chemosensor and their application for highly sensitive detection of nitroaromatics', *Sensors and Actuators B: Chemical*, **255**, pp. 2628–2634. doi: 10.1016/j.snb.2017.09.073.

Teicher, B. A. (2008) 'Next generation topoisomerase I inhibitors: Rationale and biomarker strategies', *Biochemical Pharmacology*, **75**(6), pp. 1262–1271. doi: 10.1016/j.bcp.2007.10.016.

Teicher, B. A., Holden, S. A. and Cathcart, K. N. S. (1987) 'Efficacy of Pt(Rh-123)₂ as a radiosensitizer with fractionated x rays', *International Journal of Radiation Oncology*, **13**(8), pp. 1217–1224. doi: 10.1016/0360-3016(87)90197-0.

Theodossiou, T. A., Sideratou, Z., Katsarou, M. E. and Tsiourvas, D. (2013) 'Mitochondrial delivery of doxorubicin by triphenylphosphonium- functionalized hyperbranched nanocarriers results in rapid and severe cytotoxicity', *Pharmaceutical Research*, **30**(11), pp. 2832–2842. doi: 10.1007/s11095-013-1111-7.

Thomas, H. and M.Coley, H. (2003) 'Overcoming multidrug resistance in cancer: An update on the clinical strategy of inhibiting P-glycoprotein', *Cancer Control*, **10**(2), pp. 159–165. doi: 10.1177/107327480301000207.

Torchilin, V. (2009) 'Intracellular delivery of protein and peptide therapeutics', *Drug Discovery Today: Technologies*, **5**(2–3). doi: 10.1016/j.ddtec.2009.01.002.

Turnbull, A. (2003). 'Design and development of novel DNA topoisomerases inhibitors'. PhD, Edinburgh Napier University.

Varadwaj, P., Misra, K., Sharma, A. and Kumar, R. (2010) 'Mitoxantrone : an agent with promises for anticancer therapies', *Electronic Journal of Biology*, **6**(2), pp. 36–42.

Verschoor, M. L., Ungard, R., Harbottle, A., Jakupciak, J. P., Parr, R. L. and Singh, G. (2013) 'Mitochondria and cancer: Past, present, and future', *BioMed Research International*, **2013**. doi: 10.1155/2013/612369.

Via, L. D., Garcia-Argaez, A. N., Martinez-Vazquez, M., Grancara, S., Martinis, P. and Toninello, A. (2014) 'Mitochondrial permeability transition as target of anticancer drugs.', *Current pharmaceutical design*, **20**(2), pp. 223–44. doi: 10.2174/13816128113199990033.

Wang, J., Gao, R., Li, Q., Xie, S. and Zhao, J. (2012) 'Synthesis , Cytotoxicity , and Cell Death Profile of Polyaminoanthraquinones as Antitumor Agents', *Chemical Biology and Drug Discovery*, **80**, pp. 909–917. doi: 10.1111/cbdd.12038.

Wang, X.-H., Peng, H.-S., Yang, L., You, F.-T., Teng, F., Tang, A.-W., Zhang, F.-J. and Li, X.-H. (2013) 'Poly-l-lysine assisted synthesis of core-shell nanoparticles and conjugation with triphenylphosphonium to target mitochondria', *Journal of Materials Chemistry B*, **1**(38), p. 5143. doi: 10.1039/c3tb20884b.

Wang, Y., Lyu, Y. L. and Wang, J. C. (2002) 'Dual localization of human DNA topoisomerase IIIalpha to mitochondria and nucleus.', *Proceedings of the National Academy of Sciences of the United States of America*, **99**(19), pp. 12114–12119. doi: 10.1073/pnas.192449499.

Warburg, O. (1956) 'On the Origin of Cancer Cells On the Origin of Cance',

Science, **123**(123), pp. 309–314. doi: 10.1126/science.123.3191.309.

Weissig, V., Boddapati, S. V, Cheng, S.-M. and D'souza, G. G. M. (2006) 'Liposomes and Liposome-like Vesicles for Drug and DNA Delivery to Mitochondria', *Journal of Liposome Research*, **16**(3), pp. 249–264. doi: 10.1080/08982100600851169.

Wolf, K. and Friedl, P. (2005) 'Functional imaging of pericellular proteolysis in cancer cell invasion', *Biochimie*, **87**, pp. 315–320. doi: 10.1016/j.biochi.2004.10.016.

Wolfram, R. K., Heller, L. and Csuk, R. (2018) 'Targeting mitochondria: Esters of rhodamine B with triterpenoids are mitocanic triggers of apoptosis', *European Journal of Medicinal Chemistry*, **152**, pp. 21–30. doi: 10.1016/j.ejmech.2018.04.031.

Wu, W., Luo, Y., Sun, C., Liu, Y., Kuo, P., Varga, J., Xiang, R., Reisfeld, R., Janda, K. D., Edgington, T. S. and Liu, C. (2006) 'Targeting Cell-Impermeable Prodrug Activation to Tumor Microenvironment Eradicates Multiple Drug-Resistant Neoplasms', *Cancer Research*, **66**(2), pp. 970–980. doi: 10.1158/0008-5472.can-05-2591.

Xie, C., Chang, J., Hao, X. D., Yu, J. M., Liu, H. R. and Sun, X. (2013) 'Mitochondrial-targeted prodrug cancer therapy using a rhodamine B labeled fluorinated docetaxel', *European Journal of Pharmaceutics and Biopharmaceutics*, **85**, pp. 541–549. doi: 10.1016/j.ejpb.2013.06.008.

Yang, X., Guo, X. and Zhao, Y. (2002) 'Development of a novel rhodamine-type fluorescent probe to determine peroxynitrite', *Talanta*, **57**, pp. 883–890.

Yu, M., Zhou, Y., Shi, Y., Ning, L., Yang, Y., Wei, X., Zhang, N., Hao, X. and Niu, R. (2007) 'Reduced mitochondrial DNA copy number is correlated with tumor progression and prognosis in Chinese breast cancer patients', *International Union of Biochemistry and Molecular Biology*, **59**(7), pp. 450–457. doi: 10.1080/15216540701509955.

Zhang, H., Barcelo, J. M., Lee, B., Kohlhagen, G., Zimonjic, D. B., Popescu, N. C. and Pommier, Y. (2001) 'Human mitochondrial topoisomerase I', *Proceedings of the National Academy of Sciences*, **98**(19), pp. 10608–10613. doi: 10.1073/pnas.191321998.

Zhang, H., Meng, L. H. and Pommier, Y. (2007) 'Mitochondrial topoisomerases and alternative splicing of the human TOP1mt gene', *Biochimie*, **89**(4), pp. 474–481. doi:

10.1016/j.biochi.2006.11.002.

Zhitomirsky, B. and Assaraf, Y. G. (2015) 'Lysosomal sequestration of hydrophobic weak base chemotherapeutics triggers lysosomal biogenesis and lysosome-dependent cancer multidrug resistance.', *Oncotarget*, **6**(2), pp. 1143–56. doi: 10.18632/oncotarget.2732.

Zhou, H., Sun, H., Lv, S., Zhang, D., Zhang, X., Tang, Z. and Chen, X. (2017) 'Legumain-cleavable 4-arm poly(ethylene glycol)-doxorubicin conjugate for tumor specific delivery and release', *Acta Biomaterialia*, **54**, pp. 227–238. doi: 10.1016/j.actbio.2017.03.019.

Zhu, L., Zhu, Y., Meng, X., Hao, J., Li, Q., Wei, Y. and Lin, Y. (2008) 'DCC-Assisted Esterification of a Polyoxometalate-Functionalized Phenol with Carboxylic Acids (DCC: Dicyclohexylcarbodiimide)', *Chemistry A European Journal*, **14**(35), pp. 10923–10927. doi: 10.1002/chem.200801836.

Ziegler, U. and Groscurth, P. (2004) 'Morphological Features of Cell Death', *Physiology*, **19**(3), pp. 124–128. doi: 10.1152/nips.01519.2004.

Chapter 2

2 Chapter 2

2.1 Aim

The main aim of this aspect of the research programme was to synthesise a novel prodrug designed to exploit the proteolytic activity of legumain, which is an asparaginyl endopeptidase (AEP) that is overexpressed in the tumour microenvironment in order to simultaneously deliver a therapeutic agent and to detect the activity of this protease (therefore to act as a theranostic). The specificity of legumain for asparagine residues at the C-terminus in the P1 position of substrates was taken advantage of in the design of the prodrug. The main goal of this prodrug is to improve the therapeutic index by reducing toxicity on healthy cells, eventually enhancing the therapy for cancer patients. The activation of the prodrug was to be determined by fluorescence spectroscopy. Additionally, this theranostic prodrug may offer a smart tool in early detection of tumours and ultimately enhance patient survival, with clear real time imaging.

2.2 Introduction

2.2.1 Tumour Microenvironment

The tumour microenvironment is rich in proteolytic activity and it is acidic and hypoxic and there is wide spectrum of proteases that include the cysteine endopeptidase legumain. The acidic character of the tumour microenvironment is due to the higher glycolytic rate of tumor cells. Also, the tumour microenvironment is a favorable environment for protease targeted alteration of prodrugs, which is from inactive compounds to potent cytotoxic agents. Additionally, the cellular microenvironment has a role in tumourigenesis which has become a major area of research (Arroyo-crespo *et al.*, 2018). It is also possible to design a drug delivery system that has the ability to accumulate within the tumour microenvironment by exploiting the acidic pH and the presence of proteases such as legumain. The tumour microenvironment plays an interesting role in the activation of targeted prodrug due to the overexpression of key proteases and then reduce the toxicity on the cells lacking expression of the target enzyme, therefore, encouraging safety on healthy cells and efficiency of tumour destruction. In summary, the activation of a prodrug in the tumour microenvironment, promises to reduce active drug access to normal tissues, improve availability to tumour cells, and consequently, significantly reduce toxicity to normal tissues (Wu *et al.*, 2006).

2.2.2 Proteases

Proteases are hydrolase enzymes that are expressed intracellularly and extracellularly. These enzymes play an important and essential role in many biological and pathological processes by proteolysis, which is an irreversible regulatory mechanism and can selectively cleave specific substrates (López-Otín and Hunter, 2010). Furthermore, proteases play effective roles in DNA replication, cell proliferation, angiogenesis, blood coagulation, immunity, and necrosis. Therefore, decontrolled alterations in proteolytic activity promote many diseases like cancer and cardiovascular disorders. Proteases are

associated with cancer development, especially invasion and metastasis because of the ability of proteases to degrade extracellular matrices and proteins. As a result, proteases play a significant role in drug development because many therapies have been designed to target and inhibit proteases that are deregulated, particularly for tumour suppression (Choi *et al.*, 2012). One of the most important peptidases is legumain, belonging to the C13 family of cysteine proteases (Løvsletten *et al.*, 2014).

2.2.3 Legumain

Legumain or asparaginyl endopeptidase (AEP) was initially recognized in leguminous seeds as a cysteine protease with specific activity for asparagine residues in the P1 position of peptide substrates. Also, legumain plays a significant role in endosomal/lysosomal degradation system (Zhou *et al.*, 2017). Chen and his colleagues first described legumain in human and other mammals in 1997 (Chen *et al.*, 1997). Mammalian legumain is clearly homologous with non-mammalian legumain. The human legumain gene encodes a preproprotein of 433 amino acids (Haugen *et al.*, 2013). Human legumain is a lysosomal cysteine protease which is a member of the clan CD protease family and it is over expressed in kidney, placenta, liver, spleen, and testis (Smith *et al.*, 2012). Legumain is synthesized as an inactive pro-enzyme which reaches full proteolytic activity after a complex series of maturation steps (Haugen *et al.*, 2013). In order to deliver the inactive AEP to the acidic compartment, the C-terminal and N-terminal of the AEP must be removed. AEP can be activated through the removal of C-terminal propeptides because the C-terminal acts as an auto-inhibitory area that covers the catalytic site, therefore, the removal of the C-terminal propeptide is crucial for the activation of AEP (Shirahama-Noda *et al.*, 2003).

Legumain is normally present intracellularly in endosome/lysosome systems and is related with intracellular protein degradation. Moreover, legumain is present extracellularly in the tumour microenvironment, related with matrix and cell surfaces and it plays an important role in the degradation of the extracellular matrix (ECM) and thus, reduces the pH of the tumour microenvironment (Wu *et al.*, 2006).

The overexpressed and up-regulation of legumain in tumour cells combined with recognition of unique substrate, makes legumain a potential candidate enzymatic target for prodrug activation and tumour destructive therapy (Haugen *et al.*, 2015). The invasive and metastatic properties of tumour cells are often associated with the cell surface proteases and overexpression of legumain. Legumain activates also the gelatinase A zymogen (pro-MMP 2), which is an important mediator of ECM degradation (Guo *et al.*, 2013), therefore, the overexpression of legumain is considerable with high invasion and metastasis and directly correlated with the degree of malignancy (Zhou *et al.*, 2017). The overexpression in colon cancer may play a role in encouraging tumour progression and may display more aggressive characteristics (Ohno *et al.*, 2013). However, in normal tissues, legumain is mainly localized in the endo-lysosomal system where its protease domain is activated due to acidic environment. Additionally, legumain translocates to the nucleus and cytosol and it is related to pathological conditions including cancer (Ammirati and Fogacci, 2017).

Therefore, legumain may exemplify a target for inhibition of progression and metastasis because of its regulation related with tumour growth.

2.2.4 **Protease activated probes**

One of the numerous aims for the design of protease-activated probes is *in vivo* molecular imaging. The probe is usually optically inhibited in its quenched state and fluorescence is released upon cleavage of the fluorophore (donor) from its acceptor (quencher) by the specific action of the targeted protease on a peptide linker, which acts as a substrate of the protease (Chang *et al.*, 2005). This method is used to detect the expression and activity of proteases for imaging purposes (Edgington *et al.*, 2011)

Some fluorescent substrate probes can be designed with specific peptide sequences with fluorophores whose spectral properties change when cleaved by an active protease. An example of a fluorogenic substrate consisting of a peptide sequence sensitive to legumain, attached at the C terminus, is the fluorophore aminomethylcoumarin (AMC) (Edgington *et al.*, 2011). The activity of proteases has been monitored by the use of

organic fluorophores in a variety of different studies. Kircher *et al.*, (2004) and Wolf and Friedl (2005) used fluorophores narrowly to auto-quench fluorescence and upon cleavage of the fluorophores by enzymatic action of the labeled substrate, fluorescence occurred (Kircher *et al.*, 2004; Wolf and Friedl, 2005). Others have employed FRET (fluorescence resonance energy transfer) where, the donor and acceptor (paired fluorophores) are linked together by a substrate targeted to a specific protease to monitor protease activity (Stockholm *et al.*, 2005). Other methodologies involving the use of fluorescent emitters linked to a non-fluorescent absorber have been established and used in imaging (Pham *et al.*, 2004). Despite advantages and promising results of these methods, there are disadvantages, including the demand for specific pairing between donor and acceptor molecules with respect to wavelength, rapid photobleaching under regular imaging circumstances and use of organic fluorophores which are sensitive to the physical environment (Chang *et al.*, 2005).

2.2.5 **Fluorescence resonance energy transfer (FRET)**

Fluorescence is a process by which the molecule in the singlet electronic ground state (S_0) absorbs a photon of appropriate energy. This makes the electrons travel to the higher energy orbitals and then quickly back to the first singlet excited state (S_1). The decay of the excitation state can go via different pathways such as: photon emission (fluorescence), in a nonradiative (NR) fashion (quenching of the fluorophore excited state by bond rotation, vibration, molecular collision and photoinduced electron transfer [PET]), forbidden intersystem crossing to the triplet excited state and relaxation by photon emission (phosphorescence) or NR (Lavis and Raines, 2008b).

In addition, there is another interesting pathway for decay of the excited state which is FRET (fluorescence resonance energy transfer), which takes its name from the scientist Forster, who first described the mechanism of this process (Forster, 1948). FRET is the energy transferred nonradiatively from an excited state donor, which is usually a fluorophore, to a proximal ground state acceptor by long-range dipole-dipole interaction

Figure 2.1. The rate of energy transfer depends on three parameters: (1) the

superposition of donor emission and acceptor absorption spectra, (2) the relative-direction of the donor absorption and acceptor transitions moments (3) the reflective index (Jares-Erijman and Jovin, 2003). Additionally, FRET is distance-dependent less than 10 nm between the acceptor and donor that are bound to the ends of the substrates (Kim and Kim, 2012).

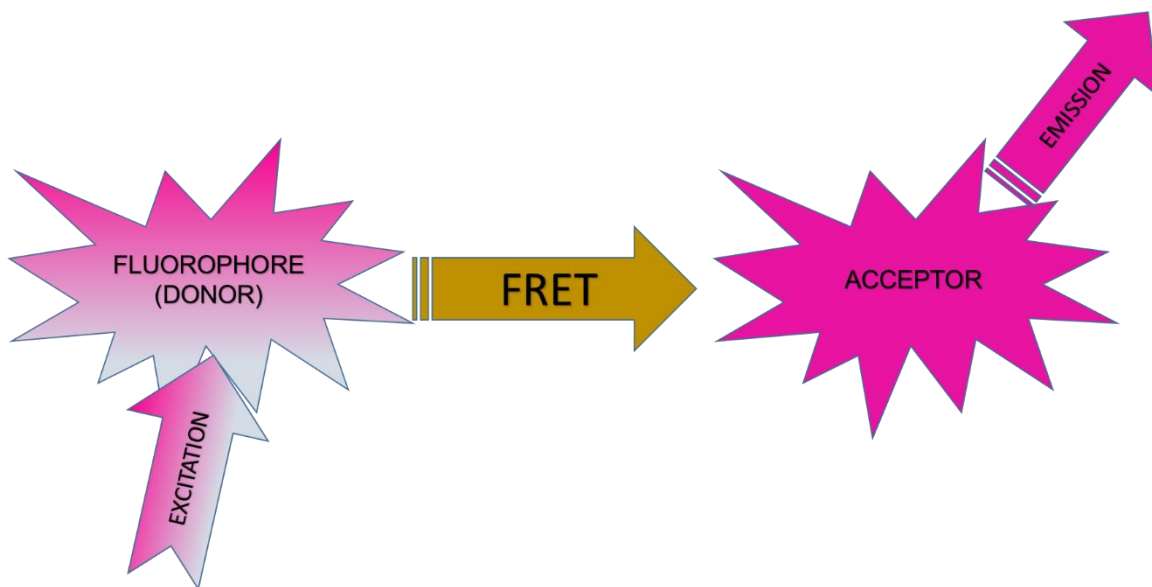


Figure 2.1: Representation of the FRET concept.

2.2.6 Rhodamine B

Rhodamine is the analogue of fluorescein and eosin dyes, which are members of the xanthene family (Beija *et al.*, 2009). This fluorophore is widely used as a dye in microscopy and in modern research such as in biological, biochemical and medicinal research due to its unique photophysical properties and structural change response to pH between opened ring (fluorescent) and closed ring (non-fluorescent). In addition, rhodamine is often utilized in biological functions because it is an inexpensive, robust molecule, with a high extinction coefficient and it is valuable for protein and peptide labelling to visualize inside cells (Birtalan *et al.*, 2011). Another important property of rhodamine is that there are different forms of rhodamine B depending on the pH and solvent polarity these forms are: cationic, zwitterionic and lactone. Additionally, in acidic solutions the rhodamine B is present as a cationic form, while in basic conditions, the

rhodamine B will be dissociated to give two forms, zwitterion and lactone forms, which are the main forms in non-polar organic solvents. However, both the cationic and zwitterionic forms are fluorescent, but there is a minor reduction in the extinction coefficient for the zwitterion compared to the cationic form, with identical change in both absorbance and fluorescence emission (Beija *et al.*, 2009). Furthermore, the lactone form is colourless and non-fluorescent (absorbs in the UV region) when compared with the cationic and zwitterion form (Karpiuk *et al.*, 1994) **Figure 2.2**.

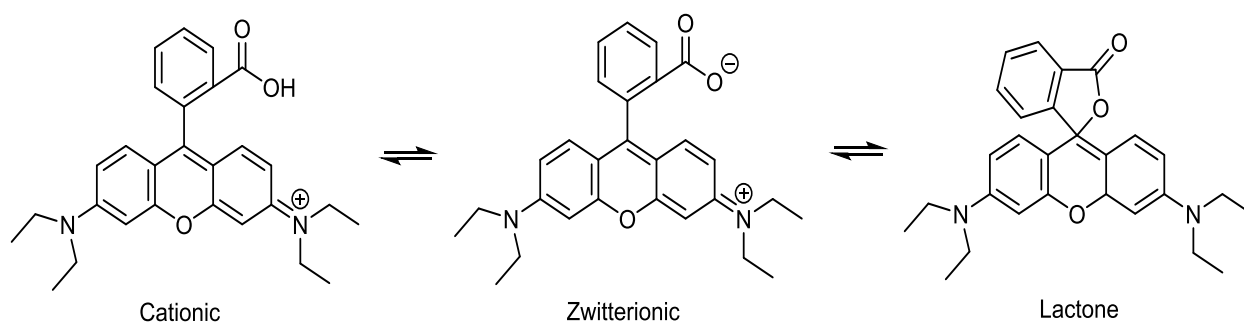


Figure 2.2: Chemical structures of three forms of rhodamine B. cationic and zwitterionic forms are fluorescent whereas the lactone form is nonfluorescent.

Rhodamine derivatives that have two nitrogen atoms substituted with two alkyl groups, can have variation (dependent) in both quantum yield and fluorescence lifetime with temperature, while rhodamine derivatives that are either have no substituent or have only one alkyl substituent at each nitrogen atom are not subject to activation and quantum yield is independent of temperature (Ferreira and Costa, 2006).

Moreover, for rhodamine to be used as a fluorescent probe, it requires some modifications such as, the modification of the 2' carboxylic acid group of rhodamines, modification of 3 and 6 positions of the amino group of xanthene and modification on positions 4' and 5' of the carboxyphenyl ring. This modification occurs by the reaction of the 2' carboxylic acid group of rhodamine with primary amines to give secondary amides. Notably, that secondary amides are normally found in their non-fluorescent, ring-closed, spirolactam form, excepting under acidic conditions or in the presence of metal cations. However, the

sensitivity of rhodamine B to pH can be altered and become low when linked to a tertiary amide and locked in the ring-open form as in Rho-Pro-OH **Figure 2.3**. The fluorescence emission for Rho-Pro-OH remains constant over the measured pH range, whereas fluorescence emission increases with increasing pH for FAM-Pro-OH. These results indicate the stability of rhodamine under different pH conditions.

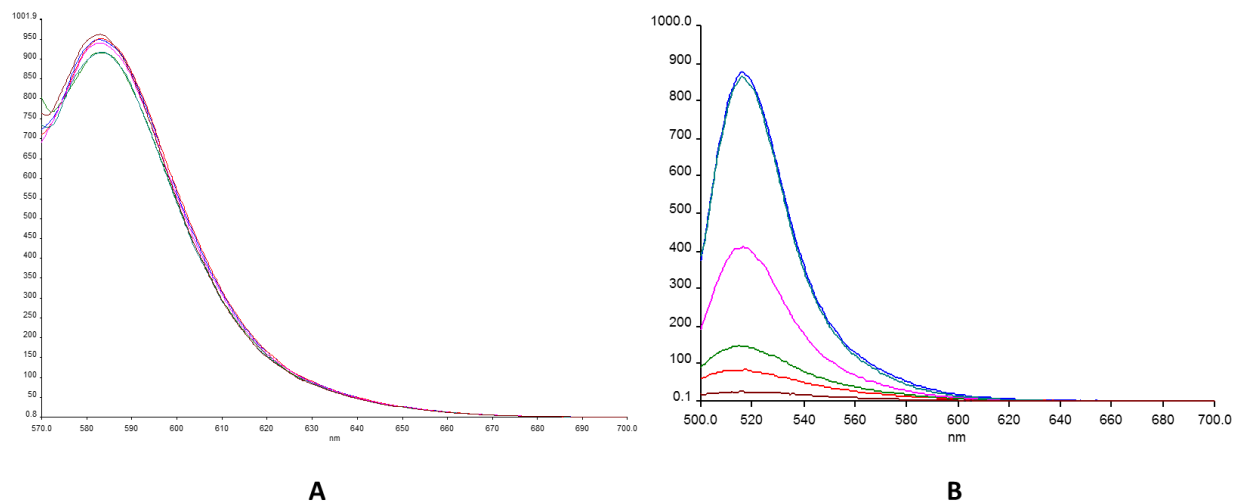


Figure 2.3: Fluorescence emission of (a) Rho-Pro-OH (10μM) and (b) FAM-Pro-OH in phosphate-citrate buffer, pH 3-8.

The modification on the amino group usually occurs using an acyl chloride or with a carboxylic acid using a carbodiimide as a coupling agent. It was noticed that the modification of the amino groups increases the nucleophilicity of the phenolic oxygen and leads to lactone formation (these rhodamine derivatives are non-fluorescent).

A study by Reungpatthanaphong *et al.*, (2003) showed that rhodamine B was well targeted specifically to the mitochondria. Reungpatthanaphong *et al.*, 2003 studied the advantage of using rhodamine B as a probe to assist the mitochondria membrane potential ($\Delta\Psi_m$) in drug-resistant and drug-sensitive cells. They used this study to determine the spontaneous changes in mitochondria function. They found that the accumulation of rhodamine B inside the cell depended on the $\Delta\Psi_m$ as a rhodamine is a lipophilic cation therefore, they suggest that rhodamine B is an appropriate probe for monitoring the mitochondrial function (Reungpatthanaphong *et al.*, 2003). Another study

by Xie *et al.*, (2013) used rhodamine B as a carrier group for the prodrug paclitaxel. As a result, the conjugation of rhodamine B with paclitaxel provided the chance to control the intracellular delivery of the prodrug and the possibility of realizing higher therapeutic efficacy by activating mitochondria related apoptosis. Xie *et al.*, (2013) showed that the conjugation of rhodamine B with another prodrug 4FDT by a biodegradable linker, would decrease the cytotoxicity of the active drug and increase intracellular delivery to mitochondria and improve the conversion of the prodrug inside the mitochondria by specific proteases (Xie *et al.*, 2013).

Additionally, Longmire *et al.*, 2008 studied the fluorescence of 4 rhodamine core based fluorescent dyes *in vivo* and *in vitro* in a mouse model of metastatic ovarian cancer **Figure 2.4**. They conjugated the 4 rhodamine core with galactosamine serum albumin (GmSA) (clinically D-galactose receptor targeting reagent). They found that carboxyrhodamine 6G (CaRG) and carboxytetramethylrhodamine (TAMRA) are superior probes for *in vivo* optical imaging due to that at low pH, CaRG produce a high fluorescence intensity and increased in fluorescence intensity of fluorophore-targeting protein. However, at low pH, TAMRA produce a high fluorescence intensity and continuous fluorescence after internalization and the most notable advantage of using TAMRA is the maximum *in vivo* signal-to-background ratios compared with other rhodamine cores (Longmire *et al.*, 2008).

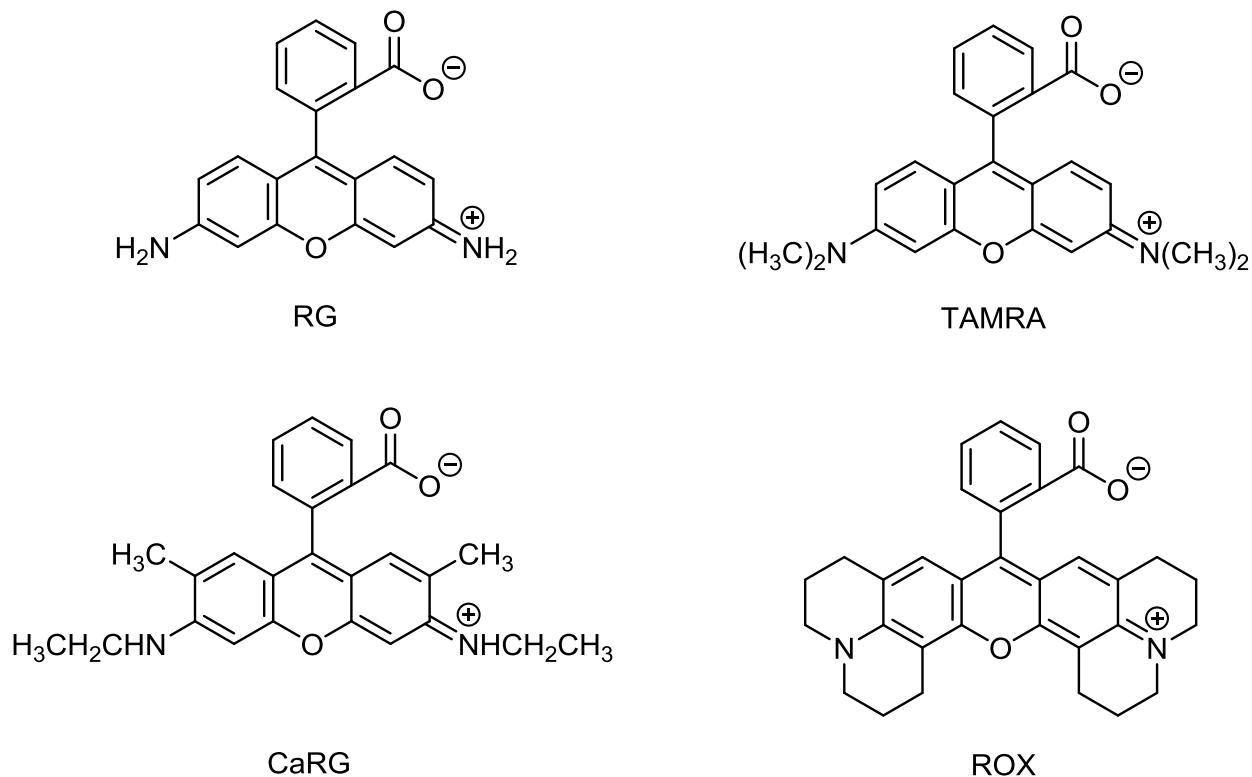


Figure 2.4: The structures of the four rhodamine core fluorophores

2.2.7 Protease activated prodrugs

A prodrug is a chemically modified form of the pharmacologically active agent, rendering it inactive, that requires one or more enzymatic and chemical transformation *in vivo* to release the active drug. The aims of a prodrug are to improve water solubility, bioavailability, chemical stability and improve drug targeting and avoid unwanted and unspecific effects. Sometimes, a prodrug may contain two pharmacologically active agents that are coupled together and each drug acts as a promoiety for the other (Rautio *et al.*, 2008). Once a prodrug has been activated by its specific target it will recover its activity.

The overexpression of specific proteases such as legumain can be utilized for prodrug-targeting resulting in the release of the active drug (Stern *et al.*, 2009). The active form of drug is usually bonded to a biodegradable linker (peptide sequence, which is a substrate for the targeting protease) to control the translation of the prodrug into the active drug. It is therefore important that the peptide sequence is stable until it reaches its target, which

increases the availability of active drug at the site of action and decreases the cytotoxicity of the active drug (Xie *et al.*, 2013).

Legumain is active only at low pH (4-6) and it is inactive at physiological neutral pH, therefore, it can specifically catalyze prodrug activation in acidic tumour cells and in the acidic tumour microenvironment. Liu *et al.*, (2011) and Wu *et al.*, (2006) designed legumain-activated prodrugs by covalently linking a cell-impermeable succinyl blocked substrate peptide to the aminoglycoside of doxorubicin. This prodrug is inactive and nontoxic until activated by legumain in the acidic tumour microenvironment. The result *in vivo* showed markedly reduced toxicity and enhanced efficacy in compared with doxorubicin alone. Additionally, the pharmacokinetic indication supports the tumour microenvironment-activated prodrug approach (Wu *et al.*, 2006; Liu *et al.*, 2012).

Following the discovery of overexpression of legumain in the tumour microenvironment and in tumour tissues when compared with normal tissue (Liu *et al.*, 2003) and the discovery of its high cleavage specificity (Haugen *et al.*, 2015), it was important to focus on the design of legumain substrates. Løvsletten and colleagues (2014), synthesized a legumain-cleavable prodrug by conjugating N-Boc-Ala-Ala-Asn-Val-OH with deacetyl colchicine to produce Suc-Ala-Ala-Asn-Val-colchicine **Figure 2.5**. They used different cell lines with different expressions and activities of legumain to study the specificity, efficacy and toxicity of the microtubule inhibitor colchicine and the legumain-cleavable colchicine prodrug. They found that the prodrug was more toxic to the colorectal cancer HCT116 cells (expressing both the active legumain and prolegumain) than SW620 cells (only expressing the prolegumain). Also, the toxicity of the prodrug was higher in monoclonal legumain over-expressing HEK293 cells when compare with native HEK293 cells. This indicated the specificity of legumain to cleave the C-terminal of asparagine and the relationship between the activity of legumain in the cells and the toxicity of the prodrug (Løvsletten *et al.*, 2014).

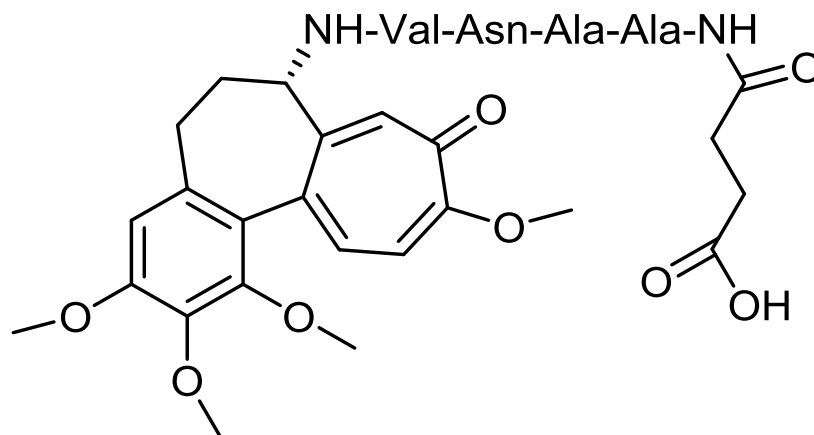


Figure 2.5: Structure of Suc-Ala-Ala-Asn-Val-colchicine

Chen and colleagues (2015), designed and synthesized a novel doxorubicin (Dox) prodrug, N-benzyloxycarbonyl-Ala-Ala-Asn-Doxorubicin (CBZ-AAN-Dox) by linking the tripeptide Ala-Ala-Asn with amino acylation of doxorubicin **Figure 2.6**. They reported that CBZ-AAN-Dox was specific for targeting tumor cells with reduced toxicity to normal cells and induced apoptosis on tumor cells upon the cleavage by legumain and released doxorubicin under hypoxic conditions. In addition, the IC_{50} of the prodrug in human cervical carcinoma cell line (SiHa) was much higher compared with doxorubicin alone (Chen *et al.*, 2015).

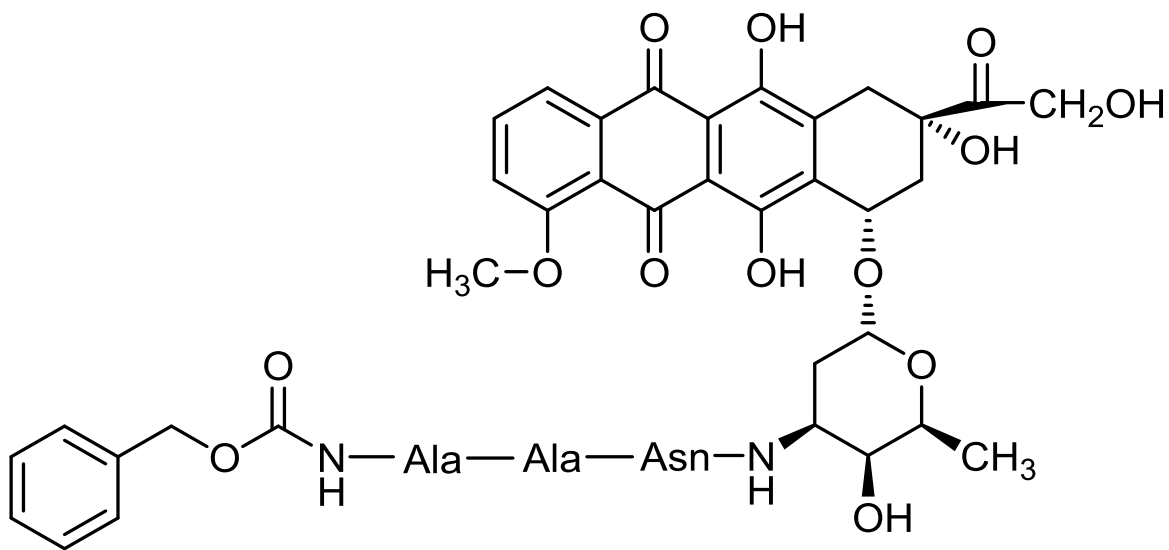


Figure 2.6: Structure of CBZ-AAN-Dox

Furthermore, Mathur (2017) designed and synthesized the first legumain-based theranostic prodrug (diagnostic and therapeutic) ALS5 targeted to the overexpression of legumain in cancer cells. In ALS5, a Rho-Pro-Ala-Asn tripeptide was conjugated with a cytotoxic agent Propyl-Pip-Propyl-AQ(4-OH) (ALS1) via an amide bond **Figure 2.7**. The release of cytotoxic agent and rhodamine-based fluorophore tripeptide was studied *in vitro* upon the addition of recombinant human legumain, which showed an increase in relative fluorescence intensity with the time, which demonstrates that the prodrug ALS5 was cleaved by legumain resulting in the release of fluorescent rhodamine B-tripeptide. Mathur *et al.*, (2017) studied the cytotoxicity of prodrug AL5 and its legumain cleaved fragment ALS1 using MTT assay in PC-3 cell line. The IC₅₀ value for prodrug ALS5 was 41.15 ± 0.09 μM, and it is less potent than ALS1 which was 1.21 ± 0.12 μM (Mathur *et al.*, 2017).

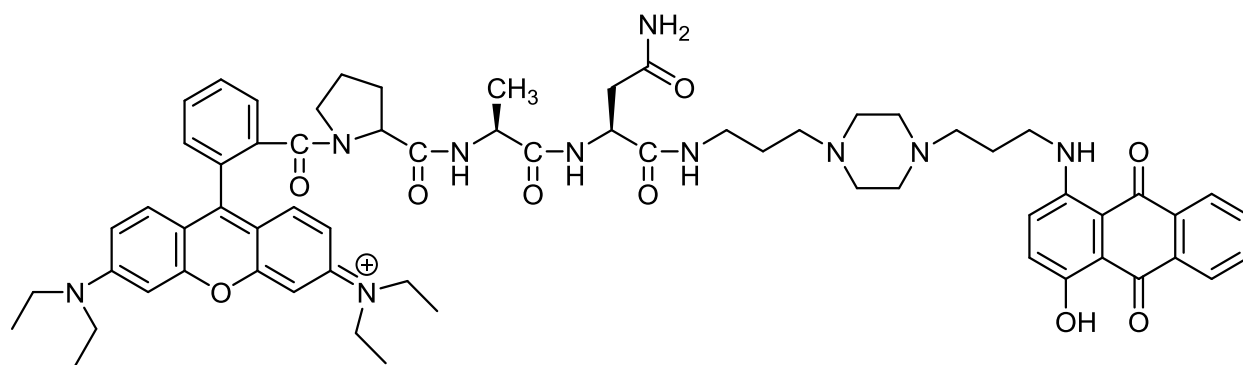


Figure 2.7: Structure of ALS5

Therefore, in this research programme, the dual properties of a diagnostic and therapeutic (theranostic) were designed to improve this concept of legumain-activated prodrug. The theranostic system was designed through the use of NU:UB 51 (an available experimental toxic drug with *in vivo* activity; a therapeutic), which also acts as a quencher (FRET-based pair) and by synthesis of tripeptide (Pro-Ala-Asn), which acts as a legumain substrate together with labelling with rhodamine B (fluorophore) which acts as a donor and plays a role in the activation process as a reporter molecule (with future potential in the diagnosis process).

2.2.8 NU:UB 51 (Gly-APA-AQ)

NU:UB 51 is a bis-hydroxylated propyl-spaced glycine conjugate **Figure 2.8**. NU:UB 51 belonging to the wide range of NU:UB compounds of spacer-linked anthraquinone-amino acid conjugates. These compounds were developed and synthesized within the Anticancer Drug Design and Delivery Research Group at Napier Edinburgh University as rationally designed topoisomerase inhibitors (Mincher, 1999). The majority of NU:UB compounds are amino substituted at the 1-position of the anthraquinone. The leader of these compounds showed a broad-spectrum activity *in vitro* at low micromolar concentrations and have also been shown to inhibit DNA topoisomerases I and II (Mincher *et al.*, 1999; Pettersson, 2004).

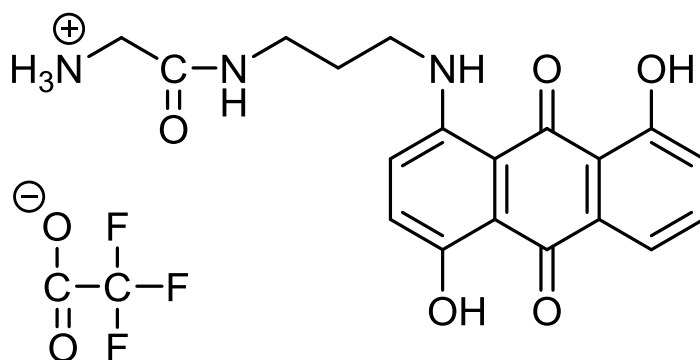


Figure 2.8: Chemical structure of NU:UB 51

NU:UB 51 can act as an acceptor in the FRET process and as an active agent after the asparagine cleavage of the prodrug by legumain to give both rhodamine B and NU:UB 51. After cleavage, the active agent NU:UB 51 (Mincher, 1999; Turnbull, 2003) will be released and it has the ability to inhibit both topoisomerase I and topoisomerase II. Topoisomerase I cut a single strand of double-stranded DNA to allow relaxation of the DNA for replication of the DNA and the single strand break is then religated, therefore restoring the DNA double strands (Teicher, 2008). While topoisomerase II cuts both strands of DNA (Zhang *et al.*, 2001). Once NU:UB 51 is released, it inhibits topoisomerase II α and II β mediated decatenation and relaxation of DNA and it inhibits topoisomerase I mediated DNA-relaxation (Mincher, 1999; Turnbull, 2003).

However, tumour cells have developed resistance to classical inhibitors of topoisomerase, therefore, the need to develop new inhibitors, such as NU:UB 51, which shows reduced resistance of tumour cells to this drug (Mincher, 1999; Turnbull, 2003). This novel anthraquinone shows notably different behaviour to other anthraquinones such as, mitoxantrone and doxorubicin. NU:UB 51 produces a tumour volume reduction and significant growth delay in a colon tumour model, whereas mitoxantrone and doxorubicin produce a simple growth delay with no reduction in tumour volume as shown in **Figure 2.9** (Mincher, 1999).

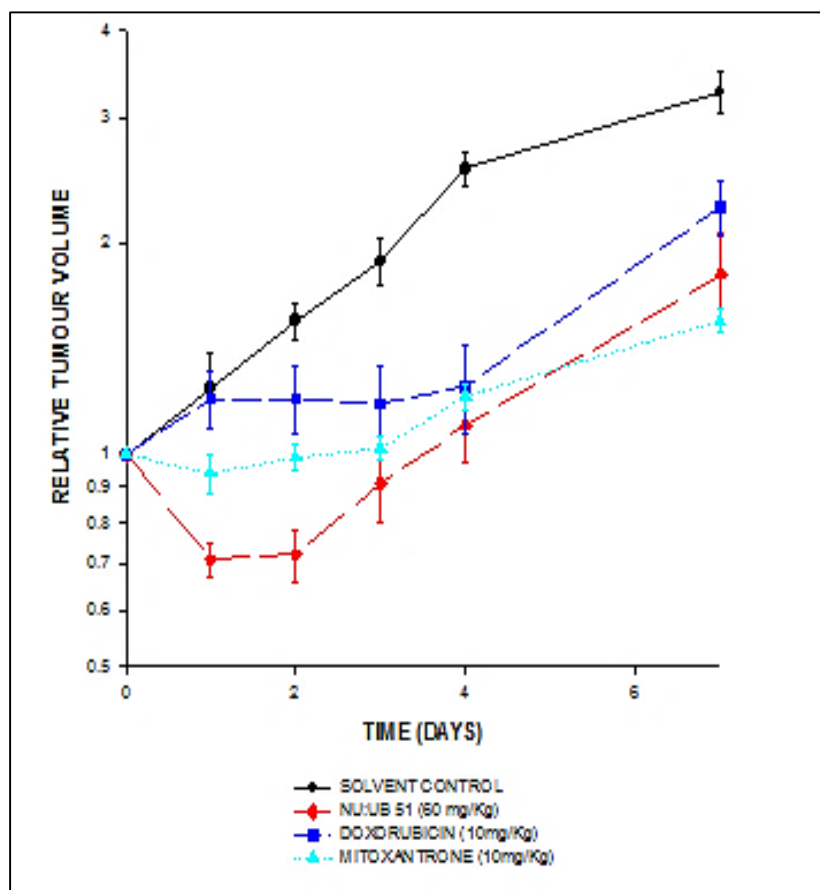


Figure 2.9: Comparison of NU:UB 51, doxorubicin and mitoxantrone *in vivo* chemosensitivity against MAC15A adenocarcinoma of the colon.

Chapter 2

Results and discussion

2.3 Results and discussion

This chapter describes the design and synthesis of a novel theranostic prodrug Rho-Pro-Ala-Asn-Gly-APA-AQ(4,8-di-OH) (OM50) **Figure 2.10** by solution phase peptide synthesis and solid phase peptide synthesis. The following sections in this chapter describes the rational design, synthetic strategy, synthesis, purification and characterization of OM50 and its legumain-mediated cleavage products: Rho-Pro-Ala-Asn-OH and Gly-APA-AQ(4,8-di-OH) (NU:UB 51). *In vitro* evaluation of the prodrug is then presented together with studies of incubation of OM50 with recombinant human legumain (rh-legumain), a fluorescence study and demonstration of the sub-cellular localization of the intact prodrug and NU:UB 51 using confocal microscopy.

2.3.1 Rational design

The prodrug Rho-Pro-Ala-Asn-Gly-APA-AQ(4,8-di-OH) (OM50) (proposed theranostic) was designed and synthesized to exploit the proteolytic activity of legumain. The legumain-targeted prodrug OM50 employs a three component design which are a cytotoxic topoisomerase inhibitor (NU:UB 51) as the active agent and quencher, a tripeptide Pro-Ala-Asn (substrate sequence) and rhodamine B (fluorophore) **Figure 2.10**. Theranostics is a technology that combines therapeutic modalities with diagnostic imaging which in turn can increase drug delivery kinetics, drug efficacy and local response (Bhuniya *et al.*, 2014). Therefore, this technology allow to monitor the release of drug at the targeted site to study drug release kinetics, drug delivery and response location (Kim *et al.*, 2014). Therefore, this technique was employed in the design of OM50 in which rhodamine B was used to label the N-terminus of Pro-Ala-Asn (legumain substrate) and cytotoxic topoisomerase inhibitor NU:UB 51 was linked with C-terminus of Asparagine.

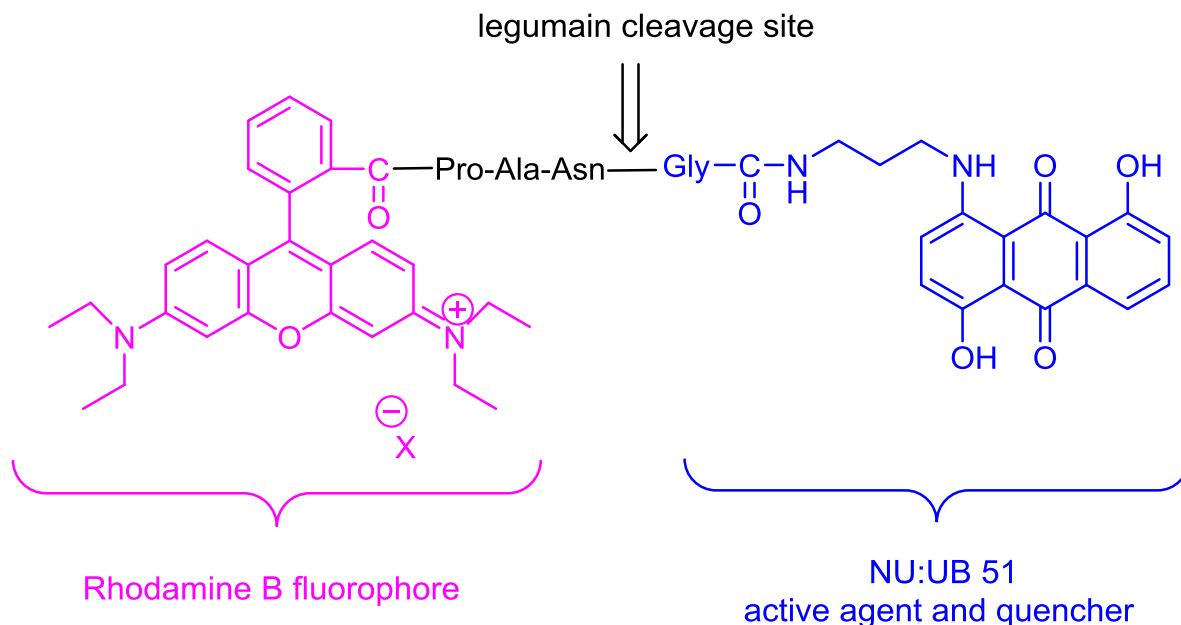


Figure 2.10: General structure of Rhodamine labeled prodrug OM50 (a theranostic)

In the design of theranostic prodrug Rho-Pro-Ala-Asn-Gly-APA-AQ(4,8-di-OH) (OM50), the quencher aminoanthraquinone NU:UB 51 [Gly-APA-AQ(4,8-di-OH)] was selected as it is non-fluorescent and used as a quencher, thus remove any fluorescence that may appear from the fluorophore rhodamine B. Also, it has the ability to quench a wide range of fluorophores due to the fact that aminoanthraquinone has a wide absorption region (λ_{\max} 550-700nm) (May *et al.*, 2005). Kodama and colleagues (2006), designed a fluorescent probe consisting of a fluorophore (fluorescein; donor) and anthraquinone as a quencher. They found that the oligoDNA probes quenched the excitation of the fluorophore efficiently and the emission of the fluorophore (λ_{\max} 520nm) interfered with the absorption spectrum of anthraquinone (λ_{\max} 520nm) (Kodama *et al.*, 2006). Therefore, NU:UB 51 should quench the fluorescence generated by rhodamine B and can work as an energy acceptor.

In addition, the selection of the amino acid residues at the *N*- and *C*- terminal is a key step toward the synthesis of OM50. Therefore, Asparagine (Asn) was used at position P1, due to the fact that asparagine is important for recognition and cleavage by legumain at the C-terminus (Chen *et al.*, 1997; Stern *et al.*, 2009). Proline was chosen for position

P3 to maintain constant fluorescence once cleaved by legumain because proline has a secondary amine, therefore the conjugation of proline with rhodamine B should lock the rhodamine B in a ring open form by linking it through a tertiary amide bond (Beija *et al.*, 2009; Choe *et al.*, 2006). Therefore, to make the prodrug OM50 recognized and cleaved by legumain, it was critical to introduce asparagine (Asn) at position P1 to be recognized by legumain. Alanine (Ala) and Proline (Pro) were decided to be in positions P2 and P3 respectively for the maximum fluorescence.

Furthermore, Wu *et al.*, (2006), used the amino acids Ala-Asn at positions P2 and P1 respectively in their prodrug LEG-3 (N-succinyl-h-alanyl- L-alanyl-L-asparaginyll-L-leucyl-doxorubicin), same as the positions of the amino acids P2 and P1 in the prodrug OM50. They revealed that the prodrug LEG-3 was cleaved by overexpressed legumain at the tumour site resulting in the release of Leu-doxorubicin (Wu *et al.*, 2006). Stern *et al.*, (2009) synthesized another prodrug targeted to the overexpression of legumain by linking the chemotherapeutic agent etoposide to legumain substrate CBZ-Ala-Ala-Asn-ethylenediamine-etoposide. In their prodrug, the amino acids at positions P2 and P1 was Asn and Ala, which they also found that this prodrug was recognized and cleaved by legumain (Stern *et al.*, 2009). These results from the literature encouraged us to e synthesized our prodrug Rho-Pro-Ala-Asn-Gly-APA-AQ(4,8-di-OH) (OM50) with the same amino acids sequences. Therefore, we hypothesized that the prodrug OM50 will be a substrate for legumain and has the prospect to exploit the proteolytic activity of overexpression of legumain at the tumour site.

2.3.2 **Synthetic strategy**

2.3.2.1 **NU:UB 51 quencher**

The first step is the synthesis of the anthraquinone spacer compound is the synthesis of APA-AQ (4,8-di-OH) NU:UB 59, which is an aminoanthraquinone derivative and prepared to use as rhodamine B fluorescence quencher. This compound will be prepared via reaction of leuco-5-hydroxyquinizarin with diaminopropane in dichloromethane. Oxidation

and purification by column chromatography should afford the free base of NU:UB 59 **Figure 2.11**. The next step was the synthesis of NU:UB 51, which acts as a cytotoxic agent and a quencher for rhodamine B fluorescence. The reaction of NU:UB 59 with Boc-Gly-OH followed by removal of Boc₂O group and purification, to afford the spacer-linked anthraquinone NU:UB 51.

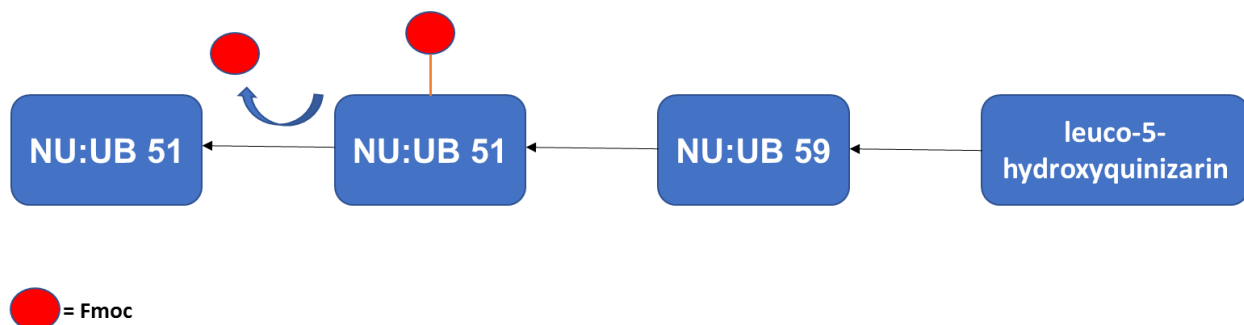


Figure 2.11: Schematic presentation of NU:UB 51 synthesis.

2.3.3 Peptide coupling

The next step was the peptide sequence synthesis by both solution and solid phase peptide synthesis. Using commercially available, suitably protected amino acid derivatives and established peptide coupling and deprotection methods (Montalbetti and Falque, 2005). The legumain peptide substrate was built onto the free amino group of NU:UB 59 to give NH-Pro-Ala-Asn~Gly-SP-AQ. In the solution phase peptide method, the amino acids were completely protected except the reacting end of the amino acids. In order to react multiple amino acids to get the desired length of the peptide, the α -amino protecting group should be removed and then reacted with the next C-activated, N-protected amino terminus. This process was continued until the desired length of the peptide is achieved. Finally, to afford the final peptide sequence, all protecting groups were removed (Kent, 2008) **Figure 2.12**.

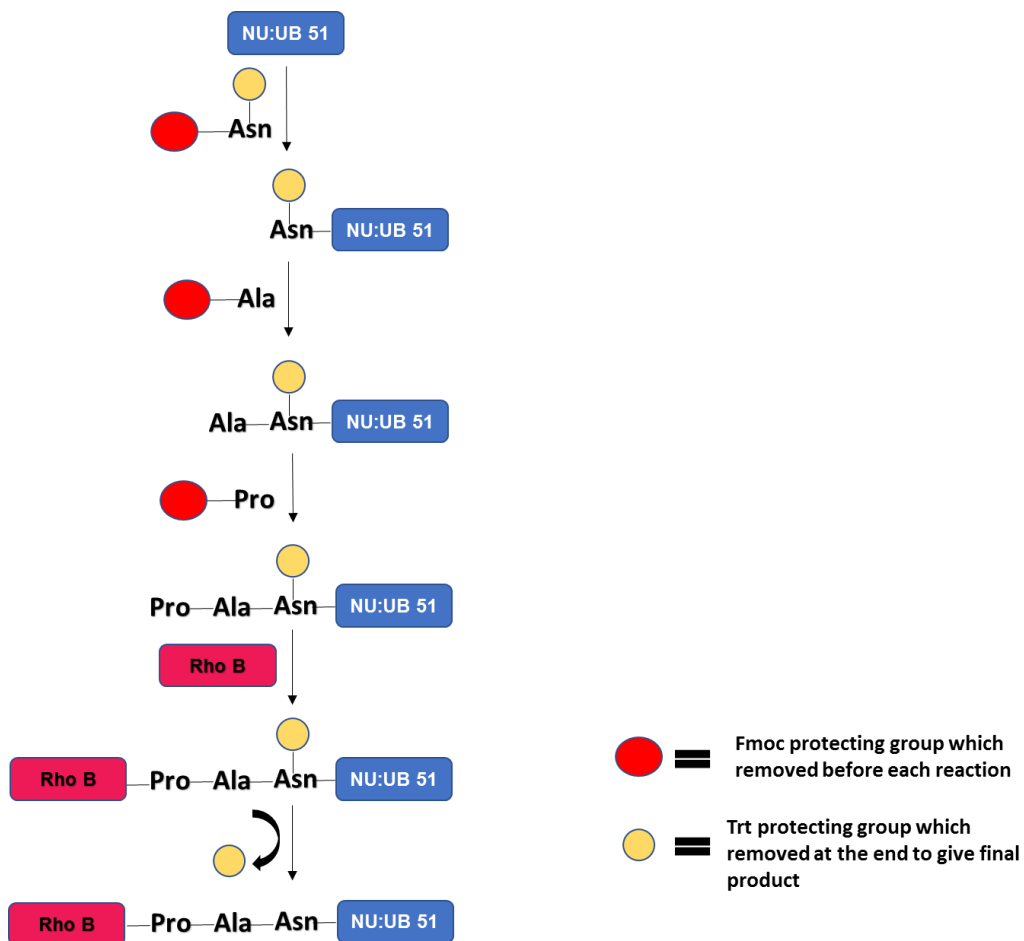


Figure 2.12: Solution phase peptide synthesis schematic representation

In solid phase peptide synthesis (SPPS), the first amino acid in the peptide chain is added to a resin followed by continuous addition of other protected α -amino acid residues. Fmoc-SPPS was used instead of Boc-SPPS because Fmoc is commercially available and release fluorene when deprotected which is an important indicator for the successful reaction (Sheppard, 2003; Behrendt *et al.*, 2016). In addition, the removal of Boc₂O group with TFA could cleave any other side chain protecting group or loss of the peptide from the resin (Behrendt *et al.*, 2016).

Herein, the side chain of Asparagine (Asn) was protected with triphenylmethyl (Trt) to avoid any possible side reaction under chemical conditions used in the peptide coupling and other reaction. The C-terminous of the (Asn) was attached with resin, which will be

removed once this terminus ready for the final reaction. The carboxyl group of the amino acids was activated by using PyBOP, PyClox, HOBt and DIPEA. The removal of the Fmoc protecting group was performed by using 20% piperidine (v/v) in DMF (Carpino, 1987). However, SPPS gives a low percentage yield compared with solution phase peptide synthesis, but SPPS method has been estimated to be fifty times easier than the solution phase peptide synthesis when preparing the same synthetic peptide (Kent, 2008)

Figure 2.13.

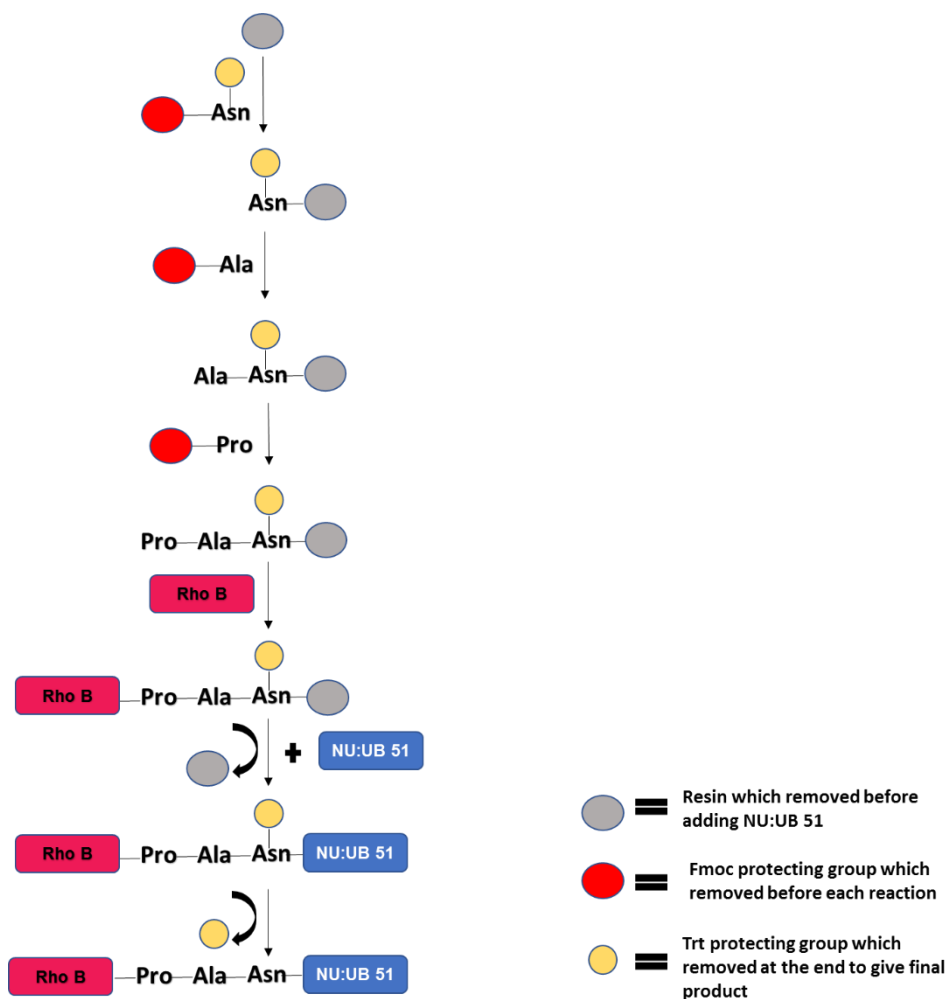


Figure 2.13: Solid phase peptide synthesis schematic representation

2.3.3.1 Fluorophore coupling

Rhodamine B was chosen over other fluorophore dye due to its great photostability, has high quantum yield, has long excited wavelength and been used widely in the biological system study (Yang *et al.*, 2002). Rhodamine B is inexpensive dye, widely used to label peptides and proteins, microscopy and cell imaging. Also, the structural changes of rhodamine Between open ring (fluorescent) and closed ring (non-fluorescent) according to the pH change and high extinction coefficient (Birtalan *et al.*, 2011). These properties give rhodamine B priority to be used in this research over other fluorescent dye

The final step in the solution phase peptide synthesis was attaching rhodamine B fluorophore to the free amino group of the tripeptide legumain substrate. Then, the trityl protecting group was removed from the side chain of asparagine (deprotection) to afford the target fluorescently labeled prodrug **Figure 2.12**. The ability of legumain to cleave at the C-terminal side of asparagine resulting in release of both fluorescence and the toxic drug.

Additionally, in SPPS, rhodamine B was reacted with the free amino group of the resin bound tripeptide. Rho-Pro-Ala-Asn(Trt) was cleaved from the resin using 0.5% TFA in dichloromethane then, the C-terminus of (Asn) was reacted with the free amino group of NU:UB 51, to afford the final prodrug OM50 **Figure 2.13**.

2.3.4 Synthesis of legumain targeted theranostic prodrug

Rho-Pro-Ala-Asn-Gly-APA-AQ(4,8-di-OH) (OM50)

Two different synthetic strategies were adopted towards the synthesis of the target prodrug OM50 **Figure 2.14**, in order to investigate which method would give the greater yield of final product and also take in consideration any potential solubility and purification problems that might be encountered. These two methods were; (1) solution phase peptide synthesis in which the linear peptide synthesis was carried out on the free amino group of NU:UB 51 using suitably protected amino acids and standard peptide coupling conditions and deprotection strategies. (2) Solid phase peptide synthesis (SPPS), in this

approach, Rho-Pro-Ala-Asn-(Trt) was synthesized on resin using standard phase peptide synthesis methods. The Rhodamine labeled tripeptide was cleaved from resin and reacted with NU:UB 51.

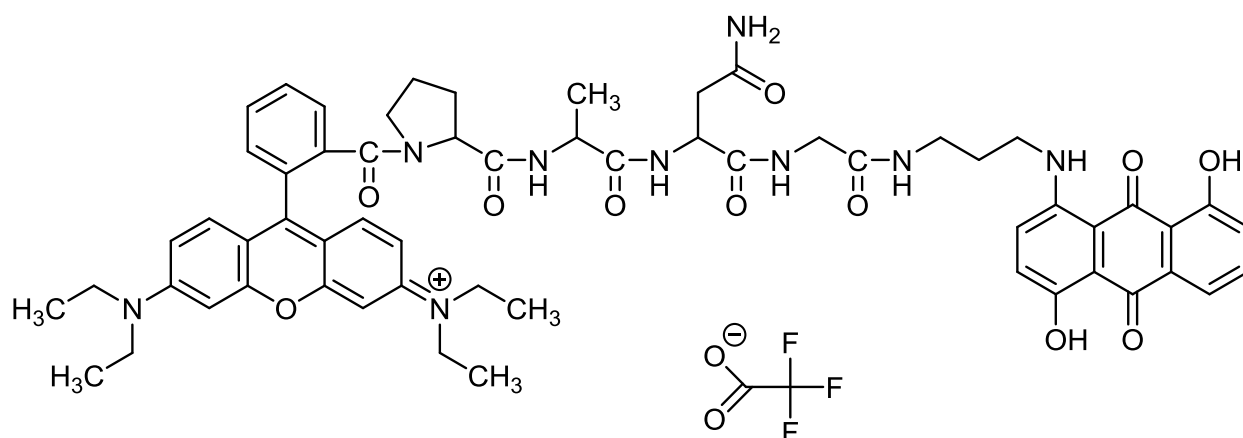


Figure 2.14: Chemical structure of the target compound Rho-Pro-Ala-Asn-Gly-APA-AQ(4,8-di-OH) (OM50)

2.3.4.1 Synthesis of anthraquinone spacer compound APA- AQ(4,8-di-OH) (NU:UB 59)

The first step in the synthesis of the legumain substrate prodrug (OM50) involved preparation of APA-AQ (4,8-di-OH) (NU:UB 59) which is an aminoanthraquinone derivative, designed to serve as the quencher and starting point in the building of the legumain synthetic peptide sequence and the rhodamine B fluorophore.

Leuco-5-hydroxyquinizarin was dissolved in dichloromethane and 1,3-diaminopropane was added and heated for 1.5 hours **Figure 2.15**. The reaction was monitored by TLC, which showed that a new purple spot had formed after adding a small spot of triethylamine with one drop of the reaction mixture to oxidize the product indicating that the reaction was complete. After that, the entire reaction mixture was oxidized using triethylamine and aeration. The product was then isolated by chloroform and water solvent extraction to remove excess amine and stop the reaction. The lower layer which was purple contained

the product APA-AQ (4,8-di-OH) (NU:UB 59). NU:UB 59 was dried at room temperature and collected.

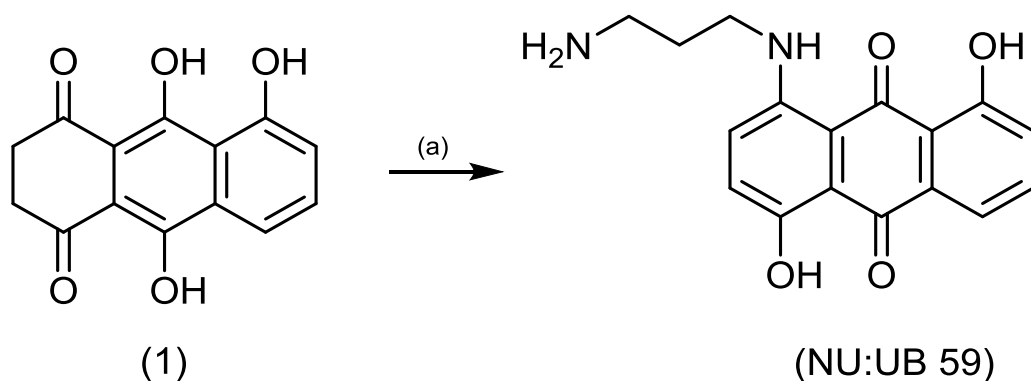


Figure 2.15: Reaction of leuco-5-hydroxyquinizarin (1) with 1,3-diaminopropane. (a) 1,3-diaminopropane, dichloromethane, 40°C, triethylamine, O₂, 1.5 h.

2.3.4.2 Synthesis of Boc-Gly-APA-AQ(4,8-di-OH) (NU:UB 51-Boc)

The synthesis of bis-hydroxylated propyl spaced glycine conjugate Gly-APA-AQ(4,8-di-OH) NU:UB 51 is a key step in the design of the theranostic system because NU:UB 51 can act both as a toxic drug to inhibit both topoisomerase I and II and act as the potential quencher (acceptor) of rhodamine B (donor) fluorescence in the final target fluorogenic prodrug.

Boc-Gly-OH was coupled to the anthraquinone spacer compound NU:UB 59 using PyBOP in DMF with DIPEA **Figure 2.16**. The reaction was monitored by TLC which showed the conversion of NU:UB 59 to NU:UB 51-Boc. Once most of NU:UB 59 was converted to NU:UB 51-Boc the product was partially purified by solvent extraction, using sodium bicarbonate in one of the washes to remove any acidic impurities. The product was then purified by silica gel column chromatography and dichloromethane solvent was used initially. Then the solvent was changed to the more polar solvent dichloromethane: ethyl acetate (4:1) + 2% methanol to accelerate the elution. Finally, the polarity of the solvent was increased through increasing the percentage of methanol to 6% to elute the pure product.

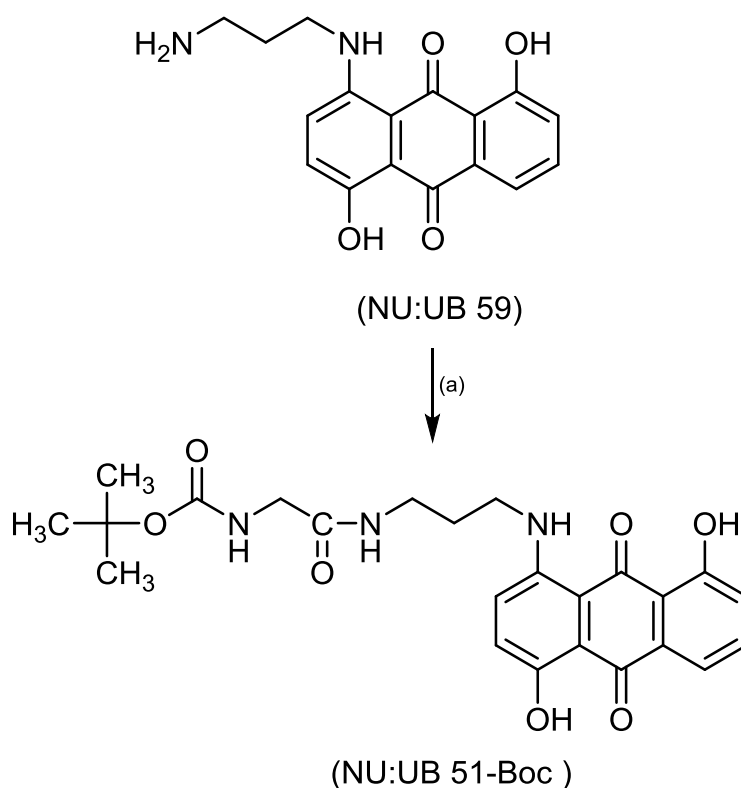


Figure 2.16: Reaction of NU:UB 59 with Boc-Gly-OH. (a) Boc-Gly-OH, PyBOP, DIPEA, DMF, 1.5 h.

2.3.4.3 Synthesis of Gly-APA-AQ(4,8-di-OH) (NU:UB 51)

The removal of the Boc group was carried out by adding trifluoroacetic acid (TFA) at room temperature for 30 minutes and it was evaporated under vacuum and some ethanol was added to lower the boiling point of TFA **Figure 2.17**. Finally, diethyl ether was added to precipitate the product NU:UB 51 and it was filtered and collected. The purity of the product was confirmed by TLC after deprotection of NU:UB 51 by TFA and it was shown that the Boc group had been removed successfully.

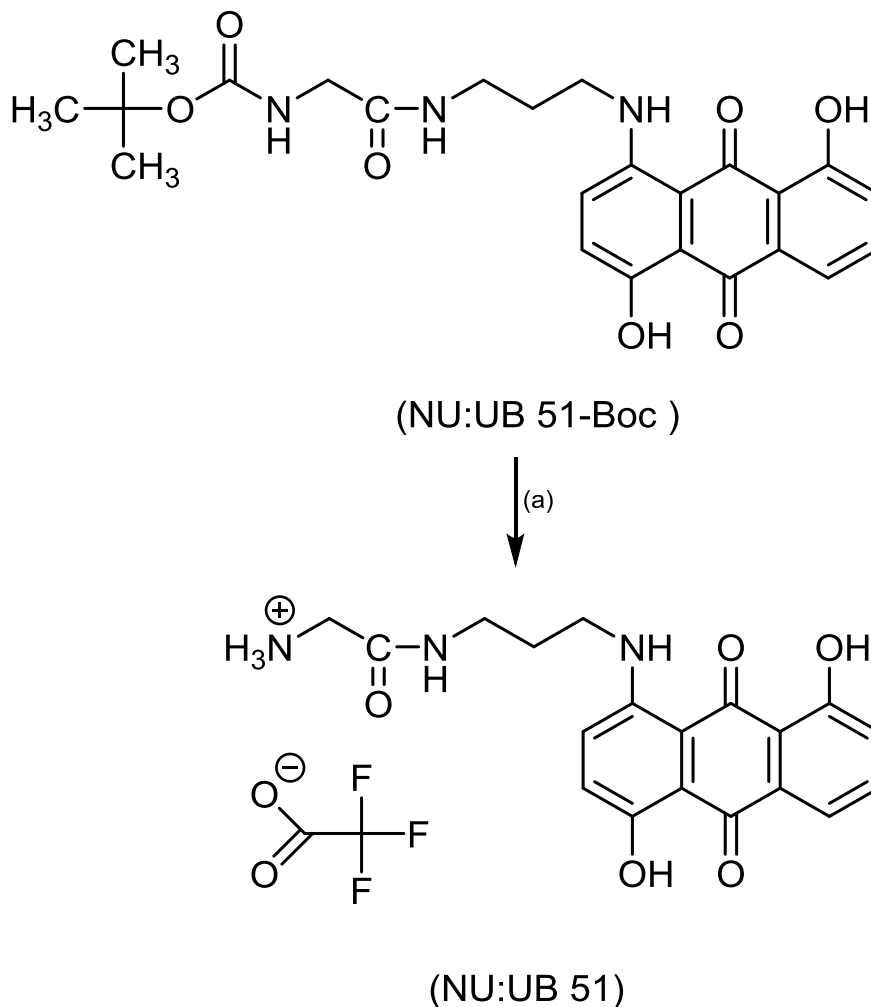


Figure 2.17: Reaction of NU:UB 51-Boc with TFA. (a) TFA, 30 min, room temperature

2.3.5 Synthesis of prodrug OM50, Rho-Pro-Ala-Asn-Gly-APA-AQ(4,8-di-OH), by solution phase peptide synthesis

2.3.5.1 Synthesis of Fmoc-Asn(Trt)-Gly-APA-AQ(4,8-di-OH) (OM43)

The synthesis of Fmoc-Asn(Trt)-Gly-APA-AQ(4,8-di-OH) (OM43) was an important step to introduce asparagine into the peptide substrate because the proteolytic action of

legumain is exclusively located at the C-terminus of this amino acid (Bajjuri *et al.*, 2011). The incorporation of asparagine in peptide synthesis requires the use of N-terminal and side chain protection to avoid complications during peptide coupling reactions.

Fmoc-Asn(Trt)-OH and coupling agents (PyBOP and HOBt) were dissolved in DMF to activate Fmoc-Asn(Trt)-OH then DIPEA was added and allowed to react for 15 minutes at room temperature. The activation takes place when PyBOP attaches to the carboxyl group of the asparagine, which is then replaced by the HOBt group. The asparagine was activated and it was added to NU:UB 51 pre-dissolved in DMF and allowed to react at room temperature for 1.5 hours **Figure 2.18**. The TLC was eluted using chloroform: methanol (4:1) to detect the end of reaction and formation of OM43. According to the TLC and in comparison with NU:UB 51, a new spot had formed and moved higher than NU:UB 51, this indicates the formation of OM43. The compound was partially purified by solvent extraction.

Chloroform was used initially for silica gel column chromatography and later the solvent was changed to more polar solvent chloroform: methanol (4:1) and 5% methanol. The target compound was obtained after chromatography and the TLC was carried out on different fractions to find out where the product OM43 ran.

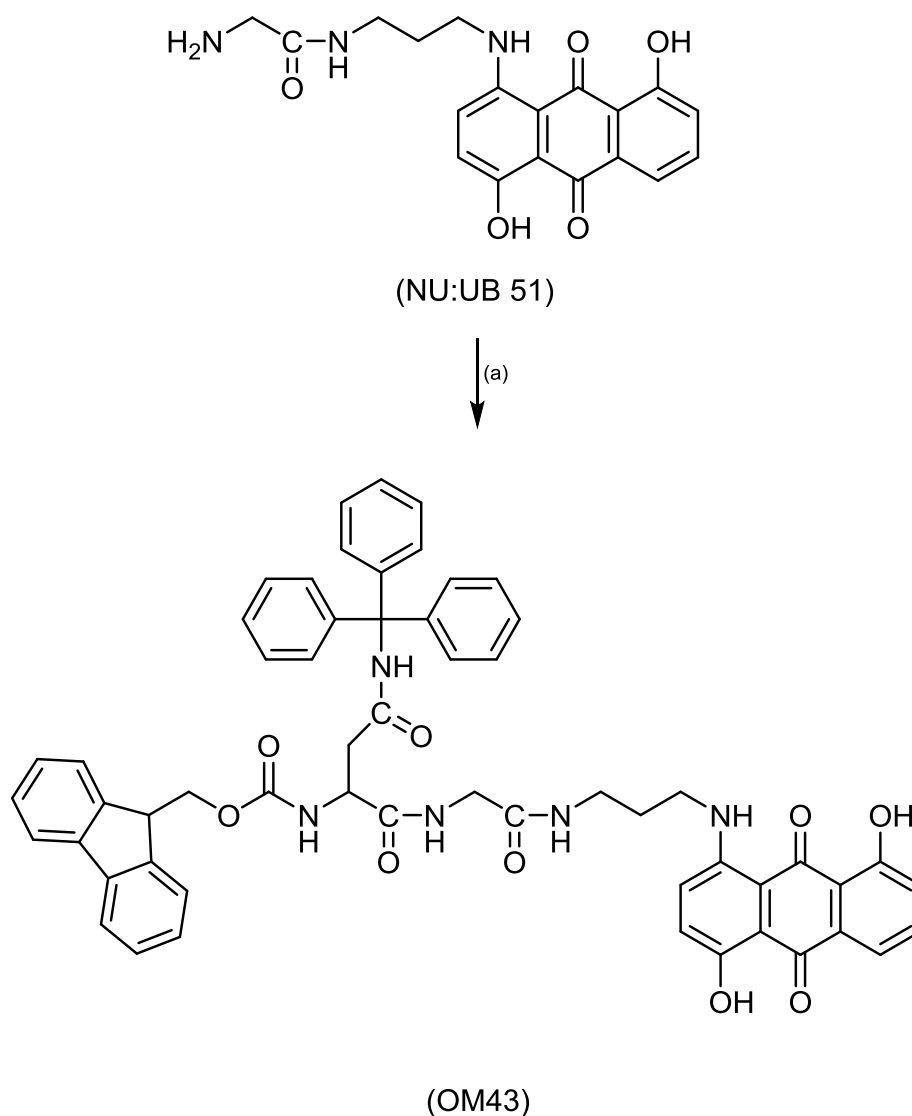


Figure 2.18: Reaction of NU:UB 51 with Fmoc-Asn(Trt)-OH. (a) Fmoc-Asn(Trt)-OH, PyBOP, HOBT, DIPEA, DMF, 1.5 h.

In this reaction, the (Trt) group, was used to protect the alpha-amino group of asparagine. The trityl group (Trt), is very important because it prevented the dehydration of the primary amine to a nitrile group in the side chain of asparagine. Therefore, the trityl group was left attached to the asparaginyl residue, until no further reactions that could cause dehydration of this group. The trityl group is relatively stable when exposed to a range of deprotecting reagents, for this reason, Trt was preferred over other protecting groups (Isidro-Llobet *et al.*, 2009). Care was taken to protect the asparaginyl side chain because

loss of the primary amide in the side chain would result in a non-productive insertion into the active site S1 pocket of legumain and no further recognition would occur.

Finally, the structure of the target compound OM43 was confirmed by high resolution electrospray (+) mass spectrum which clearly showed a signal at m/z 948.3609 which corresponded to the expected molecular mass of the 947.3530 $[M+H]^+$. Also, there was a good correlation between the observed data and the theoretical isotope model for $C_{57}H_{49}N_5O_9$ $[M+H]^+$ **Figure 2.19**. Therefore, this result confirms the successful addition of Fmoc-Asn(Trt)-OH to NU:UB 51 and it was now possible to remove the Fmoc group prior to addition of the second amino acid alanine.

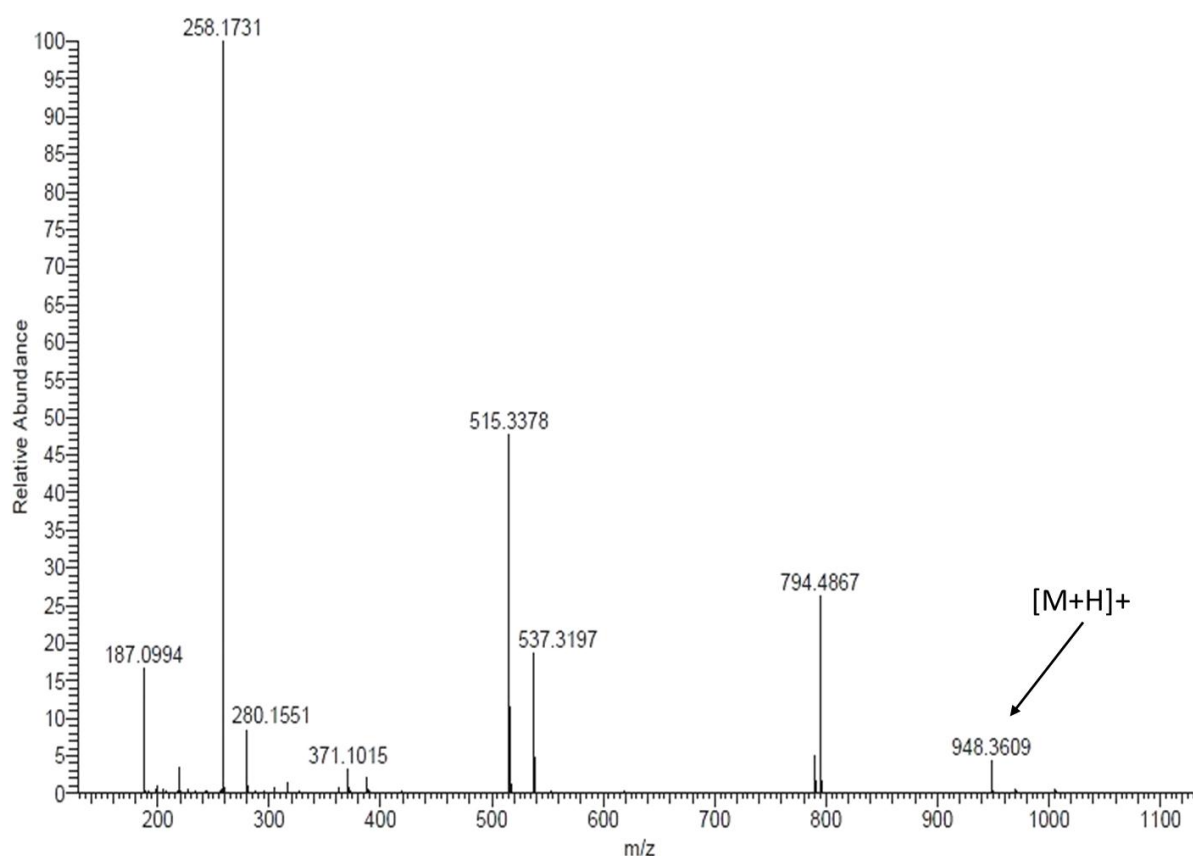


Figure 2.19: The mass spectrum of the OM43

2.3.5.2 Synthesis of H-Asn(Trt)-Gly-APA-AQ(4,8-di-OH) (OM44)

The Fmoc group was removed from OM43 by dissolving it in piperidine (20% in DMF) and allowing it to react for 15 minutes **Figure 2.20**. Piperidine was chosen over other reagents because it takes few minutes at room temperature to remove the Fmoc group and piperidine has no effect on the trityl (Trt) group. In addition, the Fmoc group is very stable to acidic reagents, but under specific basic conditions, Fmoc group is cleaved easily (Fields, 1994).

The reaction was monitored by TLC in chloroform: methanol (4:1) solvent system which shown that new spot has been formed indicating that Fmoc group has been removed from OM43 and OM44 [H-Asn(Trt)-Gly-APA-AQ(4,8-di-OH)] has been formed. The DMF was removed using chloroform/water extraction.

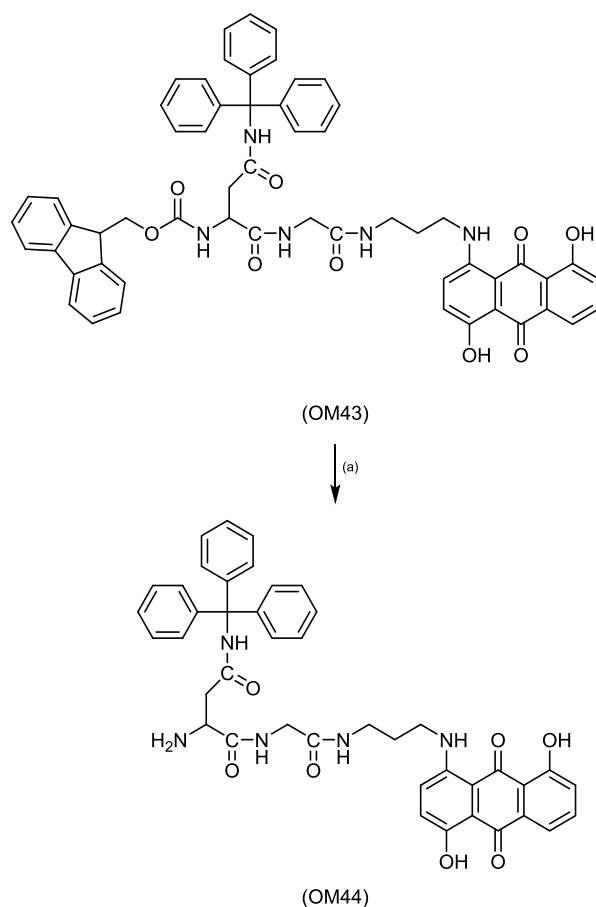


Figure 2.20: Reaction of OM43 with piperidine (20% in DMF). (a) piperidine (20% in DMF), 15 min, room temperature.

OM44 was purified by silica gel chromatography column after the Fmoc group had been removed by using in the beginning chloroform to ensure that the more mobile Fmoc-piperidine side product (pale yellow color) of the reaction was completely removed. After all the yellow color had been removed, the solvent system was changed to 4:1 chloroform: ethyl acetate and 10% methanol, since OM44 was more mobile in this ratio of mixed solvent. Finally, the TLC was checked for different fractions in 4:1 chloroform: methanol system.

As a result, the deprotection of asparagine would afford the free amino group and it is ready to be coupled with the next amino acid residue, alanine which would occupy the P2 position of the substrate.

2.3.5.3 Synthesis of Fmoc-Ala-Asn(Trt)-Gly-APA-AQ(4,8-di-OH) (OM45)

The next step was the addition of the Fmoc-Ala-OH to the deprotected alpha amino group of the asparagine residue to complete the tripeptide sequence. Fmoc-Ala-OH was coupled to OM44 using PyBOP and HOBt in DMF with DIPEA **Figure 2.21**. The TLC was checked and after confirmation of a new spot, and most of OM44 converted to OM45 [Fmoc-Ala-Asn(Trt)-Gly-APA-AQ(4,8-di-OH)], the product was partially purified by solvent extraction. At this stage, silica gel chromatography column was not applied because the product was considered to be pure enough for further reaction. Therefore, the product was evaporated and 20% piperidine in DMF was added to remove the Fmoc group.

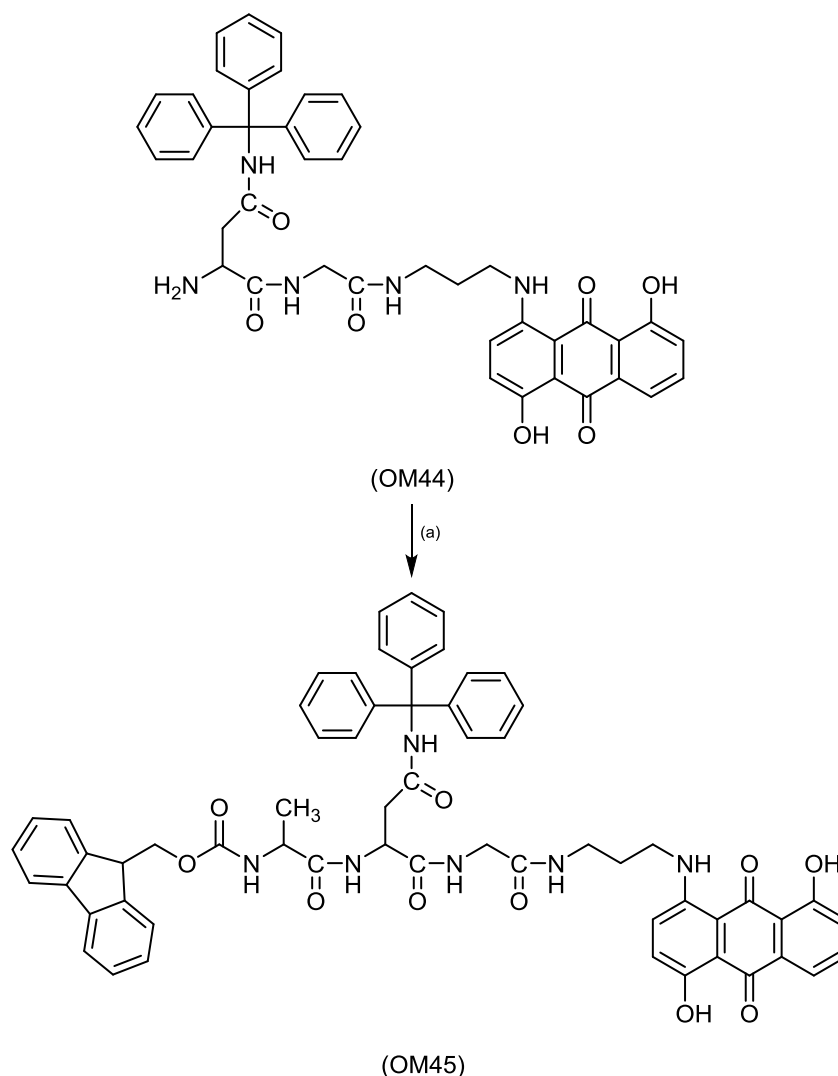


Figure 2.21: Reaction of OM44 with Fmoc-Ala-OH. (a) Fmoc-Ala-OH, PyBOP, HOBT, DIPEA, DMF, 1.5 h.

2.3.5.4 Synthesis of H-Ala-Asn(Trt)-Gly-APA-AQ(4,8-di-OH) (OM46)

The Fmoc group was removed from OM45 to give OM46 [H-Ala-Asn(Trt)-Gly-APA-AQ(4,8-di-OH)] and the TLC was checked in comparison with protected OM45 and it showed that the Fmoc group had been removed successfully. The product was partially purified by solvent extraction. The volume of solvents was reduced before purifying by silica gel column chromatography. Initially, chloroform was used to ensure that all the side product (Fmoc-piperidine) of the reaction was fully removed. Then, the solvent was turned to 4:1 chloroform: ethyl acetate and 10% methanol because OM46 was more mobile in

this ratio. The fractions were checked by TLC using chloroform: methanol (4:1) solvent system. The product was then evaporated, and there was some DMF that was not evaporated by the rotary evaporator and did not mix with diethyl ether (two layers formed), therefore, some ethanol was added because it is able to mix with DMF and ether as well. Finally, the product was left in the fridge (4°C) to obtain a solid, which was filtered to afford the final product OM46 as shown in **Figure 2.22**.

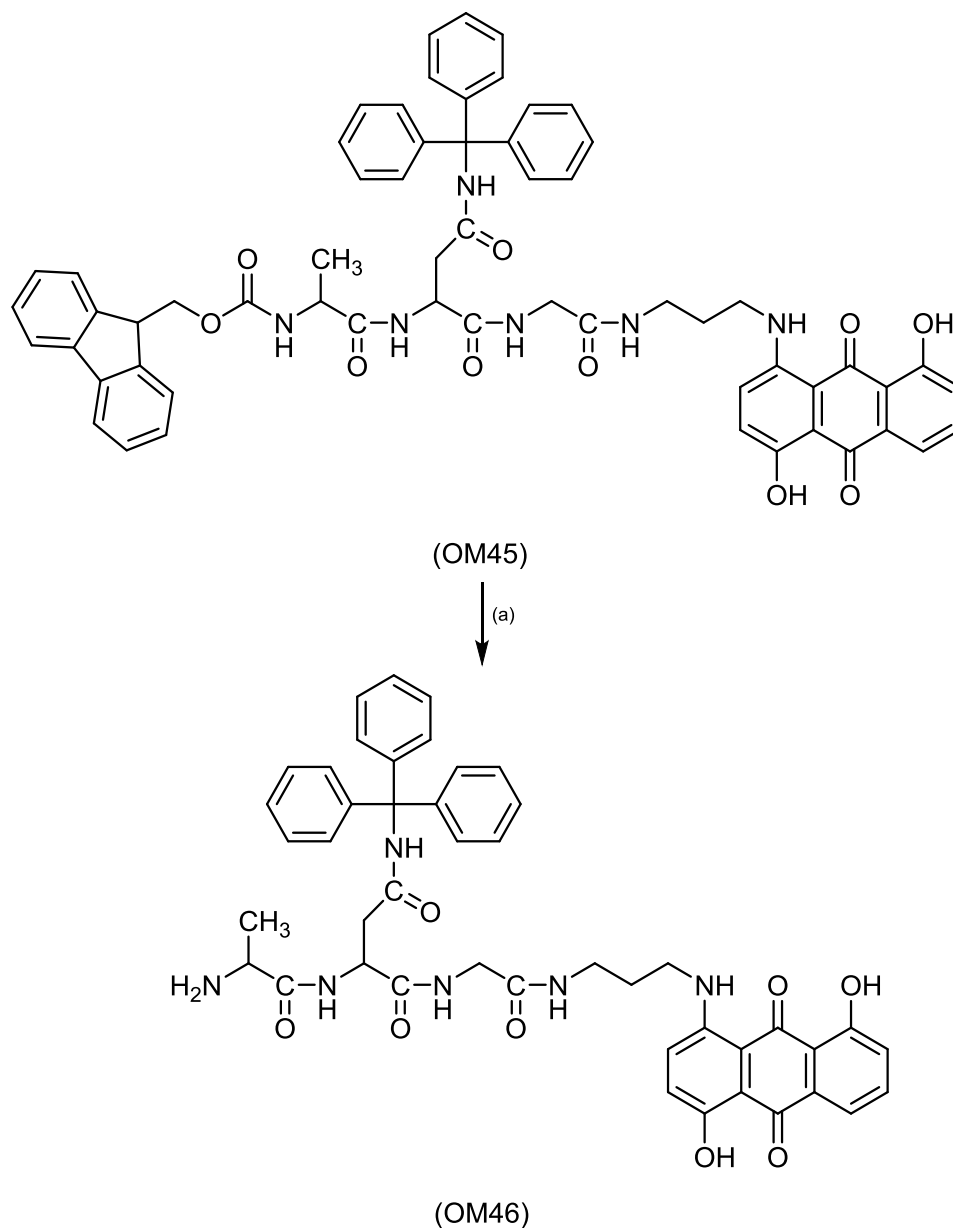


Figure 2.22: Reaction of OM45 with piperidine (20% in DMF). (a) piperidine (20% in DMF), 15 min, room temperature.

2.3.5.5 Synthesis of Fmoc-Pro-Ala-Asn(Trt)-Gly-APA-AQ(4,8-di-OH) (OM47)

Fmoc-Pro-OH was added to complete the tetrapeptide sequence and to occupy the position P3 of the protease substrate. In this step, PyClock was used as a coupling agent instead of PyBOP because PyClock has been reported to be faster than ByBOP in activating the amino acid and to increase coupling rate in few minutes (Albericio, 2008).

Fmoc-Pro-OH was coupled with OM46 pre-dissolved in DMF using PyClock in DMF with DIPEA **Figure 2.23**. The end of the reaction was monitored by TLC using 4:1 chloroform: methanol.

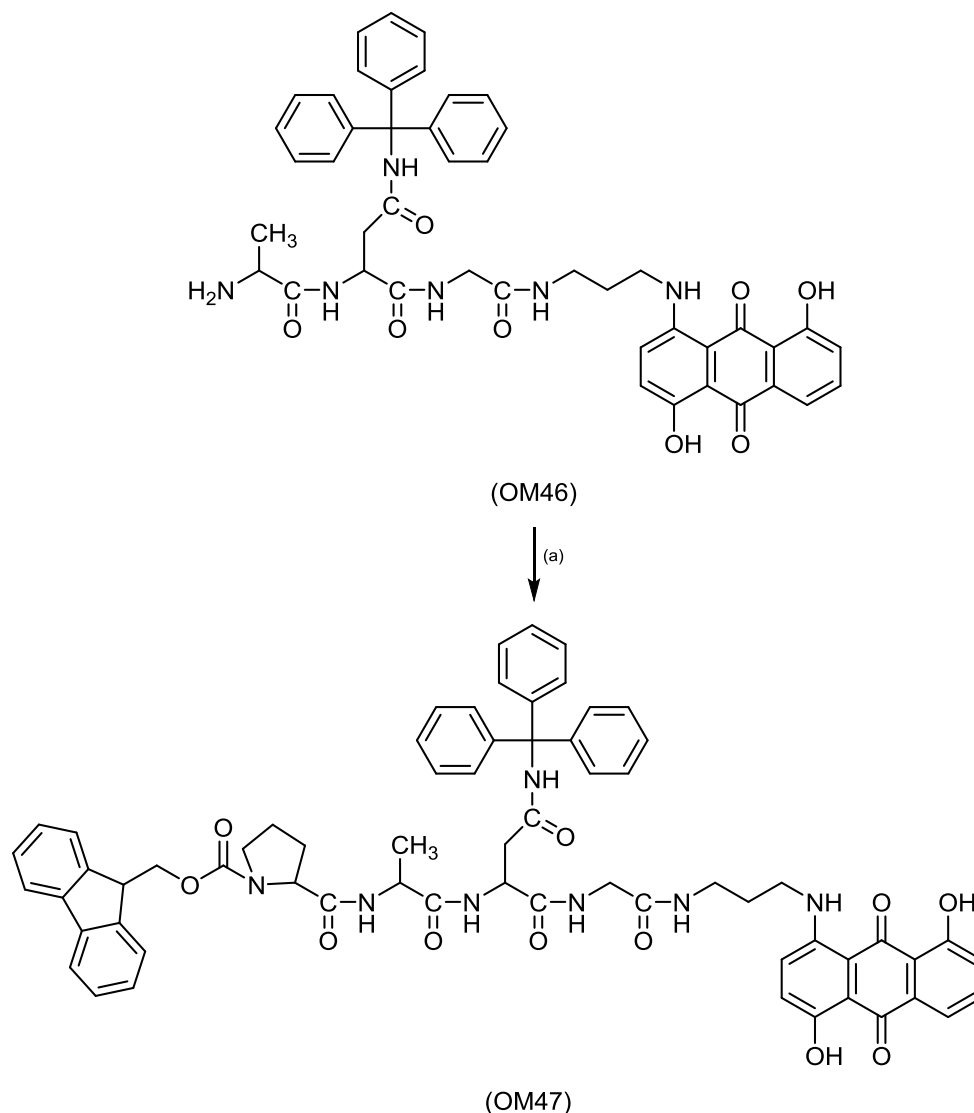


Figure 2.23: Reaction of OM46 with Fmoc-Pro-OH. (a) Fmoc-Pro-OH, PyClock, DIPEA, DMF, 1.5 h.

2.3.5.6 Synthesis of H-Pro-Ala-Asn(Trt)-Gly-APA-AQ(4,8-di-OH) (OM48)

The Fmoc group was removed from OM47 using 20% piperidine in DMF **Figure 2.24**. TLC test was used to check the deprotection of OM47 by using 4:1 chloroform: methanol and it showed that the Fmoc group has been removed successfully from OM47. The

product was purified by silica gel column chromatography using dichloromethane at the beginning to ensure that all Fmoc-piperidine was completely removed and then, the solvent was turned to dichloromethane: ethyl acetate and 10% methanol until OM48 [H-Pro-Ala-Asn(Trt)-Gly-APA-AQ(4,8-di-OH)] has been removed from the column and the product was completely pure.

Finally, the product was evaporated and diethyl ether was added to precipitate the product OM48. The product was then ready for the final step in the synthesis of the target compound which was the addition of rhodamine B.

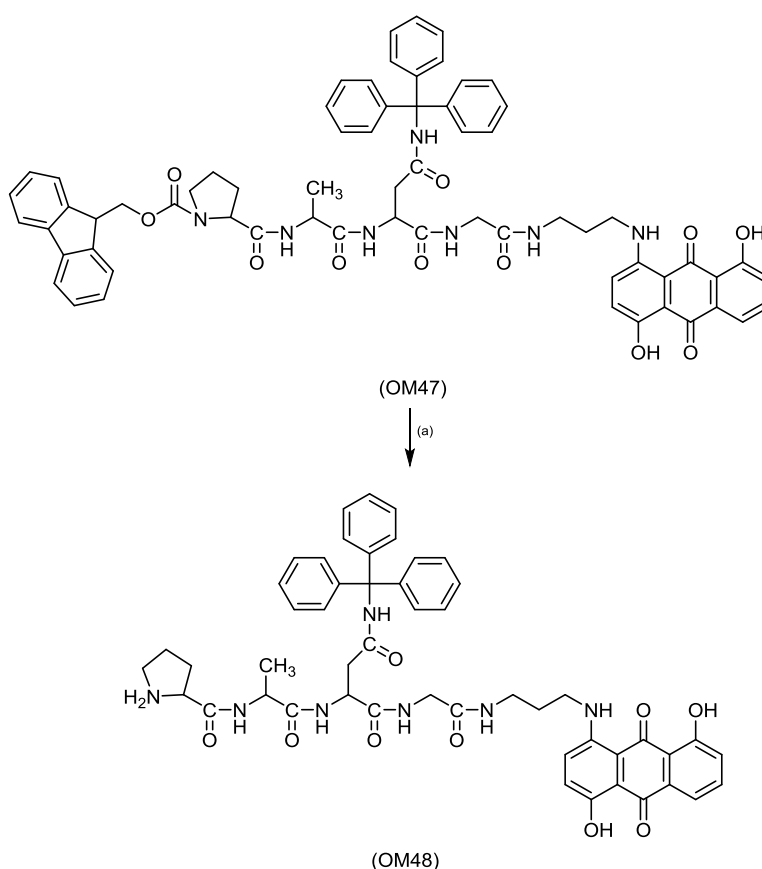


Figure 2.24: Reaction of OM47 with piperidine (20% in DMF). (a) piperidine (20% in DMF), 15 min, room temperature.

2.3.5.7 Synthesis of Rho-Pro-Ala-Asn(Trt)-Gly-APA-AQ(4,8-di-OH) (OM49)

The final step in the synthesis of the theranostic system was the addition of rhodamine B to OM48 to form OM49 [Rho-Pro-Ala-Asn(Trt)-Gly-APA-AQ(4,8-di-OH)], which is the overall

target fluorogenic probe designed for activation by legumain (after removal of the Trt group). It is hypothesized that the fluorescence of rhodamine B will be quenched by the amino anthraquinone NU:UB 51. The preparation involved the activation of the fluorophore of the carboxylic acid group and reaction with N-terminal of proline.

Rhodamine B was coupled to OM48 using PyClock in DMF with DIPEA **Figure 2.25**. The reaction was shown to be complete by using TLC, which showed a new purple product spot with pink spot (activated rhodamine B) close to the purple spot had formed in 4:1 chloroform: methanol. The compound was partially purified using chloroform/water solvent extraction. Evaporation was performed before purified by silica gel column chromatography. The solvent used in the purification was chloroform: ethyl acetate (4:1) and 5% methanol to ensure all rhodamine B had been removed. However, there was still some rhodamine B with the final product, indicating that the final product was not completely pure therefore, the silica gel column chromatography was performed again to remove all rhodamine B by using the same solvent.

After the second run of column chromatography, most of the rhodamine B had been removed and the percentage of methanol was increased to 15% to make the product move faster and elute the product from the column. However, the percentage of methanol was increased again to 30% because the product was precipitating from solution in ethyl acetate, therefore, the silica was removed from the column and 100% methanol was added and left for 15 minutes. Filtration was performed to remove the product from the silica and the TLC was checked in 4:1 chloroform: methanol to ensure that the product was pure, but there was some rhodamine B. Therefore, the product was purified for the third time by using 9:1 chloroform: methanol solvent system. The purification was monitored by TLC, which showed that there was no rhodamine B remaining

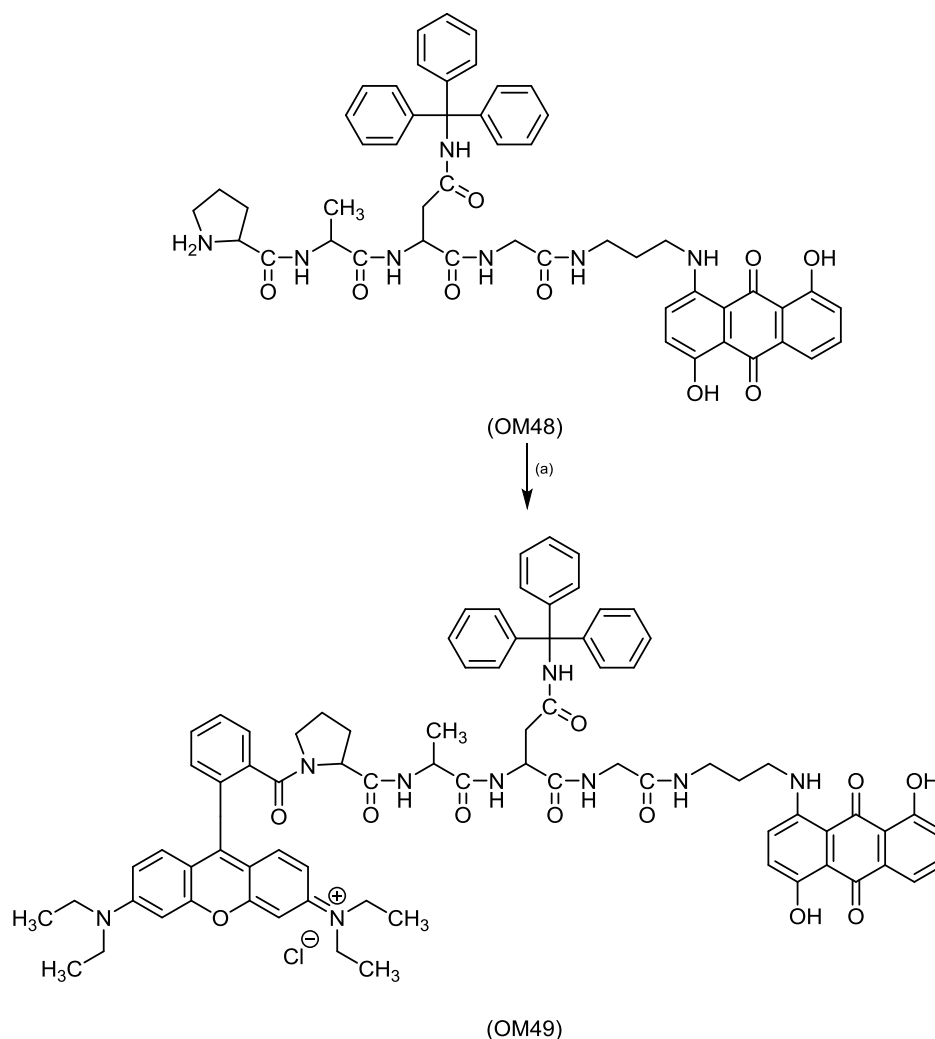


Figure 2.25: Reaction of OM48 with rhodamine B. (a) rhodamine B, PyClock, DIPEA, DMF, 1.5 h.

2.3.5.8 Removal of the trityl (Trt) group

After the product had been purified, the trityl (Trt) group was removed by exposing the product to TFA for longer time (more than 3 hours) in contrast to the removal of the Boc group which takes only few minutes (Isidro-Llobet *et al.*, 2009). The end of the reaction was monitored by TLC using 4:1 chloroform: methanol solvent system and it was shown that a new lower spot was formed, this indicated that the reaction was complete and the trityl group had been removed successfully **Figure 2.26**. The product was purified by column chromatography using 9:1 chloroform: methanol solvent system and it was checked by TLC using 9:1 chloroform: methanol. Finally, the solution was evaporated and

ether was added to aid in solidification. Filtration was performed on the resulting suspension and the solid was dried to afford OM50 [Rho-Pro-Ala-Asn-Gly-APA-AQ(4,8-di-OH)] as a purple solid **Figure 2.26**.

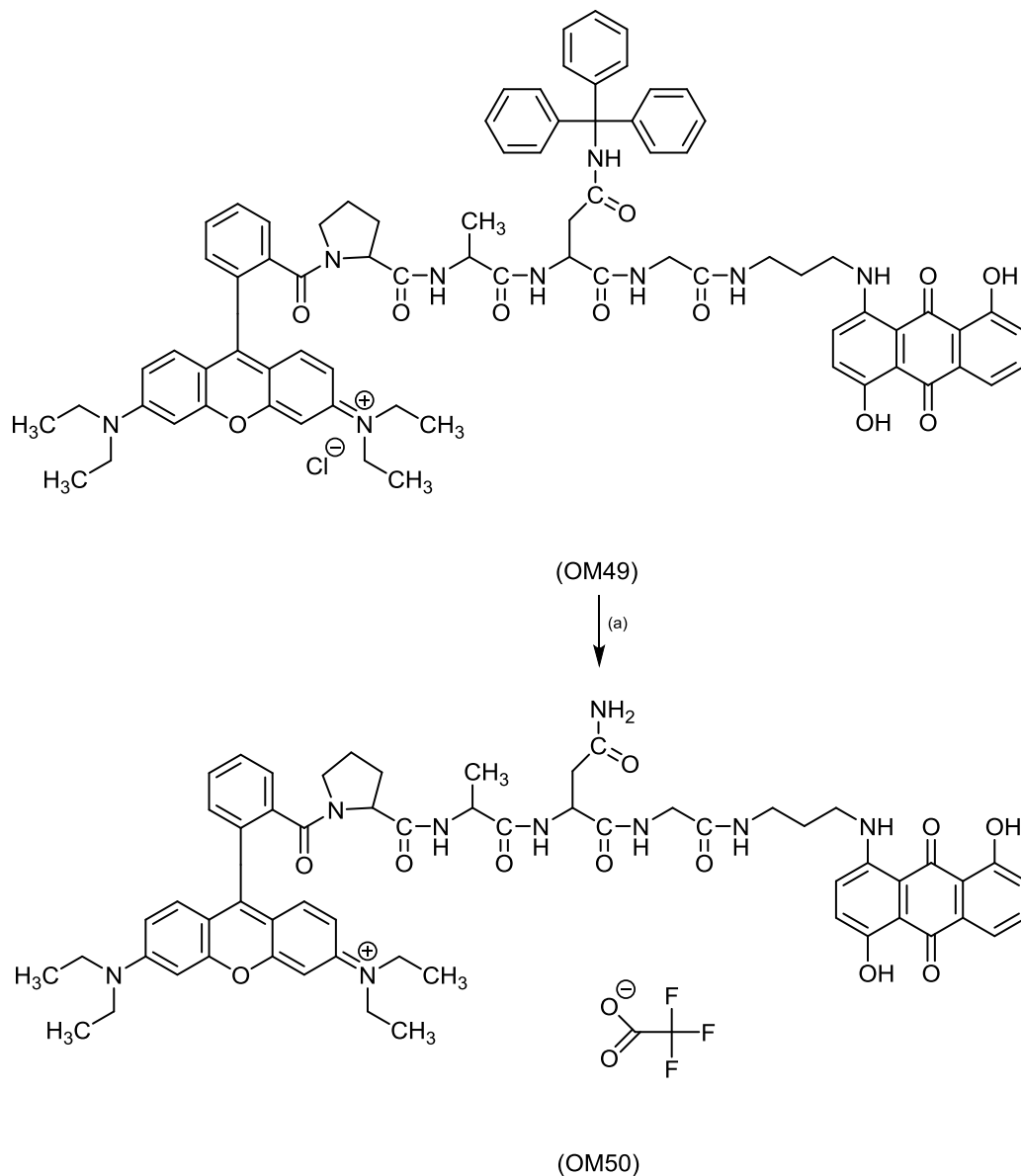


Figure 2.26: Reaction of OM49 with TFA. (a) TFA, ~ 3 h, room temperature.

Finally, the structure of the target compound OM50 was confirmed by the high resolution electrospray (+) mass spectrum which clearly showed a signal at m/z 1076.4855 which corresponded to the expected molecular mass of the 1076.4876 cation (+). Also, there

was a good correlation between the observed data and the theoretical isotope model for $C_{59}H_{66}N_9O_{11}$ **Figure 2.27**. Therefore, this result confirmed the successful synthesis of OM50.

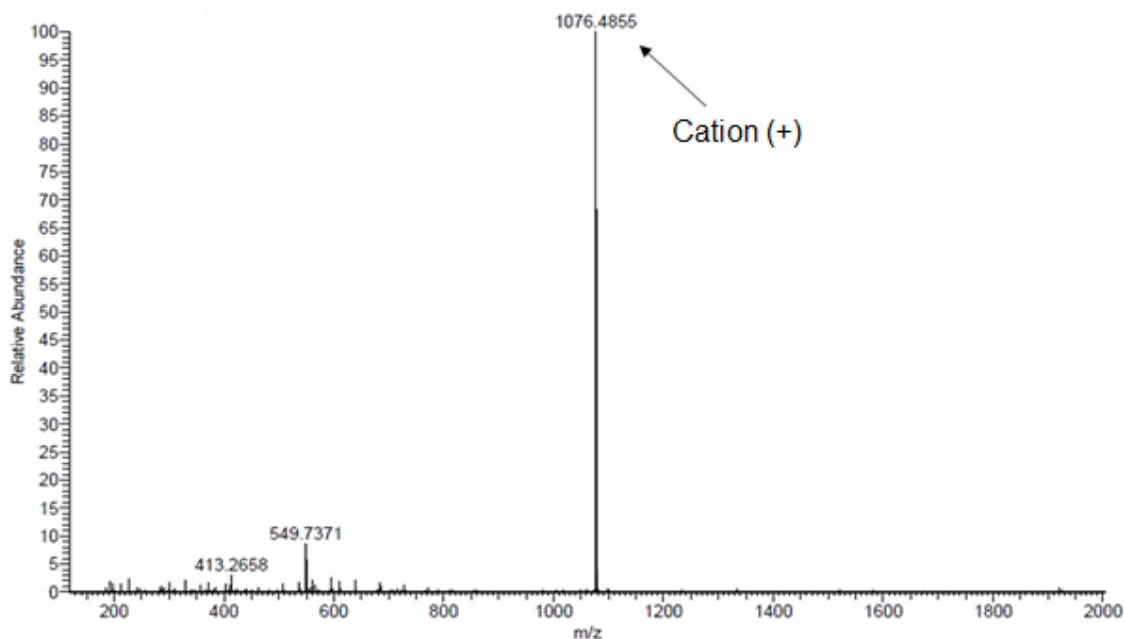


Figure 2.27: The mass spectrum for OM50

2.3.6 Synthesis of the target compound Rho-Pro-Ala-Asn-Gly-APA-AQ(4,8-di-OH) (OM50) by solid phase peptide synthesis

The fluorescent tripeptide sequence Rho-Pro-Ala-Asn(Trt)-OH was synthesized by solid phase peptide synthesis in addition to the solution phase peptide synthesis to compare the results from this process with the results from solution phase in order to determine the best synthesis method for the target compound OM50. Solid phase peptide synthesis is the process by which peptide synthesis can be carried out on solid support (Merrifield, 1963). The main advantages of this process over other processes are all reagents can be simply washed away each step, quicker time for synthesis and the synthetic

intermediates do not have to be isolated. By contrast, in solution phase peptide synthesis, all synthetic intermediates require isolation. The Fmoc-amino acids was used due to it is high quality Fmoc-building block, commercially available with minimum cost and the deprotection conditions is suitable with modified peptide in contrast with Boc₂O protection which lack the differentiation in cleavage of Boc₂O group and any other side chain protecting group (Behrendt *et al.*, 2016). In addition, the deprotection of Fmoc result in releases of fluorene which is a UV absorption properties, indicating the successful synthetic reaction (Sheppard, 2003). Fmoc-Pro-Ala-Asn(Trt)-OH was synthesized by five steps: (1) resin swelling (2) peptide coupling (3) color test to detect the presence or absence of free primary amino group (4) deprotection (removal of Fmoc group) (5) cleavage of Novasyn TGT.

2.3.6.1 Resin swelling

Fmoc-Asn(Trt)-Novasyn TGT resin was transferred to the SPPS vessel and 10ml dichloromethane was added and was shaken for 1 hour to maximize its surface for peptide coupling. Dichloromethane was drained off and the resin was washed 2 times by DMF.

2.3.6.2 Deprotection of amino acid

The Fmoc protecting group of the growing resin must be removed before the next amino acid can be attached. This process was achieved by adding 20% piperidine in DMF to the SPPS vessels and shaken for 10 mins (3 times). The reagents were drained off and the resin was washed by DMF for 3 times. This process was repeated after each coupling.

2.3.6.3 Colour test

This test was used to indicate the addition of new amino acid and after the removal of Fmoc group. HZ22 test was used instead of Kaiser Test (**Appendix**). Red beads indicate

the presence of free amino group whereas, clear beads indicate that the amino group is protected by Fmoc group.

HZ22 was added to a small number of resin beads and left for 15 minutes at room temperature and the beads were then washed with dichloromethane and filtered. After the beads were filtered, if red beads were observed there is a free amino group (after Fmoc deprotection) and clear beads if the amino group was protected by Fmoc group

Figure 2.28.

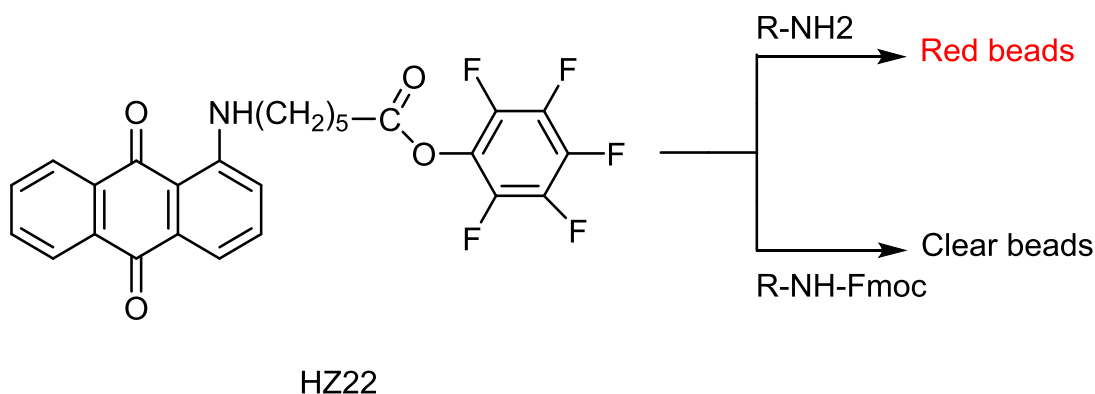


Figure 2.28: The mechanism of colour test

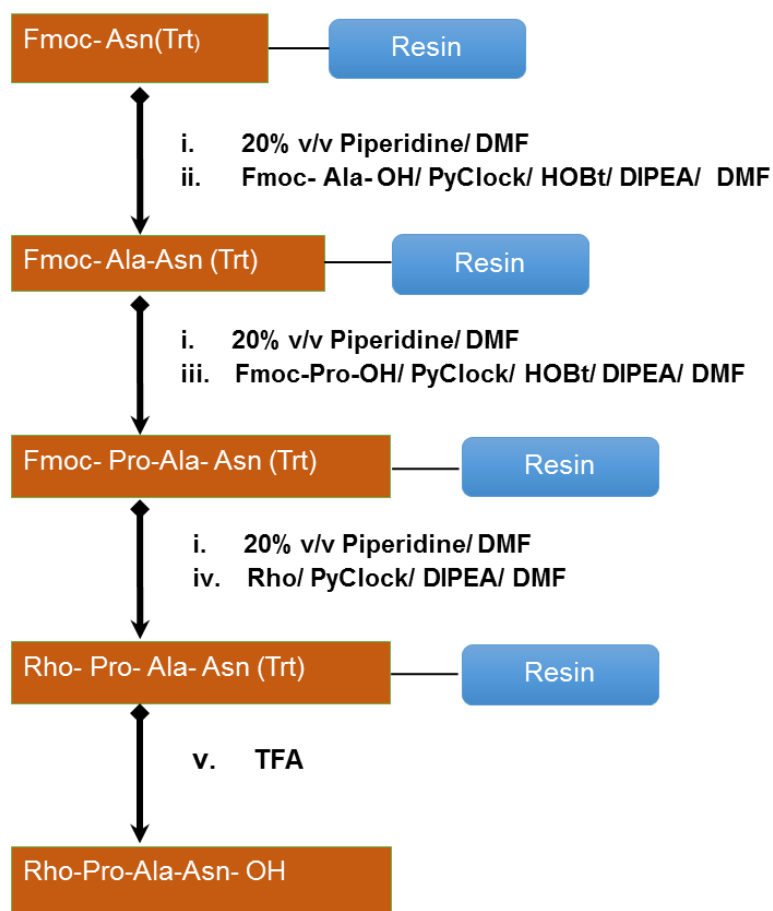
2.3.6.4 Peptide coupling

At this stage, an amide bond is formed between the free carboxylic acid group of the Fmoc-protected amino acid and the free amino terminus of the growing peptide on the resin. By using suitable coupling agents, under basic conditions, an active ester will be generated during the coupling reaction **Figure 2.29.**

Fmoc-Ala was added to the SPPS vessel to couple with NH-Asn(Trt)-resin using PyClock and HOBt in DMF with DIPEA two times and shaken each time for 40 minutes. The reagents were drained and the resin was washed with DMF three times. The color test was performed to confirm the completion of peptide coupling which showed clear beads. Finally, the Fmoc group was removed by adding 20% piperidine in DMF to the resin, drained and repeated 2 times and the resin was washed with DMF 3 times. The color test was applied to the removal of Fmoc group and it showed red beads.

After the removal of Fmoc group, the resin was ready for next coupling step which was the addition of Fmoc-Pro-OH. Fmoc-Pro-OH and coupling agents in DMF with DIPEA was added to the SPPS vessel and shaken for 40 minutes. Same amount of the amino acid and coupling reagents were added again to the vessel and shaken for another 40 minutes to ensure that the amino terminus of the resin was completely reacted with the Fmoc-Pro-OH. The reagents were drained and the resin was washed with DMF (x3). At the end of the reaction, the color test was performed and it showed clear beads indicating that there was no free amino group. Finally, Fmoc group has been removed and another colour test was performed and it showed red resin beads, indicating that Fmoc group has been removed successfully and the compound is ready for the addition of rhodamine B.

The free amino terminus of proline was ready to react with rhodamine B. Rhodamine B was coupled with tripeptide-resin using PyClock in DMF with DIPEA. The color of the resin was not completely pink, therefore, rhodamine B and coupling reagents were added again to get deep pink resin beads. The coupling reagents were drained and the resin was washed several times with dichloromethane until clear solvent was obtained.



Scheme: reagents and condition:

- i. 20% v/v Piperidine/ DMF, 10 mins (x3)
- ii. Fomc-Ala-OH/ PyClock/ HOBt/ DIPEA/ DMF, 40 mins (x2)
- iii. Fomc-Pro- OH/ PyClock/ HOBt/ DIPEA/ DMF, 40 mins (x2)
- iv. Rhodamine B/ PyClock/ DIPEA/ DMF, 40 mins (x2)
- v. 0.5% TFA in DCM

Figure 2.29: The five steps of the solid phase peptide synthesis.

2.3.6.5 Rho-Pro-Ala-Asn(TRT)-resin cleavage

After tripeptide coupling, the Rho-Pro-Ala-Asn(Trt)-OH was removed from the resin for the conjugation with Gly-APA-AQ (NU:UB 51). Novasyn TGT is very sensitive to acid and hence the resin was cleaved by adding 0.5% of trifluoroacetic acid in 100 ml dichloromethane to the resin in small portions. However, triethylamine (base) was added with the same quantity of the TFA to neutralize the product and avoid the removal of Trityl group (Trt) from asparagine **Figure 2.29**.

The filtrates containing Rho-Pro-Ala-Asn(TRT)-OH were dried using a rotary evaporator and diethyl ether was added to aid in solidification along with a little 1,4-dioxane (to prevent two layers forming). Then, diethyl ether was added again and the product was left in the fridge to get more solid. During the filtration, more ether was added because the product was very sticky. The product was collected after filtration and drying **Figure 2.30**.

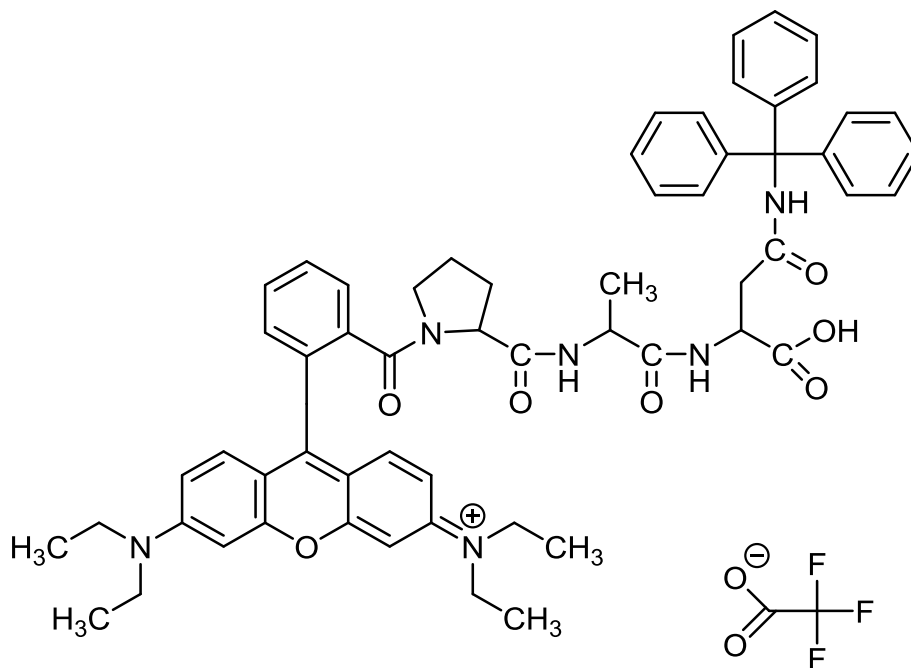


Figure 2.30: The chemical structure of the Rho-Pro-Ala-Asn(TRT)-OH

Finally, the structure of the target compound Rho-Pro-Ala-Asn(Trt)-OH was confirmed by the high resolution electrospray (+) mass spectrum which clearly showed a signal at m/z 967.4752 which corresponded to the expected molecular mass of the 967.4753 Da cation (+). Also, there was a good correlation between the observed data and the theoretical isotope model for $C_{59}H_{63}N_6O_7$ cation (+) **Figure 2.31**. Therefore, this result confirmed the successful addition of rhodamine B to the tripeptide and it was ready to react with Gly-APA-AQ(4,8-di-OH) (NU:UB 51) to give the target compound Rho-Pro-Ala-Asn-Gly-APA-AQ(4,8-di-OH) (OM50).

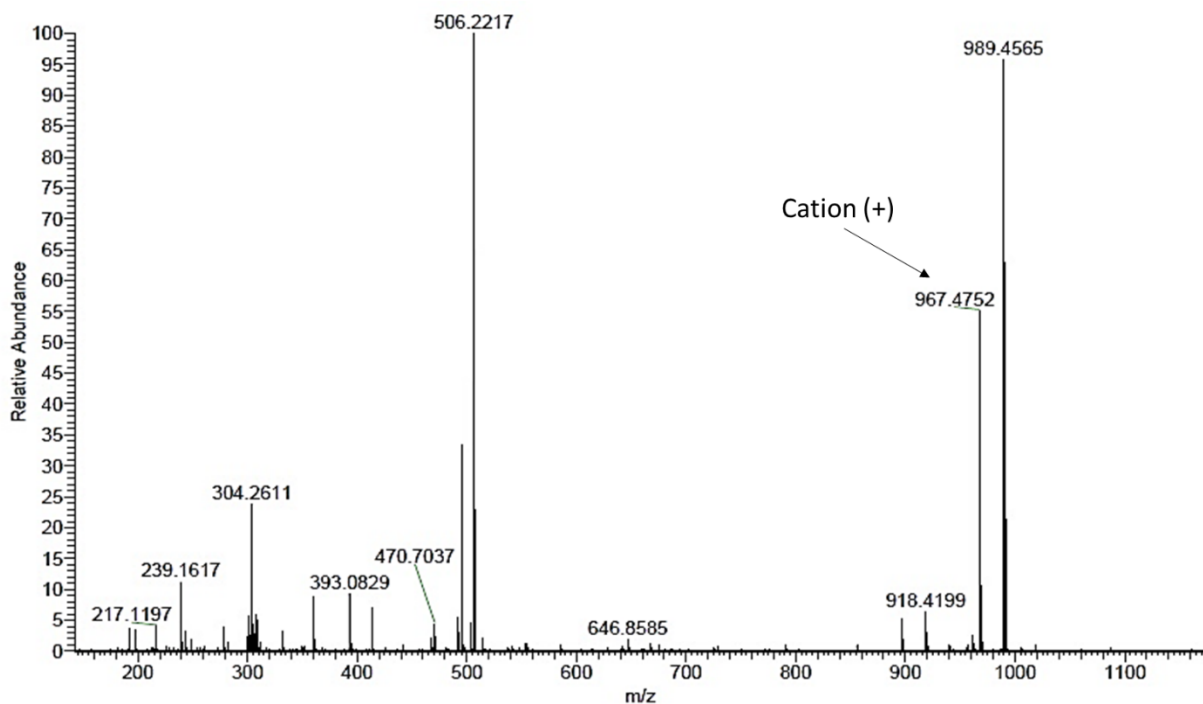


Figure 2.31: Mass spectrum for Rho-Pro-Ala-Asn(Trt)-OH

2.3.6.6 Reaction of Rho-Pro-Ala-Asn(Trt)-OH with Gly-APA-AQ(4,8-di-OH) [NU:UB 51] to give OM49

Rho-Pro-Ala-Asn(Trt)-OH was reacted with NU:UB 51 [Gly-APA-AQ(4,8-di-OH)] using HATU as a coupling agent with DIPEA. The product was then isolated from DMF using chloroform/water extraction. The reaction was monitored by TLC which showed purple spot with some close running rhodamine B derived impurities. Silica gel column chromatography was performed to purify OM49 and remove rhodamine with several attempts and using different solvents system. Firstly, 4:1 chloroform: ethyl acetate + 5% methanol solvent system was used. TLC was achieved for different fractions which showed that OM49 was not completely pure and there was some rhodamine B. Secondly, 9:1 chloroform: methanol was used and the result was better and there was less rhodamine B but OM49 was still contaminated by fluorescence. Finally, the product was subjected to column chromatography for a third purification using 4:1 chloroform: ethyl acetate + 5% methanol to ensure that all rhodamine B had been removed. After a third

purification, there was less rhodamine B derived fluorescence but the product was still fluorescent and not completely quenched.

After the attempted purification, the trityl group (Trt) was removed by adding trifluoroacetic acid (TFA) to OM49 and it was left overnight. The TLC showed that Trt had been removed successfully from OM49. Finally, the product was purified by repeated column chromatography using 9:1 chloroform: methanol solvent system. However, OM50 was still contaminated by background fluorescence after several purification attempts and the reason for this fluorescence is still unknown.

Finally, the structure of the target compound OM50 from the solid phase peptide was confirmed by the high-resolution electrospray (+) mass spectrum which clearly showed a signal at m/z 1076.4868 which corresponded to the expected molecular mass of 1076.4876 Da for cation (+). Also, there was a good correlation between the observed data and the theoretical isotope model for $C_{59}H_{66}N_9O_{11}$ cation (+) **Figure 2.32**. Therefore, this result confirms the successful synthesis of OM50 by solid phase. However, the presence of the major peak in the spectrum at m/z 810.4183 confirmed that the product was not pure and as yet the structure of the rhodamine derived fluorescent impurities not known as shown in **Figure 2.32**.

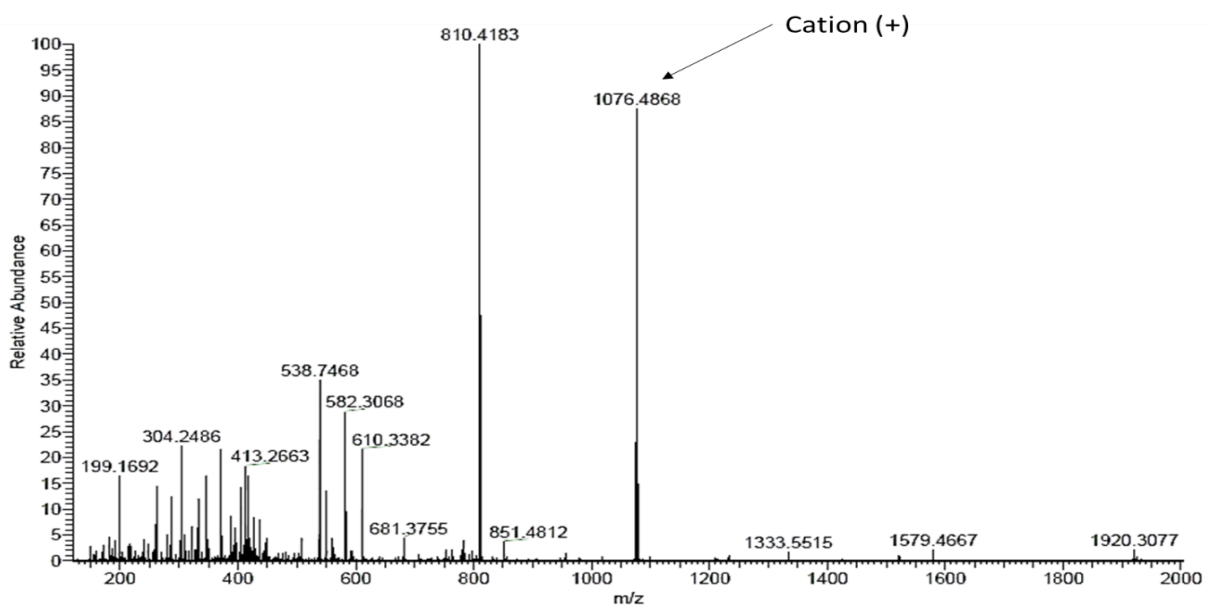


Figure 2.32: The mass spectrum for OM50 from solid phase peptide synthesis

2.3.7 FRET and legumain studies

After the structure and purity of OM50 was confirmed by mass spectrometry, the following experiment was carried out to detect that Gly-APA-AQ(4,8-di-OH) (NU:UB 51) was quenching the rhodamine B fluorophore. FRET is a distance dependent -transfer of energy from a rhodamine B (the donor), which is in an excited state, to an acceptor molecule NU:UB 51 by nonradiative dipol-dipole interaction (Taya *et al.*, 2018). Legumain assay buffer (50 mM MES hydrate, 250 mM NaCl, pH 5.0) was used in all absorbance and emission assays and ensured that all absorbance and emission assays were carried out at the same pH (pH 5) because this process could be pH sensitive.

2.3.7.1 UV-Visible absorption assays

2.3.7.2 Rhodamine B-Pro-Ala-Asn-OH and NU:UB 51

The maximum absorbance wavelength of Rho-Pro-Ala-Asn-OH was measured as it is the same compound that would be released upon cleavage of OM50 by legumain. **Figure 2.33** shows the UV-Visible absorption spectrum for the Rho-Pro-Ala-Asn-OH and NU:UB 51.

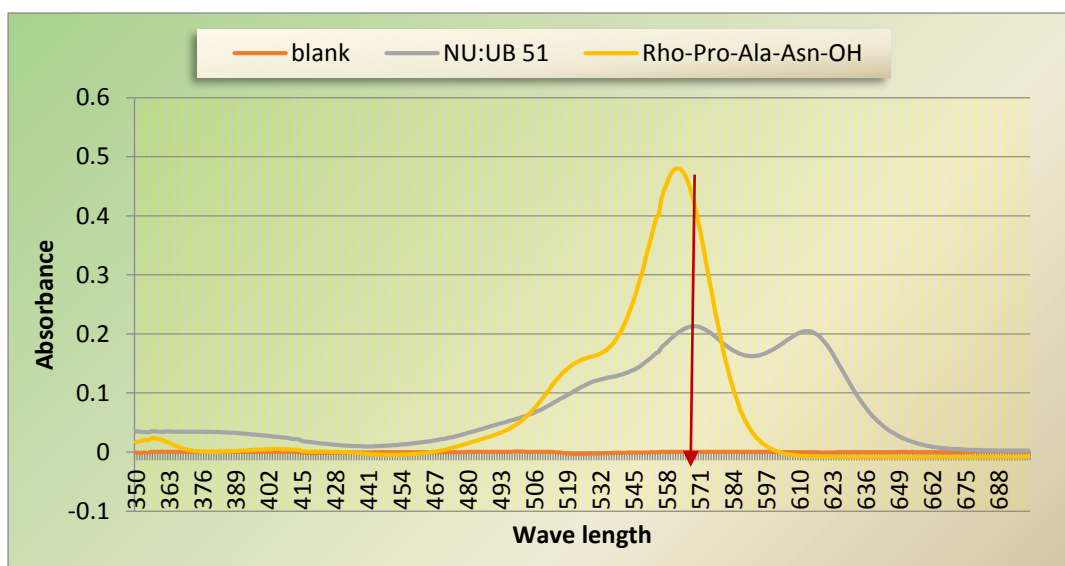


Figure 2.33: UV-Vis absorption assay of Rho B-Pro-Ala-Asn-OH and NU:UB 51. Concentration: 20 μ M of NU:UB 51 and 5 μ M of rho B-Pro-Ala-Asn- in legumain assay buffer (50 mM MES hydrate, 250 mM NaCl, pH 5.0) , Red arrow indicates the maximum absorbance

The maximum absorbance wavelength of the fluorophore was determined at 562 nm and then this was used as the excitation wavelength for the following fluorescence spectroscopy assays. Additionally, as the efficiency of the FRET was dependent on the overlap between the emission of the fluorophore (rhodamine B) and the absorbance of the acceptor NU:UB 51, it was important to characterize the absorbance of NU:UB 51. The maximum absorbance wavelength for NU:UB 51 was at 569 nm.

2.3.7.3 Fluorescence spectroscopy assays

The emission of Rho-Pro-Ala-Asn-Gly-APA-AQ(4,8-di-OH) (OM50) has been established by fluorescence assay to ensure that completely quenches the emission of Rho-Pro-Ala-Asn-OH when excited at the maximum wavelength 562 nm, due to the overlap of the absorbance of NU:UB 51 with the emission of the rhodamine B. The emission range of Rho-Pro-Ala-Asn-OH was determined when excited at a wavelength of 562 nm and is shown in **Figure 2.34**.

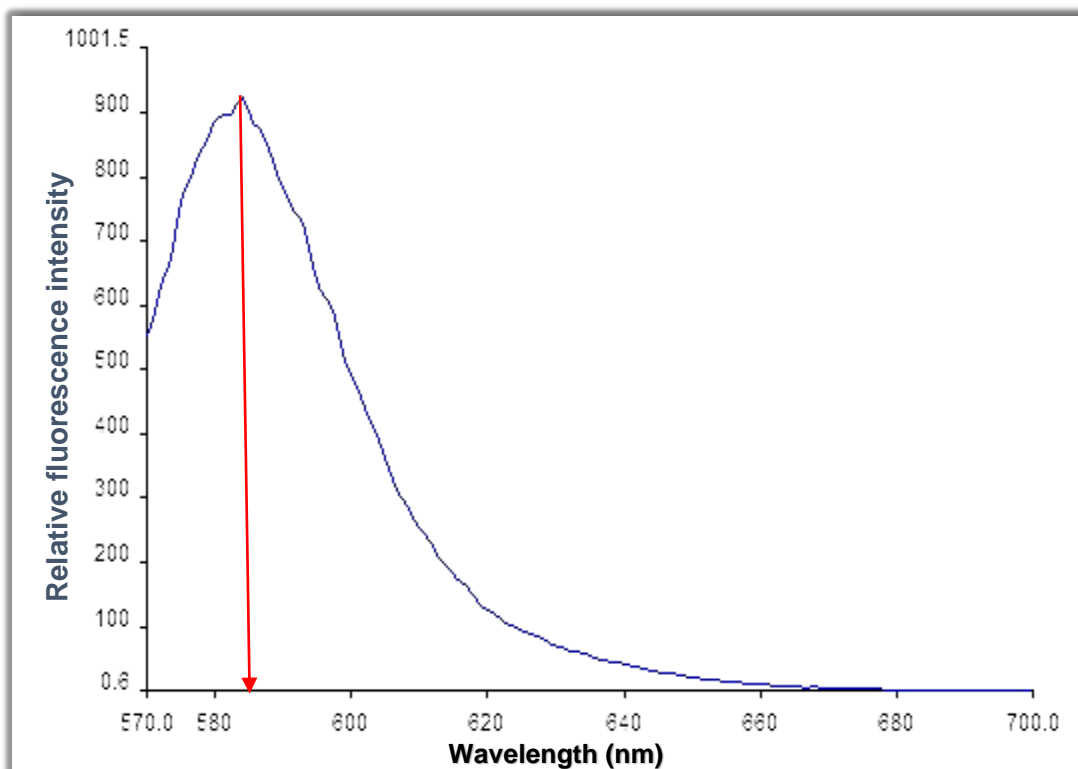


Figure 2.34: Fluorescence intensity spectrum of Rho-Pro-Ala-Asn-OH. Concentration: 0.5 μ M in legumain assay buffer (50 mM MES hydrate, 250 mM NaCl, pH 5.0). Excitation wavelength: 562 nm. Red arrow: maximum fluorescence intensity at 583 nm.

Rho-Pro-Ala-Asn-OH gave a strong fluorescence emission which reached a maximum at 583 nm as shown in **Figure 2.34** (indicated by red arrow). This value was the wavelength at which fluorescence would be expected to increase with the incubation of OM50 with legumain following cleavage of OM50 by legumain.

However, to determine whether or not there was a significant fluorescence emission by OM50 when compared with free fluorophore, the assay was carried out at a concentration of 0.5 μ M of OM50. The result indicates that OM50 emitted almost no fluorescence, as shown by a relative fluorescence intensity value of 3 (red line) when compared with the Rho-Pro-Ala-Asn-OH which was 921 at the same wavelength of 583 nm as shown in **Figure 2.35**.

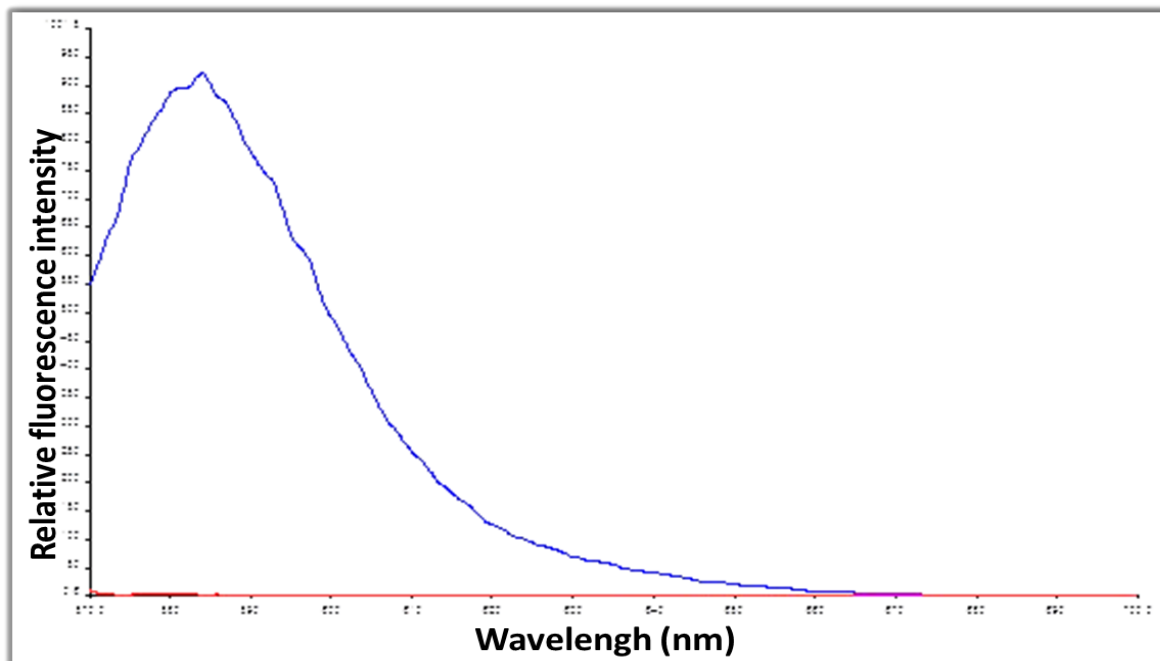


Figure 2.35: Fluorescence emission spectrum of OM50 (red line) compared with Rho-Pro-Ala-Asn-OH (blue line). Concentration 0.5 μ M each in legumain assay buffer. Excitation wavelength: 562 nm

As a result, it was concluded that rhodamine B fluorophore is completely quenched by and OM50 has an extremely low emission level which once cleaved by legumain would release a rhodamine B labelled tripeptide (fluorescence compound) with maximum fluorescence emission at 583 nm, permitting the detection and localization of the activated protease (*in vivo*) and the concurrently released NU:UB 51, which would exert its therapeutic effects (*in vivo*).

2.3.7.4 Incubation of OM50 with legumain

Human recombinant legumain at 37°C in legumain assay buffer (50 mM MES hydrate, 250 mM NaCl, pH 5.0) was used to investigate the quenching of the fluorogenic prodrug (OM50) and restoration of rhodamine B fluorescence upon incubation with legumain. The aim of this study was to indicate whether OM50 is a substrate for legumain or not. The ability of legumain to cleave at the C-terminal of asparagine will result in release of both rhodamine B (fluorescence) and NU:UB 51 as a toxic drug **Figure 2.36**.

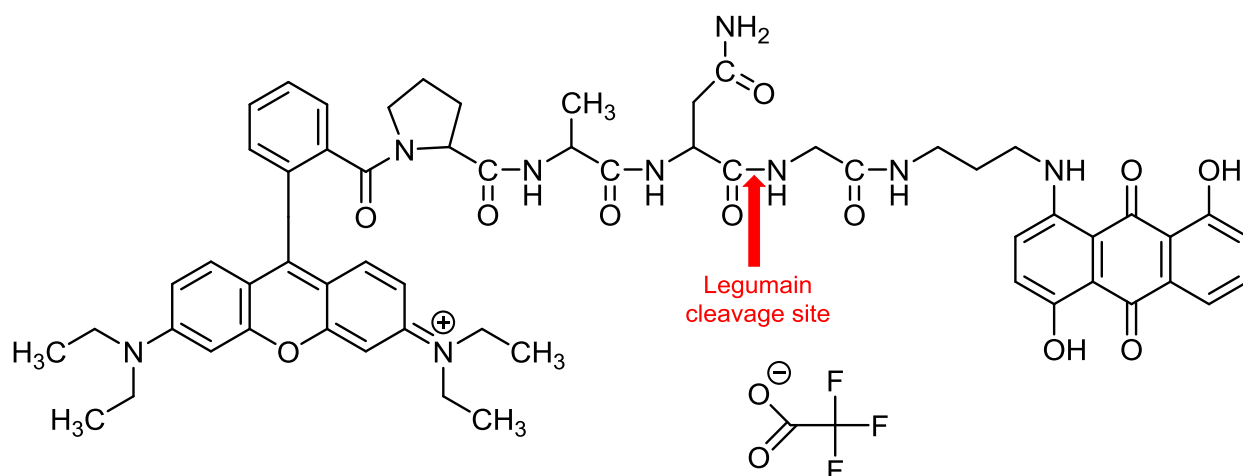


Figure 2.36: The cleavage site of legumain at the C-terminal of asparagine

The legumain was activated by incubation in activation buffer for 2 hours at 37°C and then it was diluted with legumain assay buffer (pH5). The fluorescence test was set for 2 hours at 37°C to detect how much fluorescence was released over time. **Figure 2.37** shows the fluorescence emission spectra of the incubation of OM50 with activated legumain for 2 hours. The fluorescence emission increased gradually over the first 65 minutes and then there was no further increase in fluorescence after 65 minutes which indicates that no more cleavage of OM50 was taking place. The results indicates that the fluorescence emission increased gradually over the first 65 minutes and then there was no further increase in fluorescence after 65 minutes which indicates that no more cleavage of OM50 was taking place.

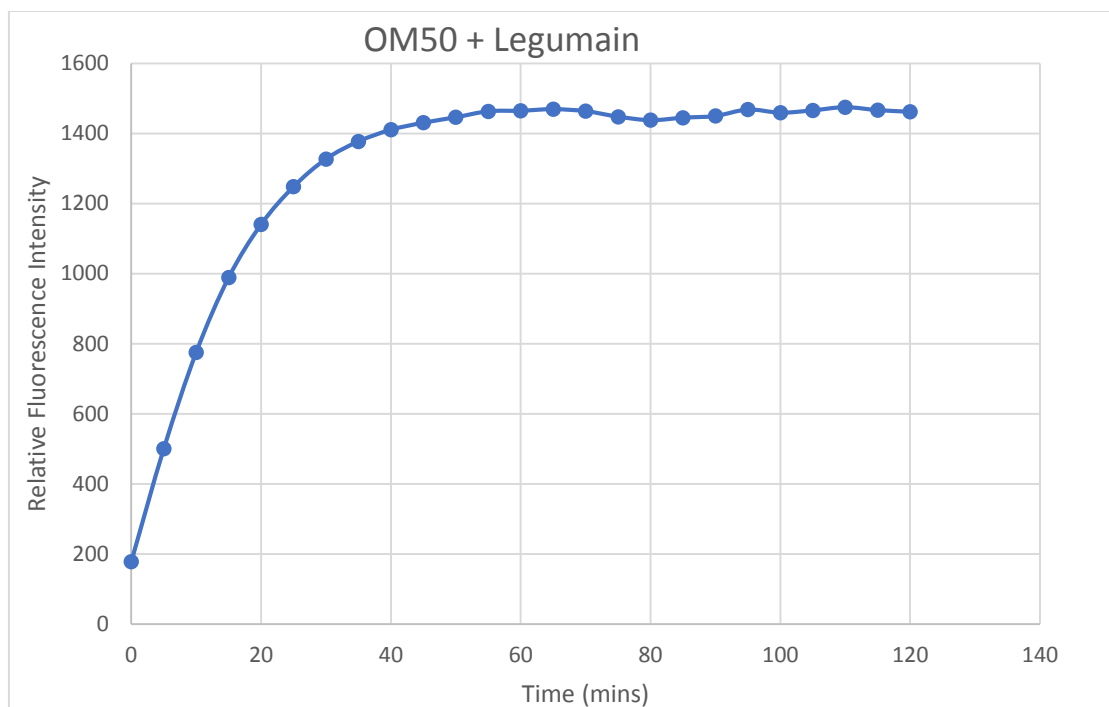


Figure 2.37: Cleavage of Prodrug OM50 by recombinant human legumain. Variation in RFI (Relative Fluorescence Intensity) with time for OM50 [Rho-Pro-Ala-Asn-Gly-APA-AQ(4,8-di-OH)] upon incubation with legumain (40 ng) in legumain assay buffer (50 mM MES hydrate, 250 mM NaCl, pH 5.0), 2 h.

Fluorescence intensity increased with the time verifying that cleavage of OM50 was taking place by legumain. The relative fluorescence as shown in **Figure 2.37** increased from ~300 (RFI) at 0 hours to ~1569 at 65 minutes resulting in a 5-fold increase in fluorescence.

2.3.8 Cellular uptake and localization

Confocal live cell imaging using a confocal microscope was performed to study the cellular uptake and localization of the prodrug Rho-Pro-Ala-Asn-Gly-APA-AQ(4,8-di-OH) (OM50) and active agent Gly-APA-AQ(4,8-di-OH) (NU:UB 51) in live colon carcinoma cells (HCT-116) in the presence of MitoTracker green FM (fluorescent dye for mitochondrial staining) and LysoTracker green DND26 (fluorescent dye for lysosome staining). **Figure 2.38** shows the cellular uptake of NU:UB 51 after 90 minutes of live cell imaging. The results confirmed that NU:UB 51 was detected in both mitochondria and

lysosomes. NU:UB 51 showed a clear staining HCT-116 cell line (**panel A**) and a clear yellow dots (**panel C**), which is the merge image for panel **A** (NU:UB 51) and **B** (MitoTracker Green FM and LysoTracker green DND26), confirming the colocalization of NU:UB 51 with mitochondria and lysosomes.

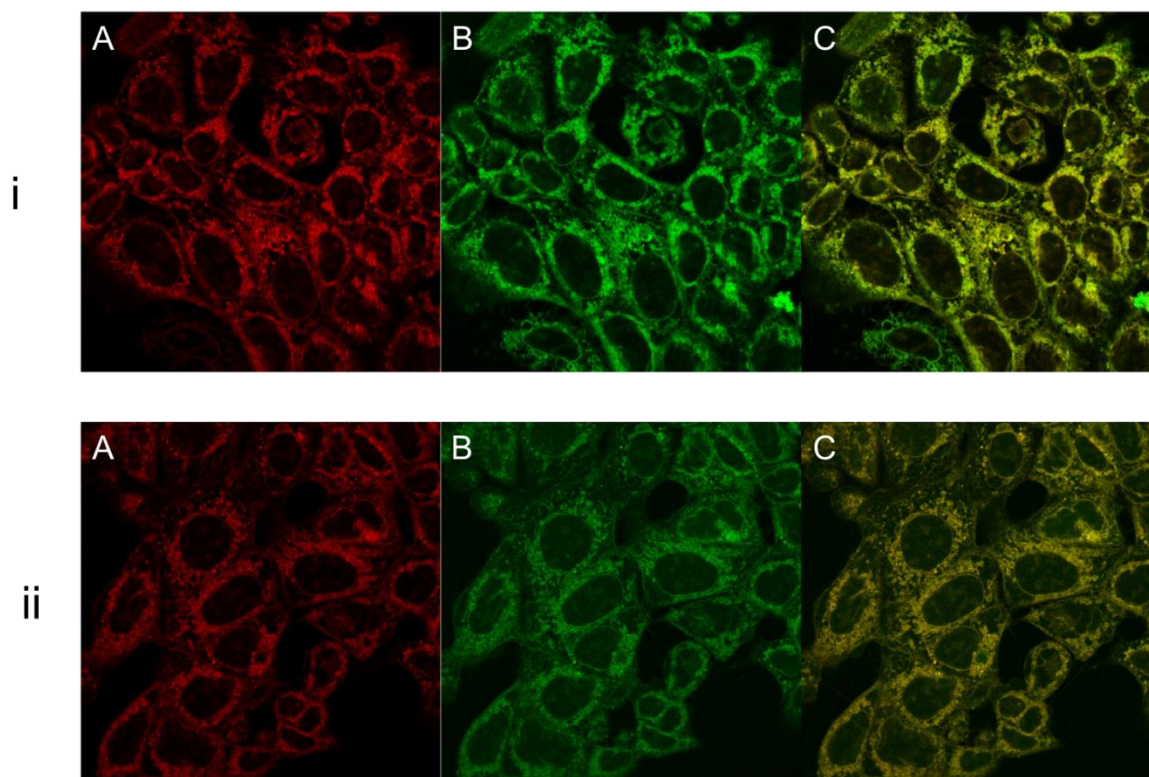


Figure 2.38: Localization of NU:UB 51 in HCT-116 cell. NU:UB 51(5 μM) localized to the mitochondria and lysosome within 90 min as measured by live cell imaging. The localisation of NU:UB 51 in mitochondria shown in (i) (A) NU:UB 51 stained with (B) MitoTracker Green FM and (c) merged image. The localisation of NU:UB 51 in lysosomes shown in (ii) (A) NU:UB 51 stained with (B) LysoTracker Green DND26 and (c) merged image. Images were captured at 63 x magnification.

However, **Figure 2.39** shows that the prodrug OM50 was not taken up by the cells and localized outside the cells after 90 min of live cell imaging. There was no localization of the OM50 within the mitochondria or lysosome. OM50 showed a clear staining HCT-116 cell line (**panel A**) and a clear red dots (**panel C**), which is the merge image for panel **A** (OM50) and **B** (LysoTracker green DND26), confirming that OM50 was not taken up by mitochondria or lysosome, indicating that OM50 localized extracellularly. In tumours, it has been reported that legumain is overexpressed extracellularly or located on the cell

surface of tumour cells (Guo *et al.*, 2013; Haugen *et al.*, 2015). Liu *et al.*, 2012, design and synthesized a legumain prodrug $\alpha\beta3$ inhibitor-NHAla-Ala-Asn-PABC-monomethylauristatin E (MMAE), which is upon the cleavage by legumain, MMAE bound to cell surface glycoprotein integrin $\alpha\beta3$ and induce cell death. They found that the prodrug was cleaved and activated by legumain on the cell surface and MMAE efficiency induced death of MDA-MB-435 human breast cancer (Liu *et al.*, 2012). Therefore, the overexpression of legumain extracellularly or on the cell surface would cleave the prodrug OM50 resulting in the release of cytotoxic NU:UB 51, which in turn could enter the cell and be localized either in the lysosomes or mitochondria as shown in **Figure 2.38**.

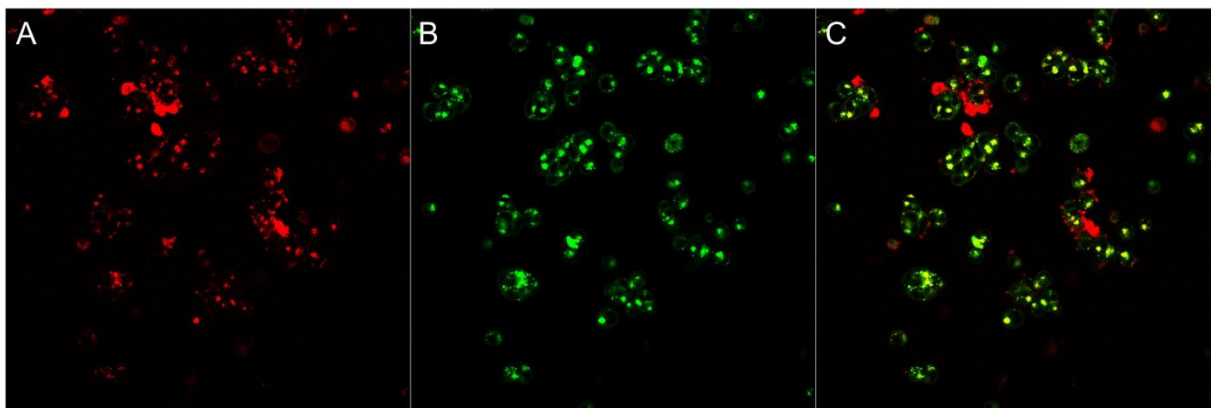


Figure 2.39: live cell imaging of OM50 in HCT-116 cell lines stained with LysoTracker Green DND26. The colocalization of OM50 with LysoTracker Green shows the localization of OM50 (1 μM) outside the cell with no localization in the mitochondria and lysosome within 90 min as measured by live cell imaging. (A) OM50, (B) LysoTracker Green DND26 and (C) merged image. Images were captured at 63 x magnification

2.3.9 **Conclusion**

The over expression of legumain in different types of cells, such as breast, colon and prostate cancers was used as a promising target for tumour activated prodrugs. The aim was to increase the drug selectivity and decrease the toxicity to the normal cells. The anthraquinone derivative Gly-APA-AQ(4,8-di-OH) (NU:UB 51) was used as the potent cytotoxic active agent and conjugated with legumain peptide substrate. The rhodamine B fluorophore was attached to the free amino group of the tripeptide legumain substrate (Pro-Ala-Asn) and the trityl protecting group was removed from the side chain of asparagine to afford the target fluorescently labeled prodrug Rho-Pro-Ala-Asn-Gly-APA-AQ(4,8-di-OH) (OM50).

In this project, two different synthetic strategies were adopted for the synthesis of the final target prodrug (OM50). The first route of synthesis of the target legumain substrate OM50 was solution phase peptide synthesis. A bis-hydroxylated propyl spaced glycine conjugate NU:UB 51 was first synthesized and the tripeptide was built on to the free amino group of glycine. The final step of the synthesis was the conjugation of rhodamine B with the free amino group of tripeptide. A good yield of OM50 was achieved (0.04 g) by solution phase synthesis and the prodrug was purified by column chromatography. The synthesis of the target compound OM50 was successful and the structure of the purified product was confirmed by mass spectrometry.

In a second approach, solid phase peptide synthesis was also considered. The tripeptide H₂N-Pro-Ala-Asn(Trt)-OH was synthesized by SPPS. Rhodamine B was then reacted with the free amino group of the tripeptide, whilst still on resin. The rhodamine labelled tripeptide was cleaved from the resin and reacted with NU:UB 51. The synthesis of the target compound OM50 was successful and the structure of OM50 was confirmed by mass spectrometry. However, the purification of the target product from this method was difficult and unsuccessful and there was an unknown (highly fluorescent) impurity with the main compound which should be identified in a future study. Therefore, according to the results from both solid phase and solution phase methods, it was better to synthesise the prodrug OM50 by solution phase peptide synthesis rather than solid phase.

The protection of the side chain of the asparagine, which should insert into the active site S1 pocket of legumain, was successful with no complications or byproducts such as the dehydration of the primary amide to a nitrile group. Therefore, the trityl group was the best choice as a protecting group of the asparagine side chain which was stable enough to withstand the coupling conditions and the action of the deprotecting agents such as piperidine, used for the removal of the Fmoc group. Mass spectrometry and TLC confirmed a very pure product and no evidence was found for byproducts from dehydration reaction of the asparagine side chain. In addition, the choice of protecting groups Fmoc and Boc group over other protecting groups was a good choice because the easier removal of these groups and easier chromatography due to their greater solubility over other groups.

The UV-visible absorption and fluorescence spectroscopy assays confirmed that the chromophore NU:UB 51 quenches fluorescence emitted by the rhodamine B. The overlap of the acceptor's (NU:UB 51) UV-visible absorption with the fluorescence emission spectrum of the rhodamine B was complete and the rationale design was valid and effective. Upon incubation of OM50 with recombinant human legumain there was an increase in fluorescence with time at an emission wavelength of 562 nm. This result gave a clear indication that OM50 was a good substrate for legumain because it clearly shows an increase in the fluorescence intensity upon incubation with recombinant human legumain with increasing time.

In addition, in this study, although rhodamine B was used as a carrier to aid cell permeability and subcellular localisation, herein, the confocal study showed that NU:UB 51 was not taken up at all into cells.. Also, the confocal studies showed clear localization of NU:UB 51 in both mitochondria and lysosomes. Therefore, cleavage of OM50 outside the cell by overexpressed legumain would result in release of the cytotoxic agent NU:UB 51, which could then enter the cell and localise in lysosomes or mitochondria which in turn, potentially causing lysosomal disruption or inhibition of both mitochondrial topoisomerase I or topoisomerase II.

Chapter 2

Experimental

2.4 Experimental

2.4.1 Synthesis of legumain targeted theranostic prodrug

Rho-Pro-Ala-Asn-Gly-APA-AQ(4,8-di-OH) (OM50)

2.4.1.1 Synthesis of anthraquinone spacer compound APA-AQ(4,8-di-OH) (NU:UB 59)

Leuco-1,4,5-trihydroxyanthraquinone (leuco-5-hydroxyquinizarin) (1 g, 3.87 mmol) was dissolved in CH₂Cl₂ (50 mL) and 1,3-diaminopropane (1 mL, 11.6 mmol) was added and heated at 40°C for 1.5 h. The product was then oxidized by aeration with the addition of triethylamine (Et₃N, 0.5 mL). The product NU:UB 59 (R_f 0.43) was then isolated by chloroform/water solvent extraction [general method A] and the organic extracts were left overnight to dry. Yield 30%, 0.5 g. The crude product was then used for further reaction without further purification.

TLC of the crude mixture (chloroform: methanol, 4:1): R_f 0.77 (green), 0.43 (purple) NU:UB 59, 0.90 (orange) 5-hydroxyquinizarin.

2.4.1.2 Synthesis of Boc-Gly-APA-AQ(4,8-di-OH) (NU:UB 51-Boc)

Boc-Gly-OH (0.42 g, 2.4 mmol) and PyBOP (1.248 g, 2.4 mmol) were dissolved in DMF (10 mL) and DIPEA (0.834 mL, 4.8 mmol) was added and allowed to react at rt for 15 min. The coupling agent and amino acid were then added to NU:UB 59 (0.5 g, 1.6 mmol) in DMF (5 mL) and allowed to react for 1.5 h. The product NU:UB 51-Boc was isolated from DMF using chloroform/water solvent extraction [general method A]. NU:UB 51-Boc was washed with sodium bicarbonate to remove any acidic impurities and it was dried using sodium sulphate anhydrous. The product was then filtered and applied to a silica gel chromatography column using neat CH₂Cl₂ at the beginning and then the polarity of the solvent was increased by using CH₂Cl₂: ethyl acetate + 6% methanol. Fractions

containing OM41 were filtered and evaporated to dryness. The crude product was then used for further reaction without solidification.

TLC of NU:UB 51-Boc (chloroform: methanol, 4:1): R_f 0.53 (purple) NU:UB 51-Boc.

2.4.1.3 Synthesis of Gly-APA-AQ(4,8-di-OH) [(NU:UB 51)]

The Boc-protected compound (OM41) was dissolved in trifluoroacetic acid (TFA) (5 mL) for 45 min. The solvent was evaporated and addition of diethyl ether (50 mL) gave a precipitate of NU:UB 51, which was filtered off and dried. Yield 45%, 0.25 g.

TLC of NU:UB 51 (chloroform: methanol, 4:1) R_f 0.08 (purple) NU:UB 51.

2.4.2 Synthesis of Synthesis of prodrug OM50, Rho-Pro-Ala-Asn-Gly-APA-AQ(4,8-di-OH), by solution phase peptide synthesis

2.4.2.1 Synthesis of Fmoc-Asn(Trt)-Gly-APA-AQ(4,8-di-OH) (OM43)

Fmoc-Asn(Trt)-OH (0.37 g, 0.62 mmol), PyBOP (0.312 g, 0.6 mmol) and HOBt (0.081 g, 0.6 mol) were dissolved in DMF (10 mL) and DIPEA (0.398 mL, 2.3 mmol) was added and allowed to react for 15 min then added to NU:UB 51 (0.25 g, 0.5 mmol) in DMF (5 mL) and was left at rt to react for 1.5 h. The product was separated from DMF using chloroform/water solvent extraction [general method A]. OM43 was applied to a silica gel chromatography column using neat chloroform initially and then more polar solvent chloroform: ethyl acetate + 5% methanol was used. OM43 was filtered and evaporated to dryness. The crude product was then used for further reaction without solidification.

TLC of OM43 (chloroform: methanol, 4:1) R_f 0.6 (purple) OM43, 0.11 (blue) NU:UB 51

HRMS (ESI) (+) m/z : 948.3609 (5%) $[M+H]^+$. Calculated for $[C_{57}H_{49}N_5O_9]^+$ 948.05; Found 948.3609.

2.4.2.2 Synthesis of Asn(Trt)-Gly-APA-AQ(4,8-di-OH) (OM44)

Piperidine in DMF (20% v/v) (10 ml) was added to OM43 to remove Fmoc group and allowed to react for 15 min. The reaction mixture was isolated using chloroform/water solvent extraction [general method A] and it was purified by silica gel column chromatography using neat chloroform to ensure that all Fmoc-piperidine was completely removed. The solvent was then changed to more polar solvent 4:1 chloroform: methanol + 10% methanol. OM44 was filtered and dried under vacuum and ether was added to aid in solidification of OM44. Yield 54%, 0.20 g.

TLC of OM44 (chloroform: methanol, 4:1) R_f 0.14 (purple) OM44.

2.4.2.3 Synthesis of Fmoc-Ala-Asn(Trt)-Gly-APA-AQ(4,8-di-OH) (OM45)

Fmoc-Ala-OH (0.15 g, 0.4 mmol), PyBOP (0.25 g, 0.4 mmol) and HOBt (0.067 g, 0.4 mmol) was dissolved in DMF (10 mL) and DIPEA (0.211 mL, 1.5 mmol) was added. After 15 min, Fmoc-Ala-OH and coupling agents was added to OM44 (0.20 g, 0.2 mmol) in DMF (5 mL) and allowed to react at rt for 1.5 h. OM45 was isolated using chloroform/water solvent extraction [general method A]. OM45 was filtered and the solvent was evaporated under vacuum. The crude product was then used for further reaction without solidification.

TLC of OM45 (chloroform: methanol, 4:1) R_f 0.48 (purple) OM45

2.4.2.4 Synthesis of Ala-Asn(Trt)-Gly-APA-AQ(4,8-di-OH) (OM46)

Fmoc group was removed from OM45 by adding 20% piperidine in DMF (10 mL) and allowed to react for 15 min. OM46 was isolated with chloroform/water solvent extraction [general method A]. OM46 was filtered and concentrated to low volume before applied to silica gel column chromatography using neat chloroform initially and then 4:1 chloroform: methanol +10% methanol was used. After that, the solvents were filtered and evaporated to dryness. OM46 was precipitated by adding ether and the product was filtered and collected. Yield 86%, 0.19 g.

TLC of OM46 (chloroform: methanol, 4:1) R_f 0.15 (purple) OM46

2.4.2.5 Synthesis of Fmoc-Pro-Ala-Asn(Trt)-Gly-APA-AQ(4,8-di-OH) (OM47)

Fmoc-Pro-OH (0.119 g, 0.3518 mmol) and PyClock (0.195 g, 0.3518 mmol) were dissolved in DMF (10 mL) and DIPEA (0.183 mL, 1.05 mmol) was added and allowed to react for 15 min at rt then added to OM46 (0.19 g, 0.234 mmol) in DMF (5 mL) and allowed to react for 1.5 h at rt. The reaction mixture was isolated from DMF using chloroform/water extraction [general method A]. The solvent was then evaporated under vacuum. The crude product was then used for further reaction without solidification.

TLC of OM47 (chloroform: methanol, 4:1) R_f 0.53 (purple) OM47.

2.4.2.6 Synthesis of Pro-Ala-Asn(Trt)-Gly-APA-AQ(4,8-di-OH) (OM48)

Piperidine in DMF (20% v/v) (10 mL) was added to remove Fmoc group and allowed to react for 15 min. The product was then isolated using chloroform/water solvent extraction [general method A] and it was purified by column chromatography using firstly neat CH_2Cl_2 to ensure that all Fmoc-piperidine was completely removed. After that, the solvent was changed to more polar solvent 4:1 CH_2Cl_2 : ethyl acetate + 10% methanol. OM48 was then filtered and dried under vacuum and diethyl ether was added to aid in solidification. Yield 66%, 0.14 g.

TLC of OM48 (chloroform: methanol, 9:1) R_f 0.17 (purple) OM48.

2.4.2.7 Synthesis of Rho-Pro-Ala-Asn(Trt)-Gly-APA-AQ(4,8-di-OH) (OM49)

Rhodamine B (0.070 g, 0.14 mmol), PyClock (0.111 g, 0.2 mmol) were dissolved in DMF (10 mL) and DIPEA (0.088 mL, 0.508 mmol) was added and allowed to react for 15 min then added to OM48 (0.14 g, 0.15 mmol) in DMF (5 mL) and allowed to react for 1 h. The reaction mixture was separated from DMF using chloroform/water extraction [general method A] and filtered. The filtrate was concentrated to low volume and applied to silica

gel column chromatography using 4:1 chloroform: ethyl acetate + 5% methanol. For the second column chromatography purification, 4:1 chloroform: ethyl acetate +5% methanol. However, the percentage of methanol was increased to 15% after all pink color (rhodamine B) has been removed. For third column chromatography purification, 9:1 chloroform: methanol was used. The solvents were evaporated under vacuum. The crude product was then used for further reaction without solidification.

TLC of OM49 (chloroform: methanol, 9:1) R_f 0.33 (purple) OM49.

2.4.2.8 Synthesis of Rho-Pro-Ala-Asn-Gly-APA-AQ(4,8-di-OH) (OM50)

Trifluoroacetic acid (TFA) (5 mL) was added to OM49 and allowed to react overnight at rt to remove Trityl group. After that, the product was purified by silica gel column chromatography using 9:1 chloroform: methanol solvent system. The solvents were evaporated under vacuum and ether was added to precipitate OM50. The solid OM50 was then filtered and collected. Yield 25%, 0.04 g.

TLC of OM50 (chloroform: methanol 6:1) R_f 0.33 (purple) OM50.

HRMS (ESI) (+) m/z : 1076.4855 (100%). Calculated for $[C_{59}H_{63}N_6O_7]^+$ 1077.23; Found 1076.4855 (M+H)⁺.

2.4.3 Synthesis of the target compound Rho-Pro-Ala-Asn-Gly-APA-AQ(4,8-di-OH) (OM50) by solid phase peptide synthesis

2.4.3.1 Resin swelling

Fmoc-Asn(Trt)-Novasyn TGT (1 g, 0.3 mmol/g) was transferred to a solid phase peptide synthesis vessel, CH_2Cl_2 (10 mL/g of resin) was added and was shaken for 1 h. CH_2Cl_2 was drained off and the resin was washed with DMF two times.

2.4.3.2 Fmoc deprotection

Piperidine in DMF (20% v/v) (~10 mL/g of resin) was added to the resin and shaken for 10 min each time (x2). The resin was washed with DMF three times. The successful removal of Fmoc group was indicated by red resin beads in colour test.

2.4.3.3 Colour test

A small number of resin beads were transferred to a small sample vial. Few drops of HZ22 (in DMF) was added to the resin and allowed the mixture to react at rt for 15 min. A few drops of CH₂Cl₂ were added to dilute the mixture. The mixture was then filtered using Whatman No. 1 filter paper and red beads were observed if there is a free amino group (after Fmoc deprotection) and clear beads if the amino group was protected by the Fmoc group.

2.4.3.4 Peptide coupling and Fmoc deprotection addition of alanine residue

Fmoc-Ala-OH (0.186 g, 0.6 mmol), PyClock (0.315 g, 0.57 mmol), HOBt (0.071 g, 0.57 mmol) and DIPEA (0.312 mL, 1.8 mmol) were dissolved in DMF (10 mL). The solution was transferred to the SPPS vessel and shaken for 50 min. After 50 min, the solution was drained off and additional coupling agents and Fmoc-Ala-OH were added and shaken for another 50 min. The solution was drained off and was washed with DMF (3x5 mL). A positive color test was achieved (red beads). The Fmoc-Ala-Asn(Trt)-resin was then deprotected by adding 20% piperidine in DMF (10 mL) and ready for the coupling of next amino acid.

2.4.3.5 Peptide coupling and Fmoc deprotection: addition of proline residue

Fmoc-Pro-OH (0.2022 g, 0.6 mmol) was coupled to the Ala-Asn(Trt)-resin by the same procedure as above (**section 2.4.3.4**).

2.4.3.6 Synthesis of Rho-Pro-Ala-Asn(Trt)-resin

Rhodamine B (0.215 g, 0.448 mmol) and PyClock (0.249 g, 0.449 mmol) were dissolved in DMF (10 mL) and DIPEA (0.156 mL, 0.897 mmol) was added and then the solution was transferred to the SPPS vessel and shaken for 1 h. After 1 h, the solution was drained off and the same quantity of rhodamine B, PyClock and DIPEA were added and shaken for another 1 h. After that, the solution was drained off and the resin was washed 3 times with DMF and several times with CH₂Cl₂.

2.4.3.7 Rho-Pro-Ala-Asn(Trt)-resin cleavage

A 0.5% trifluoroacetic acid in 100 mL CH₂Cl₂ solution was prepared and 10 mL of the solution was added to the vessel, shaken and drained quickly to avoid the removal of Trityl group. This process was repeated until no pink color was coming out from the vessel. Triethylamine (base) was added to make the filtrates neutral. The filtrates were transferred into a round bottomed flask and evaporated to dryness under vacuum. Diethyl ether was added to precipitate the product, however, as the solvent does mix with diethyl ether therefore, 1,4-dioxane was added and then ether was added and it was left overnight at 4°C to precipitate the product. The product was then dried and collected. Yield 0.19 g.

HRMS (ESI) (+) m/z: 967.4752 (55%). Calculated for [C₅₉H₆₃N₆O₇]⁺ 967.4753; Found 967.4752 cation (+).

2.4.3.8 Synthesis of Rho-Pro-Ala-Asn(Trt)-Gly-APA-AQ(4,8-di-OH) (OM49)

Rho-Pro-Ala-Asn(Trt)-OH (0.156 g, 0.14 mmol) and HATU (0.053 g, 0.13 mmol) was dissolved in DMF (10 mL) and DIPEA (0.0754 mL, 0.43 mmol) was added and allowed to react at rt for 15 min. The solution was then added to NU:UB 51 (0.07 g, 0.145 mmol) in DMF (5mL) and allowed to react for 1 h. After 1 h, the product was isolated from DMF using chloroform/water solvent extraction [general method A]. The attempted purification of the product was carried out 3 times by column chromatography using 4:1 chloroform:

ethyl acetate, 9:1 chloroform: methanol and 4:1 chloroform: ethyl acetate + 5% methanol Sequentially.

TLC of OM49 (chloroform: methanol, 9:1) R_f 0.53 (purple) OM49, 0.46 (pink) Rho-Pro-Ala-Asn(Trt)-OH

2.4.3.9 Synthesis of Rho-Pro-Ala-Asn-Gly-APA-AQ(4,8-di-OH) (OM50)

Trifluoroacetic acid (5 mL) was added to OM49 and it was left overnight at rt to remove Trityl group. After that, the product was purified by silica gel column chromatography using 9:1 chloroform: methanol solvent system. The solvents were evaporated and ether was added to aid in solidification. The solid OM50 was then filtered and collected. The compound was dissolved in ethanol (100 μ L) and applied to a thick layer chromatography plate (20cm \times 20cm \times 0.1cm) and the plate was developed using chloroform: methanol, 4:1 as the running solvent. The purple band was scraped from the plate and the product extracted into methanol, filtered, evaporated and dried.

TLC of OM50 (chloroform: methanol, 9:1) R_f 0.24 (purple) OM50.

HRMS (ESI) (+) m/z: 1076.4868 (87%). Calculated for [C₅₉H₆₆N₉O₁₁]⁺ 1077.23; Found 1076.4868 (M+H)⁺.

2.4.4 UV-visible absorption assay

2.4.4.1 Materials

Legumain assay buffer: 50 mM MES hydrate (Sigma, M2933), 250 mM NaCl, pH 5.0; Gly-APA-AQ(4,8-di-OH) (NU:UB 51) and Rho-Pro-Ala-Asn-OH 1mg/mL stock in DMSO ;3 mL cuvettes.

2.4.4.2 Method

UV-visible absorption spectra of Rho-Pro-Ala-Asn-OH and a bis-hydroxylated propyl spaced glycine conjugate (NU:UB 51) was recorded on a DU 800 spectrophotometer, 3 mL cuvettes. The final concentration of Rho-Pro-Ala-Asn-OH and NU:UB 51 was 20 μ M in legumain assay buffer and the volume was 3000 μ L. The blank legumain assay buffer was 3 mL. The wavelength scan was selected and the wavelength range was set between 350.0 to 700.0 nm and scan speed was set at 1200 nm/min.

2.4.5 Fluorescence spectroscopy assay

2.4.5.1 Materials

Legumain assay buffer: 50 mM MES hydrate (Sigma, M2933), 250 mM NaCl, pH 5.0; Rho-Pro-Ala-Asn-Gly-APA-AQ(4,8-di-OH) (OM50) and Rho-Pro-Ala-Asn-OH 1 mg/mL stock in DMSO; 3 mL cuvettes.

2.4.5.2 Methods

Perkin Elmer LS50B luminescence spectrometer was used to measure the fluorescence spectra for OM50 and Rho-Pro-Ala-Asn-OH. The maximum excitation wavelength for Rho-Pro-Ala-Asn-OH was found to be at 562 nm. The emission was measured in the wavelength range between 570 nm and 700 nm; Ex slit: 5.5 nm, Em slit: 5.5 nm and scan speed 700 nm/min.

A solution of Rho-Pro-Ala-Asn-OH concentration 100 μ M was made from 1 mg/mL stock solution. 15 μ L of this solution was mixed with 2985 μ L of legumain assay buffer to produce a final solution of (3000 μ L, 0.5 μ M) in the cuvette. In addition, a solution of OM50 concentration 100 μ M was also prepared from 1 mg/mL stock solution and 15 μ L of this solution was mixed with 2985 μ L of assay buffer to produce a final product of (3000 μ L, 0.5 μ M) in the cuvette. The assay of both Rho-Pro-Ala-Asn-OH and OM50 was run

separately, however, fluorescence intensity measurements were plotted on the same graph to allow for more simplistic comparison between both of them.

2.4.6 Fluorescence spectroscopy assay of OM50 with recombinant human legumain

2.4.6.1 Materials

Activation buffer: 50 mM Sodium Acetate, 100 mM NaCl, pH 4.0; Recombinant human legumain (R&D systems, 2199-CY-010); Assay buffer: 50 mM MES hydrate (Sigma, M2933), 250 mM NaCl, pH 5.0; Substrate: Probe OM50, 1mg/mL stock in DMSO; Fluorophore: Rho-Pro-Ala-Asn-OH, 1mg/mL stock in DMSO then diluted to 100 μ M in assay buffer; F16 Black Maxisorp 96 well Plate; FluoStar Omega multi-mode Microplate Reader.

2.4.6.2 Method

Activation buffer (100 μ L) (pH 4) was added to recombinant human legumain (10 μ g) and stored at -78°C . aliquot was incubated in a water bath for 2 h at 37°C then diluted to 1 ng/ μ L in assay buffer (pH 5).

	1	2	3	4
E	B	B+R	B+OM50	B+OM50+L
F	B	B+R	B+OM50	B+OM50+L
G	B	B+R	B+OM50	B+OM50+L

Table 2.1: Arrangement on black 96-well plate for Fluorimetric Assay

As shown in **Table 2.1**, in each well:

E1-G1 100 μ L assay buffer (B)

E2-G2 90 μ L assay buffer (B) + 10 μ L 100 μ M Rho-Pro-Ala-Asn-OH (R)

E3-G3 98.8 μL assay buffer (B) + 1.2 μL 841 μM fluorogenic probe OM50

E4-G4 58.9 μL assay buffer (B) + 1.2 μL 841 μM fluorogenic probe OM50 + 40 μL 1 ng/ μL Legumain stock solution (L)

The final concentrations in each well are: 10 μM of Rho-Pro-Ala-Asn-OH (E2-G2), 10 μM of OM50 (E3-G3 + E4-G4) and 40 ng of legumain (E4-G4).

Emission spectra were recorded at 5 min intervals on a FluoStar Omega multi-mode Microplate Reader. The emission was measured in the wavelength range between 544 nm and 590 nm. Fluorescence intensity measurements were plotted on the same graph to allow for more simplistic differentiation between them.

2.4.7 Confocal microscopy

2.4.7.1 Materials

HCT-116 (Human colon carcinoma), RPMI 1640 medium containing phenol red; sterile NaCl; 35 mm glass bottomed micro well dish (Ibidi/Thistle Scientific); compounds: Gly-APA-AQ(4,8-di-OH) (NU:UB 51) and Rho-Pro-Ala-Asn-Gly-APA-AQ(4,8-di-OH) (OM50). LysoTracker Green DND 26 probe and MitoTracker Green FM probe. Live cell imaging was performed using Zeiss LSM800 confocal laser scanning microscope with HCX PL APO lambda blue (63.0 x 1.4 oil objective). Lasers used were: diode (405 nm), Argon (458 nm, 488 nm and 514 nm), HeNe (543 nm), HeNe (543 nm), HeNe (594 nm) and HeNe (633 nm).

2.4.7.2 Method

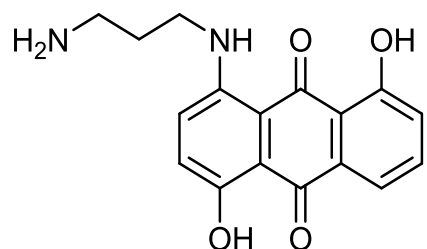
Stock solutions of tested compounds (1 mg/mL) were prepared in DMSO. HCT-116 (2 x 10⁵) were seeded in 35 mm glass bottomed micro well dish and incubated for 24 h. Cells were washed with PBS x3. For the LysoTracker Green DND 26, a solution of dye (60 nM) was added to the cell culture medium and incubated at 37°C for 20 min. After 20 min the

medium was removed and the cells were washed with sterile NaCl. Then tested compound solution was applied to cell culture medium and were imaged live using a Zeiss LSM800 confocal laser scanning microscope. For MitoTracker Green FM, a solution of dye (50 nM) was added to the cell culture medium and incubated at 37°C for 20 min. After 20 min the medium was removed and the cells were washed with sterile NaCl. Then tested compound solution was applied to cell culture medium and were imaged live using a Zeiss LSM800 confocal laser scanning microscope. Lens used was a 63.0 x 1.4 oil-immersion objective. Image analysis (field of view) was performed using Image J software.

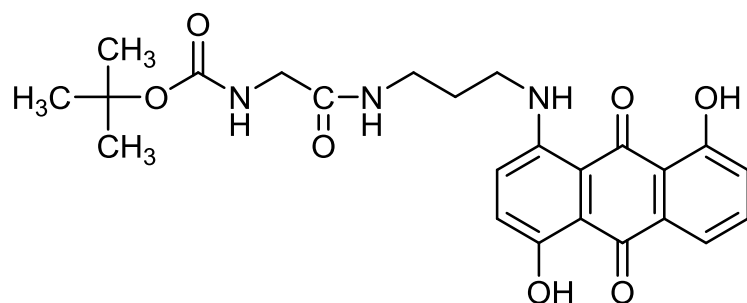
Chapter 2

Structure library

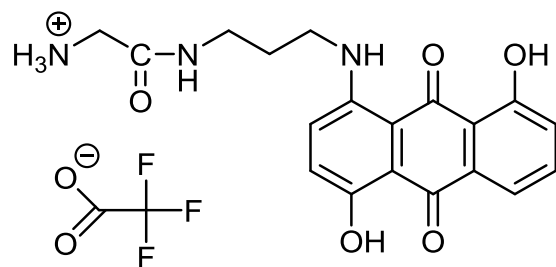
2.5 Structure library



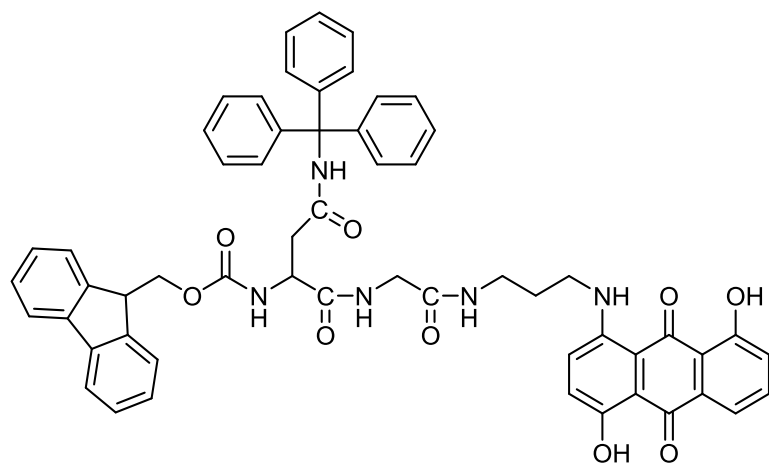
APA-AQ(4,8-di-OH) (NU:UB 59)



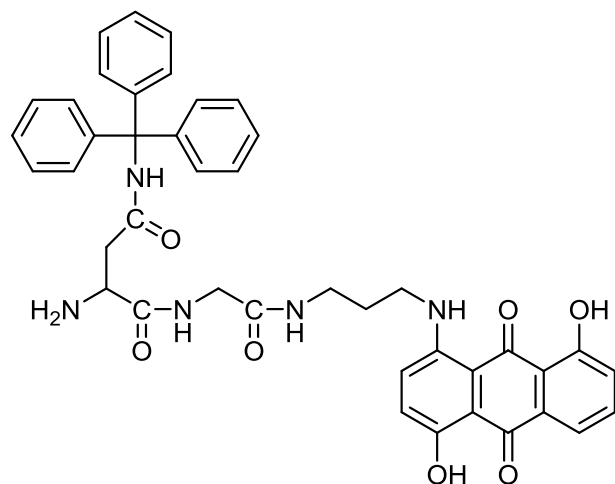
Boc-Gly-APA-AQ(4,8-di-OH) (NU:UB 51-Boc)



Gly-APA-AQ(4,8-di-OH) (NU:UB 51)

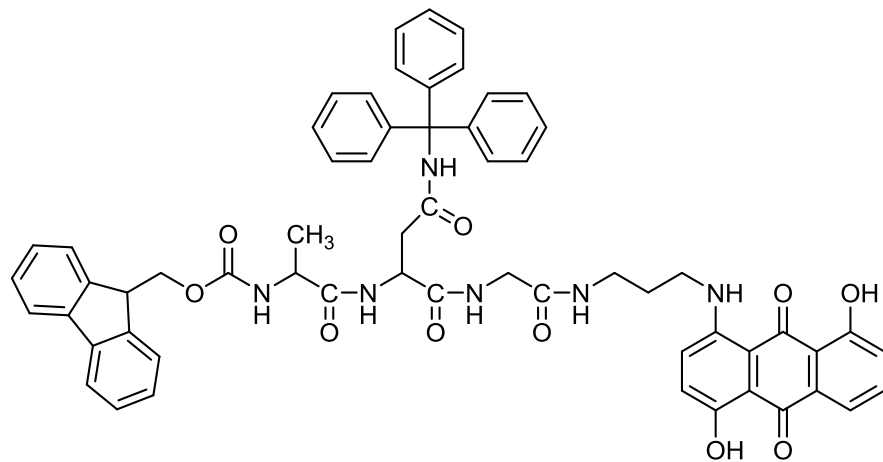


Fmoc-Asn(Trt)-Gly-APA-AQ(4,8-di-OH) (OM43)

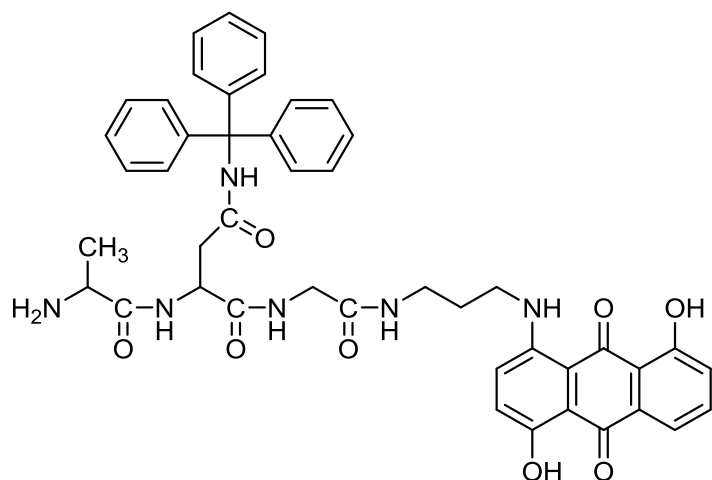


(OM44)

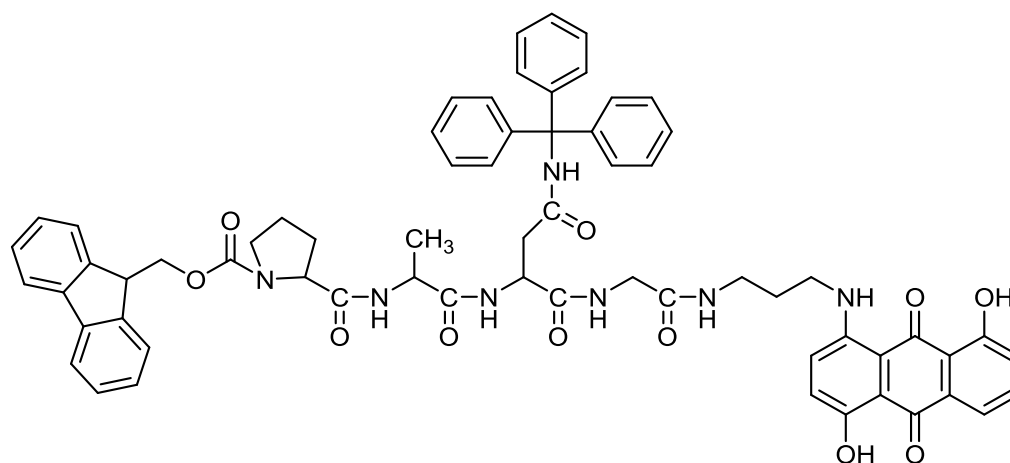
Asn(Trt)-Gly-APA-AQ(4,8-di-OH) (OM44)



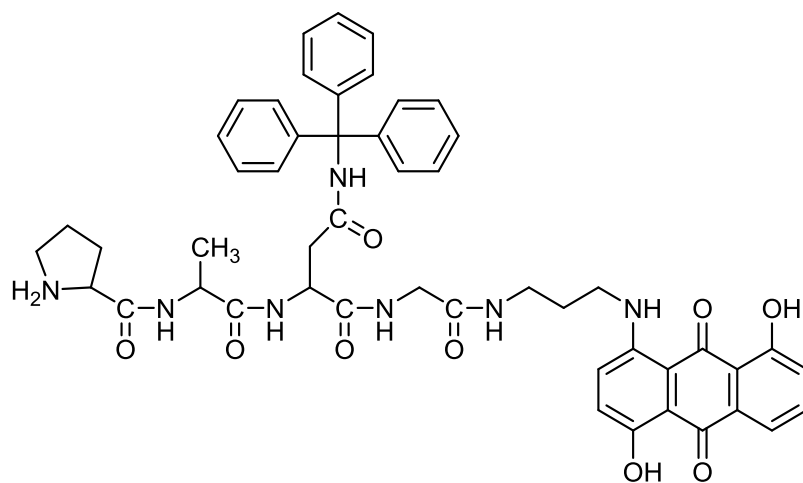
Fmoc-Ala-Asn(Trt)-Gly-APA-AQ(4,8-di-OH) (OM45)



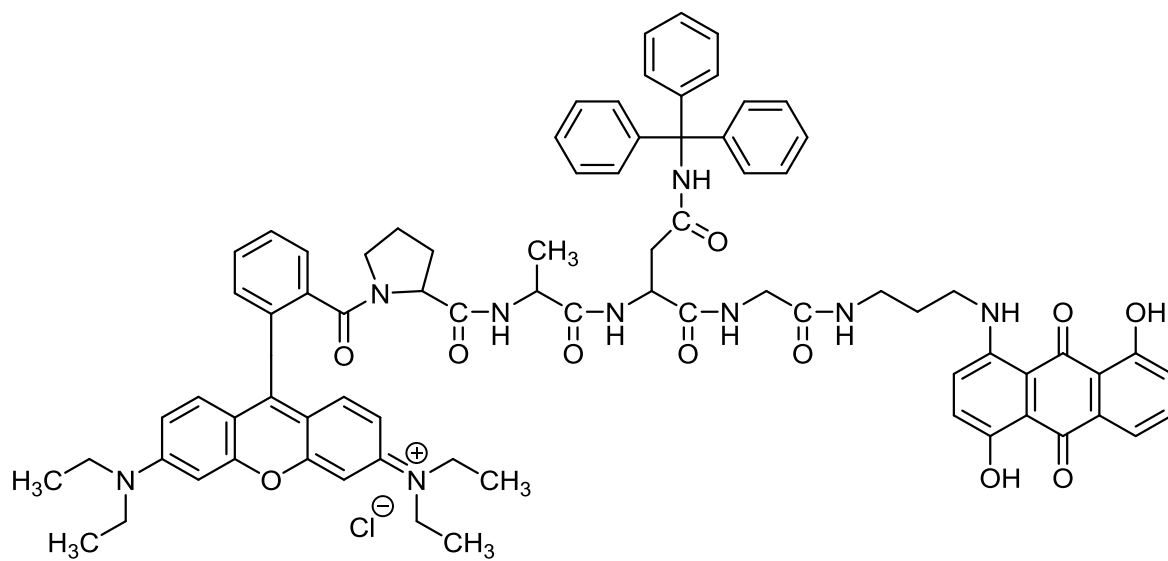
Ala-Asn(Trt)-Gly-APA-AQ(4,8-di-OH) (OM46)



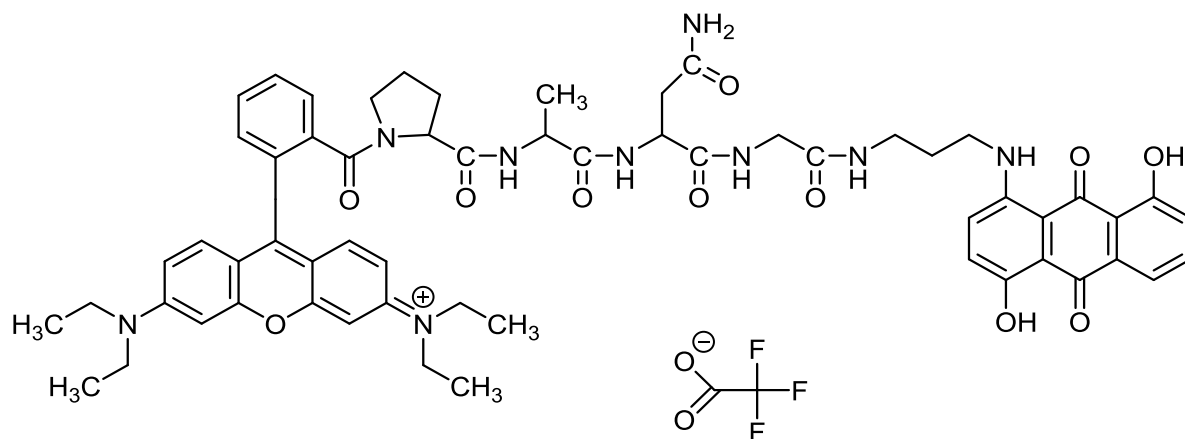
Fmoc-Pro-Ala-Asn(Trt)-Gly-APA-AQ(4,8-di-OH) (OM47)



Pro-Ala-Asn(Trt)-Gly-APA-AQ(4,8-di-OH) (OM48)



Rho-Pro-Ala-Asn(Trt)-Gly-APA-AQ(4,8-di-OH) (OM49)



Rho-Pro-Ala-Asn-Gly-APA-AQ(4,8-di-OH) (OM50)

2.6 References

- Adhikari, A. and Mahar, K. S. (2016) 'DNA targeted anthraquinone derivatives: An important anticancer agents', *International Journal of Pharmacy and Pharmaceutical Sciences*, **8**(6), pp. 17–25.
- Aftab, S., Shah, A., Nadhman, A., Kurbanoglu, S., Aysil Ozkan, S., Dionysiou, D. D., Shukla, S. S. and Aminabhavi, T. M. (2018) 'Nanomedicine: An effective tool in cancer therapy', *International Journal of Pharmaceutics*, **540**(1–2), pp. 132–149. doi: 10.1016/j.ijpharm.2018.02.007.
- Agostinis, P., Berg, K., Cengel, K. a, Foster, T. H., Girotti, A. W., Gollnick, S. O., Hahn, S. M., Hamblin, M. R., Juzeniene, A., Kessel, D., Korbelik, M., Moan, J., Mroz, P., Nowiz, D., Piette, J., Willson, B. C. and Golab, J. (2011) 'Photodynamic Therapy of Cancer : An Update', *American Cancer Society*, **61**, pp. 250–281. doi: 10.3322/caac.20114.Available.
- Al-Otaibi, J. S., Teesdale Spittle, P. and El Gogary, T. M. (2017) 'Interaction of anthraquinone anti-cancer drugs with DNA:Experimental and computational quantum chemical study', *Journal of Molecular Structure*, **1127**, pp. 751–760. doi: 10.1016/j.molstruc.2016.08.007.
- Albericio, F. (2008) 'PyClock, the phosphonium salt derived from 6-Cl-HOBt', *Chimica Oggi*, **26**(4), pp. 10–12.
- Alonso, A., Almendral, M. J., Curto, Y., Criado, J. J., Rodríguez, E. and Manzano, J. L. (2006) 'Determination of the DNA-binding characteristics of ethidium bromide, proflavine, and cisplatin by flow injection analysis: Usefulness in studies on antitumor drugs', *Analytical Biochemistry*, **355**(2), pp. 157–164. doi: 10.1016/j.ab.2006.06.004.
- Ambudkar, S. V, Dey, S., Hrycyna, C. A., Ramachandra, M., Pastan, I. and Gottesman, M. M. (1999) 'Biochemical, cellular, and pharmacological aspects of the multidrug transporter', *Annual Review of Pharmacology and Toxicology*, **39**(1), pp. 361–398. doi: 10.1146/annurev.pharmtox.39.1.361.

Ammirati, E. and Fogacci, F. (2017) 'Clinical relevance of biomarkers for the identification of patients with carotid atherosclerotic plaque: Potential role and limitations of cysteine protease legumain', *Atherosclerosis*, **257**, pp. 248–249. doi: 10.1016/j.atherosclerosis.2017.01.003.

Anderson, S., Bankier, A. T., Barrell, B. G., de Bruijn, M. H. L., Coulson, A. R., Drouin, J., Eperon, I. C., Nierlich, D. P., Roe, B. A., Sanger, F., Schreier, P. H., Smith, A. J. H., Staden, R. and Young, I. G. (1981) 'Sequence and organization of the human mitochondrial genome', *Nature*, **290**, pp. 457–465. doi: 10.1038/290457a0.

Apostolova, N. and Victor, V. M. (2015) 'Molecular Strategies for Targeting Antioxidants to Mitochondria: Therapeutic Implications', *Antioxidants & Redox Signaling*, **22**(8), pp. 686–729. doi: 10.1089/ars.2014.5952.

Arroyo-crespo, J. J., Armiñán, A., Charbonnier, D., Balzano-nogueira, L., Huertas-lópez, F., Martí, C., Tarazona, S., Forteza, J., Conesa, A. and Vicent, M. J. (2018) 'Tumor microenvironment-targeted poly-L-glutamic acid-based combination conjugate for enhanced triple negative breast cancer treatment', *Biomaterials*, **186**, pp. 8–21. doi: 10.1016/j.biomaterials.2018.09.023.

Bailly, C., Routier, S., Bernier, J. L. and Waring, M. J. (1996) 'DNA recognition by two mitoxantrone analogues: Influence of the hydroxyl groups', *FEBS Letters*, **379**(3), pp. 269–272. doi: 10.1016/0014-5793(95)01528-0.

Bajjuri, K. M., Liu, Y., Liu, C. and Sinha, S. C. (2011) 'The Legumain Protease-Activated Auristatin Prodrugs Suppress Tumor Growth and Metastasis without Toxicity', *ChemMedChem.*, **6**(1), pp. 54–59. doi: 10.1002/cmdc.201000478.The.

Behrendt, R., White, P. and Offer, J. (2016) 'Advances in Fmoc solid-phase peptide synthesis', *Journal of Peptide Science*, **22**(1), pp. 4–27. doi: 10.1002/psc.2836.

Beija, M., Afonso, C. A. M. and Martinho, J. M. G. (2009) 'Synthesis and applications of Rhodamine derivatives as fluorescent probes', *Chemical Society Reviews*, **38**, p. 2410. doi: 10.1039/b901612k.

Bellosillo, B., Colomer, D., Pons, G. and Gil, J. (1998) 'Mitoxantrone, a topoisomerase II inhibitor, induces apoptosis of B- chronic lymphocytic leukaemia cells', *British Journal of Haematology*, **100**(1), pp. 142–146. doi: 10.1046/j.1365-2141.1998.00520.x.

Bhuniya, S., Maiti, S., Kim, E.-J., Lee, H., Sessler, J. L., Hong, K. S. and Kim, J. S. (2014) 'An Activatable Theranostic for Targeted Cancer Therapy and Imaging', *Angewandte Chemie International Edition*, **53**(17), pp. 4469–4474. doi: 10.1002/anie.201311133.

Bielski, E. R., Zhong, Q., Brown, M. and Da Rocha, S. R. P. (2015) 'Effect of the Conjugation Density of Triphenylphosphonium Cation on the Mitochondrial Targeting of Poly(amidoamine) Dendrimers', *Molecular Pharmaceutics*, **12**(8), pp. 3043–3053. doi: 10.1021/acs.molpharmaceut.5b00320.

Birtalan, E., Rudat, B., Kolmel, D. K., Fritz, D., Vollrath, S. B. L., Schepers, U. and Brase, S. (2011) 'Investigating rhodamine B-labeled peptoids: Scopes and limitations of its applications', *Biopolymers*, **96**(5), pp. 694–701. doi: 10.1002/bip.21617.

Biswas, S., Dodwadkar, N. S., Deshpande, P. P. and Torchilin, V. P. (2012) 'Liposomes Loaded with Paclitaxel and Modified with Novel Triphenylphosphonium-PEG-PE Conjugate Possess Low Toxicity, Target Mitochondria and Demonstrate Enhanced Antitumor Effects In Vitro and In Vivo', *Journal of Controlled Release*, **159**(3), pp. 393–402. doi: 10.1016/j.jconrel.2012.01.009.Liposomes.

Bogman, K., Peyer, A. K., Török, M., Küsters, E. and Drewe, J. (2001) 'HMG-CoA reductase inhibitors and P-glycoprotein modulation', *British Journal of Pharmacology*, **132**(6), pp. 1183–1192. doi: 10.1038/sj.bjp.0703920.

Boya, P. (2012) 'Lysosomal Function and Dysfunction: Mechanism and Disease', *Antioxidants & Redox Signaling*, **17**(5), pp. 766–774. doi: 10.1089/ars.2011.4405.

Callaghan, R., Luk, F. and Bebawy, M. (2014) 'Inhibition of the multidrug resistance P-glycoprotein: Time for a change of strategy?', *Drug Metabolism and Disposition*, **42**(4), pp. 623–631. doi: 10.1124/dmd.113.056176.

Carpino, L. A. (1987) 'The 9-Fluorenylmethyloxycarbonyl Family of Base-Sensitive Amino-Protecting Groups', *Accounts of Chemical Research*, **20**(11), pp. 401–407. doi:

10.1021/ar00143a003.

Chakraborty, A. and Jana, N. R. (2015) 'Design and synthesis of triphenylphosphonium functionalized nanoparticle probe for mitochondria targeting and imaging', *Journal of Physical Chemistry C*, **119**(5), pp. 2888–2895. doi: 10.1021/jp511870e.

Chang, E., Miller, J. S., Sun, J., Yu, W. W., Colvin, V. L., Drezek, R. and West, J. L. (2005) 'Protease-activated quantum dot probes', *Biochemical and Biophysical Research Communications*, **334**, pp. 1317–1321. doi: 10.1016/j.bbrc.2005.07.028.

Chatterjee, A., Mambo, E. and Sidransky, D. (2006) 'Mitochondrial DNA mutations in human cancer', *Oncogene*, **25**(34), pp. 4663–4674. doi: 10.1038/sj.onc.1209604.

Chen, H., Liu, X., Clayman, E. S., Shao, F., Xiao, M., Tian, X., Fu, W., Zhang, C., Ruan, B., Zhou, P., Liu, Z., Wang, Y. and Rui, W. (2015) 'Synthesis and Evaluation of a CBZ-AAN-Dox Prodrug and its in vitro Effects on SiHa Cervical Cancer Cells under Hypoxic Conditions', *Chemical Biology and Drug Design*, **86**, pp. 589–598. doi: 10.1111/cbdd.12525.

Chen, J.-M., Watts, C., Dando, P. M., Rawlings, N. D., Hewitt, E., Brown, M. A., Barrett, A. J., Stevens, R. A. and Young, N. E. (1997) 'Cloning, Isolation, and Characterization of Mammalian Legumain, an Asparaginyl Endopeptidase', *Journal of Biological Chemistry*, **272**(12), pp. 8090–8098. doi: 10.1074/jbc.272.12.8090.

Choe, Y., Leonetti, F., Greenbaum, D. C., Lecaille, F., Bogoy, M., Bromme, D., Ellman, J. A. and Craik, C. S. (2006) 'Substrate Profiling of Cysteine Proteases Using a Combinatorial Peptide Library Identifies Functionally Unique Specificities', *Journal of Biological Chemistry*, **281**(18), pp. 12824–12832. doi: 10.1074/jbc.m513331200.

Choi, C.-H. (2005) 'ABC transporters as multidrug resistance mechanisms and the development of chemosensitizers for their reversal.', *Cancer Cell International*, **5**, pp. 1–13. doi: 10.1186/1475-2867-5-30.

Choi, K. Y., Swierczewska, M., Lee, S. and Chen, X. (2012) 'Protease-Activated Drug Development', *Theranostics*, **2**(2). doi: 10.7150/thno.4068.

Cole, S. P. C. (2014) 'Targeting Multidrug Resistance Protein 1 (MRP1, *ABCC1*): Past,

Present, and Future', *Annual Review of Pharmacology and Toxicology*, **54**(1), pp. 95–117. doi: 10.1146/annurev-pharmtox-011613-135959.

Constance, J. E. and Lim, C. S. (2012) 'Targeting malignant mitochondria with therapeutic peptides.', *Therapeutic delivery*, **3**(8), pp. 961–79. doi: 10.4155/tde.12.75.

Cornbleet, M. A., Stuart-Harris, R. C., Smith, I. E., Coleman, R. E., Rubens, R. D., McDonald, M., Mouridsen, H. T., Rainer, H., Van Oosterom, A. T. and Smyth, J. F. (1984) 'Mitoxantrone for the treatment of advanced breast cancer: Single-agent therapy in previously untreated patients', *European Journal of Cancer*, **20**(9), pp. 1141–1146. doi: 10.1016/0277-5379(84)90122-6.

Cummings, J., Macpherson, J. S., Meikle, I. and Smyth, J. F. (1996) 'Development of anthracenyl-amino acid conjugates as topoisomerase I and II inhibitors that circumvent drug resistance', *Biochemical Pharmacology*, **52**(7), pp. 979–990. doi: 10.1016/0006-2952(96)00301-2.

Dean, M., Hamon, Y. and Chimini, G. (2001) 'The Human ATP-Binding Cassette transporter superfamily', *Journal of Lipid Research*, **42**, pp. 1007–1017. doi: 10.1101/gr.184901.The.

Denizot, F. and Lang, R. (1986) 'Rapid colorimetric assay for cell growth and survival Modifications to the tetrazolium dye procedure giving improved sensitivity and reliability' *Journal of Immunological Methods*, **89**, pp. 271–277.

Detmer, S. A. and Chan, D. C. (2007) 'Functions and dysfunctions of mitochondrial dynamics', *Nature Reviews Molecular Cell Biology*, **8**(11), pp. 870–879. doi: 10.1038/nrm2275.

Diehn, M., Cho, R. W., Lobo, N. A., Kalisky, T., Jo, M., Kulp, A. N., Qian, D., Lam, J. S., Ailles, L. E., Wong, M., Joshua, B., Kaplan, M. J., Wapnir, I., Dirbas, F., Somlo, G., Paz, B., Shen, J., Lau, S. K., Quake, S. R., Martin, J., Weissman, I. L. and Clarke, M. F. (2009) 'Association of Reactive Oxygen Species Levels and Radioresistance in Cancer Stem Cells', *Nature*, **458**, pp. 780–783. doi: 10.1038/nature07733.Association.

Doonan, F. and Cotter, T. G. (2008) 'Morphological assessment of apoptosis', *Methods*,

44(3), pp. 200–204. doi: 10.1016/j.ymeth.2007.11.006.

Duchen, M. R. (2004) 'Mitochondria in health and disease: Perspectives on a new mitochondrial biology', *Molecular Aspects of Medicine*, **25**(4), pp. 365–451. doi: 10.1016/j.mam.2004.03.001.

Edgington, L. E., Verdoes, M. and Bogyo, M. (2011) 'Functional imaging of proteases : recent advances in the design and application of substrate-based and activity-based probes', *Current Opinion in Chemical Biology*, **15**(6), pp. 798–805. doi: 10.1016/j.cbpa.2011.10.012.

Ehninger, G., Schuler, U., Proksch, B., Zeller, K. P. and Blanz, J. (1990) 'Pharmacokinetics and metabolism of mitoxantrone. A review.', *Clinical pharmacokinetics*, **18**(5), pp. 365–380.

Elmore, S. (2007) 'Apoptosis: A Review of Programmed Cell Death', *Toxicologic Pathology*, **35**(4), pp. 495–516. doi: 10.1080/01926230701320337.

Enache, M., Ionescu, S. and Volanschi, E. (2015) 'Studies on the anticancer drug mitoxantrone-DNA-sodium dodecyl sulfate system', *Journal of Molecular Liquids*, **208**, pp. 333–341. doi: 10.1016/j.molliq.2015.05.006.

Endo, T. and Yamano, K. (2010) 'Transport of proteins across or into the mitochondrial outer membrane', *Biochimica et Biophysica Acta*, **1803**(6), pp. 706–714. doi: 10.1016/j.bbamcr.2009.11.007.

Feofanov, A., Sharonov, S., Fleury, F., Kudelina, I. and Nabiev, I. (1997) 'Quantitative confocal spectral imaging analysis of mitoxantrone within living K562 cells: Intracellular accumulation and distribution of monomers, aggregates, naphthoquinoline metabolite, and drug-target complexes', *Biophysical Journal*, **73**(6), pp. 3328–3336. doi: 10.1016/S0006-3495(97)78357-7.

Ferreira, J. A. B. and Costa, S. M. B. (2006) 'Activationless nonradiative decay in rhodamines: Role of NH and lower frequency vibrations in solvent kinetic isotope effects', *Chemical Physics*, **321**, pp. 197–208. doi: 10.1016/j.chemphys.2005.08.069.

Fields, G. B. (1994) 'Methods for Removing the Fmoc Group', *Methods in Molecular*

Biology, **35**. doi: 10.1385/0-89603-273-6.

Filion, M. C. and Phillips, N. C. (1998) 'Major limitations in the use of cationic liposomes for DNA delivery', *International Journal of Pharmaceutics*, **162**(1), pp. 159–170. doi: [https://doi.org/10.1016/S0378-5173\(97\)00423-7](https://doi.org/10.1016/S0378-5173(97)00423-7).

Forster, T. (1948) 'Zwischenmolekulare Energiewanderung und Fluoreszenz', *Die Naturwissenschaften*, **33**(6), pp. 166–175. doi: 10.1007/BF00585226.

Fotakis, G. and Timbrell, J. A. (2006) 'In vitro cytotoxicity assays: Comparison of LDH, neutral red, MTT and protein assay in hepatoma cell lines following exposure to cadmium chloride', *Toxicology Letters*, **160**(2), pp. 171–177. doi: 10.1016/j.toxlet.2005.07.001.

Fulda, S., Galluzzi, L. and Kroemer, G. (2010) 'Targeting mitochondria for cancer therapy', *Drug Discovery*, **9**(5), pp. 476–489. doi: 10.1002/em.20552.

Galluzzi, L. and Kroemer, G. (2008) 'Necroptosis: A Specialized Pathway of Programmed Necrosis', *Cell*, **135**(7), pp. 1161–1163. doi: 10.1016/j.cell.2008.12.004.

Galluzzi, L., Morselli, E., Kepp, O., Vitale, I., Rigoni, A., Vacchelli, E., Michaud, M., Zischka, H., Castedo, M. and Kroemer, G. (2010) 'Mitochondrial gateways to cancer', *Molecular Aspects of Medicine*, **31**(1), pp. 1–20. doi: 10.1016/j.mam.2009.08.002.

Gewirtz, D. A. (1999) 'A critical evaluation of the mechanisms of action proposed for the antitumor effects of the anthracycline antibiotics adriamycin and daunorubicin', *Biochemical Pharmacology*, **57**(7), pp. 727–741. doi: 10.1016/S0006-2952(98)00307-4.

Goffart, S., Hangan, A. and Pohjoismäki, J. L. O. (2019) 'Twist and turn—topoisomerase functions in mitochondrial DNA maintenance', *International Journal of Molecular Sciences*, **20**(8). doi: 10.3390/ijms20082041.

Goldstein, L. J., Galski, H., Fojo, A., Willingham, M., Lai, S.-L., Gazdar, A., Pirker, R., Green, A., Crist, W., Brodeur, G. M., Lieber, M., Cossman, J., Gottesman, M. M. and Pastan, I. (1989) 'Expression of Multidrug Resistance Gene in Human Cancers', *Journal of the National Cancer Institute*, **81**(2), pp. 116–124. Available at: <http://dx.doi.org/10.1093/jnci/81.2.116>.

Gotink, K. J., Broxterman, H. J., Labots, M., De Haas, R. R., Dekker, H., Honeywell, R. J., Rudek, M. A., Beerepoot, L. V., Musters, R. J., Jansen, G., Griffioen, A. W., Assaraf, Y. G., Pili, R., Peters, G. J. and Verheul, H. M. W. (2011) 'Lysosomal sequestration of sunitinib: A novel mechanism of drug resistance', *Clinical Cancer Research*, **17**(23), pp. 7337–7346. doi: 10.1158/1078-0432.CCR-11-1667.

Gottesman, M. M. (2002) 'Mechanisms of cancer drug resistance', *annual review of medicine*, **53**, pp. 615–627.

Green, D. R. and Kroemer, G. (2004) 'The Pathology of Mitochondrial Cell Death', *Science*, **305**(2004), pp. 626–629. doi: 10.1126/science.1099320.

Guo, P., Zhu, Z., Sun, Z., Wang, Z., Zheng, X. and Xu, H. (2013) 'Expression of legumain correlates with prognosis and metastasis in gastric carcinoma.', *Plos One*, **8**(9). doi: 10.1371/journal.pone.0073090.

Guzman-villanueva, D., Mendiola, M. R., Nguyen, H. X. and Weissig, V. (2015) 'Influence of Triphenylphosphonium (TPP) Cation Hydrophobization with Phospholipids on Cellular Toxicity and Mitochondrial Selectivity', *SOJ Pharm Pharm Sci*, **2**(1), pp. 1–9.

Hacker, G. (2000) 'The morphology of apoptosis', *Cell and Tissue Research*, **301**, pp. 5–17. doi: 10.1007/s004410000193.

Hajihassan, Z. and Rabbani-Chadegani, A. (2009) 'Studies on the binding affinity of anticancer drug mitoxantrone to chromatin, DNA and histone proteins', *Journal of Biomedical Science*, **16**(1), pp. 1–7. doi: 10.1186/1423-0127-16-31.

Halaby, R. (2015) 'Role of lysosomes in cancer therapy', *Research and Reports in Biology*, **6**, pp. 147–155. doi: dx.doi.org/10.2147/RRB.S83999.

Han, M., Vakili, M. R., Abyaneh, H. S., Molavi, O., Lai, R. and Lavasanifar, A. (2014) 'Mitochondrial Delivery of Doxorubicin via Triphenylphosphine Modification for Overcoming Drug Resistance in MDA-MB-435/DOX Cells', *American Chemical Society*, **11**, pp. 2640–2649.

Haugen, M. H., Boye, K., Nesland, J. M., Pettersen, S. J., Egeland, E. V., Tamhane, T., Brix, K., Maelandsmo, G. M. and Flatmark, K. (2015) 'High expression of the cysteine

proteinase legumain in colorectal cancer - Implications for therapeutic targeting', *European Journal of Cancer*, **51**(1), pp. 9–17. doi: 10.1016/j.ejca.2014.10.020.

Haugen, M. H., Johansen, H. T., Pettersen, S. J., Solberg, R., Brix, K., Flatmark, K. and Maelandsmo, G. M. (2013) 'Nuclear Legumain Activity in Colorectal Cancer', *Plos One*, **8**(1). doi: 10.1371/journal.pone.0052980.

Heerdt, B. G., Houston, M. A. and Augenlicht, L. H. (2005) 'The intrinsic mitochondrial membrane potential of colonic carcinoma cells is linked to the probability of tumor progression', *Cancer Research*, **65**(21), pp. 9861–9867. doi: 10.1158/0008-5472.CAN-05-2444.

Higgs, H. N. and Peterson, K. J. (2005) 'Phylogenetic analysis of the formin homology 2 domain.', *Molecular biology of the cell*, **16**(1), pp. 1–13. doi: 10.1091/mbc.E04.

Hong, S. K., Starenki, D., Wu, P. K. and Park, J. I. (2017) 'Suppression of B-Raf V600E melanoma cell survival by targeting mitochondria using triphenyl-phosphonium-conjugated nitroxide or ubiquinone', *Cancer Biology and Therapy*, **18**(2), pp. 106–114. doi: 10.1080/15384047.2016.1250987.

Horobin, R. W., Trapp, S. and Weissig, V. (2007) 'Mitochondriotropics: A review of their mode of action, and their applications for drug and DNA delivery to mammalian mitochondria', *Journal of Controlled Release*, **121**(3), pp. 125–136. doi: 10.1016/j.jconrel.2007.05.040.

Horton, K. L., Stewart, K. M., Fonseca, S. B., Guo, Q. and Kelley, S. O. (2008) 'Mitochondria-Penetrating Peptides', *Chemistry and Biology*, **15**(4), pp. 375–382. doi: 10.1016/j.chembiol.2008.03.015.

Hosoya, N. and Miyagawa, K. (2014) 'Targeting DNA damage response in cancer therapy', *Cancer Science*, **105**(4), pp. 370–388. doi: 10.1111/cas.12366.

Hoye, A. T., Davoren, J. E., Wipf, P., Fink, M. P. and Kagan, V. E. (2008) 'Targeting Mitochondria', *Accounts of Chemical Research*. American Chemical Society, **41**(1), pp. 87–97. doi: 10.1021/ar700135m.

Hu, Z., Sim, Y., Kon, O. L., Ng, W. H., Ribeiro, A. J. M., Ramos, M. J., Fernandes, P. A.,

Ganguly, R., Xing, B., García, F. and Yeow, E. K. L. (2017) 'Unique Triphenylphosphonium Derivatives for Enhanced Mitochondrial Uptake and Photodynamic Therapy', *Bioconjugate Chemistry*, **28**(2), pp. 590–599. doi: 10.1021/acs.bioconjchem.6b00682.

Isidro-Llobet, A., Álvarez, M. and Albericio, F. (2009) 'Amino Acid-Protecting Groups', *Chemical Reviews*, **109**(6), pp. 2455–2504. doi: 10.1021/cr800323s.

Jares-Erijman, E. A. and Jovin, T. M. (2003) 'FRET imaging', *Nature Biotechnology*, **21**(11), pp. 1387–1395. doi: 10.1038/nbt896.

Kamal, A., Ramu, R., Tekumalla, V., Khanna, G. B. R., Barkume, M. S., Juvekar, A. S. and Zingde, S. M. (2007) 'Synthesis, DNA binding, and cytotoxicity studies of pyrrolo[2,1-c][1,4]benzodiazepine-anthraquinone conjugates', *Bioorganic and Medicinal Chemistry*, **15**(22), pp. 6868–6875. doi: 10.1016/j.bmc.2007.08.026.

Kang, B. H., Plescia, J., Song, H. Y., Meli, M., Colombo, G., Beebe, K., Scroggins, B., Neckers, L. and Altieri, D. C. (2009) 'Combinatorial drug design targeting multiple cancer signaling networks controlled by mitochondrial Hsp90', *The Journal of Clinical Investigation*, **119**(3), pp. 454–464. doi: 10.1172/JCI37613DS1.

Kapuscinski, J. and Darzynkiewicz, Z. (1986) 'Relationship between the pharmacological activity of antitumor drugs Ametantrone and mitoxantrone (Novatrone) and their ability to condense nucleic acids.', *Proceedings of the National Academy of Sciences*, **83**(17), pp. 6302–6306. doi: 10.1073/pnas.83.17.6302.

Kapuscinski, J., Darzynkiewicz, Z., Traganos, F. and Melamed, M. R. (1981) 'Interactions of a new antitumor agent, 1,4-dihydroxy-5,8-bis[[2-[(2-hydroxyethyl)amino]-ethyl]amino]-9,10-anthracenedione, with nucleic acids', *Biochemical Pharmacology*, **30**(3), pp. 231–240. doi: [https://doi.org/10.1016/0006-2952\(81\)90083-6](https://doi.org/10.1016/0006-2952(81)90083-6).

Karpiuk, J., Grabowski, Z. R. and De Schryver, F. C. (1994) 'Photophysics of the lactone form of rhodamine 101', *Journal of Physical Chemistry*, **98**, pp. 3247–3256. doi: 10.1021/j100064a001.

Katayama, K., Noguchi, K. and Sugimoto, Y. (2014) 'Regulations of P-

glycoprotein/ABCB1/MDR1 in Human Cancer Cells', *New Journal of Science*, **2014**, pp. 1–10. doi: 10.1155/2014/476974.

Kelley, S. O., Stewart, K. M. and Mourtada, R. (2011) 'Development of novel peptides for mitochondrial drug delivery: Amino acids featuring delocalized lipophilic cations', *Pharmaceutical Research*, **28**(11), pp. 2808–2819. doi: 10.1007/s11095-011-0530-6.

Kent, S. B. H. (2008) 'Total chemical synthesis of proteins', *Chemical Society Reviews*, **38**(2), pp. 338–351. doi: 10.1039/B700141J.

KERR, J. F. R., WYLLIE, A. H. and CURRIE, A. R. (1972) Apoptosis: A Basic Biological Phenomenon with Wideranging Implications in Tissue Kinetics ", *British Journal of Cancer*, **26**, pp. 239–257. doi: 10.1111/j.1365-2796.2005.01570.x.

Ketterer, B., Neumcke, B. and Lauger, P. (1971) 'Transport mechanism of hydrophobic ions through lipid bilayer membranes', *The Journal of Membrane Biology*, **5**(3), pp. 225–245. doi: 10.1007/BF01870551.

Khiati, S., Rosa, I. D., Sourbier, C., Ma, X., Rao, V. A., Neckers, L. M., Zhang, H. and Pommier, Y. (2014) 'Mitochondrial topoisomerase i (Top1mt) is a novel limiting factor of doxorubicin cardiotoxicity', *Clinical Cancer Research*, **20**(18), pp. 4873–4881. doi: 10.1158/1078-0432.CCR-13-3373.

Kikuchi, M., Yamagishi, T. and Hida, M. (1982) 'Kinetic studies on the amination of leucoquinizarin', *Bulletin Of The Chemical Society Of Japan*, **55**(4), pp. 1209–1212. doi: 10.1246/bcsj.55.1209.

Kim, E. J., Bhuniya, S., Lee, H., Kim, H. M., Cheong, C., Maiti, S., Hong, K. S. and Kim, J. S. (2014) 'An activatable prodrug for the treatment of metastatic tumors', *Journal of the American Chemical Society*, **136**(39), pp. 13888–13894. doi: 10.1021/ja5077684.

Kim, G. B. and Kim, Y. P. (2012) 'Analysis of protease activity using quantum dots and resonance energy transfer', *Theranostics*, **2**(2), pp. 127–138. doi: 10.7150/thno.3476.

Kircher, M. F., Weissleder, R. and Josephson, L. (2004) 'A Dual Fluorochrome Probe for Imaging Proteases', *Bioconjugate Chemistry*, **15**, pp. 242–248. doi: 10.1021/bc034151d.

- Kodama, S., Asano, S., Moriguchi, T., Sawai, H. and Shinozuka, K. (2006) 'Novel fluorescent oligoDNA probe bearing a multi-conjugated nucleoside with a fluorophore and a non-fluorescent intercalator as a', *Bioorganic and Medicinal Chemistry Letters*, **16**(10), pp. 2685–2688. doi: 10.1016/j.bmcl.2006.02.016.
- Kroemer, G. (2006) 'Mitochondria in cancer', *Oncogene*, **25**(34), pp. 4630–4632. doi: 10.1038/sj.onc.1209589.
- Kühlbrandt, W. (2015) 'Structure and function of mitochondrial membrane protein complexes', *BMC Biology*, **13**(1), pp. 1–11. doi: 10.1186/s12915-015-0201-x.
- Kundu, S., Maity, S., Bhadra, R. and Ghosh, P. (2011) 'Trans-dichlorobis(N-p-tolylpyridin-2-amine)palladium(II): Synthesis, structure, fluorescence features and DNA binding', *Indian Journal of Chemistry*, **50**, pp. 1443–1449.
- Lampidis, T. J., Kolonias, D., Podona, T., Israel, M., Safa, A. R., Lothstein, L., Savaraj, N., Tapiero, H. and Priebe, W. (1997) 'Circumvention of P-GP MDR as a Function of Anthracycline Lipophilicity and Charge', *Biochemistry*. American Chemical Society, **36**(9), pp. 2679–2685. doi: 10.1021/bi9614489.
- Lavis, L. D. and Raines, R. T. (2008) 'Bright ideas for chemical biology', *ACS chemical biology*, **3**(3), pp. 142–55. doi: 10.1021/cb700248m.
- Leo, A., Hansch, C. and Elkins, D. (1971) 'Partition coefficients and their uses', *Chemical Reviews*, **71**(6), pp. 525–616. doi: 10.1021/cr60274a001.
- Li, J., Wang, Y., Zhu, Y. and Oupický, D. (2013) 'Recent advances in delivery of drug–nucleic acid combinations for cancer treatment', *Journal of Controlled Release*, **172**(2), pp. 589–600. doi: <https://doi.org/10.1016/j.jconrel.2013.04.010>.
- Li, N., Ma, Y., Yang, C., Guo, L. and Yang, X. (2005) 'Interaction of anticancer drug mitoxantrone with DNA analyzed by electrochemical and spectroscopic methods', *Biophysical Chemistry*, **116**(3), pp. 199–205. doi: 10.1016/j.bpc.2005.04.009.
- Liscovitch, M. and Lavie, Y. (2002) 'Cancer multidrug resistance: a review of recent drug discovery research.', *IDrugs: the investigational drugs journal*, **5**(4), pp. 349–355.

Liu, C., Sun, C., Huang, H., Janda, K. and Edgington, T. (2003) 'Overexpression of legumain in tumors is significant for invasion/metastasis and a candidate enzymatic target for prodrug therapy', *Cancer Research*, **63**, pp. 2957–2964.

Liu, Y., Bajjuri, K. M., Liu, C. and Sinha, S. C. (2012) 'Targeting cell surface alpha(v)beta(3) integrin increases therapeutic efficacies of a legumain protease-activated Auristatin Prodrug', *Molecular Pharmaceutics*, **9**, pp. 168–175. doi: 10.1021/mp200434n.

Longmire, M. R., Ogawa, M., Hama, Y., Kosaka, N., Regino, C. A. S., Choyke, P. L. and Kobayashi, H. (2008) 'Determination of Optimal Rhodamine Fluorophore for in Vivo Optical Imaging', *Bioconjugate Chemistry*, **19**(8), pp. 1735–1742. doi: 10.1021/bc800140c.

Longo-Sorbello, G. and Bertino, J. R. (2001) 'Current understanding of methotrexate pharmacology and efficacy in acute leukemias. Use of newer antifolates in clinical trials', *haematologica*, **86**, pp. 121–127.

López-Otín, C. and Hunter, T. (2010) 'The regulatory crosstalk between kinases and proteases in cancer', *Nature Reviews Cancer*, **10**(4), pp. 278–292. Available at: <https://doi.org/10.1038/nrc2823>.

Løvsletten, R., Alexander, O., Åstrand, H., Minh, L., Elvestrand, T., Hagelin, G., Solberg, R., Thidemann, H. and Rongved, P. (2014) 'Synthesis of a novel legumain-cleavable colchicine prodrug with cell-specific toxicity', *Bioorganic & Medicinal Chemistry*, **22**(13), pp. 3309–3315. doi: 10.1016/j.bmc.2014.04.056.

Mahato, R., Tai, W. and Cheng, K. (2011) 'Prodrugs for Improving Tumor Targetability and Efficiency', *Advanced Drug Delivery Reviews*, **63**(8), pp. 659–670. doi: 10.1111/j.1743-6109.2008.01122.x.Endothelial.

Majno, G. and Joris, I. (1995) 'Apoptosis, oncosis, and necrosis', *The American journal of pathology*, **146**(1), pp. 3–15. doi: 7856735.

Mansour, O. C., Evison, B. J., Sleebs, B. E., Watson, K. G., Nudelman, A., Rephaeli, A., Buck, D. P., Collins, J. G., Bilardi, R. A., Phillips, D. R. and Cutts, S. M. (2010) 'New anthracenedione derivatives with improved biological activity by virtue of stable drug-DNA

adduct formation', *Journal of Medicinal Chemistry*, **53**(19), pp. 6851–6866. doi: 10.1021/jm901894c.

May, J. P., Brown, L. J., Van Delft, I., Thelwell, N., Harley, K. and Brown, T. (2005) 'Synthesis and evaluation of a new non-fluorescent quencher in fluorogenic oligonucleotide probes for real-time PCR', *Organic and Biomolecular Chemistry*, **3**(14), pp. 2534–2542. doi: 10.1039/b504759e.

McKnight, R. E., Zhang, J. and Dixon, D. W. (2004) 'Binding of a homologous series of anthraquinones to DNA', *Bioorganic and Medicinal Chemistry Letters*, **14**(2), pp. 401–404. doi: 10.1016/j.bmcl.2003.10.054.

Meerlo, J. van, Kaspers, G. J. L. and Cloos, J. (2011) 'Cell Sensitivity Assays: The MTT Assay', *Cancer Cell Culture*, **731**, pp. 237–245. doi: 10.1385/1592594069.

Meng, Q., Yu, M., Zhang, H., Ren, J. and Huang, D. (2007) 'Synthesis and application of N-hydroxysuccinimidyl rhodamine B ester as an amine-reactive fluorescent probe', *Dyes and Pigments*, **73**(2), pp. 254–260. doi: 10.1016/j.dyepig.2005.12.008.

Merrifield, R. B. (1963) 'Solid Phase Peptide Synthesis. I. The Synthesis of a Tetrapeptide', *Journal of the American Chemical Society*, **85**(14), pp. 2149–2154. doi: 10.1021/ja00897a025.

Mincher, DJ. (1999). 'Anthracene derivatives for use as anticancer agents', Publ.

Modica-Napolitano, J. S. and Aprille, J. R. (2001) 'Delocalized lipophilic cations selectively target the mitochondria of carcinoma cells', *Advanced Drug Delivery Reviews*, **49**(1–2), pp. 63–70. doi: 10.1016/S0169-409X(01)00125-9.

Montalbetti, C. A. G. N. and Falque, V. (2005) 'Amide bond formation and peptide coupling', *Tetrahedron*, **61**(46), pp. 10827–10852. doi: 10.1016/j.tet.2005.08.031.

Mordente, A., Meucci, E., Silvestrini, A., Martorana, G. E. and Giardina, B. (2012) 'Anthracyclines and Mitochondria', *Advances in Experimental Medicine and Biology*, **942**, pp. 385–419. doi: 10.1007/978-94-007-2869-1_18.

Morris, G. A., Mullah, K. B. and Sutherland, J. K. (1986) 'Some experiments with

aminodihydroxyanthraquinones', *Tetrahedron*, **42**(12), pp. 3303–3309. doi: [https://doi.org/10.1016/S0040-4020\(01\)87394-4](https://doi.org/10.1016/S0040-4020(01)87394-4).

Mosmann, T. (1983) 'Rapid Colorimetric Assay for Cellular Growth and Survival: Application to Proliferation and Cytotoxicity Assays', *Journal of Immunological Methods*, **65**, pp. 55–63.

Mottram, L. F., Forbes, S., Ackley, B. D. and Peterson, B. R. (2012) 'Hydrophobic analogues of rhodamine B and rhodamine 101: Potent fluorescent probes of mitochondria in living *C. elegans*', *Beilstein Journal of Organic Chemistry*, **8**, pp. 2156–2165. doi: [10.3762/bjoc.8.243](https://doi.org/10.3762/bjoc.8.243).

Mrschlik, M. and Ryan, K. M. (2015) 'Lysosomal proteins in cell death and autophagy', *FEBS Journal*, **282**(10), pp. 1858–1870. doi: [10.1111/febs.13253](https://doi.org/10.1111/febs.13253).

Muli, D. K., Rajaputra, P., You, Y. and McGrath, D. V. (2014) 'Asymmetric ZnPc-rhodamine B conjugates for mitochondrial targeted photodynamic therapy', *Bioorganic and Medicinal Chemistry Letters*, **24**(18), pp. 4496–4500. doi: [10.1016/j.bmcl.2014.07.082](https://doi.org/10.1016/j.bmcl.2014.07.082).

Murphy, M. P. (1997) 'Selective targeting of bioactive compounds to mitochondria', *Trends In Biotechnology Cell Press*, **15**(8), pp. 326–330.

Murphy, M. P. (2008) 'Targeting lipophilic cations to mitochondria', *Biochimica et Biophysica Acta*, **1777**(7–8), pp. 1028–1031. doi: [10.1016/j.bbabi.2008.03.029](https://doi.org/10.1016/j.bbabi.2008.03.029).

Nass, M. M. K. and Nass, S. (1963) 'Fibers with DNA characteristics I. Fixation and electron staining reactions', *The Journal of Cell Biology*, **19**, pp. 593–611.

Ndolo, R. A., Luan, Y., Duan, S., Forrest, M. L. and Krise, J. P. (2012) 'Lysosomotropic Properties of Weakly Basic Anticancer Agents Promote Cancer Cell Selectivity In Vitro', *Plos One*, **7**(11), pp. 1–9. doi: [10.1371/journal.pone.0049366](https://doi.org/10.1371/journal.pone.0049366).

Neises, B. and Steglich, W. (1978) 'Simple Method for the Esterification of Carboxylic Acids', *Angewandte Chemie International Edition in English*, **17**(7), pp. 522–524. doi: [10.1002/anie.197805221](https://doi.org/10.1002/anie.197805221).

- Ngen, E. J., Rajaputra, P. and You, Y. (2009) 'Evaluation of delocalized lipophilic cationic dyes as delivery vehicles for photosensitizers to mitochondria', *Bioorganic and Medicinal Chemistry*, **17**(18), pp. 6631–6640. doi: 10.1016/j.bmc.2009.07.074.
- Nguyen, T. and Francis, M. B. (2003) 'Practical synthetic route to functionalized rhodamine dyes', *Organic Letters*, **5**(18), pp. 3245–3248. doi: 10.1021/ol035135z.
- Nitiss, J. (2009) 'Targeting DNA topoisomerase II in cancer chemotherapy', *Nature Reviews Cancer*, **9**(5), pp. 338–350. doi: 10.1038/nrc2607.Targeting.
- Nurgali, K., Jagoe, R. T. and Abalo, R. (2018) 'Editorial: Adverse Effects of Cancer Chemotherapy: Anything New to Improve Tolerance and Reduce Sequelae?', *Frontiers in Pharmacology*, **9**, pp. 1–3. doi: 10.3389/fphar.2018.00245.
- Ohno, Y., Nakashima, J., Izumi, M., Ohori, M., Hashimoto, T. and Tachibana, M. (2013) 'Association of legumain expression pattern with prostate cancer invasiveness and aggressiveness', *World Journal of Urology*, **31**(2), pp. 359–364. doi: 10.1007/s00345-012-0977-z.
- Van Oven, M. and Kayser, M. (2009) 'Updated comprehensive phylogenetic tree of global human mitochondrial DNA variation.', *Human mutation*, **30**(2). doi: 10.1002/humu.20921.
- Ozben, T. (2006) 'Mechanisms and strategies to overcome multiple drug resistance in cancer', *FEBS Letters*, **580**(12), pp. 2903–2909. doi: 10.1016/j.febslet.2006.02.020.
- Palchaudhuri, R. and Hergenrother, P. J. (2007) 'DNA as a target for anticancer compounds: methods to determine the mode of binding and the mechanism of action', *Current Opinion in Biotechnology*, **18**(6), pp. 497–503. doi: 10.1016/j.copbio.2007.09.006.
- Panousis, C. and Phillips, D. R. (1994) 'DNA sequence specificity of mitoxantrone.', *Nucleic acids research*, **22**(8), pp. 1342–1345. doi: 10.1093/nar/22.8.1342.
- Parker, B. S., Buley, T., Evison, B. J., Cutts, S. M., Neumann, G. M., Iskander, M. N. and Phillips, D. R. (2004) 'A molecular understanding of mitoxantrone-DNA adduct formation: Effect of cytosine methylation and flanking sequences', *Journal of Biological Chemistry*, **279**(18), pp. 18814–18823. doi: 10.1074/jbc.M400931200.

Paterson, J. K. and Gottesman, M. M. (2007) 'P-Glycoprotein is not present in mitochondrial membranes', *Experimental Cell Research*, **313**(14), pp. 3100–3105. doi: 10.1016/j.yexcr.2007.04.019.

Pathania, D., Millard, M. and Neamati, N. (2009) 'Opportunities in discovery and delivery of anticancer drugs targeting mitochondria and cancer cell metabolism', *Advanced Drug Delivery Reviews*, **61**(14), pp. 1250–1275. doi: 10.1016/j.addr.2009.05.010.

Paumard, P. (2002) 'The ATP synthase is involved in generating mitochondrial cristae morphology', *EMBO Journal*, **21**(3), pp. 221–230. doi: 10.1093/emboj/21.3.221.

Pelicano, H., Martin, D. S., Xu, R. H. and Huang, P. (2006) 'Glycolysis inhibition for anticancer treatment', *Oncogene*, **25**(34), pp. 4633–4646. doi: 10.1038/sj.onc.1209597.

Petersen, N. H. T., Olsen, O. D., Groth-pedersen, L., Ellegaard, A., Bilgin, M., Redmer, S., Ostenfeld, M. S., Ulanet, D., Dovmark, T. H., Lønborg, A., Vindeløv, S. D., Hanahan, D., Arenz, C., Ejsing, C. S., Kirkegaard, T., Rohde, M. and Nylandsted, J. (2013) 'Transformation-Associated Changes in Sphingolipid Metabolism Sensitize Cells to Lysosomal Cell Death Induced by Inhibitors of Acid Sphingomyelinase', *Cancer Cell*, **24**, pp. 379–393. doi: 10.1016/j.ccr.2013.08.003.

Pham, W., Choi, Y., Weissleder, R. and Tung, C. H. (2004) 'Developing a peptide-based near-infrared molecular probe for protease sensing', *Bioconjugate Chemistry*, **15**(6), pp. 1403–1407. doi: 10.1021/bc049924s.

Piccart, M., Rozenzweig, M., Abele, R., Cumps, E., Dodion, P., Dupont, D., Kisner, D. and Kenis, Y. (1981) 'Phase I clinical trial with ametantrone (NSC-287513)', *European Journal of Cancer and Clinical Oncology*, **17**(7), pp. 775–779. doi: [https://doi.org/10.1016/0014-2964\(81\)90233-4](https://doi.org/10.1016/0014-2964(81)90233-4).

Piddock, L. J. V (2006) 'Multidrug - resistance efflux pumps — not just for resistance', *Nature Reviews Microbiology*, **4**, pp. 629–636. doi: 10.1038/nrmicro1464.

Pluen, A., Boucher, Y., Ramanujan, S., McKee, T. D., Gohongi, T., di Tomaso, E., Brown, E. B., Izumi, Y., Campbell, R. B., Berk, D. A. and Jain, R. K. (2001) 'Role of tumor-host interactions in interstitial diffusion of macromolecules: Cranial vs. subcutaneous tumors',

Proceedings of the National Academy of Sciences, **98**(8), pp. 4628–4633. doi: 10.1073/pnas.081626898.

Pommier, Y., Leo, E., Zhang, H. and Marchand, C. (2010) 'DNA topoisomerases and their poisoning by anticancer and antibacterial drugs', *Chemistry and Biology*, **17**(5), pp. 421–433. doi: 10.1016/j.chembiol.2010.04.012.

Rautio, J., Kumpulainen, H., Heimbach, T., Oliyai, R., Oh, D., Järvinen, T. and Savolainen, J. (2008) 'Prodrugs: design and clinical applications', *Nature Reviews Drug Discovery*, **7**(3), pp. 255–270. doi: 10.1038/nrd2468.

Reily, C., Mitchell, T., Chacko, B. K., Benavides, G. A., Murphy, M. P. and Darley-Usmar, V. M. (2013) 'Mitochondrially targeted compounds and their impact on cellular bioenergetics', *Redox Biology*, **1**(1), pp. 86–93. doi: 10.1016/j.redox.2012.11.009.

Reungpatthanaphong, P., Dechsupa, S., Meesungnoen, J., Loetchutinat, C. and Mankhetkorn, S. (2003) 'Rhodamine B as a mitochondrial probe for measurement and monitoring of mitochondrial membrane potential in drug-sensitive and -resistant cells', *Journal of Biochemical and Biophysical Methods*, **57**, pp. 1–16. doi: 10.1016/S0165-022X(03)00032-0.

Riganti, C., Rolando, B., Kopecka, J., Campia, I., Chegaev, K., Lazzarato, L., Federico, A., Fruttero, R. and Ghigo, D. (2013) 'Mitochondrial-targeting nitrooxy-doxorubicin: A new approach to overcome drug resistance', *Molecular Pharmaceutics*, **10**(1), pp. 161–174. doi: 10.1021/mp300311b.

Rin Jean, S., Tulumello, D. V., Wisnovsky, S. P., Lei, E. K., Pereira, M. P. and Kelley, S. O. (2014) 'Molecular vehicles for mitochondrial chemical biology and drug delivery', *ACS Chemical Biology*, **9**(2), pp. 323–333. doi: 10.1021/cb400821p.

Ross, M. F., Kelso, G. F., Blaikie, F. H., James, A. M., Cochemé, H. M., Filipovska, A., Ros, T. Da, Hurd, T. R., Smith, R. A. J. and Murphy, M. P. (2005) 'Lipophilic triphenylphosphonium cations as tools in mitochondrial bioenergetics and free ... Lipophilic Triphenylphosphonium Cations as Tools in Mitochondrial Bioenergetics and Free Radical Biology', *Biochemistry*, **70**(2), pp. 222–230. doi: 10.1007/s10541-005-0104-

5.

Ross, M. F., Prime, T. A., Abakumova, I., James, A. M., Porteous, C. M., Smith, R. A. J. and Murphy, M. P. (2008) 'Rapid and extensive uptake and activation of hydrophobic triphenylphosphonium cations within cells', *Biochemical Journal*, **411**(3), pp. 633–645. Available at: <http://www.biochemj.org/content/411/3/633.abstract>.

Rossato, L. G., Costa, V. M., Dallegrave, E., Arbo, M., Silva, R., Ferreira, R., Amado, F., Dinis-Oliveira, R. J., Duarte, J. A., De Lourdes Bastos, M., Palmeira, C. and Remião, F. (2014) 'Mitochondrial cumulative damage induced by mitoxantrone: Late onset cardiac energetic impairment', *Cardiovascular Toxicology*, **14**(1), pp. 30–40. doi: 10.1007/s12012-013-9230-2.

Rozenzweig, M., Sanders, C., Rombaut, W., Crespeigne, N., Kenis, Y. and Klastersky, J. (1985) 'Phase II study of ametantrone in a human tumor cloning assay', *European Journal of Cancer and Clinical Oncology*, **21**(2), pp. 195–198. doi: [https://doi.org/10.1016/0277-5379\(85\)90173-7](https://doi.org/10.1016/0277-5379(85)90173-7).

Rudraraju, A. V., Amoyaw, P. N. A., Hubin, T. J. and Khan, M. O. F. (2014) 'Determination of log P values of new cyclen based antimalarial drug leads using RP-HPLC', *Pharmazie*, **69**(9), pp. 655–662. doi: 10.1691/ph.2014.4019.

Rutkowska, E., Pająk, K. and Józwiak, K. (2013) 'Lipophilicity - Methods of determination and its role in medicinal chemistry', *Acta Poloniae Pharmaceutica - Drug Research*, **70**(1), pp. 3–18. doi: 10.1097/00005392-199608001-00059.

Saraste, A. and Pulkki, K. (2000) 'Morphologic and biochemical hallmarks of apoptosis', *Cardiovascular Research*, **45**(3), pp. 528–537. doi: 10.1016/s0008-6363(99)00384-3.

Sauna, Z. E., Smith, M. M., Müller, M., Kerr, K. M. and Ambudkar, S. V. (2001) 'The Mechanism of Action of Multidrug-Resistance-Linked P-Glycoprotein', *Clinical and Experimental Dermatology*, **33**(6), pp. 481–491. Available at: <http://www.ncbi.nlm.nih.gov/pubmed/2689019>.

Seiter, K. (2005) 'Toxicity of the topoisomerase II inhibitors', *Expert opinion on drug safety*, **4**(2), pp. 219–234. doi: 10.1517/14740338.4.2.219.

Settanni, G., Zhou, J., Suo, T., Schöttler, S., Landfester, K., Schmid, F. and Mailänder, V. (2012) 'Design and Synthesis of a Mitochondria-Targeting Carrier for Small Molecule Drugs', *The Royal Society of Chemistry*. doi: 10.1039/x0xx00000x.

Shaul, P., Frenkel, M., Goldstein, E. B., Mittelman, L., Grunwald, A., Ebenstein, Y., Tsarfaty, I. and Fridman, M. (2013) 'The Structure of Anthracycline Derivatives Determines Their Subcellular Localization and Cytotoxic Activity', *American Chemical Society*, **4**, pp. 323–328. doi: 10.1021/ml3002852.

Shen, D.-W., Goldenberg, S., Pastan, I. and Gottesman, M. M. (2000) 'Decreased accumulation of [14c]carboplatin in human cisplatin-resistant cells results from reduced energy-dependent uptake', *Journal of Cellular Physiology*, **183**(1), pp. 108–116. doi: 10.1002/(SICI)1097-4652(200004)183:1<108::AID-JCP13>3.0.CO;2-4.

Shen, Y., Chu, Y., Yang, Y. and Wang, Z. (2012) 'Mitochondrial localization of P-glycoprotein in the human breast cancer cell line MCF-7/ADM and its functional characterization', *Oncology Reports*, **27**(5), pp. 1535–1540. doi: 10.3892/or.2012.1671.

Sheppard, R. (2003) 'The fluorenylmethoxycarbonyl group in solid phase synthesis', *Journal of Peptide Science*, **9**(9), pp. 545–552. doi: 10.1002/psc.479.

Shirahama-Noda, K., Yamamoto, A., Sugihara, K., Hashimoto, N., Asano, M., Nishimura, M. and Hara-Nishimura, I. (2003) 'Biosynthetic Processing of Cathepsins and Lysosomal Degradation Are Abolished in Asparaginyl Endopeptidase-deficient Mice', *Journal of Biological Chemistry*, **278**(35), pp. 33194–33199. doi: 10.1074/jbc.m302742200.

Skladanowski, A. and Konopa, J. (2000) 'Mitoxantrone and ametantrone induce interstrand cross-links in DNA of tumour cells', *British Journal of Cancer*, **82**(7), pp. 1300–1304. doi: 10.1054/bjoc.1999.1095.

Smith, P. J., Morgan, S. A., Fox, M. E. and Watson, J. V (1990) 'Mitoxantrone-DNA binding and the induction of topoisomerase II associated DNA damage in multi-drug resistant small cell lung cancer cells', *Biochemical Pharmacology*, **40**(9), pp. 2069–2078. doi: [https://doi.org/10.1016/0006-2952\(90\)90237-F](https://doi.org/10.1016/0006-2952(90)90237-F).

Smith, P. J., Sykes, H. R., Fox, M. E. and Furlong, I. J. (1992) 'Subcellular Distribution of

the Anticancer Drug Mitoxantrone in Human and Drug-resistant Murine Cells Analyzed by Flow Cytometry and Confocal Microscopy and Its Relationship to the Induction of DNA Damage¹, *Cancer Research*, **52**, pp. 4000–4008.

Smith, R. a J., Porteous, C. M., Gane, A. M. and Murphy, M. P. (2003) 'Delivery of bioactive molecules to mitochondria in vivo.', *Proceedings of the National Academy of Sciences of the United States of America*, **100**(9), pp. 5407–5412. doi: 10.1073/pnas.0931245100.

Smith, R., Hartley, R. and P Murphy, M. (2011) 'Mitochondria-Targeted Small Molecule Therapeutics and Probes', *Antioxidants & redox signaling*, **15**(12). doi: 10.1089/ars.2011.3969.

Smith, R., Johansen, H. T., Nilsen, H., Haugen, M. H., Pettersen, S. J., Mælandsmo, G. M., Abrahamson, M. and Solberg, R. (2012) 'Intra- and extracellular regulation of activity and processing of legumain by cystatin E/M', *Biochimie*, **94**, pp. 2590–2599. doi: 10.1016/j.biochi.2012.07.026.

Stéen, E. J. L., Nyberg, N., Lehel, S., Andersen, V. L., Di Pilato, P., Knudsen, G. M., Kristensen, J. L. and Herth, M. M. (2017) 'Development of a simple proton nuclear magnetic resonance-based procedure to estimate the approximate distribution coefficient at physiological pH (log D_{7.4}): Evaluation and comparison to existing practices', *Bioorganic and Medicinal Chemistry Letters*, **27**(2), pp. 319–322. doi: 10.1016/j.bmcl.2016.11.048.

Stern, L., Perry, R., Ofek, P., Many, A., Shabat, D. and Satchi-Fainaro, R. (2009) 'A novel antitumor prodrug platform designed to be cleaved by the endoprotease legumain', *Bioconjugate Chemistry*, **20**(3), pp. 500–510. doi: 10.1021/bc800448u.

Stockholm, D., Bartoli, M., Sillon, G., Bourg, N., Davoust, J. and Richard, I. (2005) 'Imaging Calpain Protease Activity by Multiphoton FRET in Living Mice', *Journal of Molecular Biology*, **346**, pp. 215–222. doi: 10.1016/j.jmb.2004.11.039.

Sukhai, M. A., Prabha, S., Hurren, R., Rutledge, A. C., Lee, A. Y., Sriskanthadevan, S., Sun, H., Wang, X., Skrtic, M., Seneviratne, A., Cusimano, M., Jhas, B., Gronda, M.,

MacLean, N., Cho, E. E., Spagnuolo, P. A., Sharmeen, S., Gebbia, M., Urbanus, M., Eppert, K., Dissanayake, D., Jonet, A., Dassonville-Klimpt, A., Li, X., Datti, A., Ohashi, P. S., Wrana, J., Rogers, I., Sonnet, P., Ellis, W. Y., Corey, S. J., Eaves, C., Minden, M. D., Wang, J. C. Y., Dick, J. E., Nislow, C., Giaever, G. and Schimmer, A. D. (2013) 'Lysosomal disruption preferentially targets acute myeloid leukemia cells and progenitors', *The Journal of Clinical Investigation*, **123**(1), pp. 315–328. doi: 10.1172/JCI64180DS1.

Swift, L. P., Rephaeli, A., Nudelman, A., Phillips, D. R. and Cutts, S. M. (2006) 'Doxorubicin-DNA adducts induce a non-topoisomerase II-mediated form of cell death', *Cancer Research*, **66**(9), pp. 4863–4871. doi: 10.1158/0008-5472.CAN-05-3410.

Tanabe, M., Ieiri, I., Nagata, N., Inoue, K., Ito, S., Kanamori, Y., Takahashi, M., Kurata, Y., Kigawa, J., Higuchi, S., Terakawa, N. and Otsubo, K. (2001) 'Expression of P-glycoprotein in human placenta: relation to genetic polymorphism of the multidrug resistance (MDR)-1 gene.', *The Journal of pharmacology and experimental therapeutics*, **297**(3), pp. 1137–1143.

Taya, P., Maiti, B., Kumar, V., De, P. and Satapathi, S. (2018) 'Design of a novel FRET based fluorescent chemosensor and their application for highly sensitive detection of nitroaromatics', *Sensors and Actuators, B: Chemical*, **255**, pp. 2628–2634. doi: 10.1016/j.snb.2017.09.073.

Teicher, B. A. (2008) 'Next generation topoisomerase I inhibitors: Rationale and biomarker strategies', *Biochemical Pharmacology*, **75**(6), pp. 1262–1271. doi: 10.1016/j.bcp.2007.10.016.

Teicher, B. A., Holden, S. A. and Cathcart, K. N. S. (1987) 'Efficacy of Pt(Rh-123)₂ as a radiosensitizer with fractionated x rays', *International Journal of Radiation Oncology*, **13**(8), pp. 1217–1224. doi: 10.1016/0360-3016(87)90197-0.

Theodossiou, T. A., Sideratou, Z., Katsarou, M. E. and Tsiourvas, D. (2013) 'Mitochondrial delivery of doxorubicin by triphenylphosphonium- functionalized hyperbranched nanocarriers results in rapid and severe cytotoxicity', *Pharmaceutical Research*, **30**(11), pp. 2832–2842. doi: 10.1007/s11095-013-1111-7.

- Thomas, H. and M.Coley, H. (2003) 'Overcoming multidrug resistance in cancer: An update on the clinical strategy of inhibiting P-glycoprotein', *Cancer Control*, **10**(2), pp. 159–165. doi: 10.1177/107327480301000207.
- Torchilin, V. (2009) 'Intracellular delivery of protein and peptide therapeutics', *Drug Discovery Today: Technologies*, **5**(2–3). doi: 10.1016/j.ddtec.2009.01.002.
- Turnbull, A. (2003). 'Design and development of novel DNA topoisomerases inhibitors'. PhD, Edinburgh Napier University.
- Varadwaj, P., Misra, K., Sharma, A. and Kumar, R. (2010) 'Mitoxantrone : an agent with promises for anticancer therapies', *Technology*, **6**(2), pp. 36–42.
- Verschoor, M. L., Ungard, R., Harbottle, A., Jakupciak, J. P., Parr, R. L. and Singh, G. (2013) 'Mitochondria and cancer: Past, present, and future', *BioMed Research International*, 2013. doi: 10.1155/2013/612369.
- Via, L. D., Garcia-Argaez, A. N., Martinez-Vazquez, M., Grancara, S., Martinis, P. and Toninello, A. (2014) 'Mitochondrial permeability transition as target of anticancer drugs.', *Current pharmaceutical design*, **20**(2), pp. 223–44. doi: 10.2174/13816128113199990033.
- Wang, J., Gao, R., Li, Q., Xie, S. and Zhao, J. (2012) 'Synthesis , Cytotoxicity , and Cell Death Profile of Polyaminoanthraquinones as Antitumor Agents', *Chemical Biology and Drug Design*, **80**, pp. 909–917. doi: 10.1111/cbdd.12038.
- Wang, X.-H., Peng, H.-S., Yang, L., You, F.-T., Teng, F., Tang, A.-W., Zhang, F.-J. and Li, X.-H. (2013) 'Poly-l-lysine assisted synthesis of core–shell nanoparticles and conjugation with triphenylphosphonium to target mitochondria', *Journal of Materials Chemistry B*, **1**(38), p. 5143. doi: 10.1039/c3tb20884b.
- Wang, Y., Lyu, Y. L. and Wang, J. C. (2002) 'Dual localization of human DNA topoisomerase IIIalpha to mitochondria and nucleus.', *Proceedings of the National Academy of Sciences of the United States of America*, **99**(19), pp. 12114–12119. doi: 10.1073/pnas.192449499.
- Warburg, O. (1956) 'On the Origin of Cancer Cells On the Origin of Cance', *Science*,

123(123), pp. 309–314. doi: 10.1126/science.123.3191.309.

Weissig, V., Boddapati, S. V, Cheng, S.-M. and D'souza, G. G. M. (2006) 'Liposomes and Liposome-like Vesicles for Drug and DNA Delivery to Mitochondria', *Journal of Liposome Research*, **16**(3), pp. 249–264. doi: 10.1080/08982100600851169.

Wolf, K. and Friedl, P. (2005) 'Functional imaging of pericellular proteolysis in cancer cell invasion', *Biochimie*, **87**, pp. 315–320. doi: 10.1016/j.biochi.2004.10.016.

Wolfram, R. K., Heller, L. and Csuk, R. (2018) 'Targeting mitochondria: Esters of rhodamine B with triterpenoids are mitocanic triggers of apoptosis', *European Journal of Medicinal Chemistry*, **152**, pp. 21–30. doi: 10.1016/j.ejmech.2018.04.031.

Wu, W., Luo, Y., Sun, C., Liu, Y., Kuo, P., Varga, J., Xiang, R., Reisfeld, R., Janda, K. D., Edgington, T. S. and Liu, C. (2006) 'Targeting Cell-Impermeable Prodrug Activation to Tumor Microenvironment Eradicates Multiple Drug-Resistant Neoplasms', *Cancer Research*, **66**(2), pp. 970–980. doi: 10.1158/0008-5472.can-05-2591.

Xie, C., Chang, J., Hao, X. D., Yu, J. M., Liu, H. R. and Sun, X. (2013) 'Mitochondrial-targeted prodrug cancer therapy using a rhodamine B labeled fluorinated docetaxel', *European Journal of Pharmaceutics and Biopharmaceutics*, **85**, pp. 541–549. doi: 10.1016/j.ejpb.2013.06.008.

Yang, X., Guo, X. and Zhao, Y. (2002) 'Development of a novel rhodamine-type fluorescent probe to determine peroxynitrite', *Talanta*, **57**, pp. 883–890.

Yu, M., Zhou, Y., Shi, Y., Ning, L., Yang, Y., Wei, X., Zhang, N., Hao, X. and Niu, R. (2007) 'Reduced mitochondrial DNA copy number is correlated with tumor progression and prognosis in Chinese breast cancer patients', *IUBMB Life*, **59**(7), pp. 450–457. doi: 10.1080/15216540701509955.

Zhang, H., Barcelo, J. M., Lee, B., Kohlhagen, G., Zimonjic, D. B., Popescu, N. C. and Pommier, Y. (2001) 'Human mitochondrial topoisomerase I', *Proceedings of the National Academy of Sciences*, **98**(19), pp. 10608–10613. doi: 10.1073/pnas.191321998.

Zhang, H., Meng, L. H. and Pommier, Y. (2007) 'Mitochondrial topoisomerases and alternative splicing of the human TOP1mt gene', *Biochimie*, **89**(4), pp. 474–481. doi:

10.1016/j.biochi.2006.11.002.

Zhitomirsky, B. and Assaraf, Y. G. (2015) 'Lysosomal sequestration of hydrophobic weak base chemotherapeutics triggers lysosomal biogenesis and lysosome-dependent cancer multidrug resistance.', *Oncotarget*, **6**(2), pp. 1143–56. doi: 10.18632/oncotarget.2732.

Zhou, H., Sun, H., Lv, S., Zhang, D., Zhang, X., Tang, Z. and Chen, X. (2017) 'Legumain-cleavable 4-arm poly(ethylene glycol)-doxorubicin conjugate for tumor specific delivery and release', *Acta Biomaterialia*, **54**, pp. 227–238. doi: 10.1016/j.actbio.2017.03.019.

Zhu, L., Zhu, Y., Meng, X., Hao, J., Li, Q., Wei, Y. and Lin, Y. (2008) 'DCC-Assisted Esterification of a Polyoxometalate-Functionalized Phenol with Carboxylic Acids (DCC: Dicyclohexylcarbodiimide)', *Chemistry - A European Journal*, **14**(35), pp. 10923–10927. doi: 10.1002/chem.200801836.

Ziegler, U. and Groscurth, P. (2004) 'Morphological Features of Cell Death', *Physiology*, **19**(3), pp. 124–128. doi: 10.1152/nips.01519.2004.

Chapter 3

3 Chapter 3: Summary Discussion of Research Results

3.1 Overview

All of the research and data presented in this thesis (Chapters 1 and 2) is focused on methods to improve drug selectivity for cancer cells by designing and developing novel chemotherapeutic agents that actively exploit phenotypic differences between cancer and healthy cells and which target features unique to the tumour microenvironment. If cytotoxic agents can be made to target cancer cells selectively, this will thereby reduce adverse side effects while improving therapeutic efficacy. One approach being used to achieve selectivity is to better control drug delivery by using appropriately designed drug delivery vehicles (Senapati et al., 2018). Alternatively, in this research project, to achieve selectivity, non-vehicle mediated approaches have been used to design new candidate drugs or prodrugs in the anthraquinone (anthracenedione) category of cytotoxics (the former to be directly imported into intracellular components of the cancer cell and the latter to be activated at the cancer cell surface). This chapter describes proven concepts that were achieved and summarizes the biological significance of the major research findings in relation to the primary objective of improving drug selectivity for cancer cells and collated structure-activity relationships drawn from the data.

3.2 Proof of Concepts

3.2.1 Proof of Concept 1: selectivity for cancer cell mitochondria

In this project, proof of concept has been demonstrated for selective localization of anticancer compounds inside the mitochondria of cancer cells, summarized as illustrated in proof of concept **Figure 3.1** where novel aminoanthraquinone derivatives have been conjugated with the lipophilic cationic triphenylphosphonium (TPP) and rhodamine B

residues. Attaching these cationic residues has made compounds more lipophilic, as hypothesized, to improve entry to the cell by taking advantage of the reported high membrane potential of mitochondria compared with the plasma membrane (Constance & Lim, 2012). The sub-cellular localization of novel compounds to the target mitochondria was shown by confocal microscopy studies (data in **Chapter 1 section 1.3.9**)

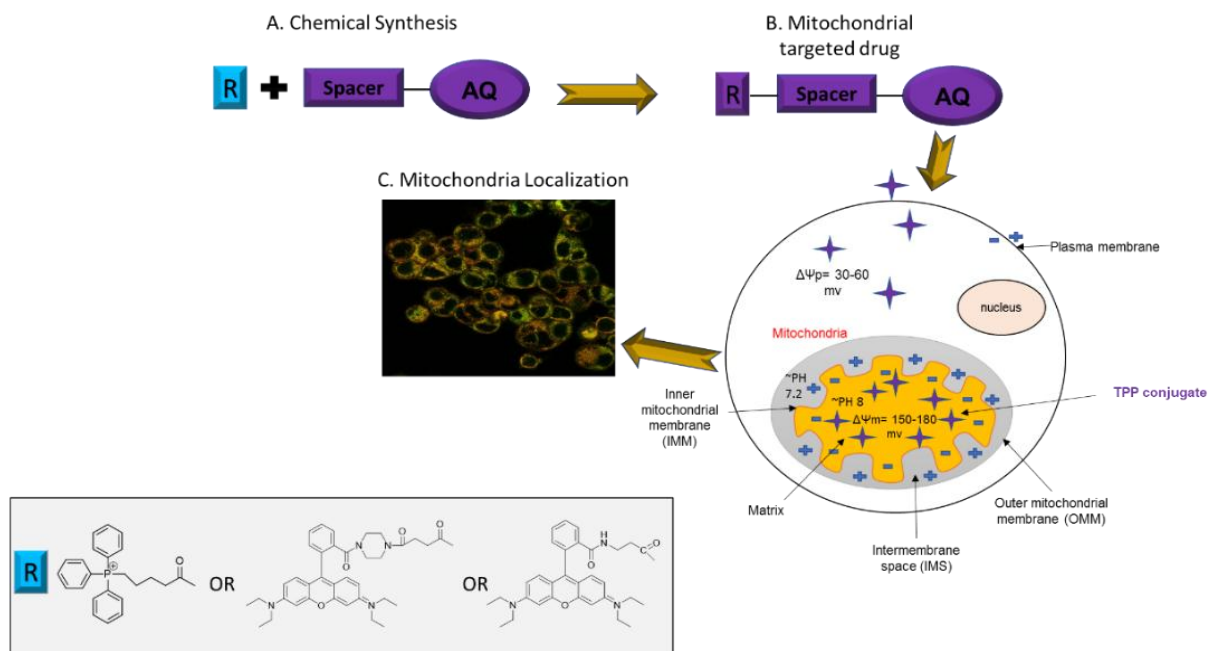


Figure 3.1: Illustration of Proof of Concept for mitochondrial targeted drugs. A. Chemical synthesis of mitochondrial targeted drug; B. mitochondrial targeted drug and C. confocal image which shows the localization of a TPP conjugate drug in mitochondria.

3.2.2 Biological significance of mitochondrial targeting and mechanistic considerations.

The failure of cancer patients to respond to specific therapeutic treatment can happen due to the fact that cancer cells become resistant to a single class of drugs by specific metabolism of a drug, loss of a cell surface receptor or transporter for a drug and modification by mutation of the specific target of a drug (Longo-Sorbello & Bertino, 2001). Also, cancer cells can develop resistance to different classes of drugs that have unrelated structure and function. This phenomenon is known as multidrug resistance (MDR) (Sauna

et al., 2001) and P-gp (drug efflux pump) is commonly involved in the development of MDR, overexpressed in the plasma membrane of cancer cells and can be found in subcellular regions including the lysosomes, mitochondria and nucleus (Roundhill & Burchill, 2012). However, the presence of P-gp is controversial; it has been reported that P-gp is not present in mitochondria (Paterson & Gottesman, 2007), but may simply be functionally inactive, therefore specific delivery of anticancer drugs to mitochondria could avoid drug resistance and consequently increase drug selectivity and efficacy.

Considerable efforts have already been invested to develop mitochondria-targeted compounds to induce cancer cells apoptosis and bypass drug resistance mechanisms. Earlier reports have shown mitochondria-specific drug delivery can be achieved by direct chemical conjugation of selective anticancer agent with mitochondriotropic ligands, that have lipophilicity and delocalization of the positive charge properties such as triphenylphosphonium (TPP) (Han *et al.*, 2014). It has been reported that the mitochondrial TPP-conjugates accumulate selectively inside the mitochondria and induce cytotoxicity even in resistant cells. In the most closely related example to the work in this thesis, Han *et al.*, 2014, conjugated the anthraquinone doxorubicin (DOX) with TPP and they studied the cellular distribution and cytotoxicity for both DOX and TPP-DOX conjugate. They found that the TPP-DOX conjugate accumulated inside the mitochondria compared with DOX alone, which was found to be localized in nucleus and cytoplasm. The TPP-DOX induced cytotoxicity in both cell lines MDA-MB-435/WT and DOX resistant MDA-MB-435/DOX. This indicates the ability of a TPP conjugate to escape the drug resistance and accumulate inside the mitochondria (Han *et al.*, 2014). In addition, Millard *et al.*, 2013, conjugated the non-anthraquinone chlorambucil with TPP. The results revealed that this TPP conjugate localized to cancer cell mitochondria where it acted on mtDNA to inhibit the cell cycle and induce cell apoptosis (Millard *et al.*, 2013). In this program of research, anthraquinones (mitoxantrone analogues) were conjugated with TPP with the aim of achieving reaching the mitochondria (avoiding the nucleus) and similarly inducing apoptosis, which for the aminoanthraquinone class points to mtDNA or possibly mtDNA-topoisomerases as targets (given these are counterparts of their known nuclear targets).

In vitro studies revealed that attaching TPP made the anticancer drugs more lipophilic and gave the ability to bypass the lipid bilayer of cancer cells and accumulate inside the mitochondria. Also, the MTT assay for novel compounds was studied in both high resistance HCT-15 and low resistance MCF-7 cell lines, to screen for compounds that have the potential to circumvent P-gp drug resistance. The results showed the ability of TPP compounds to induce cytotoxicity in both cells lines compared with the unconjugated compounds, which suggests this strategy may be able to circumvent multidrug resistance in this series.

Furthermore, lysosomes are another organelle inside the cell which offer an effective compartment for targeting anticancer drugs. Cancer cells are more vulnerable to lysosomal mediated cell death than normal cells which can be exploited in the design of new effective anticancer drugs that enhance lysosomal cell death for example, by inhibition of caspase dependent cell death (Halaby, 2019). However, lysosomes were suggested to play a significant role in MDR by sequestering protonated hydrophobic weak bases from their intracellular targeting site (Zhitomirsky & Assaraf, 2015). Therefore, this can be exploited by designing a weak base anticancer drug that can accumulate inside the lysosomes and alter its function which in turn could lead to cell death. Herein, OM22 [TPP-EAE-AQ(4-OH)] was synthesised and found to be localised in lysosomes not in the mitochondria even in the presence of an added lipophilic cation TPP, due to the presence of amine group in its side chain, which made OM22, a lipophilic amine (weak base) which was trapped or sequestered inside the acidic lysosomes. However, *in vitro* studies revealed that OM22 induced cytotoxicity at low concentration in both high resistance HCT-15 and low resistance MCF-7 cell lines. These properties may be due to the ability of OM22 to avoid drug resistance by interfering with lysosome function and induce apoptosis. In preliminary apoptotic studies, OM22 exhibited prominent growth inhibition of HCT-116 and cells were shrunken and floating indicating that the cells were dead at all tested time points. Therefore, OM22 has the ability to localise inside the lysosomes and induce cell death. Groth-pedersen & Jäättelä, 2013 reported that induction of lysosomal membrane permeabilization is an effective way to kill resistant cancer cells and the enlarged lysosomal in cancer cells make them more vulnerable to cancer drugs compared to normal cells, therefore reducing the side effects (Groth-pedersen & Jäättelä, 2013). The

combination of structural features of cationic groups and weakly-basic amine chains in OM22 is something that can be exploited further to design lysosomotropic agents and is considered worthy of expanding these studies to design more analogues in future.

As lysosomes in cancer cells are more fragile than normal cells, they are more susceptible to lysosomal membrane permeabilization LMP. This fragility may stem in part from their high lysosomal iron content (Abok *et al.*, 1983; Persson *et al.*, 2003). Reactive oxygen species (ROS) generation can result in destabilisation of lysosomal membranes through lipid peroxidation (Persson, *et al.* 2003). ROS are aerobic respiration byproducts which are responsible for maintaining redox homeostasis in cells by antioxidant enzymes, reduced thiols and NADP(H) cofactors and it is essential for cancer cells survival and progression. Cancer cells exhibit higher metabolic rates and increased iron-containing proteins, which lead to the accumulation of iron in lysosomes, which in turn affords iron-mediated sensitization to ROS and induction of LMP (Halaby, 2015). Dharmaraja, 2017, reported that quinones based compounds such as mitoxantrone and doxorubicin have the ability to induce ROS. Therefore, elevating the ROS rates led to disruption of the LMP, resulting in release of acid hydrolases, specifically the cathepsins to the cytosol, then inducing cell apoptosis (Halaby, 2019). Therefore, the well-known mechanism for iron mediated ROS production by anthraquinones and anthracyclines could be a potential mechanism of cell death by the anthraquinones OM22 and NU:UB 51.

Disruption of organelle membranes is a mechanism of cell death that can also apply to mitochondria (Via *et al.*, 2014), with outer mitochondrial membrane (OMM) permeabilisation followed by release of proteins such as cytochrome C (essential for activation of the mitochondrial apoptotic pathway) (Riganti *et al.*, 2013). As with lysosomal membrane permeability, generation of ROS have been found to play a role in OMM permeabilisation (Webster, 2013). Quinone containing compounds, for example β -lapachone, induce enhanced ROS via mitochondrial enzyme mediated redox cycling with ROS production leading to mitochondrial oxidative damage, membrane permeabilisation and apoptosis (Ma *et al.*, 2015). This mechanism of cell kill could potentially also apply to the mitochondria targeted quinone containing compounds synthesised here.

Furthermore, it is known, for example, the triterpenoid betulinic acid triggers RSO mediated apoptosis and when conjugated to TPP resulted in a significant increase in cytotoxicity compared to unconjugated betulinic acid (Nedopekina *et al.*, 2017). In addition to mitochondrial targeting, TPP conjugation to betulinic acid was also used to enhance bioavailability, a concept that also applies to many of the compounds synthesised in this research programme. For example, NU:UB 238, the aminobutanol anthraquinone precursor of SH1, is not taken up by cells and is completely inactive *in vitro* [and *in vivo* (*unpublished data*)] however upon conjugation to TPP, results in compound SH1 with the ability to bind with DNA at high affinity and induce cytotoxicity *in vitro* at low concentrations. In Addition, SH1 was found to be localized in mitochondria and induce cell morphological changes, whereas the NU:UB 238 has no ability to enter the cells **Figure 3.4.**

Uptake of a mitochondrial targeted organometallic ruthenium doxorubicin complex (Imstepf *et al.*, 2016) triggered apoptosis and disrupted mitochondrial membrane potential and also inhibited topoisomerase II; mechanisms of cell kill that incorporate these dual-targeting features could also apply to the TPP conjugates such as SH1, OM30, OM31 and OM32 and further research into these plausible mechanisms is required.

3.2.3 **Proof of Concept 2: selective prodrug activation at the cancer cell surface**

In this research programme, a theranostic (therapeutic and diagnostic) prodrug Rho-Pro-Ala-Asn-Gly-APA-AQ(4,8-di-OH) (OM50) was synthesized, where selectivity was achieved by exploiting the proteolytic activity of overexpressed legumain in the cancer cell microenvironment. Proof of concept **Figure 3.2** illustrates how the cleavage of the prodrug OM50 by legumain at the directed cleavage site, resulted in the release of the cytotoxic agent, anthraquinone derivative NU:UB 51, accompanied by a large increase in rhodamine fluorescence. Confocal microscopy and live cell imaging using HCT-116 colon cancer cells showed that the prodrug was not taken up by cells in contrast to the active

agent (data in **Chapter 2 section 2.3.8**) These properties make prodrug OM50 a good candidate for extracellular activation by secreted legumain.

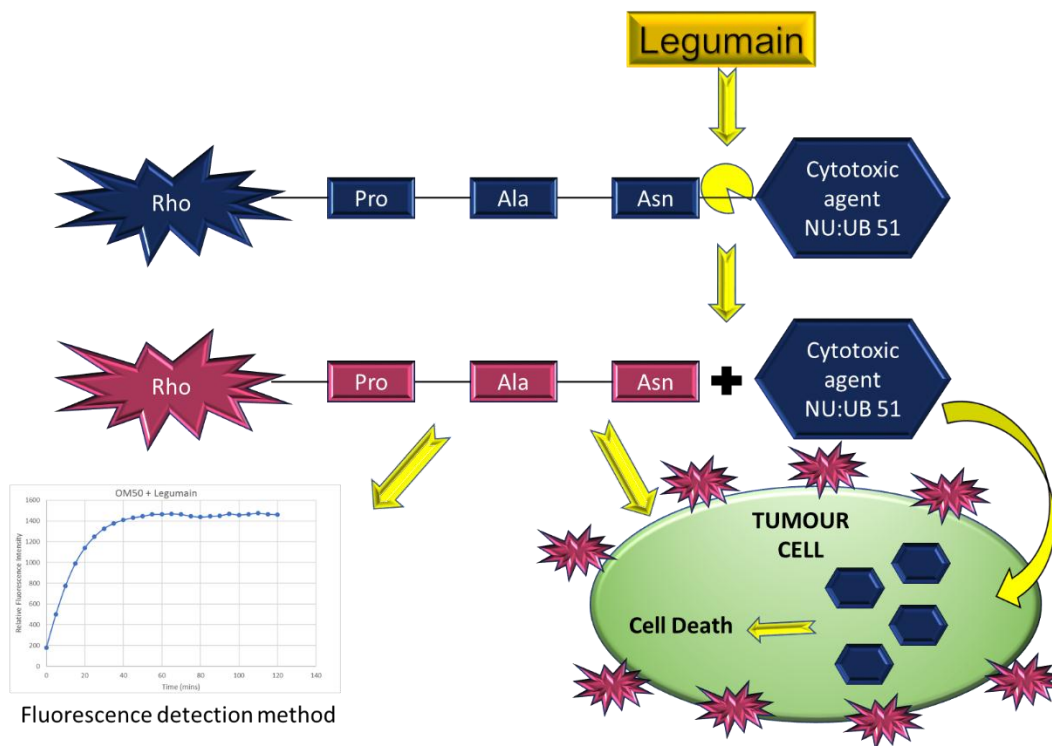


Figure 3.2: Illustration of Proof of Concept for the theranostic prodrug Rho-Pro-Ala-Asn-Gly-APA-AQ(4,8-di-OH) (OM50) and showing legumain-mediated activation of the prodrug and simultaneous release of a rhodamine B-labelled peptide (fluorescent reporter of prodrug activation) and cytotoxic agent NU:UB 51 at the tumour cell.

3.2.4 Biological significance

Cancer progression is not exclusively due to changes in cancer cells, but also includes the tumour microenvironment, which has a notable different character in in cancer cells compared with the environment surrounding normal cells. Tumour microenvironment is rich in proteolytic activity and it is acidic and hypoxic and includes a wide spectrum of proteases that include the cysteine endopeptidase legumain. The tumour microenvironment is a favourable environment for protease targeted alteration of prodrugs. Additionally, the cellular microenvironment has a role in tumourigenesis which has become a major area of research (Arroyo-crespo *et al.*, 2018). The proteolytic

specificities for peptide substrates provide a promising tool for designing prodrugs that are specifically activated by proteases (in this research, legumain) in the tumour microenvironment (Wu *et al.*, 2006). In this programme of work which focused on the anthraquinone class of compounds, it was logical to test the combination of achieving selective targeting of an anthraquinone by prodrug conversion and extracellular activation. Therefore, a theranostic prodrug Rho-Pro-Ala-Asn-Gly-APA-AQ(4,8-di-OH) (OM50) was designed and synthesized in this project. The legumain-targeted prodrug OM50 employs a three component design which are a cytotoxic topoisomerase inhibitor (NU:UB 51) as the active agent and fluorescence quencher, a tripeptide Pro-Ala-Asn (substrate sequence) and rhodamine B (as latent fluorophore). *In vitro* assays were performed by incubation of OM50 with human recombinant legumain. Increase in the fluorescence intensity of rhodamine emission with time verified that cleavage of OM50 was taking place by legumain at the predicted C-terminal of asparagine, resulting in the release of the active drug NU:UB 51 and rhodamine B-labelled peptide fragment, which in turn indicated prodrug activation.

More cellular localization studies were performed for both OM50 and the active drug NU:UB 51 to find the preferred targeting location for both. The results indicated that the prodrug OM50 was localized outside the cells in the tumour microenvironment (where the legumain is secreted). However, the active drug NU:UB 51 was found to be localized in both mitochondria and lysosomes. It has been reported that NU:UB 51 has the ability to inhibit topoisomerase II α and II β mediated decatenation and relaxation of DNA and it inhibits topoisomerase I mediated DNA-relaxation. NU:UB 51 produces a tumour volume reduction and significant growth delay in a colon tumour model, whereas mitoxantrone and doxorubicin produce a simple growth delay with no reduction in tumour volume (Mincher, 1999; Turnbull, 2003). Therefore, the new results confirmed the successful synthesis of the theranostic prodrug and its activation and these promising results could open a new field in the treatment of tumour cells by adding an extra layer of cancer cell selectivity by using a prodrug approach to the anthraquinone class with known *in vivo* activity. These results are consistent with the findings of Løvsletten *et al.*, 2014 who synthesized a legumain-cleavable prodrugs Suc-Ala-Ala-Asn-Val-colchicine. They found that the prodrug was more toxic to colorectal cancer HCT116 cells (expressing both the

active legumain and inactive, zymogen prolegumain) than SW620 cells expressing prolegumain only.

3.3 Multiple uses of rhodamine B in this research

Rhodamine B has been used in several different ways throughout this research programme and presented in each of chapters 1 and 2; as a delocalized lipophilic cation for selective mitochondrial targeting, as a capping group and as a fluorophore in theranostic applications **Figure 3.3**. Rhodamine B is a member of delocalized lipophilic cations and it has been used as a carrier for molecules targeting mitochondria because of preferential accumulation in this organelle and due to its lipophilic cationic properties (Muli *et al.*, 2014). It has been reported that accumulation of rhodamine B conjugate dyes inside the cell (mitochondria) is higher than the unconjugated ones due directly to the delocalized positive charge of rhodamine B (Ngen *et al.*, 2009). Therefore, rhodamine B was conjugated with anthraquinone derivatives for selective targeting to mitochondria. However, due to difficulty in purification and stability of rhodamine B conjugates, no further *in vitro* studies were carried out, and TPP conjugates remained the main focus.

In addition, rhodamine B was used as a fluorescent probe and required some modifications such as reaction to form a tertiary amide and locked in the ring-open form as in Rho-Pro-OH, due to the sensitivity of ring-open rhodamine B to pH causing loss of fluorescence at low pH, whereas when reacted with Pro-OH the fluorescence emission remained constant over the measured pH range. Therefore, this technique was employed in the design of OM50 in which rhodamine B was used to label the N-terminus of Pro-Ala-Asn (legumain substrate) and cytotoxic topoisomerase inhibitor NU:UB 51 was linked with the C-terminus of asparagine.

THE MULTIPLE USES OF RHODAMINE B IN THIS RESEARCH

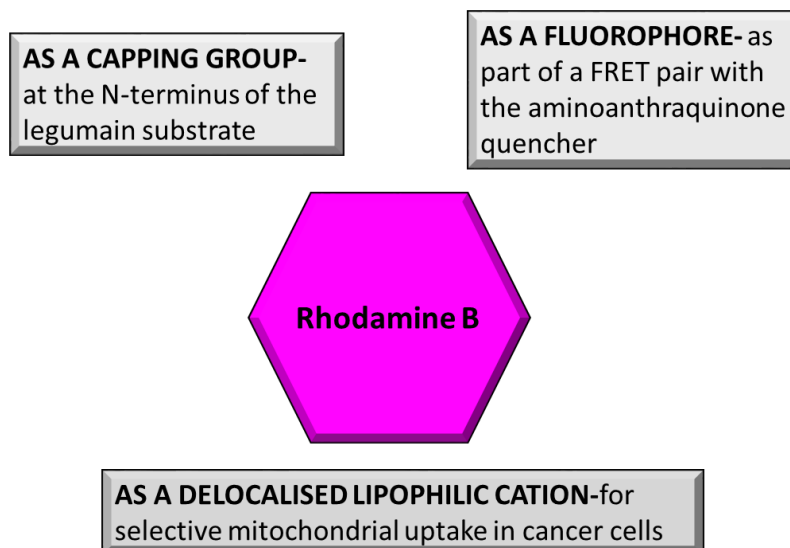


Figure 3.3: Different uses of rhodamine B in this research

3.4 Structure-activity relationships

Confocal microscopy proved invaluable when determining subcellular localisation of the novel compounds, as summarised in **Figure 3.4**. These studies indicated that even small structural changes led to very marked alterations in the subcellular distribution of the TPP conjugates. The chemical structure plays an important role in localization and activity of targeting compounds. Shaul *et al.*, (2013) studied the effect of anthracyclines structure on the cytotoxicity and the time required for these compounds to exert cytotoxic effects on tumor cells. Also the confocal studies indicated that structural differences led to differences in subcellular localization (Shaul et al., 2013). All of the TPP compounds containing hydrophobic polymethylene alkyl linkers (SH1, OM 30 and OM31) localised selectively in the mitochondria, with little or no evidence of lysosomal or nuclear accumulation. These observations proved the hypothesis that the novel TPP analogues of mitoxantrone can be delivered to and accumulate selectively in mitochondria of cancer cells *in vitro*.

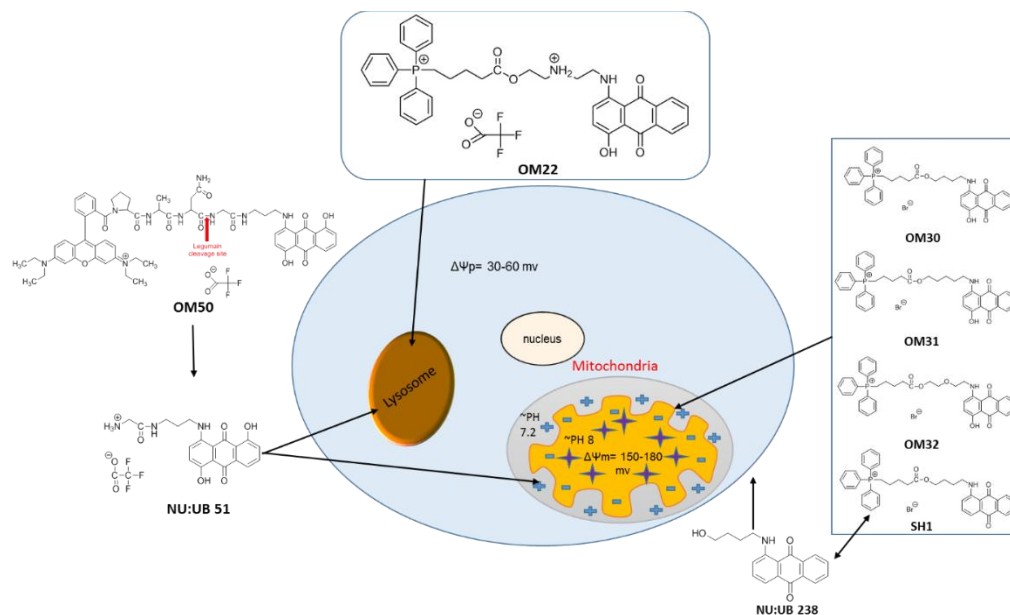


Figure 3.4: Selective delivery of novel anticancer drugs that have been synthesised in this research.

Although not for anticancer use, similar simple alkyl TPP cations were also used for selective delivery of Coenzyme Q and Vitamin E to mitochondria (Smith et al., 2003; Smith et al., 1999). In common with SH1, OM30 and OM31, MitoQ and MitoVitE selectively accumulated in mitochondria *in vitro* (Kelso et al., 2001; Smith et al., 2003) and are also low molecular weight lipophilic TPP conjugates. In addition to *in vitro* evaluation, Smith *et al* also carried out *in vivo* studies on MitoQ and MitoVitE in mice and found that not only could TPP deliver potentially therapeutic effective concentrations to mitochondria *in vivo*, the compounds were also able to cross the blood brain barrier (Smith et al., 2003). The favourable *in vivo* profile shown by MitoQ and MitoVitE offers promise for the future development of anthraquinone conjugates such as SH1, OM30 and OM31.

In complete contrast to compounds with simple alkyl linked TPP cations, OM22, containing an ethyl-amino-ethyl linker localised selectively in lysosomes **Figure 3.4**, this is despite also containing a TPP delocalised cation. The only structural difference between OM22 and the compounds which did selectively target mitochondria [SH1, OM30, OM31 and OM32 (containing central oxygen in the linker)] is the presence of the secondary amino group in the side chain which appears to lead to ‘over-riding’ of the TPP mediated mitochondrial mechanism.

This is rather surprising, as the literature confirms that TPP can be used to transport neutral, acid and basic cargos into mitochondria (Finichiu *et al.*, 2013), although the rate of accumulation was slower for amine containing compounds. As TPP compounds are first accumulated from the extracellular matrix into the cytoplasm, if subsequent uptake into mitochondria is relatively slow, there may be competition between mitochondrial and lysosomal distribution for amine containing compounds. Although delocalised lipophilic cations preferentially accumulate in mitochondria (Guzman-villanueva *et al.*, 2015; Reily *et al.*, 2013), weakly basic lipophilic drugs with localised cationic charges are extensively sequestered in acidic lysosomes (Zhitomirsky & Assaraf, 2015).

The observation that the compounds that accumulate in lysosomes are OM22 and NU:UB 51 might be linked to the presence of the secondary and primary amino groups, respectively (they are both weakly basic lipophilic drugs with localised cationic charges). It is well known from the literature that weakly basic amine containing drugs diffuse through membranes at physiological pH via passive diffusion, once inside the lysosomes, the amine containing drugs become protonated and become trapped in lysosomes in their cationic state (Derendorf, 2020; Halaby, 2019).

What is notable from the confocal studies is the absence of nuclear localisation for any of the novel anthraquinone compounds synthesised in this research programme. The principal mechanism of action for many anthraquinones and anthracyclines, including doxorubicin, is usually given as inhibition of DNA topoisomerases (Swift *et al.*, 2006; Tacar *et al.*, 2013). In fact, many anthraquinones have now been shown to also accumulate in other organelles such as lysosomes (Shaul *et al.*, 2013) and this organelle is now proposed to contain additional targets for anthraquinones and anthracyclines (Kroemer & Jäättelä, 2005; Kwok & Richardson, 2004) which might also be targets for OM22 and NU:UB 51. As these are both cationic drugs, they have the potential to induce lysosomal membrane permeability (LMP) and cell death through the release of cathepsins into the cytosol (Fennelly & Amaravadi, 2017; Groth-pedersen & Jäättelä, 2013).

Furthermore, regarding the prodrug aspects of this work, in the synthesis of the prodrug OM50, selection of the amino acid residues at the *N*- and *C*- terminal is a key point to be recognized by legumain. Therefore, asparagine (Asn) was used at position P1 for

recognition and cleavage by legumain at the C-terminus (Stern *et al.*, 2009) and proline was chosen for position P3 to maintain constant fluorescence once cleaved by legumain to lock the rhodamine B in a ring open form by linking it through a tertiary amide bond (Beija *et al.*, 2009) **Figure 3.4.**

In conclusion, by understanding of the tumour biology, structure-activity relationships and by development of specific carriers and/or designing more advanced features such as, prodrug and theranostic systems, have led to successful approaches to deliver anthraquinone chemotherapeutic agents selectively to the mitochondria or lysosomes of cancer cells.

3.5 References

- Abok, K., Hirth, T., Ericsson, J. L. E., & Brunk, U. (1983). Effect of iron on the stability of macrophage lysosomes. *Virchows Archiv B*, **43**(1), 85–101. <https://doi.org/10.1007/BF02932947>
- Arroyo-crespo, J. J., Armiñán, A., Charbonnier, D., Balzano-nogueira, L., Huertas-lópez, F., Martí, C., Tarazona, S., Forteza, J., Conesa, A., & Vicent, M. J. (2018). Tumor microenvironment-targeted poly-L-glutamic acid-based combination conjugate for enhanced triple negative breast cancer treatment. *Biomaterials*, **186**, 8–21. <https://doi.org/10.1016/j.biomaterials.2018.09.023>
- Beija, M., Afonso, C. A. M., & Martinho, J. M. G. (2009). Synthesis and applications of Rhodamine derivatives as fluorescent probes. *Chemical Society Reviews*, **38**, 2410. <https://doi.org/10.1039/b901612k>
- Constance, J. E., & Lim, C. S. (2012). Targeting malignant mitochondria with therapeutic peptides. *Therapeutic Delivery*, **3**(8), 961–979. <https://doi.org/10.4155/tde.12.75>
- Derendorf, H. (2020). Excessive lysosomal ion-trapping of hydroxychloroquine and azithromycin. *International Journal of Antimicrobial Agents*, **55**. <https://doi.org/10.1016/j.ijantimicag.2020.106007>
- Dharmaraja, A. T. (2017). Role of Reactive Oxygen Species (ROS) in Therapeutics and Drug Resistance in Cancer and Bacteria. *Journal of Medicinal Chemistry*, **60**(8), 3221–3240. <https://doi.org/10.1021/acs.jmedchem.6b01243>
- Fennelly, C., & Amaravadi, R. K. (2017). Lysosomal Biology in Cancer. *Methods in Molecular Biology*, **1594**, 179–189. <https://doi.org/10.1007/978-1-4939-6934-0>
- Finichiu, P. G., James, A. M., Larsen, L., Smith, R. A. J., & Murphy, M. P. (2013). Mitochondrial accumulation of a lipophilic cation conjugated to an ionisable group depends on membrane potential, pH gradient and pK_a: Implications for the design of mitochondrial probes and therapies. *Journal of Bioenergetics and Biomembranes*,

45(1–2), 165–173. <https://doi.org/10.1007/s10863-012-9493-5>

Groth-pedersen, L., & Jäättelä, M. (2013). Combating apoptosis and multidrug resistant cancers by targeting lysosomes. *Cancer Letters*, **332**(2), 265–274. <https://doi.org/10.1016/j.canlet.2010.05.021>

Guzman-villanueva, D., Mendiola, M. R., Nguyen, H. X., & Weissig, V. (2015). Influence of Triphenylphosphonium (TPP) Cation Hydrophobization with Phospholipids on Cellular Toxicity and Mitochondrial Selectivity. *SOJ Pharmacy & Pharmaceutical Sciences*, **2**(1), 1–9.

Halaby, R. (2015). Role of lysosomes in cancer therapy. *Research and Reports in Biology*, **6**, 147–155. <https://doi.org/dx.doi.org/10.2147/RRB.S83999>

Halaby, R. (2019). Influence of lysosomal sequestration on multidrug resistance in cancer cells. *Cancer Drug Resistance*, **2**, 31–42. <https://doi.org/10.20517/cdr.2018.23>

Han, M., Vakili, M. R., Abyaneh, H. S., Molavi, O., Lai, R., & Lavasanifar, A. (2014). Mitochondrial Delivery of Doxorubicin via Triphenylphosphine Modification for Overcoming Drug Resistance in MDA-MB-435/DOX Cells. *American Chemical Society*, **11**, 2640–2649.

Imstepf, S., Pierroz, V., Rubbiani, R., Felber, M., Fox, T., Gasser, G., & Alberto, R. (2016). Drug Targeting Organometallic Rhenium Complexes Divert Doxorubicin to the Mitochondria *Angewandte Chemie International Edition*, **55**, 2792–2795. <https://doi.org/10.1002/anie.201511432>

Kelso, G. F., Porteous, C. M., Coulter, C. V, Hughes, G., Porteous, W. K., Ledgerwood, E. C., Smith, R. A. J., & Murphy, M. P. (2001). Selective Targeting of a Redox-active Ubiquinone to Mitochondria within Cells. *The Journal OF Biological Chemistry*, **276**(7), 4588–4596. <https://doi.org/10.1074/jbc.M009093200>

Kroemer, G., & Jäättelä, M. (2005). Lysosomes and autophagy in cell death control. *Nature Reviews Cancer*, **5**(11), 886–897. <https://doi.org/10.1038/nrc1738>

Kwok, J., & Richardson, D. (2004). Examination of the Mechanism(s) Involved in Doxorubicin-Mediated Iron Accumulation in Ferritin: Studies Using Metabolic

Inhibitors, Protein Synthesis Inhibitors, and Lysosomotropic Agents. *Molecular Pharmacology*, **65**, 181–195. <https://doi.org/10.1124/mol.65.1.181>

Longo-Sorbello, G., & Bertino, J. R. (2001). Current understanding of methotrexate pharmacology and efficacy in acute leukemias. Use of newer antifolates in clinical trials. *Haematologica*, **86**, 121–127.

Løvsletten, R., Alexander, O., Åstrand, H., Minh, L., Elvestrand, T., Hagelin, G., Solberg, R., Thidemann, H., & Rongved, P. (2014). Synthesis of a novel legumain-cleavable colchicine prodrug with cell-specific toxicity. *Bioorganic & Medicinal Chemistry*, **22**(13), 3309–3315. <https://doi.org/10.1016/j.bmc.2014.04.056>

Ma, J., Lim, C., Sacher, J. R., Houten, B. Van, Qian, W., & Wipf, P. (2015). Mitochondrial targeted β -lapachone induces mitochondrial dysfunction and catastrophic vacuolization in cancer cells. *Bioorganic & Medicinal Chemistry Letters*, **25**(21), 4828–4833. <https://doi.org/10.1016/j.bmcl.2015.06.073>. Mitochondrial

Millard, M., Gallagher, J. D., Olenyuk, B. Z., & Neamati, N. (2013). A Selective Mitochondrial-Targeted Chlorambucil with Remarkable Cytotoxicity in Breast and Pancreatic Cancers. *Journal of Medicinal Chemistry*, **56**(22), 9170–9179. <https://doi.org/10.1021/jm4012438>

Muli, D. K., Rajaputra, P., You, Y., & McGrath, D. V. (2014). Asymmetric ZnPc-rhodamine B conjugates for mitochondrial targeted photodynamic therapy. *Bioorganic and Medicinal Chemistry Letters*, **24**(18), 4496–4500. <https://doi.org/10.1016/j.bmcl.2014.07.082>

Nedopekina, D. A., Gubaidullin, R. R., Odinokov, V. N., Maximchik, P. V., Zhivotovsky, B., Bel'skii, Y. P., Khazanov, V. A., Manuylova, A. V., Gogvadze, V., & Spivak, A. Y. (2017). Mitochondria-targeted betulinic and ursolic acid derivatives: synthesis and anticancer activity. *MedChemComm*, **8**(10), 1934–1945. <https://doi.org/10.1039/c7md00248c>

Ngen, E. J., Rajaputra, P., & You, Y. (2009). Evaluation of delocalized lipophilic cationic dyes as delivery vehicles for photosensitizers to mitochondria. *Bioorganic and Medicinal Chemistry*, **17**(18), 6631–6640.

<https://doi.org/10.1016/j.bmc.2009.07.074>

Paterson, J. K., & Gottesman, M. M. (2007). P-Glycoprotein is not present in mitochondrial membranes. *Experimental Cell Research*, **313**(14), 3100–3105. <https://doi.org/10.1016/j.yexcr.2007.04.019>

Persson, H. L., Yu, Z., Tirosh, O., Eaton, J. W., & Brunk, U. T. (2003). Prevention of oxidant-induced cell death by lysosomotropic iron chelators. *Free Radical Biology and Medicine*, **34**(10), 1295–1305. [https://doi.org/https://doi.org/10.1016/S0891-5849\(03\)00106-0](https://doi.org/https://doi.org/10.1016/S0891-5849(03)00106-0)

Reily, C., Mitchell, T., Chacko, B. K., Benavides, G. A., Murphy, M. P., & Darley-Usmar, V. M. (2013). Mitochondrially targeted compounds and their impact on cellular bioenergetics. *Redox Biology*, **1**(1), 86–93. <https://doi.org/10.1016/j.redox.2012.11.009>

Riganti, C., Rolando, B., Kopecka, J., Campia, I., Chegaev, K., Lazzarato, L., Federico, A., Fruttero, R., & Ghigo, D. (2013). Mitochondrial-targeting nitrooxydoxorubicin: A new approach to overcome drug resistance. *Molecular Pharmaceutics*, **10**(1), 161–174. <https://doi.org/10.1021/mp300311b>

Roundhill, E. A., & Burchill, S. A. (2012). Detection and characterisation of multi-drug resistance protein 1 (MRP-1) in human mitochondria. *British Journal of Cancer* (2012), **106**, 1224–1233. <https://doi.org/10.1038/bjc.2012.40>

Sauna, Z. E., Smith, M. M., Müller, M., Kerr, K. M., & Ambudkar, S. V. (2001). The Mechanism of Action of Multidrug-Resistance-Linked P-Glycoprotein. *Journal of Bioenergetics and Biomembranes*, **33**(6), 481–491. <http://www.ncbi.nlm.nih.gov/pubmed/2689019>

Senapati, S., Mahanta, A. K., Kumar, S., & Maiti, P. (2018). Controlled drug delivery vehicles for cancer treatment and their performance. *Signal Transduction and Targeted Therapy*, **3**(1), 1–19. <https://doi.org/10.1038/s41392-017-0004-3>

Shaul, P., Frenkel, M., Goldstein, E. B., Mittelman, L., Grunwald, A., Ebenstein, Y., Tsarfaty, I., & Fridman, M. (2013). The Structure of Anthracycline Derivatives Determines Their Subcellular Localization and Cytotoxic Activity. *ACS Medicinal*

Chemistry Letters, **4**(3), 323–328.

Smith, R. A. J., Porteous, C. M., Coulter, C. V, & Murphy, M. P. (1999). Selective targeting of an antioxidant to mitochondria. *European Journal of Pharmacology*, **263**, 709–716.

Smith, R. a J., Porteous, C. M., Gane, A. M., & Murphy, M. P. (2003). Delivery of bioactive molecules to mitochondria in vivo. *Proceedings of the National Academy of Sciences of the United States of America*, **100**(9), 5407–5412. <https://doi.org/10.1073/pnas.0931245100>

Stern, L., Perry, R., Ofek, P., Many, A., Shabat, D., & Satchi-Fainaro, R. (2009). A novel antitumor prodrug platform designed to be cleaved by the endoprotease legumain. *Bioconjugate Chemistry*, **20**(3), 500–510. <https://doi.org/10.1021/bc800448u>

Swift, L. P., Rephaeli, A., Nudelman, A., Phillips, D. R., & Cutts, S. M. (2006). Doxorubicin-DNA adducts induce a non-topoisomerase II-mediated form of cell death. *Cancer Research*, **66**(9), 4863–4871. <https://doi.org/10.1158/0008-5472.CAN-05-3410>

Tacar, O., Sriamornsak, P., & Dass, C. R. (2013). Doxorubicin: An update on anticancer molecular action, toxicity and novel drug delivery systems. *Journal of Pharmacy and Pharmacology*, **65**(2), 157–170. <https://doi.org/10.1111/j.2042-7158.2012.01567.x>

Via, L. D., Garcia-Argaez, A. N., Martinez-Vazquez, M., Grancara, S., Martinis, P., & Toninello, A. (2014). Mitochondrial permeability transition as target of anticancer drugs. *Current Pharmaceutical Design*, **20**(2), 223–244. <https://doi.org/10.2174/13816128113199990033>

Webster, K. A. (2013). Mitochondrial membrane permeabilization and cell death during myocardial infarction: roles of calcium and reactive oxygen species. *Future Cardiol*, **8**(6), 863–884. <https://doi.org/10.2217/fca.12.58>. Mitochondrial

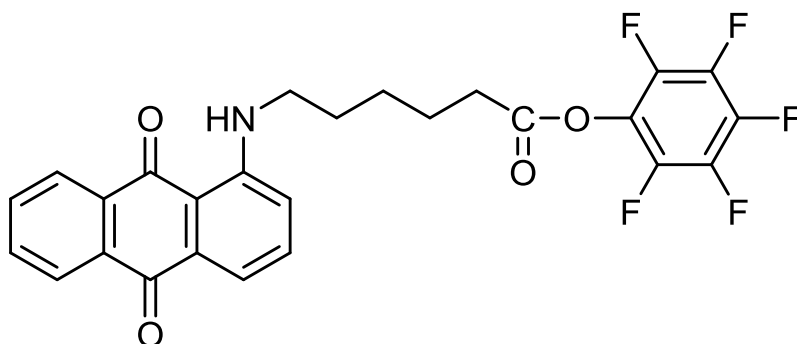
Wu, W., Luo, Y., Sun, C., Liu, Y., Kuo, P., Varga, J., Xiang, R., Reisfeld, R., Janda, K. D., Edgington, T. S., & Liu, C. (2006). Targeting Cell-Impermeable Prodrug

Activation to Tumor Microenvironment Eradicates Multiple Drug-Resistant Neoplasms. *Cancer Research*, **66**(2), 970–980. <https://doi.org/10.1158/0008-5472.can-05-2591>

Zhitomirsky, B., & Assaraf, Y. G. (2015). Lysosomal sequestration of hydrophobic weak base chemotherapeutics triggers lysosomal biogenesis and lysosome-dependent cancer multidrug resistance. *Oncotarget*, **6**(2), 1143–1156. <https://doi.org/10.18632/oncotarget.2732>

3.6 Appendix

Colour reagent test for amine deprotection and SPPS reaction monitoring



HZ22

6-(9,10-Dioxo-9,10-dihydroanthracen-1-ylamino)-hexanoic acid pentafluorophenyl ester

HZ22 is an active O-pentafluorophenolate ester, which is a safer and simpler alternative to the use of the Kaiser colour test for the detection of a free primary or secondary amino group (by amide formation). HZ22 colour test has several advantages over the Kaiser test in that it gives a positive result with secondary amines (the Kaiser test does not) and avoids the use of extremely toxic potassium cyanide and other hazardous chemicals used in the Kaiser test. HZ22 is used to import red resin beads indicate a positive test, for a primary or secondary amine. However, resin beads remain clear (not red colour) when there are no residual amino groups present.